Volume 51 Numbers 22–24 2004 ISSN 0967-0645

ELSEVIER

DEEP-SEA RESEARCH

PART II

itor:
ohn D. Milliman

est Editors:
. Turner
. Anderson
. McQuaid
.A. Nøst
. Pakhomov

The SWEDARP 1997/98 Expedition

Library
Pacific Islands Fisheries Science Center
Nat'l Marine Fisheries Service

Received Feb 2005

www.elsevier.com/locate/dsr2

DEEP-SEA RESEARCH II

http://www.elsevier.com/locate/dsr2

Editor

PROFESSOR JOHN D. MILLIMAN: *Virginia Institute of Marine Science, School of Marine Science, The College of William and Mary, P.O. Box 1346, Gloucester Point, VA 23062–1346, USA*
E-mail: milliman@vims.edu

Associate Editors

J.W. MURRAY (*Chemistry*): *School of Oceanography, WB-10, University of Washington, Seattle, WA 98195, U.S.A. E-mail: jmurray@ocean.washington.edu*

FRIEDRICH A. SCHOTT: *Institut für Meereskunde an der Universität Kiel, Düsternbrooker Weg 20, D-24105 Kiel, Germany. E-mail: fschott@ifm.uni-kiel.de*

SHARON L. SMITH: *The Rosenstiel School, University of Miami, 4600 Rickenbacker Causeway, Miami, FL 33149, USA. E-mail: ssmith@rsmas.miami.edu*

Founder Editor: DR. MARY SEARS

Publishing Offices Elsevier Ltd, The Boulevard, Langford Lane, Kidlington, Oxford OX5 1GB, UK. Tel: +44(0) 1865 843000; Fax: + 44(0) 1865 843010.

Advertising information. Advertising orders and enquiries can be sent to: ***USA, Canada and South America:*** Mr Tino DeCarlo, The Advertising Department, Elsevier Inc., 360 Park Avenue South, New York, NY 10010-1710, USA; phone: (+1) (212) 633 3815; fax: (+1) (212) 633 3820; e-mail: t.decarlo@elsevier.com. ***Europe and ROW:*** Katrina Barton, Advertising Department, Elsevier Ltd., 84 Theobald's Road, London WC1X 8RR, UK; phone (+44) 207 611 4117; fax: (+44) 207 611 4463; e-mail: k.barton@elsevier.com

USA mailing notice: *Deep-Sea Research II* (ISSN 0967-0645) is published annually in 26 issues by Elsevier Ltd. (P.O. Box 211, 1000 AE Amsterdam, The Netherlands). Annual subscription price in the USA US$ 3152 (valid in North, Central and South America), including air speed delivery.
USA POSTMASTER: Send address changes to *Deep-Sea Research II*, 655, Avenue of the Americas, New York, NY 10010.
AIRFREIGHT AND MAILING in the USA by Publications Expediting Inc., 200 Meacham Avenue, Elmont, NY 11003. Periodical postage rate paid at Jamaica, NY 11431.

Subscription Information

Published annually in 26 issues. Information on published and forthcoming issues can be found at the journal website.

Publication information: *Deep-Sea Research Part II* (ISSN 0967–0645). For 2004, volume 51 is scheduled for publication. Subscription prices are available upon request from the Publisher or from the Regional Sales Office nearest you or from this journal's website (http://www.elsevier.com./locate/dsr2). Further information is available on this journal and other Elsevier products through Elsevier's website: (http://www.elsevier.com). Subscriptions are accepted on a prepaid basis only and are entered on a calendar year basis. Issues are sent by standard mail (surface within Europe, air delivery outside Europe). Priority rates are available upon request. Claims for missing issues should be made within six months of the date of despatch.

Author enquiries. For enquiries relating to the submission of articles (including electronic submission), the preparation of electronic artwork, the status of accepted articles, author Frequently Asked Questions and any other enquiries relating to Elsevier, please consult http://authors.elsevier.com
Contact details for questions arising after acceptance of an article, especially those relating to proofs, are provided when an article is accepted for publication. Authors can also keep a track on the progress of their accepted article, and set up e-mail alerts informing them of changes to their manuscripts status, by using the "Track a paper" feature of Elsevier's Author Gateway (http: //authors.elsevier.com).

Orders, claims, and journal enquiries: please contact the Customer Service Department at the Regional Sales Office nearest you:
Orlando: Elsevier, Customer Service Department, 6277 Sea Harbor Drive, Orlando, FL 32887-4800, USA; phone: (+1) (877) 8397126 [toll free number for US customers], or (+1) (407) 3454020 [customers outside US]; fax: (+1) (407) 3631354; e-mail: usjcs@elsevier.com
Amsterdam: Elsevier, Customer Service Department, PO Box 211, 1000 AE Amsterdam, The Netherlands; phone: (+31) (20) 4853757; fax: (+31) (20) 4853432; e-mail: nlinfo-f@elsevier.com
Tokyo: Elsevier, Customer Service Department, 4F Higashi-Azabu, 1-Chome Bldg, 1-9-15 Higashi-Azabu, Minato-ku, Tokyo 106-0044, Japan; phone: (+81) (3) 5561 5037; fax: (+81) (3) 5561 5047; e-mail: jp.info@elsevier.com
Singapore: Elsevier, Customer Service Department, 3 Killiney Road, #08-01 Winsland House I, Singapore 239519; phone: (+65) 63490222; fax: (+65) 67331510; e-mail: asiainfo@elsevier.com

♾ The paper used in this publication meets the requirements of ANSI/NISO Z39. 48-1992 (Permanence of Paper).

© **2004 Elsevier Ltd. All rights reserved.**

Back Issues: Back issues of all previously published volumes are available direct from Elsevier Offices. Complete volumes and single issues can be purchased for 1999–2003. Earlier issues are available in high quality photo-duplicated copies as complete volumes only. Back volumes on microfilm are available from UMI, 300 North Zeeb Road, Ann Arbor, MI 48106-1346, USA.

Cover image: Bouvet Island — photograph courtesy of Stefan Bertilsson.

DEEP-SEA RESEARCH

PART II

Topical Studies in Oceanography

The SWEDARP 1997/98 Expedition

Guest Editors

David Turner
Department of Chemistry
Analytical and Marine Chemistry
Göteborg University
SE-412 96 Göteborg, Sweden

Leif Anderson
Department of Chemistry
Analytical and Marine Chemistry
Göteborg University
SE-412 96 Göteborg, Sweden

Christopher McQuaid
Department of Zoology and Entomology
Rhodes University
Grahamstown 6140, South Africa

Ole Anders Nøst
Norwegian Polar Institute
N-9296 Tromsø, Norway

Evgeny Pakhomov
Department of Earth and Ocean Sciences
University of British Columbia
6339 Stores Road
Vancouver BC, Canada V6T 1Z4

ELSEVIER

STATEMENT POLICY

Deep-Sea Research Part II: Topical Studies in Oceanography Publishes the topical issues arising from the many international and interdisciplinary projects which are undertaken.

Shorter research papers are welcomed for *Deep-Sea Research Part I: Oceanographic Research Papers*. Acceptable topics for papers include:

(1) the results of original scientific research
(2) theoretical work of evident oceanographic applicability
(3) the solution of some instrumental or laboratory problem with evidence of its successful use, and
(4) applications of oceanography.

Papers dealing with research on continental shelves (water depths shallower than 100–200 m) in most cases should be submitted to our sister journal *Continental Shelf Research*.

Progress reports and review articles may be invited by the Editor but these are generally more appropriate for *Progress in Oceanography*.

© 2004 Elsevier Ltd. All rights reserved.

This journal and the individual contributions contained in it are protected under copyright by Elsevier Ltd, and the following terms and conditions apply to their use:

Photocopying
Single photocopies of single articles may be made for personal use as allowed by national copyright laws. Permission of the publisher and payment of a fee is required for all other photocopying, including multiple or systematic copying, copying for advertising or promotional purposes, resale, and all forms of document delivery. Special rates are available for educational institutions that wish to make photocopies for non-profit educational classroom use.

Permissions may be sought directly from Elsevier Global Rights Department, P.O. Box 800, Oxford OX5 1DX, UK; phone: (+44) 1865 843830, fax: (+44) 1865 853333, e-mail: permissionselsevier.co.uk. You may also contact Global Rights directly through Elsevier's home page (http://www.elsevier.com), by selecting 'Obtaining Permissions'.

In the USA, users may clear permissions and make payments through the Copyright Clearance Center, Inc., 222 Rosewood Drive, Danvers, MA 01923, USA; phone: (+1) (978) 7508400, fax: (+1) (978) 7504744, and in the UK through the Copyright Licensing Agency Rapid Clearance Service (CLARCS), 90 Tottenham Court Road, London W1P 0LP, UK; phone: (+44) 20 7631 5555; fax: (+44) 20 7631 5500. Other countries may have a local reprographic rights agency for payments.

Derivative Works
Subscribers may reproduce tables of contents or prepare lists of articles including abstracts for internal circulation within their institutions. Permission of the publisher is required for resale or distribution outside the institution.

Permission of the publisher is required for all other derivative works, including compilations and translations.

Electronic Storage or Usage
Permission of the Publisher is required to store electronically any material contained in this journal, including any article or part of an article.

Except as outlined above, no part of this publication may be reproduced, stored in a retrieval system or transmitted in any form or by any means, electronic, mechanical, photocopying, recording or otherwise, without prior written permission of the publisher.

Address permissions requests to: Elsevier Global Rights Department, at the mail, fax and e-mail addresses noted above:

Notice
No responsibility is assumed by the Publisher for any injury and/or damage to persons or property as a matter of products liability, negligence or otherwise, or from any use or operation of any methods, products, instructions or ideas contained in the material herein. Because of rapid advances in the medical sciences, in particular, independent verification of diagnoses and drug dosages should be made.

Although all advertising material is expected to conform to ethical (medical) standards, inclusion in this publication does not constitute a guarantee or endorsement of the quality or value of such product or of the claims made of it by its manufacturer.

The SWEDARP 1997/98 Expedition

Volume 51 Nos. 22–24, 2004

CONTENTS

D.R. Turner, S. Bertilsson, A. Fransson and E. Pakhomov	2543	The SWEDARP 1997/98 marine expedition: overview
S. Bertilsson, P. Carlsson and W. Granéli	2557	Influence of solar radiation on the availability of dissolved organic matter to bacteria in the Southern Ocean
W. Granéli, P. Carlsson and S. Bertilsson	2569	Bacterial abundance, production and organic carbon limitation in the Southern Ocean (39–62°S, 4–14°E) during the austral summer 1997/1998
K.E. Rasmus, W. Granéli and S.-Å. Wängberg	2583	Optical studies in the Southern Ocean
E.A. Pakhomov and P.W. Froneman	2599	Zooplankton dynamics in the eastern Atlantic sector of the Southern Ocean during the austral summer 1997/1998—Part 1: Community structure
E.A. Pakhomov and P.W. Froneman	2617	Zooplankton dynamics in the eastern Atlantic sector of the Southern Ocean during the austral summer 1997/1998—Part 2: Grazing impact
P.W. Froneman	2633	Protozooplankton community structure and grazing impact in the eastern Atlantic sector of the Southern Ocean in austral summer 1998
E.A. Pakhomov	2645	Salp/krill interactions in the eastern Atlantic sector of the Southern Ocean
L.M. Jantunen, H. Kylin and T.F. Bidleman	2661	Air–water gas exchange of α-hexachlorocyclohexane enantiomers in the South Atlantic Ocean and Antarctica
D. Chen, S.-Å. Wängberg, A. Wulff and K. Borne	2673	Attenuation of biologically effective UV doses under overcast skies: a case study from the eastern Atlantic sector of the Southern Ocean
T. Tanhua, K.A. Olsson and E. Fogelqvist	2683	A first study of SF_6 as a transient tracer in the Southern Ocean
A. Wulff and S.-Å. Wängberg	2701	Spatial and vertical distribution of phytoplankton pigments in the eastern Atlantic sector of the Southern Ocean

P.W. Froneman, E.A. Pakhomov and M.G. Balarin	2715	Size-fractionated phytoplankton biomas production and biogenic carbon flux in t eastern Atlantic sector of the Southern Ocea in late austral summer 1997–1998
S.-Å. Wängberg and A. Wulff	2731	Impact of ultraviolet-B radiation on t development of phytoplankton communiti in the eastern Atlantic sector of the Southe Ocean—results from on-deck model ecosy tem experiments
K. Abrahamsson, S. Bertilsson, M. Chierici, A. Fransson, P.W. Froneman, A. Lorén and E.A. Pakhomov	2745	Variations of biochemical parameters along transect in the Southern Ocean, with speci emphasis on volatile halogenated organi compounds
A. Fransson, M. Chierici, L.G. Anderson and R. David	2757	Transformation of carbon and oxygen in th surface layer of the eastern Atlantic sector c the Southern Ocean
M. Chierici, A. Fransson, D.R. Turner, E.A. Pakhomov and P.W. Froneman	2773	Variability in pH, fCO_2, oxygen and flux o CO_2 in the surface water along a transect i the Atlantic sector of the Southern Ocean
K. Abrahamsson, A. Lorén, A. Wulff and S.-Å. Wängberg	2789	Air–sea exchange of halocarbons: the influ ence of diurnal and regional variations an distribution of pigments
A.-M. Larsson	2807	The role of mixing in an Antarctic ocea ecosystem: observations and model computa- tions of vertical distributions of relate parameters
A. Fransson, M. Chierici and L.G. Anderson	2827	Diurnal variability in the oceanic carbon dioxide system and oxygen in the Southern Ocean surface water
M. Öztürk, P.L. Croot, S. Bertilsson, K. Abrahamsson, B. Karlson, R. David, A. Fransson and E. Sakshaug	2841	Iron enrichment and photoreduction of iron under UV and PAR in the presence of hydroxycarboxylic acid: implications for phytoplankton growth in the Southern Ocean
P.L. Croot, K. Andersson, M. Öztürk and D.R. Turner	2857	The distribution and speciation of iron along 6°E in the Southern Ocean

CONTENTS direct

This journal is part of **ContentsDirect**, the ***free*** alerting service which sends tables of contents by e-mail for Elsevier books and journals. You can register for **ContentsDirect** online at: **www.elsevier.com/locate/contentsdirect**

ELSEVIER

Deep-Sea Research II 51 (2004) 2543–2556

DEEP-SEA RESEARCH
PART II

www.elsevier.com/locate/dsr2

The SWEDARP 1997/98 marine expedition: overview

David R. Turner[a,*], Stefan Bertilsson[b], Agneta Fransson[c], Evgeny Pakhomov[d,e]

[a]*Department of Chemistry, Analytical and Marine Chemistry, Göteborg University, SE-412 96 Göteborg, Sweden*
[b]*Department of Evolutionary Biology/Limnology, Uppsala University, Norbyvägen 20, SE-752 36 Uppsala, Sweden*
[c]*Climate Change Research Project, National Institute for Environmental Studies, 16-2 Onogawa, Tsukuba, Ibaraki 305-8506, Japan*
[d]*Department of Earth and Ocean Sciences, University of British Columbia, 6339 Stores Road, Vancouver, B.C., V6T 1Z4, Canada*
[e]*Zoology Department, Faculty of Science and Technology, University of Fort Hare, Private Bag X1314, Alice 5700, South Africa*

Abstract

The SWEDARP 1997/98 expedition aboard the S.A. *Agulhas* focused on three study areas along the 6°E meridian: 60°S, the location of the spring ice edge; 56°S, the location of the winter ice edge; and 50.5°S, the Antarctic Polar Front. This intensive study was preceded by a north–south transect through the area measuring surface water properties while under way. An extensive measurement programme included hydrography, tracers, nutrients, organic carbon, trace metals, bacteria, and primary and secondary producers (including production and grazing rates). Analysis of the results from the three study areas does not identify a single factor limiting primary production: water column stability and the optical regime, and probably iron supply contributed to the control of primary production. The study area acted as a sink for atmospheric CO_2 at the time of measurement, while analysis of water column carbon inventories indicated a net CO_2 source integrated over the spring season.
© 2004 Elsevier Ltd. All rights reserved.

1. Introduction

This paper provides an overview of the SWEDARP 1997/98 oceanographic expedition, which took place in the region of the southeast Atlantic Ocean between South Africa and Queen Maud Land (Fig. 1). The expedition aboard the S.A. *Agulhas* was a collaboration between the Swedish and South African Antarctic Research Programmes, with contributions from the Norwegian and Finnish Antarctic Research Programmes. The expedition also contributed to Southern Ocean JGOFS, whose aims were to (i) constrain the fluxes of carbon, both organic and inorganic, and to place these fluxes in the context of the contemporary carbon cycle, (ii) identify the factors and processes which regulate the magnitude and variability of primary production rates and the fate of biogenic materials, (iii) improve models of response to past climate changes, and (iv) predict the response of the Southern Ocean to global climate change. The specific aims of this expedition

*Corresponding author. Tel.: +46-31-772-2295; fax +46-31-772-2785
E-mail address: davidt@chem.gu.se (D.R. Turner).

0967-0645/$ - see front matter © 2004 Elsevier Ltd. All rights reserved.
doi:10.1016/j.dsr2.2003.08.006

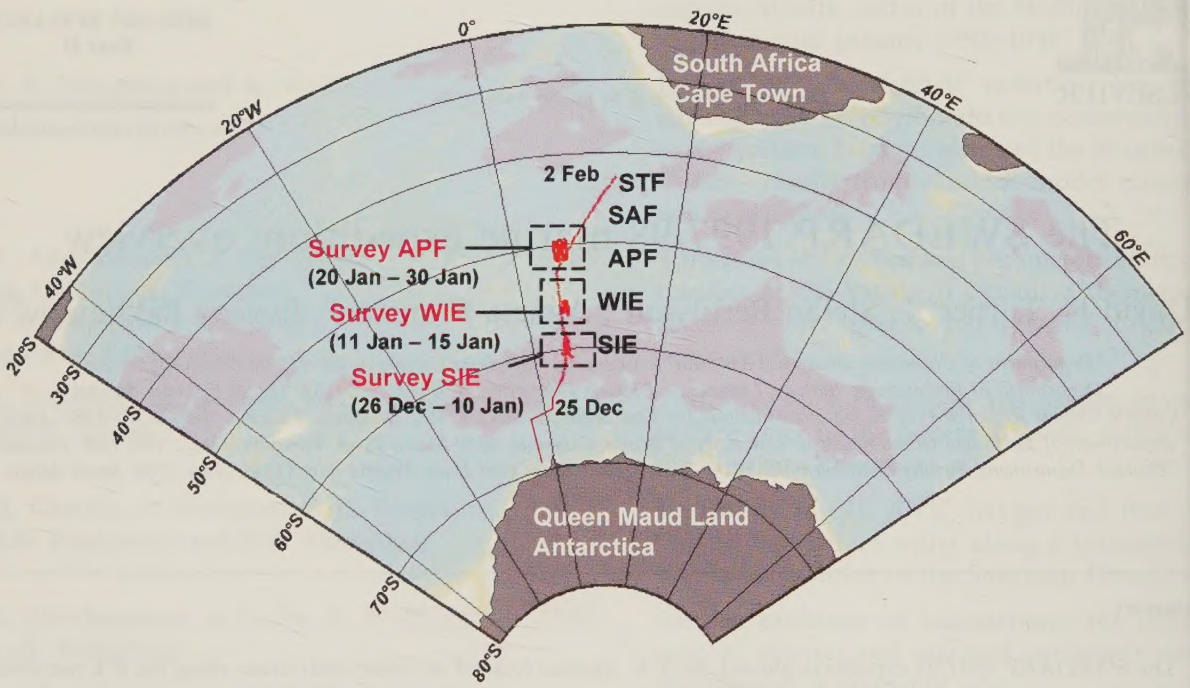

Fig. 1. Cruise track along 6°E from Cape Town to the ice edge at 61°S. Approximate positions for the detailed surveys on the north-going track are shown as well as the major fronts STF, SAF and the APF. The WIE is located around 56°S and SIE at 60°–61°S. Map prepared using Ocean Data View (Schlitzer, 2002).

were to determine the relative importance of different potential controlling factors for primary production (availability of iron and other micro-nutrients, deep mixing/upwelling, light conditions, grazing and other trophic interactions) along a transect from the Polar Front to the ice edge; and to assess the consequences of the resulting primary and secondary production for the carbon cycle.

1.1. Carbon cycling in the Southern Ocean

A significant portion of the world's oceans is characterized by low phytoplankton biomass and productivity while the major nutrients that are generally believed to limit primary production in the sea (N, P, Si) are available in high amounts. These "high-nutrient low-chlorophyll" (HNLC) areas include the equatorial and subarctic Pacific Ocean as well as the Southern Ocean (Legendre and Rassoulzadegan, 1995; Minas et al., 1986). Earlier studies have suggested that the availability of iron or other trace elements could be the factor ultimately limiting the photosynthetic activity that drives the biological carbon pump in these regions (Chavez et al., 1991; Martin et al., 1991; Morel et al., 1991), but the evidence is inconclusive and factors such as grazing, food web structure and temperature may also be important in this regard (Cavender–Bares et al., 1999; Frost, 1991; Gall et al., 2001). These regions have recently received considerable attention due to the potential for elevated primary production and a resulting higher CO_2 sequestration in response to either climate change or input of limiting nutrients such as iron (Falkowski et al., 1998; Hall and Safi, 2001; Scharek et al., 1997). Among these three major HNLC regions, the Southern Ocean has the largest potential to affect atmospheric CO_2 levels. Not only is this region the largest of the three HNLC areas, but it is also characterized by major upwelling of nutrient-rich water from the deep ocean representing a tremendous input of

macronutrients to the euphotic zone. These nutrients are only partly being utilized for biological production before the water returns to the deeper layers at the Antarctic Circumpolar Current (Falkowski et al., 1998). An uncoupling of the biological carbon pump from the current limitations could result in an elevated primary production since macronutrients are available in excess and this may in turn lead to an increase in the biological sequestration of atmospheric CO_2 which could act as a feedback mechanism that would counteract to the current increase in global atmospheric CO_2.

In addition to the above-mentioned general features of HNLC regions, the Southern Ocean is characterized by extremely low temperatures that exert considerable control over the biological community and the water chemistry. The region is also highly heterogeneous: i.e. it can be divided into several distinct water masses that differ in physical, chemical as well as biological parameters (Priddle et al., 1992). Influence from sea ice cover may also exert considerable local control of these waters (Mordy et al., 1995). Hence in order to model either the current primary production and associated carbon fluxes in the Southern Ocean, or to predict the response of the system to global change (e.g. temperature, availability of limiting nutrients, solar irradiation), there is a need for studies from many different regions sampled at different time points. Controlled experimental manipulations may also provide crucial information in this regard, since a wide range of factors such as zooplankton and protozoan grazing, competition for macronutrients and trace elements between different primary producers and heterotrophic microorganisms, and inhibition by ultraviolet radiation may have a significant impact on the ability of the phytoplankton community to act as a biological carbon pump in these waters.

1.2. Hydrographic description of the area

According to earlier investigations, biological activity in the Southern Ocean is strongly linked to frontal systems (Allanson et al., 1981; Bathmann et al., 1997; Froneman et al., 2000; Laubscher et al., 1993; Lutjeharms, 1985; Lutjeharms and Valentine, 1984; Pakhomov et al., 2000; Pollard et al., 2002; Read et al., 2002; Smetacek et al., 1997), where the Subtropical and Polar Fronts are shown to be the areas of most intense activity (Pakhomov and McQuaid, 1996, 2000).

1.2.1. Subtropical Front

The northern boundary of the Southern Ocean is confined by the Subtropical Front (STF), where it separates the warm and salty temperate surface waters and the cold subantarctic waters (Orsi et al., 1995; Stramma and Peterson, 1990; Whitworth and Nowlin, 1987). This front has previously been observed at various positions between 41°S and 42°S, defined by its large salinity and temperature gradients, where also elevated chlorophyll *a* (Chl-*a*) concentrations have been found (Lutjeharms, 1985; Lutjeharms and Valentine, 1984; Pollard et al., 2002; Read et al., 2002).

1.2.2. Subantarctic Front

South of the STF is the eastward flowing Antarctic Circumpolar Current (ACC), which is one of the most prominent features of the Southern Ocean. The ACC is dominated by two major fronts, the Subantarctic Front (SAF) and the Antarctic Polar Front (APF) (Orsi et al., 1995; Pollard et al., 2002; Whitworth and Nowlin, 1987). The SAF plays an important role as a biogeographical boundary, which separates the Antarctic and subantarctic/subtropical groups of zooplankton (Froneman et al., 1995; Pakhomov and McQuaid, 1996; Pakhomov et al., 2000). The position of the SAF has been reported between 45°S and 48°S in this region (6°W–6°E) (Lutjeharms, 1985; Lutjeharms and Valentine, 1984; Pakhomov et al., 2000; Pollard et al., 2002; Read et al., 2002; Whitworth and Nowlin, 1987) depending on the definition used.

The zone between the STF and the SAF is referred to as the Subantarctic Zone (SAZ), and surface water stratification in this region is controlled mainly by temperature (Orsi et al., 1995; Pollard et al., 2002). Silicate has been suggested to limit biological production in the SAZ, but also across the ACC (Pollard et al., 2002).

1.2.3. Antarctic Polar Front

Depending on definition, subsurface or surface expressions for temperature, the location of the APF can vary between 49°S and 51.5°S in this region (Belkin and Gordon, 1996; Gordon, 1967; Lutjeharms, 1985; Lutjeharms and Valentine, 1984; Orsi et al., 1995; Pakhomov et al., 2000; Pollard et al., 2002; Read et al., 2002; Veth et al., 1997; Whitworth and Nowlin, 1987). The cold surface water in the APF, termed the Antarctic Surface Water (AASW), reaches all the way to the Antarctic Continental Shelf (Orsi et al., 1995). Below this cold water lies a warmer, saltier and more nutrient-rich layer, called Circumpolar Deep Water (CDW) (Orsi et al., 1995). The CDW is derived from the North Atlantic Deep Water (NADW) and covers most of the area from the APF to the Weddell Gyre (Veth et al., 1997). Macronutrients such as nitrate and phosphate do not limit the biological production in these waters (de Baar et al., 1995), but deep mixing during winter may still be an important regulator of primary production through transport of iron and other limiting trace elements to the surface layer (de Baar et al., 1995; Veth et al., 1997). However, the depth of the mixed layer also affects primary production through the light regime, a shallow mixed layer creating a more favourable light regime than a deep mixed layer.

The area between the SAF and the APF is referred to as the Polar Frontal Zone (PFZ) (Belkin and Gordon, 1996; Pollard et al., 2002; Whitworth and Nowlin, 1987), where salinity is as important as temperature in regulating surface water stratification, and primary production has been shown to be limited by silicate availability (Pollard et al., 2002).

1.2.4. ACC south of the APF

The southern boundary of ACC is defined where the upper part of the CDW (UCDW) signal enters the surface mixed layer at around 56°S, where it mixes with AASW (Orsi et al., 1995; Pollard et al., 2002; Whitworth and Nowlin, 1987), which coincides with a frontal feature separating the ACC and the Weddell Gyre (Veth et al., 1997). When UCDW water mixes with surface water, macronutrients and iron become available for biological production.

The Antarctic Zone (AAZ) is the area between the APF and the southern boundary of the ACC where salinity contributes most to the stratification of the surface layer (Pollard et al., 2002). South of this boundary, between 56°S and the continent, in the Weddell Gyre (Veth et al., 1997), also referred to as the zone south of the ACC (SACCZ) by Pollard et al. (2002).

1.3. Sea ice coverage

In this region, the area between the APF and the Antarctic ice shelf is subject to seasonal sea-ice. The northernmost winter sea-ice expansion in the Atlantic sector is located between 53°S and 54°S (Pakhomov et al., 2000; Veth et al., 1997), thereby influencing the area between the ACC and the Weddell Gyre (Veth et al., 1997). During the spring season, the ice edge has commonly retreated to around 60°S (Comiso, 1993; Pakhomov et al., 2000).

1.4. Expedition plan

The passage from Cape Town to Queen Maud Land was primarily a transport leg, with no opportunity for station sampling. However, a range of underway surface measurements were made on this transect (Table 1), and also along the 6°E meridian on the later northbound leg. In addition to this surface transect, the main, northbound leg of the expedition combined a transect of deep (3000 m) CTD stations with more detailed surveys of three selected areas. These included two areas selected for relatively high biological production, the APF (Bathmann et al., 1997; Froneman et al., 2000; Lutjeharms, 1985; Lutjeharms and Valentine, 1984; Pakhomov et al., 2000; Pollard et al., 2002; Read et al., 2002; Smetacek et al., 1997), the spring ice edge (SIE) (Jennings et al., 1984; Pakhomov et al., 2000; Smith and Nelson, 1990); and the winter ice edge (WIE), an area with significantly lower primary productivity (Pakhomov et al., 2000). The measurement programme in each of these areas consisted of an areal survey comprising Scanfish transects and

Table 1
Measurement programme

Parameter	Transect leg 1	Deep CTD section	Area surveys	Biostations	Shallow CTD sections	Reference(s) or responsible scientist
Hydrography						
Salinity	X	X	X	X	X	Support data
Temperature	X	X	X	X	X	Support data
Fluorescence	X	X	X	X	X	Support data
Transmittance		X		X	X	Support data
Water column radiation				X	X	Rasmus et al. (2004)
ADCP			X			L. Djurfeldt
Tracers						
Freons		X			X	Tanhua et al. (2004)
Sulphur hexafluoride		X			X	Tanhua et al. (2004)
Meteorology, atmosphere						
Incident radiation	X	X	X	X	X	Chen et al. (2004)
Atmospheric mercury	X	X	X	X	X	L. Jantunen
Atmospheric organochlorines						Jantunen et al. (2004)
Nutrients, CO_2, O_2						
Nitrate, nitrite, silicate		X		X	X	Support data
Ammonium, urea	X			X	X	F. Sörensson
Total inorganic carbon	X	X	X	X	X	Fransson et al. (2004a,b)
Alkalinity	X	X	X	X	X	Fransson et al. (2004a,b)
pH	X	X	X	X	X	Chierici et al. (2004)
fCO_2	X		X	X	X	Chierici et al. (2004)
Oxygen	X	X	X	X	X	Chierici et al. (2004); Fransson et al. (2004a,b)
Hydrogen peroxide	X			X	X	K. Abrahamsson
Organic carbon						
TOC		X	X		X	M. Wedborg
POC	X					F. Sörensson
Humic substances		X	X		X	M. Wedborg
Colloidal organic carbon		X			X	Hassellöv (submitted)
Carbohydrates		X			X	G. Hulthe
Organochlorines	X					Jantunen et al. (2004)
Biogenic halocarbons				X		Abrahamsson et al. (2004a,b)
Trace metals						
Iron		X	X	X	X	Croot et al. (2004)
Copper		X	X	X	X	P. Croot
Biological standing stocks						
Bacterial numbers	X	X		X	X	Granéli et al. (2004)
Chl-*a*	X	X	X	X	X	Support data
Plant pigments	X			X	X	Wulff and Wängberg (2004)
Phytoplankton counts	X	X		X	X	B. Karlson
Zooplankton abundance				X	X	Froneman (2004); Pakhomov and Froneman (2004a)
Biological rate processes						
Bacterial production						Granéli et al. (2004)
Primary production				X		Froneman et al. (2004)
New production				X		F. Sörensson

Table 1 (*continued*)

Parameter	Transect leg 1	Deep CTD section	Area surveys	Biostations	Shallow CTD sections	Reference(s) or responsible scientist
Zooplankton grazing				X		Pakhomov, (2004); Pakhomov and Froneman (2004b)

Measured parameters are marked by a cross. Data published in this volume or elsewhere are indicated by references. Parameters used as supporting data in several publications are marked as "support data"; where data are unpublished, the lead scientist's name is given. This table does not include the incubation experiments focusing on the effects of UV-radiation on the plankton community (Wängberg et al., 2004), on iron bioavailability (Özturk et al., 2004), and on DOC availability in relation to photochemistry (Bertilsson et al. 2004), each of which included an extensive multidisciplinary measurement programme.

underway surface measurements; a series of shallow CTD stations along the 6°E meridian; and one or more 36-h stations for diurnal studies and biological incubations (Biostations, see Table 2 for details).

Fig. 2 shows the location of these elements in each of the study areas. This measurement programme was complemented by two programmes of long-term incubation experiments focusing on the effects of UV radiation, and on iron–organic carbon interactions on primary productivity. The complete measurement programme is summarized in Table 1.

2. Results and discussion

2.1. Hydrography

The positions of the major frontal systems were identified from the temperature and salinity sections (Figs. 3 and 4).

The presence of the Subtropical Front was indicated by a significant surface temperature change from 12 to 10 °C close to 43°S, accompanied by a sharp decrease in the surface salinity from about 34.95 to 34.2 (Chierici et al., 2004): these changes cannot be discerned in Figs. 3 and 4 since they occur at the edge of the contour sections. According to Belkin and Gordon (1996), the STF is defined at the position where the temperature decreases from 12 to 10 °C at 200 m depth, which would locate the STF in our study further to the north, where lack of data makes it difficult to give an exact position for the STF.

The SAF was identified by a sharp surface water temperature change of 2 °C (from about 8 °C to 6 °C), accompanied by a sharp surface salinity change, between 46°S and 47°S (Fig. 4). Peaks in Chl-*a* have earlier been observed at this location (Pakhomov et al., 2000; Read et al., 2002), and were also found in our study (Chierici et al., 2004).

The APF was located between 50°S and 51°S using the sub-surface temperature minimum of 2 °C at 200 m as a proxy (Orsi et al., 1995) (Fig. 4). However, a sharp change in surface water temperature locates the APF in our study closer to 52°S (Fig. 4). Enhanced Chl-*a* concentrations were found at the APF during this study (Chierici et al., 2004; Froneman et al., 2004), confirming earlier reports in this area (Bathmann et al., 1997; Pakhomov et al., 2000; Read et al., 2002). The area was also characterized by high zooplankton abundances (Pakhomov and Froneman, 2004a), in agreement with earlier observations (Pakhomov et al., 2000).

2.2. Sea-ice coverage

Satellite images show that the WIE in austral winter 1997 was located at 56°S, and retreated steadily between August and November 1997 (Fig. 5), resulting in the SIE at 60°S which was observed on the expedition's southbound transect. The satellite images for December and January

Table 2
Typical Biostation measurement programme

Time	Measurement/sampling
23.00	Bongo net tow
03.00	Bongo net tow
07.00	Bongo net tow
08.00	Downwelling radiation
08.30	CTD 300 m for primary productivity
09.15	Downwelling and upwelling radiation
09.45	Sampling for 15N measurements
10.15	Sampling for trace metals
10.40	Sampling for biogenic halocarbons
11.00	Bongo net tow
12.00	CTD 300 m*
13.00	Downwelling and upwelling radiation
14.00	CTD 300 m*
15.00	Bongo net tow
16.00	CTD 300 m*
16.45	Transmittance depth profile
17.00	Trace metal and biogenic halocarbon sampling
18.00	CTD 300 m*
19.00	Bongo net tow
20.00	CTD 300 m*
21.00	Sampling for biogenic halocarbons
21.30	Sampling for 15N measurements
22.00	CTD 300 m*
23.00	Bongo net tow
24.00	CTD 300 m*
01.00	Sampling for biogenic halocarbons
02.00	CTD 300 m*
03.00	Bongo net tow
04.00	CTD 300 m*
05.00	Sampling for biogenic halocarbons
06.00	CTD 300 m*
07.00	Bongo net tow
08.00	CTD 300m for primary produtctivity
09.00	Sampling for persistent organic pollutants
10.00	CTD 300 m*
11.00	Bongo net tow

*Water samples for a wide range of analyses taken from these samples (see Table 1).

(Fig. 5) indicate that the ice edge did not continue to retreat steadily, but rather thinned across a wide area and then dispersed within a short period of time during December 1997. This description is consistent with our observations from the S.A. *Agulhas*; the southward transect encountered significant ice coverage from 60°S to a coastal polynya off the ice shelf. Only two weeks later, the passage from the ice shelf (71°S) back to 60°S was essentially ice-free.

Seasonal sea-ice retreat around the Weddell Gyre has previously been suggested to result in phytoplankton blooms (Jennings et al., 1984; Pakhomov et al., 2000; Smith and Nelson, 1990). At the SIE, the rapid changes in ice coverage resulted in a shallow stratification of the surface layer. This stratification in combination with favourable light conditions and availability of macronutrients and iron, created an ideal environment for biological production with a three-fold increase in Chl-*a* and supersaturation in oxygen together with a large CO_2 undersaturation (Chierici et al., 2004; Froneman et al., 2004).

2.3. The southbound underway transect

Measurements were made from 43°S to 62°S: sampling of pumped surface water ceased at 62°S due to clogging of the water intake with ice. Surface chlorophyll concentrations varied between approximately 0.2 and 1 mg m^{-3}, with the highest concentrations occurring close to the major frontal systems. Bacterial counts decreased sharply towards the south, and were well correlated with temperature, but showed no correlation with phytoplankton abundance as assessed by chlorophyll concentrations (Abrahamsson et al., 2004a). Carbon dioxide was significantly undersaturated south of the SAF (48–62°S), the undersaturation resulting from a combination of cooling and photosynthesis. The instantaneous air–sea flux of CO_2, calculated using measured wind speeds, showed a significant sink between 50°S and 56°S, with only small CO_2 fluxes elsewhere (Chierici et al., 2004). Measurements of halocarbons showed significant spatial and temporal variability, which could not be directly related to chlorophyll or other parameters (Abrahamsson et al., 2004a).

2.4. Major study areas

2.4.1. Primary production

Twelve primary production stations were occupied in the three study regions with the highest (59–77 mmol C m^{-2} d^{-1}) and lowest (24–26 mmol C m^{-2} d^{-1}) primary production rates recorded in the APF and WIE regions, respectively. In the SIE region, intermediate values

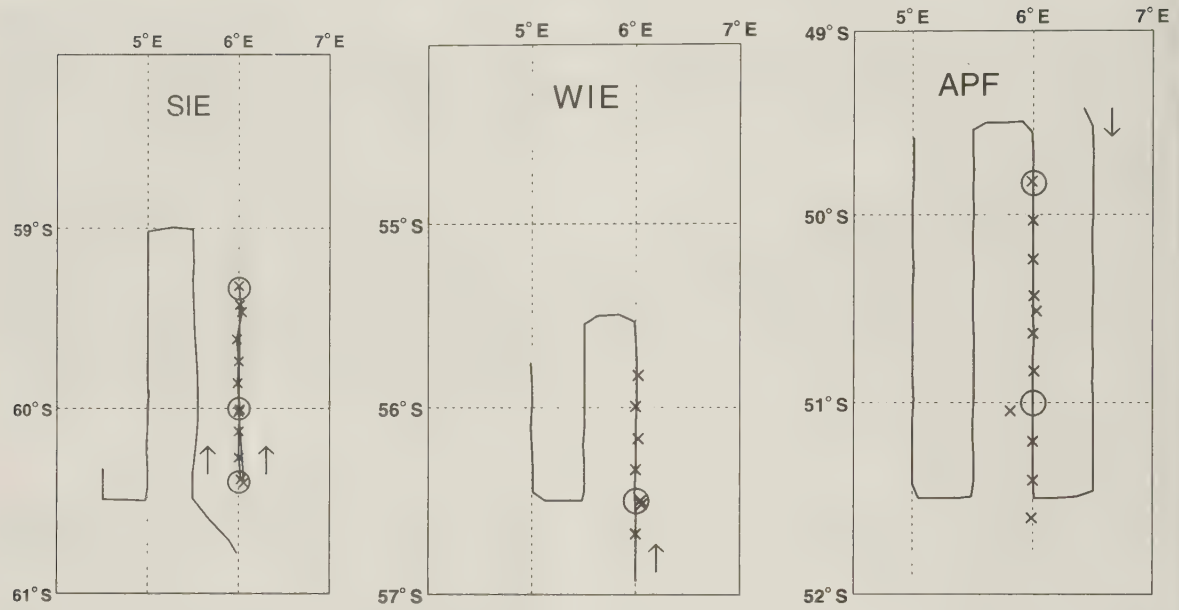

Fig. 2. Overview of the sampling programme in the three study areas: — Scanfish tow lines, × 400 m CTD stations, ○ Biostations.

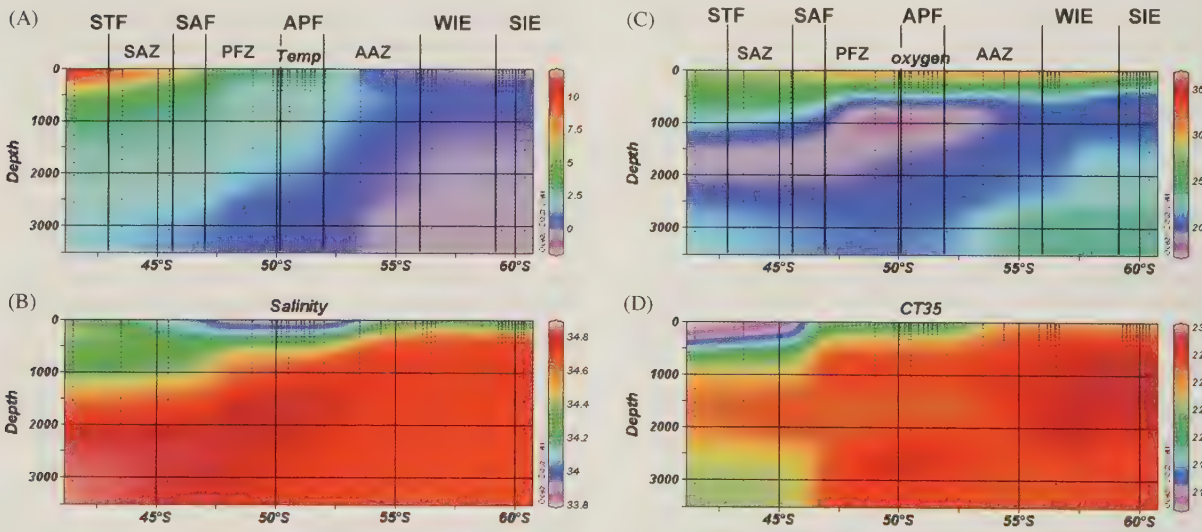

Fig. 3. Deep section plots along the 6°E transect from Cape Town (to the left) to the ice edge at 61°S (to the right) for (A) temperature, (B) salinity, (C) oxygen and (D) normalized CT ($S = 35$). The temperature and salinity diagrams show the water masses from all depths at all stations. The fronts and frontal zones (abbreviations) are marked in the figure. Plots prepared using Ocean Data View (Schlitzer, 2002).

(26–61 mmol C $m^{-2} d^{-1}$) of primary production were observed (Table 3) (Froneman et al., 2004). At stations occupied in the SIE and APF regions, the euphotic depth (ED) exceeded the mixed layer depth (MLD). In contrast, the MLD exceeded the ED depth in the WIE region. As a consequence,

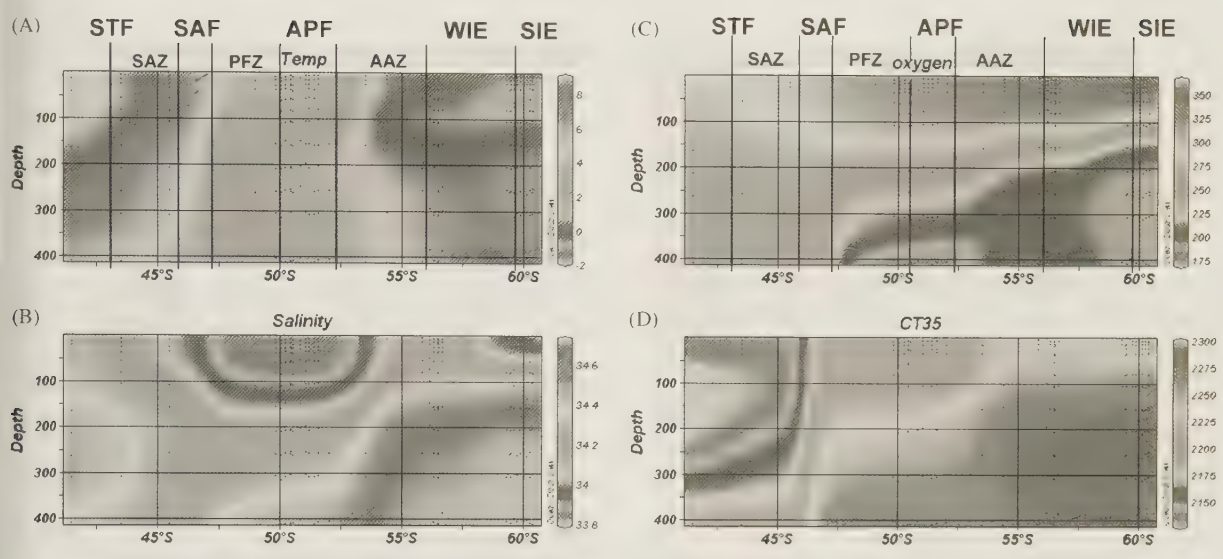

Fig. 4. Shallow section plots along the 6°E transect from Cape Town (to the left) to the ice edge at 61°S (to the right) for (A) temperature, (B) salinity, (C) oxygen and (D) normalized CT ($S=35$) in the upper 400 m. The fronts and frontal zones (abbreviations) are marked in the figure. Plots prepared using Ocean Data View (Schlitzer, 2002).

the ED/MLD ratio explained up to 53% of total variance in total primary production. Size fractionated chlorophyll-a biomass and primary production rates differed dramatically between three regions. In the regions with the highest primary production rates (APF and SIE), microphytoplankton (>20 μm) accounted for >60% of Chl-*a* standing stock and total primary production, while nano- and picophytoplankton contributed to >60% of Chl-*a* standing stock and total primary production in the WIE region (Froneman et al., 2004).

It is generally accepted that bioavailable iron is the element limiting primary production in environments with an excess of macronutrients. During the SWEDARP study, total iron concentrations at 10 m depth ranged from <0.4 to 1.6 nmol L^{-1}, with the highest concentrations in the southern region of the SIE and the lowest at the northern part of the APF region (Croot et al., 2004). Although the general spatial patterns of iron concentration and primary production were similar, no significant correlations between iron availability and primary production rates could be identified (Croot et al., 2004). This indicates that other factors are significant in the regulation of primary production in the study areas.

2.4.2. *Bacterial abundance*

Surprisingly, bacterial abundance was uniformly low south of the APF and bacterial production in the top 50-m layer only varied between 2 and 4 mmol C m^{-2} d^{-1} (Granéli et al., 2004). In situ observations demonstrated that both temperature and phytoplankton biomass had a positive influence on the heterotrophic bacterial community (Abrahamsson et al., 2004a; Granéli et al., 2004). In addition, experimental manipulations under controlled conditions showed that the availability of nitrogen, phosphorus and organic carbon were important regulators of heterotrophic bacteria (Granéli et al., 2004), whereas solar irradiation and the concentration of more recalcitrant nutrients bound in aquatic humic substances seemed only to have a minor impact (Bertilsson et al., 2004).

2.4.3. *Food web and the biological carbon pump*

The portioning of carbon between the "classical" food web and "microbial loop" has been

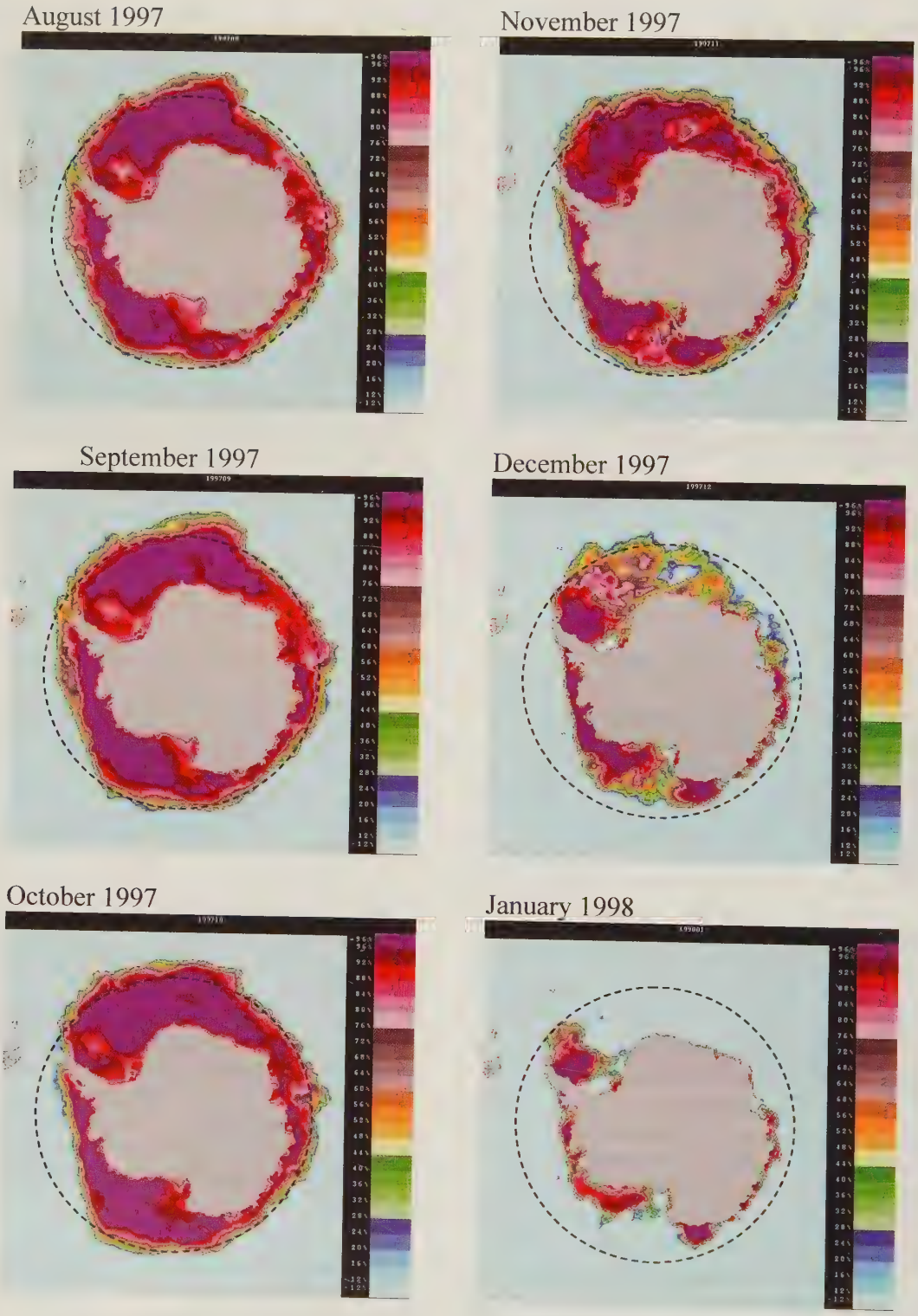

Fig. 5. Monthly ice-cover maps (Comiso, 1990). The 60°S meridian is shown as a dashed line.

Table 3
Selected mean functional characteristics of the pelagic ecosystem in the eastern Atlantic sector of the Southern Ocean during austral summer 1997/98

Parameter	Unit	APF	WIE	SIE	Reference
Sea–air CO_2 flux	$mmol\,m^{-2}\,d^{-1}$	−13	−2.5	−1.1	Fransson et al. (2004a)
Primary production	$mmol\,C\,m^{-2}\,d^{-1}$	66.7	25.4	50.1	Froneman et al. (2004)
Bacterial production (0–50 m)	$mmol\,C\,m^{-2}\,d^{-1}$	4.0	3.0	2.0	Granéli et al. (2004)
Chl-*a*	$mg\,m^{-2}$	28–51	17–23	21–55	Froneman et al. (2004)
Microzooplankton grazing	$mmol\,C\,m^{-2}\,d^{-1}$	3.8	2.2	2.7	Froneman (2004)
Mesozooplankton grazing	$mmol\,C\,m^{-2}\,d^{-1}$	18.8	13.1	2.6	Pakhomov and Froneman (2004b)
Maximum krill and salp grazing impact	$mmol\,C\,m^{-2}\,d^{-1}$	11.3	21.9	1.1	Pakhomov (2004)
Algal sinking	$mmol\,C\,m^{-2}\,d^{-1}$	3.3	1.3	2.5	Froneman et al. (2004)
Faecal pellet production	$mmol\,C\,m^{-2}\,d^{-1}$	5.6	3.9	0.8	Froneman et al. (2004)
Maximum krill and salp faecal pellet production	$mmol\,C\,m^{-2}\,d^{-1}$	1.4	4.0	0.1	Pakhomov (2004)

investigated in several papers (Froneman, 2004; Froneman et al., 2004; Pakhomov and Froneman, 2004b). Microzooplankton grazing varied between 2.2 and $3.8\,mmol\,C\,m^{-2}\,d^{-1}$ corresponding to ~5% of total primary production in the APF and SIE regions and ~10% in the WIE region (Table 3) (Froneman, 2004). It was apparent that protozooplankton alone were unable to control neither the total nor the small (<20 μm) phytoplankton stocks. This would be particularly important within the SIE, where protozooplankton was suggested to be an alternative carbon source for metazooplankton since the colonial haptophyte *Phaeocystis* spp. dominated the phytoplankton community (Froneman, 2004; Wulff and Wängberg, 2004), its chemical and/or colonial size properties making it resistant to grazing (Estep et al., 1990; Sieburth, 1960).

In general, metazoan abundance and biomass increased from the SIE to the APF region (Pakhomov and Froneman, 2004a). Copepods were the numerically dominant zooplankton group throughout the investigation, while euphausiids and tunicates were important contributors to total biomass in the WIE and APF regions (Pakhomov and Froneman, 2004a). Parallel to the increase in abundance, metazoan grazing impact increased from 2.6 to $19\,mmol\,C\,m^{-2}\,d^{-1}$ from south to north (Table 3) (Pakhomov and Froneman, 2004b). The highest phytoplankton consumption rate (~56% of total primary production) was recorded in the WIE region, while the APF region was characterized by modest (28%) grazing impact. The lowest phytoplankton removal (~5%) was observed in the SIE region (Pakhomov and Froneman, 2004b).

These results suggest that the relative efficiencies of the biological carbon pump in the three regions of investigation were related to the size structure of the phytoplankton assemblages and to the zooplankton community structure. In the SIE and APF regions, the partitioning of carbon between the microbial loop and classical food web was similar, while the classical food web dominated in the WIE, accounting for around 15% of total primary production (Froneman et al., 2004). In contrast, the larger phytoplankton assemblages in the SIE and APF regions were more resistant to mesozooplankton grazing, and consequently only 1–8% of total daily primary production could be transported to the depth via metazoan faecal pellets. In these regions, the sinking of dead or senescent phytoplankton assemblages could be an alternate route for the transfer of carbon to depth at these locations (Froneman et al., 2004). The results outlined above illustrate the substantial regional variability in the efficiency of the biological pump resulting from the size structure of the phytoplankton assemblages and grazer communities.

2.4.4. *Carbon dioxide and oxygen balances*

Air–sea fluxes of carbon dioxide and oxygen were estimated in each of the three study areas.

Spatial and diurnal variations, together with wind speed fluctuations, resulted in mean fluxes which were hardly statistically different from zero. All three areas were weak sinks for carbon dioxide in the order APF > WIE > SIE, while the APF and SIE were weak sources of oxygen to the atmosphere. The WIE was estimated to be a weak sink of oxygen (Fransson et al., 2004a). In contrast, longer-term estimates based on carbon inventories in the water column indicate that, from the preceding winter to the time of investigation, the study area has acted as a weak source of CO_2 to the atmosphere and as a weak sink for oxygen (Fransson et al., 2004b). These results, together with the observation of a strong instantaneous sink for CO_2 on the southbound transect, reinforce the importance of temporal and spatial integration when assessing air–sea fluxes of CO_2.

3. Conclusions

Significant progress has been made towards understanding the controls of carbon cycling and fluxes in the region south of the APF. Water column stability, light properties and probably also iron supply have contributed to the control of primary production in the eastern Atlantic sector of the Southern Ocean during austral summer 1997/98. In addition, zooplankton grazing, particularly grazing by large metazoans such as krill, salps and pteropods, has also contributed to the regulation of phytoplankton biomass and the fate of photosynthetically fixed carbon. While measurements of surface water CO_2 indicated that the study areas acted as a sink for atmospheric CO_2, estimates based on water column carbon inventories indicate that the study area had in fact been a weak source of CO_2 to the atmosphere during the spring season.

Acknowledgements

We thank the Swedish Polar Research Secretariat and the Sea Fisheries Research Institute of South Africa for logistical and technical support, and the officers and crew of S.A. *Agulhas* for support at sea. Financial support from the Knut and Alice Wallenberg Foundation, from the Swedish Natural Science Research Council, and from the South African Department of Environmental Affairs and Tourism through the South African National Antarctic Research Programme is gratefully acknowledged.

References

Abrahamsson, K., Bertilsson, S., Chierici, M., Fransson, A., Froneman, P.W., Lorén, A., Pakhomov, E.A., 2004a. Variations of biochemical parameters along a transect in the Southern Ocean, with special emphasis on volatile halogenated organic compounds. Deep-Sea Research II, this issue [doi: 10.1016/j.dsr2.2004.09.004].

Abrahamsson, K., Lorén, A., Wulff, A. and Wängberg, S.-Å., 2004b. Air-sea exchange of halocarbons: the influence of diurnal and regional variations and distribution of pigments. Deep-Sea Research II, this issue [doi: 10.1016/j.dsr2.2004.09.005].

Allanson, B.R., Hart, R.C., Lutjeharms, J.R.E., 1981. Observations on nutrients, chlorophyll and primary production of the Southern Ocean south of Africa. South African Journal of Antarctic Research 10 (11), 3–14.

Bathmann, U.V., Scharek, R., Klass, C., Dubischer, C.D., Smetacek, V., 1997. Spring development of phytoplankton biomass and composition in major water masses of the Atlantic sector of the Southern Ocean. Deep-Sea Research II 44, 51–67.

Belkin, M., Gordon, L., 1996. Southern Ocean fronts from the Greenwich meridian to Tasmania. Journal of Geophysical Research 101, 3675–3696.

Bertilsson, S., Carlsson, P., Granéli, W., 2004. Influence of solar radiation on the availability of dissolved organic matter to bacteria in the Southern Ocean. Deep-Sea Research II, this issue [doi: 10.1016/j.dsr2.2000.07.001].

Cavender-Bares, K.K., Mann, E.L., Chisholm, S.W., Ondrusek, M.E., Bidigare, R.R., 1999. Differential response to of equatorial Pacific phytoplankton to iron fertilization. Limnology and Oceanography 44, 237–246.

Chavez, F.P., Buck, K.R., Coale, K.H., Martin, J.H., DiTullio, G.R., Welschmeyer, N.A., Jacobson, A.C., Barber, R.T., 1991. Growth rates, grazing, sinking and iron limitation of equatorial Pacific phytoplankton. Limnology and Oceanography 44, 237–246.

Chen, D., Wängberg, S.-Å., Wulff, A., Borne, K., 2004. Attenuation of biologically effective UV doses under overcast skies: a case study from the eastern Atlantic sector of the Southern Ocean. Deep-Sea Research II, this issue [doi: 10.1016/j.dsr2.2001.02.002].

Chierici, M., Fransson, A., Turner, D.R., Pakhomov, E.A. and Froneman, P.W., 2004. Variability in pH, fCO_2, oxygen and flux of CO_2 in the surface water along a transect in the

Atlantic sector of the Southern Ocean. Deep-Sea Research II, this issue [doi: 10.1016/j.dsr2.2001.03.002].

Comiso, J., 1990. In: Maslanik J., Stroeve J. (Eds), DMSP SSM/I monthly polar gridded sea ice concentrations. National Snow and Ice Data Centre, Boulder CO, USA. WWW page, http:\\www.nsidc.org/data/nsidc-002.html.

Comiso, J., 1993. Coastal zone color scanner pigment concentrations in the Southern Ocean and relationships to geophysical surface features. Journal of Geophysical Research 98, 2419–2451.

Croot, P.L., Andersson, K., Özturk, M. and Turner, D.R., 2004. The distribution and speciation of iron along 6°E in the Southern Ocean. Deep-Sea Research II, this issue [doi: 10.1016/j.dsr2.2003.10.012].

de Baar, H.J.W., De Jong, J.T.M., Bakker, D.C.E., Löscher, B.M., Veth, C., Bathmann, U., Smetacek, V., 1995. Importance of iron for plankton blooms and carbon dioxide draw down in the Southern Ocean. Nature 373, 412–415.

Estep, K.W., Nejstgaard, J.C., Skjoldal, H.R., Rey, F., 1990. Predation by copepods upon natural populations of *Phaeocystis pouchetii* as a function of the physiological state of the prey. Marine Ecology Progress Series 67, 235–249.

Falkowski, P.G., Barber, R.T., Smetacek, V., 1998. Biogeochemical controls and feedbacks on ocean primary production. Science 281, 200–206.

Fransson, A., Chierici, M., Anderson, L.G., 2004a. Diurnal variability in the oceanic carbon dioxide system and oxygen in the Southern Ocean surface water. Deep-Sea Research II, this issue [doi: 10.1016/j.dsr2.2001.01.001].

Fransson, A., Chierici, M., Anderson, L.G., David, R., 2004b. Transformation of carbon and oxygen in the surface layer of the eastern Atlantic sector of the Southern Ocean. Deep-Sea Research II, this issue [doi: 10.1016/j.dsr2.2001.12.001].

Froneman, P.W., 2004. Protozooplankton community structure and grazing impact in the eastern Atlantic sector of the Southern Ocean in austral summer 1998. Deep-Sea Research II, this issue [doi: 10.1016/j.dsr2.2004.09.001].

Froneman, P.W., Perissinotto, R., McQuaid, C.D., Laubscher, R.K., 1995. Summer distribution of net-phytoplankton in the Atlantic sector of the Southern Ocean. Polar Biology 15, 77–84.

Froneman, P.W., Pakhomov, E.A., Perissinotto, R., McQuaid, C.D., 2000. Zooplankton structure and grazing in the Atlantic sector of the Southern Ocean in late austral summer 1993, Part 2, Biochemical zonation. Deep-Sea Research I 47, 1687–1702.

Froneman, P.W., Pakhomov, E.A., Balarin, M.G., 2004. Size-fractionated phytoplankton biomass, production and biogenic carbon flux in the eastern Atlantic sector of the Southern Ocean in late austral summer 1997–1998. Deep-Sea Research II, this issue [doi: 10.1016/j.dsr2.2002.09.001].

Frost, B.W., 1991. The role of grazing in nutrient-rich areas of the open sea. Limnology and Oceanography 36, 1616–1630.

Gall, M.P., Boyd, P.W., Hall, J., Safi, K., Chang, H., 2001. Phytoplankton processes. Part 2, Rates of primary production and factors controlling algal growth during the Southern Ocean Iron Release experiment (SOIREE). Deep-Sea Research II 48, 2571–2590.

Gordon, A.L., 1967. Structure of Antarctic Waters Between 20°W and 170°W. Antarctic Folio Map Series Folio 6. American Geographical Society, New York.

Granéli, W., Bertilsson, S., Carlsson, P., 2004. Bacterial abundance, production and organic carbon limitation in the Southern Ocean (39–62°S, 4–14°E) during the austral summer 1997/98. Deep-Sea Research II, this issue [doi: 10.1016/j.dsr2.2001.01.003].

Hall, J.A., Safi, K., 2001. The impact of in situ iron fertilization on the microbial food web in the Southern Ocean. Deep-Sea Research II 48, 2591–2613.

Jantunen, L.M., Kylin, H., Bidleman, T.F., 2004. Air-water gas exchange of α-hexachlorocyclohexane enantiomers in the South Atlantic Ocean and Antarctica. Deep-Sea Research II, this issue [doi: 10.1016/j.dsr2.2004.02.002].

Jennings, J.C., Gordon, L.I., Nelson, D.M., 1984. Nutrient depletion indicates high primary productivity in the Weddell Sea. Nature 309, 51–54.

Laubscher, R.K., Perissinotto, R., McQuaid, C.D., 1993. Phytoplankton production and biomass at frontal zones in the Atlantic sector of the Southern Ocean. Polar Biology 13, 471–481.

Legendre, L., Rassoulzadegan, F., 1995. Plankton and nutrient dynamics in marine waters. Ophelia 41, 153–172.

Lutjeharms, J.R.E., 1985. Location of frontal systems between Africa and Antarctica, some preliminary results. Deep-Sea Research 32, 1499–1509.

Lutjeharms, J.R.E., Valentine, H.R., 1984. Southern Ocean thermal fronts south of Africa. Deep-Sea Research 31, 1461–1475.

Martin, J.H., Gordon, R.M., Fitzwater, S.E., 1991. The case for iron. Limnology and Oceanography 36, 1793–1802.

Minas, H.J., Minas, M., Packard, T.T., 1986. Productivity in upwelling areas deduced from hydrographic and chemical fields. Limnology and Oceanography 31, 1182–1206.

Mordy, C.W., Penny, D.M., Sullivan, C.W., 1995. Spatial distribution of bacterioplankton biomass and production in the marginal ice-edge zone of the Weddell Scotia Sea during austral winter. Marine Ecology Progress Series 122, 9–19.

Morel, F.M.M., Hudson, R.J.M., Price, N.M., 1991. Limitation of productivity by trace metals in the sea. Limnology and Oceanography 36, 1742–1755.

Orsi, A.H., Whitworth, T., Nowlin, W.D., 1995. On the meridional extent and fronts of the Antarctic Circumpolar Current. Deep-Sea Research I 42, 641 673.

Özturk, M., Croot, P., Bertilsson, S., Abrahamsson, K., Karlson, B., David, R., Fransson, A., Sakshaug, E., 2004. Iron enrichment and photoreduction of iron under UV and PAR in the presence of hydrocarboxylic acid: implications for phytoplankton growth in the Southern Ocean. Deep-Sea Research II, this issue [doi: 10.1016/j.dsr2.2000.10.001].

Pakhomov, E.A., 2004. Salp/krill interactions in the eastern Atlantic sector of the Southern Ocean. Deep-Sea Research II, this issue [doi: 10.1016/j.dsr2.2001.03.001].

Pakhomov, E.A., McQuaid, C.D., 1996. Distribution of surface zooplankton and seabirds across the Southern Ocean. Polar Biology 16, 271–286.

Pakhomov, E.A., Froneman, P.W., 2004a. Zooplankton dynamics in the eastern Atlantic sector of the Southern Ocean during the austral summer 1997/1998. Part 1. Community structure. Deep-Sea Research II, this issue [doi: 10.1016/j.dsr2.2000.11.001].

Pakhomov, E.A. and Froneman, P.W., 2004b. Zooplankton dynamics in the eastern Atlantic sector of the Southern Ocean during the austral summer 1997/1998. Part 2. Grazing impact. Deep-Sea Research II, this issue [doi: 10.1016/j.dsr2.2000.11.002].

Pakhomov, E.A., Perissinotto, R., Froneman, P.W., 1999. Predation impact of carnivorous macrozooplankton and micronekton in the Atlantic sector of the Southern Ocean. Journal of Marine Systems 19, 47–64.

Pakhomov, E.A., Perissinotto, R., McQuaid, C.D., Froneman, P.W., 2000. Zooplankton structure and grazing in the Atlantic sector of the Southern Ocean in late austral summer 1993, Part 1, Ecological zonation. Deep-Sea Research I 47, 1663–1686.

Pollard, R.T., Lucas, M.I., Read, J.F., 2002. Physical controls on biogeochemical zonation in the Southern Ocean. Deep-Sea Research II 49, 3289–3305.

Priddle, J., Smetacek, V., Bathmann, U.V., 1992. Antarctic marine primary production, biogeochemical carbon cycles and climatic change. Philosophical Transactions of the Royal Society of London Series B 338, 289–297.

Rasmus, K.E., Granéli, W., Wängberg, S.-Å., 2004. Optical studies in the Southern Ocean. Deep-Sea Research II, this issue [doi: 10.1016/j.dsr2.2001.01.004].

Read, J.F., Pollard, R.T., Bathmann, U., 2002. Physical and biological patchiness of an upper ocean transect from South Africa to the ice edge near the Greenwich Meridian. Deep-Sea Research II 49, 3713–3733.

Scharek, R., van Leeuwe, M., de Baar, H.J.W., 199[illegible] Responses of Southern Ocean phytoplankton to th[illegible] addition of trace metals. Deep-Sea Research II 44, 209–22[illegible]

Schlitzer, R., 2002. Ocean Data View. WWW Page, aw[illegible] bremerhaven

Sieburth, J.M., 1960. Acrylic acid, an 'antibiotic' principle i[illegible] *Phaeocystis* in Antarctic waters. Science 132, 676–677.

Smetacek, V., de Baar, H.J.W., Bathmann, U.V., Lochte, K.[illegible] van der Loeff, M.M.R., 1997. Ecology and biogeochemistr[illegible] of the Antarctic Circumpolar Current during austral spring[illegible] A summary of Southern Ocean JGOFS cruise ANT X/6 c[illegible] RV Polarstern. Deep-Sea Research II 44, 1–21.

Smith, W.O., Nelson, D.M., 1990. Phytoplankton growth an[illegible] new production in the Weddell Sea marginal ice zone in th[illegible] austral spring and autumn. Limnology and Oceanograph[illegible] 35, 809 821.

Stramma, L., Peterson, R.G., 1990. The South Atlanti[illegible] Current. Journal of Physical Oceanography 20, 846 859.

Tanhua, T., Olsson, K.A. and Fogelqvist, E., 2004. A first stud[illegible] of SF_6 as a transient tracer in the Southern Ocean. Deep-Sea[illegible] Research II, this issue [doi: 10.1016/j.dsr2.2001.02.001].

Veth, C., Peeken, I., Scharek, R., 1997. Physical anatomy and[illegible] surface waters in the ACC near the 6°W meridian during[illegible] austral spring 1992. Deep-Sea Research II 44, 23–49.

Wängberg, S.-Å., Wulff, A., 2004. Impact of Ultraviolet-B[illegible] radiation on the development of phytoplankton commu-[illegible] nities in the eastern Atlantic sector of the Southern Ocean—[illegible] results from on-deck model ecosystem experiments. Deep-[illegible] Sea Research II, this issue [doi: 10.1016/j.dsr2.2001.05.001].

Whitworth, T., Nowlin, W.D., 1987. Water masses and currents[illegible] of the Southern ocean at the Greenwich Meridian. Journal[illegible] of Geophysical Research 92, 6462–6476.

Wulff, A. and Wängberg, S.-Å., 2004. Spatial and vertical[illegible] distribution of phytoplankton pigments in the eastern[illegible] Atlantic sector of the Southern Ocean. Deep-Sea Research[illegible] II, this issue [doi: 10.1016/j.dsr2.2001.01.002].

ELSEVIER

Deep-Sea Research II 51 (2004) 2557–2568

DEEP-SEA RESEARCH
PART II

www.elsevier.com/locate/dsr2

Influence of solar radiation on the availability of dissolved organic matter to bacteria in the Southern Ocean

Stefan Bertilsson[a,*], Per Carlsson[b,1], Wilhelm Granéli[c]

[a]*Department of Water and Environmental Studies, Linköping University, SE-581 83 Linköping, Sweden*
[b]*Department of Marine Sciences, Kalmar University, P. O. Box 905, SE-391 29 Kalmar, Sweden.*
[c]*Department of Ecology/Limnology, Lund University, Ecology Building, SE-223 62 Lund, Sweden*

Abstract

The influence of solar radiation on the ability of dissolved organic matter (DOM) to support bacterial growth, was studied in the eastern Atlantic sector of the Southern Ocean during the SWEDARP 1997 1998 cruise with *SA Agulhas* December 1997–February 1998. Vertical profiles of water samples (2–3000 m) were obtained from the Spring Ice Edge (SIE, 60°S, high chlorophyll-*a*) and from the Winter Ice Edge (WIE, 56 S, low chlorophyll-*a*) areas. Filter-sterilized water from each area and depth was incubated under natural solar radiation and in the dark for comparison. Photobleaching of humic substance fluorescence occurred in all studied water samples. The bleaching was typically larger in the initially more fluorescent deep waters, compared to the low-fluorescent surface waters. Both the irradiated water and the dark controls were re-inoculated with a mixed bacterial inoculum from the initially sampled water. Bacterial growth (accumulating cells) and bacterial production (protein synthesis) were monitored during a 16 19 day incubation of these cultures at near in situ temperature (2 °C). Bacterial growth in cultures prepared from SIE water was largest at the surface (2–25 m), while the growth in corresponding cultures from the WIE did not vary much over depth. In contrast to the observed photobleaching, no clear effects of the irradiation on the ability of the DOM to support bacterial growth could be observed in either of the experiments. Hence, the degradation of fluorescent structures and other photochemical alterations of the organic matter did not have a major effect on the total pool of biodegradable organic substrates. The lack of effects of photoreactions on bacterial growth potential in the present study disagrees with the short-term bacterial growth response observed in other oceanic environments. This could be due to the different experimental approaches employed (short-vs. long-term incubations) or may indicate that the impact of photoreactions on bacterial growth in the Southern Ocean differ substantially from aquatic systems that are more influenced by terrestrial environments, as well as the warmer oligotrophic oceanic environments.
© 2004 Elsevier Ltd. All rights reserved.

*Corresponding author. Present address: Department of Evolutionary Biology/Limnology, Uppsala University, Norbyv. 20, SE-75236 Uppsala, Sweden. Tel.: +46 18 471 2712; fax: +46 18 53 11 14.
E-mail address: stebe@ebc.uu.se (S. Bertilsson).
[1]Present address: Marine Biology, Lund University, Campus Helsingborg, Box 882, SE-251 08 Helsingborg, Sweden.

0967-0645/$ - see front matter © 2004 Elsevier Ltd. All rights reserved.
doi:10.1016/j.dsr2.2000.07.001

1. Introduction

Heterotrophic bacteria are ubiquitous in aquatic ecosystems and are the major degraders of organic matter. Hence they constitute an important link in the carbon cycle and have a profound influence on the flux of energy and nutrients in food webs (Azam et al., 1983; Azam and Cho, 1987; Ducklow and Carlson, 1992). In the Southern Ocean, similar to other remote oceanic environments, most of the organic matter originates from phytoplankton primary production within the system itself, while terrigenous inputs are negligible due to the remoteness from any productive terrestrial system. Therefore, the quality of the total dissolved organic matter (DOM) in this system will be distinctively different from DOM in most freshwaters and coastal waters, where the terrestrially derived component of DOM is more significant (Opsahl and Benner, 1997; Benner, 1998). The qualitative differences are also likely to influence the susceptibility of DOM to biological degradation (Pakulski and Benner, 1994). These qualitative features, combined with low ambient concentrations (often below $50\,\mu mol\,C\,l^{-1}$, Wedborg et al., 1998), low temperatures (typically below zero) and high concentrations of nitrogen and phosphorus (see Priddle et al., 1995), make the Southern Ocean a highly specialized environment for bacteria to exist in. These features also make it difficult to elucidate the role of bacteria in the Southern Ocean simply by extrapolating findings obtained from other aquatic systems (Karl, 1993).

Only a minor fraction of the total DOM pool in natural aquatic systems is directly available for heterotrophic bacterial utilization (Azam and Cho, 1987; Søndergaard and Middelboe, 1995). Still, this pool of bioavailable DOM can be increased by photochemical reactions (Lindell et al., 1995: Tranvik, 1998). These positive effects have primarily been attributed to a production of various low molecular weight organic compounds (Moran and Zepp, 1997; Bertilsson and Tranvik 2000), but it is also known that photochemical processes alter the quality of higher molecular weight DOM by degrading chromophoric structures (Skoog et al., 1996) and by inducing a decrease in the average molecular weight (Allard et al., 1994). Positi effects of solar radiation on DOM bioavailabil have almost exclusively been observed in fre waters or in coastal ecosystems with a rather lar influence of terrestrially derived DOM. Howev Benner and Biddanda (1998) also found that so radiation rendered deep-water DOM from oligotrophic marine site in the Gulf of Mexi more bioavailable. In contrast, a negative influen of irradiation on the pool of bioavailable DO was observed for surface water from the sa station, and it was suggested that the quality DOM had a key role in governing the net effects radiation on DOM bioavailability. Recentl similar results have also been obtained in t Mediterranean and the Caribbean Sea (Oberno terer et al., 1999). These authors found that sol radiation rendered DOM obtained from a chlo ophyll maximum less available to bacteria whi the opposite effect was observed for DO obtained from larger depths. A negative bacteri growth response to solar irradiation has also bee observed for an aqueous solution of algal ce debris (Tranvik and Kokalj, 1998), lakes with high algal biomass (Tranvik and Bertilsson, 200 as well as for a model protein added to seawate (Keil and Kirchman, 1994; Obernosterer et al 1999), and a peptone solution (Naganuma et a 1996). These combined findings imply that nega tive effects of radiation on DOM bioavailabilit are likely to be coupled with the occurrence o recently produced algal-derived DOM. Sinc Antarctic DOM is likely to be composed mainl of old material of phytoplankton origin, effects o solar irradiation on the bacterial availability o this material may differ from those of recentl derived algal DOM and photochemically modifie terrestrial material.

During the SWEDARP 1997/1998 expedition to the eastern Atlantic sector of the Weddel Sea during Austral summer (Turner et al., 2004 Froneman et al., 1998), we studied the influenc of solar radiation on the ability of DOM t support bacterial growth. Two areas were inves tigated, the Spring Ice Edge (SIE, 60°S) wit high concentrations of chlorophyll-*a*, and th Winter Ice Edge (WIE, 56°S) with lower chlor ophyll-*a* concentrations. An experiment wa

designed to test the initially proposed hypothesis that natural solar radiation renders surface-water DOM less available for bacterial utilization, while a positive effect on bacterial growth will be dominant when deep-water DOM of presumably older age is irradiated (Benner and Biddanda, 1998).

To estimate the net effect of solar radiation on the pool of organic substrates available for bacterial growth, we used a bioassay approach based on 16–19 day incubations of water previously exposed to solar radiation or kept in the dark. Bacterial growth was measured both as bacterial yield (e.g. accumulating bacterial cells in the stationary growth phase, i.e., when the bacteria had used all available substrates) and bacterial production, to obtain information both on the net growth and the growth rates during the incubation. In addition, the photobleaching of humic substance fluorescence was assessed to directly quantify photochemical alterations in photoreactive DOM. Hydrogen peroxide concentrations were measured after the irradiation to trace the occurrence of photochemically produced reactive species, which could exert a negative influence on bacterial growth.

2. Materials and methods

Water samples from six different depths between 2 and 3000 m (2, the depth of chlorophyll-maximum, 130, 600, 2000, and 3000 m) were taken with a 24 bottle rosette sampler equipped with a CTD probe. Sampling was made in January 1998, both at the Spring Ice Edge (SIE, 60.0°S, 6.0°E) and the Winter Ice Edge (WIE, 56.3°S, 6.0°E). Both the SIE and the WIE sampling areas were characterized by low temperatures (−0.6–1.2°C throughout the profiles), and by low bacterial abundances (less than 2.5×10^5 cells ml^{-1} for the two sampled depth profiles; see further Granéli et al., 2004). Chlorophyll-*a* concentrations, analyzed according to Wright and Jeffrey (1997), were lower at the WIE, about 1 $\mu g l^{-1}$ in the mixed surface layer, while chlorophyll-*a* was close to 4 $\mu g l^{-1}$ in the mixed surface layer at the SIE (Wulff and Wängberg, 2004).

Sampled water was immediately transported in polycarbonate containers to a cold (2°C), dark room. Within 1 h of sampling, the water was filter-sterilized through 0.2 μm membrane filters (Filtropur L) that had been prewashed with 500 ml of Milli-Q water. The first 200 ml of each filtrate was discarded and then approximately 2.5 l of filtrate were collected in a clean polycarbonate bottle and 20 ml aliquots were collected for analysis of DOC. All materials to be in contact with the seawater samples had been thoroughly washed in hot (70 °C) 0.01 M HCl and were rinsed at least 4 times in Milli-Q grade water prior to use. Initial tests showed that no detectable amounts of organic compounds were released from the washed plasticware.

Aliquots (1 l) of the filter-sterilized water were added to 2 acid-washed and autoclaved polypropylene bags, transparent to solar radiation (>90% transmittance above 280 nm). One of the duplicate bags was covered with three layers of black plastic before all bags were placed in a deck incubator with flowing surface seawater at near in situ temperature (2–4 °C). The spectral irradiance was measured at a resolution of 2 nm every 15 min, using an Optronics OL-754 spectroradiometer. The filter-sterilized water samples were incubated in the deck incubator for a total of 33 h (SIE) and 70 h (WIE), respectively. The difference in incubation time was mainly due to differences in the ambient solar irradiance between the two experiments. The estimated total accumulated irradiance for the SIE experiment was 12,735 kJ m^{-2} of PAR (400–720 nm), 1792 kJ m^{-2} of UV-A (320–400 nm) and 110 kJ m^{-2} of UV-B (280–300 nm), while the corresponding irradiance for the WIE experiment was 19485 kJ m^{-2}, 3022 and 179 kJ m^{-2}.

After this incubation in the absence of microorganisms, samples were taken for humic substance fluorescence and hydrogen peroxide concentrations. The remaining water was inoculated with a 20% addition (v/v) of a mixed bacterial inoculum from the original surface water samples (2–600 m). The inoculum had been filtered through a precombusted Whatman GFF-filter (nominal pore size 0.8 μm) at a pressure differential of <35 mbar to remove bacterivores and phytoplankton. Aliquots (200 ml) of the

inoculated water were distributed into four acid washed and autoclaved polypropylene bags. The resulting cultures were sealed with clamps, placed in the dark at 2 °C and were maintained for 16 (SIE) and 19 days (WIE), respectively.

Samples for bacterial numbers were taken after 0, 5, 8, 10, 13, and 16 days for both experiments, while a final sampling after 19 days was made for the WIE experiment. These samples were preserved by adding 0.2 μm-filtered formaldehyde to a final concentration of 2%. Samples were kept cold (4 °C) until analysis, either onboard the ship (SIE-experiment) or upon return to Sweden (WIE-experiment). Counting of bacterial cells was accomplished by flow cytometry using the green-fluorescent nucleic acid-staining dye Syto-13® (Molecular Probes, USA) according to the method described by del Giorgio et al. (1996). We used fluorescent beads (Fluoresbrite Carboxy YG 1.58 μm, Polysciences, USA) as an internal standard and cells were counted using either a FacsCalibur (SIE) or a FacsSort (WIE) flow cytometer (both supplied by Becton Dickinson), equipped with argon ion lasers (excitation at 488 nm). Bacterial cells were separated from noise and non-stained particles in a log–log scattergram of green fluorescence and side scatter. Each sample was run for 1 min or until a minimum of 5000 cells had been counted. The concentration of added fluorescent beads was monitored daily by fluorescence microscopy. Selected reference samples were also counted by fluorescence microscopy after staining cells with DAPI (Porter and Feig, 1980). The flow cytometric counts were linearly related to the microscopic counts ($r^2 > 0.95$), but the numbers in the former were on average 29% higher. This may indicate that the flow cytometer is more sensitive in detecting weakly fluorescent cells and cells of smaller size typical for the low-productive marine waters of the Southern Ocean. Finally, we could not observe any flagellates in any of the samples analyzed microscopically, suggesting an efficient removal of these potential grazers in the filtration step.

Samples for bacterial production were taken immediately after inoculation and after 5 and 10 days of incubation. Bacterial production was measured according to the leucine-incorporation centrifugation method described by Smith ar Azam (1992), except for the exclusion of tl ethanol washing-step. The omission of this st did not influence the analysis significantly (s Granéli et al., 2004). Tritiated leucine (Amersha TRK 510 diluted with non-radioactive leucine to final specific activity of 29.4 Ci mmol^{-1}) was adde to 1.7 ml water samples to a final concentration 20 nM, which was high enough to achieve satura tion of uptake (Granéli et al., 2004). For eac culture, duplicate subsamples were incubated fo 4 h at in situ temperature before terminating th incubation by adding TCA. Tests showed tha uptake was linear in time for at least 6 h. For ever sample, a TCA-killed blank was incubated i parallel and each individual sample was correcte for the average blank level.

Humic substance fluorescence, an indicator c the amount of colored DOM (Vodacek et a 1995), was measured according to the method o Wedborg et al. (1998). Briefly, a Shimadzu RF 5001 PC spectrofluorometer with a Xenon lam was used with excitation at 350 nm and emission a 450 nm (10/20 nm slit, respectively). A blank (Milli-Q water) and 3 quinine dihydrogen sulfat dihydrate standards (0.1, 0.5, and 1 μg l^{-1}) dis solved in 0.05 M sulfuric acid were used to make a standard curve ($r^2 > 0.99$). Fluorescence is given in units of μg quinine dihydrogen sulfate dihydrate liter^{-1} (QSU). DOC was analyzed in 0.2 μm filtered samples by high-temperature catalytic oxidation using a Shimadzu TOC-5000 instrument (Sugimura and Suzuki, 1988). Samples were acidified and purged for 6 min with CO_2-free air prior to injection. The coefficient of variation for each sample was below 2%.

Hydrogen peroxide was determined by the enzyme-catalyzed reaction with (para-hydroxyphenyl)acetic acid (Miller and Kester, 1988). The resulting fluorescent product was measured on a spectrofluorometer with excitation at 315 nm and emission at 400 nm (10/10 nm slit). Hydrogen peroxide was distinguished from other peroxides by correcting for the fluorescence in samples additionally treated with catalase. Quantification was made by linear regression of each sample and two additional subsamples spiked with H_2O_2 to increase levels by 50 and 100 nM, respectively.

3. Results

The depth profiles of humic-substance fluorescence (HSF) in non-irradiated samples, representing approximate levels in situ, were similar for the two sampling stations. The fluorescence was lower in the mixed surface layer (i.e. above 130 m depth) while higher HSF levels were observed at larger depths (Fig. 1). Similar to HSF, DOC was constant with depth below 600 m, with an average of 52 ± 10 μM C at the SIE and 56 ± 3.3 μM C at the WIE (average ±s.d.). The DOC in the mixed surface layer (2–130 m) was higher at both stations, with 88 ± 13 μM C at the SIE and 70 ± 6 μM C at the WIE, indicating qualitative differences in surface-water DOM compared to DOM retrieved from greater depths.

Bleaching of HSF occurred consistently in all water samples that were exposed to solar radiation. Since only single samples were analyzed for each depth and treatment, we could not make a detailed comparison of the extent of the photobleaching over depth, but whereas the bleaching was of the same magnitude in water samples below the mixed surface layer (on average 59%), DOM obtained closer to the surface appeared to be more resistant to photobleaching (Fig. 1).

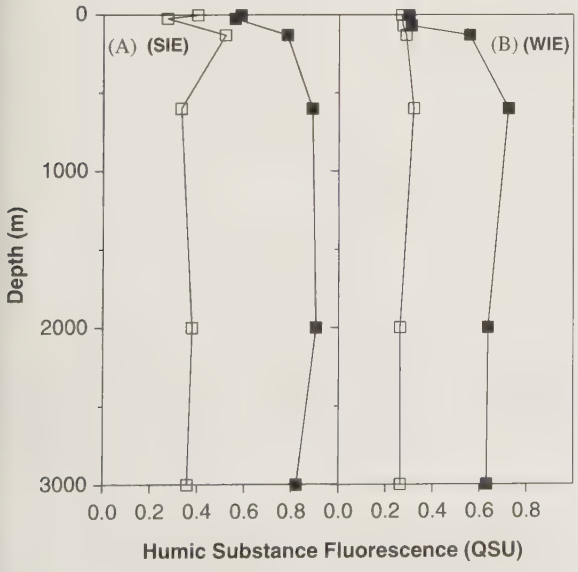

Fig. 1. (A and B) Humic substance fluorescence (QSU) in filter-sterilized water from (A) the Spring Ice Edge (SIE, 60°S) and the (B) Winter Ice Edge (WIE, 56°S) after exposure to solar radiation (open squares) and in dark controls (solid squares).

In contrast, no general increase in H_2O_2 concentrations could be observed for the irradiated samples compared to the dark controls at the time when the bioassay cultures were started ($p > 0.05$, paired t-test; Table 1). Since hydrogen peroxide typically has a longer half-life than other photochemically produced reactive oxygen species (Cooper et al., 1989), it is less likely that an increase in such harmful photoproducts influenced the results obtained in the bioassays.

In spite of the large influence of solar radiation on HSF, we did not observe any strong effects of irradiation on the ability of DOM to support bacterial growth. The bacterial growth curves in the light-and dark-treated cultures were in most instances highly correlated for each individual SIE and WIE water sample (Figs. 2 and 3). Defining the bacterial growth yields as the average number of cells in the last three samples obtained from the cultures, we could not observe any significant differences between the light and dark treatments for the WIE samples ($p > 0.05$, ANOVA). However, we did observe a negative influence of radiation on bacterial growth for some samples (e.g. 600 and 2000 m) from the SIE ($p < 0.05$, ANOVA). Due to a storm event, some of the

Table 1
Hydrogen peroxide (H_2O_2) concentrations (nM) in filter-sterilized water samples from the SIE (60°S, 6°E) and the WIE (56°S, 6°E), analyzed 3 h after exposure to solar radiation and in dark controls

Depth (m)	Spring ice edge (SIE)		Winter ice edge (WIE)	
	Irradiated	Dark	Irradiated	Dark
2	56 (5.2)	8.6 (5.6)	9.5 (2.3)	2.8 (3.8)
chl_{max}[a]	N.D.	10 (1.4)	9.0 (3.9)	5.6 (9.9)
130	3.1 (5.4)	30 (4.3)	16 (10)	5.1 (4.8)
600	N.D.	8.0 × (9.4)	8.6 (8.4)	2.7 (11)
2000	N.D.	N.D.	5.8 (10)	11 (12)
3000	517 (6.5)	N.D.	5.7 (5.1)	1.7 (11)

Standard error for the concentrations obtained from linear regressions of each standard curve is given between brackets ($n = 3$). N.D. = not detected.

[a]25 m for SIE and 70 m for WIE.

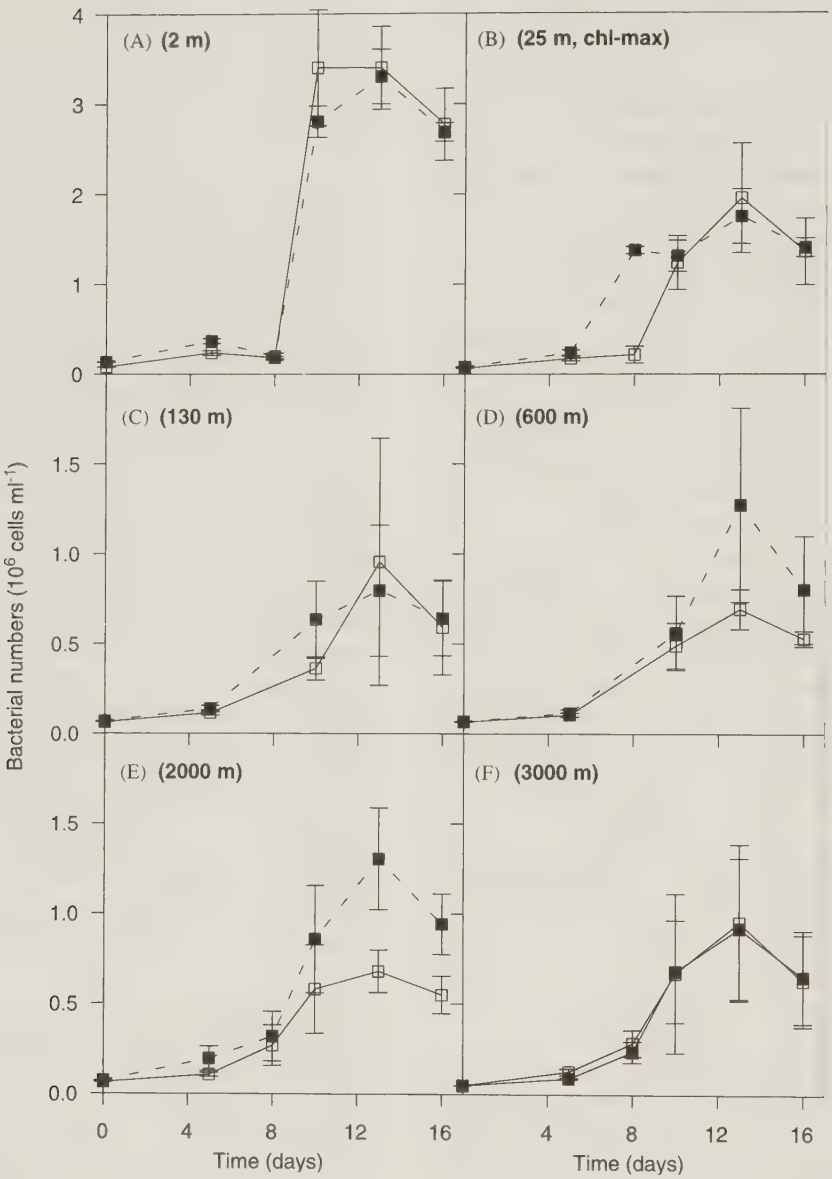

Fig. 2. (A–F) Bacterial growth (cells ml^{-1}) in re-inoculated dilution cultures of filter-sterilized light-and dark-treated water, sampled at various depths (2–3000 m) at the approximate location of the Spring Ice Edge (SIE, 60°S). Presented values are means of four replicates from cultures exposed to solar radiation (open squares, solid lines), and dark controls (solid squares, dashed lines). Error bars represent standard deviations.

replicates in the WIE experiment were lost at day 12 of the incubation. Hence from this day and onward the number of replicates was less than 4 for all water depths except 70 and 3000 m. This uncontrolled event may have influenced the obtained results to some extent.

Bacterial production in the cultures was in general agreement with the growth-curves. After 5 days of incubation, the production was significantly lower in the irradiated waters both in the SIE and WIE experiment (ANOVA, $p<0.05$; Table 2). However, this effect was only temporary,

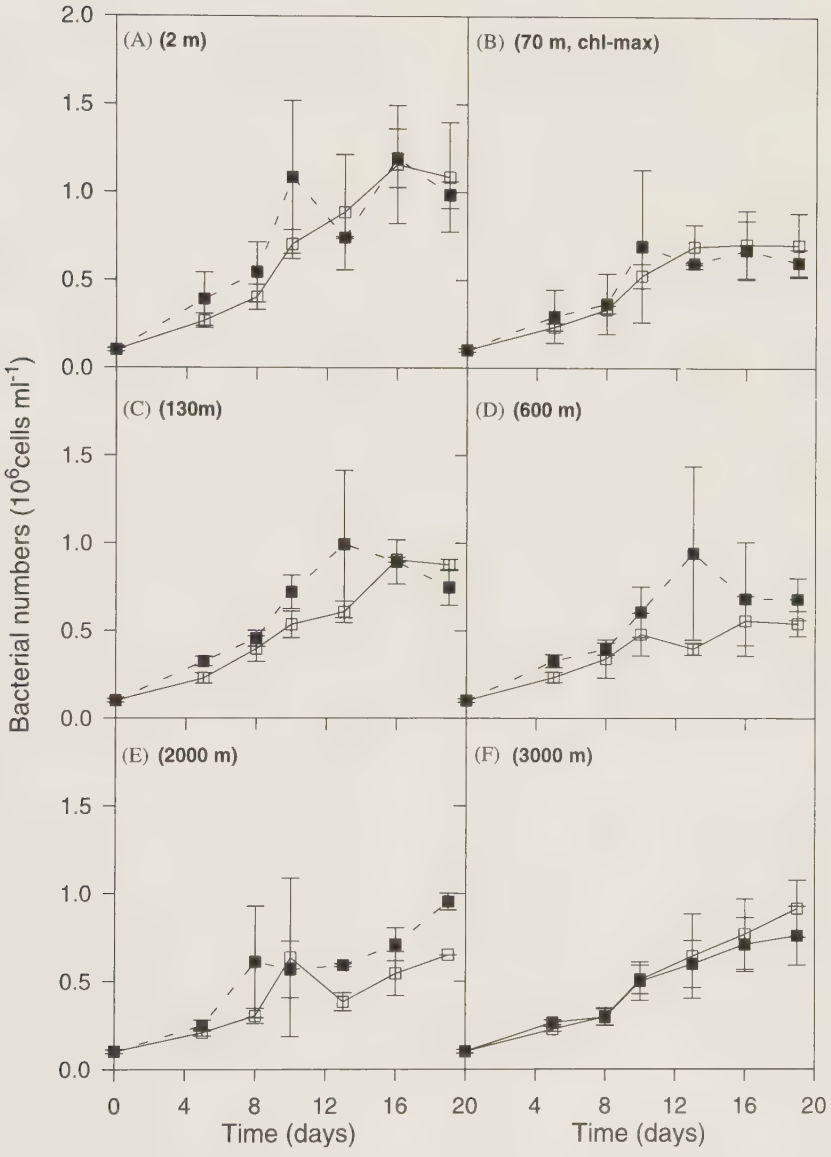

Fig. 3. (A–F) Bacterial growth (cells ml^{-1}) in re-inoculated dilution cultures of filter-sterilized light and dark treated water, sampled at various depths (2–3000 m) at the approximate location of the Winter Ice Edge (WIE, 56°S). Presented values are means of 4 replicates from cultures exposed to solar radiation (open squares, solid lines), and dark controls (solid squares, dashed lines). Error bars represent standard deviations. After 13 days of growth some replicates were lost in a storm event, hence except for the 70 and 3000 m cultures, 1–2 replicates from each treatment are missing.

and after an additional 5 days of incubation, bacterial production did not differ between the two treatments (ANOVA, $p > 0.05$; Table 2).

Bacterial growth was about twice as high in samples from the uppermost layer of the SIE compared to the other cultures. This elevated bacterial growth coincided with high levels of DOC and ambient chlorophyll-*a* due to a phytoplankton bloom, suggesting that this event was a source of substrates available for bacterial growth.

Table 2
Bacterial production (μg bacterial $C l^{-1} h^{-1}$) in dark-and light-treated water samples from the SIE (60°S, 6°E) and the WIE (56°S, 6°E after subsequent inoculation and incubation with indigenous bacteria for 5, and 10 days

Station/depth (m)	Bacterial production ($\mu g C l^{-1} h^{-1}$)			
	Irradiated		Dark	
	5 days	10 days	5 days	10 days
SIE				
2 m	0.228 (0.164)	2.543 (0.260)	2.061 (0.315)	2.450 (0.122)
chl_{max} 25 m	0.048 (0.029)	0.879 (0.663)	0.147 (0.057)	0.840 (0.376)
130 m	0.035 (0.016)	0.474 (0.067)	0.060 (0.046)	0.547 (0.456)
600m	0.023 (0.033)	0.527 (0.251)	0.020 (0.010)	0.736 (0.481)
2000 m	0.049 (0.025)	0.769 (0.392)	0.189 (0.076)	0.942 (0.460)
3000 m	0.016 (0.005)	0.754 (1.089)	0.055 (0.021)	1.212 (0.762)
WIE				
2 m	0.115 (0.045)	0.633 (0.356)	0.159 (0.036)	1.253 (1.043)
chl_{max} 70 m	0.073 (0.032)	0.760 (0.265)	0.337 (0.071)	0.697 (0.148)
130 m	0.069 (0.019)	0.537 (0.439)	0.119 (0.135)	0.760 (0.370)
600 m	0.070 (0.013)	0.499 (0.207)	0.150 (0.103)	0.527 (0.244)
2000 m	0.064 (0.030)	0.495 (0.333)	0.088 (0.123)	0.607 (0.848)
3000 m	0.072 (0.016)	0.517 (0.534)	0.082 (0.037)	0.492 (0.222)

Presented values are means with standard deviation between brackets ($n = 4$). Bacterial production immediately after inoculation (0 days) was always below 0.003 μg $C l^{-1} h^{-1}$ for the SIE and below 0.007 for the WIE.

The vertical profile of bacterial growth was less variable with depth in cultures from the WIE. In general, growth was slow in all experimental cultures. Growth-rates derived from least-square regressions of cell numbers in the exponential growth phase varied between 0.12 and 0.37 day^{-1}, and a stationary phase was not reached until after at least 10 days of incubation for either of the stations (Figs. 2 and 3).

4. Discussion

In the present study, solar radiation did not affect the ability of DOM to support bacterial growth to any larger extent, in contrast to the strong effects (positive and negative), reported for water obtained from an oligotrophic site in the Gulf of Mexico (Benner and Biddanda, 1998) and waters from the Mediterranean Sea (Obernosterer et al., 1999). As we observed a substantial photobleaching of humic substance fluorescence, these unexpected findings are less likely due to lack of effects of solar radiation on DOM chemistry in the studied waters. A more plausible interpretation is that the photochemically induced changes that resulted were not directly coupled to DOM-bioavailability. Alternatively, counteractive positive and negative effects of solar radiation on the bioavailability of DOM may have been in balance.

In studies on water from aquatic systems with a large input of terrestrially derived organic matter, solar radiation or artificial UV-radiation have in most cases had a strong positive influence of on the ability of DOM to support bacterial growth (Moran and Zepp, 1997; Tranvik and Bertilsson, 2001). The positive effects observed in these studies have mainly been attributed to the photoproduction of directly utilizable organic compounds of low molecular weight, or to photoinduced structural changes in high molecular weight organic compounds, facilitating biological hydrolysis and subsequent utilization. Only a few similar studies have been performed in oligotrophic seawaters. Mopper et al. (1991) observed a photochemical production of organic acids and

aldehydes in surface and deep water obtained from the Sargasso Sea. In a study of photoproduction and bacterial uptake of a low molecular weight compound (pyruvate) in surface waters from the same sea area, it was estimated that this photoproduct alone could account for 2–4% of the total carbon flux to heterotrophic bacteria (Kieber et al., 1989). About 20 different organic photoproducts of potential value as bacterial substrates have so far been identified in natural waters (Moran and Zepp, 1997). Hence the contribution of photochemically produced low molecular weight organic compounds to the total flux of carbon to bacteria is likely to be substantial, even in oligotrophic marine waters, and it is less likely that no such compounds were produced photochemically in the present study.

The contribution of terrestrially derived material to the total DOM in the open ocean environment is typically less than a few percent, while the dominant fraction of the DOM originates from recent or ancient phytoplankton production (Opsahl and Benner, 1997). A number of studies have shown that DOM of algal origin can be rendered less biodegradable by solar radiation (Keil and Kirchman, 1994; Naganuma et al., 1996; Tranvik and Kokalj, 1998). Therefore, such negative effects of radiation on DOM bioavailability could have been more pronounced in the present study of waters from the Southern Ocean when compared to freshwaters and marine systems more influenced by terrestrial DOM. Negative effects of radiation on bioavailability may involve condensation reactions and cross-linking of fatty acids (Kieber et al., 1997) and could counteract and possibly mask an ongoing photoproduction of LMW organic compounds (Bertilsson and Tranvik, 1999).

At present, only two studies exist, which explicitly address the influence of solar radiation on the actual ability of DOM to support bacterial growth in oligotrophic oceanic waters (Benner and Biddanda, 1998; Obernosterer et al., 1999). In both studies, oligotrophic seawater samples from the photic zone and deep waters were irradiated and then assayed for bacterial growth. Results from these two studies showed that the net effect of solar radiation on bacterial growth was negative for surface waters with a large proportion of recently produced DOM, while it was positive for water from deeper layers (>100 m). Hence, the findings in these two studies imply contrasting effects of solar radiation on the bioavailability of DOM depending on origin and character. It was concluded that the photochemical history, or at least the chemical composition of DOM, could play a fundamental role in governing the potential photoreactivity of this material.

Our results do not support such a general depth-dependent response. Instead we found negligible effects of solar radiation on the ability of the dissolved organic material to support bacterial growth, largely independent of water depth. There could be several reasons for this apparent paradox. While Benner and Biddanda (1998) and Obernosterer et al. (1999) studied the influence of solar radiation on the most rapidly utilizable DOM pool in their short-term bioassays with bacterial production as response parameter, we made long-term bioassays measuring also the influence of irradiation on the more slowly utilized but degradable organic matter, such as polymeric compounds that requires extensive hydrolysis prior to biological uptake (Tranvik, 1998). The somewhat depressed bacterial production in the beginning of our bioassays (i.e. after 5 days incubation) may suggest that the pool of the most rapidly utilizable organic compounds was photochemically transformed into material of lower availability as bacterial substrates. Such results could possibly have been caused by a negative influence of photochemically produced reactive species (e.g. singlet oxygen and hydroxyl radicals) on biological activity (Gjessing and Källkvist, 1991). However, the concentration of H_2O_2 was close to ambient levels and did not differ between irradiated and dark samples in our experiment. Hence, this explanation is less likely as H_2O_2 can be used as an indicator of levels of photochemically produced reactive species in surface waters (Cooper et al., 1989; Scully et al., 1996).

An additional explanation for the observed differences between the studies lies in the different physical—(e.g. radiation climate and temperature) and chemical environment in the different waters studied. The Southern Ocean receives a much lower input of riverine organic material from

terrestrial ecosystems compared to the Gulf of Mexico and the Mediterranean Sea. Furthermore, the Southern Ocean is much colder: the difference in ambient temperature between the study in the Southern Ocean and the Gulf of Mexico was >22 °C! Temperature is a factor that may be of central importance for bacterial metabolism and uptake affinities for various organic substrates. Wiebe et al. (1992) and Kirchman and Rich (1997) have shown that the bacterial response to additions of bioavailable DOM in water from the Equatorial Pacific is much weaker at lower temperatures. Although their experimental design differed from the present study (i.e. different temperature interval and shorter duration of bacterial cultures), the obtained results agree with the minor effects of photochemical processes on bacterial growth observed in the present study that were performed at the typically low temperatures encountered in the Southern Ocean.

We did not address direct negative effects of solar radiation on bacteria or other organisms in the present study. Photoinhibition is a well-known effect in surface waters and could be of utmost importance in the Southern Ocean due to the elevated levels of the highly energetic and photochemically active UV-B radiation that are the result of ozone depletion. In addition, the waters of the Southern Ocean are extremely clear, resulting in a deep penetration of solar radiation in the water column. We observed a strong photobleaching of humic substance fluorescence in our experiment (Fig. 1). This bleaching was particularly pronounced for deep-water DOM. Hence, photochemical processes may have the potential to alter the average radiation climate for pelagic organisms in these waters. The observed photobleaching represents a degradation of conjugated double bonds and other fluorescent structures. The impact of such a process would be most pronounced in the surface layer of the water column where the irradiance is highest. It could therefore explain the lower levels of humic substance fluorescence in the mixed surface layer of the Southern Ocean, which have been observed both in the present study (Fig. 1), as well as in a more extensive study by Wedborg et al (1998). Contrary to the depleted fluorescence observed in the top layer of oceanic water columns, DOC concentrations are typically higher in this layer (Benner et al. 1992; Guo et al. 1995; Wedborg et al. 1998), implying qualitative differences in the total DOC pool. Our results also suggest that there are differences in the DOM observed in the mixed surface layer when compared to deep waters. These differences appear to be particularly pronounced in the SIE area where chlorophyll-*a* was higher at the surface.

In conclusion, our results suggest that solar radiation exerted a minor influence on the bioavailability of total DOM in the studied areas of the Southern Ocean. These findings differ from earlier studies in the open ocean (Benner and Biddanda, 1998; Obernosterer et al., 1999). This could be due to the fact that we assessed the impact of radiation on the total pool of biodegradable DOM rather than the biologically most labile fraction, but it could also suggest that the resulting biological effects of photoreactions could be substantially different between various low-productive marine systems and that factors such as the quality of DOM and temperature could be important regulators of the response.

Acknowledgements

We thank Margareta Wedborg and Thomas Persson for skillful analysis of Humic substance fluorescence onboard the *Agulhas* and Sten-Åke Wängberg for continuously monitoring solar irradiance. Katarina Abrahamsson and Anders Lorén kindly provided us with equipment for the hydrogen peroxide measurements. Comments by three anonymous reviewers improved the manuscript substantially. Further we thank all members of the SWEDARP 1997/1998 cruise for contributing to the study in varying ways and for making the working-atmosphere enjoyable throughout the expedition. Special thanks to the expedition leader David Turner for excellent organization of the expedition. Logistic support was provided by the Swedish Polar Research Board. Financial support from the Swedish Natural Research Council (NFR) to Bert Allard (Grant no. G-AA/GU 03596-326), to Per Carlsson

(Grant no. B-PD 10890-304), and to Wilhelm Granéli (Grant no. B-AA/BU 04969-321) is gratefully acknowledged.

References

Allard, B., Borén, H., Pettersson, C., Zhang, G., 1994. Degradation of humic substances by UV-irradiation. Environment International 20, 97–101.

Azam, F., Cho, B.C., 1987. Bacterial utilization of organic matter in the sea. In: Fletcher, M., Gray, T.R.G., Jones, J.G. (Eds.), Ecology of Microbial Communities. Cambridge University Press, Cambridge, pp. 261–281.

Azam, F., Fenchel, T., Field, J.G., Gray, J.S., Meyer-Reil, L.A., Thingstad, F., 1983. The ecological role of water column microbes in the sea. Marine Ecology Progress Series 10, 257–263.

Benner, R.H., 1998. Cycling of dissolved organic matter in the ocean. In: Hessen, D.O., Tranvik, L.J. (Eds.), Aquatic Humic Substances—Ecology and Biogeochemistry. Springer, Berlin, pp. 317–331.

Benner, R., Biddanda, B., 1998. Photochemical transformations of surface and deep marine dissolved organic matter: effects on bacterial growth. Limnology and Oceanography 43, 1373–1378.

Benner, R., Pakulski, J.D., McCarthy, M., Hedges, J.I., Hatcher, P.G., 1992. Bulk chemical characteristics of dissolved organic matter in the ocean. Science 255, 1561–1564.

Bertilsson, S., Tranvik, L.J., 2000. Photochemical transformation of dissolved organic matter in lakes. Limnology and Oceanography 45, 753–762.

Cooper, W.J., Zika, R.G., Petasne, R.G., Fisher, A.M., 1989. Sunlight induced photochemistry of humic substances in natural waters: major reactive species. In: Suffet, I.H., MacCarthy, P. (Eds.), Aquatic Humic Substances: Influence on Fate and Treatment of Pollutants. American Chemical Society, Washington, pp. 333–362.

Ducklow, H.W., Carlson, C.A., 1992. Oceanic bacterial production. Advances in Microbial Ecology 12, 113–181.

Froneman, P.W., Pakhomov, E.A., Turner, D., Abrahamson, K., Karlsson, B., Godhe, A., Bertilsson, S., Granéli, W., Carlsson, P., Wangberg, S., Wulff, A., Croot, P., Andersson, K., Balarin, M., Wedborg, M., Persson, T., Rasmus, K., Özturk, M., David, R., 1998. Research cruise of the Scandinavian/South African Antarctic expedition, December 1997–February 1998. South African Journal of Science 94, 517–519.

del Giorgio, P.A., Bird, D.B., Prairie, Y.T., Planas, D., 1996. Flow cytometric determination of bacterial abundance in lake plankton with the green nucleic acid stain Syto 13. Limnology and Oceanography 41, 783–789.

Gjessing, E.T., Källkvist, T., 1991. Algicidal and chemical effect of U.V.-radiation of water containing humic substances. Water Research 25, 491–494.

Granéli, W., Bertilsson, S., Carlsson, P., 2004. Bacterial abundance, production and organic carbon limitation in the Southern Ocean (39–62°S, 4–14°E) during the austral summer 1997/1998. Deep-Sea Research II, this issue [doi:10.1016/j.dsr2.2001.01.003].

Guo, L., Santschi, P.H., Warken, K.W., 1995. Dynamics of dissolved organic carbon (DOC) in oceanic environments. Limnology and Oceanography 40, 1392–1403.

Karl, D.M., 1993. Microbial processes in the Southern Ocean. In: Friedmann, E.I., Thistle, A.B. (Eds.), Microbial Ecology—Antarctic Regions. Wiley-Liss, Inc, New York, pp. 1–63.

Keil, R.G., Kirchman, D.L., 1994. Abiotic transformation of labile protein to refractory protein in seawater. Marine Chemistry 45, 187–196.

Kieber, D.J., McDaniel, J., Mopper, K., 1989. Photochemical source of biological substrates in seawater: implications for carbon cycling. Nature 341, 637–639.

Kieber, R.J., Hydro, L.J., Seaton, P.J., 1997. Photooxidation of triglycerides and fatty acids in seawater: implication toward the formation of marine humic substances. Limnology and Oceanography 42, 1454–1462.

Kirchman, D.L., Rich, J.H., 1997. Regulation of bacterial growth rates by dissolved organic carbon and temperature in the Equatorial Pacific Ocean. Microbial Ecology 33, 11–20.

Lindell, M.J., Granéli, W., Tranvik, L.J., 1995. Enhanced bacterial growth in response to photochemical transformation of dissolved organic matter. Limnology and Oceanography 40, 195–199.

Miller, W.L., Kester, D.R., 1988. Hydrogen peroxide measurement in seawater by (*p*-hydroxyphenyl)acetic acid dimerization. Analytical Chemistry 60, 2711–2715.

Mopper, K., Zhou, X., Kieber, R.J., Kieber, D.J., Sikorski, R.J., Jones, R.D., 1991. Photochemical degradation of dissolved organic carbon and its impact on the oceanic carbon cycle. Nature 353, 60–62.

Moran, M.A., Zepp, R.G., 1997. Role of photoreactions in the formation of biologically labile compounds from dissolved organic matter. Limnology and Oceanography 42, 1307–1316.

Naganuma, T., Konishi, S., Inoue, T., Nakane, T., Sukizaki, S., 1996. Photodegradation or photoalteration? Microbial assay of the effect of UV-B on dissolved organic matter. Marine Ecology Progress Series 135, 309–310.

Obernosterer, I., Reitner, B., Herndl, G.J., 1999. Contrasting effects of solar radiation on dissolved organic matter and its bioavailability to marine bacterioplankton. Limnology and Oceanography 44, 1645–1654.

Opsahl, S., Benner, R., 1997. Distribution and cycling of terrigenous dissolved organic matter in the ocean. Nature 386, 480–482.

Pakulski, J.D., Benner, R., 1994. Abundance and distribution of carbohydrates in the ocean. Limnology and Oceanography 39, 930–940.

Porter, K.G., Feig, Y.S., 1980. The use of DAPI for identifying and counting aquatic microflora. Limnology and Oceanography 25, 943–948.

Priddle, J., Leakey, R., Symon, C., Whitehouse, M., Robins, D., Cripps, G., Murphy, E., Owens, N., 1995. Nutrient cycling by Antarctic marine microbial plankton. Marine Ecology Progress Series 116, 181–198.

Scully, N.M., McQueen, D.J., Lean, D.R.S., 1996. Hydrogen peroxide formation: the interaction of ultraviolet radiation and dissolved organic carbon in lake waters along a 43–75°N gradient. Limnology and Oceanography 41, 540–548.

Skoog, A., Wedborg, M., Fogelqvist, E., 1996. Photobleaching of fluorescence and the organic carbon concentration in a coastal environment. Marine Chemistry 55, 333–345.

Smith, D.C., Azam, F., 1992. A simple, economical method for measuring bacterial protein synthesis rates in seawater using 3H-Leucine. Marine Microbial Food Webs 6, 107–114.

Søndergaard, M., Middelboe, M., 1995. A cross-system analysis of labile dissolved organic carbon. Marine Ecology Progress Series 118, 283–294.

Sugimura, Y., Suzuki, Y., 1988. A high-temperature catalytic oxidation method for the determination of non-volatile dissolved organic carbon in seawater by direct injection of a liquid sample. Marine Chemistry 24, 105–131.

Tranvik, L.J., 1998. Degradation of dissolved organic matter in humic waters by bacteria. In: Hessen, D.O., Tranvik, L.J. (Eds.), Aquatic Humic Substances—Ecology and Biogeochemistry. Springer, Berlin, pp. 259–283.

Tranvik, L.J., Bertilsson, S., 2001. Contrasting effects of solar UV radiation on dissolved organic sources for bacterial growth. Ecology Letters 4, 458–463.

Tranvik, L., Kokalj, S., 1998. Decreased bioavailability of algal DOC due to interactive effects of UV radiation and humic matter. Aquatic Microbial Ecology 14, 301–307.

Turner, D.R., Bertilsson, S., Fransson, A., Pakhomov, E., 2004. The SWEDARP 97/98 marine expedition: overview. Deep-Sea Research II, this issue [doi:10.1016/j.dsr2.2003.08.006].

Vodacek, A., Hoge, F.E., Swift, R., Yungel, J.K., Peltzer, E.T., Blough, N.V., 1995. The use of in situ and airborne fluorescence measurements to determine coefficients and DOC concentrations in surface waters. Limnology and Oceanography 40, 411–415.

Wedborg, M., Hoppema, M., Skoog, A., 1998. On the relation between organic and inorganic carbon in the Weddell Sea. Journal of Marine Systems 17, 59–76.

Wiebe, W.J., Sheldon, W.M., Pomeroy, L.R., 1992. Bacterial growth in the cold: evidence for an enhanced substrate requirement. Applied Environmental Microbiology 58, 359–364.

Wright, S.W., Jeffrey, S.W., 1997. High-resolution HPLC system for chlorophylls and carotenoids of marine phytoplankton. In: Jeffrey, S.W., Mantoura, R.F.C., Wright, S.W. (Eds.), Phytoplankton Pigments in Oceanography. UNESCO Publishing, Paris.

Wulff, A., Wängberg, S.-Å., 2004. Spatial and vertical distribution of phytoplankton pigments in the eastern Atlantic sector of the Southern Ocean. Deep-Sea Research II, this issue [doi:10.1016/j.dsr2.2001.01.002].

ELSEVIER

Deep-Sea Research II 51 (2004) 2569–2582

DEEP-SEA RESEARCH
PART II

www.elsevier.com/locate/dsr2

Bacterial abundance, production and organic carbon limitation in the Southern Ocean (39–62°S, 4–14°E) during the austral summer 1997/1998

Wilhelm Granéli[a,*], Per Carlsson[b,1], Stefan Bertilsson[c,2]

[a]*Department of Ecology, Limnology, Ecology Building, SE-223 62 Lund, Sweden*
[b]*Department of Marine Sciences, Kalmar University, P.O. Box 905, SE-391 29 Kalmar, Sweden*
[c]*Department of Water and Environmental Studies, Linköping University, SE-581 83 Linköping, Sweden*

Abstract

Bacterial abundance and production were studied in different zones in the Southern Ocean (39–62°S, 4–14°E) during a cruise in December–January 1997/1998. The role of potential growth limitation of bacteria due to limited availability of organic carbon (glucose) or inorganic N and P was studied in parallel. A positive correlation between surface water temperatures (−2 to 18 °C) and bacterial abundance ($<0.1 \times 10^6$–1.5×10^6 cells ml^{-1}) was observed. Bacteria were studied in vertical profiles, concentrated to three areas close to 6°E: the former Spring Ice Edge (SIE, 60°S, high chlorophyll *a*), the former Winter Ice Edge (WIE, 56°S, low chlorophyll *a*) and the Antarctic Polar Front at 51°S (APF, moderate chlorophyll *a* levels). Bacterial abundance was uniformly low south of the APF, and for the upper 50 m generally below 0.3×10^6 bacteria ml^{-1}. In deeper water, bacterial abundance decreased dramatically for WIE and APF stations, but less markedly for SIE stations. The average volumetric bacterial production in the mixed layer was highest for APF stations (0.04 μg C l^{-1} h^{-1}), but only half of this value for SIE stations (0.02 μg C l^{-1} h^{-1}), with WIE in between (approximately 0.03 μg C l^{-1} h^{-1}). Below 100 m, bacterial production decreased to values close to the detection limit. None of the three areas demonstrated any systematic diurnal variations in bacterial production in surface water (2 m) or at the chlorophyll maximum (situated between 30 and 66 m). We observed a positive correlation between bacterial production and in vivo chlorophyll *a* fluorescence, but there was no correlation between this parameter and bacterial abundance, possibly indicating different control mechanisms for these two parameters. Unfiltered water samples from 20 m depth were incubated at in situ temperatures and amended with ammonium, phosphate or glucose. In all the three experiments, from warm waters (relatively poor in inorganic nitrogen and phosphorus) south of Cape Town (38°S, +18.6 °C), in the colder and inorganic nutrient-rich waters north of the APF (45°S, +7.0 °C) as well as in the cold, nutrient-rich waters at the SIE (61°S, −0.13 °C), organic carbon additions resulted in a significant increase in bacterial

*Corresponding author. Tel.: +46 46 222 8431; fax: +46 46 222 4536.
E-mail address: wilhelm.graneli@limnol.lu.se (W. Granéli).
[1]Present address: Marine Biology, Lund University, Campus Helsingborg, Box 882, SE-251 08 Helsingborg, Sweden.
[2]Present address: Department of Evolutionary Biology/Limnology, Uppsala University, Norbyvägen 20, SE-75 236 Uppsala, Sweden.

0967-0645/$ - see front matter © 2004 Elsevier Ltd. All rights reserved.
doi:10.1016/j.dsr2.2001.01.003

production. Bacterial growth rates were very different between the three regions, and the growth response in th bacterial communities to the carbon additions was very slow at low temperatures.
© 2004 Elsevier Ltd. All rights reserved.

1. Introduction

Bacterioplankton in Antarctic waters have received substantial interest in recent years, mainly for two reasons: (1) bacteria are considered major agents in the cycling and mineralization of organic carbon in the sea, and are thus important in the context of Antarctic marine food webs, as well as in the global carbon cycle, (2) bacteria are believed to be sensitive to enhanced UV-B radiation, caused by stratospheric ozone thinning. Bacterioplankton in the Southern Ocean are faced with an environment significantly different from that found in most other aquatic ecosystems on the earth: there is essentially no other source of dissolved organic matter (DOM) than phytoplankton production, since terrestrial and benthic sources of DOM are insignificant, and there is an abundant supply of macronutrients (N and P). On the other hand, concentrations of certain trace metals (especially iron) are extremely low, and temperatures are typically zero or below zero.

Bacterial growth in aquatic systems may be regulated by temperature (Shiah and Ducklow, 1994), predation (Caron, 1991), substrate supply (organic and inorganic nutrients) (Cole et al., 1988; Rivkin and Anderson, 1997) and viral infection (e.g. Proctor and Fuhrman, 1992). In oceanic environments bacteria have to rely on autochthonously produced DOM as substrates for growth. A previously observed positive correlation between phytoplankton and bacterial biomass and production has led to the suggestion that bacterial growth is limited by organic carbon supplied from phytoplankton exudation (Cole et al., 1988). Since then, several studies have shown that bacterial growth in marine environments is stimulated by the addition of organic carbon (Kirchman, 1990; Chin-Leo and Benner, 1992; Carlson and Ducklow, 1996).

However, more recently, investigators have demonstrated that bacterial growth in aquatic ecosystems can be limited by the availability of nitrogen and phosphorus, rather than the supply of organic carbon (e.g. Elser et al., 1995; Pomeroy et al., 1995; Cotner et al., 1997).

In the Southern Ocean, several frontal systems exist, which separate water masses with different characteristics (Lutjeharms, 1985). North of the Subtropical Convergence (SC) (around 41°S), the water is above 18 °C and inorganic nutrient concentrations are relatively low (Laubscher et al., 1993). North of the Antarctic Polar Front (APF) lies the Sub-Antarctic Front (around 46°S), where the water has a temperature of 3–5 °C. This water is rich in nitrate and phosphate, while ammonium concentrations are low (Laubscher et al., 1993). South of the APF, the water is usually below 0 °C and also rich in inorganic nutrients (Laubscher et al., 1993), while concentrations of dissolved organic carbon (DOC) are low (often below 50 $\mu mol\,l^{-1}$, Wedborg et al., 1998). Water temperature is often positively correlated with the seasonal bacterial abundance and production (e.g. Hoch and Kirchman, 1993; Ochs et al., 1995) and temperature has been a factor considered more important than substrate supply for the regulation of bacterial production in nature (Shiah and Ducklow, 1994).

An expedition to the Eastern Atlantic sector of the Southern Ocean was organized during the austral summer 1997/1998 within the Swedish Antarctic research program (SWEDARP) (see Turner et al., 2004; Bertilsson et al., 1999a; Froneman et al., 1998). On board the South African ice-breaking research vessel S.A. *Agulhas*, we measured bacterial abundance and production at frontal zones in the Southern Ocean. One of the main objectives was to determine if temperature, nutrients (N and P) or organic carbon availability control bacterial abundance and/or production. Our work was based on the following hypotheses:

1. Bacterial abundance and production decrease from north to south, parallel to the decrease in temperature. However, in frontal areas, e.g. at

the Spring Ice Edge (SIE), bacterial biomass and activity will be elevated.
2. Bacterial numbers and activity are very low at depths greater than 100 m.
3. Potential bacterial biomass accumulation and bacterial production in Antarctic waters are not limited by inorganic N or P availability, but by the availability of DOC. However, north of the APF, bacteria may be nutrient limited.

Fieldwork was divided between three main tasks: (1) sampling along a latitudinal transect from Cape Town into the drift ice zone (approximately 39°S, 14°E to 62°S, 4°E), (2) more detailed investigations in three areas centered along 6°E: the APF (51°S), the former SIE (60°S) and the former Winter Ice Edge (WIE, 56°S), including diurnal studies on bacterial production and numbers from surface waters and from the chlorophyll maximum, and (3) experimental investigations on potential nutrient limitation of bacterioplankton growth.

2. Materials and methods

Surface water samples were taken along a latitudinal transect between December 4 and 10, 1997. Water was sampled from the non-toxic running seawater intake of the S.A. *Agulhas* on route from Cape Town to the shelf ice. A total of 47 water samples at latitudinal intervals of one-half degree were obtained between 39° and 62°S (Fig. 1). The seawater intake system stopped functioning shortly after entering the drift ice zone, preventing sampling further south on the southbound leg. After leaving the shelf ice on the northbound leg, several stations were sampled in the former SIE, the former WIE, and at the APF, during the period December 31, 1997 to February 2, 1998 (for localization of these areas see Fig. 1). At "CTD-stations", vertical profiles from 9 depths (2, 20, 30, 50, 75, 100, 150, 200 and 400 m) were taken with a 71 rosette sampler. There were 19 complete CTD stations with respect to bacterial parameters (7 in the SIE, 4 in the WIE and 8 in the APF area). For a smaller number of "Biostations" (3 in SIE water, 1 at the WIE and 2 in APF water),

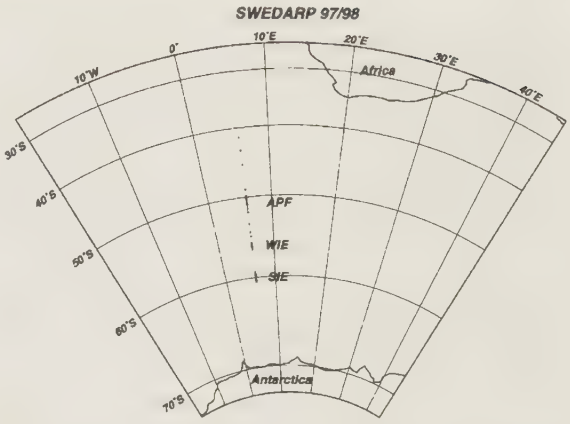

Fig. 1. Transects and intensively investigated areas. SIE (around 60°S), WIE (at 56°S) and APF (at 51°S). (From Tanhua et al., 2004.)

which were occupied for at least 24 h, we also sampled 8–9 different depths down to 200 or 400 m. Sampling depths at these stations were adjusted according to the chlorophyll fluorescence and PAR profiles. The depth of the chlorophyll maximum, as defined by in vivo fluorescence, was first determined through a CTD/fluorescence cast. PAR levels in relation to radiation at the surface were determined with a Biospherical PUV 500 underwater radiation profiling instrument (see Rasmus et al., 2004). Subsequently, some of the sampling depths were spaced in the profile at certain predetermined relative-PAR levels (e.g. 50%, 10%, 1% of surface PAR radiation), with one bottle being closed at the chlorophyll maximum. In each of the three areas, a diurnal study was made at one of the Biostations, with sampling every second hour over at least a full 24 h cycle (12–13 sampling occasions). For this diurnal profile, only 2 depths were sampled: surface (approximately 2 m) and the chlorophyll maximum (as defined by fluorescence reading from an initial CTD cast), a fixed level for the full 24 h cycle, ranging from 30 to 66 m for the three stations. In addition to the sampling stations above, we have also made measurements down to 3000 m for three CTD stations located at 45°30′, 43°30′ and 41°30′S, thus north of the APF (Fig. 1).

Water was transferred either from the running seawater or from Niskin bottles to 100 ml acid-washed and Milli-Q-rinsed polycarbonate bottles. Subsamples were immediately retrieved for quantification of bacterial numbers and bacterial protein production (BPP). For the Cape Town–shelf ice transect, only bacterial numbers were measured.

Samples (10 ml) for enumeration of bacteria were preserved with 0.2 μm filtered formaldehyde (final concentration 2%) and stored at 4 °C. Bacterial numbers were determined on board the research vessel using a Becton Dickinson FACS-Calibur flow cytometer, or after the return to Sweden using a FACSort flow cytometer according to del Giorgio et al. (1996). Subsamples (500 μl) were stained with 5 μl of a 10 × diluted solution of SYTO 13 (Molecular Probes). Internal standards were 1.58 μm fluorescent beads (Fluoresbrite Microspheres, Polysciences). Final bead concentration in the different analyses ranged from 300 to 900 beads μl^{-1}. The samples were analyzed at a low flow rate (about 12 $\mu l\,min^{-1}$). Bacterial cells and microspheres were separated in a log-log scattergram of green fluorescence intensity (FL1) and side scatter (SSC). Samples were run for 1 min, or until a minimum of 5000 cells were counted. Bacterial cell concentrations in the samples were calculated using the microspheres as an internal standard. The concentration of beads in the samples was determined on a daily basis using epifluorescence microscopy. Selected bacterial samples were also counted microscopically after staining with DAPI (Porter and Feig, 1980). Bacterial abundance assessed by flow cytometry and microscopic methods were linearly correlated ($r^2 > 0.95$, $n = 35$), but the flow cytometric estimates were on average 29% higher than the microscopic counts. Since we could not verify any errors in the subsampling, sample preparation or calculations, the flow cytometer apparently counted substantially more bacteria than the human eye. We have not found this discrepancy in lake water samples (see e.g. Bertilsson et al., 1999b). However, bacteria in the Antarctic samples were very small, and this may have resulted in the exclusion of some cells in the microscopic counting and/or a significant background noise in the flow cytometric analysis. Since any error was systematic, conclusions with respect to comparisons between different depths and stations should not be affected.

Bacterial production was measured according to the leucine centrifugation method of Smith and Azam (1992). The washing with ethanol was omitted, as preliminary tests showed that this did not affect the results. Before the measurements at the CTD and Biostations were started, leucine incorporation in relation to added leucine concentration was investigated for SIE surface bacteria. Cold and tritiated (Amersham TRK 510) specific activity 112 Ci $mmol^{-1}$) leucine were mixed to obtain final concentrations between 0 and 120 nM. Leucine incorporation was saturated at 20 nM leucine, and this concentration was used for all subsequent measurements. The specific activity of the diluted solution (total volume 5 ml) was 29.4 Ci $mmol^{-1}$. From this 5 μl was added to each sample of 1.7 ml in Eppendorf vials.

Tests at +2.0 and −1.7 °C with SIE surface water showed that the leucine incorporation was linear with time for at least 6 h. Samples from Bio- and CTD-stations were incubated for 4 h, while samples from the diurnal studies were incubated for 2 h. Duplicate samples were incubated for each depth at the CTD and Biostations, and six blanks (TCA added prior to the isotope addition) were incubated per profile. For the diurnal sampling, triplicate samples and one blank sample were incubated per depth and sampling occasion.

All bacterial production samples were incubated in darkness at the in situ temperature of the mixed layer (±0.5 °C), using a temperature-controlled water bath connected to a flow-through cooler. The temperature effect on bacterial production was investigated for one sample from the chlorophyll maximum of station D143 (WIE, 60°S, 6°E). Duplicate subsamples were incubated at eight different temperatures, ranging from −1 to 22 °C. The increase in leucine incorporation was 30% when temperature was increased from −1 to 0.2 °C. Above this temperature there was an additional 30% increase up to 14.6 °C, after which the uptake declined slightly.

After addition of liquid scintillation cocktail (1 ml of Ready Gel), samples were counted in a

Beckman LS-133 liquid scintillator on board the S.A. *Agulhas*. Counts of diluted isotopes indicated that DPM values were not reliable, i.e. the quench correction of the instrument did not work properly. Therefore, some samples were counted immediately after the expedition on a Beckman LS 6500 instrument at the Ecology department in Lund. A comparison between CPM values obtained on board the ship, and DPM values for the same samples counted in Lund, gave an r^2 value of 0.99, with DPM in Lund $= 2.0 \times$ CPM on S.A. *Agulhas*. This equation has been used to recalculate CPM values measured on board S.A. *Agulhas* to corresponding DPM values. BPP calculations are based on the assumptions of 7.3 mol% leucine in bacterial protein, an intracellular isotope dilution of 2, and a weight ratio of 0.86 between carbon and protein.

For experimental studies of nutrient limitation of bacterial growth, water from a depth of 20 m was obtained from the CTD-rosette sampling bottles at the following sites: (1) north of the SC (37°53′77″S, 15°47′85″E, 18.6 °C, 5 December 1997), (2) north of the APF (45°30′00″S, 06°00′00″E, 6.9 °C, 2 February 1998), (3) at the SIE (61°00′61″S, 05°57′12″E, −0.13 °C, 28 December 1997) (Fig 1). Subsamples were removed for determinations of initial bacterial abundance and bacterial production. Subsequently, aliquots of 300 ml were transferred to acid-washed polypropylene plastic bags and inorganic nitrogen (20 μmol l^{-1} as NH_4Cl), inorganic phosphorus (2 μmol l^{-1} as NaH_2PO_4) or glucose (100 μmol l^{-1} C) were added (control (no addition), +N, +P, +C). In one experiment (north of the APF) the following combination treatments were also used: +CP, +CN, +NP, +CNP. All treatments were incubated in triplicate. The bags were sealed with plastic clips and placed in a water bath kept dark close to the in situ water temperature (±0.5 °C). Subsamples were removed after 24, 55, 72 or 144 h of incubation (depending on the water temperature) for analyses of bacterial abundance and production. Bacterial abundance was analyzed as described above, while samples for bacterial production were incubated for 1 h and for each experimental incubation, duplicate samples and one blank was performed.

3. Results

There was a decline in bacterial numbers from 1.5×10^6 ml^{-1} at 39°S, north of the APF, where temperatures were above 10 °C, to less than 0.1×10^6 ml^{-1} in the drift ice zone at 60°S, at temperatures around −1 °C (Fig. 2). At approximately 60°30′S, entering the SIE, the temperature dropped steeply from −1 to −1.7 °C, coinciding with a reduction in salinity. This correlated with an increase in bacterial abundance in the surface waters, to approximately 0.15×10^6 ml^{-1}. Surface water temperatures (2–10 m) on the northbound leg were close to those measured on the southbound transect, although they were slightly higher at SIE and WIE. Also bacterial abundances were somewhat elevated at SIE and WIE compared to the southbound leg. Bacterial abundance was closely related to temperature (Fig. 3).

Bacterial abundances in the vertical profiles from all three regions were rather uniform above 100 m depth (Figs. 4 and 5). Maximal abundance values did not differ dramatically between the three areas, but an average APF profile showed somewhat higher bacterial numbers in the 0–50 m layer when compared to SIE and WIE water, which were more similar to each other in this aspect. Maximal bacterial concentrations for water in the APF were less than 0.4×10^6 ml^{-1}. In the WIE and APF areas, bacterial numbers decreased

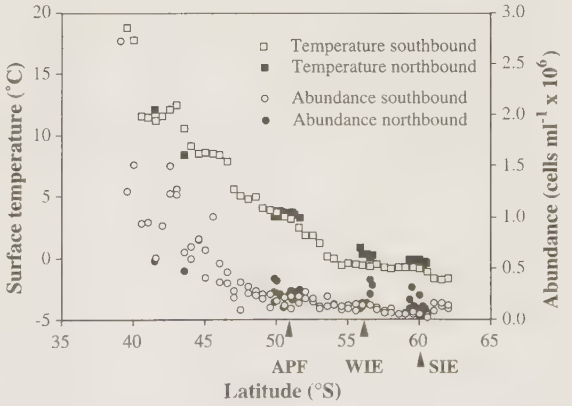

Fig. 2. Temperature and bacteria abundance in surface water (taken from the running sea water system of S.A. *Agulhas* on the southbound leg and from bottles representing surface water (2–10 m) on the northbound leg). Abbreviations as in Fig. 1.

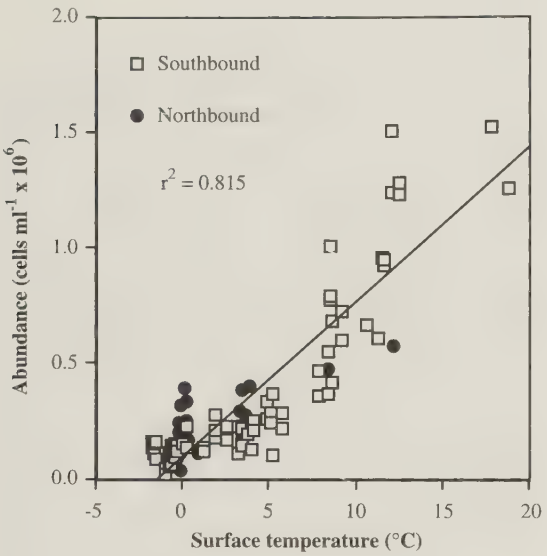

Fig. 3. Correlation between temperature and bacterial abundance. Data from both south- and northbound legs included.

markedly below 100 m depth, to less tha 0.1×10^6 ml^{-1}, while for the SIE stations, bacteri numbers were more uniform throughout the dep profile. Water samples obtained from greate depths (e.g. 600, 2000 and 3000 m) had less tha 0.05×10^6 bacterial cells ml^{-1} (data not shown For two stations north of the APF (located aroun 51°S), at 43°30′ and 41°30′S, bacterial numbe varied between 0.4 and 0.9×10^6 ml^{-1} in the mixe layer, confirming results from the southboun transect, sampled during the first half of Decembe (Fig. 2).

Overall, BPP levels were low and did not exceed 0.1 μg C l^{-1} h^{-1} (Figs. 4 and 5) The differences between areas were larger for bacterial productio than for bacterial numbers, with much lowe values for the SIE stations compared to station at the APF and the WIE. The three stations north of the APF did not show any elevated bacteria production compared to the APF stations (data

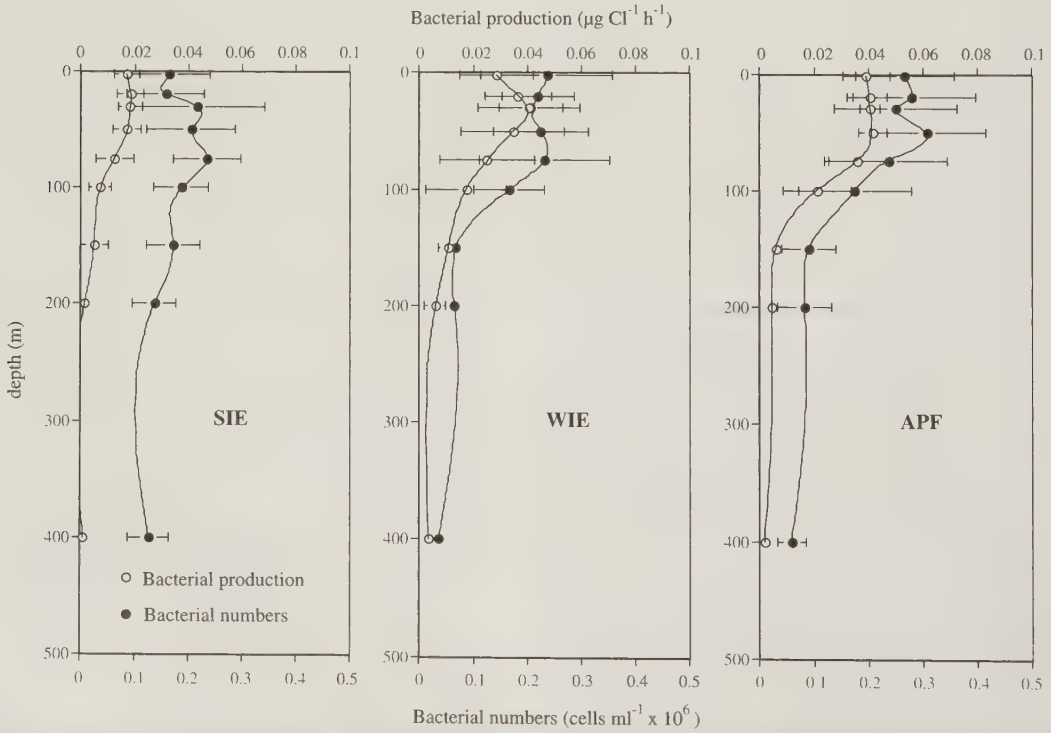

Fig. 4. Bacterial abundances and production for all SIE (around 60 S, 10 stations), WIE (at 56°S, 5 stations) and APF (at 51°S, 10 stations) stations, error bars = 1$x \pm$s.d.

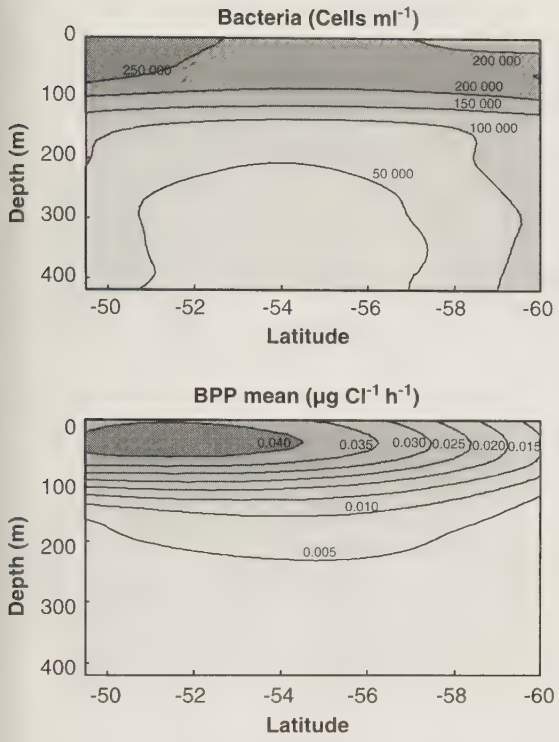

Fig. 5. Bacterial abundance and production between 50 and 60°S and 0–400 m depth.

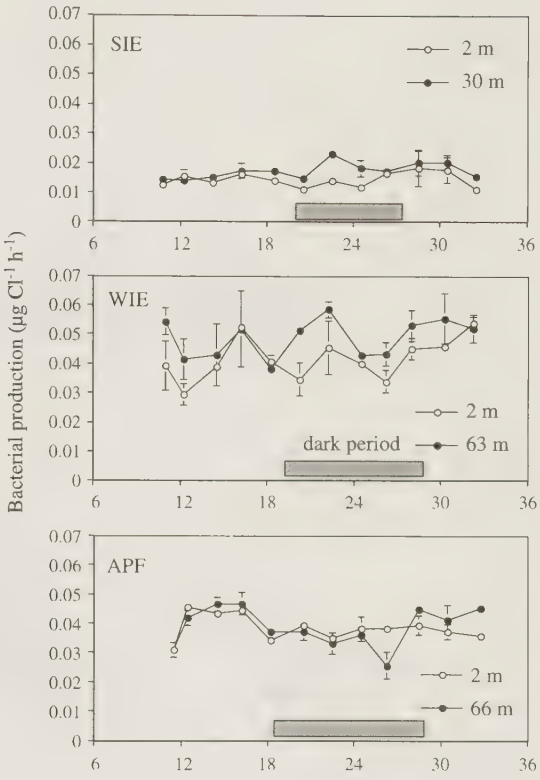

Fig. 6. Diurnal variations in bacterial production for water from the surface (2 m) and the chlorophyll maximum (range 30–66 m depth) at three stations in (A) the SIE area, (B) the WIE area and (C) at the APF area. The dark bars represent light less than 50 µE m^{-2} s^{-1}. Abbreviations as in Fig. 1.

not shown). Similar to bacterial counts, production decreased markedly below 100 m depth, with the most dramatic decrease for the APF stations. These stations had a rather equal bacterial production at depths between 2 and 75 m. A pattern similar to this was also seen in the SIE profiles (above 50 m depth), while the bacterial production at WIE stations peaked at intermediate depths (around 30 m). BPP was very low at depths below 400 m, averaging 0.002 µg Cl^{-1} h^{-1}. The depth integrated, areal average bacterial production estimated for the top 150 m of the water column was approximately 40, 90 and 100 mg C m^{-2} d^{-1} for the SIE, WIE and APF, respectively, assuming no systematic diurnal variations in bacterial production.

Bacterial production varied during the 24 h diurnal studies (Fig. 6). This was especially pronounced for the APF and the WIE Biostations. However, these fluctuations did not appear to be systematic with respect to the time of day.

Both in warmer waters, north of the SC, and in colder waters at the SIE, organic carbon additions resulted in a significant increase in bacterial production, indicating that bacterial growth was limited by the availability of organic carbon (Fig. 7). However, the slower growth rates in the colder waters delayed the bacterial response to the additions.

Initial bacterial density differed significantly between the three regions. North of the SC, the initial density was 0.87×10^6 cells ml^{-1}, while it was 1.32×10^6 cells ml^{-1} north of the APF and a very low bacterial density was obtained at the SIE (around 0.1×10^6 cells ml^{-1}). Initial bacterial production was highest north of the SC (0.152 µg Cl^{-1} h^{-1}), and lower north of the APF (0.047 µg Cl^{-1} h^{-1}) and very low at the SIE (0.021 µg Cl^{-1} h^{-1}).

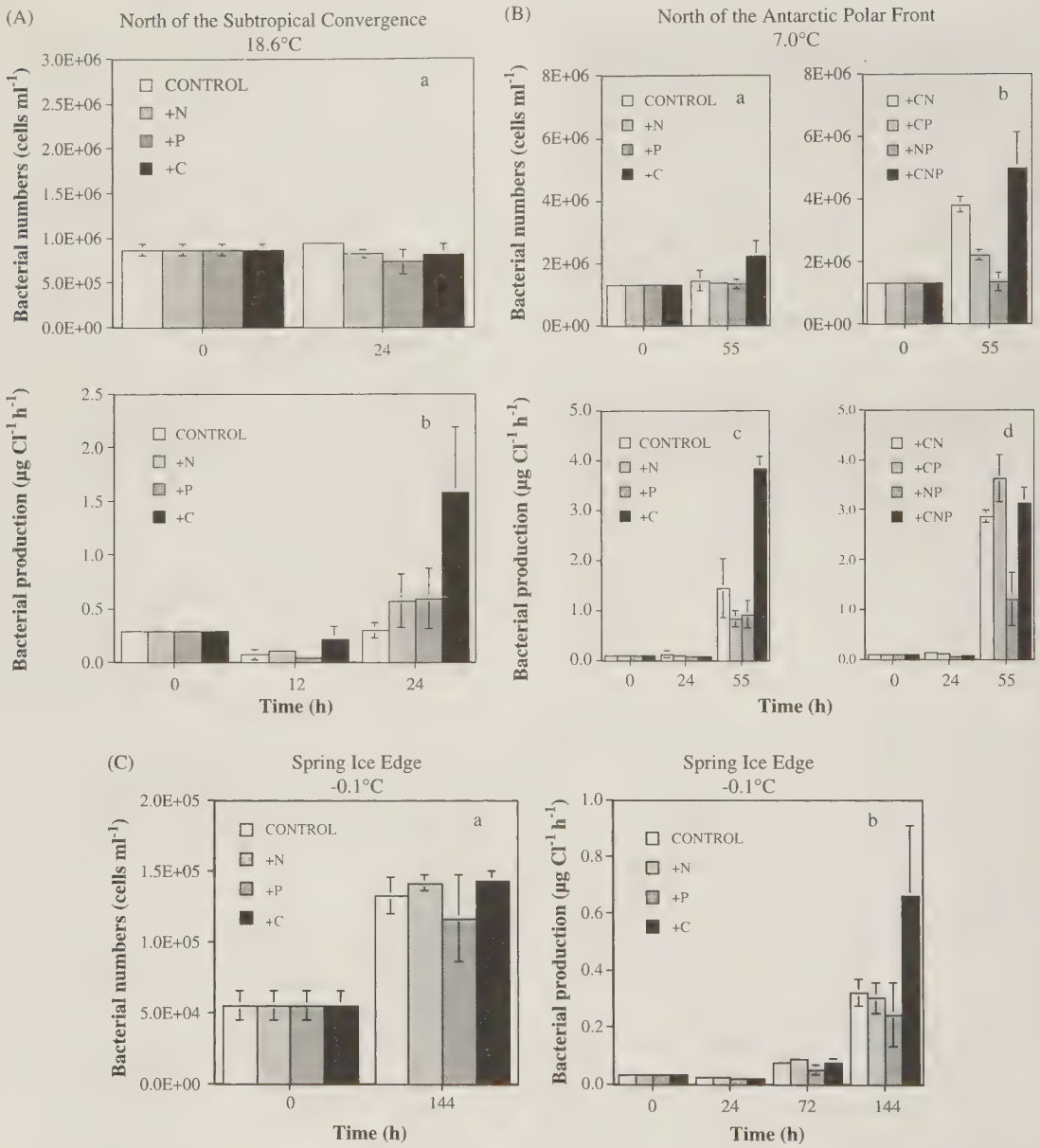

Fig. 7. Bacterial numbers (cells ml^{-1}) and bacterial production ($\mu g\,C\,l^{-1}\,h^{-1}$) from (A) the nutrient amendment experiment north of the SC (37°53′77″S, 15°47′85″E), (B) the experiment north of the APF (45°30′00″S, 06°00′00″E) and (C) the experiment at the SIE (61°00′61″S, 05°57′12″E). Control = no addition. Additions: $+N = 20\,\mu mol\,l^{-1}\ NH_4^+$, $+P = 2\,\mu mol\,l^{-1}\ PO_4^{3-}$ and $+C = 100\,\mu mol\,l^{-1}$ C as glucose. Presented data are means of three replicates and error bars represent one standard deviation.

In experiment 1 (north of the SC), bacterial numbers remained constant during the 24 h incubation (Fig. 7A). In contrast, the bacterial production in this experiment showed a significant stimulation when carbon was added ($p < 0.05$, ANOVA). This stimulation was significant already after 12 h of incubation.

In experiment 2 (north of the APF), there was no significant response in bacterial production after 24 h of incubation for any of the treatments

(Fig. 7B). However, after 55 h, there was a response both in bacterial numbers and bacterial production. In all treatments where carbon was added (+C, +CN, +CP and +CNP) bacterial production and abundance increased significantly compared to the controls ($p<0.05$, ANOVA). None of the treatments with only N and/or P added enhanced bacterial numbers or production compared to the controls.

In experiment 3 (at the SIE), there was no significant response in bacterial production to any of the treatments, even after 72 h ($p>0.05$, ANOVA) (Fig. 7C). However, after an extended incubation (144 h), bacterial numbers increased equally, both in controls and in all treatments (no significant differences $p>0.05$, ANOVA). On the other hand, bacterial production was significantly higher in the +C treatment as compared to all other treatments (including the control) ($p<0.05$, ANOVA).

4. Discussion

In this study, bacterial abundance was quantified with flow cytometry. This resulted in values that were on average 30% higher compared to our microscopic counts (see Section 2). Still, the bacterial abundances obtained in the present study, using flow cytometric methods, were in the same range as those found by other authors for Antarctic waters, i.e. $0.1–0.5\times10^6\,ml^{-1}$ (Karl, 1993; Grossmann, 1994; Grossmann and Dieckmann, 1994; Delille et al., 1995; Delille and Rosiers, 1996; Leakey et al., 1996; Heinänen et al., 1997) or Arctic marine waters (Mueller-Niklas and Herndl, 1996). However, these are total counts, and a more or less large fraction of the bacterial cells may not be active or may even be dead "ghosts". The proportion of these may vary between stations and different depths in the water column. In the Weddell Sea, microautoradiographic studies revealed that during a phytoplankton bloom only 13% of the bacteria in the euphotic zone took up leucine, while 50% of the cells at 400 m were active, even though they were growing very slowly (Grossmann, 1994). When the natural bacterial community was separated from bacterial predators and incubated at the in situ temperature, bacterial numbers increased between 5 and 20 times in 10–20 days (see Bertilsson et al., 2004). This large increase in bacterial numbers must have taken place as the active proportion of the bacterial community increased in numbers and shows the ability of the available substrates to support bacterial growth in the absence of loss factors such as grazing.

There was a general trend of decreasing bacterial abundance from 39° to 62°S and bacterial abundance was well correlated with temperature (Fig. 3). On the southbound leg (the Cape Town–shelf ice transect), bacterial numbers increased in the marginal ice zone, which may be due to enrichment of surface waters with bioavailable substrates from the melting sea ice, which contains exudates and cellular constituents from senescing ice algae. Alternatively, this effect could be due to a stabilization of the water column through meltwater, decreasing vertical mixing and thus improving conditions for phytoplankton growth.

With respect to bacterial production there was a clearer difference between the investigated areas than for bacterial abundance. BPP in the SIE mixed-layer water was only about half the rate in APF water (Fig. 4 and 5). BPP at SIE and WIE stations were in the same range as previously obtained leucine incorporation rates in the Weddell Sea (Kuparinen and Björnsen, 1992). These estimates were obtained at a similar latitude (57–62°S, 47–49°W), although the mixed layer-depth in the present study was probably much more shallow. Furthermore, the BPP in the present study was an order of magnitude lower than e.g. values from the Arctic (Mueller-Niklas and Herndl, 1996) and summertime values for temperate waters (Heinänen, 1992; Karlson et al., 1996).

Since phytoplankton production should be the only available source of organic substrates for bacterioplankton growth in the offshore parts of the Southern Ocean, it is expected that bacterial abundance and/or production would be related to phytoplankton biomass and/or production. This correlation should be particularly strong, since phosphorus and nitrogen, which may limit bacterioplankton growth in many marine and freshwater systems (see below), are

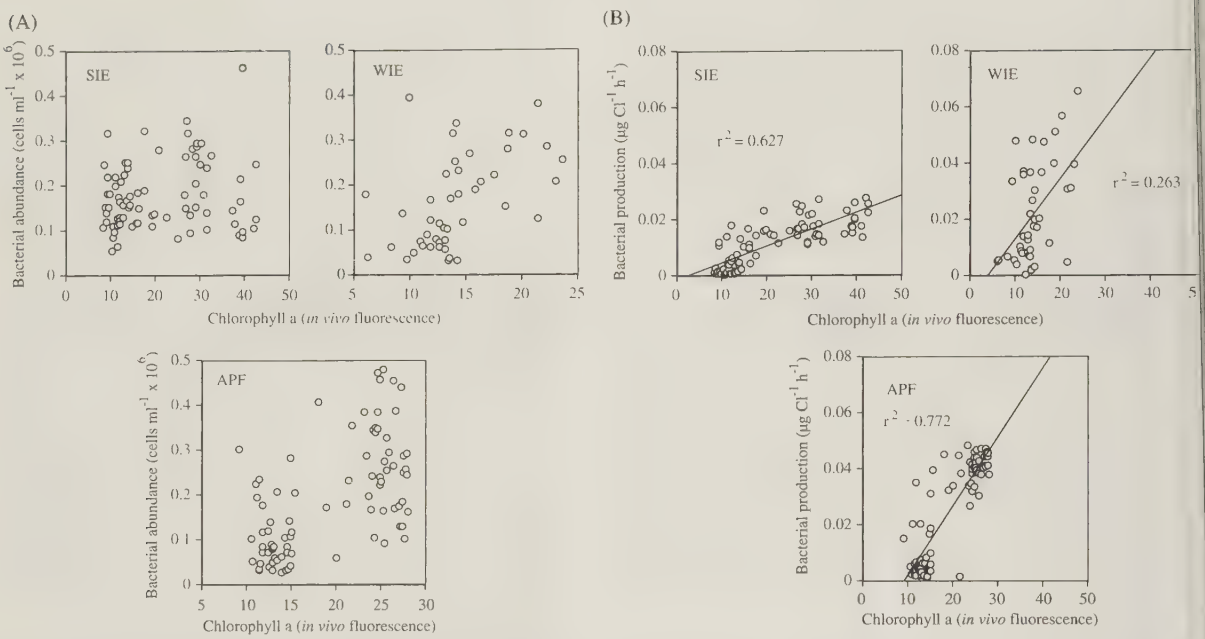

Fig. 8. Relation between in vivo chlorophyll fluorescence and bacterial abundances (A) and bacterial production (B). Abbreviations as in Fig. 1.

found in high concentrations in the Southern Ocean. On the other hand, bacteria may be limited by iron (see Özturk et al., 2004; Boyd et al., 2000). A good correlation between bacterial and phytoplankton abundance has been found in several earlier studies (e.g. Kuparinen and Björnsen, 1992; Gleitz et al. 1994; Delille et al., 1995; Heinänen et al., 1997). However, contrary to our expectations we did not find any correlation between bacterial numbers and chlorophyll *a* concentrations, neither for the combined data set nor for individual water masses (SIE, WIE and APF; Fig. 8).

On the other hand, bacterial production was positively correlated to chlorophyll *a* in vivo fluorescence. This could indicate that even if bacterial production is enhanced by algal-derived organic substrates, this increase is not reflected in an elevated bacterial biomass. The reason for this could, for example, be increased predation on bacteria. These results agree with observations made in bacterial cultures where potential grazers were removed by selective filtration (Bertilsson et al., 2004). In this study, bacterial growth potential was highest in surface waters obtained from the SIE area, where chlorophyll *a* levels were high.

When calculating daily rates of bacterial production, and integrating over depth, it is essential that there are no systematic diurnal variations, since incubation times are usually not longer than a few hours for the leucine method, and since sampling and incubation on a cruise may take place during any time of the day. This was tested for two depths at each of three stations and we could not detect any systematic changes in leucine uptake over 24 h periods, neither for surface (2 m) nor for chlorophyll maximum water (Fig. 6). This is in accordance with thymidine incorporation studies made at the Weddell–Scotia confluence by Kuparinen and Björnsen (1992). However, since our short-term incubations were made in darkness, we may have underestimated direct negative effects of UV radiation on bacteria. Incubations carried out for 5–7 h around noon in Antarctic, near-shore waters showed that bacterioplankton were strongly inhibited by UV radiation down to 9.5 m (Helbling et al., 1995). In offshore waters this inhibition probably reaches even deeper, although the effect may not be as strong as for fixed-depth incubations, since bacteria are transported randomly up and down in the mixed layer.

UV damage may be compensated for by various repair mechanisms and there may even be a positive effect of solar radiation on bacterial growth due to photochemical alterations in the amount and quality of the pool of organic substrates available for bacterial utilization (Bertilsson et al., 2004). It must also be stressed that there is no guarantee that the water was sampled from the same water mass during the entire 24 h diurnal sampling.

All three nutrient enrichment experiments showed that additions of organic carbon stimulated bacterial production. This is in accordance with several earlier investigations in different marine systems (Wheeler and Kirchman, 1986; Carlson and Ducklow, 1996). However, it has also been shown that phosphate or ammonium additions may stimulate bacterial growth in marine waters (Zweifel et al., 1993; Rivkin and Anderson, 1997). This is particularly marked if phosphate concentrations are undetectable or very low, and often correlates with a high phosphatase activity in situ (Cotner et al., 1997). The concentration and/or availability of phosphate and ammonium at all three main sampling areas (SIE, WIE, APF) were probably high enough to sustain bacterial growth without these compounds being limiting. In the warm-water area (north of the SC), quite high concentrations of phosphate (0.3–0.5 μmol l^{-1}) and ammonium (0.6–1.0 μmol l^{-1}) are found, and in the other areas there are typically even higher concentrations of ammonium and phosphate during the austral summer (Laubscher et al., 1993).

Since all the components of the microbial food web (microzooplankton and phytoplankton) were incubated in the limitation experiments, the observations of bacterial growth stimulation by addition of organic carbon is a net result of the processes taking place in the microbial food web, i.e. nutrients and dissolved organic matter from grazing activity and phytoplankton would be present, and bacteria would be grazed by microzooplankton. This means that both gain and loss factors affecting the net bacterial growth and abundance were acting on the bacterial community. Toolan et al. (1991) and Cotner et al. (1997) have also used the approach of incubating the whole water from mesotrophic lake water and oligotrophic marine waters, respectively. Their results showed a significant stimulation of bacterial production by phosphate addition. In the experiment performed by Cotner et al. (1997) in the oligotrophic Sargasso Sea, phosphate concentrations in the euphotic zone were very low (<10 nmol l^{-1}) and alkaline phosphatase activities indicated P-limitation.

There were some notable differences between the different waters in the response of bacterial numbers and production to nutrient additions. In the warm waters north of the SC, bacterial numbers did not change during the 24 h incubation, while bacterial production increased in the treatments where carbon was added. North of the APF, both bacterial numbers and production increased when carbon was added. At the SIE, bacterial numbers increased equally in all treatments (including the control), but bacterial production increased more when carbon was added. The lack of change in bacterial numbers could have been due to a balance between bacterial growth and loss of cells by the action of bacterial grazers (e.g. Sanders et al., 1992) during the incubation time. However, since bacterial production was stimulated by the carbon addition in the experiment carried out north of the SC, it is probable that an increase in bacterial numbers would have been detected if the incubation had lasted longer. Not surprisingly, there was a faster response in leucine uptake and protein production than in cell division. An addition of the limiting factor (in this case carbon) can give a detectable response in protein synthesis in 12 h, while it takes a longer time for the bacterial cells to synthesize all needed cell components and perform a division. Similar results have been obtained earlier by e.g. Berman et al. (1994), who, besides a faster response in bacterial production to nutrient additions, also found that there first was a twofold increase in cell volume rather than an increase in the number of bacterial cells.

Besides substrate supply, temperature also strongly affects bacterial growth. Several studies have demonstrated the importance of temperature in regulating bacterial abundance, substrate assimilation rates and growth rates in both freshwater

and marine environments (e.g. Hoch and Kirchman, 1993; Shiah and Ducklow, 1994, 1997; Tibbles, 1996). Kirchman et al. (1993) also showed that bacterial specific growth rates in the subarctic Pacific were enhanced by both an increase in temperature and by the addition of DOM, but that the response to temperature increase was faster than for the DOM addition. We incubated our samples at in situ temperature and did not perform any experiments with increased temperature to see if the response to the carbon and nutrient amendments would have been faster. In our experiments there was a gradient in temperature spanning across almost 20 °C, and the time it took for the bacterial community to react to different experimental manipulations also increased at lower temperatures. The results from our three enrichment experiments therefore suggest that even if organic carbon seems to be limiting bacterial production in these areas of the Southern Ocean, temperature is a very important regulator of bacterial growth rates at the community level.

Acknowledgements

We thank the expedition leader David Turner for never-ending patience and energy, and excellent organization of sampling on board S.A. *Agulhas*. We also want to express our gratitude to the crew of S.A. *Agulhas*, and to our colleagues from Scandinavia and South Africa for making the expedition enjoyable. The Swedish Polar Research Board provided logistic support. Grants from NFR (the Swedish Natural Science Research Council) to Wilhelm Granéli (Grant No. B-AA/BU 04969-321), Per Carlsson (Grant No. B-PD 10890-304) and Bert Allard (Grant No. G-AA/GU 03596-326) made our participation in SWEDARP 97/98 possible.

References

Berman, T., Hoppe, H.-G., Gocke, K., 1994. Response of aquatic bacterial populations to substrate enrichment. Marine Ecology Progress Series 104, 173–184.

Bertilsson, S., Granéli, W., Carlsson, P., 1999a. Interactions between bacteria, dissolved organic matter and solar radiation in the Southern Ocean. In: Polarforskningssekr tariatets årsbok 1998, Polarforskningssekretariatet, Stoc holm, pp. 66–68.

Bertilsson, S., Stepanauskas, R., Cuadros-Hansson, R., Gra éli, W., Wikner, J., Tranvik, L., 1999b. Photochemical induced changes in bioavailable carbon and nitrogen poo in a boreal watershed. Aquatic Microbial Ecology 1 47–56.

Bertilsson, S., Granéli, W., Carlsson, P., 2004. Influence of sola radiation on coloured dissolved organic matter an bacterial growth in the Southern Ocean. Deep-Sea Researc II, this issue [doi:10.1016/j.dsr2.2000.07.001].

Boyd, P.W., Watson, A.J., Law, C.S., Abraham, E.R., Trul T., Murdoch, R., Bakker, D.C.E., Bowie, A.R., Buesseler K.O., Chang, H., Charette, M., Croot, P., Downing, K. Frew, R., Gall, M., Hadfeld, M., Hall, J., Harvey, M Jameson, G., LaRoche, J., Liddicoat, M., Ling, R. Maldonado, M.T., McKay, R.M., Nodder, S., Pickmere S., Pridmore, R., Rintoul, S., Safi, K., Sutton, P., Strzepek R., Tanneberger, K., Turner, S., Waite, A., Zeldis, J., 2000 A mesoscale phytoplankton bloom in the polar Southern Ocean stimulated by iron fertilization. Nature 407, 695–702

Carlson, C.A., Ducklow, H.W., 1996. Growth of bacterioplankton and consumption of dissolved organic carbon in the Sargasso Sea. Aquatic Microbial Ecology 10, 69–85.

Caron, D.A., 1991. Evolving role of protozoa in aquatic nutrient cycles. In: Reid, P.C., Turley, C.M., Burkill, P.H. (Eds.), Protozoa and their Role in Marine Processes. Springer, Berlin, Heidelberg, pp. 387–415.

Chin-Leo, G., Benner, R., 1992. Enhanced bacterial production and respiration at intermediate salinities in the Mississippi River plume. Marine Ecology Progress Series 87, 87–103.

Cole, J.J., Findlay, S., Pace, M.L., 1988. Bacterial production in freshwater and saltwater ecosystems: a cross system overview. Marine Ecology Progress Series 43, 1–10.

Cotner, J.B., Ammerman, J.W., Peele, E.R., Bentzen, E., 1997. Phosphorus-limited bacterioplankton growth in the Sargasso Sea. Aquatic Microbial Ecology 13, 141–149.

del Giorgio, P.A., Bird, D.F., Prairie, Y.T., Planas, D., 1996. The flow cytometric determination of bacterial abundance in lake plankton with the green nucleic acid stain SYTO 13. Limnology and Oceanography 41, 783–789.

Delille, D., Rosiers, C., 1996. Seasonal changes of Antarctic marine bacterioplankton and sea ice bacterial assemblages. Polar Biology 16, 27–34.

Delille, D., Fiala, M., Rosiers, C., 1995. Seasonal changes in phytoplankton and bacterioplankton distribution at the ice–water interface in the Antarctic neritic area. Marine Ecology Progress Series 123, 225–233.

Elser, J.J., Stabler, L.B., Hasset, R.P., 1995. Nutrient limitation of bacterial growth and rates of bacterivory in lakes and oceans: a comparative study. Aquatic Microbial Ecology 9, 105–110.

Froneman, P.W., Pakhomov, E.A., Turner, D., Abrahamsson, K., Karlson, B., Godhe, A., Bertilsson, S., Granéli, W., Carlsson, P., Wängberg, S., Wulff, A., Croot, P., Andersson, K., Balarin, M., Wedborg, M., Persson, T., Rasmus,

K., Özturk, M., David, R., 1998. Research cruise of the Scandinavian/South African Antarctic expedition, December 1997 to February 1998. South African Journal of Science 94, 517–519.

Gleitz, M., Bathmann, U.V., Lochte, K., 1994. Build-up and decline of summer phytoplankton biomass in the eastern Weddell Sea, Antarctica. Polar Biology 14, 413–422.

Grossmann, S., 1994. Bacterial activity in sea ice and open water of the Weddell Sea, Antarctica: a microautoradiographic study. Microbial Ecology 28, 1–18.

Grossmann, S., Dieckmann, G.S., 1994. Bacterial standing stock, activity, and carbon production during formation and growth of sea ice in the Weddell Sea, Antarctica. Applied and Environmental Microbiology 60, 2746–2753.

Heinänen, A., 1992. Bacterioplankton in the open Baltic Sea. Dissertation, Finnish Marine Research 260, Finnish Institute of Marine Research, Helsinki.

Heinänen, A., Rateoja, M., Lahdes, E., Leppänen, J.M., 1997. Relationships between bacterioplankton, chl *a* and temperature in Antarctic surface waters in summer. Polar Biology 18, 62–69.

Helbling, E.W., Marguet, E.R., Villafane, V.E., Holm-Hansen, O., 1995. Bacterioplankton variability in Antarctic waters as affected by solar ultraviolet radiation. Marine Ecology Progress Series 126, 293–298.

Hoch, M., Kirchman, D.L., 1993. Seasonal and inter-annual variability in bacterial production and biomass in a temperate estuary. Marine Ecology Progress Series 98, 283–295.

Karl, D.M., 1993. Microbial processes in the Southern Ocean. In: Friedmann, E.I., Thistle, A.B. (Eds.), Microbial Ecology—Antarctic Regions. Wiley-Liss, Inc., New York, pp. 1–63.

Karlson, B., Edler, L., Granéli, W., Sahlsten, E., Kuylenstierna, M., 1996. Subsurface chlorophyll maxima in the Skagerrak—processes and plankton community structure. Journal of Sea Research 35, 139–158.

Kirchman, D.L., 1990. Limitation of bacterial growth by dissolved organic matter in the subarctic Pacific. Marine Ecology Progress Series 62, 47–54.

Kirchman, D.L., Keil, R.G., Simon, M., Welshmeyer, N.A., 1993. Biomass and production of heterotrophic bacterioplankton in the oceanic subarctic Pacific. Deep-Sea Research I 40, 967–988.

Kuparinen, J., Björnsen, P.K., 1992. Spatial distribution of bacterioplankton production across the Weddell–Scotia Confluence during early austral summer 1988–89. Polar Biology 12, 197–204.

Laubscher, R.K., Perisinotto, R., McQuaid, C.D., 1993. Phytoplankton production and biomass at frontal zones in the Atlantic sector of the Southern Ocean. Polar Biology 13, 471–481.

Leakey, R.J.G., Archer, S.D., Grey, J., 1996. Microbial dynamics in coastal waters of East Antarctica: bacterial production and nanoflagellate bacterivory. Marine Ecology Progress Series 142, 3–17.

Lutjeharms, J.R.E., 1985. Location of frontal systems between Africa and Antarctica: some preliminary results. Deep-Sea Research 32, 1499–1509.

Mueller-Niklas, G., Herndl, G.J., 1996. Dynamics of bacterioplankton during a phytoplankton bloom in the high Arctic waters of the Franz-Joseph Land archipelago. Aquatic Microbial Ecology 11, 111–118.

Ochs, C.A., Cole, J.J., Likens, G.E., 1995. Population dynamics of bacterioplankton in an oligotrophic lake. Journal of Plankton Research 17, 365–391.

Öztürk, M., Croot, P., Bertilsson, S., Abrahamsson, K., Karlson, B., David, R., Fransson, A., Sakshaug, E., 2004. Iron enrichment and photoreduction of iron under UV and PAR in the presence of hydrocarboxylic acid: implications for phytoplankton growth in the Southern Ocean. Deep-Sea Research II, this issue [doi:10.1016/j.dsr2.2000.10.001].

Pomeroy, R.L., Sheldon, J.E., Sheldon Jr., W.M., Peters, F., 1995. Limits to growth and respiration of bacterioplankton in the Gulf of Mexico. Marine Ecology Progress Series 117, 259–268.

Porter, K.G., Feig, Y.S., 1980. The use of DAPI for identifying and counting aquatic microflora. Limnology and Oceanography 25, 943–948.

Proctor, L.M., Fuhrman, J.A., 1992. Mortality of marine bacteria in response to enrichments of the virus size fraction from seawater. Marine Ecology Progress Series 87, 283–293.

Rasmus, K.E., Granéli, W., Wängberg, S.-Å., 2004. Optical studies in the Southern Ocean. Deep-Sea Research II, this issue [doi:10.1016/j.dsr2.2001.01.004].

Rivkin, R.B., Anderson, M.R., 1997. Inorganic nutrient limitation of oceanic bacterioplankton. Limnology and Oceanography 42, 730–740.

Sanders, R.W., Caron, D.A., Berninger, U.-G., 1992. Relationships between bacteria and heterotrophic nanoplankton in marine and fresh waters: an inter-ecosystem comparison. Marine Ecology Progress Series 86, 1–14.

Shiah, F., Ducklow, H.W., 1994. Temperature and substrate regulation of bacterial abundance, production and specific growth rate in Chesapeake Bay, USA. Marine Ecology Progress Series 103, 297–308.

Shiah, F.-K., Ducklow, H.W., 1997. Bacterioplankton growth responses to temperature and chlorophyll variations in estuaries measured by thymidine: leucine incorporation ratio. Aquatic Microbial Ecology 13, 151–159.

Smith, D.C., Azam, F., 1992. A simple, economical method for measuring bacterial protein synthesis rates in sea water using 3H-leucine. Marine Microbial Food Webs 6, 107–109.

Tanhua, T., Olsson, K.A., Fogelqvist, E., 2004. A first study of SF_6 as a transient tracer in the Southern Ocean. Deep-Sea Research II, this issue [doi:10.1016/j.dsr2.2001.02.001].

Tibbles, B.J., 1996. Effects of temperature on the incorporation of leucine and thymidine by bacterioplankton and bacterial isolates. Aquatic Microbial Ecology 11, 239–250.

Toolan, T., Wehr, J.D., Findlay, S., 1991. Inorganic phosphorus stimulation of bacterioplankton production in a meso-eutrophic lake. Applied and Environmental Microbiology 57, 2074–2078.

Turner, D.R., Bertilsson, S., Fransson, A., Pakhomov, E., 2004. The SWEDARP 97/98 marine expedition: overview. Deep-Sea Research II, this issue [doi:10.1016/j.dsr2.2003.08.006].

Wedborg, M., Hoppema, M., Skoog, A., 1998. On the relation between organic and inorganic carbon in the Weddell Sea. Journal of Marine Systems 17, 59–76.

Wheeler, P.A., Kirchman, D.L., 1986. Utilization of inorgani and organic nitrogen by bacteria in marine systems Limnology and Oceanography 31, 998–1009.

Zweifel, U.L., Norrman, B., Hagström, Å., 1993. Consumptio of dissolved organic carbon by marine bacteria and demand for inorganic nutrients. Marine Ecology Progress Series 101 23–32.

ELSEVIER

Deep-Sea Research II 51 (2004) 2583–2597

DEEP-SEA RESEARCH
PART II

www.elsevier.com/locate/dsr2

Optical studies in the Southern Ocean

K.E. Rasmus[a,*], W. Granéli[b], S.-Å. Wängberg[c]

[a]*Division of Geophysics, Department of Physical Sciences, University of Helsinki, P.O. Box 64, FIN-00014 Helsinki, Finland*
[b]*Department of Ecology, Limnology, Ecology Building, SE-223 62 Lund, Sweden*
[c]*Botanical Institute, Göteborg University, P.O. Box 461, SE-405 30 Göteborg, Sweden*

Abstract

During the Austral summer of 1997–1998, measurements of absorption, attenuation, downwelling and upwelling irradiance were made in the Southern Ocean along a S N transect at 6 E. Measurements were made to quantify the penetration of ultraviolet B radiation (UVBR) in the water column and daily doses of UVBR at different water depths, to study the attenuation of photosynthetically active radiation (PAR), and to judge if in the investigated areas of the Southern Ocean phytoplankton are light limited. The results show that the UVBR affects a substantial portion of the upper mixed layer. The diffuse attenuation coefficients (K_{PAR}) for PAR were found to vary between 0.03 and 0.09 m^{-1}. Using the values for K_{PAR} and the definition of the Sverdrup critical depth, the studied Southern Ocean plankton systems were found not to be light limited.
© 2004 Elsevier Ltd. All rights reserved.

1. Introduction

The inherent optical properties of water, the absorption coefficient and the volume scattering function, combine with the radiant light field to produce the apparent optical properties, one of which is the diffuse attenuation coefficient. The optical properties influence many physical and biological phenomena such as phytoplankton production, radiative transfer and solar heating. Waters in which phytoplankton and their detrital products are the only optically active substances are called Case 1 waters according to Morel (1994). This study focuses on one such Case 1 water: the Southern Ocean, which is the ocean surrounding the Antarctic continent.

The objectives of this study were to quantify the vertical penetration of solar Ultraviolet B radiation (UVBR, 280–320 nm) and Photosynthetic Active Radiation (PAR, 400–700 nm) into the water, and to determine what kind of environment for plankton growth that the optical properties together with other hydrographical characteristics of the water create. The study was made as part of the Finnish Antarctic Research Program (FINNARP) and the Swedish Antarctic Research Program (SWEDARP), on cruise number 86 of the South African research vessel S.A. *Agulhas*.

*Corresponding author. Tel.: +358 9 1915 1009; fax: +358 9 1915 1000.
E-mail address: kai.rasmus@helsinki.fi (K.E. Rasmus).

0967-0645/$ - see front matter © 2004 Elsevier Ltd. All rights reserved.
doi:10.1016/j.dsr2.2001.01.004

Measurements of downwelling and upwelling irradiance, absorption and beam attenuation were made in January 1998 along 6°E between 65° and 49°S. A detailed overview of the cruise together with an in-depth description of the hydrography encountered is given in Turner et al. (2004).

1.1. Background

PAR has been defined to include only radiation between 400 and 700 nm, even though it has been shown that photosynthesis is possible at wavelengths shorter than 400 nm (e.g. Neori et al., 1988). Any portion of ultraviolet radiation (UVR 200–400 nm) or PAR may have either deleterious or beneficial effects on certain organisms, depending upon the dose absorbed by the organism (Holm-Hansen et al., 1993a).

UVR is further subdivided into UVC (200–280 nm), UVB (280–320 nm) and UVA (320–400 nm). Solar UVR, especially over the Antarctic, has been in focus for more than a decade, since the discovery of a thinning of the stratospheric ozone layer, leading to increased ground-level UVBR. UVBR has potentially harmful effects on plankton organisms, e.g. bacteria and phytoplankton (Smith et al., 1992; Weiler and Penhale, 1994). Thus, it is important to establish both UVR levels over the sea surface, as well as the vertical attenuation in the water column of UVBR.

Phytoplankton growth in the Southern Ocean is not in proportion to the high macronutrient availability. Recent studies have shown that adding iron (Fe) to the water increases production (Boyd et al., 1999; Buma et al., 1991; Helbling et al., 1991) but other possible causes of low production are the weak stratification of the Southern Ocean (Mitchell et al., 1991), resulting in light limitation, in combination with the low solar elevation (Campbell and Aarup, 1989). Nelson and Smith (1991) propose that the hydrography together with the penetration of radiation produce a self-controlling system, and so production would not increase even with an increased Fe concentration.

Since the days of Sverdrup, the notion of a critical depth (Sverdrup et al., 1942), below which the low level of light makes photosynthesis impossible, has gone relatively unchanged. Th euphotic depth, Z_e, is defined as the depth at whic the irradiance becomes 1% of its value just unde the surface of the water. Depending on th hydrography, cells can be convected to depth below Z_e, but if they go below the Sverdrup critica depth, Z_c, they become light limited because the spend too much time in darkness.

1.2. Theory

The decay of radiation in the water is describe by an exponential law:

$$E_\lambda(z) = E_\lambda(0_-)\mathrm{e}^{-\int_{z_1}^{z_2} \mathrm{d}z\, K_\lambda(z)}, \quad (1)$$

where E_λ is the downwelling spectral (vector) irradiance, z is depth and K_λ is the spectral diffuse attenuation coefficient. The 0_- denotes a depth just below the surface of the ocean. (We shall in this paper use subscripts that indicate the spectral dependence, i.e. λ indicates a dependence on wavelength, $\Delta\lambda$ indicates a waveband dependence. The waveband can be specified, i.e. it can be PAR, UVA, etc.) From Eq. (1) an expression for the average K_λ is obtained assuming that K_λ is constant at least in the depth interval $[z_1, z_2]$:

$$K_\lambda = -\frac{1}{(z_2 - z_1)} \ln\left[\frac{E_\lambda(z_2)}{E_\lambda(z_1)}\right]. \quad (2)$$

The apparent optical properties, of which K_λ is one, are linked to the inherent optical properties (see e.g. Arst et al., 1997), which are the absorption and scattering coefficients a_λ and the volume scattering function which leads to the scattering coefficient b_λ.

The absorption coefficient of water can be expressed as

$$a = a_\mathrm{w} + C_\mathrm{chl} a^*_\mathrm{chl} + C_\mathrm{ys} a^*_\mathrm{ys} + [C_\mathrm{p} a^*_\mathrm{p}]. \quad (3)$$

Here a_w is the absorption coefficient of water, C_chl is the chlorophyll a concentration, a^*_chl is the chlorophyll specific absorption coefficient (which depends on the chlorophyll concentration), C_ys is the concentration of yellow substance, a^*_ys is the yellow substance specific attenuation coefficient, C_p is the concentration of the inorganic particulate material (which is assumed to be zero for Case 1

waters) and a_p^* is its specific attenuation coefficient. We will from now on use the symbols a_λ, b_λ and c_λ to denote absorption, scattering and attenuation. These will be understood to be particulate values, i.e. values that have had the pure water values subtracted from them.

Scattering in the ocean is due to both inorganic and organic particulates, with the latter including both living cells and detrital material of biological origin. Organic particles are the dominant scatterers in the open ocean. Scattering from particulates depends on (1) the degree of external reflection and diffraction by their geometrical form and (2) on internal refraction and reflection and hence on the index of refraction of the particles. For particles small compared to the wavelength, the scattering efficiency is comparable to λ^{-4}, but for larger particles the scattering is wavelength independent (Apel, 1987). In the light of this theory it would be expected that the b_λ spectra in the visible range would show no wavelength dependence or a slight monotonous decrease with wavelength.

The value of the pigment specific beam attenuation coefficient, c^*, is defined as

$$c^* = \frac{c - c_w}{[\text{Chl}a + \text{phaeo}]}. \quad (4)$$

Here c is the measured attenuation coefficient at 660 nm, c_w is the attenuation coefficient of pure water at 660 nm and the denominator is the concentration of chlorophyll-*a* and phaeopigments which are the pigments residing outside cells or in dead cells. Case 1 water masses have a c^* value below $0.5\,\text{mg}\,\text{m}^{-2}$.

By combining above surface E_λ levels and the K_λ for the water, the light penetration down into the water was calculated. The daily dose at a depth z for a waveband was obtained by bringing the above surface E_λ through the surface and integrating Eq. (1) over a time period Δt:

$$\int_{\Delta t} \mathrm{d}t E_{\Delta\lambda}(z,t) = \int_{\Delta t} \mathrm{d}t[(1-\alpha_{\Delta\lambda})E_{\Delta\lambda}(0_-,t)\mathrm{e}^{-\int_0^z \mathrm{d}z K_{\Delta\lambda}}. \quad (5)$$

Here $\alpha_{\Delta\lambda}$ is the albedo, which is the ratio of the upwelling and downwelling E_λ above the surface of the water. Eq. (5) is valid assuming that the optical properties of the water do not change with time. The depth Z_i at which $E_{\Delta\lambda}$ assumes a value of $E'_{\Delta\lambda}$ can be calculated from Eq. (1) assuming a constant $K_{\Delta\lambda}$ with depth:

$$Z_i = -\frac{\ln\left[E'_{\Delta\lambda}/E_{\Delta\lambda}(0_-)\right]}{K_{\Delta\lambda}}. \quad (6)$$

The Z_e depth can be calculated using this equation by putting $E'_{\Delta\lambda} - 0.01E_{\Delta\lambda}(0_-)$. We have used the definition of Z_c by Nelson and Smith (1991):

$$Z_c = A\frac{\sum I_0}{K_{\text{PAR}}}. \quad (7)$$

Here K_{PAR} is the diffuse attenuation coefficient for PAR irradiance, $\sum I_0$ is the total incident irradiance integrated over 1 day (24 h). This parameter is expressed in $\text{mol}\,\text{m}^{-2}\text{d}^{-1}$. The coefficient A has a value of $0.265\,\text{m}^2\text{d}\,\text{mol}^{-1}$. When this depth is compared to the depth of the mixed layer (ML), Z_m, the light limitation can be studied.

2. Measurements and calculations

Measurements were made in the eastern part of the Atlantic sector of the Southern Ocean, at 6°E, between 60°S and 49°S. The transect was divided into three main regions: the Spring Ice Edge (SIE, at 65°S), the Antarctic Polar Front (APF, at 51°S), and the region between them, the Winter Ice Edge (WIE). See Turner et al. (2004) for a detailed description of the measurement areas and sampling strategy.

Downwelling E_λ was measured using two different radiometers: a LiCOR LI1800UW spectroradiometer, which measured between 300 and 850 nm with a 6 nm resolution, and a Biospherical Instruments PUV-500 underwater radiometer, which measured radiation at four discrete wavelength bands. These were three 10 nm wide bands centred at 305, 320, 340 and 380 nm, and PAR. The LI1800UW was also used to measure E_λ and upwelling irradiance, $E_{\lambda u}$, above the surface of the water for albedo measurements between 300 and 850 nm $E_{\lambda u}$ was also measured at different depths in the water for irradiance reflectance measurements. Irradiance reflectance, R_λ, is the ratio of

$E_{\lambda u}/E_{\lambda}$. We shall imply irradiance reflectance when we use the term reflectance.

Both radiometers were deployed from the aft end of the ship. The LI1800UW was set to measure at discrete depths (the depths to which the instrument was lowered depended on the conditions) and the PUV500 measured continuously to a maximum depth of 80 m. The radiation measurements were preferentially made around noon (± 2 h). The LI1800UW, ready for deployment into the water, is shown in Fig. 1.

The LI1800UW has a rotating filter wheel and a rotating diffraction grating, giving it a long integration time making it susceptible to changes in the ambient light field. Measurements were normalised to surface total irradiance values measured with a LiCOR LI200SA pyranometer. K_{λ} values were then calculated from the E_{λ} spectra, using Eq. (2) for all of the depths an then for the whole water mass between 1 and 15 m

The values of $E_{\lambda u}$ and E_{λ} were then integrate over PAR and added together to obtain a value fo the total PAR E_{TOT}. The diffuse attenuation fo E_{TOT} was obtained using Eq. (2), and the euphoti depth for E_{TOT}, Z_{TOT}, was obtained using Eq. (6) For phytoplankton cells, the direction of inciden photons is irrelevant. They can utilise photon coming from all directions. It must be noted tha this is an addition of two vector irradiances whic are defined as the flux through a surface area.

The PUV500 uses band pass filters for the UV wavelengths with a bandwidth of around 10 nm with peak transmission at the nominal wave length $\pm$ 1–2 nm. The PAR sensor on the PUV500 has a near ideal ($\pm 10\%$) quantum response from 400 to 700 nm, with a sharply attenuated response

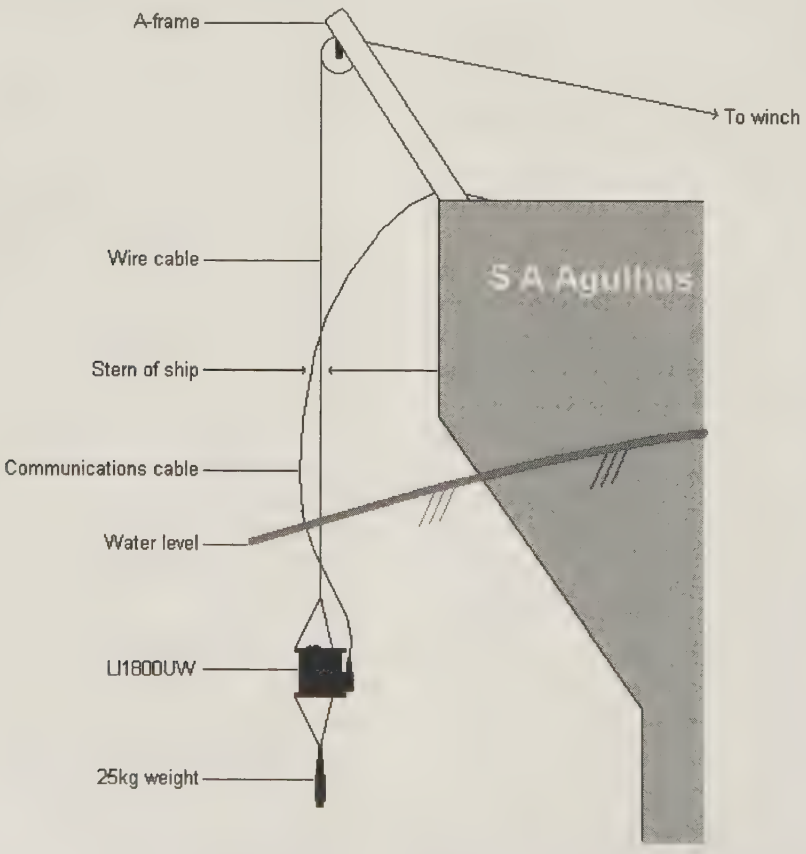

Fig. 1. The LI1800UW spectroradiometer ready for deployment.

below 400 nm and above 700 nm. The instrument measured continuously as it was lowered, but the data was packed into 1 m averages, which were used for calculations of vertical $K_{\Delta\lambda}$ values. This was done by fitting the $E_{\Delta\lambda}$ values for each 10 m interval (10 data points) to the exponential curve defined by Eq. (1). The data was, however, not normalised to surface light, as recommended by Biospherical Instruments.

Absorption and attenuation of light was measured directly at nine 10 nm wide wavelength bands centred at 412, 440, 488, 510, 532, 555, 650, 676 and 715 nm, using a WetLABS ac-9 absorption and attenuation meter. The values of a_λ and c_λ were used to calculate b_λ which is simply $c_\lambda - a_\lambda$.

The ac-9 was deployed from the starboard side of the ship to a maximum depth of 20 m. The values were then averaged for the whole surface layer. The absorption data were corrected for the infra-red absorption by water and a scattering correction was made (Pegau and Zaneveld, 1994; Zaneveld et al., 1994). The values for seawater absorption and scattering have been subtracted from the data using values obtained by Smith and Baker (1981). The prevailing conditions had no effect on the ac-9 because it operates on an internal light source.

Above surface E_λ was measured with an Optronics OL754 spectroradiometer (Optronics) between 280 and 800 nm. It was placed in a container on the uppermost deck of the ship and was connected to a cosine-collector, placed on the roof, with a fibre-optic cable (see Chen et al., 2004, for details of the set-up).

Two types of calculations were made for four wavelength bands (305, 320, 340 nm and PAR) at four locations. These were divided so that two were in the SIE region (6 and 8 January), one at the WIE (13 January) and one at the APF (27 January). Firstly the calculated daily radiation dose for a particular waveband at different depths was calculated using Eq. (5). The calculations were made only for those times when the sun angle was over 23°. The average of three α_λ measurements made around midday between 54°S and 60°S was used for the albedo calculations. Secondly, the depth at which the calculated radiation level decreased below specified levels was calculated using Eq. (6). The chosen levels were $1\,\mu W\,m^{-2}\,nm^{-1}$ for 305 nm, $1\,mW\,m^{-2}\,nm^{-1}$ for 320 nm, $10\,mW\,m^{-2}\,nm^{-1}$ for 340 nm, and $10\,\mu mol\,m^{-2}\,s^{-1}$, which is $\sim 3.8\,W\,m^{-2}$, for PAR. (Here we have used the method by Reinart et al. (1998) for changing the quantum irradiance units to energy units.) The levels for 305, 320 and 340 nm were arbitrarily chosen while for PAR it was chosen to approximately correspond with the Z_e depth.

A total of 10 spectral profiles of E_λ were measured using the LI1800UW. Of these, six were measured in the SIE zone, two in the WIE zone and two in the APF. Fifteen PUV500 profiles were obtained (nine in SIE, four in WIE and two in APF water). A total of 34 ac-9 measurements were made, which were fairly evenly distributed between the different areas. The temperature and salinity were measured using a Seabird CTD.

3. Results

Examples of an E_λ and an $E_{\lambda u}$ vertical profile measured with the LI1800UW are shown in Fig. 2. Regions with a large chlorophyll-*a* concentration showed a large attenuation at short wavelengths and at long wavelengths, compared to regions with a lowered concentration of chlorophyll-*a*. A shift can be seen in the wavelength of maximum irradiance with increasing depth. The wavelength shifts from ~450 nm at 3 m to ~490 nm at 20 m, which means that the water becomes greener.

Radiation above 700 nm is very efficiently attenuated in the first few metres of the water as can be seen from the upper figure in Fig. 2. The values of K_λ calculated from the E_λ profiles are $4\,m^{-1}$ at 800 nm in the 1–3 m layer and drop to $1\,m^{-1}$ for the deeper layers. The K_λ for the whole 1–15 m layer for all of the stations are shown for four stations in Fig. 3. They were all very similar in spectral shape. However, a station in the SIE (at 60°S) and a station in the APF (at 46°S) show almost four times stronger attenuation across the whole of the spectrum.

At 60°S this increased attenuation can be attributed to an ice edge phytoplankton bloom

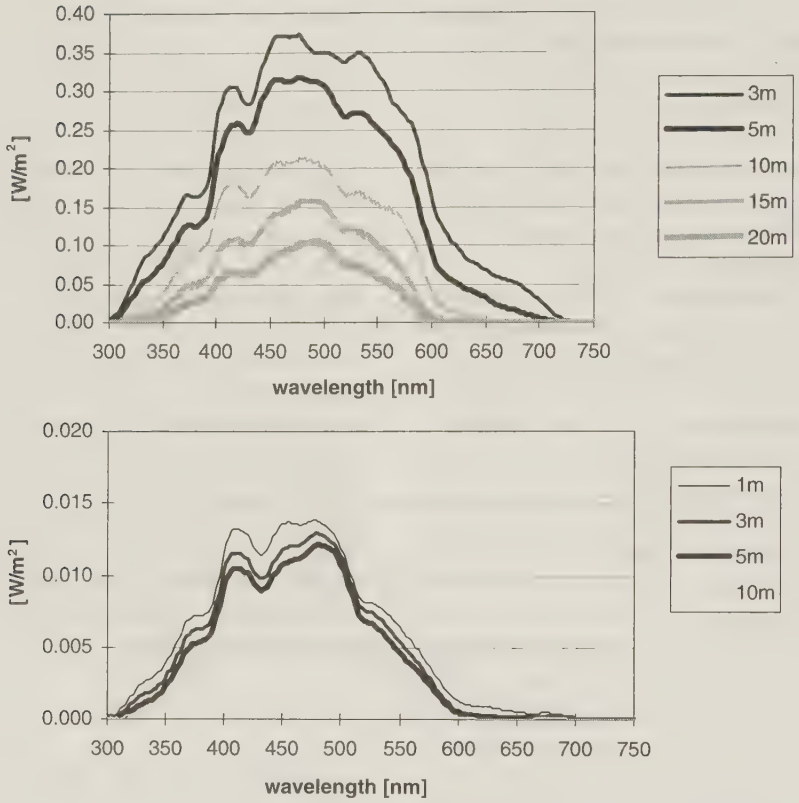

Fig. 2. A vertical profile of (A) downwelling and (B) upwelling spectral irradiance.

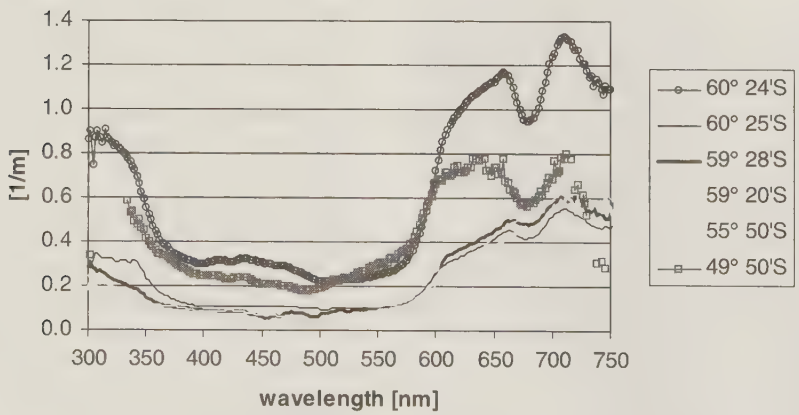

Fig. 3. Spectral diffuse attenuation coefficient for four stations.

(Wulff and Wängberg, 2004). Even though the ice edge had disappeared the surface consisted of water with a lowered salinity due to ice-melt (for the salinity field). In the APF, the presence of a convergence increases the concentrations of phytoplankton and nutrients.

The average values of the $K_{\Delta\lambda}$ for the 305, 320, 340 and 380 nm bands, as measured by the

PUV500, are shown in Fig. 4. The K_{PAR} values are shown in Fig. 5 for the different layers. The strongest attenuation was found at 305 nm, in the UVB region, and the lowest at 380 nm (Fig. 4). In general the values of $K_{\Delta\lambda}$ were lowest at the WIE, only slightly higher at the APF and highest at the SIE. There is a spike at 60°S which is visible in the 305 nm band ($0.80\,m^{-1}$) and also in the 30–40 m layer for K_{PAR} ($0.30\,m^{-1}$). At 56°S there is a steep drop in K_{PAR} of $\sim 0.05\,m^{-1}$ at all levels.

Values obtained for a_λ along the transect are shown in Fig. 6 and for b_λ in Fig. 7. The a_λ and b_λ spectra for four stations are shown in Figs. 8 and 9. The b_λ values are almost totally wavelength independent, being only slightly higher in the shorter than in the longer wavelengths. However, at two locations (56°S and 60°S) there were strong anomalies in spectral behaviour. These scattering anomalies were a residue of the way in which scattering is calculated as attenuation minus absorption. In areas of very strong absorption, the scattering values may become inaccurate.

The surface $E_{\Delta\lambda}$ values and the penetration depths Z_i are shown in Fig. 10 for four dates. The daily dose for 320 nm is shown in Fig. 11. Surface irradiance was higher on 8 January (at 60°S) than on 6 January (at 59°S), 13 January (at 56°S) or 27 January (at 51°S). The low attenuation coefficients in the WIE on 13 January caused the calculated levels of light for PAR and for the band at 340 nm to be the highest on this date for depths below 17

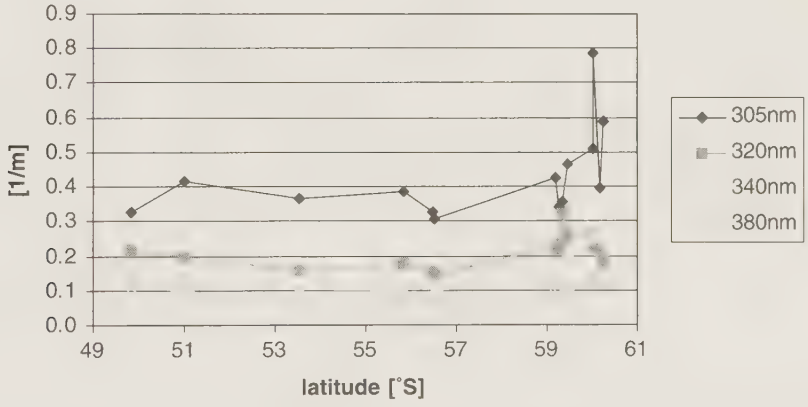

Fig. 4. The diffuse attenuation coefficient for different wavelength bands along the transect.

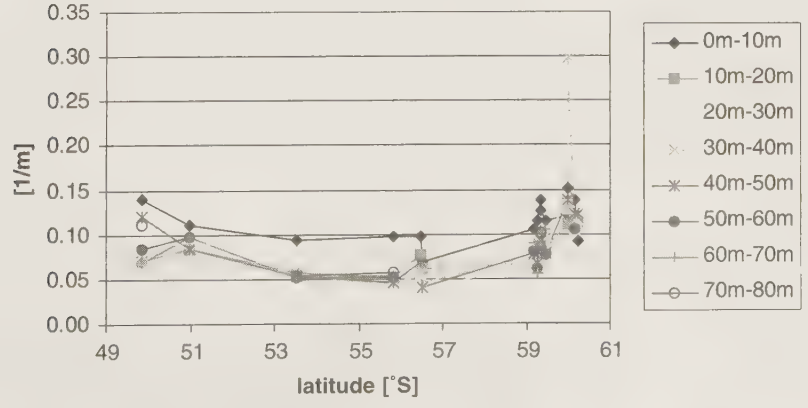

Fig. 5. The diffuse attenuation coefficient for photosynthetically active radiation along the transect in different layers.

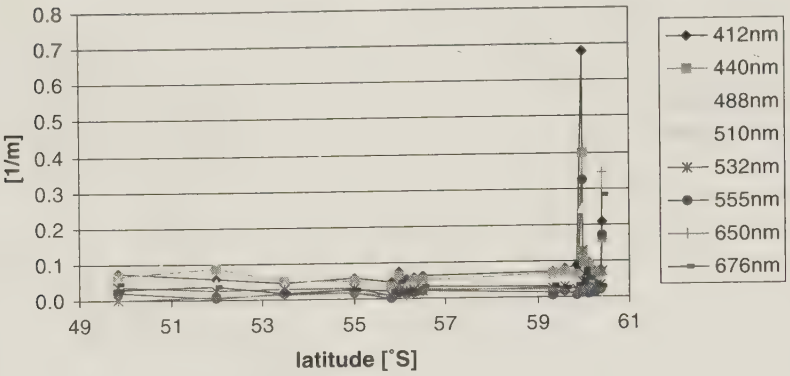

Fig. 6. Particulate absorption along the transect for different wavelengths.

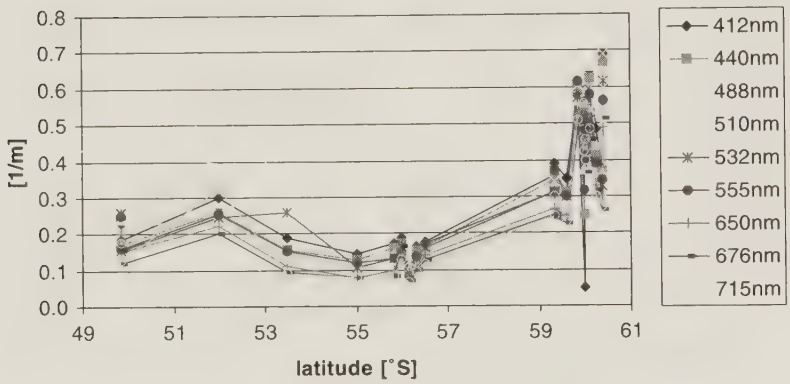

Fig. 7. Particle scattering along the transect.

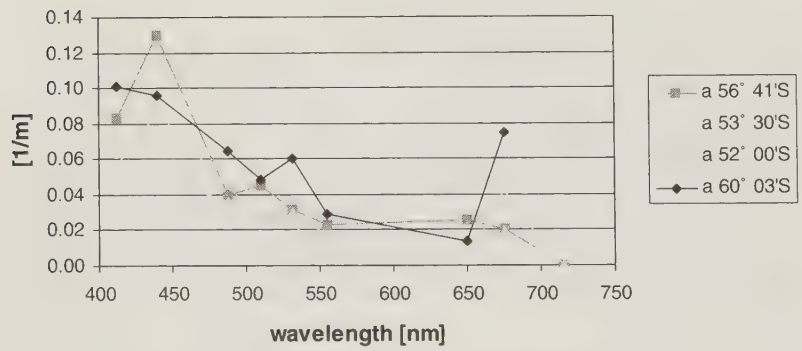

Fig. 8. Spectra of particulate absorption for five stations.

and 8 m, respectively, for the same bands. The $10\,\mu mol\,m^{-2}\,s^{-1}$ depth for PAR was also considerably higher on 13 January compared with the other dates. The calculated depths for the wavebands at 340, 320 and 305 nm (10 and 1 $mW\,m^{-2}$ showed smaller variations. The higher attenuation coefficients on 6 January resulted in considerably lower depths for both wavelengths, despite smal

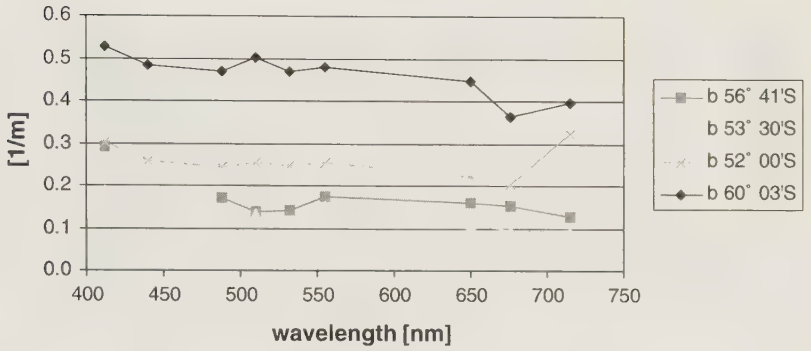

Fig. 9. Spectra of particulate scattering for 4 stations.

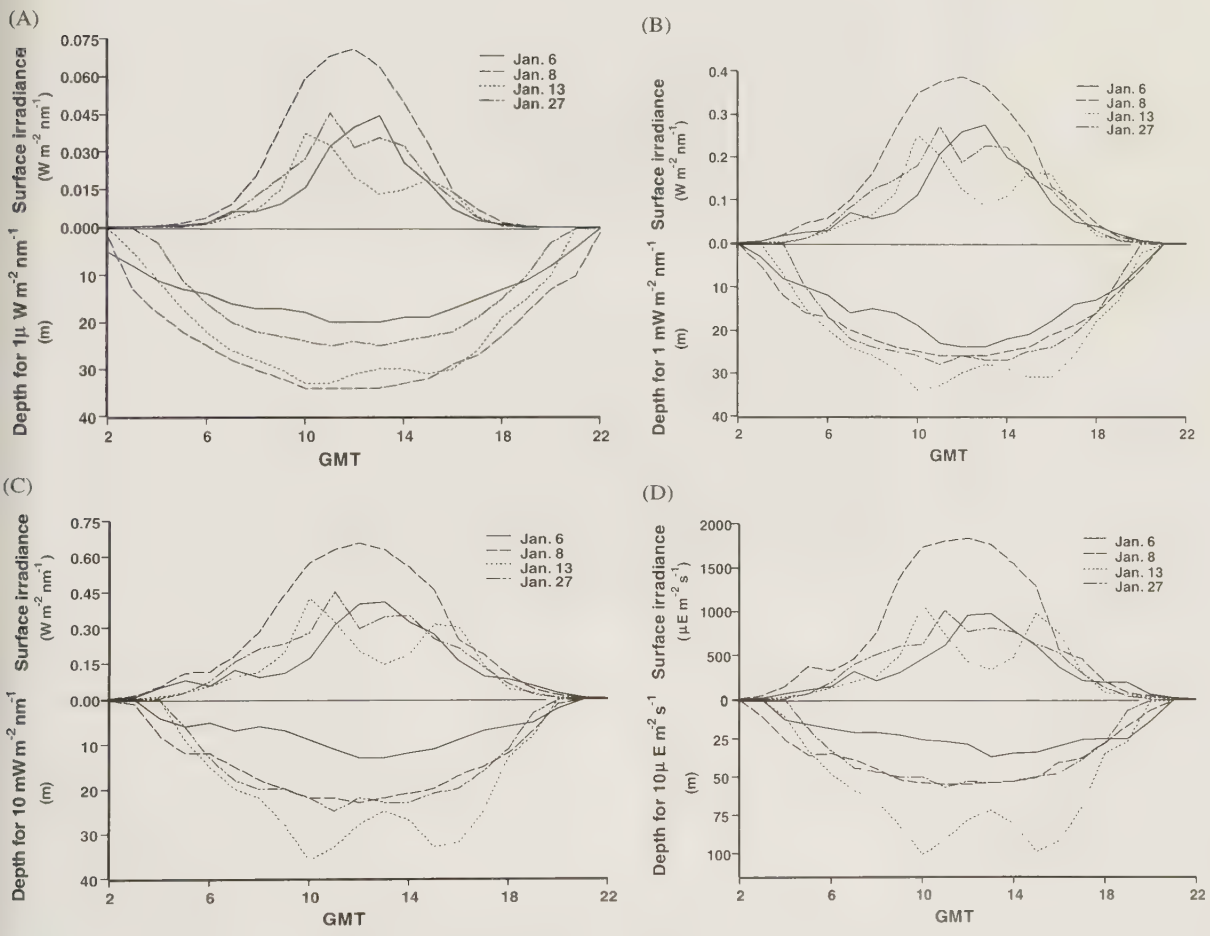

Fig. 10. Surface irradiance and calculated penetration depths for (A) 305 nm, (B) 320 nm, (C) 340 nm and (D) PAR for four dates.

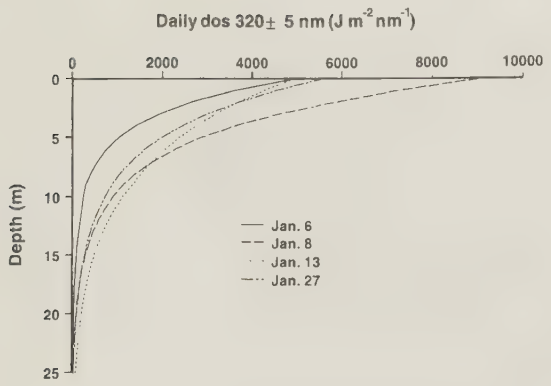

Fig. 11. Daily dose for 320 nm.

differences in surface irradiance when compared to 13 and 27 January.

The values for E_{PAR}, E_{UPAR}, E_{TOT}, Z_{TOT}, K_{TOT} and R are shown in Table 1. The mean value for R is ~3%, varying between 1% and 7%, meaning that E_{UPAR} is only 3% of E_{PAR}. This explains why the values for E_{TOT} at 10 m, Z_{TOT} and K_{TOT} do not differ remarkably from the values of E_{PAR}, Z_e and K_{PAR}.

4. Discussion

The temperature, salinity and density (σ_t) are shown in Fig. 12. It can be seen from this figure that the temperature varied from almost −2 °C at 61°S to +4 °C at 48°S, with a +3 °C increase in temperature between 53°S and 52°S indicating the position of the APF. The tongue of cold Antarctic Surface Water is visible as it dives under the Atlantic Surface Water at 54°S. At 60°S there is an eddy phenomenon and an upwelling of warmer water. The study area is at the eastern end of the Weddell Sea gyre and in the region affected by the currents of the AD system. The surface salinity varies between 33.8 and 34.6 with a maximum between 56°S and 58°S. South of 60°S the surface layer shows a very low salinity, again indicating a region of ice melt. Fig. 12 shows that salinity is the main driving force for the density. It can be seen that the σ_t field follows the salinity rather than the temperature field.

The vertical derivative in density ($\partial\sigma_t/\partial z$) shown in Fig. 13 together with Z_c. It can be see from this figure that the region of well-mixe homogeneous water, the upper mixed laye (UML) is between 75 and 100 m deep from 50° to 55°S, 50 m at 56°S dropping to 100 m at 59°S after which it decreases to 30 m around 60°S The depth of the mixed layer (ML, the dept at which the density difference becomes zer again) is between 75 and 150 m. The Z_c depth i between the UML and the ML depth. Thi means that depending on the construction of th phytoplankton cell and its buoyancy properties, i can be convected into the region between th UML and ML. But if the cells are unable t penetrate the UML, they are always above Z_c an therefore not light limited. There is a lens of low salinity water at 60°S which has originated from ice melt. This is the cause of increased stability (high values of $\partial\sigma_t/\partial z$) and a low ML depth. This area also has the remnants of an ice edge bloom which is evident in elevated a_λ, b_λ, and K_λ values A low Z_c value is the cause of these optica properties.

At the time of the cruise (January 1998) the UVBR levels were not affected by any ozone hole as the thickness of the stratospheric ozone layer was almost normal (Chen et al., 2004). The calculated UVBR levels could be compared with levels shown to reduce carbon dioxide fixation in phytoplankton. Smith et al. (1992) show that during the ICECOLOR expedition in the Belling-shausen Sea during the austral spring of 1990, reduction in the carbon dioxide fixation due to UVBR was significant at UVBR doses higher than 0.01 mol m^{-2}. We do not have the doses for the whole UVB spectrum, but assuming an even attenuation within UVBR and a constant ratio between radiation at 305 nm and the whole of UVB we can estimate the equivalent dose at 305 nm to be 52 J m^{-2}. Thus the corresponding depths of UVB doses higher than 0.01 mol m^{-2} from our calculations are 4.0 m at 60°S, 9.5 m at 59°S, 8.0 m at 56°S and 6.5 m at 51°S, for 6, 8, 13 and 27 January, respectively. When doing the same calculation for 320 nm it gives a dose of 500 J m^{-2} and corresponding depths of 7.5, 13.0, 15.0 and 12.0 m. These calculations are in accord

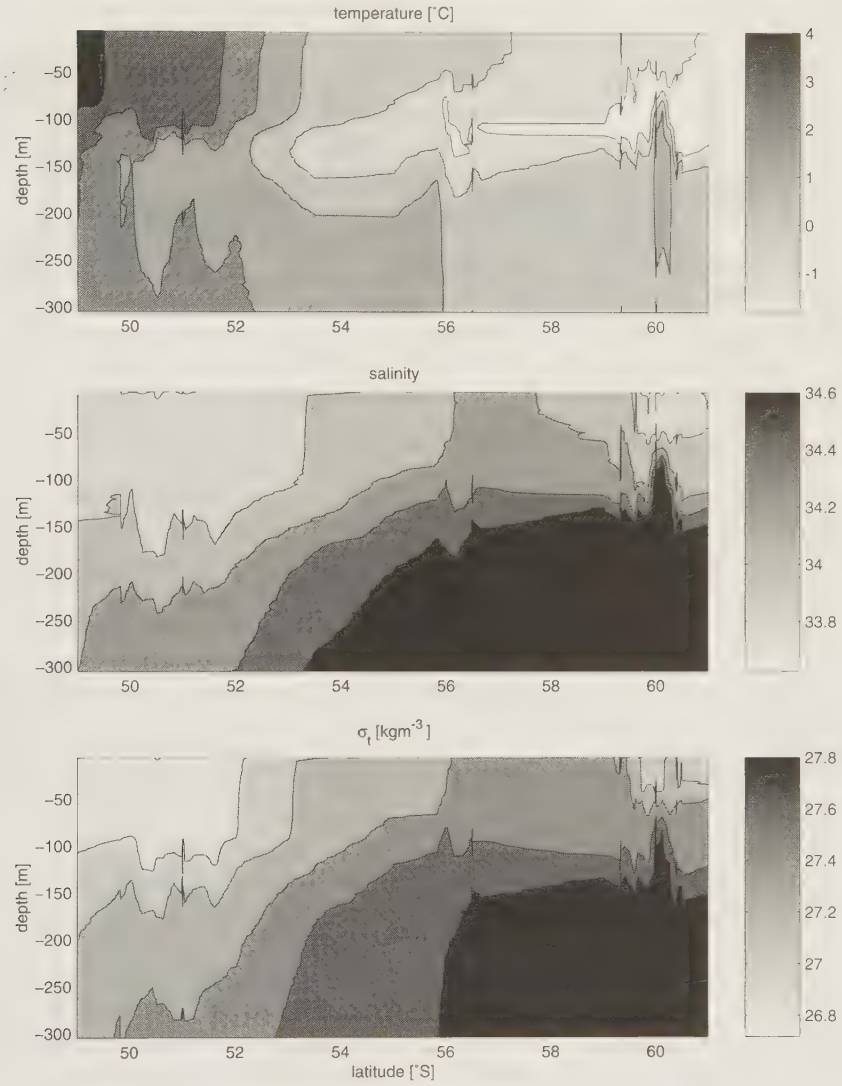

Fig. 12. Temperature, salinity and density (σ_t) for the transect.

with in situ measurements (Smith et al., 1992; Holm-Hansen et al., 1993b).

The mean thickness of the UML was 20 m in the SIE, between 30 and 75 m in WIE and 75 m at the APF. Our calculations thus show that under normal ozone levels the UVB radiation is affecting substantial parts of the UML, especially in the WIE area. They also emphasise the large influence the optics of the water have for how far the harmful radiation reaches. Despite the fact that the incident radiation was lowest on13 January the influenced depth was clearly much larger than on 6 and 27 January and almost as large as on 8 January when the incident radiation was more than two times higher. But the low stability of the water and the depth of the mixed layer are a blessing for the phytoplankton as well as a hindrance. It is possible for the cells to reside happily below the zone affected by UVR and still have enough light for photosynthesis.

The differences in K_{PAR} between regions correlates with the chlorophyll *a* concentration of the

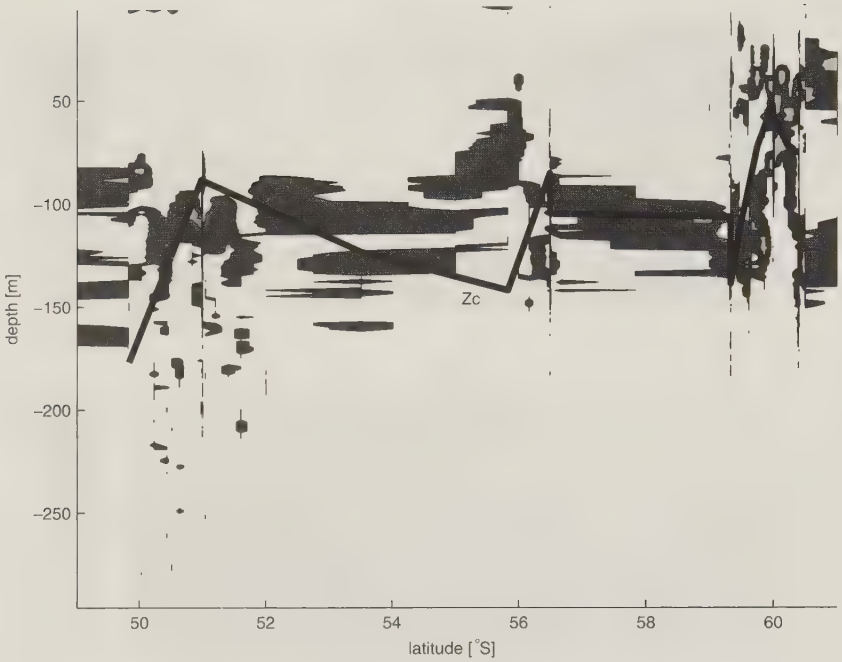

Fig. 13. Vertical density derivative and the Sverdrup critical depth. This figure shows the relationship between the upper mixed layer depth, the mixed layer depth and the Sverdrup critical depth. The different grey and black fields are fields in which the value of the derivative is nonzero, i.e. there is a difference in the density. The upper mixed layer is the layer just under the surface before the density starts to change. The mixed layer depth goes to the bottom surface of the region of change in density, i.e. where the density derivative becomes zero again.

surface water presented in detail by Wulff and Wängberg (2004). The lowest values were in the WIE region with an average of $0.20\,\mu g\,l^{-1}$ (between 0.18 and $0.23\,\mu g\,l^{-1}$) and higher values in the APF, $0.82\,\mu g\,l^{-1}$ on average (between 0.78 and $0.84\,\mu g\,l^{-1}$). The highest but also most variable values were found in the SIE, average $1.38\,\mu g\,l^{-1}$ (between 0.63 and $2.17\,\mu g\,l^{-1}$).

The K_{PAR} values were often higher for the 0–10 m layer than for deeper layers (Fig. 5). The decreases in attenuation coefficients that occur with depth may be real, but they may also be caused by selective attenuation. Wavelengths with the highest attenuation disappear first, leaving wavelengths with lower attenuation coefficients. This should especially be the case for the wide-band PAR sensor.

At 60°S (in the SIE region) there is a chlorophyll maximum that is seen in the results of all the instruments (Figs. 3, 6 and 7). The value for K_{PAR} increases dramatically at only the 30–40 m layer. This is an indication of a subsurface chlorophyll maximum, with the phytoplankton cells residing on the pycnocline.

The K_λ values generally coincide with those measured by Boucher and Prezelin (1996) in the marginal ice zone west of the Antarctic Peninsula. The two most northerly stations in Fig. 3 show K_λ values similar to those measured in the Ross Sea by Arrigo et al. (1998). They measured high values of absorption (with the effect of detritus removed) at 555 nm in waters dominated by cryptophyte species of phytoplankton. This was due to the presence of the biliprotein phycoerythrin. At some stations in the SIE region and also in the WIE, we measured a_λ spectra with maxima at 555 nm but it did not correlate with high concentrations of any phytoplankton containing phycoerytrin (Wulff and Wängberg, 2004).

The average K_λ (without the two stations showing very high attenuation) for the Southern Ocean is shown in Fig. 14 together with the pure

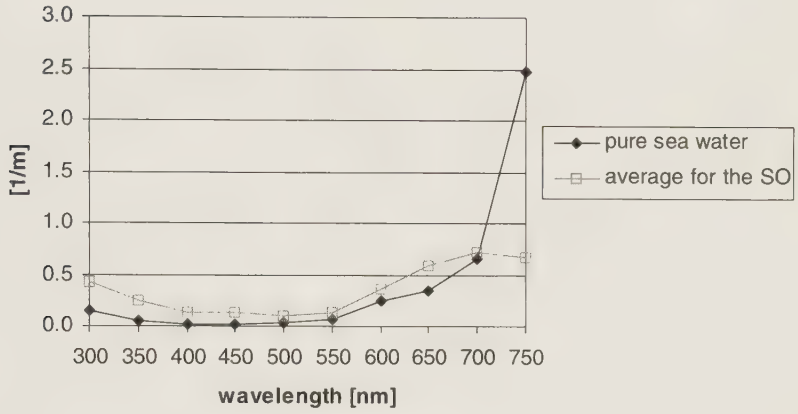

Fig. 14. Average spectral diffuse attenuation coefficient for the Southern Ocean along with values for pure water.

ocean water value for K_λ from Smith and Baker (1981). The effects of chlorophyll and yellow substance are seen in the shorter wavelengths. The strong absorption in the near infrared has deleted the radiation so the low attenuation values are not real after 700 nm.

Some optical and physical properties of the surface water masses are shown in Table 2. All of the waters studied showed a c^* value below $0.5\,\mathrm{mg\,m^{-2}}$ which indicates that all the waters were Case 1. Jerlov (1978) has classified water types according to their optical properties. The waters of the Southern Ocean could be classified as being Jerlov type III in the SIE region, and type II elsewhere. The classification was made using Austin and Petzold (1986). Classification into Jerlov types may be an old fashioned way of studying the optical properties of water but they give a simple way of making comparisons between waters from different regions. Using these classifications, the waters along 6°E are optically similar to the waters between New Zealand and Antarctica, which are influenced by the Ross Sea. Similar Jerlov water types are found in the large upwelling regions on the coast of south and North America and West Africa.

Some stations with very strong attenuation of light in the SIE and APF regions can be compared to some northern European lakes. Reinart and Herlevi (1999) have made optical studies in Finnish and Estonian lakes. Even though the attenuation is strong, the water is still Case 1 (using Eq. (4) as a guideline) because the main optically active substances are still only chlorophyll and its derivatives, mainly yellow substance. We were not able to find the Case 2 behaviour reported by Sagan et al. (1995) from the Bellingshausen Sea.

The values for the ratio a_{412}/b_{412} and the single scattering albedo at 555 nm ($\omega_0 = b_\lambda/c_\lambda$) are shown in Fig. 15. This figure shows that the transect can be divided into three sections that follow the SIE, WIE and APF regions. In the APF the scattering dominates being 5 times higher than the absorption. Yellow substance absorption is low. This would be expected of a young ice edge bloom. In the WIE region the scattering is only 2 times as large at 412 nm and only half of the total attenuation at 555 nm. In the APF region the situation is again similar to the SIE. At high a_λ/b_λ the scattering may not be correct due to the way in which it is calculated.

All of the measurement results show a large variability, especially in the SIE region. This is to be expected because of the complex dynamic structure of the region at the eastern end of the Weddell gyre.

5. Conclusions

The UVR penetration depths and daily doses were obtained for the Southern Ocean at 6°E. The depths for 320 nm doses higher than $500\,\mathrm{J\,m^{-2}\,d^{-1}}$

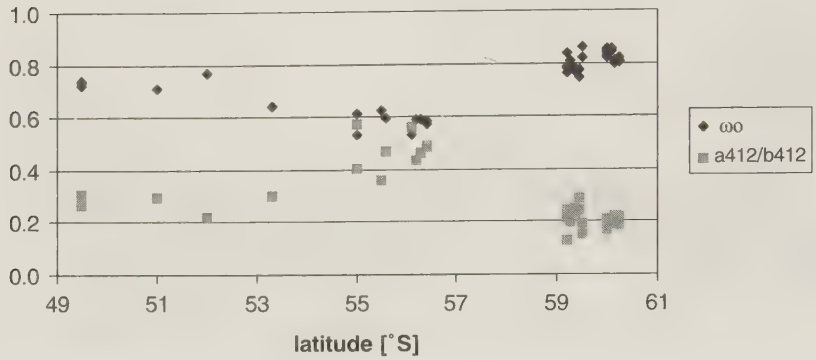

Fig. 15. Values for the ratio a_{412}/b_{412} and the single scattering albedo at 555 nm along the transect. These values include pure wate values.

were between 7.5 and 15.0 m, thus the UVR affects a large proportion of the UML. Our results concerning the critical depths (Z_e and Z_c) and Z_m show that phytoplankton in the investigated areas of the Southern Ocean were not light limited at the time of these measurements. All of the waters were classifiable as Case 1 type waters and Jerlov types II and III. The K_{PAR} values were found to vary between 0.03 and 0.09 m^{-1}. These values correlate with the concentration of chlorophyll *a*. The measured spectrum for K_λ is close to the spectrum of K_λ for pure ocean water with the absorption by chlorophyll in the wavelengths between 600 and 700 nm, and the absorption by yellow substance below 500 nm, clearly visible. The measurements were made over a period of 1 month which means that they are not entirely synoptic. The measurements are generally in accord with previous observations.

Acknowledgements

We are grateful to FINNARP and SWEDARP for providing logistic resources for our research. We would like to thank the many scientists and crew members on board the S.A. *Agulhas* who helped with the actual measurements. A special thanks to the expedition leader David Turner for never ending patience and energy, and excellent organization of sampling on board *Agulhas*. Grants from the Finnish Institute for Marine Research to Kai Rasmus, from the Swedish Council for Planning and Coordination of Research (Forskningsrådsnämnden) to Sten-Åke Wängberg, and from NFR (the Swedish Natural Science Research Council) to Wilhelm Granéli (Grant No. B-AA/BU 04969-321) made participation in the expedition possible. Kai Rasmus would also like to thank Hanna Villa for helping with the figures.

References

Apel, J.R., 1987. Introduction to Physical Oceanography. Academic Press, London.

Arrigo, K.R., Robinson, D.H., Worthen, D.L., Schieber, B., Lizotte, M.P., 1998. Bio-optical properties of the southwestern Ross Sea. Journal of Geophysical Research 103, 21683–21695.

Arst, H., Mäekivi, S., Lukk, T., Herlevi, A., 1997. Calculating irradiance penetration into water bodies from the measured beam attenuation coefficient. Limnology and Oceanography 42, 379–385.

Austin, R.W., Petzold, T.J., 1986. Spectral dependence of the diffuse attenuation coefficient of light in ocean waters. Optical Engineering 25, 471–479.

Boucher, N.P., Prezelin, B.B., 1996. Spectral modeling of UV inhibition of in situ Antarctic primary production using a field derived biological weighting function. Photochemistry and Photobiology 64, 407–418.

Boyd, P., La Roche, J., Gall, M., Frew, R., McKay, R.M.L., 1999. Role of iron, light, and silicate in controlling algal biomass in subantarctic waters SE of New Zealand. Journal of Geophysical Research 104, 13395–13408.

Buma, A.G.J., de Baar, H.J.W., Nolting, R.F., van Bennekom, A.J., 1991. Metal enrichment experiments in the Weddell–

Scotia Seas: effects of iron and manganese on various plankton communities. Limnology and Oceanography 36, 1865–1878.

Campbell, J.W., Aarup, T., 1989. Photosynthetically available radiation at high latitudes. Limnology and Oceanography 34, 1490–1499.

Chen, D., Wängberg, S.-Å., Wulff, A. and Borne, K., 2004. Attenuation of biologically effective UV doses under overcast skies: a case study from the eastern Atlantic sector of the Southern Ocean. Deep-Sea Research II, this issue [doi:10.1016/j.dsr2.2001.02.002].

Helbling, E.W., Villafañe, V., Holm-Hansen, O., 1991. Effect of iron on productivity and size distribution of Antarctic phytoplankton. Limnology and Oceanography 36, 1879–1885.

Holm-Hansen, O., Lubin, D., Helbling, E.W., 1993a. Ultraviolet radiation and its effects on organisms in aquatic environments. In: Young, A.R., et al. (Eds.), Environmental UV Photobiology. Plenum Press, New York.

Holm-Hansen, O., Helbling, E.W., Lubin, D., 1993b. Ultraviolet radiation in Antarctica: inhibition of primary production. Photochemistry and Photobiology 58, 567–570.

Jerlov, N. G., 1978. The optical classification of sea water in the Euphotic Zone. Copenhagen University, Institute of Physical Oceanography, Report No. 1, p. 10.

Mitchell, B.G., Brody, E.A., Holm-Hansen, O., McClain, C., Bishop, J., 1991. Light limitation of phytoplankton biomass and macronutrient utilization in the Southern Ocean. Limnology and Oceanography 36, 1662–1677.

Morel, A., 1994. Optics from the single cell to the mesoscale. In: Spinrad, R.W., Carder, K.L., Perry, M.J. (Eds.), Ocean Optics. Oxford University Press, Oxford.

Nelson, D.M., Smith, W.O., 1991. Sverdrup revisited: critical depths, maximum chlorophyll levels, and the control of southern ocean productivity by the irradiance-mixing regime. Limnology and Oceanography 36, 1650–1661.

Neori, A., Vernet, M., Holm-Hansen, O., Haxo, F.T., 1988. Comparison of chlorophyll far-red and red fluorescence excitation spectra with photosynthetic oxygen action spectra for photosystem II in algae. Marine Ecology Progress Series 44, 297–302.

Pegau, W. S., Zaneveld, J. R. V., 1994. Temperature dependence of the absorption coefficient of pure water in the visible portion of the spectrum. In: Ocean Optics XII, Proceedings of the Society for Photo-Optical Instrumentation in England (SPIE), 2258, pp. 44–55.

Reinart, A., Herlevi, A., 1999. Diffuse attenuation coefficient in some Estonian and Finnish lakes. Proceedings of the Estonian Academy of Sciences Biological Ecology 4, 267–283.

Reinart, A., Arst, H., Blanco-Sequeiros, A., Herlevi, A., 1998. Relation between underwater irradiance and quantum irradiance in dependence on water transparency at different depths in the water bodies. Journal of Geophysical Research 103, 7749–7752.

Sagan, S., Weeks, A.R., Robinson, I.S., Moore, G.F., Aiken, J., 1995. The relationship between beam attenuation and chlorophyll concentration and reflectance in Antarctic waters. Deep-Sea Research II 42, 983–996.

Smith, R.C., Baker, K.S., 1981. Optical properties of the clearest natural waters (200–800 nm). Applied Optics 20, 177–184.

Smith, R.C., Prezelin, B.B., Baker, K.S., Bidigare, R.R., Boucher, N.P., Coley, T., Karentz, D., MacIntyre, S., Matlick, H.A., Menzies, D., Ondrusek, M., Wan, Z., Waters, K.J., 1992. Ozone depletion: ultraviolet radiation and phytoplankton biology in Antarctic waters. Science 255, 952–959.

Sverdrup, H.U., Johnson, M.W., Fleming, R.H., 1942. The Oceans. Prentice-Hall, Englewood Cliffs, NJ.

Turner, D.R., Bertilsson, S., Fransson, A., Pakhomov, E., 2004. The SWEDARP 97/98 marine expedition: overview. Deep-Sea Research II, this issue [doi:10.1016/j.dsr2.2003.08.006].

Weiler, C.S., Penhale, P.A. (Eds.), 1994. Ultraviolet Radiation in Antarctica: Measurements and Biological Effects. Antarctic Research Series 62.

Wulff, A. and Wängberg, S.-Å., 2004. Spatial and vertical distribution of phytoplankton pigments in the eastern Atlantic sector of the Southern Ocean. Deep-Sea Research II, this issue [doi:10.1016/j.dsr2.2001.01.002].

Zaneveld, J. R. V., Kitchen, L. C., Moore, C. C., 1994. Scattering error correction of reflecting tube absorption meter. In: Ocean Optics XII, Proceedings of the Society for Photo-Optical Instrumentation in England (SPIE), 2258, pp. 44–55.

ELSEVIER

Deep-Sea Research II 51 (2004) 2599–2616

DEEP-SEA RESEARCH
PART II

www.elsevier.com/locate/dsr2

Zooplankton dynamics in the eastern Atlantic sector of the Southern Ocean during the austral summer 1997/1998—Part 1: Community structure

E.A. Pakhomov*,[1], P.W. Froneman

Southern Ocean Group, Department of Zoology and Entomology, Rhodes University, P.O. Box 94, Grahamstown 6140, South Africa

Abstract

Zooplankton abundance, biomass and community structure in the top 300 m layer were studied along the 6°E meridian between 49 and 65°S during a Scandinavian/South African Joint Global Ocean Flux Study (December 1997 January 1998) onboard the S.A. *Agulhas*. Along the transect, total abundance and biomass of zooplankton ranged from 8 to 384 ind m^{-3} and 1.4 to 64.1 mg DW m^{-3}, respectively. The general pattern in zooplankton distribution observed was an increase in density between Spring Ice Edge and the Antarctic Polar Front (APF) regions. Copepods numerically dominated zooplankton along the entire transect accounting for 68–97% of the total abundance and 24–90% of the total zooplankton standing stock. Other important contributors to total biomass, particularly within the Winter Ice Edge (WIE) and APF regions, were cnidarians and ctenophores (up to 50%), pteropods (up to 35%), tunicates (up to 30%), chaetognaths (up to 25%) and euphausiids (up to 23%). Numerical analyses identified three major zooplankton groupings, coinciding with the three regions of investigation. A dramatic change in the zooplankton composition occurred at the APF region as several copepod and euphausiid species were found on either side of the front only. A second change in the species composition was observed at the WIE, emphasizing the ecological importance of the frontal zone associated with the winter ice edge.
© 2004 Elsevier Ltd. All rights reserved.

1. Introduction

The past decade has been characterized by an increasing number of studies on the zooplankton composition and distribution in the Southern Ocean (e.g. Siegel et al., 1992; Pakhomov and McQuaid, 1996; Dubischar and Bathmann, 1997; Fransz and Gonzalez, 1997). Indeed, the south Atlantic sector, particularly in the proximity of the

*Corresponding author. Present address: Department of Earth and Ocean sciences, University of British Columbia, 6339 Stores Road, Vancouver, BC, Canada V6T 1Z4. Tel.: +1 604 827 5564; fax: +1 604 822 6088.

E-mail address: epakhomov@eos.ubc.ca (E.A. Pakhomov).

[1]Present address: Zoology Department, Faculty of Science and Technology, University of Fort Hare, Private Bag X1314, Alice 5700, South Africa.

0967-0645/$ - see front matter © 2004 Elsevier Ltd. All rights reserved.
doi:10.1016/j.dsr2.2000.11.001

Greenwich Meridian, has even received some seasonal coverage (Froneman et al., 1997; Perissinotto et al., 1997; Bathmann, 1998). Besides their relevance in understanding of the Antarctic community structure, these studies were generally conducted underlying grazing measurements of zooplankton (Dubischar and Bathmann, 1997; Froneman et al., 1997).

Extreme variability in the physico-chemical and biological processes in the different sectors of the Southern Ocean is well documented (Smetacek, 1998). To increase our understanding of the biochemical cycles of the high Antarctic, it is necessary that similarly designed mesoscale studies are conducted, which would allow comparison of results between the different regions. This paper deals with the sampling conducted along the 6°E meridian south of the Antarctic Polar Front (APF) during a Scandinavian/South African Antarctic Expedition onboard the S.A. *Agulhas* (Froneman et al., 1998). The data collected during the cruise formed part of a Southern Ocean-Joint Global Ocean Flux Study (SO-JGOFS) with the two major objectives: to determine the relative importance of various factors (including physical, chemical and biological), which control primary production, and to assess the consequences of these factors on carbon cycling (Froneman et al., 1998). The main aim of this paper is to present spatial dynamics of mesozooplankton in the top 300 m during austral summer 1997/1998 between the Marginal Ice Zone and the APF.

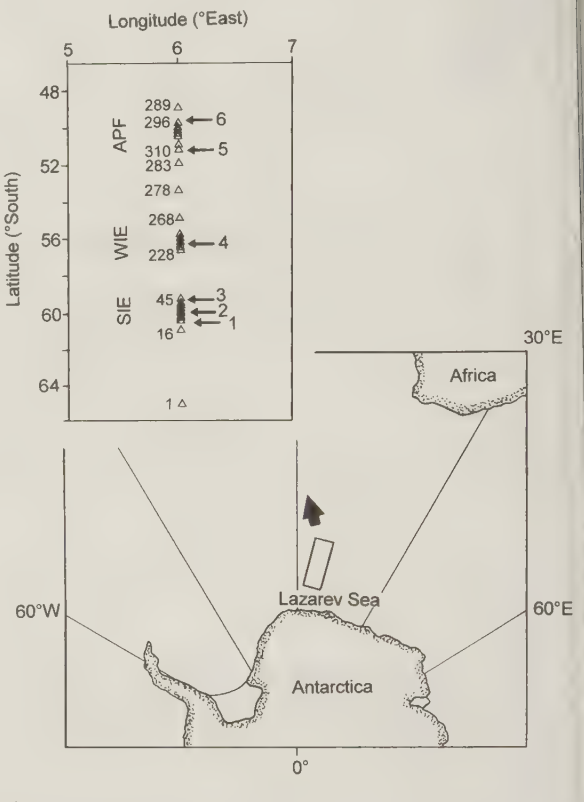

Fig. 1. Station positions occupied along the 6°E meridian in the eastern Atlantic sector of the Southern Ocean during December 1997–January 1998. Arrows indicate positions of Biostations. SIE: Spring Ice Edge region; WIE: Winter Ice Edge region; APF: Antarctic Polar Front region.

2. Materials and methods

Sampling was conducted during December 1997–January 1998 along the 6°E meridian south of the APF aboard the S.A. *Agulhas* (voyage 86). Samples were generally collected at half degree of latitude intervals (Fig. 1). Increased sampling resolution (every 10′ of latitude) was employed in three regions: the Spring Ice Edge (SIE), the Winter Ice Edge (WIE) and the APF (Fig. 1). In these areas, additional six 36 h Biostations were occupied to measure the grazing impact of zooplankton (Turner et al., 2004; Pakhomov and Froneman, 2004). The APF position was defined as the northernmost extent of the 2 °C isotherm (Turner et al., 2004). The SIE coincided with the ice edge crossed during the southbound underway transect conducted in the beginning of December 1997 (Abrahamsson et al., 2004; Turner et al., 2004). The WIE represented the northern boundary of the maximum expansion of winter ice, coinciding also with the northernmost extent of the negative subsurface isotherms (Gloersen et al., 1992; Klyausov, 1993). At each 36 h Biostation, tows were made at 4 h intervals. At Biostations, samples collected between 6 a.m. and 8 p.m. and between 8 p.m. and 6 a.m. were considered as day and night samples, respectively. Grazing results obtained at Biostations will be discussed elsewhere (Pakhomov and Froneman, 2004). Throughout the study, mesozooplankton samples

were collected using a Bongo net (total mouth area: 0.5 m^2; mesh size: 0.3 and 0.5 mm) towed obliquely from 300 m to the surface (Appendix A) and from 200 m to the surface during the 36 h Biostations (Appendix B). The net was equipped with a Universal Underwater Unit (U^4) which monitored depth and temperature continuously (Robertson et al., 1981). Towing speed varied between 1.5 and 3 knots. The volume filtered by the net was calculated using an electronic flowmeter positioned in the mouth of the 0.3 mm mesh net. The 0.3 mm mesh sample was preserved in 4–6% solution of buffered formalin. Aliquots of $\frac{1}{8}$ to $\frac{1}{32}$ (depending on the size of the sample) of the original sample were obtained with a Folsum splitter for the taxonomic and abundance analyses of zooplankton. Less numerous large zooplankters were counted from half of the sample or from the entire sample. The 0.5 mm mesh samples were used for grazing studies (Pakhomov and Froneman, 2004). In the laboratory, samples were sorted, counted and taxonomic composition assessed using the works of Razouls (1994) and Boltovskoy (1981). Euphausiid larvae of the genus *Thysanoessa* were identified and counted according to developmental stage following the procedure described by Makarov et al. (1986). Zooplankton abundance was expressed as the number of individuals per cubic meter. Dry weights of the main zooplankton species and groups were taken either from the literature (Mizdalski, 1988) or obtained from specimens that were oven-dried at 60 °C for 36 h. Samples were sorted within 2 months of collection. No adjustments were made to correct for tissue loss due to formalin preservation. Biomass was expressed as milligrams dry weight per cubic meter.

To compare plankton communities along the transect, non-metric cluster analysis was used in conjunction with the Bray-Curtis similarity index after the *log* transformation [$\log_{10}(x+1)$] of species abundance data. Significance levels and sources of difference between zooplankton assemblages associated with the different group of stations were tested using the similarity analysis programs ANOSIM and SIMPER of the Plymouth Routines In Multivariate Ecological Research (PRIMER, Clarke and Warwick, 1994) computer package, according to the procedure described by Field et al. (1982). Two-way ANOVA was run on total zooplankton abundance and biomass values at Biostations to investigate differences in zooplankton densities by time of day (day and night) and Biostation. Subsequently, Newman–Keuls multiple range tests were performed to identify differences in zooplankton densities between time of day and Biostations (Zar, 1984).

3. Results

3.1. Zooplankton abundance, biomass, distribution and composition

Along the transect, total abundance and biomass of mesozooplankton ranged from 8 to 384 ind m^{-3} and 1.4 to 64.1 mg DW m^{-3}, respectively (Fig. 2). Total zooplankton abundance was the highest at stations occupied in the WIE region (range 60–384, mean 180 ind m^{-3}). The lowest abundances of mesozooplankton (range 8–60, mean 39 ind m^{-3}) were recorded within the SIE region (Fig. 2 and Table 1). In contrast, total zooplankton biomass generally increased along the south–north transect and ranged on average from 8.4 within the SIE to 38 mg DW m^{-3} within the APF regions (Fig. 2 and Table 1). The ANOVA revealed significant ($p<0.001$) differences in zooplankton abundance between the SIE and WIE/APF Biostations conducted during both

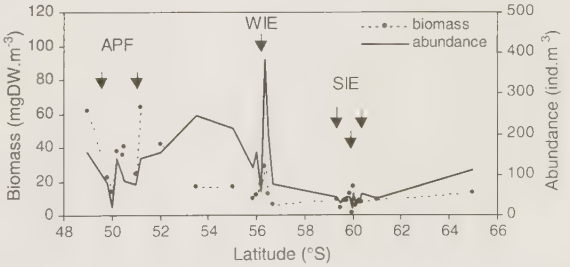

Fig. 2. Spatial distribution of abundance and biomass of zooplankton along the 6°E meridian in the eastern Atlantic sector of the Southern Ocean during December 1997–January 1998. SIE: Spring Ice Edge region; WIE: Winter Ice Edge region; APF: Antarctic Polar Front region.

Table 1
Zooplankton composition, abundance and biomass in the Spring Ice Edge (SIE), Winter Ice Edge (WIE) and Antarctic Polar Front (APF) groupings identified using cluster analysis in the Atlantic sector of the Southern Ocean during December 1997–January 1998

Groupings	Number of species	Mean abundance ind m^{-3} ($\pm$SD)	Most important contributors by abundance (%)	Mean biomass (mg DW m^{-3} $\pm$SD)	Most important contributors by mass (%)
SIE	47	39$\pm$10	*Oncaea antarctica* (27.7), *Oithona similis* (11.7), *Metridia gerlachei* (9.4), *Eukrohnia hamata* (6.9), *Calanus propinquus* (5.2), *Clausocalanus brevipes* (3.7), *Heterorabdus austrinus* (3.5), *Rhincalanus gigas* (3.4), *Oithona frigida* (3.2), Ostracoda (3.1), *Calanoides acutus* (2.9), *Ctenocalanus vanus* (2.8), *Thysanoessa macrura*, calyptopis (2.54), *Scolecithricella minor* (2.2), *Paraeuchaeta biloba* (1.8), *Sagitta gazellae* (1.5), *Rhinchonerella bongraini* (1.5), *Scaphocalanus* spp. (1.5), *Dimophies arctica* (1.1)	8.4$\pm$3.8	*P. biloba* (20.7), *R. gigas* (18.7), *S. gazellae* (6.4), *E. hamata* (6.0), *C. propinquus* (5.7), *D. arctica* (4.2), *C. acutus* (3.6), *Diphyes antarctica* (3.2), *M. gerlachei* (3.0), *H. austrinus* (2.9), *Euchirella rostromanga* (2.7), *Clio sulcata* (2.6), *Paraeuchaeta* spp. (2.4), Ostracoda (2.1), *O. antarctica* (1.9), *R. bongraini* (1.8), *T. macrura* (1.7), *Electrona* spp., larvae (1.6)
WIE	47	180$\pm$99	*O. similis* (73.5), *C. vanus* (4.8), *C. propinquus* (2.9), *Paraeuchaeta* spp. (2.3), *E. hamata* (2.2), *C. brevipes* (2.2), Nauplii copepoda (2.1), *O. frigida* (1.9), *M. gerlachei* (1.1), *C. acutus* (1.0)	15.2$\pm$6.4	*Paraeuchaeta* spp. (24.9), *O. similis* (8.2), *Salpa thompsoni* (8.0), *C. propinquus* (7.3), *R. gigas* (6.4), *C. sulcata* (6.2), *P. biloba* (5.8), *E. hamata* (5.0), *S. gazellae* (4.9), *Euphausia superba* (3.4), *C. acutus* (3.1), *D. antarctica* (2.5), *T. macrura* (1.5), *Electrona* spp., larvae (1.4), *Euphausia frigida* (1.2), *Sagitta marri* (1.0)
APF	53	105$\pm$43	*Calanus simillimus* (20.2), *C. vanus* (18.2), *O. similis* (12.2), *E. hamata* (5.7), *R. gigas* (5.5), *C. brevipes* (5.2), *O. antarctica* (3.8), Ostracoda (3.6), *Paraeuchaeta* spp. (3.2), *M. gerlachei* (2.9), *O. frigida* (2.9), *S. minor* (2.8), *Clausocalanus laticeps* (2.5), *Metridia lucens* (2.5), *C. acutus* (1.7), *P. biloba* (1.0)	38.0$\pm$15.9	*C. simillimus* (26.7), *R. gigas* (15.8), *Pleurobrachia pileus* (13.0), *S. thompsoni* (8.7), *Paraeuchaeta* spp. (8.0), *P. biloba* (6.9), *Thysanoessa vicina* (4.3), *E. hamata* (2.9), Ostracoda (1.5), *S. gazellae* (1.4), *C. acutus* (1.3), *M. lucens* (1.0)

Table 2
Mean day and night abundance (ind m $^{-3}$, ±SD) and biomass (mg DW m $^{-3}$, ±SD) of zooplankton at 36 h Biostations in the eastern Atlantic sector of the Southern Ocean during December 1997–January 1998

Density	Time of day	SIE			WIE	APF	
		1	2	3	4	5	6
Abundance	Day	13±3	14±2	15±4	154±50	162±64	167±60
	Night	22±8	23±10	15±3	259±85	175±14	231±106
Biomass	Day	33.3±47.0	21.2±28.1	6.4±1.7	12.7±2.2	55.0±23.6	65.8±26.2
	Night	6.7±2.6	16.5±12.4	10.3±4.6	51.2±26.5	67.6±8.4	66.6±34.1

SIE: Spring Ice Edge; WIE: Winter Ice Edge; APF: Antarctic Polar Front.

Table 3
Two-way ANOVA of total zooplankton abundance (ind m^{-3}) and biomass (mg DW m^{-3}) by time of day and Biostation, followed by SNK multiple comparison tests for significant results.

Source	df	MS	F	p	Significance
Abundance					
Time of day	1	13912.1	5.67	0.021	*
Biostation	5	81242.2	33.09	<0.001	**
Time × Biostation	5	3904.1	1.59	0.183	ns
SNK tests	Time of day:	Biostation 4: night > day			
		All other Biostations: night = day			
	Between Biostations (day):	1 = 2 = 3 < 4 = 5 = 6			
	Between Biostations (night):	1 = 2 = 3 < 4 = 5 = 6			
Biomass					
Time of day	1	2121.9	4.12	0.048	*
Biostation	5	4730.2	9.19	<0.001	**
Time × Biostation	5	625.1	1.21	0.318	ns
SNK tests	Time of day:	All Biostations: night = day			
	Between Biostations (day):	1 = 2 = 3 = 4 < 6; 1 = 2 = 3 = 4 = 5; 5 = 6			
	Between Biostations (night):	1 = 2 = 3 = 4; 1 = 2 = 3 < 5 = 6; 4 = 5 = 6			

*p<0.05; **p<0.001; ns: not significant.

day and night (Tables 2 and 3). Similarly with abundance, night biomass values at the SIE region were significantly lower than at the WIE and APF regions. Day biomass values did not show such clear pattern. Here, only Biostation 6 (APF) had significantly (p<0.05) higher biomass values than Biostations at the SIE and WIE regions (Tables 2 and 3).

There were no clear diel patterns in zooplankton densities, abundance and biomass, in the top 200 m layer within the SIE region, while in the WIE and APF regions zooplankton densities were often enhanced in sunset/sunrise and night tows (Fig. 3). However, with the exception of abundance values at Biostation 4, all day and night densities of total zooplankton (abundance and biomass) were not significantly different (p>0.05) at each Biostation (Table 2 and 3).

Copepods numerically dominated zooplankton along the transect accounting for 68–97% of the total abundance (Fig. 4A). Their highest contribution (>80%) was recorded within the WIE region. Copepods were followed by the chaetognaths (up to 17%) and euphausiids (up to 10%). Other

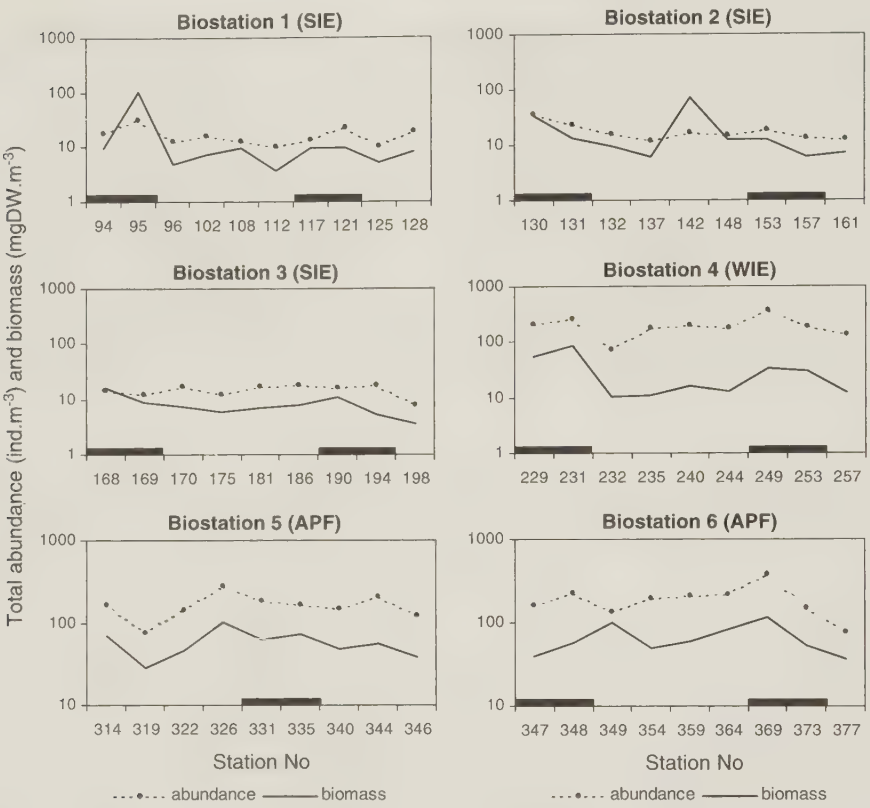

Fig. 3. Diel variability of total zooplankton abundance and biomass at Biostations conducted along the 6°E transect in the eastern Atlantic sector of the Southern Ocean during December 1997–January 1998. SIE: Spring Ice Edge region; WIE: Winter Ice Edge region; APF: Antarctic Polar Front region. The period of darkness is indicated by thickening of the horizontal axis.

groups generally accounted for <5% of the total abundance (Fig. 4A). In terms of biomass, copepods were again the most important group comprising between 24% and 90% of the total zooplankton standing stock (Fig. 4B). Other important contributors to total biomass were cnidarians and ctenophores (up to 50%), pteropods (up to 35%), tunicates (up to 30%), chaetognaths (up to 25%) and euphausiids (up to 23%). The contribution of these groups differed substantially within the three regions of investigation. Cnidarians and ctenophores, although present along the entire transect, were the most prominent group in plankton assemblages in the APF region (Fig. 4B). Tunicates were sampled mainly within the WIE and the APF regions. The contribution of pteropods was substantial only within the WIE region. Similarly, while euphausiids were represented along the entire transect, their contribution was the highest within the WIE and APF regions. Chaetognaths were also recorded along the entire transect with the lowest contribution within the APF region (Fig. 4B).

The spatial distributions of the most important zooplankton species, numerically and by biomass, are presented in Figs. 5–8. The common feature in the distribution patterns of almost all species was the extreme spatial variability in densities along the transect. However, most of the species had peaks in their densities in one or two of the regions investigated. The peak of *Oithona similis* abundance ($>50\,\mathrm{ind\,m^{-3}}$) was found within the WIE region, while highest densities of *Oithona frigida* were recorded at the southernmost stations, within the WIE and APF regions (Fig. 5A). Enhanced densities ($>7\,\mathrm{ind\,m^{-3}}$) of *Oncaea antarctica* were

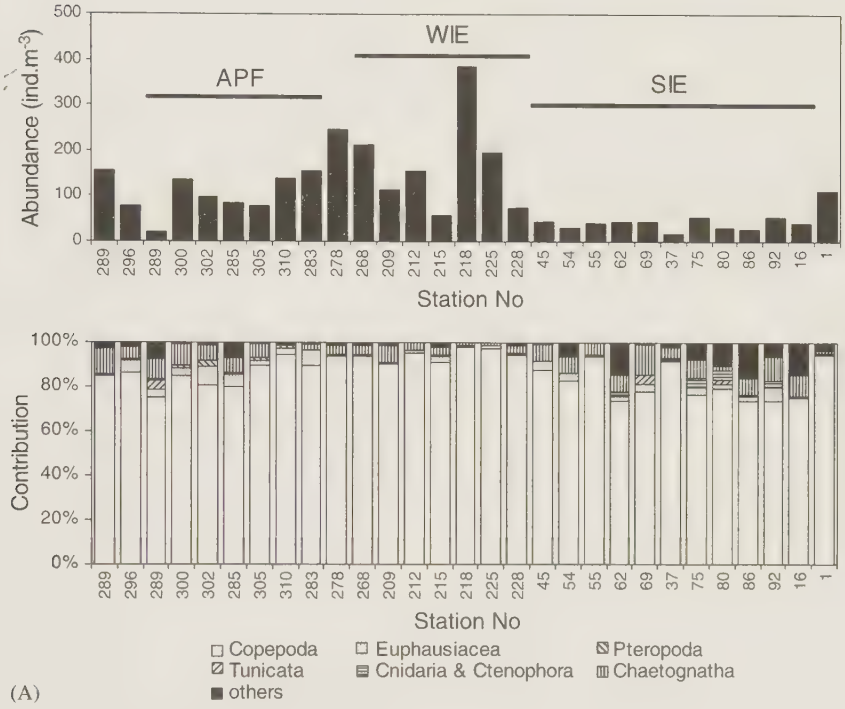

(A)

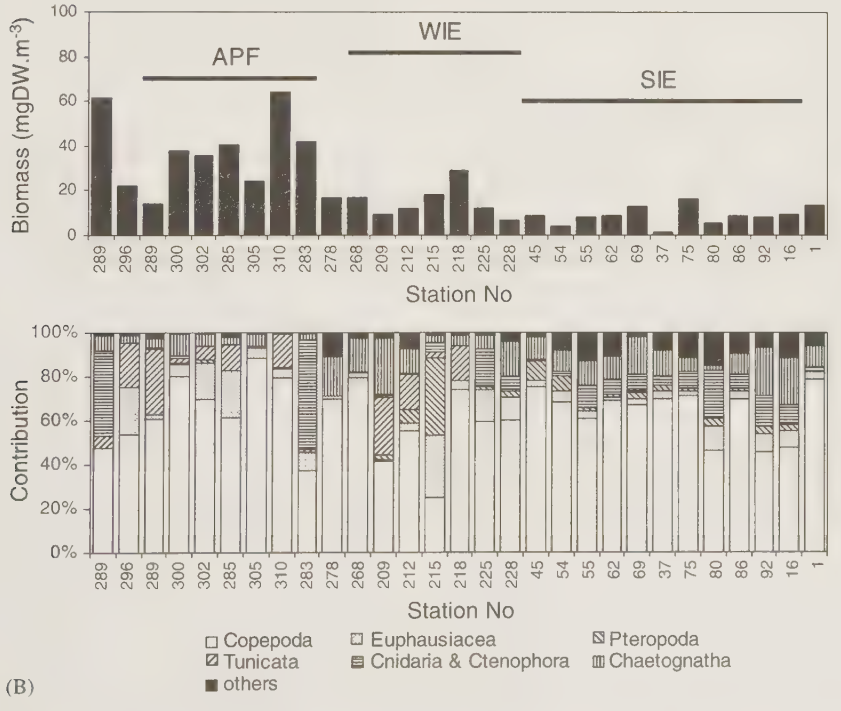

(B)

Fig. 4. Contribution of different taxonomic groups to total abundance (A) and biomass (B) along the 6°E meridian in the eastern Atlantic sector of the Southern Ocean during December 1997–January 1998. SIE: Spring Ice Edge region; WIE: Winter Ice Edge region; APF: Antarctic Polar Front region.

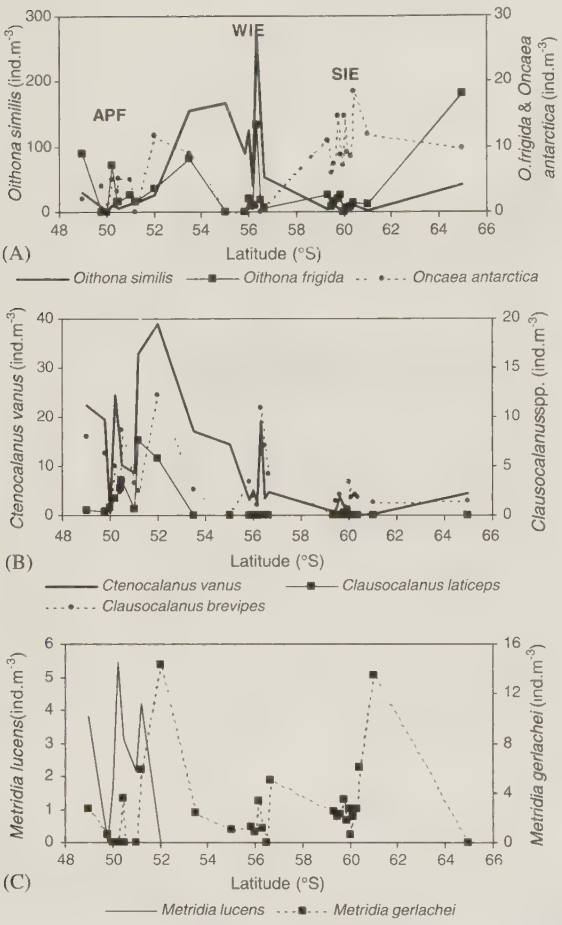

Fig. 5. Spatial variability in copepod abundance along the 6°E meridian in the eastern Atlantic sector of the Southern Ocean during December 1997–January 1998. SIE: Spring Ice Edge region; WIE: Winter Ice Edge region; APF: Antarctic Polar Front region. (A) *O. similis, O. frigida* and *O. antarctica*; (B) *C. laticeps, C. brevipes* and *C. vanus*; (C) *M. lucens* and *M. gerlachei.*

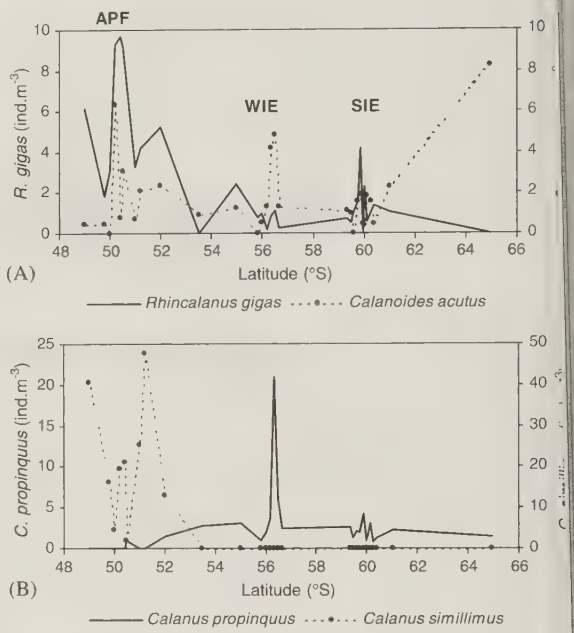

Fig. 6. Spatial variability in large calanoid copepod abundanc along the 6°E meridian in the eastern Atlantic sector of th Southern Ocean during December 1997–January 1998. SIE Spring Ice Edge region; WIE: Winter Ice Edge region; APF Antarctic Polar Front region. (A) *R. gigas* and *C. acutus*; (B) *C propinquus* and *C. simillimus.*

found within the SIE region and at the southern proximity of the APF, while its lowest densities were associated with the WIE region (Fig. 5A). Abundances of *Ctenocalanus vanus* increased northward along the transect peaking (up to 39 ind m^{-3}) at the southern proximity of the APF (Fig. 5B). Similar distribution patterns were recorded for *Clausocalanus brevipes* and *Clausocalanus laticeps*, although the latter species was found mainly between 49 and 52°S (Fig. 5B). *Metridia gerlachei* was recorded along the entire transect with two clear peaks in abundance observed at 61 and 52°S (Fig. 5C). Densities o *M. gerlachei* decreased sharply in the region of the APF, where it was replaced by *Metridia lucens* (Fig. 5C). *Rhincalanus gigas* and *Calanoides acutus* were sampled along the entire transect (Fig. 6A). Densities of *R. gigas* generally increased toward the APF with the highest abundances recorded at 51°S. The distributional pattern of *C. acutus* displayed three peaks at: the southmost station, the WIE and APF regions (Fig. 6A). Two *Calanus* species (*Calanus propinquus* and *C. simillimus*) identified along the transect had similar spatial pattern as the *Metridia* species (Fig. 6B). *C. propinquus* virtually disappeared from the samples north of the 52° parallel, while *C. simillimus* was absent south of it (Fig. 6B).

The distribution of the three *Euphausia* species showed clear overlap within the WIE region. South of this region. *Euphausia superba* numerically dominated the samples with two major

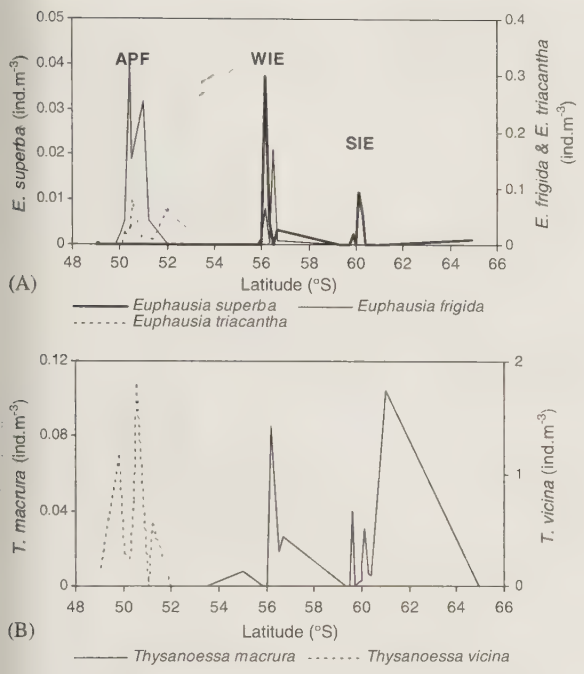

Fig. 7. Spatial variability in euphausiid abundance along the 6°E meridian in the eastern Atlantic sector of the Southern Ocean during December 1997–January 1998. SIE: Spring Ice Edge region; WIE: Winter Ice Edge region; APF: Antarctic Polar Front region. (A) *E. superba, E. frigida* and *E. triacantha*; (B) *T. macrura* and *T. vicina*.

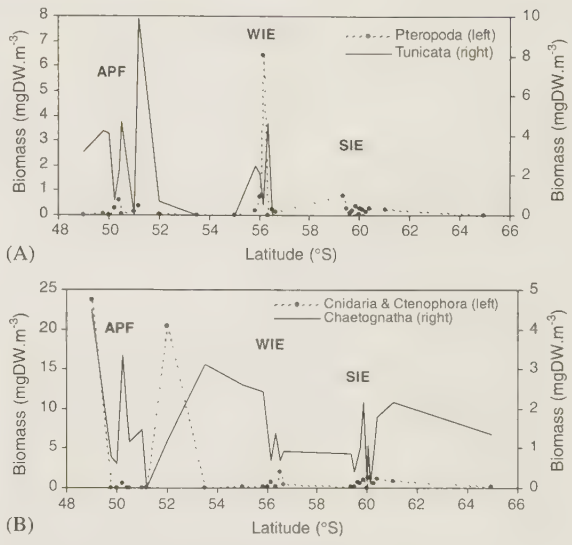

Fig. 8. Spatial distribution of biomass of pteropods and tunicates (A) and cnidarians/ctenophores and chaetognaths (B) along the 6°E meridian in the eastern Atlantic sector of the Southern Ocean during December 1997–January 1998. SIE: Spring Ice Edge region; WIE: Winter Ice Edge region; APF: Antarctic Polar Front region.

enhancements, at the SIE and WIE regions (Fig. 7A). North of the WIE region, Only *E. frigida* and *E. triacantha* were recorded. Both species had their maximum densities at the APF, while *E. frigida* also had elevated abundances at the WIE region (Fig. 7A). Similarly with the species of genera *Calanus* and *Metridia*; euphausiids of the genus *Thysanoessa*, *T. macrura* and *T. vicina*, replaced each other at the southern vicinity of the APF (Fig. 7B). Salps, mainly *Salpa thompsoni* were sampled from the WIE region northward. Their maximum densities were associated with the APF and WIE regions (Fig. 8A). Pteropods, Largely *Limacina helicina* and *Clio sulcata*, had their enhanced densities only at the WIE region (Fig. 8A). Cnidarians, comprising siphonophores and jellyfish, and ctenophores were most abundant at stations occupied in the APF region and north of the front (Fig. 8B). The distribution patterns of the chaetognaths, *Sagitta gazellae* and *Eukrohnia hamata*, were not clear along the transect (Fig. 8B).

3.2. Community structure

Results of the hierarchical cluster analysis revealed three major groupings of stations corresponding broadly to the three major regions investigated. We, therefore, named them the APF, WIE and SIE groupings, accordingly (Fig. 9). Two outliers, Stations 1 and 298, were identified. The southernmost Station 1 was characterized by the low species richness ($n = 19$) with only three copepod species, *C. acutus, O. similis* and *O. frigida*, accounting for >61% of total zooplankton abundance. Although Station 298 occupied within the APF region had the same number of species as Station 1, it was characterized by the lowest total zooplankton abundance along the entire transect (Figs. 4A and 9). The major separation of stations occurred between the APF/WIE and SIE regions (Fig. 9). ANOSIM routine (Clarke and Warwick, 1994) showed that

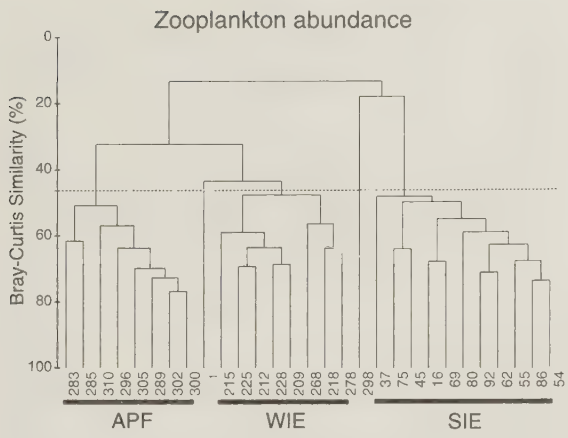

Fig. 9. Results of the cluster analysis of the zooplankton community structure along the 6°E meridian in the eastern Atlantic sector of the Southern Ocean during December 1997–January 1998. SIE: Spring Ice Edge grouping; WIE: Winter Ice Edge grouping; APF: Antarctic Polar Front grouping.

the differences between the three groups identified with the hierarchical cluster analysis were significant ($p<0.05$).

Compared to the region north of the SIE, the SIE grouping was characterized by significantly (t-test, $p<0.05$) lower average zooplankton abundance and biomass levels (Table 1). Two small cyclopoid copepods, *O. antarctica* and *O. similis*, and a calanoid copepod *M. gerlachei* numerically dominated zooplankton community at these stations accounting for almost 49% of total abundance. However, three large calanoid copepods, *Paraeuchaeta biloba, R. gigas* and *C. propinquus*, as well as two chaetognath species, *S. gazellae* and *E. hamata*, were responsible for the most (58% of the total dry mass) of the zooplankton standing stock (Table 1). The WIE grouping of stations had the highest average zooplankton abundance and intermediate biomass levels (Table 1). The species composition was similar to that identified in the SIE grouping. However, differences were evident in the relative contributions of the different species (Table 1). For example, *O. similis* was the single dominant species in the WIE realm accounting for >73% of total zooplankton counted. Although three calanoid species identified in the SIE region formed a substantial contribution total biomass, in the WIE the cyclopoid copepc *O. similis*, the salp *S. thompsoni* and the pteropc *C. sulcata* were also important contributo (together >66% of total dry mass) to tl zooplankton standing stock (Table 1). The AP grouping had the highest number of species ar average biomass values but intermediate averag abundance among the three groupings (Table 1 The calanoid copepod *C. simillimus*, together wit small copepod species *C. vanus* and *O. simil* accounted for >50% of total zooplankton count In terms of dry mass, four species includin calanoid copepods *C. simillimus* and *R. giga* ctenophore *Pleurobrachia pileus* and salp *S. thompsoni* contributed >64% to total zooplank ton biomass (Table 1).

The age composition of two copepods (*M. gerlachei* and *C. propinquus*) and a single euphau siid species (*T. macrura*) were compared betwee different regions (Figs. 10 and 11). Populations o

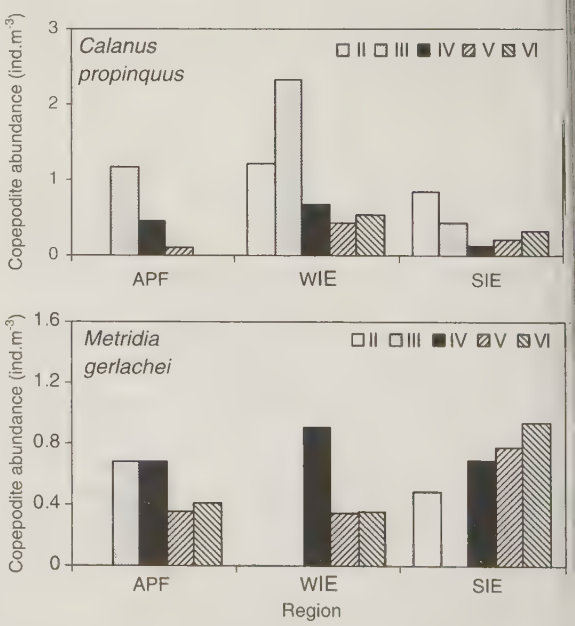

Fig. 10. Development stage composition of *C. propinquus* and *M. gerlachei* in three different regions along the 6°E meridian in the eastern Atlantic sector of the Southern Ocean during December 1997–January 1998. SIE: Spring Ice Edge region; WIE: Winter Ice Edge region; APF: Antarctic Polar Front region. (II–V) Copepodite stages II–V; (VI) adult specimens.

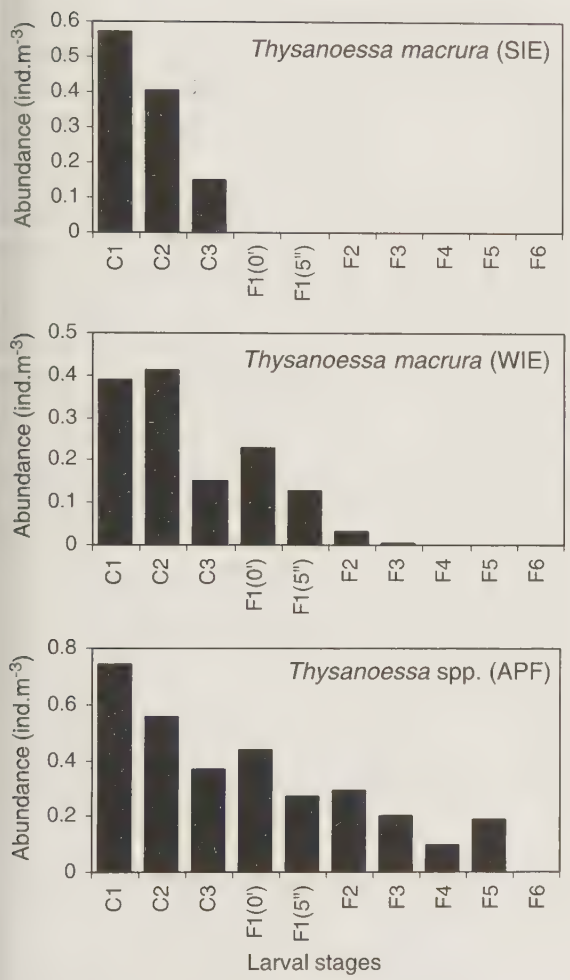

Fig. 11. Larval stage composition of *T. macrura* in three different regions along the 6°E meridian in the eastern Atlantic sector of the Southern Ocean during December 1997–January 1998. SIE: Spring Ice Edge region; WIE: Winter Ice Edge region; APF: Antarctic Polar Front region.

both copepod species within the SIE region were characterized by bimodal distributions dominated by older and younger copepodites. In the WIE region, younger copepodite stages were generally most abundant, while within the APF region mainly older copepodites and adults were encountered (Fig. 10). The developmental stage composition of *T. macrura* was the youngest within the SIE region and the oldest within the APF region (Fig. 11).

4. Discussion

As this study was mainly carried out to support grazing experiments (Pakhomov and Froneman, 2004), two main points should be addressed below: the latitudinal distribution and the structure of the zooplankton community, and its possible implications for the efficiency of the biological pump.

At stations occupied in the WIE and SIE regions, total zooplankton abundance and biomass were generally $<100\,\mathrm{ind\,m^{-3}}$ and $<20\,\mathrm{mg\,DW\,m^{-3}}$. Biomass values reported here were in the range reported previously for the region south of the APF in different sectors of the Southern Ocean (e.g. Foxton, 1956; Hopkins, 1971, 1985; Boysen-Ennen et al., 1991, Table 3; Atkinson and Shreeve, 1995; Siegel and Harm, 1996, Table 5; Fransz and Gonzalez, 1997; Voronina, 1998, Table 2; Pakhomov et al., 2000). The large mesh size (300 μm) of the nets, however, likely resulted in a substantial underestimate of the contribution of small calanoid and cyclopoid copepods to total zooplankton abundance (Fransz and Gonzalez, 1997). For example, in studies where nets with a small mesh size ($\leqslant 200\,\mu m$) were employed, average mesozooplankton abundances were at least one-order magnitude higher of those presented here (Voronina, 1984; Fransz and Gonzalez, 1997). This manuscript, therefore, mainly discusses the community structure/distribution of the larger mesozooplankton.

The general increase in zooplankton density observed along the south–north transect compares well with previous studies (Foxton, 1956; Voronina et al., 1994; Pakhomov and McQuaid, 1996; Fransz and Gonzalez, 1997; Pakhomov et al., 2000). The zooplankton densities recorded at stations occupied in the region of the APF during this study are comparable with the values identified within the localized hotspots of the Southern Ocean, such as coastal waters off the Antarctic Peninsula and South Georgia (Voronina, 1984; Hopkins, 1985; Witek et al., 1985; Atkinson et al., 1996; Pakhomov et al., 1997a, b).

Copepods were found to be the most prominent group of zooplankton along the entire transect in terms of abundance and dry mass. This finding is again in good agreement with similar studies

conducted in different sectors of the Southern Ocean indicating that copepods account for >70% of total abundance, between 25% and 95% of total biomass and the bulk of the metazoan production (Foxton, 1956; Hopkins, 1971; Maruyama et al., 1982; Voronina, 1984, 1998; Boysen-Ennen et al., 1991; Hopkins et al., 1993; Voronina et al., 1994). The contribution of other groups, e.g. euphausiids, pteropods, chaetognaths, tunicates, cnidarians and ctenophores, was highly variable and never exceeded 30% of total zooplankton abundance. In terms of biomass, the non-copepod zooplankton contribution was generally the highest within the WIE and APF regions, largely due to elevated densities of pteropods, euphausiids, chaetognaths and tunicates. This pattern conforms well to previous findings in the Atlantic sector of the Southern Ocean (Voronina, 1984; Voronina et al., 1994; Pakhomov and McQuaid, 1996; Fransz and Gonzalez, 1997; Pakhomov et al., 2000). For example, during October/November 1992 and January 1993 copepods dominated zooplankton densities by both numbers and biomass (Fransz and Gonzalez, 1997; Pakhomov et al., 2000). The contribution of copepods, however, decreased substantially in two regions, in the northern boundary of the Marginal Ice Zone at ≈60°S mainly due to the contribution of Antarctic krill and in the region of the northernmost extension of the subsurface cold water layer at ≈54°S due to high concentrations of krill and salps (Fransz and Gonzalez, 1997; Pakhomov et al., 2000).

Macro-scale zonation of the Southern Ocean epipelagic zooplankton has been investigated on several occasions (e.g. Dolzhenkov, 1982; Deacon, 1982; Grachev, 1991; Pakhomov and McQuaid, 1996; Pakhomov et al., 2000). These studies recognized the APF as being an important biogeographic boundary to the zooplankton distribution demarcating the Subantarctic and Antarctic realms of the Southern Ocean. There is some evidence in the literature to suggest that zooplankton may at times be displaced across the APF (Deacon, 1982; Pakhomov et al., 1994a). Wyrtki (1960) showed that depending on the strength of the westerly winds, the APF alternates between a divergence and convergence frontal system. When a convergent motion of the APF changes to a divergent one, a mixing zone is established resulting in mutual penetration in species of Subantarctic and Antarctic origin across the APF (Voronina, 1962). South of the APF extending up to the Antarctic continental shelf, two large-scale subsystems coinciding with the distribution of water masses and ice cover have previously been distinguished (Hempel, 1985). The first zone coincides with the ice-free oceanic West Wind Drift where copepods, salps and small euphausiids dominate. The second zone covers the seasonal pack-ice zone, where Antarctic krill is the most important species (Hempel, 1985).

During this survey, the major separation of stations along the transect occurred across the WIE region. This was particularly evident in the Antarctic krill/salp distribution and in the developmental composition of some calanoid copepods and euphausiid of the genus *Thysanoessa*. Identical patterns have previously been observed in all three sectors suggesting that the WIE region act as an important ecological boundary probably throughout most of the Southern Ocean (Casareto and Nemoto, 1986; Makarov et al., 1990; Grachev 1991; Klyausov, 1993; Pakhomov and McQuaid 1996; Pakhomov et al., 2000). This region generally represents the northernmost distributional limit for Antarctic krill, coincides with the sharp decline in *S. thompsoni* populations to the south and separates phenologically different copepod and euphausiid populations (Makarov et al., 1990; Pakhomov and McQuaid, 1996; Pakhomov et al., 1994b, 2000; Fransz and Gonzalez, 1997; this study).

Differences in the broad-scale distribution of zooplankton between surveys conducted in January 1980 and 1993 suggest high inter-annual variability in the zooplankton community dynamics (Pakhomov and McQuaid, 1996; Pakhomov et al., 2000). This variability is mainly concerned with the distribution of *E. superba* and *S. thompsoni*. Unlike the 1998 survey, enhanced Antarctic krill concentrations were observed at the northern boundary of the Marginal Ice Zone at ≈60°S during January 1980 and 1993 (Pakhomov and McQuaid, 1996; Pakhomov et al., 2000). Although during all three surveys the second peak

in Antarctic krill densities coincided with the region of the northernmost expansion of the subsurface cold layer, during 1993 it was observed at ≈56°S, while during both 1980 and 1998 it was registered at ≈54°S (Pakhomov and McQuaid, 1996; Pakhomov et al., 2000; this study). The Antarctic krill found in this area likely belong to the Weddell Drift originating from the Bellingshausen Sea and a northern branch of the Weddell Gyre (Makarov and Sysoeva, 1983; Latogursky et al., 1990). With regard to the tunicate distribution, *S. thompsoni* were occasionally found as far south as 67°S (Pakhomov et al., 1994b; Perissinotto and Pakhomov, 1998). Unfortunately, during January 1998 the southernmost station was occupied at ≈65°S. As a consequence, the areas of the most dense krill concentrations, which are generally restricted to the East Wind Drift, and salp protrusions were not covered (Makarov and Sysoeva, 1983; Solyankin et al., 1983; Pakhomov et al., 1994b).

Although some similarity in zooplankton zonation during January 1980, 1993 and 1998 was found, the region along the Greenwich Meridian and adjacent to the west and east areas is known as a region of complex oceanography. It is documented that east of Bouvet Island, the waters of the Weddell Gyre turn south (Marr, 1962; Mackintosh, 1973; Maslennikov, 1980; Grachev, 1991). It was also shown that large quantities of transformed warm circumpolar waters may be advected into the Lazarev Sea (Deacon, 1979; Gordon, 1980; Makarov and Sysoeva, 1983; Latogursky et al., 1990; Pakhomov et al., 1994b). This may result in the variable Antarctic krill distribution and the salp *S. thompsoni* advection into the areas along the Greenwich Meridian and adjacent regions (Pakhomov et al., 1994b; Perissinotto and Pakhomov, 1998). Unfortunately, the present study was conducted along the single transect and, therefore, a broader-scale spatial dynamics in krill/salp distribution cannot be properly addressed.

The phytoplankton and zooplankton community structure may be used to estimate the potential efficiency of the biological pump in areas south of the APF (Froneman et al., 2000; Pakhomov et al., 2000). The phytoplankton communities within the SIE and APF regions were dominated by microphytoplankton, while within the WIE region, nano- and picophytoplankton accounted for the bulk of phytoplankton community (Froneman et al., 2004). Despite the differences in phytoplankton size structure along the transect, microzooplankton grazing accounted for ⩽11% of daily primary production in the three regions (Froneman et al., 2004). As a consequence, the partitioning of carbon between the microbial loop and classical food web appeared to be similar in the SIE and APF regions, while the classical food web represented most important sink for primary production within the WIE (Froneman et al., 2004). The size structure of metazoan plankton in the region of investigation may provide further details on pathways of the carbon transfer. For example, copepods cannot graze efficiently on large microphytoplankton and they tend to retain carbon within the euphotic zone (Fortier et al., 1994; Bathmann, 1998). These data suggest that grazer mediated carbon transfer to depth would be minimal and that the sinking of phytoplankton cells would represent the major pathway for downward transfer of carbon in the SIE region (Froneman et al., 2004). Alternatively, the predominance of large metazoans in the WIE and APF regions, would likely result in an efficient biological pump in these regions as result of the phytoplankton sinking and grazing mediated transfer of carbon from surface waters to depth (Froneman et al., 2004; Pakhomov, 2004; Pakhomov and Froneman, 2004).

Acknowledgements

We are grateful to the South African Department of Environmental Affairs and Tourism, to Rhodes University and the Swedish Polar Secretariat for logistical and financial support of this study. We would like to thank officers and crew of the S.A. *Agulhas* and many colleagues from Göteborg University (Sweden) and Rhodes University (South Africa) for understanding and constant help during the expedition. We are also indebted to A. Grinham and B. Hunt for their invaluable assistance at sea.

Appendix A. Details of bongo sampling stations conducted along the 6°E meridian during the voyage 86 of th S.A. *Agulhas*, December 1997–January 1998

Station no.	Latitude (S)	Longitude (E)	Date (1997/1998)	Time (GMT)	Sampling depth (m)	Volume filtered (m
D001	64°57.52	5°59.73	25.12	10:20	0–311	852.12
D016	61°01.37	5°56.41	29.12	17:10	0–299	765.73
D037	59°59.68	5°58.48	30.12	20:06	0–108	353.62
D045	59°19.98	6°00.98	31.12	13:55	0–300	443.23
D054	59°28.09	6°02.85	01.01	15:18	0–301	649.1
D055	59°36.21	6°00.23	01.01	17:04	0–303	300.91
D062	59°44.87	6°01.83	02.01	07:28	0–301	411.24
D069	59°52.37	5°59.02	02.01	12:41	0–300	421.17
D075	60°01.70	6°02.90	02.01	19:36	0–300	415.54
D080	60°07.53	5°59.56	03.01	03:22	0–303	261.4
D086	60°16.67	6°00.44	03.01	11:26	0–298	618.93
D209	55°49.22	6°02.39	12.01	16:26	0–300	396.93
D212	55°59.89	6°00.71	12.01	19:23	0–301	321.53
D215	56°10.25	6°02.05	12.01	23:51	0–300	375.42
D218	56°19.78	6°00.02	13.01	04:58	0–301	191.4
D225	56°30.25	5°56.52	13.01	16:34	0–301	428.17
D228	56°40.83	5°59.65	13.01	19:06	0–302	303.78
D268	55°00.37	6°00.37	16.01	07:52	0–301	264.13
D278	53°30.93	5°58.79	17.01	17:16	0–301	356.72
D283	52°00.27	5°59.52	18.01	07:07	0–304	275.1
D285	50°30.03	6°00.31	20.01	00:11	0–304	314.95
D289	49°00.65	6°03.28	21.01	04:23	0–301	337.87
D296	49°48.90	6°00.30	24.01	09:50	0–301	354.48
D298	50°01.77	5°59.68	24.01	12:54	0–301	390.6
D300	50°14.33	6°00.23	24.01	17:47	0–304	380.53
D302	50°26.39	6°00.36	24.01	22:58	0–303	396.1
D305	51°00.18	5°59.26	26.01	07:17	0–303	222
D310	51°12.57	6°00.33	26.01	19:44	0–100	190

Appendix B. Details of Bongo sampling stations conducted along the 6°E meridian during Biostations, voyage 86 of the S.A. *Agulhas*, December 1997–January 1998

Biostation no.	Station no.	Latitude (S)	Longitude (E)	Date (1998)	Time (GMT)	Sampling depth (m)	Volume filtered (m^3)
1	D092	60°23.69	5°59.59	03.01	18:10	0–300	348.34
	D094	60°23.50	6°01.12	03.01	23:05	0–201	197.75
	D095	60°23.51	6°01.48	04.01	02:55	0–200	204.08
	D096	60°24.02	6°00.30	04.01	07:04	0–201	176.77
	D102	60°24.26	6°01.56	04.01	10:54	0–200	293.07

Appendix B. (*continued*)

Biostation no.	Station no.	Latitude (S)	Longitude (E)	Date (1998)	Time (GMT)	Sampling depth (m)	Volume filtered (m^3)
	D108	60°25.45	6°01.78	04.01	14:53	0–201	264.05
	D112	60°23.28	6°00.36	04.01	18:57	0–202	161.79
	D117	60°23.98	5°59.65	04.01	22:56	0–202	203.15
	D121	60°23.96	6°10.47	05.01	02:54	0–200	190.52
	D125	60°23.61	6°00.28	05.01	06:58	0–200	182.29
	D128	60°24.56	6°01.18	05.01	11:03	0–203	186.56
2	D130	60°00.00	5°59.78	06.01	00:26	0–201	159.06
	D131	60°00.59	6°01.13	06.01	03:32	0–199	193.57
	D132	60°00.21	5°59.97	06.01	07:00	0–202	197.87
	D137	59°59.18	6°01.69	06.01	11:05	0–201	249.96
	D142	59°59.99	5°59.53	06.01	15:02	0–200	288.99
	D148	60°00.08	6°00.20	06.01	19:10	0–200	260.23
	D153	60°00.18	6°01.26	06.01	23:01	0–201	210.25
	D157	60°00.44	6°01.07	07.01	03:01	0–202	145.28
	D161	59°59.96	5°58.78	07.01	07:03	0–209	151.62
3	D168	59°19.89	6°00.28	07.01	23:00	0–201	176.44
	D169	59°19.24	6°00.54	08.01	03:02	0–201	179.76
	D170	59°19.86	6°00.13	08.01	07:04	0–201	184.71
	D175	59°20.61	5°59.42	08.01	11:03	0–201	194.41
	D181	59°19.28	6°00.78	08.01	15:05	0–200	239.92
	D186	59°19.23	6°02.48	08.01	18:57	0–201	188.43
	D190	59°20.75	6°02.31	08.01	23:01	0–201	217.11
	D194	59°19.41	5°59.10	09.01	03:01	0–201	188.61
	D198	59°20.19	6°00.31	09.01	07:01	0–202	189.38
4	D229	56°28.35	6°01.27	13.01	23:02	0–201	287.13
	D230	56°25.45	6°03.28	14.01	00:33	0–22	140.26
	D231	56°29.43	5°59.89	14.01	02:53	0–200	237.51
	D232	56°30.43	6°00.67	14.01	06:58	0–203	167.56
	D235	56°29.40	6°02.06	14.01	11:17	0–201	277.46
	D240	56°28.90	5°58.47	14.01	14:54	0–203	257.40
	D244	56°30.02	6°00.38	14.01	19:01	0–201	224.20
	D249	56°28.75	6°00.83	14.01	22:58	0–198	235.38
	D253	56°29.63	6°01.71	15.01	02:55	0–199	247.21
	D257	56°30.15	6°01.51	15.01	06:58	0–201	224.91
5	D314	51°00.15	6°00.40	27.01	07:06	0–202	164.60
	D319	50°59.62	5°59.21	27.01	10:57	0–302	328.90
	D322	51°00.92	5°59.76	27.01	14:54	0–201	244.45
	D326	51°00.00	5°59.75	27.01	18:59	0–200	265.63
	D331	50°59.32	6°01.97	27.01	22:53	0–301	396.90
	D335	50°59.83	5°58.38	28.01	02:55	0–202	302.91
	D340	51°00.08	6°00.37	28.01	06:51	0–201	150.05

Appendix B. (*continued*)

Biostation no.	Station no.	Latitude (S)	Longitude (E)	Date (1998)	Time (GMT)	Sampling depth (m)	Volume filtered (m^3)
	D344	50°59.92	6°01.39	28.01	10:58	0–202	203.16
	D346	51°00.59	5°59.45	28.01	14:40	0–201	192.05
6	D347	49°49.44	6°01.14	28.01	22:58	0–300	553.54
	D348	49°50.53	5°59.38	29.01	02:57	0–200	225.17
	D349	49°49.79	6°00.33	29.01	06:53	0–201	184.76
	D354	49°49.55	5°59.91	29.01	10:58	0–302	390.91
	D359	49v49.64	6°00.06	29.01	14:51	0–201	321.06
	D364	49v50.35	5°59.25	29.01	18:52	0–202	195.17
	D369	49°50.61	6°00.41	29.01	23:00	0–201	284.27
	D373	49°49.52	6°00.14	30.01	02:53	0–202	155.15
	D377	49°49.75	6°00.08	30.01	06:59	0–202	181.60

References

Abrahamsson, K., Bertilsson, S., Chierici, M., Fransson, A., Froneman, P.W., Lorén, A., Pakhomov, E.A., 2004. Variations of biochemical parameters along a transect in the Southern Ocean, with special emphasis on volatile halogenated organic compounds. Deep-Sea Research II, this issue [doi:10.1016/j.dsr2.2004.09.004].

Atkinson, A., Shreeve, R.S., 1995. Response of the copepod community to a spring bloom in the Bellingshausen Sea. Deep-Sea Research II 42, 1291–1311.

Atkinson, A., Shreeve, R.S., Pakhomov, E.A., Priddle, J., Blight, S.P., Ward, P., 1996. Zooplankton response to a phytoplankton bloom near South Georgia, Antarctica. Marine Ecology Progress Series 144, 195–210.

Bathmann, U.V., 1998. Ecology and biochemistry in the Atlantic sector of the Southern Ocean during austral spring: the first JGOFS expedition aboard RV 'Polarstern'. Journal of Marine Systems 17, 77–85.

Boltovskoy, D., 1981. Atlas del zooplankton del Atlántico Suboccidental. Y métodos de trabajo con el zooplancton marino. Publicación especial del UNIDEP, Mar del Plata, Argentina.

Boysen-Ennen, E., Hagen, W., Hubold, G., Piatkowski, U., 1991. Zooplankton biomass in the ice-covered Weddell Sea, Antarctica. Marine Biology 111, 227–235.

Casareto, B.E., Nemoto, T., 1986. Salps of the Southern Ocean (Australian sector) during the 1983 84 summer, with special reference to the species *Salpa thompsoni*, Foxton 1961. Memoirs of National Institute of Polar Research 40, 221–239.

Clarke, K.R., Warwick, R.M., 1994. Change in Marine Communities: An Approach to Statistical Analysis and Interpretation. Natural Environment Research Council, Cambridge.

Deacon, G.E.R., 1979. The Weddell Gyre. Deep-Sea Research 26A, 981–995.

Deacon, G.E.R., 1982. Physical and biological zonation in the Southern Ocean. Deep-Sea Research 29, 1–15.

Dolzhenkov, V.N., 1982. Zoogeographic zonation of the surface waters in the Pacific sector of the Southern Ocean using macroplankton. In: Lubimova, T.G., Makarov, R.R., Kamenskaja, E.A. (Eds.), Fauna and Distribution of Temperate and Antarctic Crustaceans (Collected papers). DVNC AN USSR Publishers, Vladivostok, pp. 110–116 (in Russian).

Dubischar, C.D., Bathmann, U.V., 1997. Grazing impact of copepods and salps on phytoplankton in the Atlantic sector of the Southern Ocean. Deep-Sea Research II 44, 415–433.

Field, J.G., Clarke, K.R., Warwick, R.M., 1982. A practical strategy for analysing multispecies distribution patterns. Marine Ecology Progress Series 8, 37–52.

Foxton, P., 1956. The distribution and the standing crop of zooplankton in the Southern Ocean. Discovery Reports 28, 191–236.

Fortier, L., Le Fèvre, J., Legendre, L., 1994. Export of biogenic carbon to fish and to the deep ocean: the role of large planktonic microphages. Journal of Plankton Research 16, 809–839.

Fransz, H.G., Gonzalez, S.R., 1997. Latitudinal metazoan plankton zones in the Antarctic Circumpolar Current along 6°W during austral spring 1992. Deep-Sea Research II 44, 395–414.

Froneman, P.W., Pakhomov, E.A., Perissinotto, R., Laubscher, R.K., McQuaid, C.D., 1997. Dynamics of the plankton communities during seasonal ice melt in the Lazarev Sea in austral summer 1994–1995. Marine Ecology Progress Series 149, 201–214.

Froneman, P.W., Pakhomov, E.A., Turner, D., Abrahamsson, K., Karlson, B., Godhe, A., Bertilsson, S., Granéli, W., Carlsson,

P., Wängberg, S., Wulff, A., Croot, P., Andersson, K., Balarin, M., Wedborg, M., Persson, T., Rasmus, K., Özturk, M., David, R., 1998. Research cruise of the Scandinavian/South African Antarctic Expedition: December 1997 February 1998. South African Journal of Science 94, 517–519.

Froneman, P.W., Pakhomov, E.A., Perissinotto, R., McQuaid, C.D., 2000. Zooplankton structure and grazing in the Atlantic sector of the Southern Ocean in late austral summer 1993. Part 2. Biochemical zonation. Deep-Sea Research I 47, 1687–1702.

Froneman, P.W., Pakhomov, E.A., Balarin, M.G., 2004. Size-fractionated phytoplankton biomass, production and biogenic carbon flux in the eastern Atlantic sector of the Southern Ocean in late austral summer 1997–1998. Deep-Sea Research II, this issue [doi:10.1016/j.dsr2.2002.09.001].

Gloersen, P., Campbell, W.J., Cavalieri, D.J., Comiso, J.C., Parkinson, C.L., Zwally, H.J., 1992. Arctic and Antarctic Sea Ice, 1978–1987. Satellite Passive-Microwave Observations and Analysis. NASA SP-511, Washington, DC.

Gordon, A.L., 1980. Circumpolar water masses. Antarctic Journal of the United States 15, 89–91.

Grachev, D.G., 1991. Frontal zone influences on the distribution of different zooplankton groups in the central part of the Indian sector of the Southern Ocean. In: Samolova, M.S., Shumkova, S.O. (Eds.), Ecology of Commercial Marine Hydrobionts. TINRO Press, Vladivostok, pp. 19–21 (in Russian).

Hempel, G., 1985. On the biology of polar seas, particularly the Southern Ocean. In: Gray, J.S., Christiansen, M.E. (Eds.), Marine Biology of Polar Regions and Effects of Stress on Marine Organisms. Wiley, Chichester, pp. 3–33.

Hopkins, T.L., 1971. Zooplankton standing crop in the Pacific sector of the Antarctic. In: Llano, G.W., Wallen, I.E., (Eds.), Biology of the Antarctic Seas IV. Antarctic Research Series 17, 347–362.

Hopkins, T.L., 1985. Food web of an Antarctic midwater ecosystem. Marine Biology 89, 197–212.

Hopkins, T.L., Ainley, D.G., Torres, J.J., Lancraft, T.M., 1993. Trophic structure in open waters of the Marginal Ice Zone in the Scotia Weddell confluence region during spring (1983). Polar Biology 13, 389–397.

Klyausov, A.V., 1993. On the frontal zone near the northern boundary of sea ice area distribution in the Southern Ocean. Oceanology 33, 824–832.

Latogursky, V.I., Makarov, R.R., Maklygin, L.Y., Solyankin, E.V., Fedotov, A.S., 1990. Distribution and peculiarities of *Euphausia superba* Dana population structure in the area of the Weddell Gyre and adjacent waters. In: Solyankin, E.V. (Ed.), Investigations of the Weddell Gyre. Oceanographic Conditions and Peculiarities of the Development of Plankton Communities. VNIRO Publishers, Moscow, pp. 183–205 (in Russian).

Mackintosh, N.A., 1973. Distribution of post-larval krill in the Antarctic. Discovery Reports 36, 95–156.

Makarov, R.R., Sysoeva, M.V., 1983. Biological condition and distribution of *Euphausia superba* Dana in the Lazarev Sea and adjacent waters. In: Antarctic Krill. The Distribution Pattern and Environment (Collected papers). Legkaja i pishevaja promyshlennost Press, Moscow, pp. 110–117 (in Russian).

Makarov, R.R., Menshenina, L.L., Spiridonov, V.A., 1986. Methodological Recommendations for the Investigation of the ANTARCTIC Euphausiid Larvae. VNIRO Press, Moscow, pp. 1–104 (in Russian).

Makarov, R.R., Maslennikov, V.V., Menshenina, L.L., 1990. Frontal zones as ecological boundaries in the Antarctic waters. In: Solyankin, E.V. (Ed.), Investigations of the Weddell Gyre. Oceanographic Conditions and Peculiarities of the Development of Plankton Communities. VNIRO Press, Moscow, pp. 99–125 (in Russian).

Marr, J.W.S., 1962. The natural history and geography of the Antarctic krill (*Euphausia superba* Dana). Discovery Reports 32, 33–464.

Maruyama, T., Toyoda, H., Suzuki, S., 1982. Preliminary report on the biomass of macroplankton and micronekton collected with a Bongo net during the Umitaka Maru FIBEX cruise. Transactions of the Tokyo University of Fisheries 5, 145–153.

Maslennikov, V.V., 1980. Modern concepts on the large scale circulation of Antarctic waters and routes of mass drift of krill. In: Makarov, R.R. (Ed.), Biological Resources of the Antarctic Krill. VNIRO Press, Moscow, pp. 8–27 (in Russian).

Mizdalski, E., 1988. Weight and length data of zooplankton in the Weddell Sea in austral spring 1986 (ANT V/3). Berichte zür Polarforschung 55, 1–72.

Pakhomov, E.A., 2004. Salp/krill interactions in the eastern Atlantic sector of the Southern Ocean. Deep-Sea Research II, this issue [doi:10.1016/j.dsr2.2001.03.011].

Pakhomov, E.A., Froneman, P.W., 2004. Zooplankton dynamics in the eastern Atlantic sector of the Southern Ocean during the austral summer 1997/1998. Part 2. Grazing impact. Deep-Sea Research II, this issue [doi:10.1016/j.dsr2.2000.11.002].

Pakhomov, E.A., McQuaid, C.D., 1996. Distribution of surface zooplankton and seabirds across the Southern Ocean. Polar Biology 16, 271–286.

Pakhomov, E.A., Perissinotto, R., McQuaid, C.D., 1994a. Comparative structure of the macrozooplankton/micronekton communities of the Subtropical and Antarctic Polar Fronts. Marine Ecology Progress Series 111, 155–169.

Pakhomov, E.A., Grachev, D.G., Trotsenko, B.G., 1994b. Distribution and composition of macroplankton communities in the Lazarev Sea (Antarctic). Oceanology 33, 635–642.

Pakhomov, E.A., Verheye, H.M., Atkinson, A., Laubscher, R.K., Taunton-Clark, J., 1997a. Structure and grazing impact of the mesozooplankton community during late summer 1994 near South Georgia, Antarctica. Polar Biology 18, 180–192.

Pakhomov, E.A., Perissinotto, R., Froneman, P.W., McQuaid, C.D., 1997b. Energetics and feeding dynamics of *Euphausia superba* in the South Georgia region during the summer of 1994. Journal of Plankton Research 19, 399–423.

Pakhomov, E.A., Perissinotto, R., McQuaid, C.D., Froneman, P.W., 2000. Zooplankton structure and grazing in the Atlantic sector of the Southern Ocean in late austral summer 1993. Part 1. Ecological zonation. Deep-Sea Research I 47, 1663–1686.

Perissinotto, R., Pakhomov, E.A., 1998. The trophic role of the tunicate *Salpa thompsoni* in the Antarctic marine ecosystem. Journal of Marine Systems 17, 361–374.

Perissinotto, R., Pakhomov, E.A., McQuaid, C.D., Froneman, P.W., 1997. In situ grazing rates and daily ration of the Antarctic krill *Euphausia superba* feeding on phytoplankton at the Antarctic Polar Front and the Marginal Ice Zone. Marine Ecology Progress Series 160, 77–91.

Razouls, C., 1994. Manuel d'identification des principales espèces de copépodes pélagiques antarctiques et subantarctiques. Annales de l'Institut Océanographique 70, 3–204.

Robertson, A.A., Alexander, D.G.W., Miller, D.G.M., 1981. Modified collapsible opening and closing midwater trawls (RMT-8 and RMT-2). Fisheries Bulletin of South Africa 14, 103–113.

Siegel, V., Harm, U., 1996. The composition, abundance, biomass and diversity of the epipelagic zooplankton communities of the southern Bellinshausen Sea (Antarctic) with special reference to krill and salps. Archive of Fishery and Marine Research 44, 115–139.

Siegel, V., Skibowski, A., Harm, U., 1992. Community structure of the epipelagic zooplankton community under the sea-ice of the northern Weddell Sea. Polar Biology 12, 15–24.

Smetacek, V., 1998. The "merry-go-round ecosystems" of Antarctica: a study in stability. New Zealand Natural Sciences 23 (Suppl.), 189.

Solyankin, E.V., Sysoeva, M.V., Chvatsky, N.V., 1983. Wat dynamics and conditions for appearance of krill aggreg tions in the Lazarev Sea. In: Makarov, R.R. (Ed.), Antarct Krill. Peculiarities of Distribution and Environmen Legkaya and Pichevaya Promyshlennost Press, Moscov pp. 57–66 (in Russian).

Turner, D.R., Bertilsson, S., Fransson, A., Pakhomov, E 2004. The SWEDARP 97/98 marine expedition: overvie Deep-Sea Research II, this issue [doi:10.1016/j.dsr2 2003.08.006].

Voronina, N.M., 1962. On the dependence of the character c the boundary between Antarctic and Subantarctic pelagi zones on the meteorological conditions. Geophysica Monograph 7, 160–162.

Voronina, N.M., 1984. Pelagic Ecosystems of the Souther Ocean. Nauka Press, Moscow (in Russian).

Voronina, N.M., 1998. Comparative abundance and distribu tion of major filter-feeders in the Antarctic pelagic zone Journal of Marine Systems 17, 375–390.

Voronina, N.M., Kosobokova, K.N., Pakhomov, E.A., 1994 Composition and biomass of summer metazoan plankton i the 0–200 m layer of the Atlantic sector of the Antarctic Polar Biology 14, 91–95.

Witek, Z., Kittel, W., Czykieta, H., Zmijewska, M., Presler, E. 1985. Macrozooplankton in the southern Drake Passag and in the Bransfield Strait during BIOMASS-SIBEX (December 1983–January 1984). Polish Polar Research 6 95–115.

Wyrtki, K., 1960. The Antarctic Convergence and Divergence Nature 187, 581–582.

Zar, J.H., 1984. Biostatistical Analysis. Prentice-Hall, Engle wood Cliffs, NJ, p. 718.

ELSEVIER

Deep-Sea Research II 51 (2004) 2617–2631

DEEP-SEA RESEARCH
PART II

www.elsevier.com/locate/dsr2

Zooplankton dynamics in the eastern Atlantic sector of the Southern Ocean during the austral summer 1997/1998—Part 2: Grazing impact

E.A. Pakhomov*, P.W. Froneman

Southern Ocean Group, Department of Zoology and Entomology, Rhodes University, P.O. Box 94, Grahamstown 6140, South Africa

Abstract

Zooplankton grazing impact using the gut fluorescence technique was investigated in the top 200 m water layer along the 6°E meridian between 49°50′ and 60 25′S at six Biostations during a Scandinavian South African Joint Global Ocean Flux Study (December 1997–January 1998) on board the *SA Agulhas*. Copepods were found to be the most conspicuous grazers along the entire transect, generally accounting for ≈40% of total zooplankton grazing. Pelagic pteropods, *Limacina helicina* and *Clio sulcata*, were the second most important grazers within the Seasonal Ice Edge (SIE) region, while the tunicate *Salpa thompsoni* and euphausiids, mainly *Euphausia superba* and *E. frigida*, were the second and third most important consumers of the phytoplankton production within the Winter Ice Edge (WIE) and Antarctic Polar Front (APF) regions. The overall ingestion rates of the zooplankton community ranged from 24 to 277 mg C m^{-2} day^{-1}. The lowest and highest ingestion rates were recorded within the SIE and APF regions. The zooplankton grazing impact was low within the SIE region accounting for <10% of daily primary production. The highest phytoplankton consumption rate (56% of daily primary production) was observed in the WIE region, while the APF region was characterized by modest (23–33%) grazing impact of zooplankton.
© 2004 Elsevier Ltd. All rights reserved.

1. Introduction

The Marginal Ice Zone (MIZ) is one of the most dynamic environments in the Southern Ocean (Smith et al., 1988; Sullivan et al., 1993). It is now recognized that phytoplankton blooms associated with the seasonal ice retreat contribute substantially to the biochemical cycling in the region south of the Antarctic Polar Front (Smith and Nelson, 1986; Savidge et al., 1996). The release of epontic cells during the ice melt combined with increased water column stability and high nutrient and trace metal concentrations are thought to be vital in triggering phytoplankton blooms in regions of retreating ice (Sakshaug, 1989; de Baar

*Corresponding author. Present address: Department of Earth and Ocean Sciences, University of British Columbia, 6339 Stores Road, Vancouver, BC, Canada, V6T 1Z4 and Zoology Department, Faculty of Science and Technology, University of Fort Hare, Private Bag X1314, Alice 5700, South Africa. Tel.: +1 604 827 6654; fax: +1 604 822 6088.

E-mail address: epakhomov@eos.ubc.ca (E.A. Pakhomov).

0967-0645/$ - see front matter © 2004 Elsevier Ltd. All rights reserved.
doi:10.1016/j.dsr2.2000.11.002

et al., 1990; Priddle et al., 1992). It has been suggested that zooplankton grazing may at times control phytoplankton composition and the development of such phytoplankton blooms (Smetacek et al., 1990; Dubischar and Bathmann, 1997; Perissinotto and Pakhomov, 1998). The factors (physical, chemical and biological) controlling phytoplankton production and subsequent carbon partitioning within the pelagic ecosystem are of particular interest in determining the total carbon budget of the Southern Ocean. During a collaborative Scandinavian/South African Joint Global Ocean Flux Study (JGOFS) carried out in the eastern Atlantic sector of the Southern Ocean, we conducted zooplankton grazing experiments to determine the role of herbivores in controlling phytoplankton growth. Three major regions along the 6°E meridian, the Spring Ice Edge (SIE, ≈60°S), the Winter Ice Edge (WIE, ≈56°S) and the Antarctic Polar Front (APF, ≈50°S) regions, were targeted for grazing measurements (Froneman et al., 1998). The study regions and techniques employed were similar to those of previous studies conducted along the 6°W meridian during the SO-JGOFS-*Polarstern* cruise in October/November 1992 (Dubischar and Bathmann, 1997) and along the Greenwich Meridian during the second South African Antarctic Marine Ecosystem Study on board of the *SA Agulhas* in January 1993 (Froneman et al., 2000). A comparison of results obtained in the different regions could, therefore, be made.

2. Materials and methods

Sampling was conducted during December 1997–January 1998 along the 6°E meridian between 49°50′S and 60°25′S aboard the *SA Agulhas* (voyage 86). In total, six 36 h Biostations were occupied (Turner et al., 2004). Three Biostations within the SIE centred at 60°S were conducted approximately 20 nautical miles apart, a single Biostation was occupied within the WIE at 56°30′S and two Biostations were carried out within the region of the APF between 51°S and 49°50′S (Pakhomov and Froneman, 2004). At each Biostation, tows were made at 4 h intervals. In addition to 36 h Biostations, several gut evacuation ra and gut pigment degradation experiments we conducted at stations along the 6°E meridia (Pakhomov and Froneman, 2004). Detailed in formation on sampling procedures and statio positions are presented in Pakhomov and Fron man (2004). For the purpose of the grazing impac calculations, zooplankton abundance and bio mass values were averaged over the 24 h cycl and expressed as ind m^{-2} and mg DW m^{-2}, re spectively.

Following JGOFS-protocols (JGOFS, 1989) zooplankton ingestion rates were determined usin the gut fluorescence technique (Mackas an Bohrer, 1976). After each tow, individuals of th most abundant herbivorous species from th 0.5 mm mesh sample were taken for grazin studies. For the gut pigment analyses, the mos abundant copepodite stages of copepods wer selected. For euphausiids, furcilia, juveniles, sub adults and adults were studied separately, whil for salps specimens of total length size classes <1 1–2, 2–3, 3–5, 6–7 and 7–13 cm were analyzed Animals for measurements of gut pigment conten were sorted immediately after capture (pteropods juvenile to adult euphausiids and salps) or froze in liquid nitrogen (euphausiid furcilia and cope pods) and sorted within 1–2 h after capture Specimens were placed in plastic centrifuge tube with 8 ml or in case of larger salps in jars with up to 50 ml of 90% acetone and stored at −20 °C for ≈24 h. Gut pigments were extracted from a single salp or pteropod or juvenile to adult euphausiid, while 3–10 copepods or euphausiid furcilia were combined per tube. Five to ten replicates (tubes) per species were generally used. After centrifugation (5000 rpm), chlorophyll-*a* and phaeopigments, were measured with a Turner Designs fluorometer, before and after acidification (Mackas and Bohrer, 1976). Gut contents were expressed in terms of pigment equivalents per individual and calculated according to Strickland and Parsons (1968) as modified by Conover et al. (1986). When the chlorophyll-*a*: phaeopigment ratio of the gut content was higher than 0.25, total pigment levels were corrected according to Baars and Helling (1985). Background fluorescence levels, determined for animals starved for 24–36 h in filtered

seawater with charcoal particles, were subtracted from gut pigment data of all species investigated.

To estimate the gut evacuation rate (k), freshly caught animals were gently placed into a 20 l plastic bucket filled with 0.2 μm filtered seawater to which non-fluorescent charcoal powder ($\leqslant 100$ μm, diameter) was added to keep the animals under continuous feeding conditions (Willason and Cox, 1987; Perissinotto, 1992; Perissinotto and Pakhomov, 1996). Containers with experimental animals were kept in darkness on deck at ambient temperature. The duration of these incubations ranged from 40 min to 8 h and the decline in gut content was monitored at intervals of 5–20 min for the first hour and 0.5–2 h thereafter. Gut evacuation rate (k, h^{-1}) was derived from the slope of the regression of the natural logarithm of gut pigments versus time (Dam and Peterson, 1988) following recommendations of Perissinotto and Pakhomov (1996).

Independent measurements of gut pigment loss were made to estimate the gut degradation efficiency. In each experiment, animals were first allowed to empty their gut of pigments for 4–24 h in filtered seawater with charcoal powder. One to ten animals, depending on taxonomic group and size, were then incubated for 1–2 h in 1 l bottles filled with natural seawater. A two-compartment pigment budget approach was employed by comparing the decrease in pigment content in the grazing bottles with the increase in gut pigment levels of animals incubated in these bottles (Lopez et al., 1988; Mayzaud and Razouls, 1992; Perissinotto, 1992).

Daily ingestion rates (I, ng (pigm) $ind^{-1} d^{-1}$) were estimated from the relation: $I = kG/(1-b')$, where G is an integrated value (over a 24 h period) of gut pigment content (ng (pigm) ind^{-1}), k is the gut evacuation rate constant (h^{-1}) and b' is a non-dimensional index of the loss of pigment during digestion (Wang and Conover, 1986; Perissinotto, 1992). As direct estimates of b' were not available for all species, for selected species values were derived from the literature or an average value of 0.5 was assumed (Mayzaud and Razouls, 1992; Perissinotto, 1992).

To estimate community grazing impact, zooplankton abundance data were combined with individual ingestion rates. To convert chlorophyll-*a* concentration into autotrophic carbon an average chlorophyll-*a*: carbon ratio of 50 was employed (Atkinson, 1996). Areal chlorophyll-*a* biomass and primary production rates in the euphotic zone (depth of 1% of surface irradiance) were obtained by trapezoidal integration (Froneman et al., 2004). The grazing impact expressed as mg (pigm) $m^{-2} day^{-1}$ and mg C $m^{-2} day^{-1}$ was then expressed as a percentage of integrated phytoplankton standing stock or the daily primary production removed per day.

3. Results

3.1. Zooplankton structure

Detailed description of the zooplankton species composition, abundance and biomass along the 6°E meridian is presented elsewhere (Pakhomov and Froneman, 2004). Here, only a brief summary of zooplankton densities at the six Biostations is presented. Total zooplankton abundances and biomass ranged from 2981 to 39 080 ind m^{-2} and from 1621 to 13 235 mg DW m^{-2} (Table 1). Within the SIE region, zooplankton densities were an order of magnitude lower than in the WIE and APF regions (Table 1; Fig. 1). Species used for grazing measurements generally accounted for 43–51% of total zooplankton abundance within the SIE region. Their contribution was higher (55–67%) within the APF region, while they accounted for >94% of total zooplankton abundance in the WIE region. In biomass terms, the highest contribution of species used for grazing studies (89%) was again recorded in the WIE region. This followed by the SIE (30–76%) and APF (35%) regions (Table 1; Fig. 1). Carnivorous species accounted for the majority >80% of remaining densities (Pakhomov and Froneman, 2004). Among the species used for grazing studies, copepods dominated zooplankton abundances and biomass (Fig. 1), with exception of Biostations 1 (SIE) and 4 (WIE). Here, euphausiids, *Thysanoessa macrura* and *Euphausia superba* together with *E. frigida*, accounted for 55% and 72% of total zooplankton standing stock (Table 1). Pteropods

Table 1
Numerical abundance (A) and biomass (B) estimates (both in % of the total) of major species of the mesozooplankton community
Biostations conducted in the Atlantic sector of the Southern Ocean using a Bongo net (0–200 m) during December 1997–January 19

Taxa	Biostations											
	1 (SIE)		2 (SIE)		3 (SIE)		4 (WIE)		5 (APF)		6 APF)	
	A	B	A	B	A	B	A	B	A	B	A	B
Calanoides acutus	5.6	1.8	6.1	1.5	6.5	3.2	0.8	0.6	1.4	1.0	0.7	0.5
Calanus propinquus	6.5	3.8	13.4	9.4	12.5	7.3	3.2	4.2	—	—	—	—
Clausocalanus/Ctenocalanus	1.3	0.1	0.7	<0.1	0.5	<0.1	8.1	0.4	29.7	1.6	27.0	1.5
Rhincalanus gigas	5.8	8.5	10.1	11.1	4.9	10.8	0.2	0.6	3.8	11.9	3.2	10.5
Metridia spp.	14.8	1.6	9.6	0.8	19.5	2.9	0.4	0.2	2.8	1.3	5.3	2.7
Pleuromamma spp.	—	—	—	—	—	—	—	—	0.5	0.3	0.5	0.3
Oithona spp.	5.7	0.1	0.4	<0.1	0.9	<0.1	78.5	2.1	13.5	0.4	25.8	0.7
Euphausia superba	<0.1	0.6	<0.1	0.5	<0.1	0.3	0.2	56.5		—	—	-
E. frigida	—	—	<0.1	<0.1	<0.1	<0.1	0.9	15.7	<0.1	0.4	0.7	1.3
E. triacantha	—	—	—	—	—	—	—	—	<0.1	0.5	<0.1	0.4
Thysanoessa macrura	6.9	54.6	0.4	1.7	0.6	4.4	0.4	1.2	0.5	0.2	-	-
Thysanoessa spp.	—	—	—	—	—	—	—	—	0.1	1.1	0.2	1.9
Euphausia furcilia	3.5	0.8	1.3	0.3	2.9	1.6	1.1	1.1	1.8	1.9	2.4	2.8
Clio sulcata	0.2	4.1	0.2	4.4	0.3	13.1	<0.1	2.6	—	-		
Limacina helicina	0.2	0.1	0.3	0.1	0.3	0.1	<0.1	<0.1	0.3	0.2	0.8	0.5
Salpa thompsoni	—	—	—	—	0.6	6.8	0.2	3.5	0.2	14.0	0.2	11.9
Other zooplankton	49.5	23.9	57.4	70.1	50.4	49.4	5.9	11.3	45.3	65.2	33.1	65.0
Total abundance (ind m^2)	3995		3581		2981		37,270		33,020		39,080	
Total biomass (mg DW m^2)		3268		3819		1621		13,118		11,565		13,23

SIE: Spring Ice Edge region; WIE: Winter Ice Edge region; APF: Antarctic Polar Front region.

and tunicates were important contributors only within the SIE and the APF regions, respectively (Fig. 1).

3.2. Ingestion rates

In all regions investigated, the majority of copepod, euphausiid and pteropod species used in grazing studies demonstrated pronounced diel variability in their gut pigment contents (Figs. 2–4). Only *Thysanoessa* spp. and *Salpa thompsoni* (all size-classes) did not display clear diel pattern in gut pigments (Figs. 3 and 5). In total, 50 gut evacuation rate measurements for 20 species or size groups were conducted. Gut evacuation rate constants (k) varied between 0.39 and 2.99 h^{-1} for copepods, between 0.29 and 0.88 h^{-1} for euphausiids and between 0.25 and 0.95 h^{-1} for salps (Table 2). An average k value of 0.25 h^{-1} for pteropods, determined during the January 1995 in the Lazarev Sea (E.A. Pakhomov unpublished), was used for the ingestion rate calculations. Gut pigment destruction rates were determined for 10 species on 19 occasions (Table 3). Generally, pigment destruction rates were highest in copepods, ranging from 38% to 89% of the total pigment ingested, and lowest in salps, only 4% (Table 3). In situ individual ingestion rates of species used in grazing studies are summarized in Table 4. The lowest ingestion rates (29–32 ng (pigm) $ind^{-1} day^{-1}$) were determined for euphausiid furcilia and the cyclopoid copepod, *Oithona* spp. Ingestion rates of copepods, euphausiids *Thysanoessa* spp., *E. frigida* and juvenile *E. superba* generally varied between 100 and 500 ng (pigm) $ind^{-1} day^{-1}$ (Table 4). Daily food intake of larger euphausiids, including subadults and adults of *E. superba* and *E. triacantha*, the pteropod *Limacina helicina* and the salp *S. thompsoni* with total length <3 cm

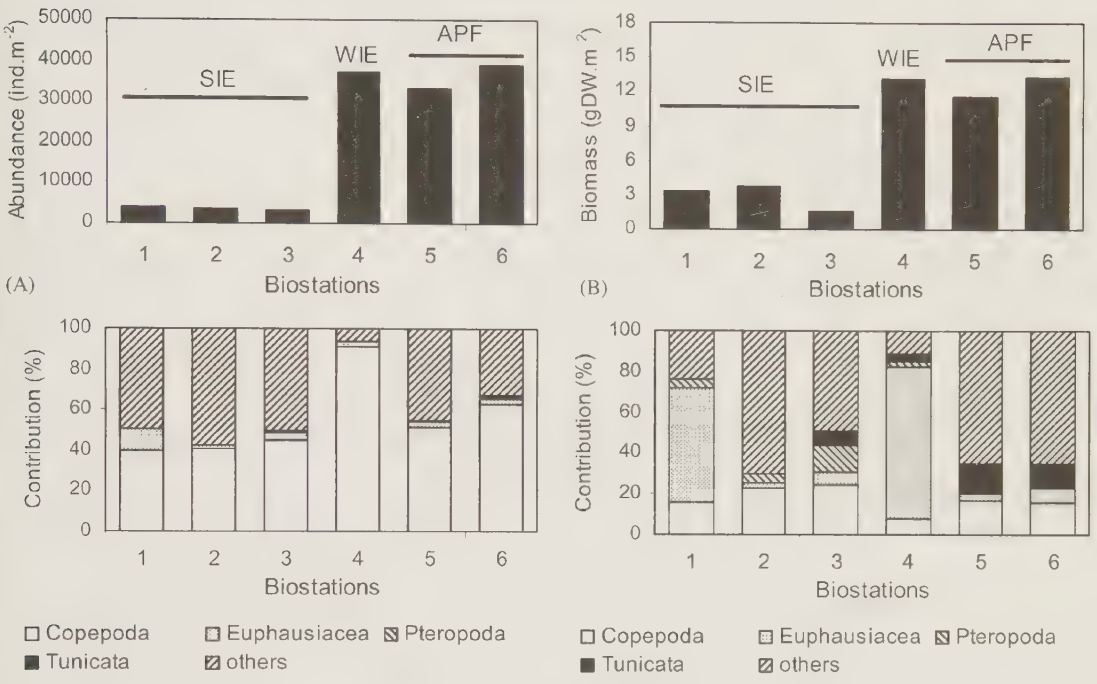

Fig. 1. Zooplankton abundance (A), biomass (B) and composition at Biostations conducted along the 6°E meridian in the eastern Atlantic sector of the Southern Ocean during December 1997–January 1998. SIE: Spring Ice Edge region; WIE: Winter Ice Edge region; APF: Antarctic Polar Front region.

ranged from 704 to 12 512 ng (pigm) $ind^{-1} day^{-1}$. Larger salps (>3 cm) and the pteropod *Clio sulcata* had the highest individual ingestion rates varying between 13 895 and 124 923 ng (pigm) $ind^{-1} day^{-1}$ (Table 4).

3.3. Grazing impact

Abundance data of each herbivorous species combined with their individual ingestion rates at each Biostation yielded community ingestion rates ranging from 0.483 to 5.542 mg (pigm) $m^{-2} day^{-1}$ or between 24 and 277 mg C $m^{-2} day^{-1}$ (Table 5). The lowest grazing rates were recorded within the SIE region, while one order of magnitude higher rates were determined within the WIE and APF regions (Fig. 6). With the exception of the SIE stations, where the contribution of pteropods and copepods was equal (on average 45% for each group), copepods dominated (>60%) total community consumption (Table 5; Fig. 6). The contribution of euphausiids was substantial (up to 22%) only at Biostation 1 in the SIE, while salps accounted for 19–32% of total community ingestion within the WIE and APF regions (Fig. 6). Using data on chlorophyll biomass and primary production rates presented elsewhere (Froneman et al., 2004) and summarized in Table 5, daily grazing impact varied between 0.9% and 15.7% of the phytoplankton standing stock, or between 3.3% and 51.4% of the daily primary production (Table 5; Fig. 6). The highest and lowest grazing impact was recorded within the WIE and the SIE regions, respectively.

4. Discussion

Over the past decade, a large number of single species grazer (mainly copepods and euphausiids) studies have been conducted in the Southern Ocean south of the APF (for example, Drits and Semenova, 1989; Huntley and Escritor, 1991, 1992; Atkinson et al., 1992, 1996; Drits and

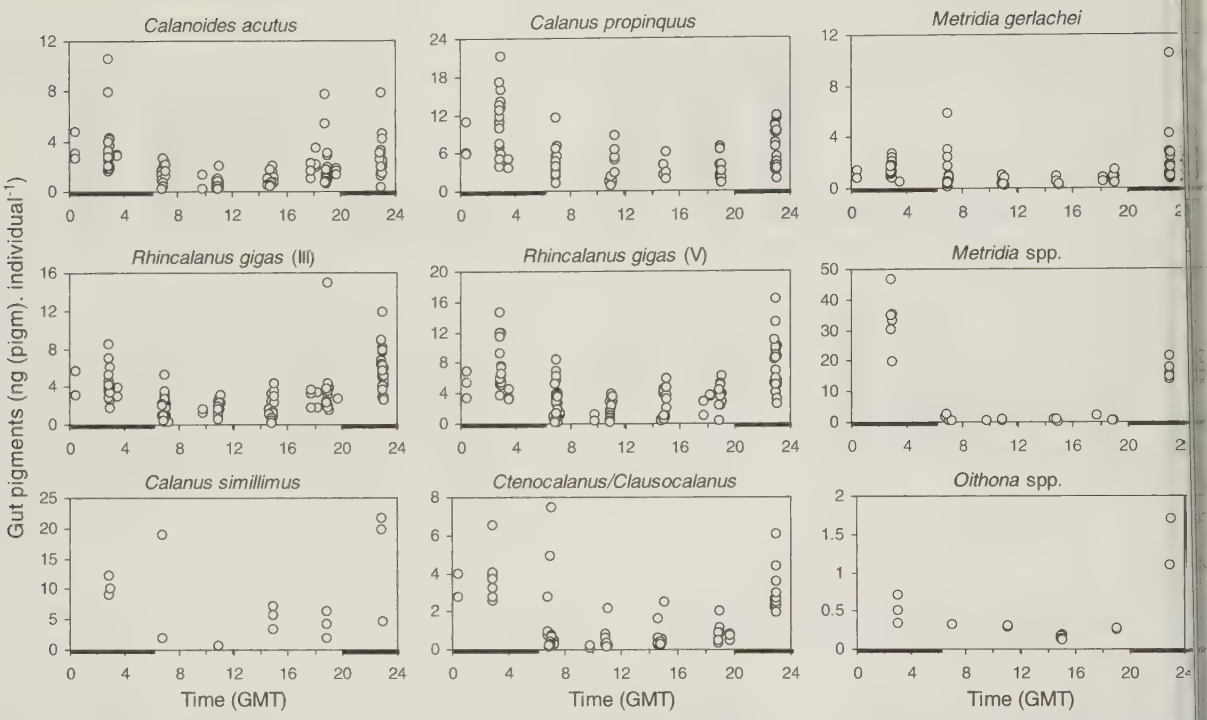

Fig. 2. Diel pattern of gut pigment contents of the copepods along the 6° E meridian in the eastern Atlantic sector of the Souther Ocean during December 1997 January 1998. Data from all Biostations pooled to show diel pattern. The period of darkness is indicate by thickening of the horizontal axis.

Pasternak, 1993; Atkinson and Shreeve, 1995; Pakhomov et al., 1997a; Perissinotto et al., 1997; Perissinotto and Pakhomov, 1998). Only a few studies have attempted to estimate the grazing impact of the entire mesozooplankton community (e.g. Ward et al., 1995; Dubischar and Bathmann, 1997; Froneman et al., 1997, 2000; Pakhomov et al., 1997b). To our knowledge, therefore, this study represents one of the most comprehensive data sets yet collected in the Antarctic zone, as the majority of the herbivorous groups of mesozooplankton were studied simultaneously using the same technique. However, whilst a similar technique was used to estimate impact on the phytoplankton standing stock, the grazing budget obtained in our study should be treated with caution. Despite all efforts to include the entire copepod community, we most likely underestimated the grazing impact of small calanoid and cyclopoid copepods due to sampling gear employed (Fransz and Gonzalez, 1997; Pakhomov and Froneman, 2004). Previous studies hav shown that small mesozooplankton may accoun for up to 50% of total grazing while contributing <10% to the total copepod stock (Schnack et al. 1985; Morales et al., 1991; Atkinson et al., 1996 Head et al., 1999). As a consequence, grazing values obtained in our study correspond mainly to the larger fraction of the zooplankton community (Pakhomov and Froneman, 2004).

In general, gut pigment contents, gut evacuation and gut pigment destruction rates, and overall individual ingestion rates of the copepods, krill and salps during this study agree with similar measurements in other studies in the Atlantic sector of the Southern Ocean (Drits and Semenova, 1989; Huntley and Escritor, 1991, 1992; Atkinson et al., 1992, 1996; Drits and Pasternak, 1993; Atkinson and Shreeve, 1995; Ward et al., 1995; Pakhomov and Perisinotto, 1996; Dubischar and Bathmann, 1997; Froneman et al., 1997, 2000; Pakhomov et al., 1997a, b; Perissinotto et al., 1997;

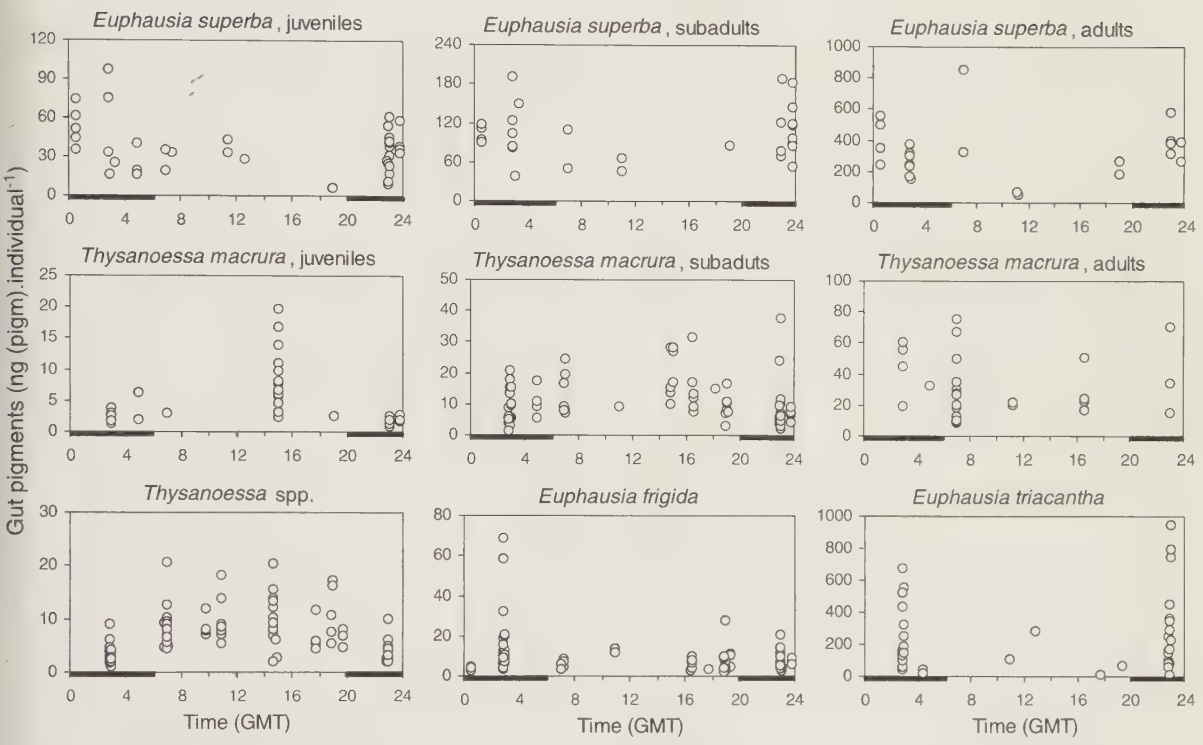

Fig. 3. Diel pattern of gut pigment contents of the euphausiids along the 6°E meridian in the eastern Atlantic sector of the Southern Ocean during December 1997–January 1998. Data from all Biostations pooled to show diel pattern. The period of darkness is indicated by thickening of the horizontal axis.

Perissinotto and Pakhomov, 1998). Considering the enormous spatio-temporal variability in the measured rates and parameters, a detailed comparison between our estimates and those in the literature was not attempted here.

It is worth nothing that the ingestion rates of many zooplankton species increased from south to north. This was particularly evident for the copepods, although a similar trend was also observed in the euphausiids and the salps (Table 4). This trend may reflect two major processes: an increase in food availability from south to north (particularly particle concentration and size composition changes) and/or in feeding activity of the zooplankton. Total chlorophyll-*a* concentrations were the highest (generally $>0.5\,mg\,m^{-3}$) at stations occupied in the SIE and APF regions (Froneman et al., 2004). This does not support an increase in food concentration from south to north. The contribution of microphytoplankton (cells $>20\,\mu m$), however, was the highest (average 73% of total) within the SIE region. It decreased dramatically (to 28%) within the WIE region and increased again (to 49%) within the APF region (Froneman et al., 2004). The biomass of the small ($<20\,\mu m$) phytoplankton fraction, which is considered to be the main food source of copepods (Fortier et al., 1994), thus displayed the same trend as ingestion rates increasing on average from $11.2\,mg\,m^{-2}$ in the SIE region to $20.8\,mg\,m^{-2}$ in the APF region (Froneman et al., 2004). These findings suggest that copepod feeding may be constrained by the phytoplankton size structure in the SIE and APF regions and by food availability within the SIE region.

Although the gut pigment contents of copepods did not show significant differences between the three regions investigated ($p<0.05$), the gut turnover time ($1/k$) decreased substantially from south

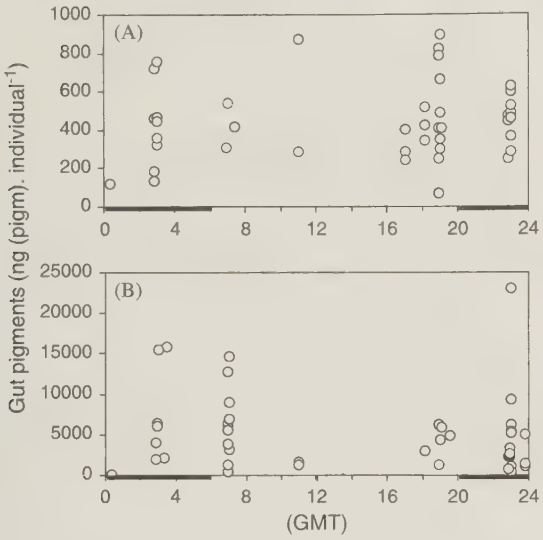

Fig. 4. Diel pattern of gut pigment contents of *L. helicina* (A) and *C. sulcata* (B) along the 6°E meridian in the eastern Atlantic sector of the Southern Ocean during December 1997 January 1998. Data from all Biostations pooled to show diel pattern. The period of darkness is indicated by thickening of the horizontal axis.

to north (see Table 2). This provides evidence that feeding activity of copepods increased along the transect likely reflecting the increase in average water temperature in the top 200 m between the SIE and APF regions (Froneman et al., 1998). Alternatively, the decrease in gut turnover time may also be associated with the seasonal succession of mesozooplankton as the population structure of copepods within the SIE, WIE and APF regions differed substantially (Pakhomov and Froneman, 2004). Although the euphausiids and salps also showed a substantial increase in their gut pigment contents from south to north, the differences were not significant ($p > 0.05$). Since the same evacuation rate constant was employed in calculations in both regions, it is evident that the increase in the ingestion rates was a function of the increase in gut pigment content. This may indicate that ingestion rates of euphausiids and salps may be biased, as they do not take into account the effect of temperature on metabolic activity. On the other hand, it has been shown that changes in ingestion rates of large metazoan grazers occur in response to increased food availability.

The ingestion rate estimates of the tw most abundant pteropod species *L. helicina* a *C. sulcata* should be discussed separately as thi were obtained for the first time in this study. T only available estimate of *Limacina* sp. ingestio rate was obtained in a study conducted around t sub-Antarctic Prince Edward Islands (Perissinott 1992). The average daily ration of the 0.2 mg d wt specimen of *Limacina* sp. in this environme was 161 ± 110 ng (pigm) ind^{-1} day^{-1} (rang 31–302 ng (pigm) ind^{-1} day^{-1}) (Perissinott 1992). During our study, the ingestion rate *L. helicina* was at least one-order magnitud higher, 2103 ng (pigm) ind^{-1} day^{-1}. This is like the result of the average individual dry mass *L. helicina* (mean 2.2 mg dry wt ind^{-1}) during ou study being at least one-order of magnitud higher. To our knowledge there are no simila estimates of ingestion rates for *C. sulcata* in th literature. Its ingestion rates were extremely hig and were only comparable to daily ratio estimated for the 3–5 cm long salp *S. thompson* (Dubischar and Bathmann, 1997; Perissinotto an Pakhomov, 1998; this study). These finding underline the importance of this group in th calculation of the total grazing budget in th Antarctic zone, as pelagic pteropods are alway present in background numbers in the regio south of the APF (Piatkowski, 1987; Pakhomov 1989; Pakhomov and Froneman, 2004). Thei density may, however, increase dramatically a locally pteropods can be extremely numerous. Fo example, densities of >1 ind m^{-3} for *C. sulcat* have been documented within the seasonal MIZ and *Limacina* spp. concentrations >100 ind m^{-} were regularly observed around the Antarcti islands (Tesch, 1913; Atkinson et al., 1996 Pakhomov et al., 1997b).

Previous studies suggested that copepods are regarded as the most important contributors to the total community grazing in both hemispheres due to their numerical domination in the total zoo-plankton stock (Morales et al., 1991; Ward et al., 1995; Zhang et al., 1995; Atkinson et al., 1996; Froneman et al., 1997, 2000; Pakhomov et al., 1997b; Head et al., 1999). During our study, copepods were dominant grazers ($\geq 60\%$ to total grazing) only within the WIE and APF regions.

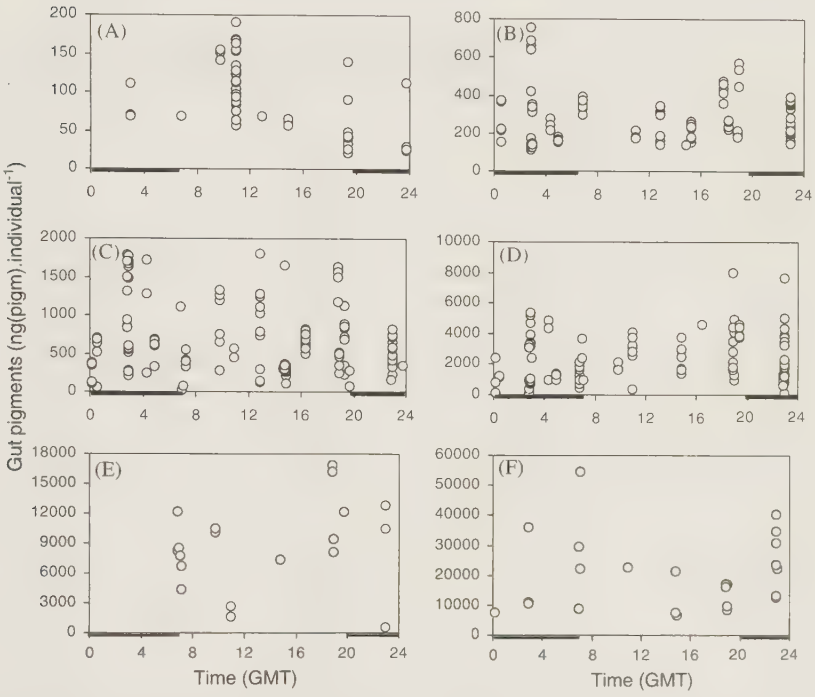

Fig. 5. Diel pattern of gut pigment contents of the salp *S. thompsoni* (different sizes) along the 6°E meridian in the eastern Atlantic sector of the Southern Ocean during December 1997–January 1998. Data from all Biostations pooled to show diel pattern. The period of darkness is indicated by thickening of the horizontal axis. (A) <10 mm; (B) 10–20 mm; (C) 20–30 mm; (D) 30–50 mm; (E) 60–70 mm; (F) >70 mm.

Due to their relatively low abundance within the SIE region, the overall copepod contribution to total grazing was ≤50% (Fig. 6). In this region, pteropods on average accounted for ≈50% of zooplankton grazing impact. Only, at the southern station (Biostation 1) did the euphausiid *T. macrura* contribute substantially (≈20%) to total daily grazing. Within the WIE and APF region, the second most important grazer was the unicate *S. thompsoni* accounting for 20–35% of total phytoplankton consumption (Fig. 6).

It is generally accepted that in the Antarctic one, particularly during phytoplankton blooms, ooplankton grazing impact accounts for ≪10% f the primary production (Atkinson et al., 1996). ubstantial community grazing impact (50–90% f daily primary production) has only been ecorded in the shelf regions of Antarctic islands, uch as South Georgia, outside periods of ex-ensive phytoplankton blooms (Ward et al., 1995; akhomov et al., 1997b). Under conditions when zooplankton were able to control phytoplankton biomass in the oceanic waters of the Antarctic zone, large metazoan grazers, such as *E. superba* and *S. thompsoni*, generally dominated (Drits and Semenova, 1989; Drits and Pasternak, 1993; Pakhomov et al., 1997a; Perissinotto et al., 1997; Perissinotto and Pakhomov, 1998).

In this study, the grazing impact of zooplankton on daily primary production was low (generally <10%) within the SIE region and substantial (25–50%) in the regions north of it. Low grazing impact estimated within the SIE region agrees well with previous estimates in the same area during austral spring (<1% of daily primary production, Dubischar and Bathmann, 1997) and summer (range 4–25%, mean 10.5%, Froneman et al., 1997, 2000), and in the ice-edge zone of the Bellingshausen Sea during early summer (<8%, Atkinson and Shreeve, 1995). The results obtained here, therefore, provide further support to the notion that copepod grazing within the MIZ is not

Table 2
Gut evacuation rate constant (k) of zooplankton during December 1997 January 1998 in the Atlantic sector of the Southern Ocea

Species	Region	Station No	k (h^{-1})	R^2
Calanoides acutus	SIE	D092	1.1608	0.660
	SIE	D148	1.7280	0.735
	APF	D300	1.8837	0.750
Calanus propinquus	SIE	D094	1.2333	0.836
	SIE	D117	1.2484	0.874
	SIE	D130	0.9183	0.688
	SIE	D142	1.3621	0.354
	SIE	D168	1.3241	0.863
	WIE	D235	1.3661	0.625
	WIE	D249	2.3768	0.854
Ctenocalanus spp.	APF	D296	2.9928	0.295
Rhincalanus gigas, III	SIE	D092	0.6497	0.743
	APF	D296	1.6773	0.395
	APF	D302	2.1606	0.797
	APF	D331	1.9509	0.829
Rhincalanus gigas, V	SIE	D092	0.8732	0.701
	SIE	D108	0.6426	0.217
	SIE	D142	0.6656	0.611
	SIE	D169	1.0989	0.765
	APF	D296	1.2607	0.398
	APF	D302	0.5167	0.686
	APF	D319	1.2576	0.772
	APF	D331	1.0913	0.907
Metridia gerlachei	SIE	D094	1.7943	0.283
	SIE	D102	0.3943	0.455
	SIE	D148	1.5493	0.742
	SIE	D169	1.6954	0.512
	WIE	D249	1.3340	0.414
Metridia spp.	APF	D300	1.4144	0.901
	APF	D319	1.3966	0.534
	APF	D346	2.1252	0.502
Pleuromamma spp.	APF	D331	1.1856	0.859
Euphausia frigida	WIE	D249	0.2918	0.214
Euphausia triacantha	APF	D302	0.8836	0.527
Euphausia superba, juveniles	WIE	D229	0.5030	0.666
Euphausia superba, subadults	WIE	D229	0.5538	0.902
Euphausia superba, adults	WIE	D229	0.4182	0.504
	WIE	D231	0.3784	0.638
Thysanoessa macrura, juveniles	SIE	D181	0.8702	0.496
Thysanoessa macrura, subadults	SIE	D095	0.3827	0.512
	SIE	D108	0.3899	0.241
	WIE	D249	0.8504	0.274
Thysanoessa spp., subadults	APF	D346	0.7371	0.527
Salpa thompsoni, <1 cm	APF	D347	0.9538	0.856
Salpa thompsoni, 1–2 cm	SIE	D054	0.3026	0.854
	SIE	D168	0.2919	0.911
	APF	D335	0.5284	0.774
Salpa thompsoni, 2–4 cm	APF	D335	0.3388	0.717
	APF	D347	0.5294	0.859
Salpa thompsoni, 5–7 cm	APF	D347	0.2511	0.526

SIE: Spring Ice Edge region; WIE: Winter Ice Edge region; APF: Antarctic Polar Front region.

Table 3
Pigment destruction rates of zooplankton during December 1997–January 1998 in the eastern Atlantic sector of the Southern Ocean identified using the two-compartment (phytoplankton and grazer) pigment budget approach

Species	Region	Station No	Percentage of pigments destroyed		
			Mean (±SD)	Range	*n*
Calanoides acutus	SIE	D121	79.2±6.2	74.9–83.6	2
	SIE	D153	82.8±6.8	75.6–89.2	3
	APF	D300	85.4±10.6	77.9–92.9	2
	APF	D302	88.7±5.5	85.1–95.1	3
Calanus propinquus	SIE	D121	77.2±4.3	72.2–80.1	3
	SIE	D130	47.4	—	1
	WIE	D249	71.6±6.8	66.8–76.5	2
Ctenocalanus spp.	APF	D322	86.5±0.4	86.3–86.8	2
Rhincalanus gigas	SIE	D121	87.0±3.6	83.6–91.5	4
	SIE	D130	38.2	—	1
	APF	D300	77.6±18.9	55.9–90.1	3
	APF	D302	59.0±32.7	35.8–82.1	2
	APF	D322	85.5±3.0	81.9–87.6	3
Metridia gerlachei	SIE	D153	62.2±8.2	53.3–73.1	4
Metridia spp.	WIE	D249	67.4±3.3	65.0–69.7	2
Euphausia frigida	WIE	D249	35.8±50.5	0–71.5	2
Euphausia superba	WIE	D231	19.9±28.6	0–84.0	12
Thysanoessa macrura	SIE	D108	80.1±22.9	45.9–94.1	4
Salpa thompsoni, 1–2 cm	APF	D300	4.0	—	1

SIE: Spring Ice Edge region; WIE: Winter Ice Edge region; APF: Antarctic Polar Front region.

sufficient to limit the development of phytoplankton blooms (Lancelot et al., 1993; Atkinson and Shreeve, 1995; Froneman et al., 1997).

In a similar study conducted along the Greenwich Meridian during January 1993, zooplankton grazing impact could reach 89% of daily primary production in the APF region (Froneman et al., 2000) and exceeded 100% of primary production in the southern part of the Antarctic Circumpolar Current in October/November 1992 (Dubischar and Bathmann, 1997). It should be noted that on both occasions chlorophyll-*a* concentrations $\leqslant 0.5\,\mathrm{mg\,m^{-3}}$ and primary production rates $<400\,\mathrm{mg\ C\,m^{-2}\,day^{-1}}$ were observed (Bathmann et al., 1997; Pakhomov et al., 2000). This suggests that low primary production rates coupled with high grazing pressure appeared to constrain phytoplankton biomass in these regions. In our study, the high grazing pressure recorded in the WIE region was largely the result of high densities of copepods, particularly *Oithona* species, the Antarctic krill and salps (Table 1). Furthermore, in this region the herbivorous zooplankton overwhelmingly dominated total zooplankton standing stock both numerically and by biomass. This region also coincided with the lowest phytoplankton standing stock and primary production levels (Froneman et al., 2004). Indeed, if maximum density values of both Antarctic krill and salps were used to calculate the total grazing impact (Pakhomov, 2004), the overall metazoan grazing may exceed total daily primary production. Furthermore, microzooplankton grazing has been suggested as a major sink of primary production in the Southern Ocean (e.g. Froneman and Perissinotto, 1996a, b). Although, microzooplankton grazing measured in parallel to our study never exceeded 11% of daily primary production (Froneman et al., 2004), the above findings suggest that the phytoplankton community could be constrained by zooplankton in this region (Pakhomov, 2004). If the same could be applied to the APF region, the total grazing impact would increase to $\approx 50\%$ of primary production. This

Table 4
Individual daily ingestion rates (ng (pigm) $ind^{-1}day^{-1}$) of the most abundant zooplankton species estimated at Biostations using th gut fluorescence technique in the eastern Atlantic sector of the Southern Ocean during Dec 1997–Jan 1998

Species	SIE				WIE	APF		Biostations
	1	2	3	1–3	4	5	6	4–6
Copepoda								
Calanoides acutus	185.6	271.2	264.0	—	—	266.5	321.9	—
Calanus propinquus	318.0	199.3	543.5	—	577.3	—	—	
Calanus simillimus	—	—	—	—	—	—	391.9	
Clausocalanus spp.	—	—	—	266.2	—	—	—	
Ctenocalanus spp.	—	—	—	—	—	151.8	211.5	—
Rhincalanus gigas, III	122.2	192.8	329.5	—	—	456.2	407.2	—
Rhincalanus gigas, V	163.8	160.6	388.2	—	—	208.8	403.9	—
Metridia gerlachei	106.4	67.6	108.0	—	247.8	—	—	—
Metridia lucens	—	—	—	—	—	135.9	—	—
Pleuromamma spp.	—	—	—	—	—	585.0	—	—
Oithona spp.	—	—	—	32.3	—	—	—	—
Euphausiacea								
Euphausia furcilia	—	—	—	—	—	—	28.9	—
Thysanoessa macrura, juv	—	—	—	446	79.1	—	—	
T. macrura, subadults	—	—	—	480	248.5	—	—	—
T. macrura, adults	—	—	—	—	453	—	—	—
Thysanoessa spp.	—	—	—	—	—	232.1	231.7	—
Euphausia frigida	—	—	—	—	91.8	67.4	132.2	—
Euphausia triacantha	—	—	—	—	—	3828	12512	—
Euphausia superba, juv	—	—	—	513	618.7	—	—	—
E. superba, subadults	—	—	—	—	1583	—	—	—
E. superba, adults	—	—	—	—	3556	—	—	
Pteropoda								
Clio sulcata	—	—	—	27757	16627	—	—	—
Limacina helicina	—	—	—	2103	—	—	—	
Tunicata								
Salpa thompsoni, <1 cm	—	—	—	—	704	1043.5	—	—
S. thompsoni, 1–2 cm	—	—	—	1918	1391	3579	3184	
S. thompsoni, 2–3 cm	—	—	—	—	4942	5992	7233	—
S. thompsoni, 3–5 cm	—	—	—	—	22197	13895	23795	
S. thompsoni, 6–7 cm	—	—	—	—	—	36692	50639	—
S. thompsoni, 7–13 cm	—	—	—	—	—			124923

SIE: Spring Ice Edge region; WIE: Winter Ice Edge region; APF: Antarctic Polar Front region.

grazing pressure is, however, insufficient to prevent phytoplankton accumulation (Pakhomov, 2004).

The findings of our study are in good agreement with similar investigations conducted during austral summer along the Greenwich Meridian, which showed that in the MIZ (SIE), the sinking of dead/senescent phytoplankton cells, rather than grazing, represented the most important mechanism for transporting carbon to depth (Froneman et al., 1997, 2000; Rabouille et al., 1998). This is because copepods tend to retain carbon in the euphotic zone through coprophagy and coprohexy (Fortier et al., 1994). However, in the WIE and APF regions, large metazoan grazers, including euphausiids and tunicates, probably represented the major pathway of transport of carbon to the deep ocean due to their high abundances and individual

Table 5
Grazing impact (% of the total) of major mesozooplankton groups at Biostations occupied in the Atlantic sector of the Southern Ocean during December 1997–January 1998

	Biostations					
	SIE			WIE	APF	
	1	2	3	4	5	6
Zooplankton groups						
Copepods	38.5	45.8	51.2	72.4	73.4	61.1
Euphausiids	21.6	1.7	1.5	3.9	1.8	1.2
Pteropods	39.9	52.5	40.6	5.0	5.6	5.6
Tunicates	—	—	6.7	18.7	19.2	32.1
Total ingestion rate						
(mg(pigm) m^{-2} day^{-1})	0.63	0.48	0.74	3.14	3.46	5.54
% of Chl-*a* biomass	1.3	0.9	3.1	15.7	9.0	12.8
(mgC m^{-2} day^{-1})	31.7	24.15	36.95	157.1	173.0	277.1
% of primary production	4.8	3.3	9.2	51.4	23.2	32.5
Chl-*a* biomass (mg(pigm) m^{-2})	47.21	53.85	24.12	20.00	38.44	43.22
Primary production (mg C m^{-2} day^{-1})	664.9	738.1	400.5	305.4	746.5	853.4

SIE: Spring Ice Edge region; WIE: Winter Ice Edge region; APF: Antarctic Polar Front region.

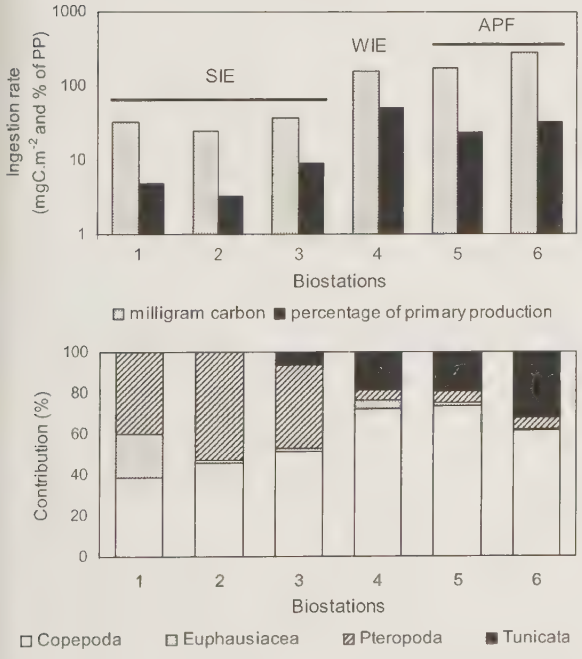

Fig. 6. Grazing impact and contribution of major zooplankton groups at Biostations conducted along the 6°E meridian in the eastern Atlantic sector of the Southern Ocean during December 1997–January 1998. SIE: Spring Ice Edge region; WIE: Winter Ice Edge region; APF: Antarctic Polar Front region.

ingestion rates (Dubischar and Bathmann, 1997; Froneman et al., 2000, 2004).

Acknowledgments

We are grateful to the South African Department of Environmental Affairs and Tourism, to Rhodes University and to the Swedish Polar Secretariat for logistical and financial support of this study. We would like to thank officers and crew of the *SA Agulhas* and our colleagues from Göteborg University (Sweden) and Rhodes University (South Africa) for understanding and constant help during the expedition.

References

Atkinson, A., 1996. Subantarctic copepods in an oceanic, low chlorophyll environment: ciliate predation, food selectivity and impact on prey populations. Marine Ecology Progress Series 130, 85–96.

Atkinson, A., Shreeve, R.S., 1995. Response of the copepod community to a spring bloom in the Bellingshausen Sea. Deep-Sea Research II 42, 1291–1311.

Atkinson, A., Ward, P., Williams, R., Poulet, S.A., 1992. Feeding rates and diel vertical migration of copepods near South Georgia: comparison of shelf and oceanic sites. Marine Biology 114, 49–56.

Atkinson, A., Shreeve, R.S., Pakhomov, E.A., Priddle, J., Blight, S.P., Ward, P., 1996. Zooplankton response to a phytoplankton bloom near South Georgia, Antarctica. Marine Ecology Progress Series 144, 195 210.

Baars, M.A., Helling, G.R., 1985. Methodological problems in the measurements of phytoplankton ingestion rate by gut fluorescence. Hydrobiological Bulletin 19, 81–88.

Bathmann, U.V., Scharek, R., Klaas, C., Dubischar, C.D., Smetacek, V., 1997. Spring development of phytoplankton biomass and comparison in major water masses of the Atlantic sector of the Southern Ocean. Deep-Sea Research II 44, 51–67.

Conover, R.J., Durvasula, R., Roy, S., Wang, R., 1986. Probable loss of chlorophyll-derived pigments during passage through the gut of zooplankton and some of the consequences. Limnology and Oceanography 31, 878–887.

Dam, H.G., Peterson, W.T., 1988. The effect of temperature on the gut clearance rate constant of planktonic copepods. Journal of Experimental Marine Biology and Ecology 123, 1–14.

de Baar, H.J.W., Buma, A.G.J., Nothing, R.F., Cadee, G.C., Jaques, G., Treguer, P.J., 1990. On iron limitation of the Southern Ocean: experimental observations in the Weddell and Scotia Seas. Marine Ecology Progress Series 65, 105–122.

Drits, A.V., Pasternak, A.F., 1993. Feeding of dominant species of the Antarctic herbivorous zooplankton. In: Voronina, N.M. (Ed.), Pelagic Ecosystems of the Southern Ocean. Nauka Press, Moscow, pp. 250–259 (in Russian).

Drits, A.V., Semenova, T.N., 1989. Trophic characteristics of major planktonic phytphages from South Shetland Islands region during early spring. In: Ponomareva, L.A. (Ed.), Complex Investigations of the Pelagic Zone of the Southern Ocean. Shirshov Institute Oceanology Publishers, Moscow, pp. 66–78 (in Russian).

Dubischar, C.D., Bathmann, U.V., 1997. Grazing impact of copepods and salps on phytoplankton in the Atlantic sector of the Southern Ocean. Deep-Sea Research II 44, 415–433.

Fortier, L., Le Fèvre, J., Legendre, L., 1994. Export of biogenic carbon to fish and to the deep ocean: the role of large planktonic microphages. Journal of Plankton Research 16, 809–839.

Fransz, H.G., Gonzalez, S.R., 1997. Latitudinal metazoan plankton zones in the Antarctic Circumpolar Current along 6°W during austral spring 1992. Deep-Sea Research II 44, 395–414.

Froneman, P.W., Perissinotto, R., 1996a. Microzooplankton grazing in the Southern Ocean: implications for the carbon flux. Marine Ecology 17, 99–115.

Froneman, P.W., Perissinotto, R., 1996b. Microzooplankton grazing and protozooplankton community structure in the South Atlantic and in the Atlantic sector of the Southern Ocean. Deep-Sea Research I 43, 703–721.

Froneman, P.W., Pakhomov, E.A., Perissinotto, R., Laubscher, R.K., McQuaid, C.D., 1997. Dynamics of the plankton communities during seasonal ice melt in the Lazarev Sea in austral summer 1994–1995. Marine Ecology Progress Series 149, 201–214.

Froneman, P.W., Pakhomov, E.A., Turner, D., Abrahamsson K., Karlson, B., Godhe, A., Bertilsson, S., Granéli, W., Carlsson, P., Wängberg, S., Wulff, A., Croot, P., Andersson, K., Balarin, M., Wedborg, M., Persson, T., Rasmus K., Özturk, M., David, R., 1998. Research cruise of the Scandinavian/South African Antarctic Expedition: December 1997 to February 1998. South African Journal of Science 94, 517–519.

Froneman, P.W., Pakhomov, E.A., Perissinotto, R., McQuaid C.D., 2000. Zooplankton structure and grazing in the Atlantic sector of the Southern Ocean in late austral summer 1993. Part 2. Biochemical zonation. Deep-Sea Research I 47, 1687–1702.

Froneman, P.W., Pakhomov, E.A., Balarin, M.G., 2004. Size-fractionated phytoplankton biomass, production and biogenic carbon flux in the eastern Atlantic sector of the Southern Ocean in late austral summer 1997–1998. Deep-Sea Research II, this issue [doi:10.1016/j.dsr2.2002.09.001].

Head, R.N., Harris, R.P., Bonnet, D., Irigoien, X., 1999. A comparative study of size-fractionated mesozooplankton biomass and grazing in the North East Atlantic. Journal of Plankton Research 21, 2285–2308.

Huntley, M., Escritor, F., 1991. Dynamics of *Calanoides acutus* (Copepods: Calanoida) in Antarctic coastal waters. Deep-Sea Research 38, 1145–1167.

Huntley, M., Escritor, F., 1992. Ecology of *Metridia gerlachei* Giesbrecht in western Bransfield Strait, Antarctica. Deep-Sea Research 39, 1027–1055.

JGOFS, 1989. Core measurements protocols, reports of the core measurement working groups. In: Tidmarsh, E. (Ed.), SCOR JGOFS Report, vol. 6, 40pp.

Lancelot, C., Mathot, S., Veth, C., de Baar, H., 1993. Factors controlling phytoplankton ice-edge blooms in the marginal ice-zone of the northwestern Weddell Sea during the sea ice retreat 1988: field observations and mathematical modeling. Polar Biology 13, 377–387.

Lopez, M.D.G., Huntley, M.E., Sykes, P.F., 1988. Pigment destruction by *Calanus pacificus*: impact on the estimation of water column fluxes. Journal of Plankton Research 10, 715–734.

Mackas, D., Bohrer, R., 1976. Fluorescence analysis of zooplankton gut contents and an investigation of diel feeding patterns. Journal of Experimental Marine Biology and Ecology 25, 77–85.

Mayzaud, P., Razouls, S., 1992. Degradation of gut pigment during feeding by a subantarctic copepod: importance of feeding history and digestive acclimation. Limnology and Oceanography 37, 393–404.

Morales, C.E., Bedo, A., Harris, R.P., Tranter, P.R.G., 1991. Grazing of copepod assemblages in the north-east Atlantic: the importance of the small size fraction. Journal of Plankton Research 13, 455–472.

Pakhomov, E.A., 1989. Macroplankton distribution in the central part of the Indian sector of Antarctica during summer of 1984–1986. The Antarctic (Nauka Press, Moscow) 28, 145–158 (in Russian with English abstract).

Pakhomov, E.A., 2004. Salp/krill interactions in the eastern Atlantic sector of the Southern Ocean. Deep-Sea Research II, this issue [doi:10.1016/j.dsr2.2001.03.001].

Pakhomov, E.A., Froneman, P.W., 2004. Zooplankton dynamics in the eastern Atlantic sector of the Southern Ocean during the austral summer 1997/1998. Part 1. Community structure. Deep-Sea Research II, this issue [doi:10.1016/j.dsr2.2000.11.001].

Pakhomov, E.A., Perisinotto, R., 1996. Antarctic neritic krill *Euphausia crystallorophias*: spatio-temporal distribution, growth and grazing rates. Deep-Sea Research I 43, 59–87.

Pakhomov, E.A., Perissinotto, R., Froneman, P.W., McQuaid, C.D., 1997a. Energetics and feeding dynamics of *Euphausia superba* in the South Georgia region during the summer of 1994. Journal of Plankton Research 19, 399–423.

Pakhomov, E.A., Verheye, H.M., Atkinson, A., Laubscher, R.K., Taunton-Clark, J., 1997b. Structure and grazing impact of the mesozooplankton community during late summer 1994 near South Georgia, Antarctica. Polar Biology 18, 180–192.

Pakhomov, E.A., Perissinotto, R., McQuaid, C.D., Froneman, P.W., 2000. Zooplankton structure and grazing in the Atlantic sector of the Southern Ocean in late austral summer 1993. Part 1. Ecological zonation. Deep-Sea Research I 47, 1663–1686.

Perissinotto, R., 1992. Mesozooplankton size-selectivity and grazing impact on the phytoplankton community of the Prince Edward Archipelago (Southern Ocean). Marine Ecology Progress Series 79, 243–258.

Perissinotto, R., Pakhomov, E.A., 1996. Gut evacuation rates and pigment destruction in the Antarctic krill *Euphausia superba*. Marine Biology 125, 47–54.

Perissinotto, R., Pakhomov, E.A., 1998. The trophic role of the tunicate *Salpa thompsoni* in the Antarctic marine ecosystem. Journal of Marine Systems 17, 361–374.

Perissinotto, R., Pakhomov, E.A., McQuaid, C.D., Froneman, P.W., 1997. In situ grazing rates and daily ration of the Antarctic krill *Euphausia superba* feeding on phytoplankton at the Antarctic Polar Front and the Marginal Ice Zone. Marine Ecology Progress Series 160, 77–91.

Piatkowski, U., 1987. Zoogeographische Untersuchungen und Gemeinschaftanalysen an antarktischem Makroplankton. Berichte zur Polarforschung 34, 1–150.

Priddle, J., Smetacek, V., Bathmann, U., 1992. Antarctic marine primary production, biochemical carbon cycles and climatic change. Philosophical Transactions of the Royal Society of London B 338, 289–297.

Rabouille, C., Gaillard, J., Relexans, J., Treguer, P., Vincendeau, M., 1998. Recycling of organic matter in Antarctic sediments: a transect through the polar front in the Southern Ocean (Indian sector). Limnology and Oceanography 43, 420–432.

Sakshaug, E., 1989. The physiological ecology of polar phytoplankton. In: Rey, L., Alexander, V. (Eds.), Proceedings of the Sixth Conference of the Comite Arctique International. E.J. Brill, Leiden, pp. 61–89.

Savidge, G., Priddle, J., Gilpin, L.C., Bathmann, U., Murphy, E.J., Owens, N.J.P., Pollard, R.T., Turner, D.R., Veth, C., Boyd, P., 1996. An assessment of the role of the Marginal Ice Zone in the carbon cycle of the Southern Ocean. Antarctic Science 8, 349–358.

Schnack, S., Smetacek, V., von Bodungen, B., Stegmann, P., 1985. Utilization of phytoplankton by copepods in Antarctic waters during spring. In: Grat, J.S., Christiansen, M.E. (Eds.), Marine Biology of Polar Regions and Effects of Stress on Marine Organisms. Wiley, London, pp. 65–81.

Smetacek, V., Scharek, R., Nothing, E.-M., 1990. Seasonal and regional variations in the pelagial and its relationship to the life history cycle of krill. In: Kerry, K.R., Hempel, G. (Eds.), Antarctic Ecosystems. Ecological Change and Conservation. Springer, Berlin, pp. 103–114.

Smith Jr., W.O., Nelson, D.M., 1986. Importance of ice edge phytoplankton production in the Southern Ocean. BioScience 36, 251–257.

Smith Jr., W.O., Keene, N.K., Comiso, J.C., 1988. Interannual variability in estimated primary productivity of the Antarctic Marginal Ice Zone. In: Sahrhage, D. (Ed.), Antarctic Ocean and Resources Variability. Springer, Berlin, pp. 131–139.

Strickland, J.D.H., Parsons, T.R., 1968. A practical handbook of seawater analysis. Bulletin of the Fisheries Research Board of Canada 167, 1–311.

Sullivan, C.W., Arrigo, K.R., McClain, C.R., Comiso, J.C., Firestone, J., 1993. Distribution of phytoplankton blooms in the Southern Ocean. Science 262, 1832–1837.

Tesch, J.J., 1913. Pteropoda. Das Tierreich 36, 1–154.

Turner, D.R., Bertilsson, S., Fransson, A., Pakhomov, E., 2004. The SWEDARP 97/98 marine expedition: overview. Deep-Sea Research II, this issue [doi:10.1016/j.dsr2.2003.08.006].

Wang, R., Conover, R.J., 1986. Dynamics of gut pigment in the copepod *Temora longicornis* and the determination of in situ grazing rates. Limnology and Oceanography 31, 867–877.

Ward, P., Atkinson, A., Murray, A.W.A., Wood, A.G., Williams, R., Poulet, S.A., 1995. The summer zooplankton community at South Georgia: biomass, vertical migration and grazing. Polar Biology 15, 195–208.

Willason, S.W., Cox, J.L., 1987. Diel feeding, laminarinase activity and phytoplankton consumption by euphausiids. Biological Oceanography 4, 1–24.

Zhang, X., Dam, H.G., White, J.R., Roman, M.R., 1995. Latitudinal variations in mesozooplankton grazing and metabolism in the central tropical Pacific during the US JGOFS EqPac study. Deep-Sea Research II 42, 695–714.

ELSEVIER

Deep-Sea Research II 51 (2004) 2633–2643

DEEP-SEA RESEARCH
PART II

www.elsevier.com/locate/dsr2

Protozooplankton community structure and grazing impact in the eastern Atlantic sector of the Southern Ocean in austral summer 1998

Pierre Willliam Froneman*

Southern Ocean Group, Department of Zoology and Entomology, Rhodes University, P.O. Box 94, Grahamstown 6140, South Africa

Abstract

The protozooplankton community structure and grazing impact within the winter ice-edge zone (WIE), spring ice-edge zone (SIE) and in the vicinity of the Antarctic Polar Front (APF) in the eastern Atlantic sector of the Southern Ocean was investigated in austral summer (December 97—January 98). Total chlorophyll-*a* (Chl-*a*) concentrations in the vicinity of the SIZ and APF were always $>0.5\,\mu g\,l$ while at stations within the SIE total pigment concentrations were always $<0.3\,\mu g\,l^{-1}$. Protozooplankton communities throughout the investigation were dominated by nanoflagellates with densities varying between 2050 and 2750 ind. l^{-1} in the SIE, between 2525 and 3100 ind. l^{-1} in the WIE and between 2750 and 3350 ind. l^{-1} in the region of the APF. The $>20\,\mu m$ fraction was always dominated by ciliates comprising aloricates and tintinnids and dinoflagellates. The contribution of the larger components to the total was, however, always $<40\%$ of the total. Protozooplankton biomass estimated from biovolume:carbon ratios ranged from 0.4 to $1.5\,\mu g\,C\,l^{-1}$. Protozooplankton herbivory throughout the study was highest within the $<20\,\mu m$ chlorophyll fraction. Instantaneous grazing coefficients of protozooplankton within this chlorophyll fraction ranged between 0.04 and $0.28\,d^{-1}$ corresponding to a grazing impact equivalent to up to 24% (range 4–24%) of the chlorophyll standing stock. These rates are equivalent to a community ingestion rate of between 0.55 and $1.89\,\mu g\,C\,l^{-1}$ or between 13% and 35% of the daily production within the $<20\,\mu m$ Chl-*a* fraction. Protozooplankton were unable to control the growth of the larger microphytoplankton. The highest impact of the protozooplankton was recorded in the WIE where small phytoplankton cells comprised $>60\%$ of total pigment. These results suggest that the grazing impact of the protozooplankton was largely mediated by the contribution of the small phytoplankton cells to total pigment.
© 2004 Elsevier Ltd. All rights reserved.

1. Introduction

The fate of photosynthetically fixed carbon in marine environments can dramatically affect the magnitude of particulate flux, and hence the efficiency of the biological pump in the draw-down

*Tel.: +27 603 8524; fax: +27 46 622 4377.
E-mail address: w.froneman@ru.ac.za (P.W. Froneman).

0967-0645/$ - see front matter © 2004 Elsevier Ltd. All rights reserved.
doi:10.1016/j.dsr2.2004.09.001

of atmospheric CO_2 (Longhurst and Harrison, 1989; Longhurst, 1991; Fortier et al., 1994). In the open waters, grazing by larger zooplankton is thought to represent the primary biological route for the transfer of organic carbon from the surface waters to the interior of the ocean. The role of grazers in determining the vertical flux of carbon is, however, strongly determined by the partitioning of photosynthetically fixed carbon between the various size classes of grazers (Michaels and Silver, 1988; Roman et al., 1993, Fortier et al., 1994; Froneman and Perissinotto, 1996a; Froneman et al., 1997). Large grazers such as macro- and mesozooplankton generally contribute to particle flux through the production of large, compact and fast-sinking faecal pellets which have a high carbon content (Schnack, 1985; Fortier et al., 1994). Carbon flux beneath the zone of regeneration is further enhanced as many of the larger herbivores undertake vertical migrations from the surface waters where they feed to below the zone of regeneration (Fortier et al., 1994). Production originating in the surface waters is, therefore, transported to depth. In contrast, phytoplankton production entering the microbial loop (which comprises bacteria, small phytoplankton and protozoa) contributes less to particulate flux because the close coupling between protozoans and bacteria results in the recycling of nutrients within the zone of regeneration (Sherr and Sherr, 1988). Furthermore, protozoans produce small faecal pellets (minipellets), which remain in suspension for long periods (Nöthig and von Bodungen, 1989; Elbrächter, 1991; Fortier et al., 1994). As a consequence, there is little carbon available for the export to depth. Indeed, a study conducted in the Gulf of Mexico showed that when protozooplankton constituted the major grazers of phytoplankton production, $<1\%$ of the total production sedimented to depth (Fahnenstiel et al., 1995).

The Southern Ocean is a major repository of macronutrients, an important region of deep-water formation and a major sink for dissolved carbon dioxide (Siegenthaler and Sarmiento, 1993). As a consequence, the role of the Southern Ocean in the global carbon cycle is at present a leading concern in physical and biological oceanographic studies. Although phytoplankton production in the open waters of the Southe Ocean is generally low (El-Sayed, 1988; Jacque 1989), there are areas characterised by hig production. These include the Marginal Ice Zor (Smith and Nelson, 1986; Smith and Sakshau 1990; Sullivan et al., 1993; Froneman et al., 1997 neritic waters of Antarctica (Laubscher et al 1993) and frontal regions (El-Sayed, 1988; Jac ques, 1989; Laubscher et al., 1993; Sullivan et al 1993). The partitioning of photosynthetically fixe carbon within the areas of higher production is c particular interest in understanding the biochem ical cycles of the Southern Ocean.

The role of protozooplankton in the Souther Ocean carbon cycle has been the subject of severa investigations (Garrison, 1991; Burkill et al., 199 Atkinson, 1995; Froneman and Perissinotto 1996a, b; Froneman et al., 1997). The results o these studies have emphasised the importance o these organisms in the plankton assemblages of th Southern Ocean (Garrison and Buck, 1989 Garrison, 1991; Garrison et al., 1991, 1993 Edwards et al., 1998), and have demonstrated their importance as grazers of phytoplankton production (Taylor and Haberstroh, 1988; Burkil et al., 1995; Froneman et al., 1996, 1997). Indeed at times particularly when small phytoplankton cells dominate total chlorophyll, the protozoo-plankton grazing impact exceeds that of the larger zooplankton (Froneman et al., 1997). More recently, protozooplankton have also been shown to be an important carbon source for larger zooplankton and can, therefore, be regarded as important trophic intermediates between small phytoplankton ($<20\,\mu m$) on which they feed and larger zooplankton (Hopkins et al., 1993; Atkinson, 1995; Froneman et al., 1996). Despite these findings, the role of protozooplankton within the Southern Ocean carbon cycle is poorly understood largely because of the extreme variability in physico-chemical and biological parameters within the ocean.

In this paper, the protozooplankton community structure and grazing impact within three different environments, the winter ice-edge (WIE), spring ice-edge (SIE) and within the vicinity of Antarctic Polar Front (APF) in the eastern Atlantic sector of the Southern Ocean in austral summer (December 1997–January 1998) are described.

2. Materials and methods

The protozooplankton (2–200 μm) community structure and grazing impact at 10 stations within the SIE zone, WIE zone and in the vicinity of the APF were investigated during the collaborative Scandinavian/South African Antarctic cruise conducted to the region of the eastern Atlantic sector of the Southern Ocean austral summer (December 97–January 98) on board the research vessel *SA Agulhas* (Fig. 1). Water samples for the experiments were collected at 08:00 each morning with 20 l carboys from the surface. The water in the carboys was then gently passed through a 200 μm mesh to isolate the protozooplankton community. Particle-free water was obtained by passing surface water obtained using a shipboard metal-free Iwaki Magnetic Pump (operated at a flow rate of $\approx 5\,l\,min^{-1}$) through a 0.2 μm Milli Q (Millipore) filtration system. Dilution series in ratios of 1:0; 3:1; 1:1 and 1:3 of unfiltered to filtered seawater were then prepared in 2 l dialysis bags. The dialysis bags were employed to minimise bottling effects such as nutrient enrichment and the buildup of metabolic waste products. The dilution series were incubated on deck for 24 h in Perspex incubators cooled with running surface water and screened with shade cloth (neutral spectral transmission) to simulate light intensity at the depth of collection. Water temperatures within the incubators were maintained to within 1 °C of the surface seawater temperature.

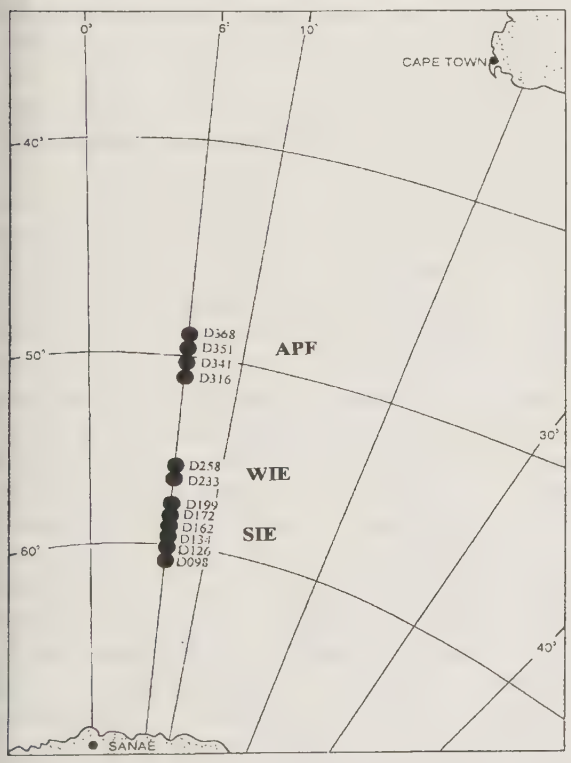

Fig. 1. Cruise track and position of grazing stations occupied during the collaborative Scandinavian/South African expedition conducted to the region of the Lazarev Sea in austral summer (December 1997–January 1998).

Before the incubations were begun, water samples (250 ml) were taken for the initial chlorophyll-*a* (Chl-*a*) concentration. The bottles were sampled again at the end of the incubation to determine the final Chl-*a* concentrations. Chl-*a* was fractionated into the >20 and <20 μm fractions by serial filtration. Chl-*a* concentrations were determined fluorometrically (Turner 10 AU fluorometer) after extraction in 90% cold acetone for 24 h (Holm-Hansen and Riemann, 1978).

To identify and enumerate the various components of the protozooplankton communities at each grazing station, a 250 ml sample of natural seawater was passed gently through a 200 μm mesh and fixed with 10% Lugols' solution (Leakey et al., 1994a; Stoecker et al., 1994). No differentiation between the autotrophic and heterotrophic components of the protozooplankton were made. Only athecate dinoflagellates were counted as these are regarded as heterotrophic (Tomas, 1996). All ciliates were considered heterotrophic. For the taxonomic analysis of the microphytoplankton standing stock, a 250 ml seawater sample obtained from the scientific seawater supply was fixed in 2% buffered formalin. The water samples were then examined using the Utermöhl settling technique, employing a Nikon-TMS inverted microscope operated at 400× magnification (Reid, 1983). A minimum of 500 cells or 100 fields was counted for each sample.

To estimate the biomass of the protozooplankton community, biovolume to carbon conversion factors of Lessard (1991) and Putt and Stoecker (1989) were employed. The biovolume of the

various components of the protozooplankton assemblage was estimated by applying simple geometric configurations to 100 individuals from each group. It should be noted that these values should be regarded with caution as cell shrinkage as much as 25% have been recorded in samples preserved with Lugols' solution (Leakey et al., 1994a).

The protozooplankton grazing impact on phytoplankton standing stock was estimated from the slope of the regression between the dilution factor and apparent growth using the exponential model of Landry and Hassett (1982):

$$P_t = P_0 e^{-g}, \quad (1)$$

where P_t is Chl-*a* concentration at time t; P_0 is initial Chl-*a* concentration and g is the instantaneous grazing coefficient determined from the slope of the regression. The % standing stock removed per day by the protozooplankton was then converted to biomass assuming a Chl-*a*: carbon ratio of 50 (Atkinson, 1995). The % biomass removed each day was then expressed as % daily primary production consumed per day employing the data collected during fractionated primary production studies conducted in parallel to this study (Froneman et al., 2004).

Correlation analysis was performed to identify possible relationships between grazing rate, temperature and chlorophyll. Grazing rate data, expressed as % initial standing stock and potential primary production removed per day, was transformed using arcsin transformation (Sokal and Rolhf, 1969), while chlorophyll concentration values were transformed using the factor: $\log(x+1)$ (Legendre and Legendre, 1983). The computer package Statgraphics, Version 5.0, was used for this analysis.

3. Results

3.1. Physical oceanography

A detailed description of the oceanographic conditions during the survey is presented elsewhere in this issue (Turner et al., 2004). Here the conditions at the grazing stations are briefly described. The three regions surveyed during th study could be divided into two distinct regime Stations occupied in the vicinity of the SIE ar APF were characterised by relatively high wat column stability and shallow mixed layer dep (<100 m). The water column stability in the SI appeared to be related to sea-ice melt, whic imparts water column stability within the vicini of the retreating ice. In the region of the API water column stability appeared to be related t the physical attributes between the interactin water masses in the region of the front (Fronema et al., 2004). In contrast, stations occupied withi the region of the WIE were characterised by lo water column stability with a deep mixed laye (±100 m) (Froneman et al., 2004).

3.2. Chlorophyll

Total Chl-*a* in the surface waters ranged fro 1.52 to 2.09 $\mu g l^{-1}$ at the stations in vicinity of th SIE, between 0.167 and 0.206 $\mu g l^{-1}$ in the WI and between 0.427 and 0.636 $\mu g l^{-1}$ at station occupied in the vicinity of the APF (Fig. 2). Onl at stations occupied within the vicinity of the SI did microphytoplankton dominate total Chl-a concentrations. Here microphytoplankton com prised on average 75% (range 75–80%) of th total and was dominated by the colonial hapto phyte, *Phaeocystis* spp. Within the WIE and APF the <20 μm chlorophyll fraction dominated tota pigment comprising >55% of the total. Ar exception was found at station D378 occupiec within the vicinity of the APF where microphyto plankton comprised 54% of the total chlorophyl (Fig. 2). In the region of the APF and WIE microphytoplankton was dominated by small chain forming diatoms of the genera *Chaetoceros*, *Fragilariopsis* and *Nitzschia* spp. Within the APF, larger diatoms such as *Proboscia alata* and *Thalassiosira* spp. were also well represented. A detailed description of the microphytoplankton assemblages during the survey is presented in Froneman et al. (2004). Flagellates dominated the nano- and picophytoplankton assemblages throughout the study. Also well represented in the nanophytoplankton were small diatoms of the genera *Fragilariopsis* and *Chaetoceros*.

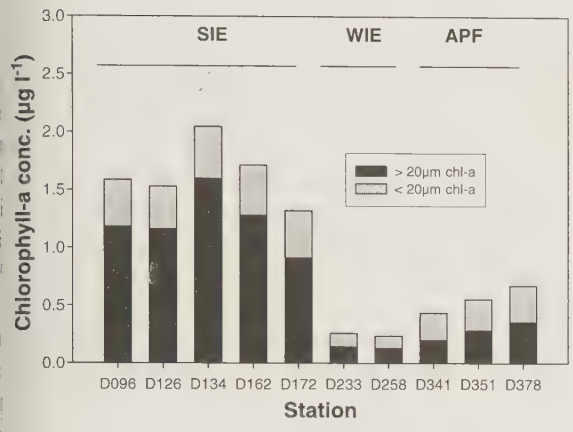

Fig. 2. Surface size-fractionated Chl-*a* concentrations at grazing stations occupied in the vicinity of the winter ice zone (WIE), spring ice zone (SIE) and APF in the Lazarev Sea during austral summer (December 1997–January 1998).

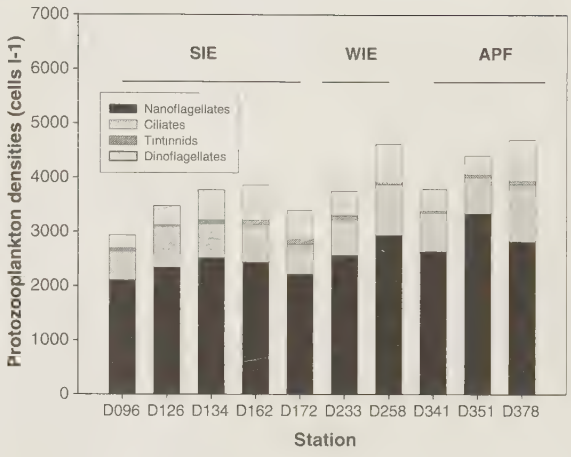

Fig. 3. Protozooplankton community structure and abundances at grazing stations occupied within the winter ice-edge (WIE), spring ice-edge (SIE) and APF in austral summer 1998.

3.3. *Protozooplankton species composition and abundances*

Throughout the investigation, nanoflagellates numerically dominated protozooplankton counts (Fig. 3). Densities of nanoflagellates ranged between 2050 and 2750 ind. l^{-1} within the SIE, between 2525 and 3100 ind. l^{-1} within the WIE and between 2750 and 3350 ind. l^{-1} at stations in the region of the APF (Fig. 3). The $>20\,\mu m$ fraction was always dominated by ciliates. Densities of ciliates at stations occupied within the SIE and WIE ranged between 525 and 750 ind. l^{-1} and between 600 and 950 ind. l^{-1}, respectively. Tintinnid ciliates within these two regions were always <100 ind. l^{-1} (Fig. 3). At stations in the vicinity of the APF, ciliate densities ranged from 650 to 1050 ind. l^{-1} while tintinnid densities ranged from 25 to 150 ind. l^{-1} (Fig. 3). Dinoflagellate densities ranged between 350 and 650 ind. l^{-1} within the SIE, between 450 and 700 ind. l^{-1} within the WIE and between 350 and 750 ind. l^{-1} in the APF (Fig. 3).

Throughout the investigation, protozooplankton species composition was similar. Generally, unidentifiable flagellates dominated the smaller nanoflagellates. Among the larger protozooplankton ($>20\,\mu m$), the most well represented taxa were species of aloricate choreotrichs and oligotrichs of the genera *Lohmaniella*, *Strombidium* and *Strombilidium*. Tintinnid ciliates were represented by species of the genera *Codonellopsis*, *Laackmaniella* and *Cymatocylis*. The contribution of the tintinnid ciliates to total was, however, always $<10\%$. Dinoflagellates well represented included species belonging to the genera *Protoperidinium* and *Gyrodinium*, which are considered heterotrophic. Also, well represented among the dinoflagellates were representatives of the genera *Gonyaulax* and *Prontoctiluca*.

Assuming a mean cell volume ($n = 100$ for each group) of $3.4 \times 10^1\,\mu m^3$ for the nanoflagellates, $8.7 \times 10^3\,\mu m^3$ for ciliates and $2.7 \times 10^4\,\mu m^3$ for the dinoflagellates, the total biomass of protozooplankton during this study ranged from 0.3 to 1.5 $\mu g\,l^{-1}$. Generally, protozooplankton biomass displayed the same distribution pattern as the abundance data with the lowest values recorded at stations within the SIE (range 0.1–0.9 $\mu g\,C\,l^{-1}$) and highest biomass values recorded at stations in the vicinity of the APF (range 0.8–1.5 $\mu g\,C\,l^{-1}$). Total protozooplankton biomass at grazing stations within the WIE ranged from 0.4 to 1.3 $\mu g\,C\,l^{-1}$.

Pearson correlation analysis showed that there were no significant correlations between total

Chl-*a* concentration and protozooplankton abundance and biomass ($P<0.05$).

3.4. Protozooplankton grazing impact

Initial Chl-*a* concentrations, instantaneous grazing coefficients of the protozooplankton derived from the seawater dilution experiments and daily phytoplankton production rates of the <20 μm fraction are shown in Table 1. In all dilution experiments, the relationship between apparent growth rate and dilution was significantly linear ($P<0.05$ in all cases). Throughout the investigation, no decrease in the >20 μm chlorophyll fraction was measured over the 24 h incubation period. As a consequence, only the results of the grazing impact of the protozooplankton on the <20 μm fraction are presented here.

The daily production of the nano- and picophytoplankton during the experiments were highest at stations occupied in the vicinity of the SIE. Here the growth was estimated at between 5.08 and 10.77 $\mu g C l^{-1} d^{-1}$ (Table 1). At stations occupied within the WIE and APF, the daily production rates of the <20 μm fraction were lower and ranged between 3.66 and 4.08 $\mu g C l^{-1} d^{-1}$ a between 2.60 and 7.25 $\mu g C l^{-1} d^{-1}$, respectiv (Table 1). Instantaneous grazing coefficients protozooplankton on the <20 μm chloroph fraction ranged from 0.04 to 0.09 per day in t SIE, between 0.19 and 0.28 per day in the WIE a between 0.04 and 0.08 per day in the APF. The rates correspond to a loss of between 4.9% a 8.6% of the initial standing stock within the S and between 17.8% and 24.3% of the standi stock within the WIE (Table 1). At statio occupied in the vicinity of the APF, the grazi impact was equivalent to a loss of up to 7.8 (range 4.2%–7.85%) of the standing stock.

Based on the percentage standing stock r moved, the daily ingestion rate was estimated to b between 0. 98 and 1.32 $\mu g C l^{-1} d^{-1}$ in the SI between 0.9 and 1.41 $\mu g C l^{-1} d^{-1}$ in the WIE a between 0.91 and 1.24 $\mu g C l^{-1} d^{-1}$ at the AP These ingestion rates correspond to a loss of up 26.1% (range 11.1–26.1%) of the daily productio in the <20 μm fraction at stations occupied in th SIE. Within the WIE and APF, the grazing impa of the protozooplankton was equivalent to a lo of between 25.6% and 34.5% and between 13

Table 1
Results of protozooplankton grazing experiments on the <20 μm chl-*a* fraction in the three regions of investigation

Station	Chl-*a* conc. ($\mu g l^{-1}$)	Grazing coeff. (g) (d^{-1})	Standing stock removed (d^{-1})	Carbon ingested d^{-1} ($\mu g C l^{-1}$)	Production ($\mu g C l^{-1}$)	Production removed (%)
Spring ice-edge						
D098	0.395	0.07	6.7	1.323	5.078	26.1
D126	0.361	0.07	6.6	1.191	10.767	11.1
D134	0.441	0.09	8.6	1.896	6.641	18.5
D162	0.430	0.04	4.9	0.982	7.385	11.6
D172	0.401	0.05	4.9	0.982	6.565	15.0
Winter ice-edge						
D233	0.116	0.28	24.3	1.410	4.081	34.5
D258	0.101	0.19	17.8	0.901	3.656	25.6
Antarctic Polar Front						
D341	0.232	0.08	7.8	0.905	6.913	13.0
D351	0.263	0.04	4.2	0.552	2.595	21.3
D378	0.319	0.08	7.7	1.244	7.251	17.1

Protozooplankton grazing coefficients (g) were determined employing the seawater dilution technique. In all dilution experiments a significant correlation between apparent growth rate and dilution were obtained ($P<0.05$ in all cases). Phytoplankton growth rate were estimated from ^{14}C incorporation experiments.

nd 17.1% of the daily phytoplankton production, espectively (Table 1).

Pearson correlation analysis indicated that there were no significant correlations between grazing mpact of protozooplankton and the protozoo-plankton abundance or biomass ($P>0.05$ in all ases). Multiple range test performed after a one way analysis of variance (ANOVA) test indicated hat the grazing impact of the protozooplankton in he WIE was significantly higher than that ecorded in the region of the APF and SIE ($F=1.03$; $P<0.05$).

. Discussion

Studies on the importance of protozooplankton s grazers of phytoplankton production in the outhern Ocean have largely been derived from nvestigations employing the seawater dilution echnique (Landry and Hassett, 1982; Taylor and Haberstroh, 1988; Froneman and Perissinotto, 996a, b). Despite the wealth of grazing data that as been derived from the dilution experiments, here is some evidence in the literature to suggest hat the rates measured should be considered with aution due to possible artefacts (Li, 1990). These nclude bottling effects and nutrient enrichment ssociated with cell breakage (Cullen et al., 1986; Taguchi et al., 1993). In addition, there is some ebate as to whether changes in clearance rates f protozooplankton in response to changes in rey densities occur (Gifford, 1988; Gallegos, 989). Although no data are available to deter-nine whether a change in response to the hange in prey densities occurred during these xperiments, possible bottling effects, including utrient enrichment, would have been minimised y utilising the dialysis bags. These facts suggest hat the rates measured during this study can be onsidered as a true reflection of the natural ommunity.

Protozooplankton communities throughout the urvey were dominated by nanoflagellates and iliates (Fig. 3). The species composition and bundances recorded during this study are con-istent with previous studies conducted in different ectors of the Southern Ocean (Garrison and Buck, 1989; Garrison, 1991; Leakey et al., 1994b; Burkill et al., 1995; Froneman and Perissinotto, 1996a, b). The lack of a positive significant correlation between protozooplankton abundance/biomass and total Chl-*a* concentration during this study can probably be related to the fact that no clear distinctions between autotrophic and heterotrophic forms were made ($P>0.05$). Alternatively, cell shrinkage associated with the preservation of the samples may have underestimated the protozooplankton biomass (Leakey et al., 1994a). Protozooplankton biomass ranged from 0.5 to 1.5 $\mu g\,C\,l^{-1}$. Despite possible sources of error, e.g. cell shrinkage (Leakey et al., 1994a), the estimates of protozooplankton biomass presented here are in the range reported for other regions of the Southern Ocean (Garrison, 1991; Garrison and Buck, 1989; Leakey et al., 1994b; Burkill et al., 1995; Edwards et al., 1998). Recent studies conducted in the Bellingshausen Sea have shown that sea-ice has a dramatic effect of the species composition and abundances of protozoo-plankton (Burkill et al., 1995; Edwards et al., 1998). Furthermore, these studies have shown that the protozooplankton abundances increase from the sea-ice to open waters. Although no sea-ice was observed during the study, the increase in protozooplankton abundance along the south-north transect in the ice-edge zone (Fig. 3) suggest that the effect of sea-ice persisted after it had retreated. This hypothesis is supported by the composition of the microphytoplankton and zooplankton along the transect (Froneman et al., 2004; Pakhomov and Froneman, 2004).

The grazing impact of the protozooplankton on the $<20\,\mu m$ chlorophyll fraction during the study was substantial within the three regions of investigation, accounting for up to 24% (mean $=9.4\%\pm6.2$) of the standing stock or up to 35% (mean $=19.4\%\pm7.2$) of the daily phytoplankton production (Table 1). The estimates of grazing impact presented here are in the same range as previous studies conducted in the Southern Ocean which have shown that in regions dominated by small phytoplankton, grazing by protozooplankton is substantial (Garrison et al., 1993; Froneman and Perissinotto, 1996a, b;

Froneman et al., 1997). The highest impact was recorded in the WIE (Table 1). The grazing impact of protozooplankton on phytoplankton can be related to several factors including the phytoplankton size composition and growth, protozooplankton species composition and numerical abundance. The high grazing impact of the protozooplankton in the WIE coincided with low phytoplankton growth rates and high protozooplankton abundances (Table 1; Fig. 3). Finally, it is well documented that ciliates and nanoflagellates, which numerically dominated the counts, preferentially consume particles $<20\,\mu m$ (Rassoulzadegan et al., 1988; Hansen et al., 1994). At all stations within the WIE, small nano- and picophytoplankton comprised $>60\%$ of the total pigment (Table 2).

Throughout the survey, protozooplankton were unable to control the growth of the larger microphytoplankton. This result is consistent with recent studies conducted in the region of the sea-ice in the Lazarev Sea (Froneman et al., 1996; Froneman et al., 1997) and indeed in other subsystems of the Southern Ocean (Froneman and Balarin, 1998). Several criteria may l involved in food selection by protozooplankto including feeding mode, prey size, motility, surfa characteristics or biochemical compositio Among these, prey size is generally believed play a major role. Hansen et al. (1994) showed th a linear size ratio between planktonic predato and prey existed. These were calculated to be 8: for ciliates, 1:1 for dinoflagellates and 3:1 for oth flagellates (including nanoflagellates). Throughou the investigation, the microphytoplankton assem blages were dominated by chain forming species c the genera *Chaetoceros* and *Fragilariopsis* (Fron man et al., 2004). Since nanoflagellates and ciliate numerically dominated total protozooplankto counts within the region of investigation (Fig. 3 the lack of grazing impact within the large microphytoplankton is hardly surprising Although dinoflagellates have been shown at time to consume prey larger than themselves (Lessarc 1991; Hansen et al., 1994), they only formed minor component of the protozooplankton assem blages during this investigation (Fig. 3). As consequence, no detectable decrease in standin stock of microphytoplankton was observed durin the study. Lancelot et al. (1993) suggested tha grazing by protozooplankton was sufficient t control the development of a phytoplankto bloom in the region of the retreating ice. The results of this study, however, suggest that the importance of protozooplankton in controllin phytoplankton growth will largely be deter-mined by the size structure of the phytoplankto community.

The partitioning of carbon between the "classi-cal" food web dominated by large metazoans and the "microbial" loop is central in determining the localised efficiency of the biological pump (Long-hurst, 1991; Legendre and Michaud, 1998). Results of the protozooplankton herbivory experiments indicate that the grazing impact was highest within the winter-ice zone. Here grazing removed between 18.7% and 21.7% of the total daily phytoplankton production (Table 2). In the region of the SIE, $<10\%$ of the total production was removed by the larger zooplankton. These facts suggest that in the vicinity of the WIE and APF, total daily phytoplankton production

Table 2
Surface phytoplankton production and protozooplankton grazing impact at grazing stations occupied during the collaborative Scandinavian/South African Antarctic expedition conducted to the region of the eastern Atlantic sector of the Southern Ocean in austral summer (Dec 1997–Feb 1998)

Station	Phytoplankton prod. ($\mu g\,C\,l^{-1}\,d^{-1}$)	Daily ingestion ($\mu g\,C\,l^{-1}\,d^{-1}$)	Daily prod. removed (%)
Spring ice-edge			
DO98	16.32	1.32	8.1
D126	30.80	1.19	3.8
D134	24.18	1.89	7.8
D162	29.90	0.98	3.2
D172	28.26	0.98	3.5
Winter ice-edge			
D233	6.51	1.41	21.7
D258	4.82	0.90	18.7
Antarctic Polar Front			
D341	14.29	0.91	6.3
D351	5.99	0.55	9.2
D378	12.14	1.24	10.2

appeared to be channelled through the classical food web. In contrast within the region of the SIE, the sinking of senescent or dead phytoplankton cells is probably primarily responsible for carbon flux to depth.

The importance of protozooplankton as grazers of phytoplankton production has been emphasised in several studies (Burkill et al., 1995; Froneman and Perissinotto, 1996a, b; Froneman and Balarin, 1998). Lancelot et al. (1993) suggested that grazing by protozooplankton was sufficient to control the development of a phytoplankton bloom in the region of the retreating ice. Results of this study, however, suggest that the protozooplankton were unable to control phytoplankton growth largely as a result of the size structure of the local phytoplankton community which was dominated by microphytoplankton. Unfortunately, Lancelot et al. (1993) did not present data on the size structure of the phytoplankton assemblages. As a consequence, no comparison between the two studies can be made.

Acknowledgements

I would like to thank the South African Department of Environmental Affairs and Tourism (DEAT) and the Swedish Polar Secretariat for providing funds and facilities for this study. My thanks also go to the officers and crew of the *SA Agulhas* for their co-operation at sea. Finally, I would like to thank Brian Hunt for his invaluable assistance at sea.

References

Atkinson, A., 1995. Omnivory and feeding selectivity in five copepod species during spring in the Bellingshausen Sea, Antarctica. Journal of Marine Science 52, 385–396.

Burkill, P.H., Edwards, E.S., Sleigh, M.A., 1995. Microzooplankton and their role in controlling phytoplankton growth in the marginal ice zone of the Bellingshausen Sea. Deep-Sea Research II 42, 1277–1290.

Cullen, J.J., Zhu, M., Pierson, D.C., 1986. A technique to assess the harmful effects of sampling and containment for determining primary production. Limnology and Oceanography 31, 1364–1373.

Edwards, E.S., Burkill, P.H., Sleigh, M.A., 1998. Microbial community structure in the marginal ice zone of the Bellingshausen Sea. Journal of Marine Systems 17, 87 96.

Elbrächter, M., 1991. Faeces production by dinoflagellates and other small flagellates. Marine Microbial Food Webs 5, 189–204.

El-Sayed, S.Z., 1988. Productivity in the Southern Ocean: a closer look. Comparative Biochemical Physiology 90, 489–498.

Fahnenstiel, G.L., McCormick, M.J., Lang, G.A., Radlaje, D.G., Lohrenz, S.E., Marcowitz, M., Wagoner, B., Garrick, H.J., 1995. Taxon specific growth and loss rates for dominant phytoplankton populations from the northern Gulf of Mexico. Marine Ecology Progress Series 117, 229–239.

Fortier, L., Le Fevre, J., Legendre, L., 1994. Export of biogenic carbon to fish and the deep ocean: the role of large planktonic microphages. Journal of Plankton Research 16, 809–839.

Froneman, P.W., Balarin, M.G., 1998. Structure and grazing impact of the protozooplankton community in the waters surrounding the subantarctic Prince Edward Islands. Polar Biology 20, 198 205.

Froneman, P.W., Perissinotto, R., 1996a. Structure and grazing of the microzooplankton communities of the Subtropical Convergence and a warm-core eddy in the Atlantic sector of the Southern Ocean. Marine Ecology Progress Series 135, 237–245.

Froneman, P.W., Perissinotto, R., 1996b. Microzooplankton grazing and protozooplankton community structure in the south Atlantic and Atlantic sector of the Southern Ocean. Deep-Sea Research I 43, 703–721.

Froneman, P.W., Pakhomov, E.A., Perissinotto, R., McQuaid, C.D., 1996. The role of microzooplankton in the diet and daily ration of Antarctic zooplankton species during austral summer. Marine Ecology Progress Series 143, 15–23.

Froneman, P.W., Pakhomov, E.A., Perissinotto, R., Laubscher, R.K., McQuaid, C.D., 1997. Dynamics of the plankton communities of the Lazarev Sea (Southern Ocean) during seasonal ice melt. Marine Ecology Progress Series 149, 210–214.

Froneman, P.W., Pakhomov, E.A., Balarin, M.G., 2004. Size- fractionated phytoplankton biomass, production and biogenic carbon flux in the eastern Atlantic sector of the Southern Ocean in late austral summer 1997–1998. Deep-Sea Research II, this issue [doi:10.1016/j.dsr2.2002.09.001].

Gallegos, D.L., 1989. Microzooplankton grazing on phytoplankton in the Rhode River, Maryland: nonlinear feeding kinetics. Marine Ecology Progress Series 57, 23–33.

Garrison, D.L., 1991. An overview of the abundance and role of protozooplankton in Antarctic waters. Journal of Marine Systems 2, 17–331.

Garrison, D.L., Buck, K.R., 1989. Protozooplankton in the Weddell Sea: abundance and distribution in the ice-edge zone. Polar Biology 9, 341–351.

Garrison, D.L., Buck, K.R., Gowing, M.M., 1991. Plankton assemblages in the ice edge zone of the Weddell Sea during austral winter. Journal of Marine Systems 2, 123–130.

Garrison, D.L., Buck, K.R., Gowing, M.M., 1993. Winter plankton assemblage in the ice edge zone of the Weddell and Scotia Seas: composition, biomass and spatial distributions. Deep-Sea Research II 40, 311–338.

Gifford, D.J., 1988. Impact of grazing by microzooplankton in the Northwest Arm of Halifax Harbour, Nova Scotia. Marine Ecology Progress Series 47, 249–258.

Hansen, B., Bjornsen, P.K., Hansen, P.J., 1994. The size ratio between planktonic predators and their prey. Limnology and Oceanography 39, 395–403.

Holm-Hansen, O., Riemann, B., 1978. Chlorophyll-a determination: improvements in methodology. Oikos 30, 438–447.

Hopkins, T.L., Ainley, D.G., Torres, J.J., Lancraft, T.M., 1993. Trophic structure in open waters of the marginal ice zone in the Scotia–Weddell confluence region during spring (1983). Polar Biology 13, 389–397.

Jacques, G., 1989. Primary production in the open Antarctic Ocean during austral summer. A review. Vie Milieu 39, 1–17.

Lancelot, C., Mathot, S., Veth, C., de Baar, H.J.W., 1993. Factors controlling phytoplankton ice-edge blooms in the marginal ice zone of the northwest Weddell Sea during ice retreat 1988: field observations and mathematical modelling. Polar Research 13, 377–387.

Landry, M.R., Hassett, R.P., 1982. Estimating the grazing impact of marine microzooplankton. Marine Biology 67, 283–288.

Laubscher, R.K., Perissinotto, R., McQuaid, C.D., 1993. Phytoplankton production and biomass at frontal zones in the Atlantic sector of the Southern Ocean. Polar Biology 13, 471–481.

Leakey, J.G., Burkill, P.H., Sleigh, M.A., 1994a. A comparison of fixatives for the estimation of abundance and biovolume of marine planktonic ciliate populations. Journal of Plankton Research 16, 375–389.

Leakey, R.J.G., Fenton, N., Clarke, A., 1994b. The annual cycle of planktonic ciliates in the near shore waters of Signy Island. Journal of Plankton Research 16, 841–856.

Legendre, L., Legendre, P., 1983. Numerical Ecology. Elsevier, Amsterdam.

Legendre, L., Michaud, J., 1998. Flux of biogenic carbon in oceans: size dependant regulation by pelagic food webs. Marine Ecology Progress Series 164, 1–11.

Lessard, E.J., 1991. The trophic role of heterotrophic dinoflagellates in diverse marine environments. Marine Microbial Food Webs 5, 49–58.

Li, W.K.W., 1990. Particles in particle-free seawater: growth of ultraphytoplankton and implications for dilution experiments. Canadian Journal of Aquatic Sciences 47, 1258–1268.

Longhurst, A.R., 1991. Role of the marine biosphere in the global carbon cycle. Limnology and Oceanography 36, 1507–1526.

Longhurst, A.R., Harrison, W.G., 1989. The biological pum profiles of plankton production and consumption in t upper ocean. Progress in Oceanography 22, 47–123.

Michaels, A.F., Silver, M.W., 1988. Primary productio sinking fluxes and the microbial food web. Deep-S Research I 35, 473–490.

Nöthig, E., von Bodungen, B., 1989. Occurrence and vertic flux of faecal pellets of probably protozoan origin in t southeastern Weddell Sea (Antarctica). Marine Ecolo Progress Series 56, 281–289.

Pakhomov, E.A., Froneman, P.W., 2004. Zooplankton d namics in the eastern Atlantic sector of the Southern Ocea during the austral summer 1997/1998. Part 1. Communi structure. Deep-Sea Research II, this issue [doi:10.101 j.dsr2.2000.11.001].

Putt, M., Stoecker, D.K., 1989. A experimentally determine carbon: volume ratio for marine oligotrichous ciliates fro estuarine and coastal waters. Limnology and Oceanograph 34, 1097–1103.

Rassoulzadegan, F., Lavalpeuto, M., Sheldon, R.W., 198 Partitioning of the food ration of marine ciliate between picoplankton and nanoplankton. Hydrobiologi 159, 75–88.

Reid, F.M.H., 1983. Biomass estimation on components of th marine nanoplankton and picoplankton by the Utermoh settling technique. Journal of Plankton Research 5 235–252.

Roman, M.L., Dam, H.G., Gauzens, A.L., Napp, J.M. 1993. Zooplankton biomass and grazing at the JGOF Sargasso Sea time series station. Deep-Sea Research I 40 883–901.

Schnack, S.B., 1985. A note on the sedimentation of particulate matter in Antarctic waters during summer. Meersforschung 30, 306–315.

Sherr, E., Sherr, B., 1988. Role of microbes in pelagic fooc webs: a revised concept. Limnology and Oceanography 33 1225–1227.

Siegenthaler, U., Sarmiento, J.L., 1993. Atmospheric carbon dioxide and the ocean. Nature 365, 119–125.

Smith, W.O., Nelson, D.M., 1986. Importance of ice edge phytoplankton production in the Southern Ocean Bioscience 36, 251–256.

Smith, W.O., Sakshaug, E., 1990. Polar phytoplankton. In: Smith, W.O. (Ed.), Polar Oceanography. Academic Press, San Diego.

Sokal, F.J., Rolhf, R.R., 1969. Statistical Tables. Freeman & Co., San Francisco.

Stoecker, D.K., Gifford, D.J., Putt, M., 1994. Preservation of marine planktonic ciliates: losses and cell shrinkage during fixation. Marine Ecology Progress Series 110, 293–299.

Sullivan, C.W., Arrigo, K.R., McClain, C.R., Comiso, J.C., Firestone, J., 1993. Distribution of phytoplankton blooms in the Southern Ocean. Science 262, 1832–1837.

Taguchi, S., Laws, E.A., Bigidare, R.R., 1993. Temporal variability in chlorophyll-a and phaeopigment concentrations

during incubations in the absence of grazers. Marine Ecology Progress Series 45, 45–53.

Taylor, G.T., Haberstroh, P.R., 1988. Microzooplankton grazing and planktonic production in the Bransfield Strait observed during the RACER programme. Antarctic Journal of the United States 23, 125–128.

Tomas, C.R., 1996. Identifying Marine Diatoms and Dinoflagellates. Academic Press, San Diego.

Turner, D.R., Bertilsson, S., Fransson, A., Pakhomov, E., 2004. The SWEDARP 97/98 marine expedition: overview. Deep-Sea Research II, this issue [doi:10.1016/j.dsr2.2003.08.006].

ELSEVIER

Deep-Sea Research II 51 (2004) 2645–2660

DEEP-SEA RESEARCH
PART II

www.elsevier.com/locate/dsr2

Salp/krill interactions in the eastern Atlantic sector of the Southern Ocean

E.A. Pakhomov*

Southern Ocean Group, Department of Zoology and Entomology, Rhodes University, P.O. Box 94, Grahamstown 6140, South Africa

Abstract

Spatial distribution and feeding ecophysiology of the Antarctic krill, *Euphausia superba*, and the tunicate, *Salpa thompsoni*, were investigated along the 6°E meridian between 49 and 65°S. Krill and salps displayed pronounced spatial segregation along the transect. Salps clearly dominated north of the 56°S parallel, while krill dominated south of it. Overlap in krill/salp distribution occurred only at ≈56°S. This region coincided with the northernmost expansion of the subsurface cold water layer and with the Winter Ice Edge (WIE) region suggesting a clear biotopical separation of these key-stone species in the Antarctic pelagic food web. Krill and salp grazing rates determined using the in situ gut fluorescence technique were low (<1% of daily primary production) to moderate (<25%) in the areas south and north of the WIE region. However, in the region of their overlap, krill and salps alone consumed up to 86% of daily primary production. Assuming that all faecal pellets produced sink, krill and salp would be able to re-package and remove from surface layers <2%, up to 37% and 3–12% of primary production per day in the regions south, within and north of the WIE, respectively. In real terms, krill/salp mediated in situ carbon flux range from 0.01 to 3.7 and from 9.6 to 23.8 mg C $m^{-2}d^{-1}$ south and north of the WIE region, respectively, and would be as high as 48 mg C $m^{-2}d^{-1}$ in the WIE region.
© 2004 Elsevier Ltd. All rights reserved.

1. Introduction

The Antarctic krill, *Euphausia superba*, and the tunicate, *Salpa thompsoni*, are regarded as two of the most important filter-feeding metazoans of the Southern Ocean, ranking after only copepods in terms of total dry pelagic biomass (Voronina, 1998). These two species are also recognized as two of the most efficient re-packagers of small particles into larger ones, thereby playing a major role in channelling biogenic carbon into long-living pools and to the ocean's interior and seafloor via production of fast sinking faeces (Huntley et al., 1989; Fortier et al., 1994; Schnack-Schiel and Mujica, 1994; Pakhomov et al., 1997; Le Fèvre et al., 1998; Perissinotto and Pakhomov, 1998a). As a consequence, the ecological role of these two key

*Present addresses: Department of Earth and Ocean Sciences, University of British Columbia, 6339 Stores Road, Vancouver, BC, Canada V6T 1Z4 and Zoology Department, Faculty of Science and Technology, University of Fort Hare, Private Bag X1314, Alice 5700, South Africa. Tel.: +1 604 827 5564; fax: +1 604 822 6088.

E-mail address: epakhomov@eos.ubc.ca (E.A. Pakhomov).

0967-0645/$ - see front matter © 2004 Elsevier Ltd. All rights reserved.
doi:10.1016/j.dsr2.2001.03.001

species in the Antarctic pelagic food web has recently received much attention (e.g. Nishikawa et al., 1995; Siegel and Harm, 1996; Dubischar and Bathmann, 1997; Kawaguchi et al., 1998; Ross et al., 1998). It has been suggested that krill and salps may be in direct competition with one another in some areas off the Antarctic Peninsula (Loeb et al., 1997) and in the Lazarev and Cooperation Seas (Perissinotto and Pakhomov, 1998a, b).

In the Southern Ocean, *S. thompsoni* are generally restricted to the warmer water masses (Nast, 1986; Siegel et al., 1992; Pakhomov, 1993; Park and Wormuth, 1993; Kawamura et al., 1994; Nishikawa et al., 1995). With the exception of only a few areas such as Antarctic Peninsula region, spatial segregation of Antarctic krill and salps has been documented (Pakhomov et al., 1994; Hosie, 1994; Voronina, 1998). It has been postulated that if the increase in seawater temperature, already observed in the Antarctic Peninsula region continues (Zwally, 1991; Rott et al., 1996), salps may spread into the high Antarctic regions, which may have important implications for the regional carbon flux (Perissinotto and Pakhomov, 1998a, b). The studies on the community structure of zooplankton conducted in the vicinity of the Greenwich meridian indicated that Antarctic krill and salps often overlap in their distribution south of the Antarctic Polar Front (Fransz and Gonzalez, 1997; Pakhomov et al., 2000). Feeding studies conducted in this region provided evidence that these species may at times consume the entire daily primary production (Dubischar and Bathmann, 1997; Perissinotto et al., 1997; Perissinotto and Pakhomov, 1998a; Froneman et al., 2000). However, despite the increasing number of grazing measurements undertaken separately on each species, the krill/salp trophic/spatial interactions are poorly documented. The main aim of this paper was to study the distribution and feeding ecophysiology of Antarctic krill *E. superba* and salp *S. thompsoni* in the eastern Atlantic sector of the Southern Ocean south of the Antarctic Polar Front.

2. Materials and methods

Krill and salps were collected during December 1997 and January 1998 along the 6°E meridian between 49 and 65°S during a Scandinavian/South African Antarctic Expedition onboard the *S.A. Agulhas* (Froneman et al., 1998). To study zooplankton quantitative distribution, samples were generally collected every half degree of latitude. An increased sampling resolution, every 10′ of latitude, at the Spring Ice Edge (SIE, 60°S), at the Winter Ice Edge (WIE, 56°S) and at the Antarctic Polar Front (APF, 51°S) was applied (Fig. 1). The APF position was defined as the northernmost extent of the 2 °C isotherm (Turner et al., 2004). The SIE coincided with the ice edge crossed during the southbound underway transect conducted in the beginning of December 1997 (Abrahamsson et al., 2004; Turner et al., 2004). The WIE represented northern boundary of the maximum expansion of winter ice, which coincided with the northernmost extent of the negative

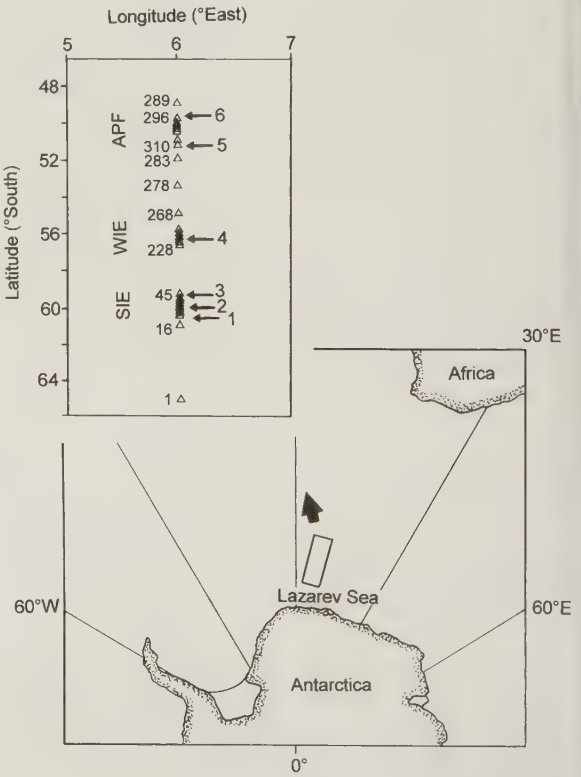

Fig. 1. Station positions occupied along the 6°E meridian in the eastern Atlantic sector of the Southern Ocean during December 1997–January 1998. Arrows indicate positions of 36 h stations (Biostations). SIE: Spring Ice Edge region; WIE: Winter Ice Edge region; APF: Antarctic Polar Front region.

subsurface isotherms (Gloersen et al., 1992; Klyausov, 1993).

Zooplankton samples were collected using a Bongo net (total mouth area: 0.5 m^2, mesh size: 0.3 and 0.5 mm, the 0.5 mm net was equipped with a 2 l plastic cod end) towed obliquely from 300 m to the surface along the transect and from 200 m to the surface during the 36 h stations. The net was equipped with a Universal Underwater Unit (U^4, Robertson et al., 1981) which monitored depth and temperature continuously. Towing speed varied between 1.5 and 3 knots. Salps for in vitro incubations were collected by additional near surface Bongo net tows conducted at the speed <1 knot. The volume filtered by the net was calculated using electronic flow meter data positioned in the 0.3 mm mesh net. The 0.3 mm mesh sample was preserved in 4–6% buffered formalin for the taxonomic, abundance and dry mass analyses of zooplankton. Detailed description of the zooplankton community structure presented in Pakhomov and Froneman (2004a). The 0.5 mm mesh samples were used for the grazing experiments (Pakhomov and Froneman, 2004b). In the laboratory, Antarctic krill *E. superba* and the salp *S. thompsoni* were counted and measured. Dry weights were obtained by oven-drying fresh specimens for 36 h at 60 °C. Krill and salp densities were expressed as the number of individuals and milligrams dry weight per cubic meter.

To measure ingestion rates of krill and salps, the in situ gut fluorescence technique (Mackas and Bohrer, 1976; JGOFS, 1989) and in vitro (only for salps) on deck incubations were employed. Detailed results of grazing studies using the gut fluorescence technique described in Pakhomov and Froneman (2004b). In order to estimate the grazing impact, krill and salp abundance data (in accordance with the size group) were combined with individual ingestion rates. To convert chlorophyll-*a* concentration into autotrophic carbon an average chlorophyll-*a*: carbon ratio of 50 was employed (Atkinson, 1996). Areal chlorophyll-*a* concentration and primary production rates in the euphotic zone (water column between surface and the depth of 1% of surface irradiances) were obtained by trapezoidal integration (Froneman et al., 2004). The grazing impact expressed as mg (pigm) m^{-2} day^{-1} and mg C m^{-2} day^{-1} was then calculated as a percentage of integrated phytoplankton standing stock and daily primary production removed per day.

For in vitro incubations, immediately after the tow, intact, actively swimming salps were placed into 20 l containers filled with surface seawater. Containers with experimental animals were kept in darkness on deck at sea surface temperature (0.6–1.0 °C at the WIE and 3–4 °C at the APF region). One or two salps (size range 30–40 mm) were incubated for 24 h. Initial and final, as well as every 4–10 h during the experiment, chlorophyll-*a* concentrations were measured in duplicate or triplicate by filtering 250 ml aliquots of water onto GF/F Whatman filters. Pigments were extracted for 24 h in polyethylene tubes with 8 ml of 90% acetone and concentrations measured with a Turner Designs fluorometer according to Strickland and Parsons (1968), as modified by Conover et al. (1986). Specimens were then frozen (−20 °C) for the dry weight analysis. Every 4–10 h during the course of the 24 h experiment, faecal pellets were counted and gently collected (1–5 pellets per filter) onto GF/F filters for pigment extractions described above. It was observed that faecal pellet production (FFP) of freshly caught salps was the highest during the first 4–8 h of incubation. Therefore, after the first 24 h in vitro experiment with 40 mm *S. thompsoni*, a second 24 h run using the same specimen was performed. During the second 24 h experiment, water in the incubation container was changed every 8 h and initial and final chlorophyll-*a* concentrations, as well as faecal pigment contents were determined for every time interval. In addition to these incubations, short incubations (2–6 h) were conducted with salps of different size to determine faecal pellet pigment concentration and production using the technique described above. Depending on salp size, between 1 and 10 specimens were incubated in 20 l containers.

3. Results

3.1. Spatial distribution and size structure

Along the transect, *E. superba* were collected between 56 and 65°S with densities <0.05 ind m^{-3}

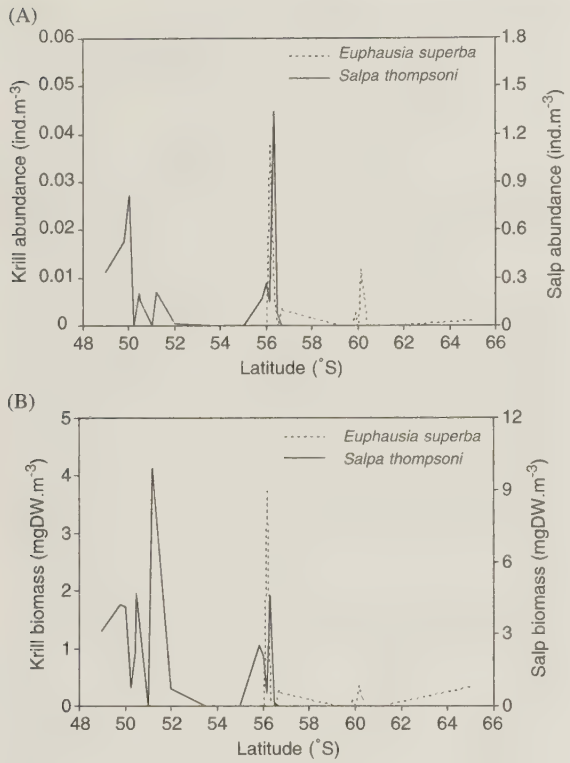

Fig. 2. Spatial distribution of abundance (A) and biomass (B) of *S. thompsoni* and *E. superba* along the 6°E meridian in the eastern Atlantic sector of the Southern Ocean during December 1997–January 1998.

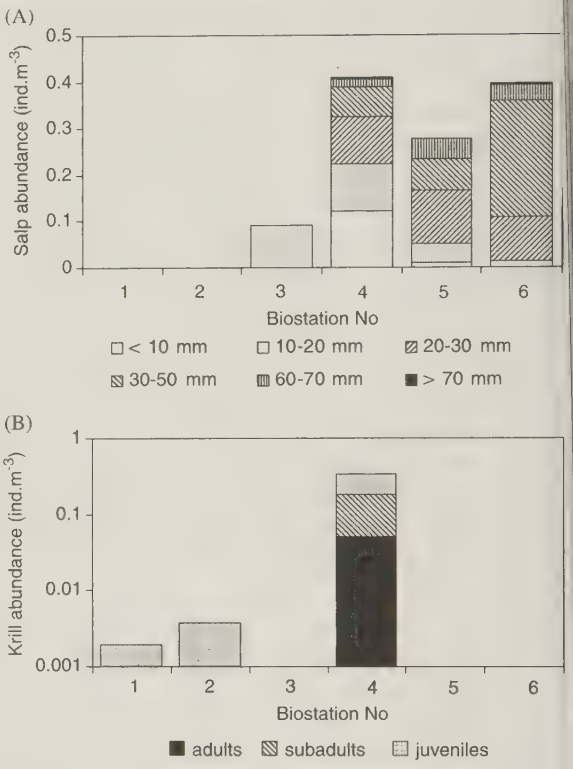

Fig. 3. Size composition of *S. thompsoni* (A) and *E. superba* (B) at Biostations conducted along the 6°E meridian in the eastern Atlantic sector of the Southern Ocean during December 1997–January 1998.

and $<4\,\mathrm{mg\,DW\,m^{-3}}$ (Fig. 2). A peak in krill density was recorded at 56°10′S within the WIE region. Krill juveniles dominated ($\approx 100\%$) along the transect and at the SIE Biostations (Fig. 3B). In the WIE region, subadults and adult krill were also well represented (Fig. 3). *S. thompsoni* were generally found in the samples collected between 49° and 56°20′S and were abundant (up to $1.4\,\mathrm{ind\,m^{-3}}$ and $10\,\mathrm{mg\,DW\,m^{-3}}$) within the WIE and APF regions (Fig. 2). Also, a few specimens ($<0.05\,\mathrm{ind\,m^{-3}}$) of *S. thompsoni* were sampled at Biostation 3 at 59°20′S. Salps were more abundant within the WIE region, while their maximum biomass levels were recorded in the APF region (Fig. 2). The main trend in salp size distribution was an increase in size from the WIE to the APF region (Fig. 3A). The overlap in krill and salp spatial distribution occurred within the WIE region. In this region, krill accounted for 56.5% of total biomass but <0.2% of total abundance. Outside of the WIE region, krill contribution to total zooplankton was negligible accounting for <0.6% of total dry biomass and <0.1% of total abundance (Fig. 4A). Salp contribution to total abundance was low along the transect and not exceeded 0.6% of total zooplankton counts. However, in terms of biomass, salps comprised between 4% and 14% of the total zooplankton standing stock (Fig. 4). Pronounced diel variability in krill and salp densities was observed at Biostations with maximum values always observed during the night (Fig. 5).

3.2. Feeding ecophysiology

Ingestion rates of krill and salps estimated using the gut fluorescence technique are discussed in detail elsewhere (Pakhomov and Froneman,

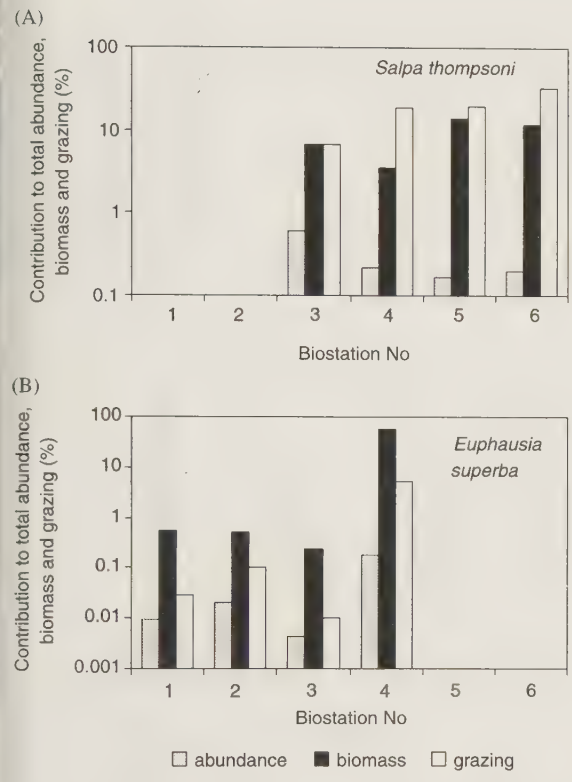

Fig. 4. Contribution to total zooplankton abundance, biomass and grazing of *S. thompsoni* (A) and *E. superba* (B) at biostations conducted along the 6°E meridian in the eastern Atlantic sector of the Southern Ocean during December 1997–January 1998.

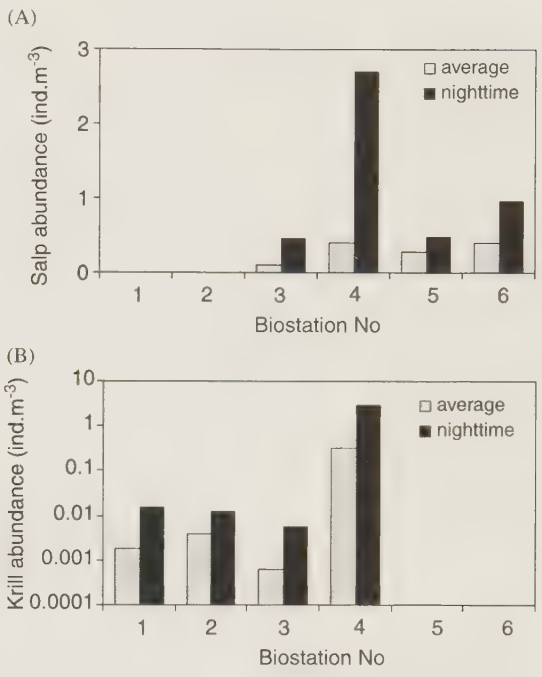

Fig. 5. Comparison between average and maximum contribution of *S. thompsoni* (A) and *E. superba* (B) to total zooplankton abundance at Biostations conducted along the 6°E meridian in the eastern Atlantic sector of the Southern Ocean during December 1997–January 1998.

2004b). In summary, the ingestion rates of krill juveniles, subadults and adults were 513–619, 1583 and 3556 ng (pigm) $ind^{-1} d^{-1}$, respectively. Using the in situ chlorophyll-*a* concentrations, individual clearance rates of juveniles, subadults and adults of krill were equal to 175, 449 and 1008 ml h^{-1}, respectively. In situ daily ingestion of *S. thompsoni* also increased with body size from 704 ng (pigm) $ind^{-1} d^{-1}$ in 10 mm salps to 125 μg (pigm) $ind^{-1} d^{-1}$ for salps 100 mm in size (Fig. 6). Using the in situ chlorophyll-*a* concentrations, salp individual clearance rates were estimated to average 147 ± 75, 265 ± 116, 812 ± 510, 3061 ± 2500, 3393 ± 208 and 9766 ml h^{-1} for 10, 20, 30, 50, 60 and 100 mm salps.

Faecal pellet pigment concentration of *S. thompsoni* increased with the salp size and dry mass (Fig. 7). Two types of faecal pellets, dense (normal) and transparent, were observed during FPP experiments. Although on most occasions 3–5 faecal pellets were pooled to measure pigment composition, in one experiment pigment content of dense and transparent pellets of 30 mm *S. thompsoni* was measured. Pigment content of dense faecal pellets (108 ± 41 ng (pigm) $pellet^{-1}$, $n = 7$) was significantly ($p < 0.01$) higher than that of transparent pellets (41.5 ± 9.8 ng (pigm) $pellet^{-1}$, $n = 5$).

The daily FPP of *S. thompsoni* expressed as number of pellets per individual did not correlated with either the salp size or dry mass. However, when the daily FPP was expressed as amount of pigments per individual, it was significantly ($p < 0.05$) positively correlated with the salp size and dry mass (Fig. 8). Two in vitro grazing/FPP experiments and one FPP experiment revealed a diel cycle in the feeding and FPP activity

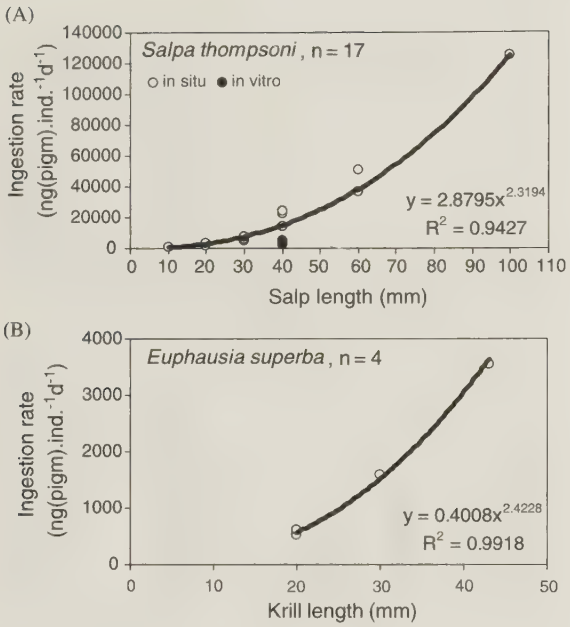

Fig. 6. Ingestion rates of *S. thompsoni* (A) and *E. superba* (B) as a function of body length.

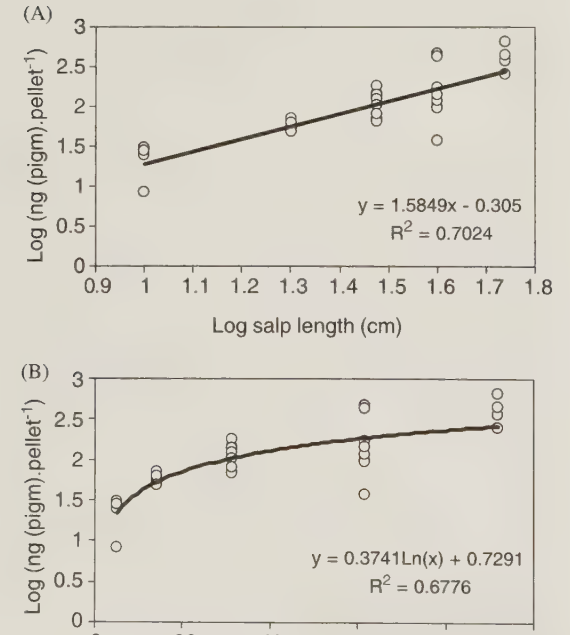

Fig. 7. Pigment contents of faecal pellets of *S. thompsoni* as a function of body length (A) and individual dry mass (B).

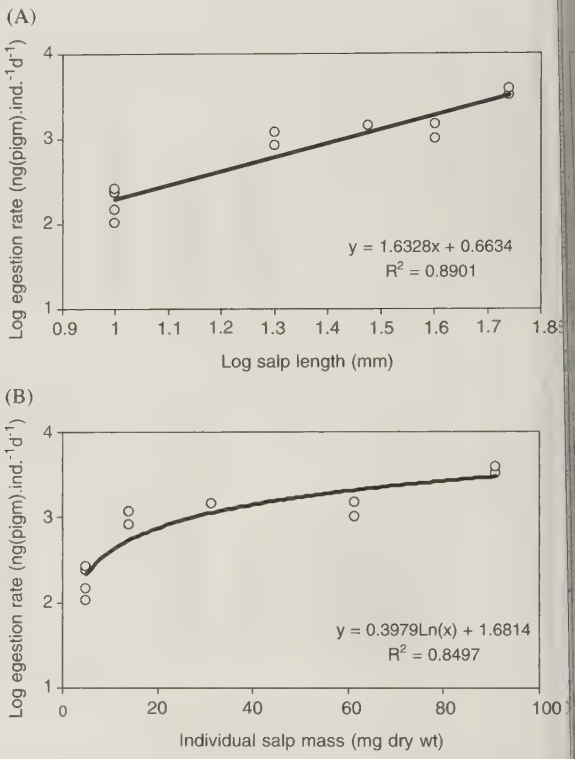

Fig. 8. FPP of *S. thompsoni* as a function of body length (A) and individual dry mass (B).

of *S. thompsoni* (Fig. 9). The lowest FPP rates for both acclimated and non-acclimated 40 mm salps, expressed as amount of pigments per individual per hour, were observed during the late afternoon. This pattern was, however, not always obvious from the number of faecal pellets produced per hour (Fig. 9). In both in vitro experiments conducted with freshly caught salps, the FPP was the highest during the first 4–8 h (Fig. 9). Daily in situ FPP, estimated from Fig. 8A and expressed as percentage of in situ ingestion rates (Fig. 6), showed high variability ranging between 7% in 100 mm salp and 33% in 10 mm salp (Table 1). In comparison, daily in vitro FPP of 40 mm salps, expressed as % of in vitro ingestion rates, ranged from 39% in the experiment with the acclimated salp to 64% in the experiment with the not acclimated salp (Table 1; Fig. 10).

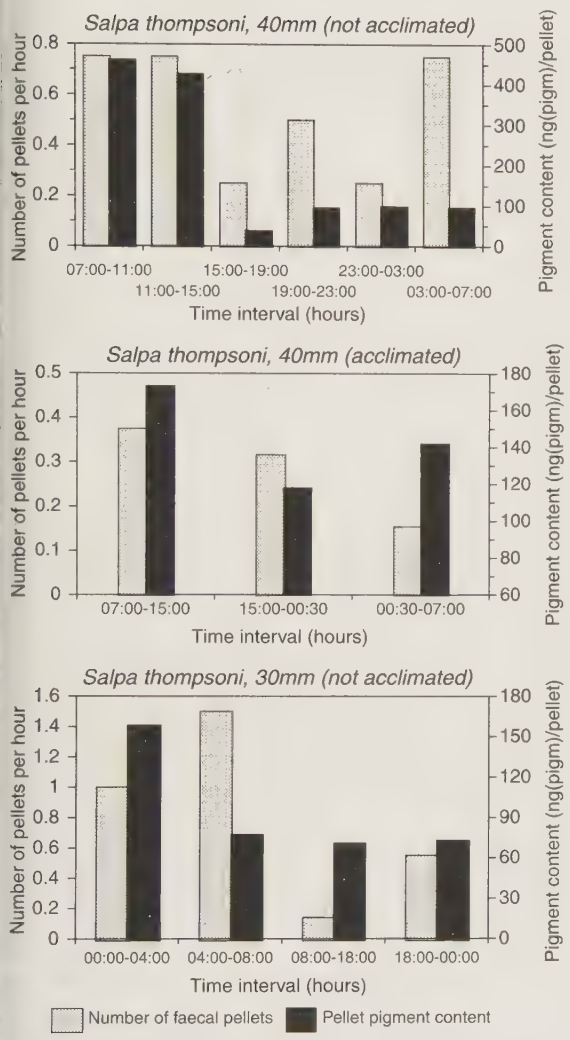

Fig. 9. Diel variability in FPP of *S. thompsoni* during in vitro incubations. Initial chlorophyll-*a* concentration in the incubating buckets was 0.64 ± 0.10 and $0.93 \pm 0.01\ \mu l^{-1}$ in experiments with 40 and 30 mm salps, respectively.

3.3. Grazing impact and carbon flux

Within the SIE region, overall daily grazing impact of Antarctic krill was very low, accounting for $<0.1\%$ of the phytoplankton standing stock and primary production (Table 2). Krill contribution to total grazing within the WIE was 0.6% of phytoplankton standing stock or 2.7% of primary production daily (Table 2). If maximum (night time) densities of krill were employed, the daily impact would increase to 6.9% and 22.7% of the phytoplankton stock and primary production, respectively (Table 2). Overall, the krill contribution to total zooplankton grazing did not exceed 5% within the SIE and WIE regions (Fig. 4). However, if maximum (night time) density data are employed, it could reach 18% of total zooplankton grazing within the WIE region.

Based on average densities, *S. thomsoni* grazing impact varied between 0.2% and 4.1% of phytoplankton standing stock and between 0.6% and 10.4% of primary production per day (Table 2). This accounted for 7–32% of the total zooplankton grazing within the WIE and APF regions (Fig. 4). If maximum (night time) salp densities are employed to estimate the grazing impact, salps would remove between 1% and 19% of the phytoplankton stock or between 3% and 63% of the daily primary production (Table 2). Using these values, the salp contribution to total zooplankton grazing would be equivalent to between 26% and 53% of the total (Fig. 4).

In order to calculate the FPP of Antarctic krill, literature sources on krill egestion rates were reviewed (Table 3). As chlorophyll values within the WIE region were the lowest along the entire transect (Froneman et al., 2004; Pakhomov and Froneman, 2004b), an average minimum egestion rate of $0.3\ \mu g\ C\ mgDW^{-1}d^{-1}$ in combination with krill biomass was used to calculate the krill FPP (1 approach) at Biostations. For a comparison, the potential particle flux through faecal pellets was also assessed using average assimilation efficiency (2 approach) of 70% for krill (Pakhomov et al., 1997) and 52% for salps (Table 1). Krill and salp FPP generally accounted for $<0.8\%$ (max 7%) and for $<5\%$ (max 30%) of daily primary production, respectively (Table 4). The highest proportion of primary production removed (up to 37%) by both species through faeces was observed within the WIE region (Table 4).

4. Discussion

4.1. Krill/salp spatial separation

Data collected during austral summer 1997–98 along the 6°E meridian indicated that the spatial

Table 1
Ingestion rates (IR) and faecal pellet production (FPP) of *S. thompsoni* estimated during in situ and in vitro experiments

Salp length (mm)	In situ IR[a] ($\mu g(pigm)\,ind^{-1}\,d^{-1}$)	In situ FPP[b] ($\mu g(pigm)\,ind^{-1}\,d^{-1}$)	% of IR	In vitro IR ($\mu g(pigm)\,ind^{-1}\,d^{-1}$)	In vitro FPP ($\mu g(pigm)\,ind^{-1}\,d^{-1}$)	% of IR
10	0.601	0.198	32.9	nd	nd	nd
20	2.999	0.613	20.4	nd	nd	nd
30	7.680	1.189	15.5	nd	nd	nd
40	14.967	1.902	12.7	2.590(a)/5.130(na)	1.015(a)/3.276(na)	39.2(a)/ 63.9(na)
60	38.332	3.688	9.6	nd	nd	nd
100	125.348	8.492	6.8	nd	nd	nd

nd: not determined; (a): acclimated salp; (na): not acclimated salp.
[a]In situ IR was calculated using equation $IR = 2.8795 \times \text{salp length}^{2.3194}$ from Fig. 6A.
[b]In situ FPP was calculated using equation $\log FPP = 1.6328 \times \log(\text{salp length}) + 0.6634$ from Fig. 8A.

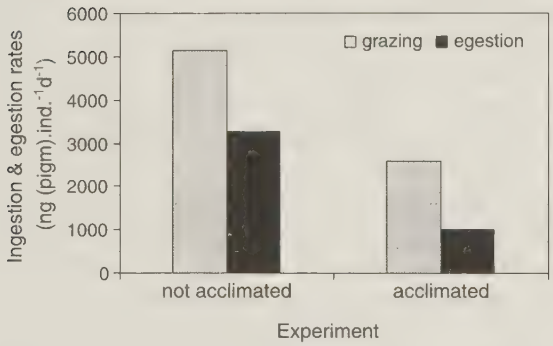

Fig. 10. Comparison between grazing and FPP of 40 mm *S. thompsoni* estimated during in vitro incubations with not acclimated and acclimated specimens.

overlap in distribution of the Antarctic krill and tunicate, *S. thompsoni*, was minimal and occurred only within the WIE region at approximately 56°S. Salps virtually disappeared from the samples south of the WIE region, while krill were not sampled north of it. Here, the highest densities of both species were observed. It is worth noting that the major separation in the zooplankton assemblages along this transect coincided with the WIE region suggesting that different water masses were sampled to the north and south of this region (Pakhomov and Froneman, 2004a). With respect to the oceanographic environment, the WIE region was characterized by disappearance of the subsurface cold water layer as the northernmost limit of the subsurface zero isotherm being foun between 55 and 56°S (Turner et al., 2004). Thi region also coincided more or less with th northernmost expansion of the winter sea-ic (Gloersen et al., 1992; Turner et al., 2004).

Similar studies conducted along the Greenwic and 45°E meridians and in the Pacific sector of th Southern Ocean also showed the ecologica importance of the subsurface frontal featur associated with the northernmost limit of the zer isotherm and winter ice expansion (Casareto an Nemoto, 1986; Terazaki and Wada, 1986; Gra chev, 1991; Klyausov, 1993; Pakhomov an McQuaid, 1996; Pakhomov et al., 2000). Indeed in the Southern Ocean, *S. thompsoni* are generall restricted to the warmer waters or layers and thei density declines sharply as ice cover increase (Foxton, 1966; Siegel et al., 1992; Pakhomov 1993; Park and Wormuth, 1993; Hosie, 1994). The inability of *S. thompsoni* to complete successfully its reproduction cycle in the high Antarctic waters (Casareto and Nemoto, 1986; Chiba et al., 1999) indicates that at higher latitudes this species probably survive in conditions close to its ther mo-physiological limits. During summer *S. thomp soni* may, however, be observed as far south as 68°S (Pakhomov, 1991; Pakhomov et al., 1994; Perissinotto and Pakhomov, 1998a, b). On these occasions, *S. thompsoni* were, however, associated with warmer (>0 °C) water layers derived from the upwelling/advection of Antarctic deep water or

Table 2
Krill and salp grazing at Biostations conducted in the eastern Atlantic sector of the Southern Ocean during December 1997 January 1998

Species	Grazing impact (units)	SIE 1	SIE 2	SIE 3	WIE 4	APF 5	APF 6
E. superba	mg (pigm) $m^{-2} d^{-1}$	<0.01	<0.01	<0.01	0.124	—	—
		<0.01	**<0.01**	**<0.01**	**1.385**	—	—
	% of phytoplankton stock	<0.1	<0.1	<0.1	0.6	—	—
		<0.1	**<0.1**	**<0.1**	**6.9**	—	—
	% of primary production	<0.1	<0.1	<0.1	2.7	—	—
		<0.1	**<0.1**	**<0.1**	**22.7**	—	—
S. thompsoni	mg (pigm) $m^{-2} d^{-1}$	—	—	0.050	0.585	0.666	1.779
			—	**0.247**	**3.867**	**1.144**	**4.287**
	% of phytoplankton stock	—	—	0.2	2.9	1.7	4.1
			—	**1.0**	**19.3**	**3.0**	**9.9**
	% of primary production	—	—	0.6	9.5	4.5	10.4
			—	**3.1**	**63.3**	**7.7**	**25.1**

Bold numbers represent values calculated using maximum (night time) abundance data (see text for further explanation). SIE: Spring Ice Edge region; WIE: Winter Ice Edge region; APF: Antarctic Polar Front region.

Table 3
Antarctic krill *E. superba* egestion rates

Mean krill mass (mg dry wt)	Egestion rate ($\mu g C mg^{-1} d^{-1}$)	Source
243.6±20.0	Mean 0.287 Max 2.258	(Antezana et al., 1982)
144.0	4.583 43.083	(Clarke et al., 1988)
154.9±23.2	Mean 0.298 Max 0.393	(Ponomareva and Kuznetsova, 1989)
45.3±16.6	Mean 10.0 Max 55.0	(Nordhausen and Huntley, 1990)
137.0±31.4	Mean 7.131	(Pakhomov et al., 1997)

Carbon content of faecal pellets was assumed to account in average for 11% of their dry mass (Pakhomov et al., 1997)

as a result of summer capping (Pakhomov, 1991, 1993). Conversely, the distribution of Antarctic krill is restricted to the high Antarctic water masses and its life cycle is closely linked to the seasonal sea-ice biotope (Knox, 1994; Loeb et al., 1997). Therefore, the spatial segregation of Antarctic krill and *S. thompsoni* throughout the Southern Ocean is most likely the result of biotopical separation of these species. It is documented that in the Atlantic sector of the Southern Ocean, particularly in the Antarctic Peninsula region, krill and salps clearly overlap in their summer macro-scale distribution range (e.g. Witek et al., 1985; Piatkowski, 1987; Ross et al., 1998). However, during surveys when meso- and micro-scale sampling resolution was applied, on most occasions krill and salps were spatially, horizontally or vertically, separated (Park and Wormuth, 1993; Brinton, 1984; Nast, 1986; Maklygin and Pakhomov, 1993; Pakhomov, 1993; Siegel and Harm, 1996; Nishikawa et al., 1995; Ross et al., 1998).

Table 4
Krill and salp contribution to vertical carbon flux as estimated using faecal pellet production rates at Biostations in the eastern Atlan sector of the Southern Ocean during December 1997–January 1998

Species	Faecal pellet production (units)	SIE 1	SIE 2	SIE 3	WIE 4	APF 5	AP 6
E. superba	$mg\,C\,m^{-2}\,d^{-1}$	0.005	0.006	0.001	2.223	—	—
		0.050	**0.020**	**0.011**	**15.565**	—	—
	% primary production (1)	<0.1	<0.1	<0.1	0.7	—	—
		<0.1	**<0.1**	**<0.1**	**5.2**	—	
	% primary production (2)	<0.1	<0.1	<0.1	0.8	—	—
		<0.1	**<0.1**	**<0.1**	**6.8**	—	—
S. thompsoni	$mg\,C\,m^{-2}\,d^{-1}$	—	—	0.733	4.895	5.550	9.81
		—	—	**3.728**	**32.41**	**9.610**	**23.8**
	% primary production (1)	—	—	0.2	1.6	0.7	1.2
		—	—	**0.9**	**10.6**	**1.3**	**2.8**
	% primary production (2)	—	—	0.3	4.6	2.0	4.9
		—	—	**1.5**	**30.4**	**3.7**	**12.0**

Bold numbers represent values calculated using maximum (night time) abundance data. (1): calculations made using faecal pell production (FPP) data; for salps FPP calculated using equation from Fig. 8A combined with size class abundance data; for krill FF calculated using minimum mean value of $0.3\,\mu gC\,mg\,DW^{-1}\,d^{-1}$ from Table 3 combined with biomass data; (2): calculations ma using grazing rate estimates presented in Table 2 assuming average assimilation efficiency of 70% for krill (Pakhomov et al., 1997) a 52% for salps (Table 1). SIE: Spring Ice Edge region; WIE: Winter Ice Edge region; APF: Antarctic Polar Front region.

4.2. Krill/salp feeding dynamics

Gut pigment contents, daily in situ ingestion and clearance rates of both the Antarctic krill and salps increased dramatically with increasing in size and were found to be among the highest estimates recorded for these species (Reinke, 1987; Drits and Semenova, 1989; Huntley et al., 1989 (Table 6); Drits and Pasternak, 1993; Pakhomov et al., 1997 (Table 6); Perissinotto et al., 1997; Dubischar and Bathmann, 1997; Perissinotto and Pakhomov, 1998a, b; Ross et al., 1998). In situ grazing estimates showed that *S. thompsoni* exhibited the highest individual ingestion and clearance rates ($\approx 125\,\mu g$ (pigm) $ind^{-1}\,d^{-1}$ and $9766\,ml\,ind^{-1}\,d^{-1}$) compared to any other primary production consumer in the Antarctic pelagic community. These were only comparable to ingestion rates obtained for the same species (and similarly sized specimens) in the Antarctic Circumpolar Current (max $16\,\mu g$ (pigm) $ind^{-1}\,d^{-1}$; Dubischar and Bathmann, 1997) and in the Lazarev Sea (up to $160\,\mu g$ (pigm) $ind^{-1}\,d^{-1}$; Perissinotto and Pakhomov, 1998a, b).

In contrast with Antarctic krill (Table 3), ver little information is available on the FPP rates c *S. thompsoni*. To date, only a single experimen near the Antarctic Peninsula during austra summer 1983/84 has been conducted (Huntle et al., 1989). The estimates showed that a 21 mm blastozoid of *S. thompsoni* egested 10.2% of bod carbon and 6.6% of body nitrogen per day, whic accounted for 40.7% and 48.8% of ingeste carbon and nitrogen, respectively (Huntley et al. 1989). The average in situ FPP rates obtained i the present study for similar size individuals usin pigment budget ($\approx 20\%$ of ingested pigments Table 1) are only about half of estimates presente above. This could be due to the methodologica constrains as average ingestion and egestion rate were obtained independently. The Huntley et a (1989) estimates are, however, almost identical t the value (39.2%, Table 1) derived from in vitr experiment conducted during this study wit acclimated *S. thompsoni*. The higher relative FP (64% of the ingestion rate) was observed in no acclimated salp specimens. As mentioned in th results, the highest FPP rates were obtained durin

he first 4–8 h of incubation using salps that have ot been acclimated. Consequently, elevated FPP ates at the beginning of incubation, representing robably in situ rates, would most likely bias total n vitro daily FPP. This also suggests that under atural conditions specimens of *S. thompsoni* feed n higher phytoplankton concentrations utilizing robably the natural fine-scale patchiness of food esources. Thus, the FPP rates calculated using the n situ measurements are likely more realistic Table 1). The data presented in Fig. 9 and Table suggest that, whilst the absolute FPP rates ncrease significantly with the salp size, the smaller alp specimens (<30 mm) may possibly be in verage 2.4 fold more efficient in re-packaging uspended particles than larger (>30 mm) salps.

Diel variability in Antarctic krill and salp ensities, observed during the Biostations Fig. 5), resulted in 2–10 fold differences in grazing npact and FPP calculations (Tables 2 and 4). As his would have important implications for the ownward flux, the validity of the data sets btained using different densities should be erified. The Antarctic krill is a well-known ertical migrator within the top 200 m layer (e.g. Marr, 1962; Everson, 1983; Klusek and Godlewska, 1988; Pakhomov, 1995). Krill disperse in he top layer to feed during the night and swarm ithin the water column during the day (Everson nd Ward, 1980). Known as a good swimmer, Antarctic krill successfully avoid nets, even large ets such as RMT-8, during the day (Miller and Hampton, 1989). There is no doubt, therefore, that he grazing impact calculations estimated employng the densities of Antarctic krill obtained during he night are more reliable. Salps, on the other and, do not exhibit pronounced net avoidance. Their diel vertical migrations may cover up to 000 m of the water column and, therefore, day/ ight differences in salp densities could reflect their bsence in the top layer (Foxton, 1966; Casareto nd Nemoto, 1986; Pakhomov, 1991). However, he most recent studies conducted along the Greenwich meridian south of the APF, showed hat the bulk of the *S. thompsoni* population during the austral summer undertakes vertical migrations within the top 200 m, concentrating ear the surface during the night (Perissinotto and Pakhomov, 1998a, b). The high degree of variability in densities of *S. thompsoni* is, therefore, likely a result of extreme natural patchiness as they mostly are found in large colonies (Foxton, 1966; Everson and Ward, 1980). The recorded variability would be further enhanced if small sampling devices, such as Bongo net, are used to collect salps. As a consequence, maximum salp densities obtained during the night will represent an overestimate of their average density and subsequently potential maximum grazing and FPP rates at any particular location.

Total grazing impact on primary production of Antarctic krill and *S. thompsoni* was negligible (<0.1% of total) to modest (3–25%) within the SIE and APF regions. In contrast, in the area of overlap (WIE region), these two species could potentially consume up to 86% of daily primary production (Table 2). The above grazing impact likely reflects the spatial coincidence of krill and salps with the lowest primary production rates along the entire transect (Froneman et al., 2004). If grazing impact of other zooplankton groups, e.g. copepods (37% of daily primary production) and pteropods (3%) included (from Pakhomov and Froneman, 2004b), total zooplankton grazing would exceed the total daily primary production, consequently controlling the phytoplankton biomass build-up in the WIE region.

The contribution of mesozooplankton (mainly copepods) to the downward particle flux through faeces is thought to be limited due to fact that their faecal pellets may be largely recycled within the euphotic zone (Fortier et al., 1994; Bathmann, 1998). On the other hand, salps and krill (and probably pteropods), by producing large, fast sinking faecal pellets may be major contributors to the downward particulate carbon flux (Fortier et al., 1994; Le Fèvre et al., 1998). Indeed, assuming that all faecal pellets sink, krill and salps alone would re-package and transfer to depth per day <2%, ≈37% and 3–12% of primary production within the SIE, WIE and APF regions, respectively. Krill and salp mediated in situ average carbon flux would range from 0.01 to 3.7 and from 9.6 to 23.8 mg C m^{-2} d^{-1} within the SIE and APF regions, respectively, and would be as high as 48 mg C m^{-2} d^{-1} in the WIE region. This

constitutes a downward transport of biogenic carbon higher than the average carbon flux in many oceanic areas (Fisher et al., 1988) and would be equivalent to 1–60% of the particulate organic carbon flux in various areas of the Southern Ocean obtained from sediment trap collections (Schnack, 1985; von Bodungen, 1986; von Bodungen et al., 1986; Nöthig and von Bodungen, 1989; Bathmann et al., 1991; Gonzalez, 1992).

4.3. Krill/salp interactions

Increasing interest in krill/salp interactions in the Southern Ocean (Loeb et al., 1997), has led to several hypotheses being proposed to explain their spatial segregation. Firstly, salps may prey (filter out) on eggs and early larval stages of krill, thus, affecting krill recruitment (Huntley et al., 1989). This hypothesis was supported by findings of krill debris and larvae in food boluses of *S. thompsoni* (Hopkins, 1985; Hopkins and Torres, 1989; Lancraft et al., 1991; Hopkins et al., 1993). This appeared, however, to be negligible due to vertical segregation of krill eggs/early stages and salps (Perissinotto and Pakhomov, 1998b) and in any case would only be noticeable in latter years. Secondly, salps may produce distasteful metabolic products which may drive other organisms, including krill, away (Fraser, 1962). Although the above cannot be discounted, recent observations suggest that the exactly opposite response occurs in the areas of the krill/salp spatial overlap. It has been shown that Antarctic krill were attracted to salp extracts and, in fact, were able to successfully prey on salps with a rate of up to 0.5 salp per krill per day (Kawaguchi and Takahashi, 1996). Thirdly, Antarctic krill may be excluded from the areas of high salp densities because salps deprive other zooplankton, including krill, from food (Fraser, 1962). Indeed, salps are efficient in retaining particles within a wide size range, from 1 to 1000 μm (Drits and Semenova, 1989; Fortier et al., 1994), while Antarctic krill prey mainly on food particles >10 to <50 μm (Meyer and El-Sayed, 1983; Drits and Semenova, 1989; Maciejewska, 1993; Opalinski et al., 1997). Also, salps may at times control phytoplankton biomass consuming the entire daily primary production (Huntley et al., 1989; Perissinot and Pakhomov, 1998a, b; Ross et al., 199 However, no direct interaction between the pr portion of green krill (intensively feeding krill) a salp density was observed, suggesting a negligi competition for phytoplankton between krill a salps (Kawaguchi et al., 1998). Lastly, the spati segregation in krill and salp populations may due to the advection of different water masses the region. This hypothesis has already be discussed above and seems to explain limit spatial overlap in krill/salp distribution outsi the Antarctic Peninsula region. A noticeab synchronized pattern between salp density a elevated sea-surface temperatures was also o served around Antarctic Peninsula (Piatkowsk 1989). In the Lazarev and Cosmonaut Seas, sal may occasionally be found as far south as 68°S b only in association with the warmer water intr sions into the region (Pakhomov, 1991; Pakhom et al., 1994; Perissinotto and Pakhomov, 1998a).

The waters surrounding Elephant Island (Sout Shetland Islands) are well known as a region krill and salp spatial overlap (Loeb et al., 199 This is hardly surprising as oceanographic da indicate that this region is one of the most comple areas of the Southern Ocean, where water mass of different origin are often mixed togeth (Maslennikov and Solyankin, 1979; Maslennikov 1980; Sahrhage, 1988). Most recent analysis o long-term data sets on krill biomass, krill spawn ing and recruitment, salp biomass and sea-ic cover in the vicinity of the Elephant Islan revealed significant correlations between thes parameters (Loeb et al., 1997). It was postulate that winters characterized with poor sea-ice cove would promote extensive salp blooms and poo krill spawning during the following summer and as a consequence, poor krill recruitment th following year. A long-term warming trend wa suggested to be responsible for the increase occurrence of "salp" years around Elephant Islan (Loeb et al., 1997). As the warming trend in ai temperature is generally coupled with seawate temperature increase (Priddle et al., 1988; Fedou lov et al., 1996), changes in the pelagic biotop may occur around Elephant Island. Indeed although it is not absolutely clear due to limite

data sets, "salp" years showed good coincidence with the highest mean sea water temperature for the region (Siegel and Loeb, 1995).

Particle concentrations may be an additional environmental factor affecting salp distribution. Salps generally dominate in the oligotrophic, warmer waters (Foxton, 1966; Voronina, 1984, 1998; Casareto and Nemoto, 1986; Nishikawa et al., 1995). When salps are advected far south, high phytoplankton concentrations may cause clogging in their filtering apparatus resulting in salp disappearance to the advantage of other zooplankton, such as krill, which are adapted to feed in the presence of high particle densities (Perissinotto and Pakhomov, 1997, 1998b).

The regional ecological consequences of years of high salp densities, as discussed above, may be dramatic and if the warming trend spread into other areas of the Southern Ocean, salps would probably play a more prominent role in the trophic structure of the Antarctic marine ecosystem. This could probably be coupled with the dramatic decrease in krill productivity largely due to decrease in the spatial extension of the krill biotope.

Acknowledgements

I am grateful to the South African Department of Environmental Affairs and Tourism, to Rhodes University and to the Swedish Polar Secretariate for logistical and financial support of this study. I would like to thank officers and crew of the *SA Agulhas* and many my colleagues from Göteborg University (Sweden) and Rhodes University (South Africa) for understanding and constant help during the expedition. I am particularly indebted to P.W. Froneman, A. Grinham and M. Balarin for their help in conducting some grazing experiments.

References

Abrahamsson, K., Bertilsson, S., Chierici, M., Fransson, A., Froneman, P.W., Lorén, A., Pakhomov, E.A., 2004. Variations of biochemical parameters along a transect in the Southern Ocean, with special emphasis on volatile halogenated organic compounds. Deep-Sea Research II, this issue [doi:10.1016/j.dsr2.2004.09.004].

Antezana, T., Ray, K., Melo, C., 1982. Trophic behavior of *Euphausia superba* Dana in laboratory conditions. Polar Biology 1, 77–82.

Atkinson, A., 1996. Subantarctic copepods in an oceanic, low chlorophyll environment: ciliate predation, food selectivity and impact on prey populations. Marine Ecology Progress Series 130, 85–96.

Bathmann, U.V., 1998. Ecology and biochemistry in the Atlantic sector of the Southern Ocean during austral spring: the first JGOFS expedition aboard RV *Polarstern*. Journal of Marine Systems 17, 77–85.

Bathmann, U., Fischer, G., Müller, P.J., Gerdes, D., 1991. Short-term variations in particular matter sedimentation off Kapp Norvegia, Weddell Sea, Antarctica: relation to water mass advection, ice cover, plankton biomass and feeding activity. Polar Biology 11, 185–195.

Brinton, B., 1984. Observations of plankton organisms obtained by Bongo nets during the November–December 1983 ice-edge investigations. Antarctic Journal of the US 19, 113–115.

Casareto, B.E., Nemoto, T., 1986. Salps of the Southern Ocean (Australian sector) during the 1983–84 summer, with special reference to the species *Salpa thompsoni*, Foxton 1961. Memoirs of the National Institute for Polar Research 40, 221–239.

Chiba, S., Ishimaru, T., Hosie, G., Wright, S.W., 1999. Population structure change of *Salpa thompsoni* from austral mid-summer to autumn. Polar Biology 22, 341–349.

Clarke, A., Quetin, L.B., Ross, R.M., 1988. Laboratory and field estimates of the rate of faecal pellet production by Antarctic krill, *Euphausia superba*. Marine Biology 98, 557–563.

Conover, R.J., Durvasula, R., Roy, S., Wang, R., 1986. Probable loss of chlorophyll-derived pigments during passage through the gut of zooplankton and some of the consequences. Limnology and Oceanography 31, 878–887.

Drits, A.V., Pasternak, A.F., 1993. Feeding of dominant species of the Antarctic herbivorous zooplankton. In: Voronina, N.M. (Ed.), Pelagic Ecosystems of the Southern Ocean. Nauka Press, Moscow, pp. 250–259 (in Russian).

Drits, A.V., Semenova, T.N., 1989. Trophic characteristics of major planktonic phytophages from South Shetland Islands region during early spring. In: Ponomareva, L.A. (Ed.), Complex Investigations of the Pelagic Zone of the Southern Ocean. Shirshov Institute Oceanology Publishers, Moscow, pp. 66–78 (in Russian).

Dubischar, C.D., Bathmann, U.V., 1997. Grazing impact of copepods and salps on phytoplankton in the Atlantic sector of the Southern Ocean. Deep-Sea Research II 44, 415–433.

Everson, E., 1983. Variations in vertical distribution and density of krill swarms in the vicinity of South Georgia. Memoirs of the National Institute for Polar Research 27, 84–92.

Everson, E., Ward, P., 1980. Aspects of Scotia Sea zooplankton. Biological Journal of the Linnean Society 14, 93–101.

Fedoulov, P.P., Murphy, E., Shulgovsky, K.E., 1996. Environment–krill relations in the South Georgia marine ecosystem. CCAMLR Science 3, 13–30.

Fisher, G., Fütterer, D.R., Gersonde, R., Honjo, S., Ostermann, D., Wefer, G., 1988. Seasonal variability of particle flux in the Weddell Sea and its relation to ice cover. Nature 335, 426–428.

Fortier, L., Le Fèvre, J., Legendre, L., 1994. Export of biogenic carbon to fish and to the deep ocean: the role of large planktonic microphages. Journal of Plankton Research 16, 809–839.

Foxton, P., 1966. The distribution and life history of *Salpa thompsoni* Foxton with observations on a related species, *Salpa gerlachei* Foxton. Discovery Reports 34, 1–116.

Fransz, H.G., Gonzalez, S.R., 1997. Latitudinal metazoan plankton zones in the Antarctic Circumpolar Current along 6°W during austral spring 1992. Deep-Sea Research II 44, 395–414.

Fraser, J.H., 1962. The role of ctenophores and salps in zooplankton production and standing crop. Rapports et Proces-Verbaux des Reunions, Conseil International pour l'Exploration de la Mer 153, 121–123.

Froneman, P.W., Pakhomov, E.A., Turner, D., Abrahamsson, K., Karlson, B., Godhe, A., Bertilsson, S., Granéli, W., Carlsson, P., Wängberg, S., Wulff, A., Croot, P., Andersson, K., Balarin, M., Wedborg, M., Persson, T., Rasmus, K., Özturk, M., David, R., 1998. Research cruise of the Scandinavian/South African Antarctic Expedition: December 1997 to February 1998. South African Journal of Science 94, 517–519.

Froneman, P.W., Pakhomov, E.A., Perissinotto, R., McQuaid, C.D., 2000. Zooplankton structure and grazing in the Atlantic sector of the Southern Ocean in late austral summer 1993. Part 2. Biochemical zonation. Deep-Sea Research I 47, 1687–1702.

Froneman, P.W., Pakhomov, E.A., Balarin, M.G., 2004. Size-fractionated phytoplankton biomass, production and biogenic carbon flux in the eastern Atlantic sector of the Southern Ocean in late austral summer 1997–1998. Deep-Sea Research II, this issue [doi:10.1016/j.dsr2.2002.09.001].

Gloersen, P., Campbell, W.J., Cavalieri, D.J., Comiso, J.C., Parkinson, C.L., Zwally, H.J., 1992. Arctic and Antarctic sea ice, 1978–1987: satellite passive-microwave observations and analysis. NASA SP-511, Washington, DC.

Gonzalez, H.E., 1992. The distribution and abundance of krill faecal material and oval pellets in the Scotia and Weddell Seas (Antarctica) and their role in particle flux. Polar Biology 12, 81–91.

Grachev, D.G., 1991. Frontal zone influences on the distribution of different zooplankton groups in the central part of the Indian sector of the Southern Ocean. In: Samolova, M.S., Shumkova, S.O. (Eds.), Ecology of Commercial Marine Hydrobionts. TINRO Press, Vladivostok, pp. 19–21 (in Russian).

Hopkins, T.L., 1985. Food web of an Antarctic midwater ecosystem. Marine Biology 89, 197–212.

Hopkins, T.L., Torres, J.J., 1989. Midwater food web in t vicinity of a marginal ice zone in the western Weddell Se Deep-Sea Research 36, 543–560.

Hopkins, T.L., Ainley, D.G., Torres, J.J., Lancraft, T.M., 19 Trophic structure in open waters of the marginal ice zone the Scotia Weddell confluence region during spring (198 Polar Biology 13, 389–397.

Hosie, G.W., 1994. The macrozooplankton communities in t Prydz Bay region, Antarctica. In: El-Sayed, S.Z. (Ed Southern Ocean Ecology: the BIOMASS Perspectiv Cambridge University Press, Cambridge, pp. 93–123.

Huntley, M.E., Sykes, P.F., Marin, V., 1989. Biometry ar trophodynamics of *Salpa thompsoni* Foxton (Tunicat Thaliacea) near the Antarctic Peninsula in Austral summe 1983–1984. Polar Biology 10, 59–70.

JGOFS, 1989. Core measurements protocols, reports of th core measurement working groups. In: Tidmarsh, E. (Ed SCOR JGOFS Report, vol. 6, 40pp.

Kawaguchi, S., Takahashi, Y., 1996. Antarctic krill (*Euphausi superba* Dana) eat salps. Polar Biology 16, 479–481.

Kawaguchi, S., Ichii, T., Naganobu, M., de la Mare, W.K 1998. Do krill and salps compete? Contrary evidence fro the krill fisheries. CCAMLR Science 5, 205–216.

Kawamura, A., Michimori, K., Moto, J., 1994. Marked invers distribution of salps to other macrozooplankton in wate adjacent to the South Shetland Islands. Proceedings of th NIPR Symposium on Polar Biology 7, 70–81.

Klusek, Z., Godlewska, M., 1988. Depth distribution and day night migrations of krill (BIOMASS III, October–Novem ber, 1986, January, 1987). Polish Polar Research 9, 349–356

Klyausov, A.V., 1993. On the frontal zone near the northern boundary of sea ice area distribution in the Southern Ocean Oceanology 33, 824–832.

Knox, G.A., 1994. The Biology of the Southern Ocean Cambridge University Press, Cambridge.

Lancraft, T.M., Hopkins, T.L., Torres, J.J., Donnelly, J., 1991 Oceanic micronektonic/macro-zooplanktonic community structure in ice covered Antarctic waters during the winte (AMERIEZ 1988). Polar Biology 11, 157–167.

Le Fèvre, J., Legendre, L., Rivkin, R.B., 1998. Fluxes o biogenic carbon in the Southern Ocean: roles of large microphagous zooplankton. Journal of Marine Systems 17, 325–345.

Loeb, V., Siegel, V., Holm-Hansen, O., Hewitt, R., Fraser, W., Trivelpiece, W., Trivelpiece, S., 1997. Effects of sea-ice extent and krill or salp dominance on the Antarctic food web. Nature 387, 897–900.

Maciejewska, K., 1993. Feeding of Antarctic krill *Euphausia superba* in Weddell Sea. Polish Polar Research 14, 52–54.

Mackas, D., Bohrer, R., 1976. Fluorescence analysis of zooplankton gut contents and an investigation of diel feeding patterns. Journal of Experimental Marine Biology and Ecology 25, 77–85.

Maklygin, L.G., Pakhomov, E.A., 1993. Vertical distribution and diurnal migrations of Antarctic macrozooplankton (February–March 1989, Atlantic sector of the Southern Ocean). In: Klekowski, R.Z., Opalinski, K.W. (Eds.), The

Second Polish–Soviet Antarctic Symposium. Polish Academy of Sciences, Institute Ecology Publishing Office, Dziekanów Lesny, pp. 145–150.

Marr, J.W.S., 1962. The natural history and geography of the Antarctic krill (*Euphausia superba* Dana). Discovery Reports 32, 33–464.

Maslennikov, V.V., 1980. Modern concepts on the large scale circulation of Antarctic waters and routes of mass drift of krill. In: Makarov, R.R. (Ed.), Biological Resources of the Antarctic Krill. VNIRO Press, Moscow, pp. 8–27 (in Russian).

Maslennikov, V.V., Solyankin, Y.V., 1979. Interannual displacements of the zone of interaction of Weddell Sea waters with the Antarctic Circumpolar Current. The Antarctic 18, 118–122 (in Russian).

Meyer, M.A., El-Sayed, S.Z., 1983. Grazing of *Euphausia superba* Dana on natural phytoplankton populations. Polar Biology 1, 193–197.

Miller, D.G.M., Hampton, I., 1989. Biology and ecology of the Antarctic krill (*Euphausia superba* Dana): a review. BIOMASS Scientific Series 9, 1–166.

Nast, F., 1986. Changes in krill abundance and in other zooplankton relative to the Weddell–Scotia Confluence around Elephant Island in November 1983, November 1984 and March 1985. Archiv für Fischereiwissenschaft 37, 73–94.

Nishikawa, J., Naganobu, M., Ichii, T., Ishii, H., Terazaki, M., Kawaguchi, K., 1995. Distribution of salps near the South Shetland Islands during austral summer, 1990–1991 with special reference to krill distribution. Polar Biology 15, 31–39.

Nordhausen, W., Huntley, M.E., 1990. RACER: carbon egestion rates of *Euphausia superba*. Antarctic Journal of the United States 25, 161–162.

Nöthig, E.-M., von Bodungen, B., 1989. Occurrence and vertical flux of faecal pellets of probably protozoan origin in the southeastern Weddell Sea (Antarctica). Marine Ecology Progress Series 56, 281–289.

Opalinski, K.W., Maciejewska, K., Georgieva, L.V., 1997. Notes on food selection in the Antarctic krill, *Euphausia superba*. Polar Biology 17, 350–357.

Pakhomov, E.A., 1991. Antarctic macroplankton and feeding of the Demersal Fish. Ph.D. Thesis, PP. Shirshov Institute of Oceanology library, Russian Academy of Sciences, Moscow, 263pp. (in Russian).

Pakhomov, E.A., 1993. Macrozooplankton communities in the Cooperation Sea, Antarctica. The Antarctic 32, 94–110 (in Russian).

Pakhomov, E.A., 1995. Diel vertical migration of the Antarctic macroplankton (euphausiids and hyperiids). In: Ponomareva, L.A. (Ed.), The Pelagic Ecosystems in the Atlantic Sector of the Antarctic. Shirshov Institute Oceanology Publishers, Moscow, pp. 127–136 (in Russian).

Pakhomov, E.A., McQuaid, C.D., 1996. Distribution of surface zooplankton and seabirds across the Southern Ocean. Polar Biology 16, 271–286.

Pakhomov, E.A., Froneman, P.W., 2004a. Zooplankton dynamics in the eastern Atlantic sector of the Southern Ocean during the austral summer 1997/1998. Part 1. Community structure. Deep-Sea Research II, this issue [doi:10.1016/j.dsr2.2000.11.001].

Pakhomov, E.A., Froneman, P.W., 2004b. Zooplankton dynamics in the eastern Atlantic sector of the Southern Ocean during the austral summer 1997/1998. Part 2. Grazing impact. Deep-Sea Research II, this issue [doi:10.1016/j.dsr2.2000.11.002].

Pakhomov, E.A., Grachev, D.G., Trotsenko, B.G., 1994. Distribution and composition of macroplankton communities in the Lazarev Sea (Antarctic). Oceanology 33, 635–642.

Pakhomov, E.A., Perissinotto, R., Froneman, P.W., McQuaid, C.D., 1997. Energetics and feeding dynamics of *Euphausia superba* in the South Georgia region during the summer of 1994. Journal of Plankton Research 19, 399–423.

Pakhomov, E.A., Perissinotto, R., McQuaid, C.D., Froneman, P.W., 2000. Zooplankton structure and grazing in the Atlantic sector of the Southern Ocean in late austral summer 1993. Part 1. Ecological zonation. Deep-Sea Research I 47, 1663–1686.

Park, C., Wormuth, J.H., 1993. Distribution of Antarctic zooplankton around Elephant Island during the austral summers of 1988, 1989, and 1990. Polar Biology 13, 215–225.

Perissinotto, R., Pakhomov, E.A., 1997. Feeding association of the copepod *Rhincalanus gigas* with the tunicate *Salpa thompsoni* in the Southern Ocean. Marine Biology 127, 479–483.

Perissinotto, R., Pakhomov, E.A., 1998a. Contribution of salps to carbon flux of marginal ice zone of the Lazarev Sea, Southern Ocean. Marine Biology 131, 25–32.

Perissinotto, R., Pakhomov, E.A., 1998b. The trophic role of the tunicate *Salpa thompsoni* in the Antarctic marine ecosystem. Journal of Marine Systems 17, 361–374.

Perissinotto, R., Pakhomov, E.A., McQuaid, C.D., Froneman, P.W., 1997. In situ grazing rates and daily ration of the Antarctic krill *Euphausia superba* feeding on phytoplankton at the Antarctic Polar Front and the Marginal Ice Zone. Marine Ecology Progress Series 160, 77–91.

Piatkowski, U., 1987. Zoogeographische Untersuchungen und Gemeinschaftanalysen an antarktischem Makroplankton. Berichte zur Polarforschung 34, 1–150.

Piatkowski, U., 1989. Macroplankton communities in Antarctic surface waters: spatial changes related to hydrography. Marine Ecology Progress Series 55, 251–259.

Ponomareva, L.A., Kuznetsova, I.A., 1989. Feeding and rations of *Euphausia superba* in the south part of the Scotia Sea. In: Ponomareva, L.A. (Ed.), Complex Investigations of the Pelagic Zone of the Southern Ocean. Shirshov Institute Oceanology Publishers, Moscow, pp. 86–93 (in Russian).

Priddle, J., Croxall, J.P., Everson, I., Heywood, R.B., Murphy, E.J., Prince, P.A., Sear, C.B., 1988. Large-scale fluctuations in distribution and abundance of krill—a discussion of possible causes. In: Sahrhage, D. (Ed.), Antarctic Ocean and

Resources Variability. Springer, Berlin, Heidelberg, pp. 169–182.

Reinke, M., 1987. On the feeding and locomotory physiology of *Salpa thompsoni* and *Salpa fusiformis*. Berichte zur Polarforschung 36, 1–89.

Robertson, A.A., Alexander, D.G.W., Miller, D.G.M., 1981. Modified collapsible opening and closing midwater trawls (RMT-8 and RMT-2). Fisheries Bulletin of South Africa 14, 103–113.

Ross, R.M., Quetin, L.B., Haberman, K.L., 1998. Interannual and seasonal variability in short-term grazing impact of *Euphausia superba* in nearshore and offshore waters west of the Antarctic Peninsula. Journal of Marine Systems 17, 261–273.

Rott, H., Skvarca, P., Nagler, T., 1996. Rapid collapse of northern Larsen Ice Shelf, Antarctica. Science 271, 788–792.

Sahrhage, D., 1988. Some indications for environmental and krill resources variability in the Southern Ocean. In: Sahrhage, D. (Ed.), Antarctic Ocean and Resources Variability. Springer, Berlin, Heidelberg, pp. 33–40.

Schnack, S.B., 1985. Feeding by *Euphausia superba* and copepod species in response to varying concentrations of phytoplankton. In: Siegfried, W.R., Condy, P.R., Laws, R.M. (Eds.), Antarctic Nutrient Cycles and Food Webs. Springer, Berlin, Heidelberg, pp. 311–323.

Schnack-Schiel, S.B., Mujica, A., 1994. The zooplankton of the Antarctic Peninsula region. In: El-Sayed, S.Z. (Ed.), Southern Ocean Ecology: the BIOMASS Perspective. Cambridge University Press, Cambridge, pp. 79–92.

Siegel, V., Harm, U., 1996. The composition, abundance, biomass and diversity of the epipelagic zooplankton communities of the southern Bellingshausen Sea (Antarctic) with special reference to krill and salps. Archive of Fishery and Marine Research 44, 115–139.

Siegel, V., Loeb, V., 1995. Recruitment of Antarctic krill *Euphausia superba* and possible causes for its variability. Marine Ecology Progress Series 123, 45–56.

Siegel, V., Skibowski, A., Harm, U., 1992. Communi structure of the epipelagic zooplankton community und the sea-ice of the northern Weddell Sea. Polar Biology 1 15–24.

Strickland, J.D.H., Parsons, T.R., 1968. A practical handboo of seawater analysis. Bulletin of the Fisheries Researc Board of Canada 167, 1–311.

Terazaki, M., Wada, M., 1986. Euphausiids collected from th Australian sector of the Southern Ocean during th BIOMASS SIBEX cruise (KH-83-4). Memoirs of th National Institute for Polar Research 40, 97–109.

Turner, D.R., Bertilsson, S., Fransson, A., Pakhomov, E 2004. The SWEDARP 97/98 marine expedition overview. Deep-Sea Research II, this issue [doi:10.1016 j.dsr2.2003.08.006].

von Bodungen, B., 1986. Phytoplankton growth and kri grazing during spring in the Bransfield Strait, Antarctica— implications from sediment trap collections. Polar Biolog 6, 153–160.

von Bodungen, B., Smetacek, V.S., Tilzer, M.M., Zeitzschel, B. 1986. Primary production and sedimentation during spring in the Antarctic Peninsula region. Deep-Sea Research 33 177–194.

Voronina, N.M., 1984. Pelagic Ecosystems of the Southern Ocean. Nauka Press, Moscow (in Russian).

Voronina, N.M., 1998. Comparative abundance and distribution of major filter-feeders in the Antarctic pelagic zone Journal of Marine Systems 17, 375–390.

Witek, Z., Kittel, W., Czykieta, H., Zmijewska, M., Presler, E., 1985. Macrozooplankton in the southern Drake Passage and in the Bransfield Strait during BIOMASS-SIBEX (December 1983–January 1984). Polish Polar Research 6, 95–115.

Zwally, H.J., 1991. Breakup of Antarctic ice. Nature 350, 274.

ELSEVIER

Deep-Sea Research II 51 (2004) 2661–2672

DEEP-SEA RESEARCH
PART II

www.elsevier.com/locate/dsr2

Air–water gas exchange of α-hexachlorocyclohexane enantiomers in the South Atlantic Ocean and Antarctica

Liisa M. Jantunen[a,*], Henrik Kylin[b], Terry F. Bidleman[a]

[a]*Centre for Atmospheric Research Experiments, Meteorological Service of Canada, 6248 Eighth Line, Egbert, Ont., Canada L0L 1N0*
[b]*Department of Environmental Assessment, Swedish University of Agricultural Sciences, P.O. Box 7050, S-750 07, Uppsala, Sweden*

Abstract

Between November 1997 and February 1998, air and water samples were collected on the African side of the South Atlantic Ocean to Antarctica, on board the S.A. *Agulhas*, to determine the spatial distribution of α-hexachlorocyclohexane (α-HCH) and the net direction of air/water gas exchange. The α-HCH concentrations in air and surface water were much lower than in Arctic regions, consistent with the historically lower usage of technical HCH in the Southern Hemisphere. The water/air fugacity ratios of α-HCH were $\leqslant 1.0$, indicating steady state or net deposition conditions. The α-HCH in water was enantioselectively metabolized, with resulting enantiomer fractions (EFs) that differed from the racemic (0.500) value of the technical product. The EFs decreased from >0.500 at the lower latitudes to <0.500 farther south, indicating preferential loss of (−)α-HCH or (+)α-HCH in different ocean regions. EFs in the air boundary layer reflected those in surface water, showing the bidirectional nature of gas exchange.
© 2004 Elsevier Ltd. All rights reserved.

1. Introduction

Organochlorine (OC) contamination in the Southern Hemisphere (SH) has been studied less extensively than in the Northern Hemisphere (NH) but OC residues, including hexachlorocyclohexanes (HCHs), have been found in Antarctic air (Bidleman, et al., 1993; Iwata et al., 1993; Kallenborn et al., 1998; Lakaschus et al., 2002; Larsson et al., 1992; Weber and Montone, 1990), water (Iwata et al., 1993; Lakaschus et al., 2002), fish, penguins (DeBoer and Wester, 1991) and birds (Van den Brink, 1997). Technical HCH is a mixture of several isomers: 60–70% α-HCH, 5–12% β-HCH, 10–15% γ-HCH and other minor isomers (Iwata et al., 1993). Only γ-HCH, also known as lindane, is insecticidally active, and many industrialized countries have restricted the use of the technical product in favor of the purified lindane.

Some countries in the SH continue to use OC pesticides that have been banned or restricted in the NH industrialized nations. As of 1990, technical HCH had been banned in most SH

*Corresponding author. Tel.: +1 705 458 3318; fax: +1 705 458 3301.
E-mail address: liisa.jantunen@ec.gc.ca (L.M. Jantunen).

0967-0645/$ - see front matter © 2004 Elsevier Ltd. All rights reserved.
doi:10.1016/j.dsr2.2004.02.002

countries but not in Australia, Chile, several countries in southern Africa and in the South Pacific (Pesticide Action Network, 1995). In 1990, 90% of global α-HCH emissions were estimated to originate in the NH, over 70% from Asia (Li et al., 2000). Usage of technical HCH in the SH was approximately 5% of the NH tonnage in 1980 and 10% in 1990 (Li, 1999).

Chemicals released in the temperate and tropical zones are atmospherically transported to the colder boreal and polar zones through episodic events (Haugen et al., 1998) and cycles of deposition and re-emission ("grasshoppering") (Wania and Mackay, 1996, 1999; Wania et al., 1999), where they have the tendency to reside for long periods of time. Characteristics of HCH transport to the Arctic and distribution in Arctic Ocean water have been well established (Li et al., 2002; Macdonald et al., 2000; Harner et al., 1999; Halsall et al., 1998; Iwata et al., 1993; Jantunen and Bidleman, 1995, 1996, 1998; Lakaschus et al., 2002; Wania et al., 1999).

Since usage of technical HCH is being phased out globally, studying its behavior contributes to an understanding of how the atmosphere and oceans respond. Global models for α-HCH have been published (Koziol and Pudykiewicz, 2001; Wania and Mackay, 1999; Wania et al., 1999; Strand and Hov, 1996), but there are few measurements of α-HCH in air and water of the SH to compare with model results and many of the SH measurements were made during the 1980s and early 1990s (Iwata et al. (1993) and papers cited therein). Concentrations of HCHs in Antarctic air and water (Bidleman, et al., 1993; Iwata et al., 1993; Kallenborn et al., 1998; Lakaschus et al., 2002; Larsson et al., 1992; Tatsukawa et al., 1990; Weber and Montone, 1990) are approximately an order of magnitude lower than those in the Arctic. The α-HCH/γ-HCH ratio in air is generally >1 in the NH (except in situations involving transport of fresh lindane) but is <1 in the SH, reflecting a preference for lindane usage (Lakaschus et al., 2002; Schreitmüller and Ballschmiter, 1995; Wania et al., 1999; Walker et al., 1999). The exchange of α-HCH between hemispheres in the lower troposphere was estimated to be very slow by measuring the ratio of α-HCH/γ-HCH in air (Ballschmiter, 1992). Schreitmüller and Ballschmiter (1995) found a concentration ratio of ~40 for α-HCH in air of the NH and SH westwind belts.

The α-HCH isomer is a chiral compound consisting of two enantiomers, which are degraded at different rates by microbial action. The enantiomer fraction EF is defined as the amounts of (+)/[(+)+(−)] enantiomers and equal amounts (racemic) are denoted by EF = 0.5. Investigations in arctic and subarctic waters have found that (−)α-HCH is preferentially metabolized in the Bering and Chukchi seas (EF > 0.5), while (+)α-HCH is depleted in the central and eastern Arctic Ocean (Falconer et al., 1995a; Harner et al., 1999; Jantunen and Bidleman, 1996, 1998). The (+) enantiomer is also preferentially degraded in arctic lakes and wetlands (Falconer et al., 1995b; Helm et al., 2000; Law et al., 2001).

Enantiomer measurements show that α-HCH is being re-emitted from some areas of the Arctic Ocean and its marginal seas (Jantunen and Bidleman, 1996; Harner et al., 1999), the Great Lakes (Ridal et al., 1997; Shen et al., 2004) and the east coast of Canada (Shen et al., 2004). As usage of technical HCH declines in the coming years, such re-emission processes will become increasingly important in supplying α-HCH to the global atmosphere. Including enantiomer signatures in measurement programs and models will provide useful information for distinguishing "new" and "old" sources (Shen et al., 2004).

In December 1997–February 1998, air and water samples were collected from the South African S.A. *Agulhas* in the South Atlantic to Antarctica to determine the spatial trends and gas exchange of α-HCH enantiomers. No previous investigations of α-HCH enantioselective degradation have been made in SH oceans.

1.1. Cruise track

The S.A. *Agulhas* left Cape Town, South Africa on November 30, 1997 and proceeded south along 6°E reaching the South African National Antarctic Expedition (SANAE) Base (70°S, 3°E) on December 13, 1997 and then returned to Cape Town on February 7, 1998. The cruise track is shown in Fig. 1 of Turner et al. (2004).

2. Materials and methods

Water samples of 20–80 l were collected via a submersible pump beneath the ship (~10 m below the surface). The line running from the pump was stainless steel tubing lined with glass. Deeper samples were also collected via a 100 l polytetrafluoroethylene-lined Glo–Flo bottle. The water was stored in pressurizable stainless steel cans, filtered through a glass fiber filter (Whatman, 47 and 142 mm, nominal cutoff 0.7 μm) and then extracted by two different methods, XAD-2 resin (Amberlite, Supelco Corp.) or ENV+ cartridges (polystyrene-divinylbenzene copolymer, International Sorbent Technology). XAD-2 was used to process large volumes of water (~100 l) and the ENV+ cartridges were used for smaller volumes (~20 l). In both cases the water was pulled through the adsorbent by a peristaltic pump at a flow rate of 150 and 15 ml min^{-1}, respectively. Collection data are listed in Table 1.

Before use, the XAD-2 was sieved under tap water and cleaned by Soxhlet extraction in acetone, petroleum ether and dichloromethane, each for 48 h, and was stored in chromatographic grade water (BDH, Omnisolv). The ENV+ cartridges were cleaned with hexane and conditioned with methanol immediately before use. The filters were cleaned by baking at 400 °C in a muffle furnace for 24 h.

After sampling, the XAD-2 was placed in 100 ml bottles and stored in the refrigerator and ENV+ cartridges were placed in sealed bags and frozen. Upon returning to the laboratory, the XAD-2 and ENV+ adsorbents were extracted with 350 and 20 ml dichloromethane, respectively, and the XAD-2 extracts were dried over anhydrous granular sodium sulfate. The filters were Soxhlet extracted with dichloromethane for 18 h. Rotary evaporation and gentle nitrogen blowdown were used to concentrate the extracts into isooctane. The XAD-2 extracts were cleaned up and fractionated on an alumina–silicic acid column to separate polychlorinated biphenyls from HCHs and other chlorinated pesticides. The column consisted of 3 g silicic acid (deactivated with 3% water), overlaid with 1 g neutral alumina (deactivated with 6% water) and topped with 1 cm anhydrous granular sodium sulfate (Keller and Bidleman, 1984). The column was prewashed with 30 ml dichloromethane and then 30 ml petroleum ether. The sample was eluted with 20 ml petroleum ether and then 30 ml dichloromethane (this fraction contained α-HCH and other chlorinated pesticides). Extracts from the ENV+ cartridges were cleaned up on a 1-g column of neutral alumina (deactivated with 6% water) topped with anhydrous granular sodium sulfate and eluted with 10 ml of 10% dichloromethane in petroleum ether. The column eluates were reduced into isooctane as above, and subjected to further clean up by shaking with 18 mole l^{-1} sulfuric acid. The final volume was 1.0 ml for quantitative analysis and 100 μl for enantiomeric analysis. The water and solvents used were chromatographic quality.

Air samples were collected by drawing 700–1500 m^3 of air through a glass fiber filter (Whatman EPM 2000, 20 × 25 cm^2, >99% collection of particles >0.3 mm) followed by two polyurethane foam plugs (PUFs, 7.8 cm diameter × 7.5 cm thick). The PUFs were cleaned by rinsing with deionized water then Soxhlet extracting in acetone and petroleum ether, each for 48 h. One PUF from each batch of eight was checked for cleanliness by chromatographic analysis. After sampling, the PUFs were Soxhlet extracted in petroleum ether for 12 h. The air filters were cleaned and extracted by the same method as the water filters. Extracts were transferred to isooctane, fractionated on alumina–silicic acid columns and cleaned up with sulfuric acid, as described above.

Quantitative and chiral analyses were done on a Hewlett Packard 5890 GC-5989B MS Engine operated in the electron capture negative ion (ECNI) mode with methane reagent gas at a nominal pressure of 1.2 Torr. Selected monitoring of the 255/257 (target/qualifier) ions was used for α-HCH and 261/263 for the added surrogate α-HCH-d_6 (see below). For acceptable quantitative analysis and to ensure peak purity, the target/qualifier ion ratio was required to be within ±20% of values found for standards. Mirex was added to extracts just prior to injection as a volume correction internal standard and monitored at m/z 404. Random samples were checked for native

Table 1
Concentrations and enantiomer fractions of α-HCH in water

Sample[a]	Lat. S	Long. E	Temp. (°C)	Salinity (psu)	Depth (m)	α-HCH ($pg\,l^{-1}$)	EF of α-HCH[b]		Me
							BGB	BDX	
ENV-008	42.0	6.0	11.16	34.3	Surface	6.5			
ENV-009	40.2	8.0	14.40	34.7	Surface	8.4	0.522	0.519	0.52
ENV-U5	44.0	11.7	9.20	34.3	Surface	12.4			
ENV-U9	45.0	11.0	8.62	34.2	Surface	14			
XAD-031	45.5	6.0	6.80	33.8	50	34	0.501	0.502	0.50
ENV-U13	46.0	10.2	8.48	34.2	Surface	12			
ENV-U17	47.0	9.5	5.69	34.8	Surface	19			
ENV-U25	49.0	8.0	4.14	33.8	Surface	14			
ENV-006	49.1	6.0	4.08	33.8	Surface	16			
ENV-007	49.1	6.0	4.08	33.8	Surface	8.9			
XAD-029	49.8	6.0	3.59	33.8	Surface	NA	0.507	0.510	0.50
XAD-028	49.9	6.0	3.40	33.8	50	20	0.502	0.500	0.50
ENV-U29	50.0	7.2	3.75	33.9	Surface	14			
ENV-004	50.3	6.0	3.85	33.8	Surface	9.3			
ENV-005	50.3	6.0	3.85	33.8	Surface	14			
XAD-024	50.8	6.0	3.57	33.8	Surface	11	0.489	0.487	0.48
XAD-025	50.8	5.5	3.87	33.8	Surface	11	0.495	0.492	0.49
XAD-026	51.0	5.8	3.85	33.8	Surface	28	0.491	0.495	0.49
XAD-027	51.0	6.0	3.73	33.7	Surface	NA	0.506	0.505	0.50
ENV-U37	52.0	5.6	1.85	33.7	Surface	9.5			
XAD-023	52.0	6.0			Surface	9.4	0.493	0.495	0.49
ENV-U41	53.0	5.0	1.16	33.8	Surface	12			
ENV-U47	54.3	5.0	−0.57	34.1	Surface	6.7			
ENV-U49	55.0	5.0	−0.20	34.1	Surface	5.7			
XAD-017	55.9	5.0	0.93	34.0	Surface	6.5	0.497	0.495	0.49
XAD-021+022	56.0	6.0	−0.50	34.2	60/80	10	0.482	0.485	0.48
XAD-019	56.4	6.1	0.26	34.2	Surface	14	0.493	0.495	0.49
XAD-020	56.5	6.0	0.19	34.2	Surface	8.1	0.495	0.497	0.49
ENV-U57	57.0	5.0	−0.54	34.2	Surface	5.5			
ENV-U61	58.0	5.0	−0.77	34.2	Surface	6.1			
ENV-U65	59.0	5.0	−0.73	34.3	Surface	10			
XAD-014	59.2	6.0	0.59	34.1	Surface	7.1	0.475	0.482	0.479
XAD-015	59.2	6.0			50	9.0	0.505	0.502	0.504
XAD-016	59.2	6.0			50	8.8	0.495	0.497	0.496
XAD-006	59.4	6.0	0.05	33.9	Surface	6.7	0.482	0.479	0.481
ENV-D036	59.6	6.0	−0.23	33.7	Surface	17			
XAD-012	60.0	5.6	−0.02	33.8	Surface	7.2	0.493	0.490	0.491
XAD-013	60.0	6.0			30	9.9	0.509	0.507	0.508
XAD-007	60.1	5.6	−0.33	33.7	Surface	7.3	0.482	0.487	0.485
XAD-010	60.2	6.0	−0.12	33.8	Surface	11	0.492	0.495	0.494
XAD-008	60.2	6.0	0.70	34.8	75	5.7			
XAD-009	60.2	6.0	0.70	34.1	200	3.5	0.490	0.485	0.487
ENV-U136	60.4	5.7	−0.60	33.8	Surface	14			
ENV-134	60.5	6.0	0.90	33.8	Surface	12			
XAD-004	60.5	5.6	−1.90	34.2	75	11	0.499	0.500	0.500
XAD-005	60.5	5.6	−1.60	34.7	200	4.4	0.482	0.485	0.483
XAD-003	61.0	5.6	−1.14	33.8	Surface	7.4	0.497	0.500	0.499
ENV-003	61.0	6.0	−1.14	33.8	Surface	12			
ENV-U77	62.0	4.3	−1.67	33.9	Surface	8.8			
XAD-002	62.0	6.0	−1.22	33.6	Surface	7.6	0.502	0.505	0.504
XAD-001	64.6	6.1	−1.04	33.9	25	9.6			
ENV-001	64.4	5.8	−1.04	33.9	Surface	5.1	0.476	0.479	0.478
ENV-002	65.0	6.0	−1.05	33.8	Surface	7.5			

NA: not analyzed quantitatively.

[a]ENV and XAD refer to samples collected by the two methods, see text. ENV-008, 009 and U5, and ENV-001 and 002 were combined for chiral analysis.

[b]Chiral analysis was only done on XAD-2 samples, except for the following: ENV-008, 009 and U5, and ENV-001 and 002 were combined for chiral analysis.

nirex and found negative. The column used for quantitative analysis was a DB-5 MS (J&W Scientific Co., 60 m × 0.25 mm i.d., 0.25 μm film thickness) operated at a helium carrier gas flow of 40 cm s^{-1}. The temperature program was: initial temperature 90 °C, 15 °C min^{-1} to 160 °C, 2.0 °C min^{-1} to 210 °C, hold 1.0 min, 20 °C min^{-1} to 260 °C hold 5.0 min. Sample volumes of 2 μl were injected splitless (split opened after 1.5 min). Other conditions were: injector and transfer line temperature 250 °C, ion source temperature 150 °C and quadrupole temperature 100 °C. Quantification was carried out against five standards that spanned the concentration range of the samples, using the HP MS Chemstation software.

Enantiomer separations were carried out on two different chiral columns that reversed the elution order of the two α-HCH enantiomers: Betadex-120 (BDX: 20% permethylated β-cyclodextrin in polydimethylsiloxane, 30 m × 0.25 mm i.d., 0.25 μm film thickness, Supelco Corp.) and BGB-172 (BGB: 20% tert-butyldimethylsilylated β-cyclodextrin in OV-1701, 30 m × 0.25 mm i.d., 0.25 μm film thickness, BGB Analytik AG, Switzerland). The (+)α-HCH elutes first on the BDX column and (−)α-HCH elutes first on the BGB column (Jantunen and Bidleman, 1996, 1998). The temperature program was the same for both columns: initial temperature 90 °C, hold for 1.0 min, 15 °C min^{-1} to 140 °C, 1.0 °C min^{-1} to 175 °C, 20 °C min^{-1} to 220 °C hold for 5.0 min. Both columns were operated at a helium carrier gas flow of 30 cm s^{-1}. Other conditions were: splitless injection (split opened after 1.5 min), injector temperature 220 °C, ion source temperature 150 °C, transfer line temperature 220 °C and quadrupole temperature 100 °C.

3. Results and discussion

3.1. Quality control

Initially, the intent was to measure both the α- and γ-HCH isomers. However, due to apparent shipboard contamination with lindane, measurements of γ-HCH were compromised and therefore are not reported. No contamination was evident for α-HCH.

Two PUFs were spiked with 100 ng of α-HCH, recoveries were >85%. Recovery experiments were also done for XAD and ENV+ by spiking 20–100 l water with 45 ng of α-HCH. Average recoveries were 83 ± 12% ($n = 5$), after correcting for the native amounts in the seawater. Before concentration on the sorbents, the water samples were spiked with a surrogate of α-HCH-d_6; recoveries averaged 79 ± 12% ($n = 52$). Blanks for α-HCH in water were done by passing 200 ml of deionized water through XAD and ENV+ and averaged 11 ± 6 pg ($n = 6$). Air blanks were done by placing clean PUFs in the sampling apparatus and drawing air for 30 s, resulting an average blank of 24 ± 13 pg ($n = 3$). All samples were greater than the mean blank values plus three times their standard deviations. Back and front PUFs were analyzed separately to check for breakthrough of α-HCH. Only 4 out of 28 air samples showed a small degree of breakthrough, and the average back PUF/front PUF percentage for these four samples was 6.2%.

Quality control issues in chiral analysis are precise integration of enantiomer peaks and elimination of interferences. Racemic standards were repeatedly injected on the two columns to determine the reproducibility of measuring the EF values. Average EFs were 0.500 on the BGB column ($n = 11$) and 0.497 on the BDX column ($n = 9$), with a relative standard deviation of ±0.003. The criterion used for peak purity was agreement of the target/qualifying (255/257) ion ratio within ±5% of the standard values (Falconer et al., 1997). Enantiomer elution order was confirmed by injecting an enriched (+)α-HCH standard (Ehrenstorfer Laboratories, Germany) on both columns. The average absolute difference in EF values between the BGB and BDX columns was 1.4 ± 1.0% ($n = 20$) for air samples and 0.6 ± 0.3% ($n = 27$) for water samples.

3.2. α-HCH concentrations in water

The α-HCH was predominately found in the dissolved phase with <0.5% on the glass fiber filter. Measurements of α-HCH in water and

hydrographic information are given in Table 1. Concentrations of α-HCH in surface water generally ranged from 5.1 to 19 pg l^{-1}, with 28 pg l^{-1} for one sample. A slight trend with latitude was noted in which concentrations maximized between 47° and 51°S and again around 60°S, then declined toward Antarctica (Fig. 1). The first maximum occurred near the Subantarctic Front and the Antarctic Polar Front, which on this expedition were identified between 46–47°S and 50–51°S, respectively. The second maximum occurred near the spring ice edge (Turner et al., 2004). Ten samples at 25–80 m and two at 200 m depth were also taken during the expedition. Concentrations of α-HCH were 5.7–34 pg l^{-1} in the 25–80 m depth range and 3.5–4.4 pg l^{-1} at 200 m. Lakaschus et al. (2002) noted that a slight maximum in α-HCH surface water concentrations consistently appeared between 40° and 50°S for samples collected on expeditions from 1993 to 1999.

Concentrations of α-HCH in surface water were not correlated with water temperature ($r^2 = 0.05$) nor salinity ($r^2 = 0.02$). This contrasts strongly with the situation in the NH, where the "cold condensation effect" has been hypothesized to account for observed concentrations of α-HCH in surface water that increase by an order of magnitude from subtropical waters to the Arctic Ocean (Harner et al., 1999; Lakaschus et al., 2002; Macdonald et al., 2000; Wania and Mackay, 1996; Wania et al., 1999).

Table 2 gives a comparison of α-HCH measur ments in surface water from the Agulhas expec tion (5.1–28 pg l^{-1}) with other measurements in t SH. Concentrations reported by Lakaschus et a (2002) from expeditions in 1997 and 1999 range from 3.6–15 pg l^{-1} to 2.0–9.6 pg l^{-1}, respectivel The authors reported that α-HCH in surface wat of the South Atlantic declined by about four-fo between 1993 and 1999. Schreitmüller and Ballsch miter (1995) collected samples in the Sou Atlantic in 1990 and found α-HCH ranging fro 6.7 to 17 pg l^{-1}. Concentrations of α-HCH in t Ross Sea in 1990 were higher, 18–43 pg l^{-1} (Iwat et al., 1993). A global distribution model for α HCH predicted surface water concentrations in t SH ranging from 1 to 4 pg l^{-1} in 1997–1999 and to 11 pg l^{-1} in 1993 (Lakaschus et al., 2002).

In arctic and subarctic waters, α-HCH range from about 350 to 6000 pg l^{-1} (Harner et al., 199 Jantunen and Bidleman, 1995, 1996, 1998; La kaschus et al., 2002; Li et al., 2002), reflecting th historically much higher usage of technical HCH in the NH.

3.3. HCH concentrations in air

Concentrations of gaseous α-HCH (PUF plugs are listed by sample in Table 3 and shown as a function of latitude in Fig. 2. The α-HCH on the glass fiber filters was below the detection limi of 0.024 m^3 for a 1000 m^3 air sample. The

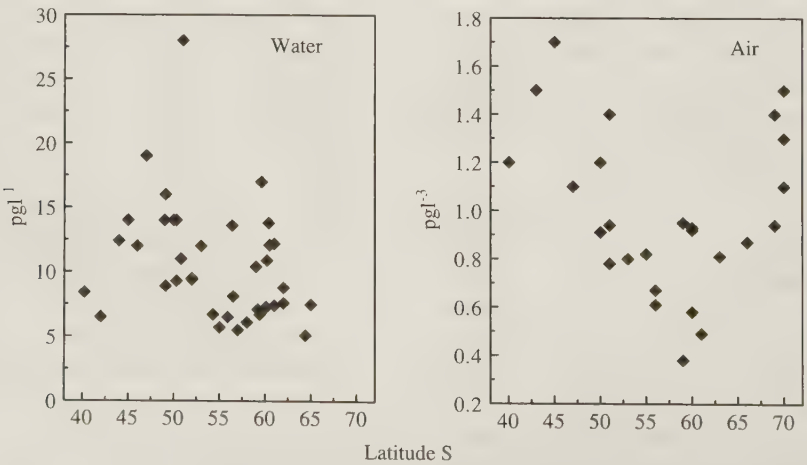

Fig. 1. Concentrations of α-HCH in surface water (pg l^{-1}) and air (pg m^{-3}) versus latitude.

Table 2
Concentrations of α-HCH in air and surface water of the Southern Hemisphere

Year	Location	Range	Reference
Air ($pg\,m^{-3}$)			
1997–1998	African side	0.38–1.7	This work
1999–2000	African side	0.3–3.3	Lakaschus et al. (2002)
1990	African side	1.8–4.8	Schreitmüller and Ballschmiter (1995)
1990	Australian side	2.7–6.7	Bidleman, et al. (1993)
1989–1990	Ross Sea	6.6–40	Iwata et al. (1993)
1994–1995	Signy Island	<0.9–8.4	Kallenborn et al. (1998)
Water ($pg\,l^{-1}$)			
1997–1998	African side	5.1–28	This work
1999–2000	African side	2.0–9.6	Lakaschus et al. (2002)
1997	African side	3.6–15	Lakaschus et al. (2002)
1990	African side	6.7–15	Schreitmüller and Ballschmiter (1995)
1989–1990	Australian side	18–43	Iwata et al. (1993)

Concentration of α-HCH in air ranged from 0.38 to 1.7 $pg\,m^{-3}$ and showed no significant trend with latitude when analyzed by simple linear regression ($r^2 = 0.012$, $p > 0.5$). Fig. 2 shows that concentrations tend to be higher in subtropical latitudes and near Antarctica, and minimal between about 55° and 60°S.

Table 2 compares the results found here (0.38–1.7 $pg\,m^{-3}$) with other measurements in the South Atlantic and the Southern Ocean between New Zealand and Antarctica. Three groups measured α-HCH in air between 1989 and 1990. Iwata et al. (1993) found higher concentrations ranging from 6.6 to 40 $pg\,m^{-3}$. Measurements by Schreitmüller and Ballschmiter (1995) and Bidleman et al. (1993) were lower than those of Iwata et al., and ranged from 1.8 to 6.7 $pg\,m^{-3}$. The lowest concentrations (0.3–3.3 $pg\,m^{-3}$) have been measured in 1997–1999 (Lakaschus et al., 2002 and this work). The global distribution model of Wania et al. (1999) predicted 1–10 $pg\,m^{-3}$ of α-HCH in SH air.

Concentrations of α-HCH in the air of arctic and subarctic regions are much higher, with annual means ranging from 40 to 79 $pg\,m^{-3}$ in the mid-1990s (Hung et al., 2002; Li et al., 2002). Concentrations of α-HCH in arctic air have dropped by over an order of magnitude from 700 to 900 $pg\,m^{-3}$ measured in the early 1980s. This decline corresponds closely to estimated reductions in technical HCH usage (largely in Asian countries) over that time period (Bidleman et al., 1995; Li et al., 1998; Li and Bidleman, 2003).

3.4. Air–water gas exchange

The net direction of air–water gas exchange was estimated by using the fugacity approach (Harner et al., 1999; Jantunen and Bidleman, 1996). The water/air fugacity ratio (f_w/f_a) was calculated from average air and water concentrations in 5° latitude bands using the equations below, and results are presented in Table 4.

$$f_w = 10^{-9} C_w H / M, \quad (1)$$

$$f_a = 10^{-9} C_a R T_a / M, \quad (2)$$

$$f_w/f_a = C_w H / C_a R T_a, \quad (3)$$

where f_w and f_a are the fugacities in water and air (Pa), C_w and C_a are the concentrations of the dissolved and gaseous HCHs in water and air ($ng\,m^{-3}$), R is the gas constant (8.314 $Pa\,m^3\,deg^{-1}\,mol^{-1}$), T_a is the air temperature (K), H is the Henry's law constant ($Pa\,m^3\,mol^{-1}$) at the temperature of the surface water and M is the molecular mass (291 $g\,mol^{-1}$). A value of $f_w/f_a = 1.00$ indicates a steady-state situation in which deposition and volatilization take place at equal

Table 3
Concentrations and enantiomer fractions of α-HCH in air

Sample	Latitude S on/off	Average Lat. S	Longitude E on/off	α-HCH (pg/m^{-3})	EF of α-HCH		M
					BGB	BDX	
031	40.21/40.21	40	8.00/8.00	1.2	0.505	0.491	0.4
030	45.21/40.21	43	5.00/8.00	1.5	0.518	0.513	0.5
002	42.10/48.30	45	12.59/8.22	1.7	0.507	0.502	0.5
029	49.50/45.42	47	5.59/6.00	1.1	0.502	0.501	0.5
028	51.05/49.50	50	6.00/6.00	1.2	0.494	0.481	0.4
024	50.31/50.17	50	6.00/6.00	0.91			
024+025[a]		50			0.500	0.487	0.4
025	50.17/51.29	51	6.00/5.15	1.4			
027	50.38/51.00	51	6.00/6.00	0.78			
026	51.29/50.38	51	5.15/6.00	0.94			
026+027[a]		51			0.490	0.492	0.4
003	48.40/56.21	52	8.09/5.00	NR	0.507	0.510	0.5
023	55.00/50.31	53	6.00/6.00	0.80	0.512	0.502	0.5
013	51.53/60.54	55	5.59/5.54	0.82	0.488	0.485	0.4
022	56.30/55.00	56	6.00/6.00	0.67			
020	56.06/56.10	56	6.00/6.00	0.61	0.479	0.474	0.4
015	59.41/59.19	59	5.00/6.00	0.38			
016	59.19/59.36	59	6.00/6.00	0.95			
014	60.59/59.41	60	5.54/5.00	0.58			
014+015[a]		60			0.488	0.478	0.48
016+017[a]		60			0.496	0.480	0.48
019	60.02/59.20	60	6.00/6.00	0.93	0.502	0.485	0.4
017	60.24/60.23	60	5.56/6.00	0.92			
004	56.21/67.34	61	5.00/0.22	0.49	0.485	0.482	0.48
012	64.53/61.53	63	6.00/5.59	0.81	0.506	0.500	0.50
011	68.15/64.53	66	0.40/6.00	0.87	0.482	0.487	0.48
005	67.34/70.16	69	0.02/2.47	0.94	0.483	0.485	0.48
010	70.09/68.15	69	2.51/0.40	1.4	0.496	0.500	0.49
006	70.16/70.16	70	2.47/2.47	1.3			
006+007[a]		70			0.497	0.502	0.50
007	70.16/70.16	70	2.47/2.47	1.3			
008	70.16/70.17	70	2.47/2.48	1.1			
009	70.17/70.09	70	2.48/2.51	1.5			

NR: not reported due to analytical interference.
[a]Samples were combined for chiral analysis.

rates; $f_w/f_a > 1.00$ and < 1.00 imply net volatilization and deposition, respectively.

Temperatures on the *Agulhas* expedition ranged from 12 to −3 °C (air) and 14 to −1.7 °C (water). Two sets of Henry's law constants for α-HCH were used in the calculations. Kucklick et al. (1991) determined Henry's law constants as a function of temperature in distilled water and artificial seawater of salinity = 35. No difference between the two water types was found at temperatures below 15 °C, although higher Henry's law constants in seawater due to a "salting out" effect wer observed at 25–45 °C. Sahsuvar et al. (2002 determined Henry's law constants in distille water as a function of temperature using tw techniques, with good agreement. Since Kucklic et al. (1991) found no salt effect in the temperatur range encountered on this expedition, no adjust ment was made to the Sahsuvar values, which ar about 40% lower than Kucklick's (Table 4).

Fugacity ratios of α-HCH ranged from 0.39 t 1.12 using Kucklick's Henry's law constants, an

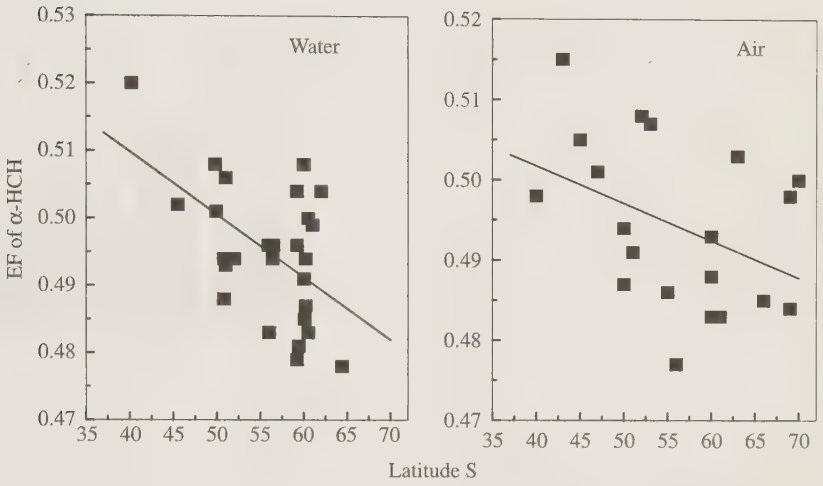

Fig. 2. Enantiomer fractions (EFs) of α-HCH in surface water and air versus latitude.

ıble 4
ıgacity calculations for α-HCH, averaged by 5° latitude bands

ıtitude S	Water temp. (K)	C_w (ng m^{-3})	C_a (ng m^{-3})	H^a (Pa m^3 mol^{-1})	f_w/f_a	SD[b]	H^c (Pa m^3 mol^{-1})	f_w/f_a	SD[b]
–44	288	9.1	0.0013	0.374	1.12	0.48	0.237	0.71	0.30
–49	282	14	0.0014	0.230	0.96	0.42	0.143	0.60[d]	0.26
–54	279	11	0.00091	0.180	0.94	0.52	0.111	0.58[d]	0.32
–59	278	8.9	0.00068	0.154	0.87	0.47	0.094	0.53[d]	0.28
–64	276	10	0.00074	0.130	0.80[d]	0.34	0.079	0.48[d]	0.20
–69	275	7.5	0.0011	0.126	0.39[d]	0.18	0.076	0.24[d]	0.11

[a]Henry's law constants from Kucklick et al. (1991).
[b]Standard deviation derived by propagation of errors in C_w, C_a and H.
[c]Henry's law constants from Sahsuvar et al. (2002).
[d]Significantly different from 1.00.

.24–0.71 using Sahsuvar's constants, indicating et deposition or near steady-state conditions Table 4). Uncertainties in the fugacity calculaons were determined by propagation of errors in ıe water and air concentrations (standard deviaons for multiple samples taken within a latitude and) and the Henry's law constants. The latter ere assumed to have a relative error of 20% Kucklick et al., 1991; Sahsuvar et al., 2002). The ropagated relative errors in the fugacity ratios nged from 43% to 56% and absolute errors in ıgacity ratios ranged from 0.11 to 0.52 (Table 4). *t*-test was used to judge whether the fugacity ıtios were significantly different from steady state (1.00), using the appropriate degrees of freedom for the number of air and water samples taken within a latitude band. The fugacity ratios based on Kucklick's Henry's law constants were significantly different ($p>0.05$) from 1.00 in regions south of 60°, but not at lower latitudes. Using Sahsuvar's Henry's law constants, fugacity ratios were significantly different from 1.00 in all latitude bands except 40°–44°S. Lakaschus et al. (2002) estimated that the gas exchange direction of α-HCH was near steady state in the tropical South Atlantic, net volatilization at about 45°S, and net deposition from 55° to 65°S. Schreitmüller and Ballschmiter, (1995) found that α-HCH was near

steady state or undergoing net deposition between 24° and 52°S. Both of these studies employed Kucklick's Henry's law constants in their assessments.

Fugacity ratios indicated net volatilization of α-HCH in some arctic and subarctic regions in 1993–1994 (Jantunen and Bidleman, 1995, 1996; Sahsuvar et al., 2002). Gas exchange of α-HCH was close to steady state in the eastern Arctic Ocean in 1996 (Harner et al., 1999). In the Arctic there has been a reversal in the net air–water gas exchange direction for α-HCH, from net deposition in the late 1980s to steady state or net volatilization in the mid-1990s. This reversal has been caused by the drop in atmospheric levels of α-HCH (Bidleman et al., 1995; Jantunen and Bidleman, 1995, 1996; Sahsuvar et al., 2002). As inputs of α-HCH to SH waters decline, a similar oceanic source of to the atmosphere is likely to emerge.

3.5. Enantiomer composition of α-HCH in air and water

The EFs of α-HCH ranged from 0.477 to 0.515 ($n = 20$) in air and 0.478–0.520 in water ($n = 27$), Tables 1 and 3, and Fig. 2. EFs for two samples that were collected at 200 m and 60°S were 0.483 and 0.487, within the range of EFs in surface water at that latitude. A slight tendency was noted for EFs to be racemic or reflect preferential degradation of the (−) enantiomer (EFs >0.500) at the lower latitudes, versus racemic or depletion of the (+) enantiomer (EFs <0.500) at higher latitudes (Fig. 2). Regression of EF versus latitude was significant ($p = 0.005$, $r^2 = 0.28$). A similar, though weaker, trend was suggested in a plot for the air samples (Fig. 2), but the data were more scattered than in the case of water and the regression of EF vs. latitude was not significant ($p = 0.078$, $r^2 = 0.16$). The tendency for EFs in air to reflect those in water is also shown in Fig. 3, where the EFs have been averaged by 5° latitude bands. Even though the fugacity ratio indicates that α-HCH in the air and water was depositional or in steady state in most sampling regions, α-HCH can enter the air boundary layer due to the bidirectional nature of gas exchange. Thus, a

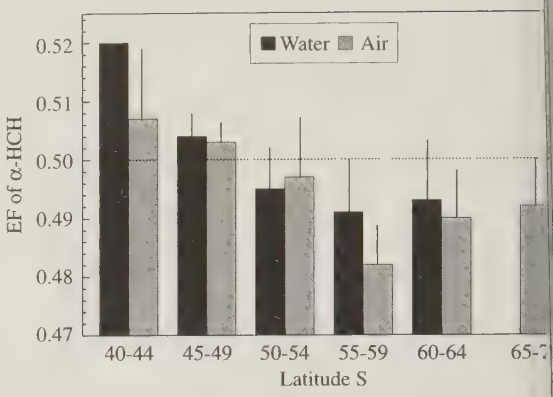

Fig. 3. Enantiomer fractions (EFs) of α-HCH in surface wa and air, averaged by 5° latitude bands.

portion of the α-HCH in the boundary lay consists of α-HCH volatilized from the water, ev in situations where there is no net gas exchange the net exchange direction is depositional (Jant nen and Bidleman, 1996; Ridal et al., 1997).

In the Arctic, a similar reversal was seen for t EFs of α-HCH in paired air and water sampl that were taken on a transect from the Beri Strait to the Greenland Sea, over the North Pol The ERs were >0.500 in the Bering and Chukc seas and <0.500 in the central Arctic Ocean ar Greenland Sea (Jantunen and Bidleman, 199 Faller et al. (1991) also found a reversed degrad tion preference for the (+) or (−) enantiomers different regions of the North Sea. The range EFs in arctic and subarctic surface wate (0.415–0.551) was greater than found on th expedition, and EFs in the Arctic Ocean decreas with depth below the Polar Mixed Layer (Jant nen and Bidleman, 1996, 1998; Harner et al., 199 2000). Enantiomer measurements suggest th microbial degradation exceeds hydrolysis removing HCHs from the Arctic Ocean (Harn et al., 1999, 2000).

It is unknown what parameters affect rates enantioselective microbial degradation in t ocean. The range of EFs in the Arctic Ocean w about the same as in the North Sea where it warmer (Faller et al., 1991), so no temperatu effect on the rate of enantioselective degradati can be assessed. Greater enantioselectivity w found in freshwater wetlands of arctic a

mperate regions and in oligotropic freshwater lakes mpared to mesotrophic lakes (Helm et al., 2000; aw et al., 2001). Law et al. (2001) hypothesized that ntioselectivity for α-HCH degradation is favored nder oligotrophic conditions.

cknowledgments

We thank the Southern Oceans Group at hodes University, Grahamstown, South Africa nd fellow scientists on board the S.A. *Agulhas* for elp during sampling and the Swedish Polar esearch Secretariat for organizing the expedition. unding for this project was provided by the rafoord Foundation and the Swedish Natural cience Research Council.

eferences

allschmiter, K., 1992. Transport and fate of organic compounds in the global environment. Angewandte Chemie, International Edition in English 31, 487 664.

idleman, T.F., Walla, M.D., Roura, R., Carr, E., Schmidt, S., 1993. Organochlorine pesticides in the atmosphere of the Southern Ocean and Antarctica, January–March, 1990. Marine Pollution Bulletin 26, 258–262.

idleman, T.F., Jantunen, L.M., Falconer, R.L., Barrie, L.A., 1995. Decline of hexachlorocyclohexane in the arctic atmosphere and reversal of air sea gas exchange. Geophysical Research Letters 22, 219–222.

eBoer, J., Wester, P., 1991. Chlorobiphenyls and organochlorine pesticides in various sub-Antarctic organisms. Marine Pollution Bulletin 22, 441–447.

alconer, R.L., Bidleman, T.F., Gregor, D.J., 1995a. Air–water gas exchange and evidence of metabolism of hexachlorocyclohexanes in Resolute Bay, NWT. Science of the Total Environment 160/161, 65 74.

alconer, R.L., Bidleman, T.F., Gregor, D.J., Semkin, R., Teixeira, C., 1995b. Enantioselective breakdown of α-hexachlorocyclohexane in a small arctic lake and its watershed. Environmental Science and Technology 29, 1297–1302.

alconer, R.L., Bidleman, T.F., Szeto, S.Y., 1997. Chiral pesticides in soils of the Fraser Valley, British Columbia. Journal of Agricultural and Food Chemistry 45, 1946–1951.

aller, J., Hühnerfuss, H., König, W., Lugwig, P., 1991. Gas chromatographic separation of the enantiomers of marine pollutants. Distribution of α-HCH enantiomers in the North Sea. Marine Pollution Bulletin 22, 82 86.

alsall, C.J., Bailey, R., Stern, G., Barrie, L.A., Fellin, P., Muir, D.C.G., Rosenberg, B., Rovinsky, F.Ya., Kononov, E.Ya., Pastukhov, B., 1998. Multiyear observations of organohalgen pesticides in the Arctic Atmosphere. Environmental Pollution 102, 51 62.

Harner, T., Kylin, H., Bidleman, T.F., Strachan, W.M.J., 1999. Removal of α-hexachlorocyclohexane and enantiomers of α-HCH in the eastern Arctic Ocean. Environmental Science and Technology 33, 1157–1164.

Harner, T., Jantunen, L.M.M., Bidleman, T.F., Barrie, L.A., Kylin, H., Strachan, W.M.J., Macdonald, R.W., 2000. Microbial degradation is a key elimination pathway of hexachlorocyclohexanes from the Arctic Ocean. Geophysical Research Letters 27, 1155–1158.

Haugen, J.-E., Wania, F., Ritter, N., Schlabach, M., 1998. Hexachlorocyclohexanes in air in southern Norway. Temporal variations, source allocation and temperature dependence. Environmental Science and Technology 32, 217–224.

Helm, P.A., Diamond, M.L., Semkin, R., Bidleman, T.F., 2000. Degradation as a loss mechanism in the fate of α-hexachlorocyclohexane in arctic watersheds. Environmental Science and Technology 34, 812–818.

Hung, H., Halsall, C.J., Blanchard, P., Li, H.H., Fellin, P., Stern, G., Rosenberg, B., 2002. Temporal trends of organochlorine pesticides in the Canadian arctic atmosphere. Environmental Science and Technology 36, 862 868.

Iwata, H., Tanabe, S., Sakai, N., Tatsukawa, R., 1993. Distribution of persistent organochlorine pollutants in oceanic air and surface seawater and the role of ocean on their global transport and fate. Environmental Science and Technology 27, 1080–1098.

Jantunen, L., Bidleman, T.F., 1995. Reversal of the air–water gas exchange direction of hexachlorocyclohexanes in the Bering and Chukchi seas, 1993 versus 1998. Environmental Science and Technology 29, 1081–1089.

Jantunen, L., Bidleman, T.F., 1996. Air–water gas exchange of hexachlorocyclohexanes (HCHs) and the enantiomers of α-HCH in arctic regions. Journal of Geophysical Research (corrections Jantunen and Bidleman, 1997. 102, 19279–19282).

Jantunen, L., Bidleman, T.F., 1998. Organochlorine pesticides and enantiomers of chiral pesticides in Arctic Ocean water. Archives of Environmental Contamination and Toxicology 35, 218 228.

Kallenborn, R., Oehme, M., Wynn-Williams, D.D., Schlabach, M., Harris, J., 1998. Ambient air levels and atmospheric long-range transport of persistent organochlorines to Signey Island, Antarctica. Science of the Total Environment 220, 167–180.

Keller, C.D., Bidleman, T.F., 1984. Collection of airborne polycyclic aromatic hydrocarbons and other organics with a glass fiber filter-polyurethane foam systems. Atmospheric Environment 18, 837–845.

Koziol, A.S., Pudykiewicz, J.A., 2001. Global-scale environmental transport of persistent organic pollutants. Chemosphere 45, 1181 1200.

Kucklick, J.R., Hinkley, D.A., Bidleman, T.F., 1991. Determination of Henry's Law constants for hexachlorocyclohex-

anes in distilled water and artificial seawater as a function of temperature. Marine Chemistry 34, 197–209.

Lakaschus, S., Weber, K., Wania, F., Bruhn, R., Schrems, O., 2002. The air–sea equilibrium and time trend of hexachlorocyclohexanes in the Atlantic Ocean between the Arctic and Antarctica. Environmental Science and Technology 36, 138–145.

Larsson, P., Järnmark, C., Södergren, A., 1992. PCBs and chlorinated pesticides in the atmosphere and aquatic organisms of Ross Island, Antarctica. Marine Pollution Bulletin 25, 9–12.

Law, S.A., Diamond, M.L., Helm, P.A., Jantunen, L.M., Alaee, M., 2001. Factors affecting the occurrence and enantiomeric degradation of hexachlorocyclohexane isomers in northern and temperate aquatic systems. Environmental Toxicology and Chemistry 20, 2690–2698.

Li, Y.F., 1999. Global technical hexachlorocyclohexane usage inventories using a global cropland as a surrogate. Journal of Geophysical Research 104, 23785–23797.

Li, Y-F., Bidleman, T.F., 2003. Correlation between global emissions of alpha-HCH and its concentrations in Arctic air. Journal of Environmental Informatics 1, 52–57.

Li, Y.-F., Barrie, L.A., Bidleman, T.F., McConnell, L.L., 1998. Global hexachlorocyclohexane use trends and their impact on the arctic atmosphere. Geophysical Research Letters 25, 39–41.

Li, Y.-F., Scholtz, M.T., Van Heyst, B.J., 2000. Global gridded emission inventory of α-hexachlorocyclohexane. Journal of Geophysical Research 105, 6621–6632.

Li, Y-F., Macdonald, R.W., Jantunen, L.M.M., Harner, T., Bidleman, T.F., Strachan, W.M.J., 2002. The transport of β-hexachlorocyclohexane to the western Arctic Ocean: a contrast to α-HCH. The Science of the Total Environment 291, 229–246.

Macdonald, R.W., Barrie, L.A., Bidleman, T.F., Diamond, M.L., Gregor, D.J., Semkin, R.G., Strachan, W.M.J., Li, Y.F., Wania, F., Alaee, M., Alexeeva, L.B., Backus, S.M., Bailey, R., Bewers, J.M., Gobeil, C., Halsall, C.J., Harner, T., Hoff, J.T., Jantunen, L.M.M., Lockhart, W.L., Mackay, D., Muir, D.C.G., Pudykiewicz, J., Reimer, K.J., Smith, J.N., Stern, G.A., Schroeder, W.H., Wageman, R., Yunker, M.B., 2000. Contaminants in Canadian Arctic: five years of progress in understanding sources, occurrence and pathways. Science of the Total Environment 254, 93–234.

Pesticide Action Network North America "PANNA", 1995. Demise of the Dirty Dozen. WWW Page, http://www.panna.org/resources/documents/dirtyDozenChart.dv.html.

Ridal, J.J., Bidleman, T.F., Kerman, B., Fox, M.E., Strachan, W.M.J., 1997. Enantiomers of α-hexachlorocyclohexane as tracers of air–water gas exchange in Lake Ontario. Environmental Science and Technology 31, 1940–1945.

Sahsuvar, L., Helm, P.A., Jantunen, L.M., Bidleman, T. 2002. Henry's Law constants for α-, β- and γ-hexachl ocyclohexanes (HCHs) as a function of temperature and exchange in Arctic regions. Atmospheric Environment 983–992.

Schreitmüller, J., Ballschmiter, K., 1995. Air–water equilibri of hexachlorocyclohexanes and chloromethoxybenzenes the North and South Atlantic. Environmental Science a Technology 29, 207–215.

Shen, L., Wania, F., Lei, Y.D., Teixeira, C., Muir, D.C. Bidleman, T.F., 2004. Hexachlorocyclohexanes in the No American Atmosphere. Environmental Science and Tec nology 38, 965–975.

Strand, A., Hov, Ø., 1996. A model strategy for the simulati of chlorinated hydrocarbon distribution in the glo environment. Water Air and Soil Pollution 86, 283–316.

Tatsukawa, R., Yamaguichi, T., Kawano, Y., Kannan, N Tanabe, S., 1990. Global monitoring of organochlori insecticides: an eleven-year case study (1975–1985) of HCI and DDTs in the open ocean atmosphere and hydrosphe In: Kurtz, D.A. (Ed.), Long-Range Transport of Pesticid Lewis Publishers, Chelsea, Michigan, pp. 127–141.

Turner, D.R., Bertilsson, S., Fransson, A., Pakhomov, E 2004. The SWEDARP 97/98 marine expedition: overvie Deep-Sea Research II, this issue [doi:10.101 j.dsr2.2003.08.006].

Van den Brink, N.W., 1997. Direct transport of volati organochlorine pollutants to polar regions: the effect c the contamination pattern of Antarctic seabirds. Science the Total Environment 198, 43–50.

Walker, K., Vallero, D.A., Lewis, R.G., 1999. Factors influen ing the distribution of lindane and other hexachlor cyclohexanes in the environment. Environmental Scienc and Technology 33, 4373–4378.

Wania, F., Mackay, D., 1996. Tracking the global distributio of persistent organic pollutants. Environmental Science an Technology 30, 390–396.

Wania, F., Mackay, D., 1999. Global chemical fate of α hexachlorocyclohexane. 2. Use of a global distributio model for mass balancing source apportionment and tren prediction. Environmental Toxicology and Chemistry 18 1400–1407.

Wania, F., Mackay, D., Li, Y.F., Bidleman, T.F., Strand, A. 1999. Global chemical fate of α-hexachlorocyclohexane. 1 Evaluation of a global distribution model. Environmenta Toxicology and Chemistry 18, 1380–1389.

Weber, R.R., Montone, R.C., 1990. Distribution of organo chlorines in the atmosphere of the south Atlantic an Antarctic Oceans. In: Kurtz, D.A. (Ed.), Long Range Transport of Pesticides. Lewis Publishers, Chelsea, MI, pp 185–197.

ELSEVIER

Deep-Sea Research II 51 (2004) 2673–2682

DEEP-SEA RESEARCH
PART II

www.elsevier.com/locate/dsr2

Attenuation of biologically effective UV doses under overcast skies: a case study from the eastern Atlantic sector of the Southern Ocean

Deliang Chen[a,b], Sten-Åke Wängberg[c,*], Angela Wulff[d], Katarina Borne[a]

[a]*Earth Sciences Centre, Göteborg University, Box 460, SE-405 30 Göteborg, Sweden*
[b]*Laboratory for Climate Studies, National Climate Center, China Meteorological Administration, Beijing, China*
[c]*Botanical Institute, Göteborg University, Box 461, SE-405 30 Göteborg, Sweden*
[d]*Department of Marine Ecology, Marine Botany, Göteborg University, Box 460, SE-405 30 Göteborg, Sweden*

Abstract

This study deals attenuation of ultraviolet solar radiation measured during the SWEDARP 1997/1998 expedition in the eastern Atlantic sector of the Southern Ocean. Experimental data were measured on board a ship and theoretical computation of radiative transfer has been applied. Focus has been placed on biologically effective UV-B doses using three commonly applied biological weighting functions based on: inhibition of carbon dioxide fixation (Science 258 (1992) 646); Generalized plant effects (Stratospheric Ozone Reduction, Solar Ultraviolet Radiation and Plant Life 1986, Springer, Berlin) and DNA lesions (Proc. Nat. Acad. Sci. USA 71 (1974) 3363). The ratio of measured dose to that under clear sky condition, calculated by a model, was defined as transmittance which was studied in relation to other information. Further, the interrelationship between the biologically effective UV doses and various broadband irradiance in the UV-A, UV-B and PAR was established. It shows that the UV-B doses based on the three weighting functions are closely linked to each other and their cloud transmittances are nearly the same. The biologically effective UV-B doses can be estimated with reasonable accuracy from the broadband irradiance in the UV-A, UV-B and PAR regions, with UV-B giving the best results. Univariate analysis between the transmittance and zenith angle, total cloud cover and cloud base height was performed. It is found that attenuation is almost independent of zenith angle. Transmission is reduced by 7.7% if the cloud cover is increased by one octa. The average transmittance of the UV-B doses is 0.40, indicating that clouds have played an important role in reducing the UV radiation.
© 2004 Elsevier Ltd. All rights reserved.

1. Introduction

Amongst the various anthropogenic effects on global climate, the role played by ozone depletion is of particular concern. Ozone plays an important

*Corresponding author. Tel.: +46 31 773 2608; fax: +46 31 773 2626.
E-mail address: swa@botany.gu.se (S.-A. Wängberg).

0967-0645/$ - see front matter © 2004 Elsevier Ltd. All rights reserved.
doi:10.1016/j.dsr2.2001.02.002

role in global weather and climate as well as surface ecology through absorbing some of the biologically harmful ultraviolet radiation, therefore preventing them from reaching the earth's surface. Most of the solar radiation at wavelengths less than 280 nm, in the ultraviolet (UV-C) region, is absorbed in the atmosphere so that only very small amounts reach the earth's surface. Ozone absorption coefficients become appreciably smaller in the UV-B (280–320 nm) region and some radiation reaches the earth's surface, with the actual amount depending on total column ozone, solar zenith angle and attenuation by clouds and aerosols. Very low levels of ozone absorption occur in the UV-A region, at wavelengths between 320 and 400 nm.

An increasing number of studies have documented the impact that ultraviolet radiation may have on the ecosystem. In the marine environment biological productivity may be affected by higher levels of ultraviolet radiation (Häder, 1993; Vincent and Roy, 1993; Wängberg et al., 1996a) and in some cases, a species shift of phytoplankton may occur (Helbling et al., 1992; Davidsson et al., 1996, Wängberg et al., 1996b). Increasing levels of ultraviolet radiation have also been linked to lower crop productivity (Tevini, 1993) and a range of health problems in humans such as skin cancer (melanoma and non-melanoma) and eye cataracts (Tevini, 1993; Elwood, 1989; Lee, 1989; Hollows, 1989).

A convenient way of describing the effect of UV radiation is by means of biological weighting functions (BWF), which can be either monochromatic or polychromatic (Caldwell et al., 1986). The BWF indicates the biological effectiveness of different wavelength for a given reaction, usually normalized to 100% at 300 nm. A number of laboratory studies have produced BWF, such as that for acute reactions of the skin (erythema and photodermatoses), acute reactions of the eye (keratitis and conjunctivitis), cataracts and DNA damage. Madronich (1992) gives some of the most important BWF. This study concentrates on the UV-B region of the solar spectrum as modulated by three biologically relevant filters, Cullen's spectra for inhibition of photosynthesis in a marine diatom (Cullen et al., 1992), Caldwell's

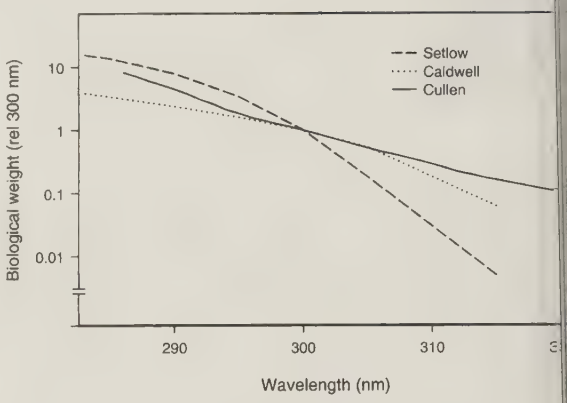

Fig. 1. Used BWF, normalized to 300 nm.

generalized plant spectrum (Caldwell, 1971) an Setlow's DNA spectrum (Setlow, 1974) (Fig. 1).

Regional UV variability can be induced b changes in total ozone, tropospheric aerosols an cloud cover. Most published data on UV radiatio in Antarctic rely on point measurements a research stations (e.g. Gautier et al., 1994) whil this study focuses on the role played by clouds i affecting the depletion of ultraviolet radiatio during an expedition far from land in the easter Atlantic sector of the Southern Ocean.

2. Data collection and processing

Data were collected during the SWEDAR (Swedish Antarctic Research Programme) 1997 1998 expedition. The expedition was a Swedish South African cooperation aiming on studies o the chemistry and biology in the Eastern Atlanti sector of the Southern Ocean. Data durin December 31, 1997 and February 2, 1998 wa used in the analysis. For the position of the shi and the measurement, the reader is referred to Fig 2 which shows that daily movement of the shi starting from 31/12 and ending at 2/2.

2.1. Radiation data

Spectroradiometer measurements were carrie out by using an Optronic spectroradiomete (OL754) in the range 280–800 nm with a resolutio of 2 nm. The 2π-sensor (submersible spher

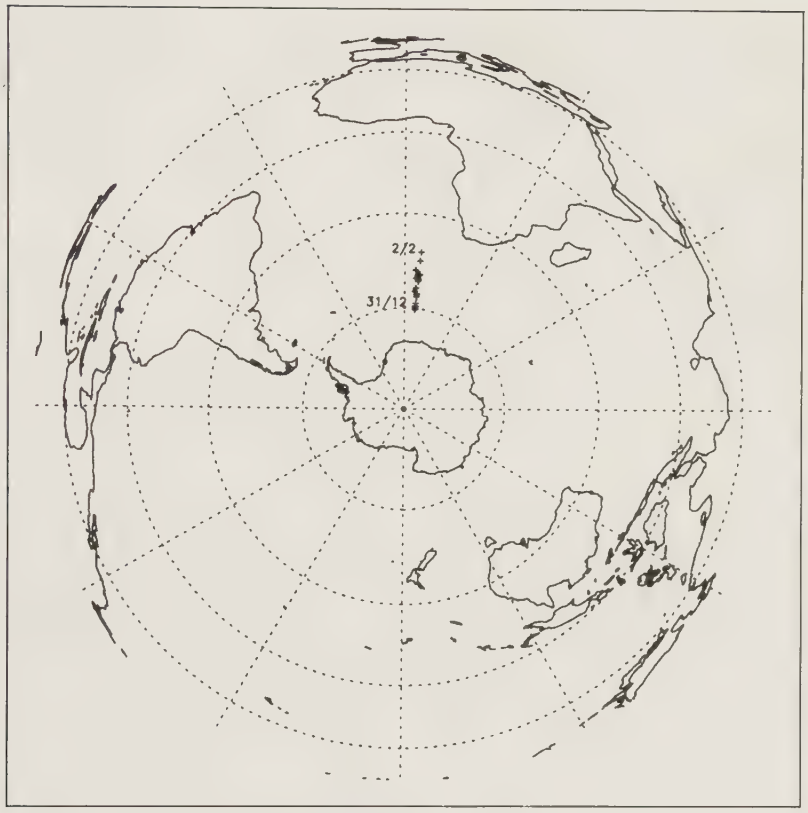

Fig. 2. Map showing the daily movement of the expedition ship during the period December 31, 1997 (59 °S, 6 °E) to February 2, 1998 (42 °S, 6 °E).

assembly, Optronics) was placed on the top of a container on the most upper deck of the ship and the light was transferred to the spectroradiometer, placed in the container, through a quartz fiber optic probe (2 m). The submersible sphere function as the normal integrating sphere with the exception that the opening is covered by a transparent dome. The spectroradiometer was calibrated in October 1997 using an OL752-10E calibration accessory (Optronics). Before starting the measurements wavelength and sensitivity check was done with OL752-150 Check source module (Optronics). UV-B, UV-A and PAR irradiance were obtained by integrating the spectrum measurements from 280 to 320 nm, from 320 to 400 nm and from 400 to 700 nm, respectively. The spectroradiometer operated continuously, starting a new scan each 15 min. Each scan took approximately 12 min. The data were processed into hourly averages to reduce differences due to short-term fluctuations in cloud cover and ship movements during scanning.

Since the data were collected on a ship that was in continued motion (changing latitude) and data from different times of a day (changing time) were used, a normalisation procedure is needed to make the data comparable. Here the clear-sky spectral model (GCS) (Green et al., 1980) was used to calculate cloudless values that were used in the normalisation. A comparison of the GCS model with a more sophisticated model UVSPEC (Kylling, 1995) shows that the difference between results from the two models is negligible.

Three BWFs were used to obtain the UV radiation effective doses with regard to inhibition of photosynthesis in a marine diatom (Cullen et al., 1992), plant damage (Caldwell, 1971) and to DNA damage (Setlow, 1974). The

relevant radiative doses (UV_1, UV_2 and UV_3) is calculated as the product of the spectral radiative irradiance (both measured and modelled) and the respective BWF, summed over all relevant wavelengths. This way the impact of a given UV radiation climatology on a given organism can be readily estimated.

The hourly transmittance (τ) is used to study the attenuation. It is defined as the measured biologically effective irradiance (UV_i) divided by the respective irradiance that would be incident on that surface for the same time under cloudless conditions (UV^c_i), i.e.

$$\tau_i = UV_i/UV^c_i, \quad (1)$$

where $i = 1, 2, 3$ for Cullen, Caldwell and Setlow spectrum, respectively. Since such processes as the ozone absorption and scattering have been taken into account in the computation of clear sky radiation, the transmittance calculated by Eq. (1) should be a good index of the influence of clouds, provided that effects of aerosol is small. Aerosol was not measured during the expedition, so its effect cannot be quantified. However, since the measurement was done in a remote area, the aerosol conditions may be assumed homogenous. Also, the transmittance is only considered as an index for cloud attenuation. This is why the transmittance is sometimes referred to as cloud transmittance in later discussion.

The working irradiance data set was finally reduced in order to correspond with zenith angles 35–60°. Outside this range, instrument errors and low irradiance signals provided too much uncertainty.

2.2. Meteorological data

Meteorological observations were done every third hour and consisted of total cloud cover, single distinctive layers (octas), cloud base height and cloud type. To ensure compatibility with the hourly radiation data, linear interpolation was applied to the three hourly data and hourly meteorological data created. Except some extreme situations, three hours are considered short for changes in cloud, which justifies the interpolation procedure.

Daily total ozone was obtained from TOM satellite data (http://jwocky.gsfc.nasa.gov/index.html) and corresponds to 12:00 GMT. Hour ozone was used for the clear sky calculation, whic was obtained by linear interpolation between t daily values at 12:00 GMT.

3. Results

3.1. Interrelationship of the radiation fluxes

Time series of the measurement of thre biologically effective UV doses, UV-A, UV-B PAR, total ozone and total cloud cover during th study period were plotted and examined. It turn out that all the radiation fluxes have a very clea diurnal cycle so that the values around noon ca be representative of the daily variability. Fig. . displays the values at 12:00 GMT, when the ozon data is available. Also plotted are the total ozon and total clouds. The influence of ozone is difficul to judge by a visual inspection of the figure. On the other side, clouds have a much more eviden impact on the radiation fluxes. It is obvious that al the radiation fluxes are fairly well correlated t each other. The correlation between the fluxes in the UV range is especially high. This points to a possibility of using one or more fluxes to estimate another. If the estimation is of reasonable accuracy, the established statistical relationship could provide an alternative to the more demanding or impossible measurement. This has a high application value if broadband instrument such as those for PAR and UV-B ranges can be useful in estimating the biologically effective UV doses, since the broadband instruments have the advantage of being low cost, simple to use, portable and weather proof.

Correlation analysis was performed to examine how well these fluxes are related. Table 1 shows results of the linear regression. Combinations of the three independent variables were also tried, but they did not give better correlation. From the table it is seen that UV-B is well correlated with UV_i ($i = 1-3$) so that a reliable estimate can be made using UV-B. When using the UV-A or PAR values the correlation is weaker especially for UV_2 and UV_3.

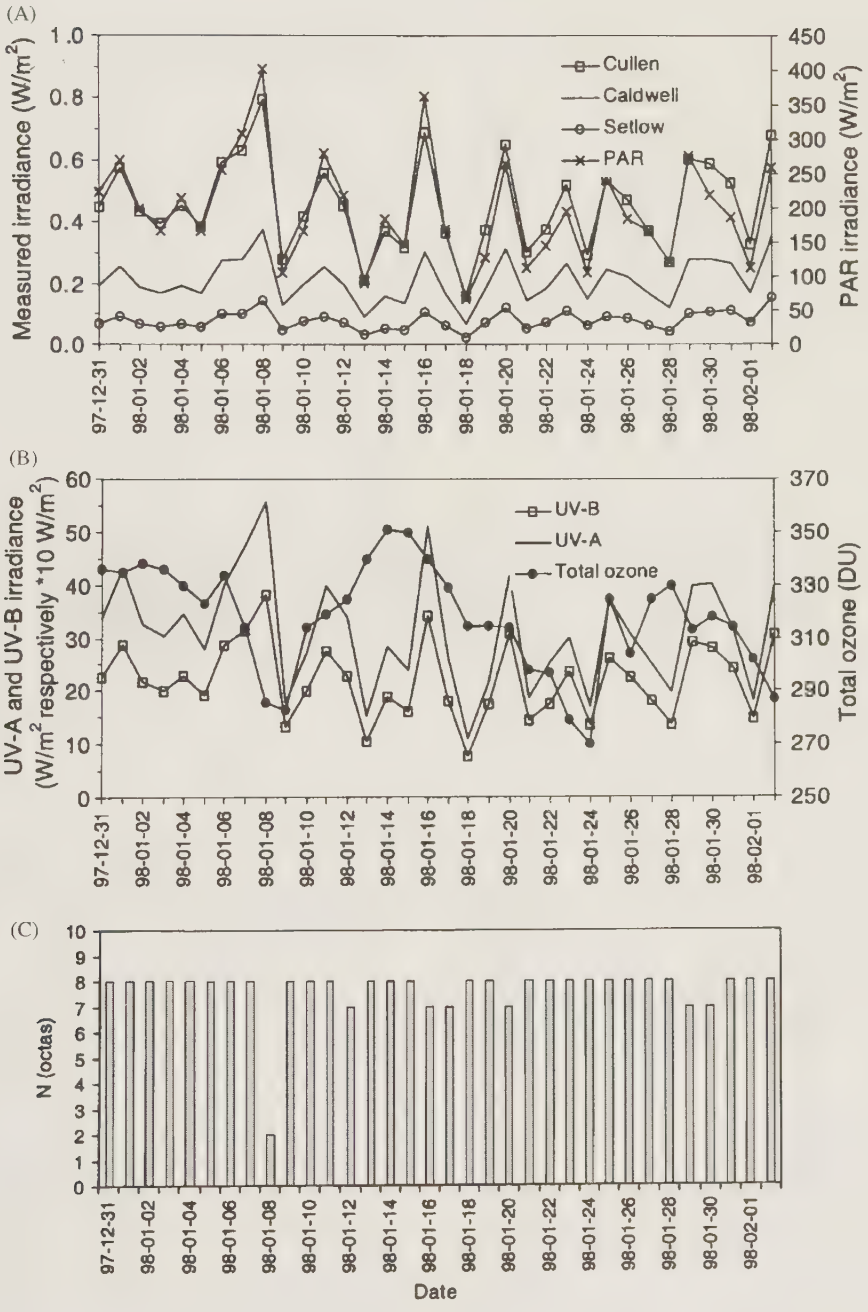

Fig. 3. Noon values (at 12:00 GMT) of the measured irradiance: (A) the three biologically effective UV-B irradiances and PAR; (B) UV-B, UV-A and total ozone; (C) total cloud cover during the study period.

Table 1
Analysis of weighted UVB irradiance as a function of UV-A, UV-B and PAR by using linear regression

	UV-A			UV-B			PAR		
	a	B	R^2	a	b	R^2	a	b	R^2
UV_1	-4.36×10^{-2}	1.49×10^{-2}	0.90	-2.43×10^{-2}	0.21	0.99	1.05×10^{-2}	1.98×10^{-3}	0.8
UV_2	-3.37×10^{-2}	7.08×10^{-3}	0.81	-2.97×10^{-2}	0.10	0.95	-6.78×10^{-3}	9.34×10^{-4}	0.7
UV_3	-1.69×10^{-2}	2.73×10^{-3}	0.73	-1.71×10^{-2}	4.14×10^{-2}	0.89	-6.11×10^{-3}	3.57×10^{-4}	0.6

BWFs used are Cullen (UV_1), Caldwell (UV_2) and Setlow (UV_3). R is the correlation coefficient, a and b are coefficients in the linea equation $y = a + bx$. The number of samples is 292.

Fig. 4. Box plot showing basic descriptive statistics of the cloud transmittance during the study period calculated for the three biological active UV irradiances respectively. The bottom of the vertical line marks the 5th percentile. The bottom of the box marks the 25th percentile, the median line marks the 50th percentile in the box, the top of the box marks the 75th percentile, and the top of the vertical line marks the 95th percentile. Note that the data with zenith angle greater than 60° were excluded.

3.2. Characteristics of transmittance

It is important to characterize transmittance's statistical property before its dependence on total cloud cover and cloud base height is examined. These two parameters are chosen because they are included in standard meteorological observation. Fig. 4 summarizes the basic descriptive statistics of the transmittances during the whole study period. Note that the data with zenith angle greater than 60° were excluded, the statistics for all three doses are similar.

A sample of 292 data points produced transmittances with an interquartile range of 0.19–0.46, 0.20–0.51, and 0.19–0.48 for UV_1, UV_2 and UV_3, respectively. For the arithmetic means (medians) the numbers are 0.38 (0.37), 0.42 (0.40), and 0.40 (0.37), respectively. The fact the medians and the arithmetic means are very close indicates that the distributions are approximately normal. An average cloud transmission of 0.7 for erythemal UV doses at Latitude 60 °N has been presented by Fredrick and Snell (1990) and Fredrick and Lubin (1988) from satellite observations. In comparison, results from this study suggest an average reduction in the three UV doses of around 60%. However, it must be noted that the data involved in this analysis is from a period when cloudy and overcast conditions dominate.

It is interesting to note that cloud transmission values greater than one did appear twice (for Caldwell it is equal to 1.08 and for Setlow 1.12) on

26 January at 7:00 GMT in the selected data set. This phenomena in the UV-B range has been reported previously (e.g. Segal and Davis, 1992). It occurred at a zenith angle of 60° and under the cover of cumulus and stratocumulus clouds. Side reflection is usually suggested as the causal factor.

3.3. Transmittance and total cloud cover

Fig. 5 shows the transmittance plotted against total cloud cover. There is much fewer data in the lower cloud coverage relative to the occasions of high cloud cover range. There appears to be a trend of decreasing transmittance with increasing cloud covers. A linear regression analysis shows that around 10% of the total variance in the transmittances can be accounted for by the linear trend with interceptions forced to 1. The correlation coefficients of the regression are statistically significant at the 99% level, which indicates that the decreasing trend is significant.

To better describe the influence of the total clouds, the total data set was divided into two groups, one with cloud cover ranging from 2 to 7 octas (low cloud cover) and another for 8 octas (high cloud cover), which includes occasions when the sky is obscured or the cloud amount cannot be estimated. Fig. 6 gives the box plot of the results. The scatters are nearly the same for all the transmittances in the two groups, while the medians are quite different between the two groups. The difference among the three transmittances are relatively small and the mean of the medians are 0.50 and 0.35 for the low and high cloud covers, respectively. It is evident that the median of the transmittances for the total data set (0.38) is biased toward the high cloud cover conditions. High cloud cover conditions corresponding to zenith angles 35–60° produce a median transmittance of 0.35, and similar to estimates reported in other studies (Paltridge and Barton, 1978; Blumthaler et al., 1996).

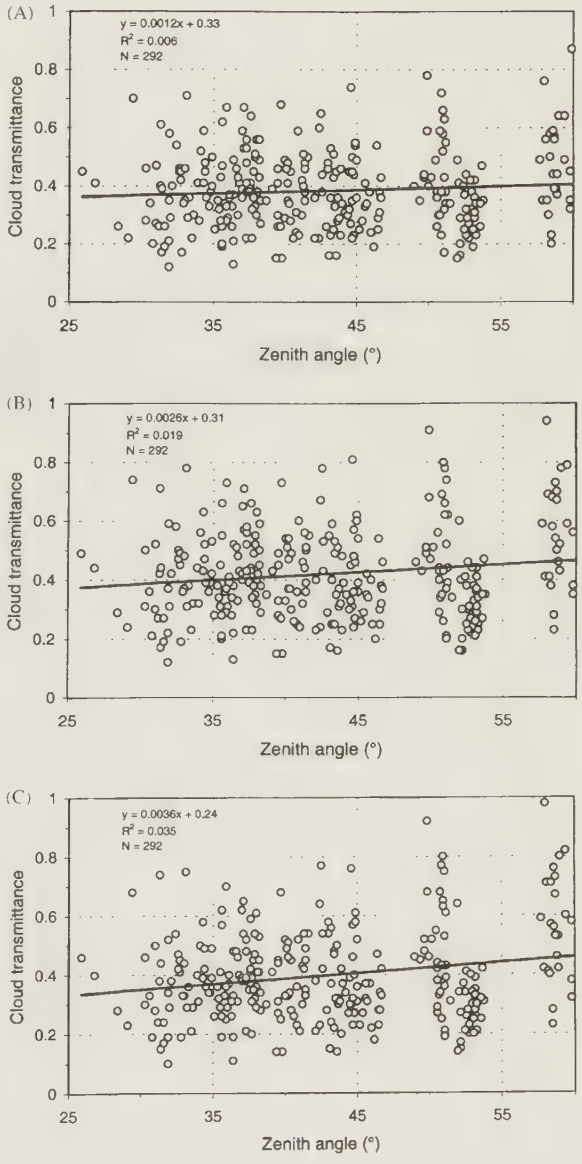

Fig. 5. Cloud transmittance for each of the three weighted UV irradiances: (A) for τ_1; (B) for τ_2; and (C) for τ_3 versus the cloud cover. The number indicating the BWF used is as same as in Fig. 3.

3.4. Transmission and cloud base height

The effects of cloud base height on the transmittances are displayed in Fig. 7 where transmittances for 5 groups with different cloud base height ranges are shown. Samples were concentrated around low altitude clouds. Median values of the first four groups indicate that the transmittances under the cloud base height of

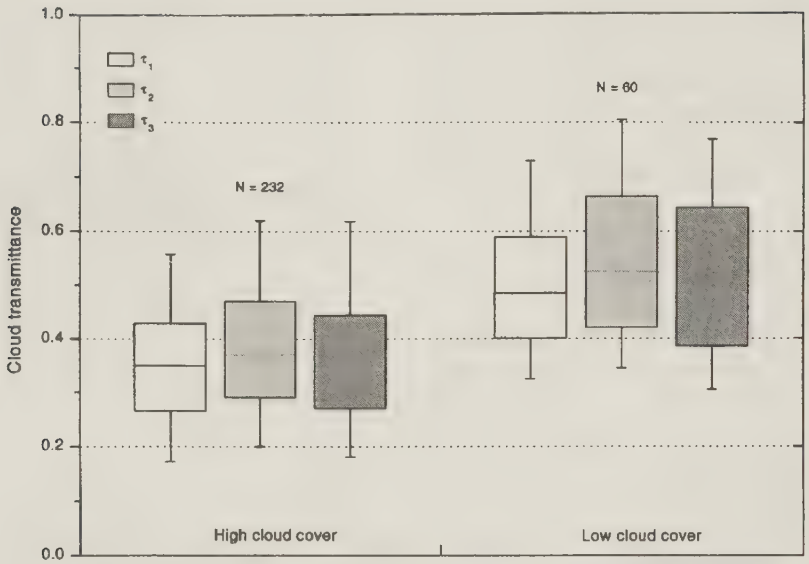

Fig. 6. Box plot showing descriptive statistics of cloud transmittance for each of the three weighted UV irradiances: (A) τ_1; (B) τ_2 and (C) τ_3. The transmittance is divided by cloud cover into two groups; one with high cloud cover (8 octas including occasions when the sky is obscured, or the cloud amount cannot be estimated) and another with relatively low cloud cover (2–7 octas). The number indicating the BWF used is as same as in Fig. 3.

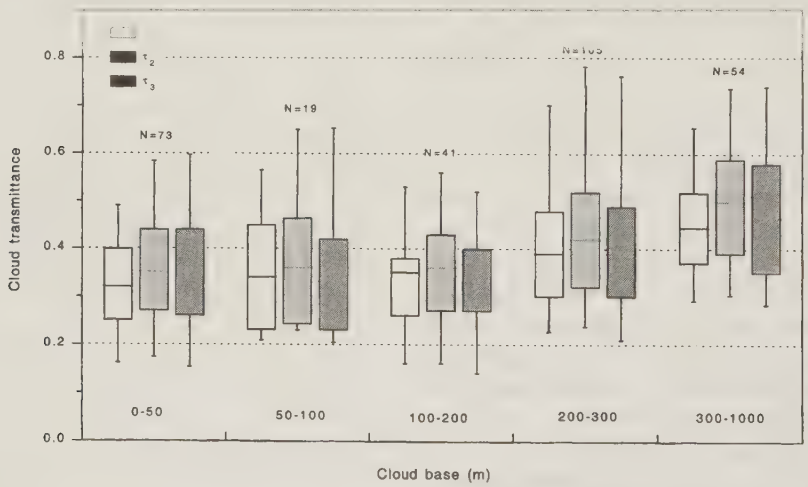

Fig. 7. Box plot showing cloud transmittance for the three weighted UV irradiances presented in groups according to five cloud base height ranges. The number indicating the BWF used is as same as in Fig. 3.

0–200 m are very similar and there is a tendency of higher transmission for higher clouds (the last group). It has been suggested by Borkowski et al. (1977) that high clouds have a much lower effect on the sky ultraviolet radiation at the ground level. However, caution is required here since the higher transmission for higher clouds may have been, at least partly, caused by lower cloud coverage associated with the high clouds.

4. Summary and conclusions

Cloud transmittance of three biologically effective UV-B irradiance during the SWEDARP 97/98 expedition to the eastern Atlantic sector of the Southern Ocean (31 December 1997 to 2 February 1998) has been examined by utilizing ship-based measurements and theoretical clear-sky model. Low clouds and high could cover were the dominant modes of cloud present during the expedition. The main purpose of this work is to characterize the impact of clouds on the radiation doses. This is achieved by studying the cloud transmittance defined as the ratio of the measured to calculated clear-sky UV doses. In addition, the biological effective UV doses are related to broadband UV-A, UV-B and PAR, while the transmittance is studied in relation to cloud characteristics. The main results can be summarized as follows:

- The UV-B doses based on the Cullen, Caldwell and Setlow BWFs are well correlated to each other. In fact, the correlation coefficients among them are so high (0.97–0.99) that one spectrum is enough to characterize the biological effect of the UV radiation. As a result, the cloud transmittances of the three doses are very similar under overcast skies.
- The interquartile range of the cloud transmittances ($N = 292$) for the Setlow spectrum is 0.19–0.48 which is almost the same as with other two spectrums. The average attenuation of the UV-B doses with Cullen, Caldwell and Setlow action spectrums are 0.38, 0.42 and 0.40. respectively. Therefore, the clouds have played a significant role in reducing the UV radiation reached the surface.
- There is one instance where the ground incident UV-B dose was above the clear-sky values. It occurred under the partial cover of cumulus and stratocumulus.
- Although the data are strongly biased toward the overcast situations, a dependence of the cloud transmission on the total cloud cover can still be identified. The linear regression between the transmittance and the cloud cover shows that transmission would be reduced by 7.7% if the cloud cover is increased by one octa.
- Greater attenuation is found for clouds whose base lies below 300 m, with average reduction (mean of the medians in the four base height ranges) being 65%. Clouds between 300 and 1000 m reduced the UV-B doses by 56%.

Acknowledgement

We would like to thank the Swedish Polar Secretariat and Göteborg Marine Research Centre (GMF), who funded the expedition. We also acknowledge the work of the crew on the Research Vessel SA Agulhas and a special thank to the expedition meteorologist, James Fletcher, who collected and gave us assess to all cloud data. Manuel Nunez is thanked for help with the radiation model.

References

Blumthaler, M., Ambach, W., Cede, A., Staehelin, J., 1996. Attenuation of erythemal effective irradiance by cloudiness at low and high altitude in the Alpine region. Photochemistry and Photobiology 63, 193–196.

Borkowski, J., Chai, A., Mo, T., Green, A., 1977. Cloud effects on middle ultraviolet global radiation. Acta Geophysica Polonica 25, 287 301.

Caldwell, M.M., 1971. Solar UV irradiation and the growth and development of higher plants. In: Giese, A.C. (Ed.), Photophysiology, vol. 6. Academic Press, New York.

Caldwell, M.M., Camp, L.B., Warner, C.W., Flint, S.D., 1986. Action spectra and their key role in assessing biological consequences of solar UV-B radiation change. In: Worrest, R.C., Caldwell, M.M. (Eds.), Stratospheric Ozone Reduction, Solar Ultraviolet Radiation and Plant Life. Springer, Berlin.

Cullen, J.J., Neal, P.J., Lesser, M.P., 1992. Biological weighting function for the inhibition of phtoplankton photosynthesis by ultraviolet radiation. Science 258, 646–650.

Davidsson, A.T., Marchant, H.J., de la Mare, W.K., 1996. Natural UVB exposure changes the species composition of Antarctic phytoplankton in mixed culture. Aquatic Microbial Ecology 10, 299 -305.

Elwood, J.M., 1989. The epidemiology of melanoma: its relationship to ultraviolet radiation and ozone depletion. Transactions of the Menzies Foundation 15, 95–108.

Fredrick, J.E., Lubin, D., 1988. The budget of biologically active ultraviolet radiation in the earth atmosphere system. Journal of Geophysical Research 93 (D4), 3825–3832.

Fredrick, J.E., Snell, H.E., 1990. Tropospheric influence of solar ultraviolet radiation: the role of clouds. Journal of Climatology 33, 373–381.

Gautier, C., He, G., Yang, S., Lubin, D., 1994. Role of clouds and ozone on spectral ultraviolet-B radiation and biologically active UV dose over Antarctica. In: Weiler, C.S., Penhale, P.A. (Eds.), Ultraviolet Radiation in Antarctica: Measurements and Biological Effects. Antarctic Research Series vol. 62, American Geophysic Union, Washington DC, pp. 83–91.

Green, A.E.S., Cross, K.R., Smith, L.A., 1980. Improved analytic characterization of ultraviolet skylight. Photochemistry and Photobiology 31, 59–65.

Häder, D.-P., 1993. Risks of enhanced solar ultraviolet radiation for aquatic ecosystems. In: Round F.E., Chapman, D.J. (Eds.), Progress in Phycological Research. Biopress Ltd., pp. 1–45.

Helbling, E.W., Villafañe, V., Ferrario, M., Holm-Hansen, O., 1992. Impact of natural ultraviolet radiation on rates of photosynthesis and on specific marine phytoplankton species. Marine Ecology Progress Series 80, 89–100.

Hollows, F.C., 1989. Ultraviolet radiation and eye diseases. Transactions of the Menzies Foundation 15, 113–120.

Kylling, A., 1995. UVspec Users's Guide, Edition 0.2 for Uvspec version vol. 1.41, May 1995.

Lee, J.A.H., 1989. Health outcomes of non-melanoma skin cancer. Transactions of the Menzies Foundation 15, 109–112.

Madronich, S., 1992. Implications of recent total atmospheric ozone measurements for biologically active ultraviolet radiation reaching the earth's surface. Geophysical R search Letter 19, 37.

Paltridge, G.W., Barton, I.J., 1978. Erythemal ultravio radiation distribution over Australia—the calculatio detailed results and input data including frequency analy of observed Australian cloud cover Division of Atmosphe Physics Technical Paper 33, Commonwealth Scientific a Industrial research Organisation, Australia.

Segal, M., Davis, J., 1992. The impact of deep cumul reflection on the ground-level global irradiance. Journal Applied Meteorology 31 (2), 217–222.

Setlow, R.B., 1974. The wavelengths in sunlight effective producing skin cancer: a theoretical analysis. Proceedings the National Academy of Science USA 71, 3363–3366.

Tevini, M., 1993. UV-B Radiation and Ozone Depletion. Lew Publishers, USA.

Vincent, W.F., Roy, S., 1993. Solar ultraviolet-B radiation an aquatic primary production: damage, protection, an recovery. Environmental Review 1, 1–12.

Wängberg, S.-Å., Selmer, J.-S., Ekelund, N., Gustavson, K 1996a. Effects of increased UV-B radiation on the Nord marine ecosystem—a literature review. Nordic Council Ministers TemaNord. 1996. 515.

Wängberg, S.-Å., Selmer, J.-S., Gustavson, K., 1996b. Effec of UV-B radiation on biomass and composition in marin phytoplankton communities. In: Figueroa, F.L., et a (Eds.), Underwater light and algal photobiology. Scienti Marina, 60 (Suppl.1), pp. 81–88.

ELSEVIER

Deep-Sea Research II 51 (2004) 2683–2699

DEEP-SEA RESEARCH
PART II

www.elsevier.com/locate/dsr2

A first study of SF_6 as a transient tracer in the Southern Ocean

Toste Tanhua*, K. Anders Olsson[1], Elisabet Fogelqvist

Department of Chemistry, Analytical and Marine Chemistry, Göteborg University, SE-412 96 Göteborg, Sweden

Accepted 20 February 2001

Abstract

Halogenated transient tracers such as the chlorofluorocarbons CFC-11, CFC-12 and CFC-113 are commonly used in oceanographic studies. These compounds enter the ocean via the atmosphere and their transient atmospheric concentrations make them valuable as oceanic tracers. The trends of rapidly rising atmospheric concentrations of these tracers are however broken, and the oceanic signal becomes increasingly more difficult to decipher. There is a need for a new transient tracer to complement the existing suit of tracers, especially for recently ventilated water masses. One compound that looks promising in this respect is sulphur hexafluoride (SF_6), an inert gas whose atmospheric concentration is rising rapidly. In this paper, the use of SF_6 as a transient tracer in recently ventilated waters is discussed and the method for determination of SF_6 in seawater is described. Tracer data from a section in the Atlantic sector of the Southern Ocean along 6°E, from 60°S to 40°S, occupied during January 1998, are presented. The Antarctic Polar Front, found close to 50°S, was studied with a densely sampled section down to 400 m depth and SF_6/CFC-12 ratios are used to deduce ventilation ages and dilution factors. A comparison of apparent ages derived from a variety of tracers is presented together with the uncertainties in these estimates. This work demonstrates that SF_6 is a useful and valuable transient tracer for waters ventilated during the last 20 years.
© 2004 Elsevier Ltd. All rights reserved.

1. Introduction

A variety of transient tracers together with more traditional physical parameters such as salinity and temperature provide complementary understanding of the ocean system. These transient tracers include the extensively used chlorofluorocarbons (CFCs). These are anthropogenic compounds that enter the sea surface from the atmosphere via air–sea exchange. The studies of CFCs dissolved in the ocean have helped to elucidate movement and mixing of water masses. There are only insignificant natural sources of CFCs (Jordan et al., 2000) and their atmospheric concentrations have been increasing until the early 1990s. This transient signal gives the CFCs their value as tracers in the sea. The atmospheric

*Corresponding author. Present address: Leibniz-Institut für Meereswissenschaften, Düsternbrooker Weg 20, D-24105 Kiel, Germany. Tel.: +49 431 600 4213; fax: +49 431 600 4202.
E-mail address: ttanhua@ifm.uni-kiel.de (T. Tanhua).
[1]Present address: Bjerknes Centre for Climate Research and Geophysical Institute, University of Bergen. Allégaten 55, N-5007 Bergen, Norway.

0967-0645/$ - see front matter © 2004 Elsevier Ltd. All rights reserved.
doi:10.1016/j.dsr2.2001.02.001

concentrations of the CFCs are well known from experimental observations for the period after the late 1970s/early 1980s (Walker et al., 2000). The atmospheric CFC concentrations for the years before that have been estimated based on industrial productions and atmospheric lifetimes (Walker et al., 2000). The solubility data for the CFCs are known as functions of salinity and temperature (Bu and Warner, 1995; Bullister and Wisegarver, 1998; Warner and Weiss, 1985). It is hence possible to estimate the time elapsed since a water parcel was in contact with the atmosphere. The first CFCs used as marine tracers and also the most widely used are CFC-11 and CFC-12 (cf. Bullister and Weiss, 1983; Warner and Weiss, 1985; Weiss et al., 1985). The use of the tracer CFC-113 was applied in the late 1970s for use in more recently ventilated water masses (cf. Bu and Warner, 1995; Wisegarver and Gammon, 1988). In a similar way, carbon tetrachloride (CCl_4) has been used for age estimates of older water masses in high latitude regions since it has been released to the atmosphere since the first decade of the 20th century (cf. Bullister and Wisegarver, 1998; Krysell, 1992; Krysell and Wallace, 1988). The use of the CFC-11, CFC-12 and CFC-113, as well as CCl_4, and any ratio between them as transient tracers in the ocean has recently been hampered by the slow rise rate, or even decline, of their atmospheric concentrations that started in the early 1990s. The ratio CFC-11/CFC-12, however, has remained virtually constant from the middle of the 1970s to the late 1980s but may again be useful for water masses ventilated from the early 1990s and onwards, since the ratio is now decreasing, as demonstrated by Min (1999). There is a need for a 'new' transient tracer, whose source function is still increasing, to add to the measurements frequently performed today.

One new transient tracer is sulphur hexafluoride (SF_6), which is a non-reactive, stable gas whose atmospheric concentration is rapidly increasing. The most important commercial use of sulphur hexafluoride is as a gaseous electrical insulator and in the processing of aluminium and magnesium, processes from which the gas is subsequently released to the atmosphere. There is only one known natural source for SF_6 and since this is a weak source, there is an extremely low natu background concentration of the compound in environment (Harnisch and Eisenhauer, 1998). fact, the background signal in the ocean can regarded as nil since it is well below the analyti detection limit of the current instrumentation. T atmospheric history of SF_6 from 1978 to presen reported by Maiss and Brenninkmeijer (19 based on measurements of archived air samp from Cape Grim, Tasmania. They also rep production estimates for SF_6 back to 1953, wh makes it possible to reproduce the early atm spheric history of SF_6. The atmospheric conce tration of SF_6 in the Southern Hemisphere w approximately 3.99 ppt in the beginning of 19 and is currently rising at a rate of 7% per ye (Maiss and Brenninkmeijer, 1998), see Fig. 1. T yearly emission of SF_6 to the atmosphere decreasing at present, from a peak value 6700 tons yr^{-1} in 1995 to 4900 tons yr^{-1} in 19 (Maiss and Brenninkmeijer, 2000). The sam authors estimate that the future emission of S to the atmosphere will be reduced to abo 750 tons yr^{-1}. Considering the long lifetime f SF_6 in the atmosphere (estimated to 3200 years this future scenario means that SF_6 will contin to rise in the atmosphere by a modest 0.03 ppt yr even after such a drastic reduction of the emissio Although such a small interannual gradient in t SF_6 concentration will make the direct use of SF as a tracer difficult, the ratios of SF_6 to the CF

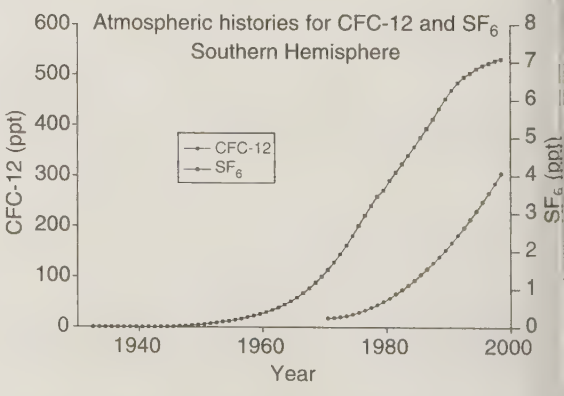

Fig. 1. Atmospheric concentrations for CFC-12 and SF_6 in th Southern Hemisphere, from Walker et al. (2000) and Maiss an Brenninkmeijer (1998), respectively.

l most likely continue to rise rapidly in the ure, since the CFCs will be decreasing. Fig. 2 ows the evolution of the atmospheric ratio of $_6$/CFC-12 in the Southern Hemisphere. The ubility of SF_6 in seawater is discussed by anninkhof et al. (1991), and in recent work by llister et al. (2002), thus providing the rce function for SF_6 in the ocean. Experiments ther suggest that SF_6 does not adsorb onto rticles and is inert in seawater (Ledwell and tson, 1991). Sulphur hexafluoride thus fulfils ny demands that are put on a transient marine cer.

Since SF_6 has low atmospheric concentration d low solubility in seawater, its concentration in ocean surface waters is typically less than mol kg^{-1} (2×10^{-15} mol kg^{-1}). However, due to h sensitivity for SF_6 by the electron capture ector (ECD), it is possible to measure even se minute quantities of the tracer in seawater. spite of many favourable properties, few studies ve so far been published where SF_6 is used as a nsient tracer in oceanographic studies, an plication suggested by Law et al. (1994). The st one is the recent work by Law and Watson 001), where SF_6 is used in the Arabian Sea to dy Persian Gulf Water inflow and associated ygen utilisation. However, several vertical pro- s of background SF_6 concentrations have been

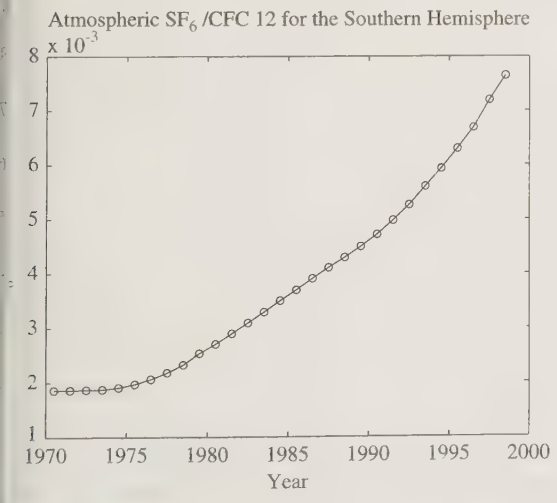

2. Atmospheric concentration ratio between SF_6 and C-12 in the Southern Hemisphere.

published in conjunction with different projects (cf. Law et al., 1994, 1998; Watson and Liddicoat, 1985).

Sulphur hexafluoride has been widely used as a deliberately released tracer in experiments such as the iron fertilisation experiment in the equatorial Pacific (Law et al., 1998) and the study of deep convection in the Greenland Sea (Watson et al., 1999). The use of SF_6 as a deliberately released tracer has somewhat hampered its use as a transient tracer in parts of the world oceans. Table 1 lists most deliberate SF_6 release experiments to date (see also Watson and Ledwell, 2000). Most of these are conducted in the surface region where the SF_6 will equilibrate with the atmosphere before being transported to the interior of the ocean and will therefore not affect the transient use of SF_6. Nevertheless, the potential of SF_6 as a transient tracer is great and its use as such will most likely increase in the future.

In this paper, we will present tracer data from a section in the Southern Ocean along 6°E from 60.5°S to 41.5°S. The SF_6 and CFC-12 data from the Antarctic Polar Front (APF) region are treated in detail.

2. Sampling and analysis

Water samples were taken at 38 stations on a section along 6°E from 60°30′S to 41°30′S in January and early February 1998 during the Swedish Antarctic Research Programme (SWEDARP) 1997/1998 expedition aboard the *S.A. Agulhas* (Turner et al., 2004). The section runs through several active frontal regions with areas of weaker stratification in between. In three areas, intense sampling down to 400 m depth was carried out: the Spring Ice Edge (SIE) the Winter Ice Edge (WIE) and the APF. See Fig. 3 for a map of the investigated area. Due to analytical difficulties the SIE section could not be completed with regard to SF_6. Water samples were collected with 8 L Niskin bottles on a rosette. The CFCs were normally the first sample to be drawn from the Niskin bottles followed by SF_6. However, no sample deeper than 3100 m could be obtained due to limitations of the ship's winch.

Table 1
Experiments where SF_6 has been used as a deliberately released tracer in the ocean

Experiment	Area	Amount released (kg)	Depth of release (m)	Reference
Mixing August/September 1985	Santa Monica Basin 34°N 119°W	0.2	790	Ledwell and Watson (1991)
Mixing May 1988	Santa Cruz Basin 34°N 119.5°W	1.45	1500	Ledwell and Bratkovich (199
CRP March 1989 October 1989	North Sea 52.5°N 3.5°W	 0.04 0.04	Surface	Watson et al. (1991)
Georges Bank Experiment	Georges Bank 41.5°N 68°W	8	20	Wanninkhof et al. (1993)
EPOCH February 1992 February 1993	North Sea 52°N 4°E	 0.045 0.034	 30 20	Nightingale et al. (2000)
NATRE May 1992	Canary Basin 25°N 29°W	139	310	Ledwell et al. (1993)
IRONEX October 1993	Equatorial East Pacific 5°S 90°W	0.0511	Surface	Martin et al. (1994)
IRONEX II May 1995	Equatorial East Pacific 3.5°S 104°W	0.07	Surface	Cooper et al. (1996)
Mixing February 1996	Brazil Basin 22°S 18°W	110	4000	Polzin et al. (1997)
FSLE April 1996	West Florida Shelf 29°N 84°W		20	Wanninkhof et al. (1997)
PRIME June 1996	Northern North Atlantic 59°N 20°W	0.05	Surface	Law et al. (2001)
ESOP August 1996	Greenland Sea 75°N 2°W	320	300	Watson et al. (1999)
ASGAMAG October 1996	North Sea 52°N 4°E		Surface	
ACSOE/MAGE June 1998	Northern North Atlantic 59°N 21°W	0.05	Surface	
SOIREE February 1999	Southern Ocean 61°S 140°E	0.165	15	Boyd et al. (2000)
CARUSO/EISENEX 2000/2001	Southern Ocean			

The analytical system used for the analysis of SF_6 is based on vacuum sparge sample extraction followed by gas chromatographic separation and detection by ECD. The system is similar to a system described by Law et al. (1994). Water samples are introduced into the system by vacuum created in the purge chamber. The samp inlet is placed into the water bottle, the purg chamber is isolated from the purge gas flow and vacuum is created in the purge chamber. The lo

g. 3. A map of the station network for water samples tained during the SWEDARP 1997/1998 campaign. The ation of the SIE, the WIE and the APF is indicated in the ure. The cruise track is from south to north starting January and ending February 2, 1998.

essure in the purge chamber during the sample troduction forces the water to spray through ur orifices in the top part of the purge chamber ereby promoting the transfer of SF_6 to the seous phase. When the water has been intro-ced into the system, nitrogen purge gas enters e purge chamber through a stainless-steel frit in e lower part of the purge chamber. The water mple is purged for a total of 300 s and close to 0% of the SF_6 is transferred from the water mple onto the trap. For this study of SF_6 as a ansient tracer approximately 350 ml of seawater as used for each analysis.

The high volatility of SF_6 makes it a difficult ecies to trap efficiently without applying very w temperatures to the trap. This can be over-me by the use of an efficient adsorbent. For this rpose eight different adsorbents were evaluated r their SF_6 retention at different temperatures. It as found that carboxen 1000 was the only one, of ose tested by us, that could retain SF_6 at mperatures above $-30\,^{\circ}C$. Carboxen 1000 did fact retain SF_6 at temperatures as high as 5 °C. Carboxen 1000 is a pyrolysed polymer with n active surface area of $1200\,m^2\,g^{-1}$, and has been sed for trapping the volatile CFC replacement compounds, hydrofluorocarbons and hydro-CFCs (O'Doherty et al., 1993a, b). For this work we used a 200 mm long 1/8″ OD (1.5 mm ID) stainless-steel tubing filled with Carboxen 1000 (45/60 mesh, Supelco). A vortex tube (ITW Vortec), (Bruno, 1993), in which compressed air is utilised for cooling, lowers the temperature of the trap to $-7\,^{\circ}C$ during the purge phase. For desorption, the trap is rapidly heated to about 250 °C by dissipating a power of 300 W across the trap. During the desorption phase, carrier gas is routed through the trap and transports the contents of the trap to the separation column. This main column consists of a 3 m long 1/8″ stainless-steel tube packed with molecular sieve 5A (80/100 mesh, Supelco). A post-column with the same material as the main column but only 30 cm long is used as a pressure buffer after the main column. The main column is kept at ambient temperatures and the post-column is located in the gas chromatograph (GC) oven at 40 °C. The SF_6 passes the columns without much retention, whereas all other compounds are retained, with oxygen eluting as a large peak shortly after the SF_6. High purity nitrogen gas is used as carrier gas at a flow of $35\,ml\,min^{-1}$, and the separation takes about 2.5 min. A complete analytical cycle takes 12 min, allowing a sample throughput of 5 injections/h. Although the analysis time is twice that reported by Law et al. (1994), 6 min, no attempts were made here to reduce the analysis time since the throughput of CFC samples was the same, i.e. $5\,h^{-1}$.

Standardisation is achieved by injection of various volumes of standard gas of concentration 48.8 ppt, either via the trap or directly onto the column, while the temperature and pressure of the sampling loop are logged. Two loops with nominal volumes of 250 and 1000 μl connected to a sampling valve facilitate the injection of different standard volumes. The response of the detector is linear for SF_6 in the low and relatively narrow concentration range encountered in seawater. Multiple injections of 1000 μl of standard gas were regularly performed to monitor the drift of the detector. The standard gas was produced by the dilution of pure SF_6 in N_2 and is calibrated against a standard gas prepared at Plymouth Marine Laboratory, England. This standard gas was in

Table 2
Performance of the analytical system during the expedition

Tracer	Analytical error	Limit of detection	Calibration error (%)	Saturation error (
CFC-12	0.7% or 0.005 pmol kg^{-1}	0.03 pmol kg^{-1}	1.5	5.5
CFC-11	1.9% or 0.006 pmol kg^{-1}	0.01 pmol kg^{-1}	0.6	4.9
CFC-113	3.6% or 0.027 pmol kg^{-1}	0.05 pmol kg^{-1}	2.0	11.3
CCl_4	2.6% or 0.006 pmol kg^{-1}	0.01 pmol kg^{-1}	0.5	5.6
SF_6	3.1% or 0.06 fmol kg^{-1}	0.05 fmol kg^{-1}	2.0	5.3

Note: The sample-to-sample precision is calculated as the standard deviation of 10 replicate measurements of the same water samp drawn from different Niskin bottles, or the system blank, whichever is the largest. The water samples were collected at 80 m depth 60°S. The calibration error is the uncertainty in the calibration gas. The saturation error reflects the variability of surface water samp collected during the entire cruise; see text.

turn calibrated against the standards used by M. Maiss, Heidelberg, Germany. For precision of the measurements and for the limits of detection, see Table 2. The detection limit of SF_6 is slightly higher compared to some other studies (Law et al., 1994, 1998; Wanninkhof et al., 1991) that report limits of detection of 0.03 fmol kg^{-1} for similar sample volumes. It is also high compared to the present conditions of the instrument. The reason for this is a small background originating from the sampling procedure, which has been compensated for. As a result of this the precisions of the measurements were affected slightly. Measurements below 0.05 fmol kg^{-1} SF_6 were rejected and set to below detection limit. One should also observe that the instrument precision is based on samples taken from different Niskin bottles on the same depth when comparing them with values derived from samples taken from the same bottle.

The detection of SF_6 is achieved by a Varian 3400 CX GC equipped with an ECD kept at 350 °C. Varian's Personal Computer (PC) chromatographic software "Star" is used to integrate the SF_6 peak, to control chromatographic events and the temperatures in the GC oven and gas sampling loops, and to monitor the trap temperature. All timed events in the purge and trap system, such as actuating valves and solenoids, heating the trap and starting data acquisition are controlled by a PC-operated relay card. The system is thus fully automated and a single command on the PC starts the whole analytical process. For a more detailed description of the analytical system see Tanhua (1997).

In addition to SF_6, five other halogenate tracers were measured on a separate analytic system during the cruise. These tracers were CFC 11, CFC-12, CFC-113, methyl chlorofor (CH_3CCl_3) and carbon tetrachloride (CCl_4). Th system consists of a dual channel purge and tra unit connected to a GC (Varian 3400) equippe with two megabore columns (J&W, DB624, 75 m and two ECDs kept at 350 °C. A volume of 30 n of seawater is purged of its CFC content by a flo of N_2 gas (80 ml min^{-1}) for 10 min. The trace were trapped in open capillary traps, kept nea liquid nitrogen temperatures and desorbed fro the trap by heating to 100 °C in boiling water. Th gas chromatographic separation was performe isothermally at 70 °C with helium as carrier ga The CFCs were standardised to the SIO93 scale b the injections of standard gas. Fogelqvist (199 describes the analysis of CFCs in seawater i detail. For information on the analytical precisio and limits of detection obtained during the cruis see Table 2.

3. Results and discussion

3.1. Apparent age/chlorofluorocarbon-ventilation age

The age of a water mass is considered to be th time elapsed since the water parcel was exposed t the atmosphere, where it can be modified b ocean/atmosphere transfer processes such as e change of heat and dissolved gases and b

biological processes in the surface layer. A water parcel that leaves the surface of the ocean will carry with it a signal that is dependent on the actual conditions at the time of exposure to the atmosphere. The length of time a water parcel is exposed to the atmosphere will affect the extent to which any transfer occurs, which in turn will affect to what degree the trace gases are saturated.

The process of obtaining the "true" age of a given water mass from its measured tracer concentration is not always straightforward. This is because a given parcel of water may actually be a mixture of fluids of differing origins, tracer concentrations and therefore ages. Since the relationship between tracer concentration and age is not a linear one, direct interpretation of the true water age from an average concentration will yield a biased true age estimate. For this reason the concept of "apparent age" is adopted. This is the age, which we obtain assuming that no mixing with other water masses has occurred. Mixing of two parcels of differing tracer concentrations and ages will lead to some weighted average tracer concentration that most likely will not represent the average age. In this paper, the apparent age concept is used, and any age referred to should be considered as an apparent age.

Provided that conditions such as temperature, salinity and saturation during formation of a water mass are known, certain calculations can be made. For instance, if a water mass is assumed not to have mixed with any other water mass, the concentration of a single CFC tracer can provide a good age estimate. This scenario is however seldom the case, and another commonly used approach is to use the ratio of two CFCs. This approach is not as sensitive to any unknown deviations from 100% saturation as is the single tracer approach. Provided that both CFCs are equally saturated, their ratio will be negligibly changed. If a recent water mass (and hence with high concentrations of CFCs) is mixed with a water mass with no or low CFC content, the CFC ratio will not change greatly and the age estimate will be heavily biased in favour for the younger component. The age derived from a single tracer will, in this example, not be biased in the same way. The mixing patterns in the ocean and the non-linear source function of the tracers are in most cases such that the age derived from tracer data is biased to yield younger ventilation ages than the "true" ventilation ages. Wallace et al. (1992) and Thiele and Sarmiento (1990) discuss some aspects of calculating apparent ages from tracer data in more detail.

Here we use the concept of equilibrium tracer mole fraction, P, to compensate for differences in solubility arising from variations in temperature and salinity. Although this effect is small in the confined APF region, there are considerable temperature gradients throughout the complete section. The value of P is calculated as follows (Doney and Bullister, 1992):

$$P = \frac{C_{\text{seawater}}}{F(\Theta, S)},$$

where C_{seawater} is the concentrations of the tracer in the water sample and $F(\Theta, S)$ is the solubility of the tracer as a function of potential temperature and salinity. For CFC-12 we have used the solubility function provided by Warner and Weiss (1985) and for SF_6 that of Bullister et al. (2002). The obtained P values are then matched to the Southern Hemisphere atmospheric history of the compound, which was obtained from Walker et al. (2000) for CFC-12 and from Maiss and Brenninkmeijer (1998) for SF_6 by ways of interpolation. We have assumed that the atmospheric pressure is 1 atm over the surveyed area. We have opted to use dry air mole fractions of the tracers rather than partial pressures. The main benefit of doing this is that the effect of water vapour of the moist air at the water-saturated interface is taken into account in the calculation of F, the solubility function, in the relationship discussed by Weiss and Price (1980) and Warner and Weiss (1985). The dry air mole fractions are further the unit in which the atmospheric histories of the CFCs and SF_6 are presented in Walker et al. (2000) and Maiss and Brenninkmeijer (1998). Thus by knowing the dry air mole fraction of a tracer in a water sample it is straightforward to asses an apparent age to this water sample, given the limitations discussed above.

The $P_{\text{CFC-12}}$ and P_{SF6} tracer ages derived by this method are plotted vs. each other in Fig. 4A. The

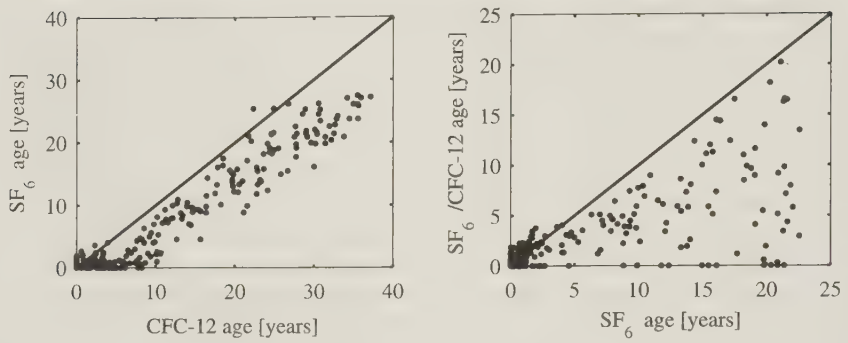

Fig. 4. Left panel shows apparent age estimates based on P_{SF6} plotted vs. estimates based on P_{CFC-12}. Right panel shows appare ventilation ages derived from the ratio P_{SF6}/P_{CFC-12} vs. the ages derived from P_{SF6} alone. All estimates are obtained making th assumption that no mixing has taken place. The deviation of the data points from the line of equal age indicates that in fact mixing d take place. Assuming mixing only between a water mass carrying the tracer signal and under-lying water with no tracer signal, it possible to calculate a dilution factor for each water sample, see text. Data are corrected for the differences in saturation between th species.

solid line with slope 1 and intercept 0 is where one would expect all data points to be centred, in an ideal case where both mole fractions give the same apparent ages. It is however clear that there is a bias towards higher apparent age derived from CFC-12 compared to that derived from SF_6. Due to the different shape of the atmospheric input functions for CFC-12 and SF_6 (Fig. 1), the calculated tracer ages will differ if applied to a mixed water mass. For instance, imagine a water mass that contain equal amounts of water equilibrated at the surface each year between 1975 and 1998, i.e. 1/23 of that water mass was equilibrated in 1975 and so forth. Such a water mass would have a true mean age of 11.5 years, if sampled in 1998, and would have a P_{CFC-12} age of approximately 11.9 years, whereas the P_{SF6} age would only be 10.2 years. The P_{CFC-12} age is thus biased to give a higher ventilation age. This effect is due to the decline in the rate of atmospheric increase rate for CFC-12. This can partly explain the difference in apparent ages of the relatively recently ventilated water samples shown in Fig. 4A. It is also clear that since the rate of increase for CFC-12 in the atmosphere is low at present (Fig. 1), a slight deviation from equilibrium with the atmosphere results in a large difference in calculated apparent age. This is also reflected in the scatter of CFC-12 apparent ages in the surface layer. Based on the data collected during the cruise, 97% saturation for CFC-12 has been use for the apparent age calculation, whereas SF_6 wa only saturated to 87%. There is a certain amoun of scatter in the saturation data, which could b due to factors such as differences in ice cover an local weather. There seems to be a tendency fo CFC-12 to be slightly under-saturated in th colder southern part of the section. The differenc in saturation between the two species can partly b explained by the differences in the rate of increas of the atmospheric concentration for the tw species and by the slightly higher piston velocity for CFC-12. Haine and Richards (1995) demon strate that the rate of atmospheric increase as wel as piston velocities influence the saturation in the mixed layer. The differences in saturation betwee CFC-12 and SF_6 are probably larger at present than it was prior to 1990 when the rates of increase of the atmospheric concentrations for the two species were similar. This could also explain some of the differences in the age estimates presented in Fig. 4A.

The other way to obtain apparent ventilation ages is to utilise the ratio between two tracers. We once again use P_{CFC-12} and P_{SF6} since the P_{SF6}/P_{CFC-12} atmospheric ratio has increased rapidly since the mid-1970s (Fig. 2). The ratio age at any date before that is uncertain due to the low concentrations of SF_6, and hence a larger uncertainty in the SF_6 analysis. The SF_6 atmospheric

history as inferred from production estimates (Maiss and Brenninkmeijer, 1998) suggests that the $P_{SF6}/P_{CFC\text{-}12}$ ratio actually decreased rather than increased with time before the mid-1960s. Considering these two facts, we have opted to filter the data and to discard those ratios derived from P_{SF6} values lower than 0.40 ppt, which corresponds to the atmospheric concentration in the mid-1970s, assuming that the saturation level of SF_6 in the water is 87%.

The $P_{SF6}/P_{CFC\text{-}12}$ ratio for the water samples is calculated and fitted to the atmospheric SF_6/CFC-12 ratio to yield a ventilation age. The ventilation age obtained in this way is plotted vs. P_{SF6} age in Fig. 4B. It is obvious that the $P_{SF6}/P_{CFC\text{-}12}$ ratio age is biased to yield younger ages compared to the age obtained from P_{SF6}. This discrepancy can be attributed to the fact that, when a water mass with a certain tracer signature mixes with a water mass that is CFC-12 and SF_6 free, the $P_{SF6}/P_{CFC\text{-}12}$ ratio will remain constant, and so will the ratio age. The P_{SF6} age will however indicate a relatively older water mass, since the SF_6 concentration now is lower due to mixing with SF_6 free water. This difference in age estimates can be used to calculate a dilution factor as described by Weiss et al. (1985). Each water sample is assigned a ventilation age as calculated from the $P_{SF6}/P_{CFC\text{-}12}$ ratio age. The corresponding atmospheric SF_6 concentration for that time is determined from the known atmospheric history, which yields the expected seawater SF_6 concentration (P_{calc}), which is to be compared with the observed SF_6 concentration ($P_{seawater}$). Both factors are expressed as equilibrium tracer mole fraction, P. The dilution factor (ξ) is then calculated as follows:

$$\xi = \frac{P_{seawater}}{P_{calc}}.$$

In a case where the entrained water mass is free of CFC-12 and SF_6, the dilution factor will give us the fraction of water that originates from the upper well-ventilated mixed layer, and hence the fraction of deeper, older, water. The conditions for these assumptions to be valid are almost true in this section of the Southern Ocean, where the waters under the pycnocline are free of SF_6 and have only low concentrations of CFC-12. The dilution factor should at least give a rough estimate of mixing across the pycnocline.

3.2. Estimates of uncertainties

Uncertainties in apparent age (δT_v) estimates are due to a number of factors. Age estimates are determined from the equilibrium tracer mole fraction (P), and uncertainties in this value will propagate into the apparent age calculation. Uncertainties in the observed equilibrium mole fraction (δP_{obs}) come from analytical errors ($\delta P_{analytical}$) and calibration errors ($\delta P_{calibration}$). In addition to that one must account for uncertainties in assessing the correct degree of saturation of the tracer in the water mass at the time of formation ($\delta P_{saturation}$). The uncertainties in the analytical procedure were determined from 10 replicate measurements of water samples from the same depth drawn from different Niskin bottles, and are determined as one standard deviation or the system blank value, whichever is the greater. The analytical errors of SF_6 and CFC-12 are regarded as independent, since these measurements were performed on two different instruments and from two different water samples. The combined analytical error to be used for the ratio SF_6/CFC-12 is then the squared sum of the fractional errors for the two measurements. In the case when the ratio age between two of the CFC species is used, e.g. CFC-12/CFC-11 or CFC-113/CFC-12, the measurements cannot be regarded as independent of each other, since the measurements are conducted on the same water sample and on the same instrument. The analytical error for those ratios is then determined as the sum of the two individual analytical fractional errors. The uncertainty in the calibration standard is derived from the calibration of the standard gases.

Possibly the largest source of error that will affect the mole fraction calculation is uncertainties in the saturation of the tracers in the surface layer. The saturation might vary on yearly and seasonal basis, mainly dependent on the depth of the seasonal mixed layer (Haine and Richards, 1995). The uncertainty in the saturation ($\delta P_{saturation}$) of this data set is estimated as one standard deviation

of the measured saturation in the top 20 m of the water column, compensated for the analytical error.

The uncertainty in assessing the observed equilibrium tracer mole fraction (δP_{obs}) is then calculated as the squared sum of the errors:

$$\delta P^2_{obs} = \delta P^2_{analytical} + \delta P^2_{calibration} + \delta P^2_{saturation}.$$

The values of the uncertainties are listed in Table 2. It is clear that uncertainty in the saturation is the dominating factor determining the total uncertainty (δP_{obs}). However, in the case when a ratio between two tracers is used to determine an age, the last term in the above equation will disappear, assuming that the saturation of the tracers are dependent and cancel each other. That is, a surface water with high saturation of CFC-11 will have a equally high saturation of CFC-12. This seems to be a valid assumption for the CFCs, based on this rather limited data set. It does not seem to be entirely justified for the SF_6 vs. the CFCs, see discussion above. The saturation uncertainties have been included in the calculation of the total uncertainty for the case of SF_6/CFC-12, but not for the case of CFC-113/CFC-12 or CFC-11/CFC-12.

How well a derived mole fraction value or ratio between two can be represented as an age is further dependent on uncertainty in the atmospheric mixing ratio over time ($\delta P_{atmhist}$). Walker et al. (2000) give the errors in the atmospheric history for the CFCs and Maiss and Brenninkmeijer (1998) for SF_6. The total uncertainty of the mole fraction calculation (δP) including comparison with historic data is then

$$\delta P^2 = \delta P^2_{obs} + \delta P^2_{atmoshist}.$$

These errors (δP) propagate into our calculation of the age by way of the time varying atmospheric source functions. The source function is usually used to express the saturation mole fraction *(P)* in terms of time of ventilation (T_v), $P = P(T_v)$. However, we invert this relationship to calculate ventilation time from a saturation mole fraction, $T_v = T_v(P)$. Thus our uncertainty in calculated ventilation time (δT_v) may be expressed in terms of (δP) as follows:

$$\delta T_v = \frac{dT_v}{dP}\,\delta P.$$

We therefore see that even at times when o uncertainty in the equilibrium tracer mo fraction (δP) is small, we may have relative large uncertainties in the age when the slop of the atmospheric source function (dP/dT_v becomes small (or rather when dT_v/dP becom large).

The uncertainties in apparent age calculation for some commonly used tracers and ratio between tracers are demonstrated in Fig. 5. It evident from the figure that each tracer or rati has a time interval where they are useful, i.e. wher dT_v/dP is small and δP is small, and sometime when they are less useful, i.e. either dT_v/dP is larg and/or δP is large. For instance, the CFC-11 is no a useful transient tracer for water equilibrate after 1990 due to ambiguity in the atmospheri source function, but is useful for about 40 year before that. Sulphur hexafluoride, on the othe hand, is useful in recently ventilated waters, bu does not have a very long atmospheric history an the analytical uncertainties become significan before 1980.

It is important to remember that the effect o mixing between water masses is not addressed i these estimates of apparent age uncertainties. It i clear that mixing will affect the age estimates, se discussion above, and also that different mixing

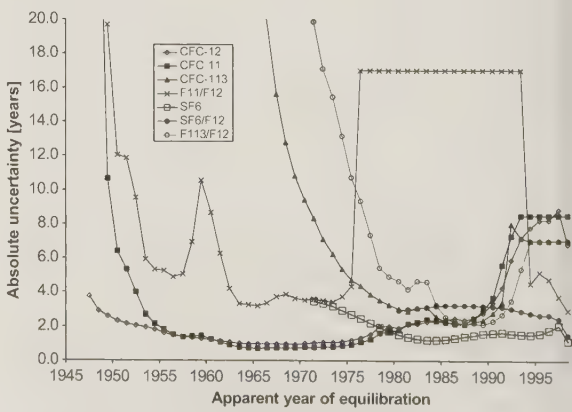

Fig. 5. Estimates of the uncertainty in age estimates using various tracers and ratios between them.

scenarios will have different impact on the age calculation depending on which tracer or ratio is used. In fact, it would be possible to find plausible mixing scenarios with the help of a suite of carefully measured tracers.

Age profiles, with error bars, for one deep station are illustrated in Fig. 6. The apparent ages are calculated using the tracers CFC-12, CFC-11, CFC-113 and SF_6, and also the ratios SF_6/CFC-12 and CFC-11/CFC-12, which are all commonly used except for the ones involving SF_6. The error bars are calculated as described above. Note that the error bars are not always symmetrical around the value. This is due to the non-linearity in the transient atmospheric signal of the tracers. The offset of the ages calculated from different tracers/ratios does primarily reflect the effect of mixing with surrounding water masses. It is evident from Figs. 5 and 6 that SF_6 and the ratio SF_6/CFC-12 are useful for recently ventilated waters when other tracer combinations fail to be very informative.

3.3. Tracer characteristics along 6°E

Along this section there is a sharp gradient in tracer concentration associated with the pycnocline (Fig. 7C). The depth of the mixed layer shoals to the south as the pycnocline becomes more pronounced. In the shallow mixed layer above the pycnocline, the tracers are more or less in equilibrium with the atmosphere. The tracer concentrations decrease rapidly with depth below the pycnocline. In the southern parts of the section, the ventilation age of the water column goes from essentially a few years old to about 40 years old within a 20–50 m depth interval. Further north, the gradient becomes less steep and some fine structure in the tracer concentration is visible within and above the pycnocline. A layer of Winter Water (WW) centred at about 100 m depth in the southern part of the section is recognised by a temperature minimum under the surface water (Fig. 7B). A salinity minimum is visible in the northern part of the section at about 500 m depth and deepens

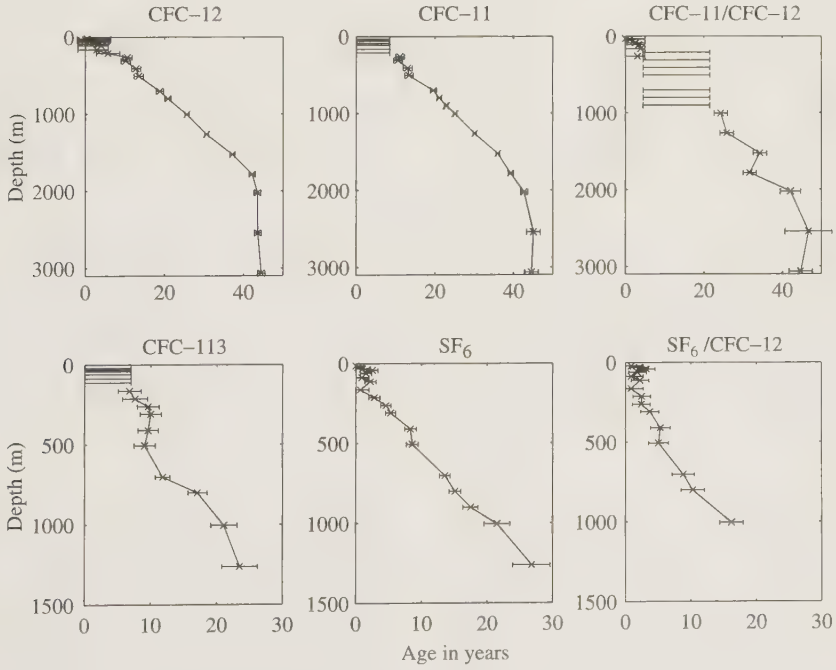

Fig. 6. Depth profiles of station 385 at 41.5°S, in where the apparent ages have been calculated using a variety of tracers/ratios of tracers. The differences in ages between the panels reflect the different responses to mixing for various tracers. Error bars are also given; see main text for details.

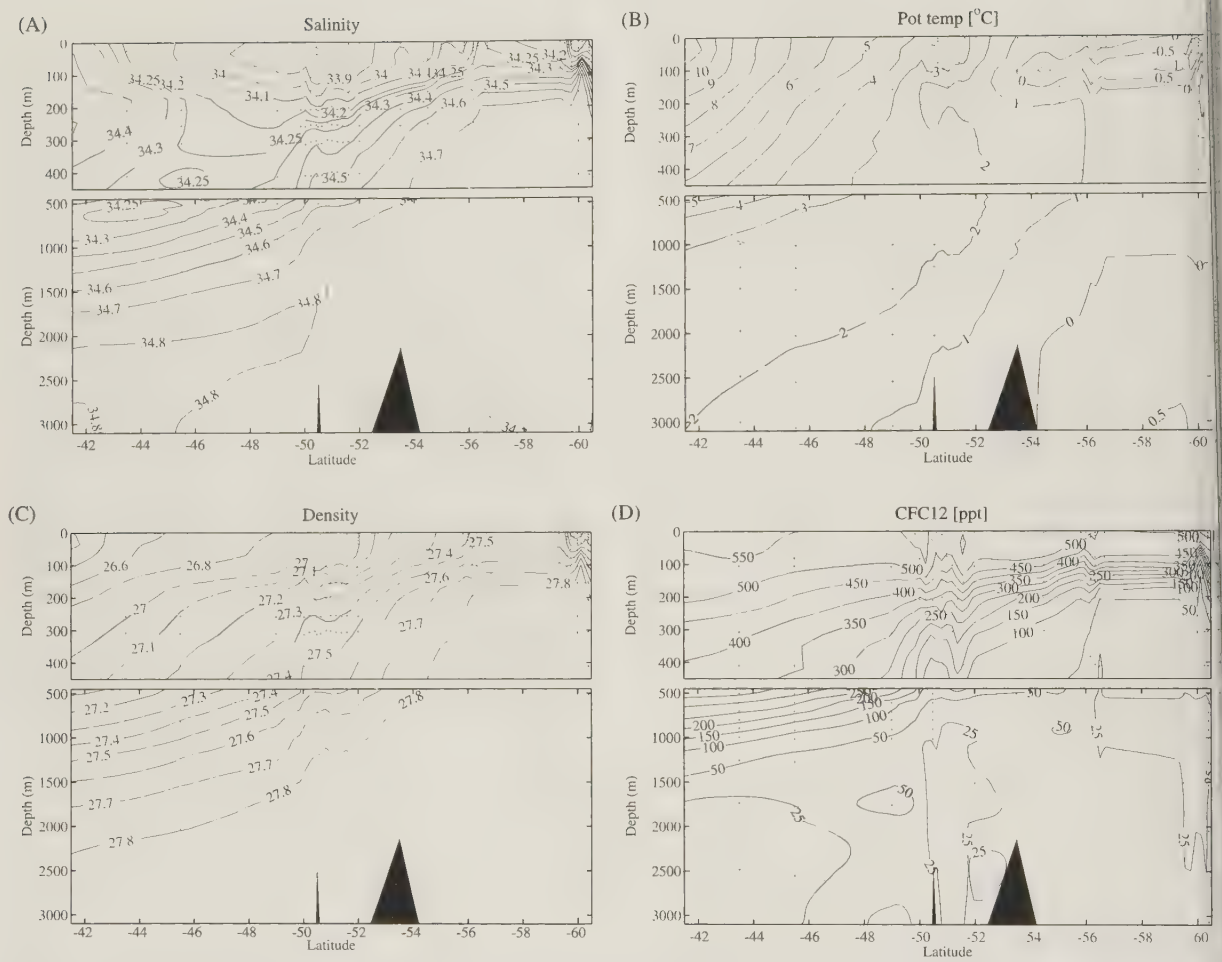

Fig. 7. (A) Salinity section along 6°E. The positions for the samples are indicated by dots and the isolines are obtained by objective interpolation with variable correlation length to account for the variable distance between stations. Note the salinity minimum in the surface region across the APF region (~50°N). Another salinity minimum at around 400 m depth north of the APF region indicates AAIW that descends to the north. (B) Temperature section, as Fig. 7a. Note the layer of cold WW at about 150 m depth in the southern part of the section. (C) Density section, as Fig. 7a. (D) CFC-12 section, as Fig. 7a. The concentration is given as equilibrium mole fraction. (E) SF_6 section, as Fig. 7a. The concentration is given as equilibrium mole fraction. (F) CFC-11 section, as Fig. 7a. The concentration is given as equilibrium mole fraction. (G) CFC-113 section, as Fig. 7a. The concentration is given as equilibrium mole fraction. (H) CCl_4 section, as Fig. 7a. The concentration is given as equilibrium mole fraction.

towards the north (Fig. 7A). This is the core of the Antarctic Intermediate Water (AAIW).

The deeper part of the section is dominated by Circumpolar Deep Water (CDW) and the tracer concentrations are more uniform within this water mass. Any penetration of SF_6 and CFC-113 through the pycnocline is prevented since the ventilation time of this deep water is longer than the atmospheric histories of the two compounds (Figs. 7E and G). CFC-11 and CFC-12, on the other hand, are present at all sampled depths (Figs. 7D and F). The apparent ventilation age of the CDW is roughly 40 years, based on average concentrations of CFC-12 and CFC-11 of 0.15 and 0.25 pmol kg^{-1}, respectively. There is a marked increase in tracer concentrations in the deepest parts of the southern portion of the section. This is probably due to mixing with newly formed

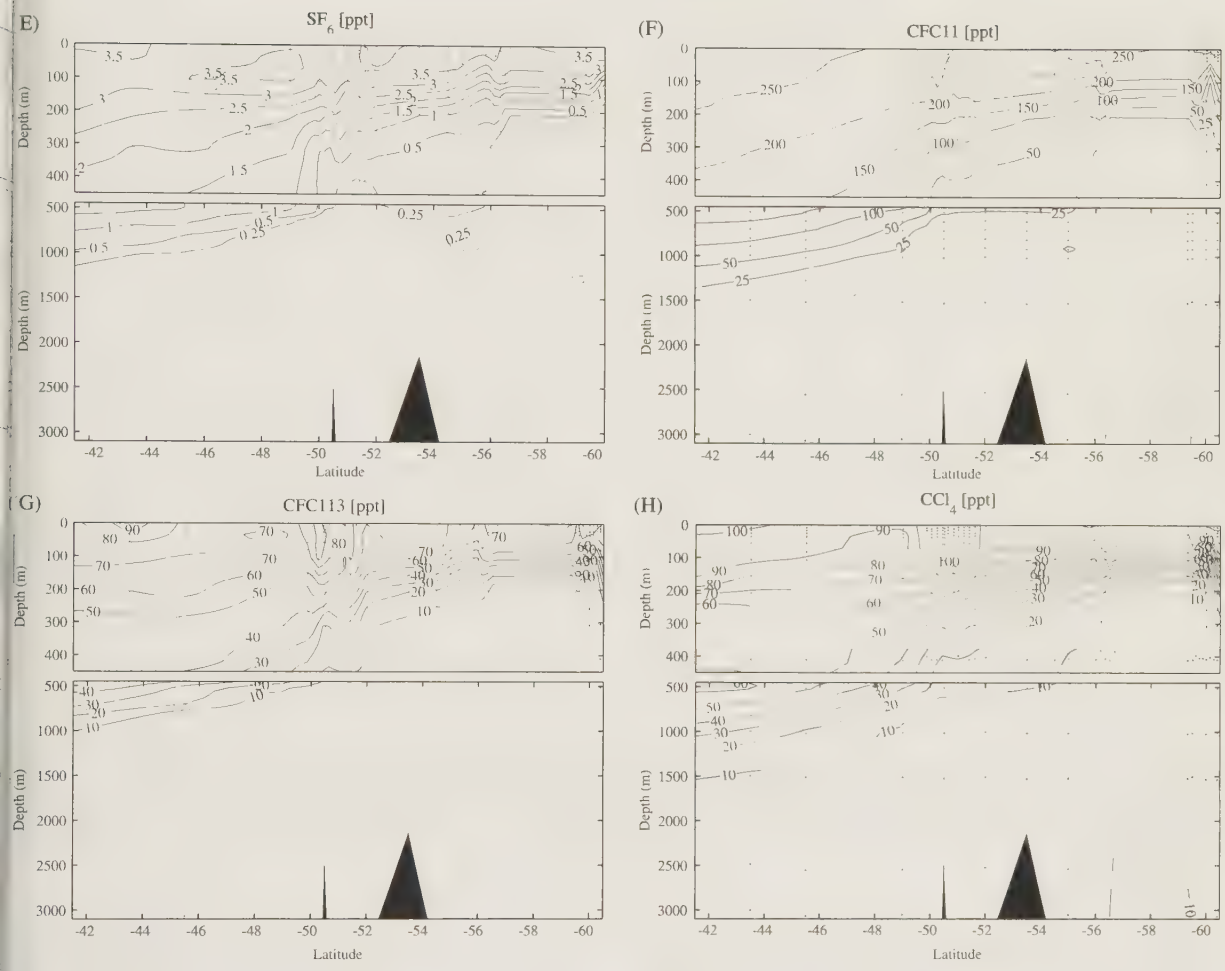

Fig. 7. (*Continued*)

Antarctic Bottom Water (AABW), but since no samples were obtained below 3000 m depth we were not able to capture the bulk of the AABW.

The CCl_4 concentrations (Fig. 7H) in the deep water (0.03–0.75 pmol kg^{-1}) do suggest a much higher apparent age than suggested by $P_{CFC\text{-}12}$ and $P_{CFC\text{-}11}$, and the ratio between them. This could be due to a non-conservative behaviour of CCl_4 or uncertainty in the source function for CCl_4. For instance, Tanhua et al. (1996) reported that CCl_4 seems to be removed in waters with oxygen concentrations of 200 μM or less, and proposed chemical reduction as a removal mechanism. Similarly, CCl_4 deficiencies were reported in the South Atlantic by Wallace et al. (1994), in the Baltic Sea by Krysell et al. (1994) and in the Weddell Sea by Meredith et al. (1996). The oxygen concentration in the deep water in this section is approximately 200 μM, suggesting a possible removal of CCl_4 in deep Antarctic Waters.

3.4. Ventilation age at the Antarctic Polar Front

The densely sampled section across the APF consists of 10 stations between 52°S and 50°S along 6°E and down to 400 m depth. The area is characterised by a salinity minimum in the surface and the temperature minimum of WW at about 200 m depth (Figs. 8C and D). This section further reveals an almost linear gradient in tracer

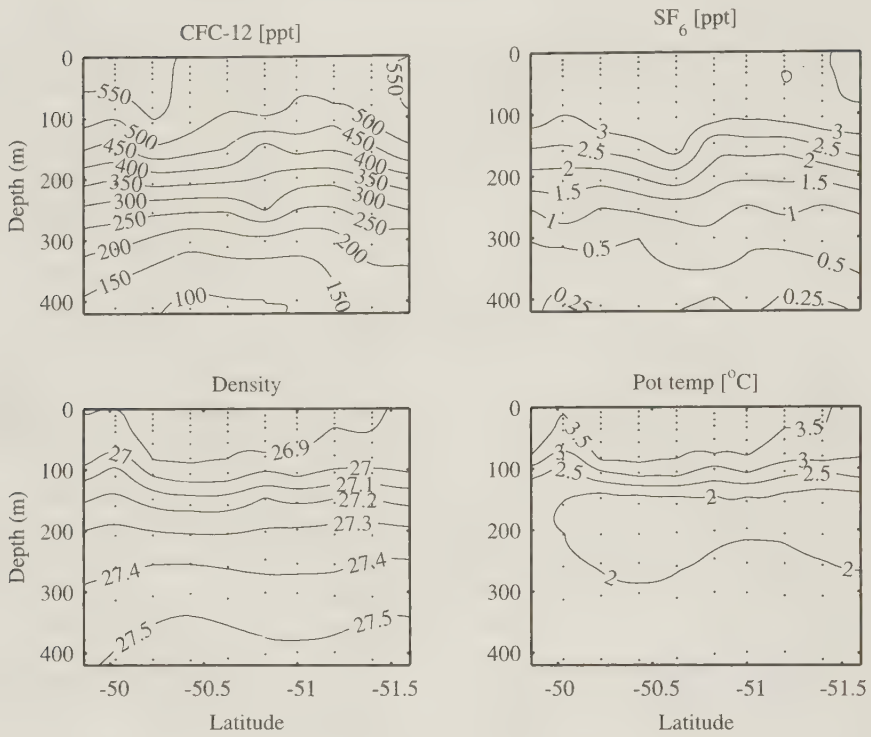

Fig. 8. Figure showing the intensely sampled APF region. The stations were occupied between January 24 and 27, 1998. The sampling points are indicated by dots. Panel a shows the CFC-12 concentration and panel b the SF_6 concentration. Note the difference in concentration range between the two species. Panels c and d display the density and temperature sections. Note the temperature minimum of WW that stretches into the section from the south at about 200 m depth.

concentrations with depth, except for the top 100 m of the water column. The CFC-12 equilibrium mole fraction ranges from saturated surface conditions to 80 ppt in the deep part of the section (Fig. 8A). The concentration of SF_6, on the other hand, ranges from under-saturated surface conditions, down to 0.16 ppt in the deep part of the section, which is at our limit of detection for SF_6 (Fig. 8B).

Apparent ventilation ages have been calculated based on the SF_6 and CFC-12 concentrations assuming no mixing with surrounding water masses (Figs. 9A and B). These calculations for CFC-12 indicate a ventilation age of the deep part of the section close to 30 years, assuming 97% saturation. The ventilation age derived from SF_6 for the same water points at slightly lower ages, about 25 years, assuming 87% saturation. The older range of this age estimate has a degree of uncertainty in it since the concentration is close to our detection limit for SF_6, and analytical errors may be of significant importance, see Fig. 5. The tendency for the $P_{SF6}/P_{CFC\text{-}12}$ ratio to yield younger ventilation ages as compared to the ages derived from P_{SF6} and $P_{CFC\text{-}12}$ is clearly shown in Fig. 9C. The ratio age for the deep water in the section barely reaches 15 years, as compared to 25 years based solely on P_{SF6} data. Based on the differences in ventilation ages between the ratio age and the P_{SF6} age we have calculated dilution factors as described above (Fig. 9D). It is interesting to note some features that are not so obvious in any of the other panels. Note especially the doming feature in the middle of the section where deep water wells up towards the surface.

It would be possible to calculate the dilution factor on this section using another tracer combination such as CFC-113 and CFC-12 in a similar manner as to the one described above. It is

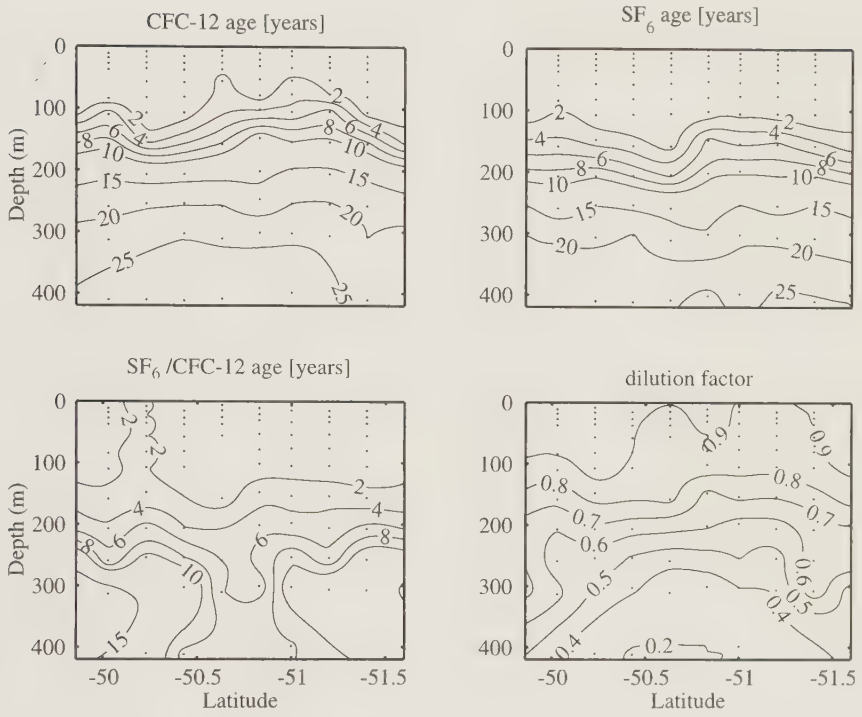

Fig. 9. Section across the APF region, panels showing the apparent ages derived from P_{SF6}, P_{CFC-12} and the ratio P_{SF6}/P_{CFC-12}. The age scale is in years and age 0 is set to January 1998. The dilution factor is the fraction of water from the surface mixed layer, assuming mixing solely between the surface mixed layer and water with low tracer content from below the pycnocline. Age estimates are corrected for the differences in saturation between the species.

However clear from the uncertainties presented in Fig. 5 that both CFC-113 and the ratio CFC-113/CFC-12 have a rather limited time period when their uncertainties are small. The use of the combination of SF_6 and CFC-12 is currently, and in the near future, the most viable tracer combination for waters with a short apparent age.

4. Summary

Sulphur hexafluoride is a promising new transient tracer for oceanographic studies to complement the established CFC tracers. Its inert properties in seawater and its rapidly growing atmospheric concentration make it a valuable tracer. One drawback of SF_6 is its low atmospheric concentration, which together with its low solubility in water makes the concentration in surface seawater about 3 orders of magnitude lower than that of CFC-11 and CFC-12. ECDs are however very sensitive to sulphur hexafluoride, which makes the analysis of "background" levels of SF_6 in seawater possible. The precision of this analysis is comparable to the analysis of the CFC tracers. The future use of SF_6 as a transient tracer is however hampered by its use as a purposefully released tracer.

It is demonstrated that while the traditional CFC tracers are ambiguous for any water mass ventilated during the last decade, SF_6 provides valuable information as a tracer. The combination of CFC-12 and SF_6 data yields information about mixing of surface water and deep water across the pycnocline in the APF region.

Acknowledgements

We are grateful to the officers and crew on *S.A. Agulhas* and to the Swedish Polar Research

Secretariat for making this experiment possible. We also recognise the invaluable effort by Prof. David Turner to co-ordinate a large expedition with a large variety of research. We gratefully acknowledge valuable comments on the manuscript from Dr. Ray F. Weiss, Dr. Stephen J. Walker and Martin Vollmer at SIO. Thanks to Dr. Wisegarver and Dr. Bullister for providing first-hand information on newly derived values for the SF_6 solubility. For an important contribution in developing the SF_6 instrument, we owe many thanks to Marie Persson. While this manuscript was prepared, T.T. was financed from The Swedish Foundation for International Co-operation in Research and Higher Education (STINT). We acknowledge the comments from two reviewers that led to a improved final version of the manuscript.

References

Boyd, P.W., Watson, A.J., Law, C.S., Abraham, E.R., Trull, T., Murdoch, R., Bakker, D.C.E., Bowie, A.R., Buesseler, K.O., Chang, H., Charette, M., Croot, P., Downing, K., Frew, R., Gall, M., Hadfeld, M., Hall, J., Harvey, M., Jameson, G., LaRoche, J., Liddicoat, M., Ling, R., Maldonado, M.T., McKay, R.M., Nodder, S., Pickmere, S., Pridmore, R., Rintoul, S., Safi, K., Sutton, P., Strzepek, R., Tanneberger, K., Turner, S., Waite, A., Zeldis, J., 2000. A mesoscale phytoplankton bloom in the polar Southern Ocean stimulated by iron fertilization. Nature 407, 695–702.

Bruno, T.J., 1993. Applications of the vortex tube in chemical analysis. 1. Introductory principles. American Laboratory 25, 15.

Bu, X., Warner, M.J., 1995. Solubility of chlorofluorocarbon 113 in water and seawater. Deep-Sea Research I 42, 1151–1161.

Bullister, J.L., Weiss, R.F., 1983. Anthropogenic chlorofluoromethanes in the Greenland and Norwegian seas. Science 221, 265–268.

Bullister, J.L., Wisegarver, D.P., 1998. The solubility of carbon tetrachloride in water and seawater. Deep-Sea Research I 45, 1285–1302.

Bullister, J.L., Wisegarver, D.P., Menzia, F.A., 2002. The solubility of sulfur hexafluoride in water and seawater. Deep-Sea Research I 49, 175–187.

Cooper, D.J., Watson, A.J., Nightingale, P.D., 1996. Large decrease in ocean-surface CO_2 fugacity in response to in situ iron fertilization. Nature 383, 511–513.

Doney, S.C., Bullister, J.L., 1992. A chlorofluorocarbon section in the eastern North Atlantic. Deep-Sea Research A 39, 1857–1883.

Fogelqvist, E., 1999. Determination of volatile halocarbons seawater. In: Grasshoff, K., Kremling, K., Ehrhardt, M (Eds.), Methods of Seawater Analysis. Wiley-VCH, Weinheim, pp. 501–519.

Haine, T.W.N., Richards, K.J., 1995. The influence of t seasonal mixed layer on oceanic uptake of CFCs. Journal Geophysical Research 100, 10727–10744.

Harnisch, J., Eisenhauer, A., 1998. Natural CF_4 and SF_6 Earth. Geophysical Research Letters 25, 2401–2404.

Jordan, A., Harnisch, J., Borchers, R., Le Guern, F.N Shinohara, H., 2000. Volcanogenic halocarbons. Enviro mental Science and Technology 34, 1122–1124.

Krysell, M., 1992. Carbon tetrachloride and methyl chlorofor as tracers of deep water formation in the Weddell Se Antarctica. Marine Chemistry 39, 297–310.

Krysell, M., Wallace, D.W.R., 1988. Arctic Ocean ventilatio studied with a suite of anthropogenic halocarbon tracer Science 242, 746–749.

Krysell, M., Fogelqvist, E., Tanhua, T., 1994. Apparen removal of the transient tracer carbon tetrachloride fro anoxic seawater. Geophysical Research Letters 2 2511–2514.

Law, C.S., Watson, A.J., 2001. Determination of Persian Gu Water transport and oxygen utilisation rates using SF_6 as novel transient tracer. Geophysical Research Letters 28 815–818.

Law, C.S., Watson, A.J., Liddicoat, M.I., 1994. Automate vacuum analysis of sulphur hexafluoride in seawater derivation of the atmospheric trend (1970–1993) an potential as a transient tracer. Marine Chemistry 48, 57–69

Law, C.S., Watson, A.J., Liddicoat, M.I., Stanton, T., 1998 Sulphur hexafluoride as a tracer of biogeochemical an physical processes in an open-ocean iron fertilisatio experiment. Deep-Sea Research II 45, 977–994.

Law, C.S., Martin, A.P., Liddicoat, M.I., Watson, A.J. Richards, K.J., Woodward, E.M.S., 2001. A Lagrangia SF_6 tracer study of an anticyclonic eddy in the North Atlantic: patch evolution, vertical mixing and nutrient supply to the mixed layer. Deep-Sea Research II 48, 705–724.

Ledwell, J.R., Bratkovich, A., 1995. A tracer study of mixing in the Santa Cruz Basin. Journal of Geophysical Research 100, 20681–20704.

Ledwell, J.R., Watson, A.J., 1991. The Santa-Monica Basin tracer experiment—a study of diapycnal and isopycnal mixing. Journal of Geophysical Research 96, 8695–8718.

Ledwell, J.R., Watson, A.J., Law, C.S., 1993. Evidence for slow mixing across the pycnocline from an open-ocean tracer-release experiment. Nature 364, 701–703.

Maiss, M., Brenninkmeijer, C.A.M., 1998. Atmospheric SF_6: trends, sources, and prospects. Environmental Science and Technology 32, 3077–3086.

Maiss, M., Brenninkmeijer, C.A.M., 2000. A reversed trend in emissions of SF_6 into the atmosphere? In: Van Ham, J., Baede, A.P.M., Meyer, L.A., Ybema, R. (Eds.), Non-CO_2 Greenhouse Gases: Scientific Understanding, Control, and Implementation. Proceedings of the Second International

Symposium, Noordwijkerhout, The Netherlands, 8–10 September 1999. Kluwer Academic Publishers, Dordrecht, pp. 199–204.

Martin, J.H., Coale, K.H., Johnson, K.S., Fitzwater, S.E., Gordon, R.M., Tanner, S.J., Hunter, C.N., Elrod, V.A., Nowicki, J.L., Coley, T.L., Barber, R.T., Lindley, S., Watson, A.J., Van Scoy, K., Law, C.S., Liddicoat, M.I., Ling, R., Stanton, T., Stockel, J., Collins, C., Anderson, A., Bidigare, R., Ondrusek, M., Latasa, M., Millero, F.J., Lee, K., Yao, W., Zhang, J.Z., Friederich, G., Sakamoto, C., Chavez, F., Buck, K., Kolber, Z., Greene, R., Falkowski, P., Chisholm, S.W., Hoge, F., Swift, R., Yungel, J., Turner, S., Nightingale, P., Hatton, A., Liss, P., Tindale, N.W., 1994. Testing the Iron Hypothesis in ecosystems of the Equatorial Pacific Ocean. Nature 371, 123–129.

Meredith, M.P., Van Scoy, K.A., Watson, A.J., Locarnini, R.A., 1996. On the use of carbon tetrachloride as a transient tracer of Weddell Sea deep and bottom waters. Geophysical Research Letters 23, 2943–2946.

Min, D.-H., 1999. Studies of large-scale intermediate and deep water circulation and ventilation in the North Atlantic, South Indian and Northeast Pacific Oceans, and in the East Sea (Sea of Japan), using chlorofluorocarbons as tracers. Ph.D. Thesis, University of California, San Diego, La Jolla.

Nightingale, P.D., Malin, G., Law, C.S., Watson, A.J., Liss, P.S., Liddicoat, M.I., Boutin, J., Upstill-Goddard, R.C., 2000. In situ evaluation of air–sea gas exchange parameterizations using novel conservative and volatile tracers. Global Biogeochemical Cycles 14, 373–387.

O'Doherty, S.J., Simmonds, P.G., Nickless, G., 1993a. Analysis of replacement chlorofluorocarbons using Carboxen microtraps for isolation and preconcentration in gas chromatography mass spectrometry. Journal of Chromatography A 657, 123–129.

O'Doherty, S.J., Simmonds, P.G., Nickless, G., Betz, W.R., 1993b. Evaluation of Carboxen carbon molecular sieves for trapping replacement chlorofluorocarbons. Journal of Chromatography 630, 265–274.

Polzin, K.L., Toole, J.M., Ledwell, J.R., Schmitt, R.W., 1997. Spatial variability of turbulent mixing in the abyssal ocean. Science 276, 93–96.

Tanhua, T., 1997. Halogenated substances as marine tracers. Ph.D. Thesis, Göteborg University, Göteborg, Sweden.

Tanhua, T., Fogelqvist, E., Bastürk, Ö., 1996. Reduction of volatile halocarbons in anoxic seawater, results from a study in the Black Sea. Marine Chemistry 54, 159–170.

Thiele, G., Sarmiento, J.L., 1990. Tracer dating and ocean ventilation. Journal of Geophysical Research 95, 9377–9391.

Turner, D.R., Bertilsson, S., Fransson, A., Pakhomov, E., 2004. The SWEDARP 97/98 marine expedition: overview. Deep-Sea Research II, this issue [doi:10.1016/j.dsr2.2003.08.006].

Walker, S.J., Weiss, R.F., Salameh, P.K., 2000. Reconstructed histories of the annual mean atmospheric mole fractions for the halocarbons CFC-11, CFC-12, CFC-113 and carbon tetrachloride. Journal of Geophysical Research 105, 14285–14296.

Wallace, D.W.R., Schlosser, P., Krysell, M., Bönisch, G., 1992. Halocarbon ratio and tritium/3He dating of water masses in the Nansen Basin, Arctic Ocean. Deep-Sea Research A 39, S435–S458.

Wallace, D.W.R., Beining, P., Putzka, A., 1994. Carbon tetrachloride and chlorofluorocarbons in the South Atlantic Ocean, 19°S. Journal of Geophysical Research 99, 7803–7819.

Wanninkhof, R., Ledwell, J.R., Watson, A.J., 1991. Analysis of sulfur hexafluoride in seawater. Journal of Geophysical Research 96, 8733–8740.

Wanninkhof, R., Asher, W., Weppernig, R., Chen, H., Schlosser, P., Langdon, C., Sambrotto, R., 1993. Gas transfer experiment on Georges Bank using two volatile deliberate tracers. Journal of Geophysical Research 98, 20237–20248.

Wanninkhof, R., Hitchcock, G., Wiseman, W.J., Vargo, G., Ortner, P.B., Asher, W., Ho, D.T., Schlosser, P., Dickson, M.L., Masserini, R., Fanning, K., Zhang, J.Z., 1997. Gas exchange, dispersion, and biological productivity on the west Florida shelf: results from a Lagrangian tracer study. Geophysical Research Letters 24, 1767–1770.

Warner, M.J., Weiss, R.F., 1985. Solubilities of chlorofluorocarbons 11 and 12 in water and sea water. Deep-Sea Research 32, 1485–1497.

Watson, A.J., Ledwell, J.R., 2000. Oceanographic tracer release experiments using sulphur hexafluoride. Journal of Geophysical Research 105, 14325–14337.

Watson, A.J., Liddicoat, M.I., 1985. Recent history of atmospheric trace gas concentrations deduced from measurements in the deep sea: application to sulphur hexafluoride and carbon tetrachloride. Atmospheric Environment 19, 1477–1484.

Watson, A.J., Upstill-Goddard, R.C., Liss, P.S., 1991. Air sea gas exchange in rough and stormy seas measured by a dual-tracer technique. Nature 349, 145–147.

Watson, A.J., Messias, M.J., Fogelqvist, E., Van Scoy, K.A., Johannessen, T., Oliver, K.I.C., Stevens, D.P., Rey, F., Tanhua, T., Olsson, K.A., Carse, F., Simonsen, K., Ledwell, J.R., Jansen, E., Cooper, D.J., Kruepke, J.A., Guilyardi, E., 1999. Mixing and convection in the Greenland Sea from a tracer-release experiment. Nature 401, 902–904.

Weiss, R.F., Price, B.A., 1980. Nitrous oxide solubility in water and seawater. Marine Chemistry 8, 347–359.

Weiss, R.F., Bullister, J.L., Gammon, R.H., Warner, M.J., 1985. Atmospheric chlorofluoromethanes in the deep equatorial Atlantic. Nature 314, 608–610.

Wisegarver, D.P., Gammon, R.H., 1988. A new transient tracer: measured vertical distribution of CCl_2FCClF_2 (F-113) in the North Pacific Subarctic gyre. Geophysical Research Letters 15, 188–191.

ELSEVIER

Deep-Sea Research II 51 (2004) 2701–2713

DEEP-SEA RESEARCH
PART II

www.elsevier.com/locate/dsr2

Spatial and vertical distribution of phytoplankton pigments in the eastern Atlantic sector of the Southern Ocean

A. Wulff[a,*], S.-Å. Wängberg[b]

[a]*Department of Marine Ecology, Göteborg University, Box 461, Göteborg SE-405 30, Sweden*
[b]*Botanical Institute, Göteborg University, Box 461, Göteborg SE-405 30, Sweden*

Abstract

The spatial and vertical distribution of phytoplankton pigments was analysed during the Scandinavian South African Southern Ocean JGOFS expedition of the S.A. *Agulhas* from 31 December 1997 to 26 January 1998. In total, seawater from 12 different stations along a transect at 6°E from 60.38 to 49.82°S were sampled at water depths of approximately 1, 10, 20, 30, 50, 75 and 100 m. Pigment concentrations were analysed using high-performance liquid chromatography. The highest chlorophyll *a* (chl *a*) concentrations were found within the Spring Ice Edge (SIE) at water depths of 2–30 m (1.5–2.0 $\mu g l^{-1}$). The lowest phytoplankton biomass (chl *a*) was found within the Winter Ice Edge (WIE) with typical values around 0.3 $\mu g l^{-1}$. While the chl *a* concentrations decreased with depth within the SIE, no apparent difference between depths was found within WIE. The same trend with similar chl *a* concentrations (0.8–1.2 $\mu g l^{-1}$) at all depths was found for the northernmost part of the Antarctic Polar Front (APF) except for samples from 100 m. Principal component analysis (PCA) and the matrix factorisation program, CHEMTAX, were used to interpret the pigment data. The PCA indicated small differences between the samples in WIE and APF, while the SIE samples were separated into three groups. At the southernmost stations a clear separation was found between surface samples and deeper samples; this was not seen at the two northernmost stations within SIE. Along the whole transect, CHEMTAX suggested a dominance of diatoms and haptophytes. In general, the haptophytes contributed more to total chl *a* further south and the diatom contribution increased from south to north. Within WIE, CHEMTAX indicated that cyanobacteria were contributing approximately 3% to the total autotrophic biomass. In APF, a more diverse phytoplankton community was found compared with WIE and SIE. The pigment patterns interpreted by CHEMTAX showed that different phytoplankton assemblages were associated with distinct water masses along the transect.
© 2004 Elsevier Ltd. All rights reserved.

*Corresponding author. Tel.: +46 31 773 2628; fax: +46 31 773 2727.
E-mail address: angela.wulff@marbot.gu.se (A. Wulff).

0967-0645/$ - see front matter © 2004 Elsevier Ltd. All rights reserved.
doi:10.1016/j.dsr2.2001.01.002

1. Introduction

Oceanic phytoplankton communities are comprised of many different taxonomic groups that have various influences on the total primary productivity and trophic interactions. According to Smetacek et al. (1990), Antarctic phytoplankton communities are generally dominated by flagellates as a background community, sometimes superimposed by diatom blooms. Occasionally, single species of small flagellates such as the colonial haptophyte *Phaeocystis* sp. may dominate these blooms (e.g. Davidson and Marchant, 1992; Peeken, 1997, and references therein).

Although phytoplankton biomass is generally low over most of the Southern Ocean (Smetacek et al., 1990) phytoplankton blooms have been reported from e.g. the marginal sea-ice zone (e.g. Smith and Nelson, 1986) and along fronts between water masses (Laubscher et al., 1993; Turner and Owens, 1995). Different factors involved in the biomass accumulation and depth distribution include vertical stabilisation of the water column (e.g. Laubscher et al., 1993), seawater temperature (e.g. Jacques, 1983) and availability of trace nutrients (e.g. de Baar et al., 1995).

Phytoplankton identification and quantification is usually obtained through microscopic examination, which is very time-consuming and requires a high level of taxonomic skill. Furthermore, small cells, especially flagellates, belonging to nano- or picophytoplankton are easily overlooked or sometimes bonded together as one group. Alternatively, photosynthetic pigments can be used for studying the composition and physiological status of phytoplankton, as certain pigments serve as taxon-specific indicators of major taxonomic groups. High-performance liquid chromatography (HPLC) can be used to separate all relevant pigments and is now a common tool, extensively used for estimating pigment concentrations in microalgal communities (e.g. Jeffrey, 1997, and references therein). For phytoplankton, the major diagnostic photopigments used are chlorophyll *b* (chlorophytes), fucoxanthin (diatoms), 19′-hexanoyloxyfucoxanthin (haptophytes), 19′-butanoyloxyfucoxanthin (pelagophytes and haptophytes), peridinin (dinophytes), alloxanthin (cryptophytes) and zeaxanthin (cyanobacteria) (e.g. Jeffrey a Vesk, 1997). In order to determine algal cl abundance from group-specific pigments Mack et al. (1996) developed the matrix factorisati program CHEMTAX. The program uses steepest-descent algorithm to determine the b fit based on an estimate of pigment/chl *a* ratios different algal classes (Mackey et al., 1996).

The aim of this study was to use mark pigments to describe the vertical and spat distribution of different phytoplankton taxonor cal groups during the Scandinavian/South Afric Southern Ocean JGOFS expedition in the easte Atlantic sector of the Southern Ocean.

2. Material and methods

Samples were collected during the SWEDAR 97/98 cruise of S.A. *Agulhas* from 31 Decemb 1997 to 26 January 1998. Five stations we sampled along a 6°E transect (59.32°S to 60.39° 31 December to 3 January) within the Spring I Edge (SIE) region, two stations (55.83°S 56.67°S, 12–13 January) within the Winter I Edge (WIE) region and another five statio (49.82°S to 51.41°S, 24–26 January) within th Antarctic Polar Front region (APF) (Fig. 1 Seawater samples were collected in 121 NISKI bottles on a 24-bottle rosette sampler attached to CTD. Approximate sampling depths were 2, 1 20, 30, 50, 75 and 100 m. Background enviro mental data for the different stations are shown Table 1.

2.1. Pigment analysis

From each depth, 1–2 l of seawater were gent filtered onto 20 mm Whatman GF/F glass fib filters. The filtration was done in dim light at 1 ° and the filters were immediately frozen and store in liquid nitrogen. After 4–8 weeks, the filters we transferred to a low-temperature freezer (−85 °C to improve extraction efficiency (cf. Wright et a 1997) and stored for up to 3 months unt analysed. One milliliter of 100% methanol w added to the filters and the extraction and HPL analysis continued according to Wright a

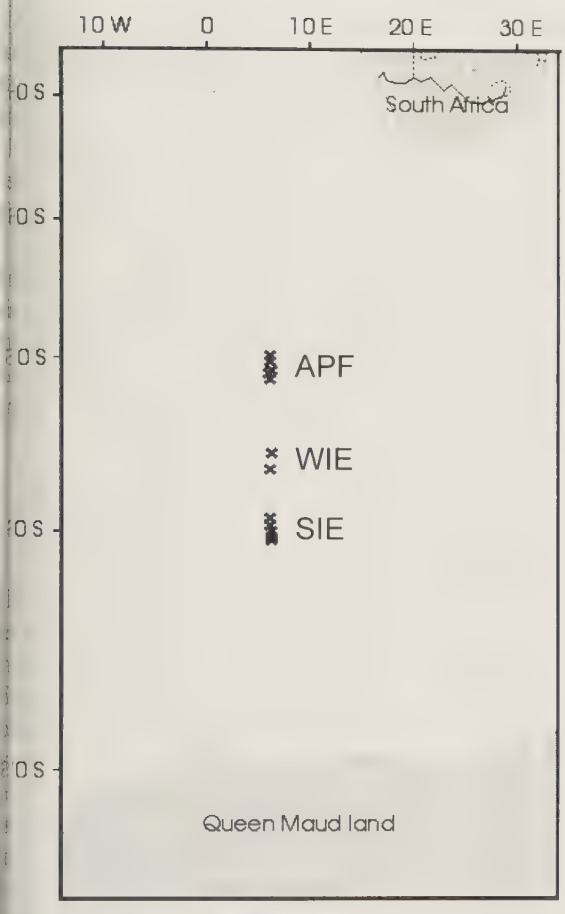

g. 1. Map of the Atlantic sector of the Southern Ocean owing the different study areas during the Scandinavian/ outh African Southern Ocean JGOFS expedition 1997/98. The ts represent individual sampling stations.

ffrey (1997), using a diode-array detector (Spec-aphysics UV6000LP), with, however, a slightly ifferent solvent composition. Solvent A was 85% ethanol and 15% ammonium acetate buffer (pH 2). Pigments were quantified as described in Wright and Jeffrey (1997). To ensure a correct identification, a spectrum (400–700 nm) was run or each sample and a mixture prepared from algal ultures with known pigment compositions was n everyday and/or the twentieth sample. Pig-ent standards were provided from the Interna-onal Agency for ^{14}C Determination, Hørsholm, enmark. Pigments are expressed as concentra-ons ($\mu g l^{-1}$). The following pigments were de-cted: chl *a*, chl *b*, chl c_3, chl c_1c_2, peridinin (*per*),

Table 1
Background data for each station, respectively

Area	Latitude, °S/date	Depth (m)	Temp (°C)	Salinity
APF	49.82, Jan 24	107	2.442	33.918
		81	3.779	33.869
		57	3.811	33.867
		36	3.810	33.867
		26	3.809	33.866
		16	3.815	33.866
		8	3.814	33.865
APF	50.24, Jan 24	107	2.946	33.854
		82	3.847	33.822
		57	3.847	33.821
		35	3.863	33.822
		26	3.863	33.822
		16	3.863	33.822
		8	3.865	33.822
APF	50.83, Jan 12	101	2.687	33.871
		78	3.645	33.826
		53	3.640	33.826
		31	3.635	33.827
		21	3.645	33.826
		11	3.641	33.826
APF	51.05, Jan 13	105	3.223	33.841
		76	3.656	33.833
		54	3.668	33.833
		34	3.686	33.833
		25	3.719	33.833
		15	3.718	33.833
		7	3.730	33.834
APF	51.41, Jan 26	106	2.344	33.883
		80	3.430	33.829
		56	3.470	33.828
		36	3.504	33.828
		25	3.529	33.822
		15	3.526	33.820
		7	3.532	33.819
WIE	55.83, Jan 12	105	−0.265	34.377
		80	−0.738	34.221
		53	−0.218	34.111
		33	0.288	34.074
		24	0.309	34.073
		12	0.386	34.073
		5	0.872	34.077
WIE	56.67, Jan 13	105	−1.084	34.368
		80	−0.600	34.290
		55	−0.043	34.270
		34	0.119	34.262
		25	0.189	34.259
		14	0.195	34.259
		6	0.222	34.260

Table 1 (*continued*)

Area	Latitude, °S/date	Depth (m)	Temp (°C)	Salinity
SIE	59.32, Dec 31	105	−1.128	34.222
		79	−0.950	34.179
		53	−0.743	34.153
		32	−0.696	34.151
		23	−0.265	34.134
		13	−0.280	34.133
		3	−0.213	34.132
SIE	59.62, Jan 02	106	−1.629	34.169
		71	−1.012	34.140
		61	−0.691	34.143
		34	−0.367	34.029
		22	−0.292	34.009
		13	−0.276	34.009
		2	−0.276	34.008
SIE	60.00, Jan 02	104	1.043	34.711
		79	−0.855	34.381
		54	−1.627	34.152
		33	−0.291	33.817
		23	−0.290	33.816
		12	−0.295	33.814
		4	−0.291	33.815
SIE	60.27, Jan 03	107	0.746	34.673
		78	−1.436	34.230
		55	−1.335	34.077
		33	−0.451	33.955
		23	−0.439	33.955
		14	−0.448	33.959
		5	−0.463	33.952
SIE	60.39, Jan 03	104	−1.785	34.199
		78	−1.820	34.156
		54	−1.711	34.071
		33	−0.466	33.961
		23	−0.407	33.936
		13	−0.321	33.940
		5	−0.339	33.938

19′-butanoyloxyfucoxanthin (19′-*but*), fucoxanthin (*fucox*), 19′-hexanoyloxyfucoxanthin (19′-*hex*), diadinoxanthin (*dd*), diatoxanthin (*dt*), alloxanthin (*allox*), violaxanthin (*violax*), zeaxanthin (*zeax*) and betacarotene. In addition, the breakdown/intermediate product chlorophyllide *a* and the breakdown products phaeophytin *a* and phaeophorbide *a* were analysed but detected in very small amounts and will therefore not be discussed further. To estimate the contribution of differ algal classes to total chl *a*, the pigment data w interpreted using the matrix factorisation progr CHEMTAX (Mackey et al., 1996; Wright et 1996). The program uses the steepest-desc algorithm to determine the best fit based on estimate of pigment/chl *a* ratios for different al classes (Mackey et al., 1996). We used an init pigment-ratio matrix derived from a Southe Ocean data set (Mackey et al., 1996) and our ent data set was computed (Wright et al., 1996).

2.2. Statistical and mathematical analyses

Principal component analysis (PCA) was us to identify similarities in patterns of pigme composition and algal classes, determined CHEMTAX, between samples. The analysis w done with the program SIMCA-P (Unimetrics A Umeå, Sweden). As input for the pigment analys the absolute concentration ($\mu g l^{-1}$) was used, a for the algal classes, the fraction in each cla multiplied with the chl *a* concentration was use The data were scaled to unit variance and ze means for each pigment (algal class). The si nificance of the principal components was dete mined by cross validation. Differences in conte of single pigments between the identified grou were tested with the nonparametric Kruskal–Wa lis ANOVA median test in which $p<0.05$ we considered significant.

2.3. Physical data

Hydrological conditions during the cruise a discussed in detail in Turner et al. (2004). Surfa water temperatures varied between −0.5 a 3.9 °C from south to north and surface salini was between 33.82 (APF) and 34.26 (WIE). Dep profiles of total dissolved organic carbon, tot alkalinity and nitrate are shown in Fransson et a (2004). Macronutrients were not limiting (Froneman et al., 2004). In December, the ice ed had retreated from 56°S to 60°S. The mean dep of the euphotic zone was about 50 m in SIE, 90 in WIE and 50 m in APF (calculated from da presented in Rasmus et al., 2004). The correspon ing mean thickness of the upper mixed layer w

), 30 and 50 m for SIE, WIE and APF, spectively (c.f. Larsson, 2004).

Results

1. Pigment data

Absolute pigment concentrations ($\mu g l^{-1}$) for the fferent marker pigments are shown in Table 2. he chl *a* concentrations varied with depth and titude. The depth distribution of chl *a* showed iat within SIE, the surface concentrations exnded to 20–30 m at the stations located furthest outh and to depths below 75 m at 59.3 and 59.6°S nd for stations within APF (Fig. 2). An even iore homogeneous water column was found ithin WIE with surface conditions extending to t least 100 m. For samples from 2–30 m depths, ie highest concentrations were found in the outhern part of SIE, ranging from 1.6 to .2 $\mu g l^{-1}$, and the lowest in WIE (ca. 0.18 $\mu g l^{-1}$). Within WIE, the chl *a* concentrations at 50–100 m ere somewhat higher than the surface values 2–30 m). The chl *a* concentrations in APF and the orthern part of SIE were similar. In APF, a orth–south gradient was found where the chl *a* oncentrations at latitudes 49.8, 50.2 and 50.8°S ere in the same range (1 $\mu g l^{-1}$) as for samples om 2 to 75 m. At a water depth of 100 m, the chl concentration increased strongly from 0.18 $\mu g l^{-1}$ t 49.8°S to 1.14 $\mu g l^{-1}$ at 51.0°S.

Along the entire transect, CHEMTAX sugested a total dominance of diatoms and haptohytes. However, the outcome differed between reas and depths. In general, the haptophytes ontributed more to total chl *a* further south and he diatom contribution increased from south to orth (Fig. 3). Dinoflagellates contributed to round 1% of total chl *a* in the SIE, increased long the transect and reached maximum values at 9.8°S. Cryptophytes showed a patchy distribution oth between depths and areas, but were virtually bsent in the SIE except for the station at 60.3°S, ll depths, and at 30 plus 50 m at 60.4°S. Within VIE and APF, cryptophytes contributed with ca. –4% of total biomass. According to CHEMTAX, yanophytes were absent in the SIE and generally constituted 0.5% of the biomass in the other areas. However, at 56.7°S within the WIE, CHEMTAX suggested values of 5–6% between 2–50 m depth and around 1% at 55.8°S, all depths. Chlorophytes were identified by the pigments *violax* and chl *b* as no other green algal pigments were detected. In SIE and WIE, chlorophytes were very patchily distributed with occasionally high biomass contributions at water depths of 75–100 m. In APF, chlorophytes constituted ca. 3–5% of total chl *a*, all depths.

3.2. PCA analysis

As the outcome of the analysis was very similar if it was done on pigment concentrations or algal classes determined by CHEMTAX, only the results from the concentrations are presented. The PCA analysis of the data set gave two significant components: the first explained 38% of the variation and the second 52%. The scores from the first component (Fig. 4a) show that all samples within APF, except some of the 100 m samples, were separated from the homogeneous WIE samples. The stations within the SIE were more diverse. At the two northernmost stations, the scores were independent of the depth whilst in the other three stations there was a clear division between the samples below 50 m and those above. To elucidate the relationship within SIE a separate PCA was done with the samples from SIE only. The pattern of scores in the second component was very similar to the first component (Fig. 4b). As reflected in the loadings, the first component explained over 50% of the variance for chl *a*, chl c_1c_2, chl c_3, *fucox* and *dd,* while for the second component it was for chl *b*, *violax*, *per*, 19′-*but*, chl *a*, chl c_1c_2, chl c_3 and 19′-*hex*. The statistical test showed significant differences in concentration between the different areas for all of these pigments, except *violax*, and, in addition, for *allox* and *zeax*.

To analyse the relationships within the SIE more closely, a second PCA was performed with samples from those five stations only. It generated only one significant component that explained 50% of the variation. The scores from that component were grouped into three groups that

Table 2
Pigment concentrations (μg l $^{-1}$) for the different signature pigments, peridinin (*per*), 19′-butanoyloxyfucoxanthin (*19′-b*
fucoxanthin (*fucox*), 19′-hexanoyloxyfucoxanthin (*19′-hex*), alloxanthin (*allox*), zeaxanthin (*zeax*) and chlorophyll *b* (chl *b*)

Area	Latitude, °S/date	Depth	Per	19′-but	Fucox	19′-hex	Allox	Zeax	Ch
APF	49.82, Jan 24	100	0.036	0.009	0.076	0.045	0.000	0.001	0.0
		75	0.074	0.079	0.365	0.385	0.005	0.002	0.0
		50	0.088	0.081	0.369	0.402	0.009	0.002	0.0
		30	0.077	0.075	0.358	0.371	0.008	0.002	0.0
		20	0.081	0.080	0.329	0.404	0.006	0.002	0.0
		10	0.076	0.073	0.348	0.379	0.008	0.001	0.0
		2	0.097	0.080	0.337	0.416	0.008	0.002	0.0
APF	50.24, Jan 24	100	0.029	0.017	0.156	0.108	0.001	0.000	0.0
		75	0.081	0.071	0.365	0.363	0.005	0.002	0.0
		50	0.089	0.073	0.363	0.375	0.007	0.002	0.0
		30	0.056	0.050	0.270	0.253	0.005	0.002	0.0
		20	0.092	0.074	0.364	0.393	0.008	0.003	0.0
		10	0.088	0.072	0.354	0.384	0.007	0.002	0.0
		2	0.085	0.074	0.373	0.362	0.000	0.002	0.0
APF	50.83, Jan 12	100	0.042	0.040	0.270	0.234	0.005	0.002	0.0
		75	0.073	0.063	0.365	0.368	0.007	0.003	0.0
		50	0.067	0.065	0.384	0.371	0.005	0.002	0.0
		30	0.051	0.046	0.262	0.268	0.005	0.002	0.0
		20	0.071	0.064	0.352	0.373	0.008	0.003	0.0
		10	0.075	0.065	0.364	0.377	0.008	0.002	0.0
APF	51.05, Jan 13	100	0.061	0.050	0.319	0.284	0.006	0.005	0.0
		75	0.068	0.062	0.340	0.337	0.008	0.005	0.0
		30	0.059	0.062	0.341	0.346	0.000	0.000	0.0
		20	0.062	0.066	0.366	0.343	0.000	0.002	0.0
		10	0.062	0.059	0.309	0.330	0.007	0.002	0.0
		2	0.061	0.063	0.339	0.323	0.004	0.002	0.0
APF	51.41, Jan 26	100	0.018	0.013	0.105	0.068	0.001	0.000	0.0
		30	0.058	0.060	0.307	0.335	0.007	0.002	0.0
		20	0.059	0.057	0.283	0.328	0.007	0.003	0.0
		10	0.060	0.054	0.276	0.329	0.007	0.002	0.0
WIE	55.83, Jan 12	100	0.003	0.047	0.108	0.125	0.002	0.001	0.0
		75	0.011	0.046	0.220	0.198	0.003	0.001	0.0
		50	0.042	0.026	0.181	0.180	0.003	0.001	0.0
		30	0.008	0.008	0.111	0.111	0.002	0.001	0.0
		20	0.007	0.008	0.115	0.095	0.001	0.001	0.0
		10	0.007	0.008	0.106	0.107	0.002	0.001	0.0
WIE	56.67, Jan 13	100	0.011	0.035	0.117	0.256	0.004	0.001	0.0
		75	0.010	0.023	0.145	0.283	0.005	0.003	0.0
		50	0.009	0.012	0.102	0.184	0.003	0.005	0.0
		30	0.006	0.010	0.085	0.164	0.002	0.005	0.0
		20	0.005	0.009	0.075	0.151	0.001	0.005	0.0
		10	0.004	0.010	0.081	0.158	0.001	0.005	0.0
		2	0.004	0.010	0.078	0.157	0.000	0.004	0.0
SIE	59.32, Dec 31	100	0.016	0.019	0.218	0.432	0.000	0.011	0.0
		75	0.020	0.022	0.340	0.508	0.000	0.002	0.0
		50	0.023	0.023	0.430	0.460	0.000	0.000	0.0
		20	0.007	0.011	0.237	0.224	0.000	0.000	0.0

able 2 (*continued*)

rea	Latitude, °S/date	Depth	Per	19′-but	Fucox	19′-hex	Allox	Zeax	Chl *b*
		10	0.009	0.013	0.265	0.273	0.000	0.000	0.000
		2	0.010	0.012	0.254	0.239	0.000	0.000	0.000
IE	59.62, Jan 02	100	0.008	0.042	0.133	0.406	0.000	0.000	0.012
		75	0.018	0.027	0.323	0.512	0.000	0.000	0.007
		50	0.017	0.022	0.363	0.363	0.000	0.000	0.000
		30	0.010	0.012	0.283	0.311	0.000	0.000	0.000
		20	0.009	0.012	0.243	0.283	0.000	0.000	0.000
		10	0.011	0.013	0.274	0.341	0.005	0.000	0.000
		2	0.012	0.015	0.276	0.361	0.005	0.000	0.000
IE	60.00, Jan 02	100	0.000	0.019	0.025	0.058	0.000	0.000	0.000
		75	0.002	0.025	0.043	0.154	0.000	0.000	0.007
		50	0.013	0.033	0.155	1.021	0.000	0.000	0.009
		30	0.024	0.034	0.507	1.870	0.000	0.002	0.005
		20	0.021	0.028	0.461	1.589	0.000	0.002	0.000
		10	0.025	0.032	0.517	1.952	0.000	0.002	0.000
		2	0.025	0.034	0.544	2.090	0.000	0.002	0.005
IE	60.27, Jan 03	100	0.000	0.029	0.034	0.074	0.001	0.000	0.005
		75	0.003	0.033	0.073	0.444	0.007	0.000	0.010
		50	0.020	0.029	0.320	1.370	0.019	0.002	0.000
		30	0.019	0.027	0.454	1.863	0.027	0.000	0.000
		20	0.018	0.022	0.382	1.511	0.022	0.000	0.000
		10	0.017	0.024	0.420	1.486	0.021	0.000	0.000
		2	0.018	0.026	0.401	1.754	0.025	0.000	0.000
IE	60.39, Jan 03	100	0.000	0.006	0.008	0.038	0.000	0.000	0.000
		75	0.002	0.032	0.048	0.228	0.000	0.000	0.008
		50	0.000	0.031	0.082	0.364	0.005	0.000	0.013
		30	0.018	0.024	0.244	1.226	0.016	0.000	0.005
		20	0.015	0.023	0.425	1.294	0.000	0.000	0.000
		10	0.018	0.025	0.396	1.270	0.000	0.000	0.000
		2	0.019	0.027	0.398	1.343	0.000	0.000	0.000

ncluded all but four samples as indicated in Fig. 4c. The component explained over 50% of the variance for chl *a*, chl c_1c_2, chl c_3, 19′-*hex*, *fucox*, *per* and *dd*. Statistically, there were no significant differences between the groups for *fucox* but significant differences were found for chl *a*, chl c_1c_2, chl c_3, 19′-*hex*, *per* and *dd* (>50% were explained in the PCA), and, in addition, for 19′-*but*, *zeax*, *violax* and chl *b*.

In summary, five different groups were identified:

(1) APF < 100 m,
(2) WIE,
(3) the northern part of SIE,
(4) surface (2–30 m) samples in the southern part of SIE and
(5) deep samples (75 and 100 m) in the southern part of SIE.

A plot of the scores for the first and second components, using the whole data set, clearly showed the separation between the first, third and fourth groups whilst there was an overlap between the second and fifth groups (Fig. 4d).

4. Discussion

The phytoplankton composition agreed with other observations in the area (Savidge et al., 1995;

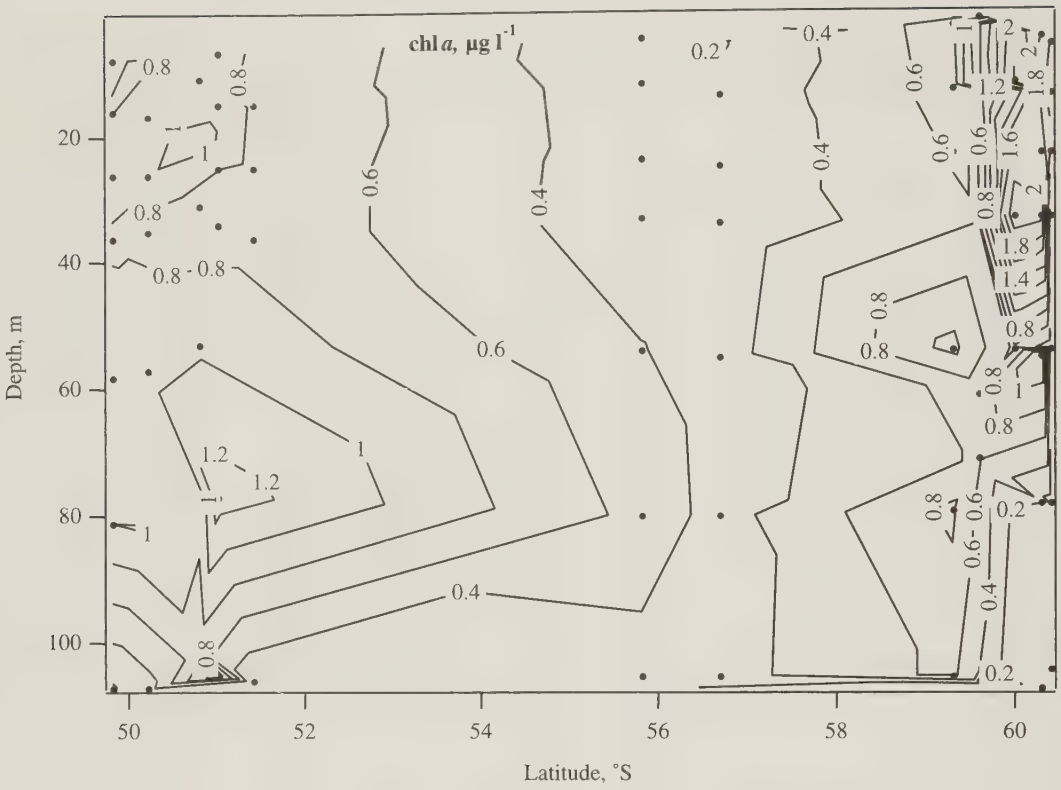

Fig. 2. Chlorophyll *a* concentrations ($\mu g l^{-1}$) with black dots representing the individual samples.

Peeken, 1997) and the pigment data were generally confirmed by microscopical data (Wängberg and Wulff, 2004; Karlson and Godhe, unpublished). However, the species analyses were limited to diatoms and dinoflagellates.

The highest chl *a* concentrations were found in samples from <50 m at SIE stations south of 60°S. They were separated as a cluster with high scores in the PCA even if there was a decreasing trend in the PCA scores going south. In contrast, the deep-water samples (75 and 100 m) in SIE had among the lowest chl *a* concentrations of all. Based on significant differences in signature pigments and PCA loadings, the surface communities were primarily composed of haptophytes and diatoms. Peridinin (*per*) is a pigment exclusively found in dinoflagellates and was observed at all stations. Our observation agrees with Peeken (1997) who found *per* in most samples between 50 and 60°S. We could not, however, distinguish between autotrophic and heterotrophic dinoflagellates an autotrophic dinoflagellates have been reported t be abundant primarily north of 50.5°S (Kopczyns ka et al., 1986). In the SIE, a higher amount of *pe* was found in the surface samples compared wit the deeper samples. The only signature pigmen with higher concentrations in 75–100 m sample compared with shallower depths was chl *b*. In bot the SIE and WIE, according to CHEMTAX chlorophytes were only present at 50–100 m depth while in the APF a more even depth distributio was found. In SIE and WIE, only very small peak of chl *b* were detected and CHEMTAX might hav overestimated the contribution of chlorophytes i these areas. Detmer and Bathmann (1997) re ported the presence of a "*Chlorella*-like" organism in the area and as chlorophytes have been found i sea-ice (Palmisano and Garrison, 1993) it possible that chl *b* containing algae were trappe in the stratified water column in the SIE an

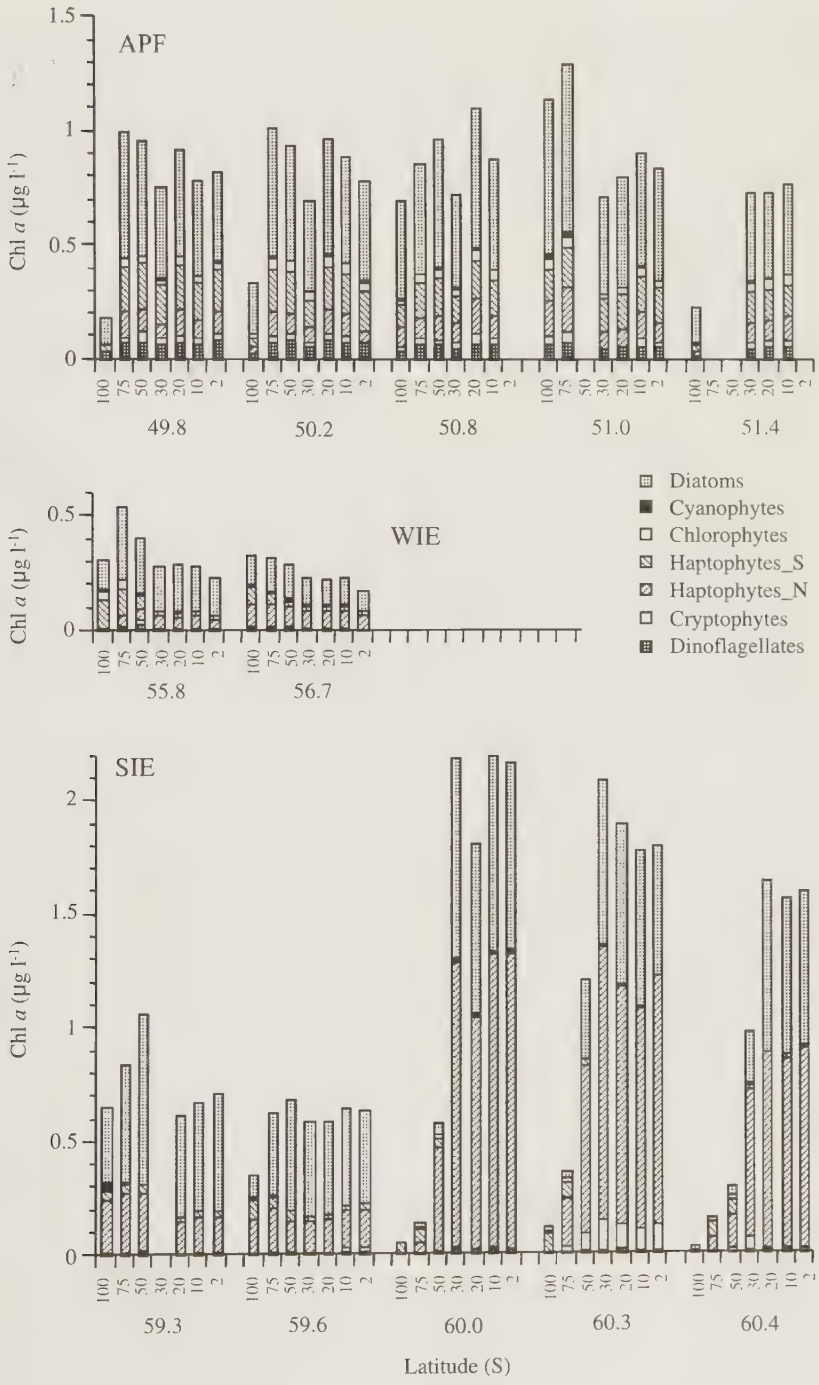

Fig. 3. Biomass of phytoplankton groups in samples from APF, WIE and SIE estimated by CHEMTAX. The *x*-axis shows the different sampling depths at each latitude (°S).

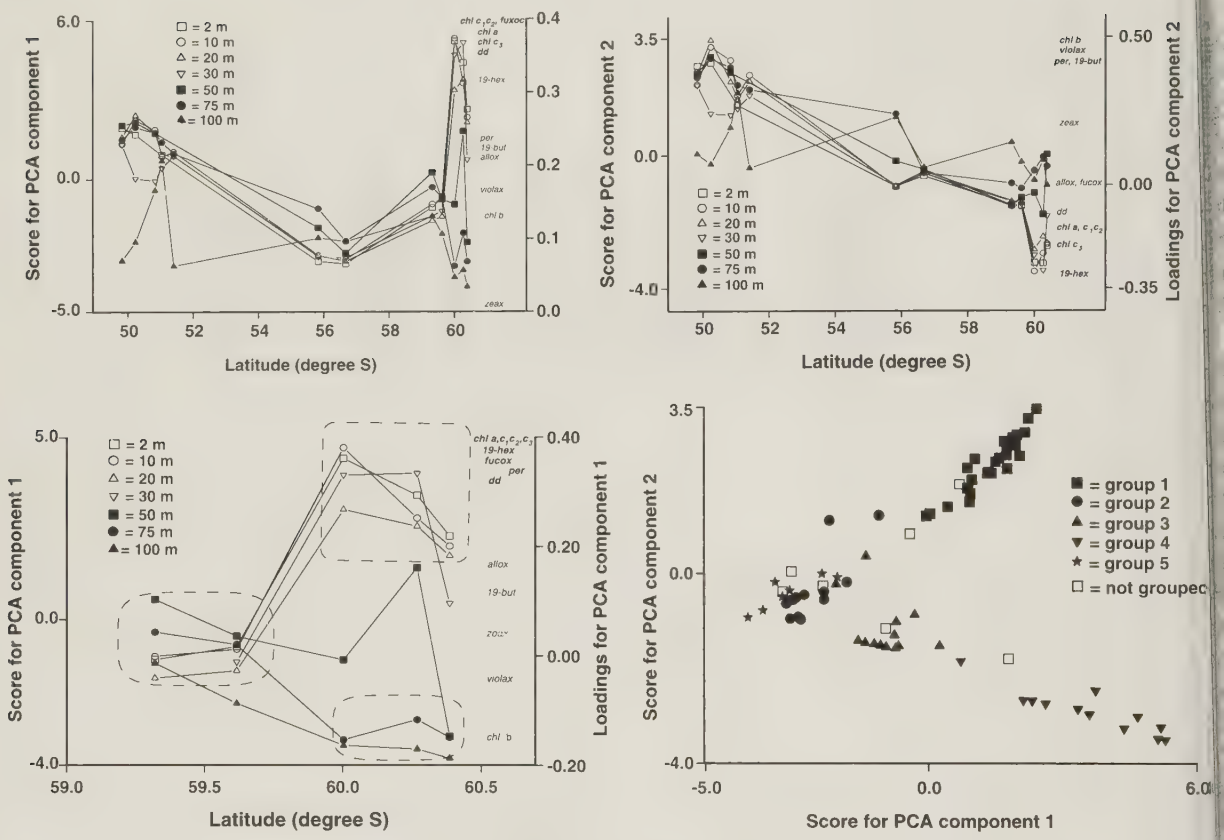

Fig. 4. Principal component analysis of pigment concentrations ($\mu g\,l^{-1}$), done with SIMCA-P. Before analysis, the pigment concentrations were scaled to unit variance. Beside the scores for the different stations (x- and left y-axes) the corresponding loadings for the pigments are shown (right y-axis). Pigments whose variance was reduced by more than 50% are written in bold style. (A) First component with the whole data set, plotted against latitude. The component explained 38% of the total variation. (B) Second component with the whole data set plotted against latitude. The component explained 52% of the total variation. (C) First component with samples from SIE only, plotted against latitude. The component explained 56% of the total variation. (D) Plot of the scores of the first and second components using the whole data set.

survived unfavourable light conditions. The *allox* distribution at the two southernmost stations could be explained by the presence of the ciliate *Mesodinium rubrum* (contains cryptophytes as endosymbionts) as Bathmann et al. (1997) found this ciliate to be fairly abundant in the SIE. This species has also been observed in other Antarctic areas often associated with sea-ice (Satoh and Watanabe, 1991; Stoecker et al., 1993). The relatively large algal biomass at water depths shallower than 50 m were probably remnants from algae earlier associated with the sea-ice. The highest chl *a* concentrations observed were, in fact, associated with the highest iron concentrations found during the expedition (dissolved Fe 1.46 nM and total Fe 1.54 nM; Croot et al., 2004; cf. de Baar et al., 1995). A stable stratification of the water column together with a shallow mixed-layer depth generated a bloom as the phytoplankton was kept within the euphotic zone. In this perspective, the decreasing trend in PCA scores with higher latitude were probably caused by ageing of the bloom as the stations within the SIE were sampled from north to south. In the two northernmost stations within the SIE, the chl *a* concentrations were more evenly distributed down to 100 m depth with values between the surface and deep samples of the other stations in SIE. The

harked difference between the southern and orthern part of SIE could be due to a smaller ontribution of ice-algae in the northern part ogether with a weaker stratification.

The WIE region had the lowest chl *a* concentrations evenly distributed from the surface to 100 m epth. The same trend was found for all other iomarker pigments except *zeax*. Similarly to the ndings of Wright et al. (1996), CHEMTAX redicted small amounts of cyanobacteria south f 50°S. Also Peeken (1997) reported small mounts of lutein/*zeax* in most samples, but the hromatographic system used in that study could ot separate lutein from *zeax*. During the same ruise, Detmer and Bathmann (1997) found cells ith autofluorescence typical for cyanobacteria nd cryptophytes, but the cells were not possible to dentify and the authors hypothesised that they ere cryptophytes. In our study, the relatively high mounts of *zeax* at 56.7°S (WIE) with the absence f other pigments typical of green algae, made ources other than cyanobacteria less likely. *Zeax* s a major pigment of prochlorophyta (Jeffrey and esk, 1997) but this group has not previously been eported in Antarctic waters. In contrast to the IE, the chl *a* concentrations in WIE were somewhat higher at 50–100 m compared with 2–30 m. A ow algal biomass is expected in this region, as lgae from melting ice or from frontal systems do ot support it. No apparent stratification was bserved above 100 m, which together with the lear water explain the higher chl *a* values in the eeper samples. Sakshaug and Holm-Hansen (1984) speculate that 50 m is the maximum depth f the mixed layer to support phytoplankton looms and the upper mixed layer in WIE was a. 30 m. The euphotic zone in WIE was, however, eeper so it is not likely that phytoplankton were ight-limited even in the deepest samples. A ossible explanation is instead the low iron concentrations in this area (Croot et al., 2004). n APF, the mixed layer was slightly deeper than he euphotic zone, but the chl *a* values were still uite high down to 75–100 m depth. Based on the PCA, no apparent differences in signature pigment composition were found in the 2–75 m depth. However, the deviation in two of the 30 m samples was caused by a lower concentration of *fucox*, 19′-*hex*, 19′-*but*, *per* and chl *b*. The lack of thermo- and pycnoclines above 100 m explains the homogeneous pigment distribution. A similar scenario with deep chl *a* concentrations was also observed by Bathmann et al. (1997) and in the Bellingshausen Sea by Turner and Owens (1995). Bathmann et al. (1997) speculate that the relatively high chl *a* values found below 40 m were due to a subduction of a plankton-rich, surface layer below the adjoining uppermost surface layer. Based on the PCA no apparent differences in signature pigment composition were found in the 2–75 m depth.

We found an increasing amount of 19′-*but* and a decreasing amount of 19′-*hex* going from south to north. Using initial pigment ratios from a Southern Ocean data set (Wright et al., 1996; Mackey et al., 1996), CHEMTAX suggested up to 80% hapto-N in the southern part and almost 90% of hapto-S in the northern part of the transect. Although the microscopical data are sparse, we observed relatively higher amounts of *Phaeocystis* sp. (colonies) in the southern stations, which contradicts with CHEMTAX results. The above contradictions could be explained as follows. (i) The amount of 19′-*but* in haptophytes has been shown to be quite variable. Total fucoxanthins range from 4 to 20% and from 0 to 24% in colonial and flagellate stages of *Phaeocystis antarctica*, respectively (Wright and van den Enden, 2000). Moreover, both Jeffrey and Wright (1994) and Schlüter et al. (2000) have reported the absence of 19′-*but* in *Phaeocystis* sp. (ii) The pigment composition varies with growth phase. In laboratory experiments, Schlüter et al. (2000) detected an increased 19′-*hex*/chl *a* ratio for *Phaeocystis* sp. in stationary growth. In the present study, on the southward transect, ca. 12 days before the return to the SIE, a dense *Phaeocystis* sp. bloom was observed in the SIE region, which appeared to be in decline (Karlson and Godhe, 1998) and could explain the proportion of 19′-*hex*. (iii) Influence of light and iron stress. Van Leeuwe and Stefels (1998) observed that the 19′-*but* concentration in *Phaeocystis* sp. varied according to light and iron stress, increasing from 0% in low light and low iron to 13% of total fucoxanthins in high light and low iron. The SIE has previously been reported to contain low iron concentrations

compared with the APF (de Baar et al., 1995; Löscher et al., 1997). During the cruise, relatively high iron concentrations were found in the SIE and APF areas but very low amounts in WIE (Croot et al., 2004). (iv) Sources other than haptophytes could explain the proportion of 19′-*but*. 19′-*but* is also found in pelagophytes and chrysophytes. The pelagophyte *Pelagococcus subviridis* is widely distributed and it is quite possible that this and related species contribute to the 19′-*but* pool also in Antarctic waters (cf. Wright and Jeffrey, 1987). Interestingly, in the present study a high correlation ($r^2 > 0.80$) was found between chl c_3 (present in both haptophytes and pelagophytes) and 19′-*hex* (not present in pelagophytes) and not between chl c_3 and 19′-*but* ($r^2 < 0.40$). Recently, species of *Parmales* with the same pigments as in type 4 haptophytes (*19′-but* and chl c_3 with or without *fucox* and 19′-*hex* and 19′-*but*/(*fucox* + 19′-*hex*) > 0.02 (Mackey et al., 1996)) were observed in large amounts in a sample from the Ross Sea (cf. Wright and van den Enden, 2000).

Though CHEMTAX has proven to be reliable, it is important to point out that the program only estimates the contribution of different algal groups to total chl *a*. Naturally, the program is dependent on the reliability of the initial pigment ratios and basic knowledge of how pigment ratios vary within and between species as well as within and between different microalgal groups are still lacking (cf. Goericke and Montoya, 1998; Schlüter et al., 2000).

In conclusion, the pigment patterns interpreted by CHEMTAX showed that different phytoplankton assemblages were associated with distinct water masses along the transect, diatoms and haptophytes being the most abundant groups. In general, the haptophytes contributed more to total chl *a* further south and the diatom contribution increased from south to north. In the APF, a more diverse phytoplankton community was found compared with the WIE and the SIE.

Acknowledgements

We would like to thank the Swedish Polar Secretariat and Göteborg Marine Research Centre (GMF), who funded the expedition. We als acknowledge the work of the crew on the Researc Vessel S.A. *Agulhas* and the invaluable help fro our Swedish and South-African colleagues. Man thanks to Dr. Peter Henriksen who assisted wit CHEMTAX analyses and Dr. Simon Wright fo valuable suggestions on pigment distributions.

References

Bathmann, U., Scharek, R., Klaas, C., Dubischar, C Smetacek, V., 1997. Spring development of phytoplankto biomass and composition in major water masses of th Atlantic sector of the Southern Ocean. Deep-Sea Researc II 44, 51–67.

Croot, P.L., Andersson, K., Özturk, M., Turner, D.R., 200 The distribution and speciation of iron along 6°E in th Southern Ocean. Deep-Sea Research II, this issu [doi:10.1016/j.dsr2.2003.10.012].

Davidson, A.T., Marchant, H.J., 1992. Protist interactions an carbon dynamics of a Phaeocystis-dominated bloom at a Antarctic coastal site. Polar Biology 12, 387–395.

de Baar, H.J.W., de Jong, J.T.M., Bakker, D.C.E., Löscher B.M., Veth, C., Bathmann, U., Smetacek, V., 1995 Importance of iron for plankton blooms and carbon dioxid drawdown in the Southern Ocean. Nature 373, 412–415.

Detmer, A., Bathmann, U., 1997. Distribution patterns o autotrophic pico- and nanoplankton and their relativ contribution to algal biomass during spring in the Atlanti sector of the Southern Ocean. Deep-Sea Research II 44 299–320.

Fransson, A., Chierici, M., Anderson, L.G., David, R., 2004 Transformation of carbon and oxygen in the surface layer o the eastern Atlantic sector of the Southern Ocean. Deep-Se Research II, this issue [doi:10.1016/j.dsr2.2001.12.001].

Froneman, P.W., Pakhomov, E.A., Balarin, M.G., 2004. Size fractionated phytoplankton biomass, production and bio genic carbon flux in the eastern Atlantic sector of th Southern Ocean in late austral summer 1997–1998. Deep Sea Research II, this issue [doi:10.1016/j.dsr2.2002.09.001]

Goericke, R., Montoya, J.P., 1998. Estimating the contributio of microalgal taxa to chlorophyll a in the field- variations o pigment ratios under nutrient- and light-limited growths Marine Ecology Progress Series 169, 97–112.

Jacques, G., 1983. Some ecophysiological aspects of th Antarctic phytoplankton. Polar Biology 2, 27–33.

Jeffrey, S.W., 1997. Application of pigment methods t oceanography. In: Jeffrey, S.W., Mantoura, R.F.C., Wright S.W. (Eds.), Phytoplankton Pigments in Oceanography UNESCO Publishing, Paris, pp. 37–84.

Jeffrey, S.W., Vesk, M., 1997. Introduction to marin phytoplankton and their pigment signatures. In: Jeffrey S.W., Mantoura, R.F.C., Wright, S.W. (Eds.), Phytoplank ton Pigments in Oceanography. UNESCO Publishing Paris, pp. 37–84.

Jeffrey, S.W., Wright, S.W., 1994. Photosynthetic pigments in the Haptophyta. In: Green, J.C., Leadbeater, B.S.C. (Eds.), The Haptophyte Algae. Clarendon Press, Oxford, pp. 111–132.

Larlson, B., Godhe, Á., 1998. Phytoplankton observations in the Atlantic sector of the Southern Ocean. In: Polarforskningssekretariatets årsbok 1998. Polarforskningssekretariatet, Stockholm, pp. 69–70.

Lopczynska, E.E., Weber, L.H., El-Sayed, S.Z., 1986. Phytoplankton species composition and abundance in the Indian sector of the Antarctic Ocean. Polar Biology 6, 161–169.

Larsson, A.-M., 2004. The role of mixing in an Antarctic ocean ecosystem: Observations and model computations of vertical distributions of related parameters. Deep-Sea Research II, this issue [doi:10.1016/j.dsr2.2004.09.006].

Laubscher, R.K., Perissinotto, R., McQuaid, C.D., 1993. Phytoplankton production and biomass at frontal zones in the Atlantic sector of the Southern Ocean. Polar Biology 13, 471–481.

Löscher, B.M., de Baar, H.J.W., de Jong, J.T.M., Veth, C., Dehairs, F., 1997. The distribution of Fe in the Antarctic Circumpolar Current. Deep-Sea Research II 44, 143–187.

Mackey, M.D., Mackey, D.J., Higgins, H.W., Wright, S.W., 1996. CHEMTAX- a program for estimating class abundances from chemical markers: application to HPLC measurements of phytoplankton. Marine Ecology Progress Series 144, 265–283.

Palmisano, A.C., Garrison, D.L., 1993. Organisms in Antarctic sea ice. In: Antarctic Microbiology. Wiley, New York, pp. 167–218.

Peeken, I., 1997. Photosynthetic pigment fingerprints as indicators of phytoplankton biomass and development in different water masses of the Southern Ocean during austral spring. Deep-Sea Research II 44, 261–282.

Rasmus, K.E., Granéli, W., Wängberg, S.-Å., 2004. Optical studies in the Southern Ocean. Deep-Sea Research II, this issue [doi:10.1016/j.dsr2.2001.01.004].

Sakshaug, E., Holm-Hansen, O., 1984. Factors governing pelagic production in polar oceans. In: Holm-Hansen, O., Bolis, L., Gilles, R. (Eds.), Marine Phytoplankton and Productivity. Springer, Berlin, pp. 1–18.

Satoh, H., Watanabe, K., 1991. A red-water bloom caused by the ciliate *Mesodinium rubrum* in the Austral summer in the fast ice near Syowa station Antarctica with notes on their photosynthetic rate. Journal of the Tokyo University of Fisheries 78, 11–18.

Savidge, G., Harbour, D., Gilpin, L., Boyd, P., 1995. Phytoplankton distributions and production in the Bellingshausen Sea, Austral spring 1992. Deep-Sea Research II 42, 1201 -1224.

Schlüter, L., Møhlenberg, F., Havskum, H., Larsen, S., 2000. The use of phytoplankton pigments for identifying and quantifying phytoplankton groups in coastal areas: testing the influence of light and nutrients on pigment/chlorophyll a ratios. Marine Ecology Progress Series 192, 49–63.

Smetacek, V., Scharek, R., Nöthig, E.-M., 1990. Seasonal and regional variation in the pelagial and its relationship to the life history cycle of krill. In: Kerry, K.R., Hempel, G. (Eds.), Antarctic Ecosystems: Ecological Change and Conservation. Springer, Berlin, pp. 103–114.

Smith, W.O., Nelson, D.M., 1986. Importance of ice edge phytoplankton production in the Southern Ocean. BioScience 36, 251–257.

Stoecker, D.K., Buck, K.R., Putt, M., 1993. Changes in the sea-ice brine community during the spring-summer transition, McMurdo Sound, Antarctica. II. Phagotrophic protists. Marine Ecology Progress Series 95, 103–113.

Turner, D.R., Owens, N.J.P., 1995. A biogeochemical study in the Bellingshausen Sea: overview of the STERNA 1992 expedition. Deep-Sea Research II 42, 907–932.

Turner, D.R., Bertilsson, S., Fransson, A., Pakhomov, E., 2004. The SWEDARP 97/98 marine expedition: overview. Deep-Sea Research II, this issue [doi:10.1016/j.dsr2.2003.08.006].

van Leeuwe, M.A., Stefels, J., 1998. Effects of iron and light stress on the biochemical composition of Antarctic *Phaeocystis* sp. (Prymnesiophyceae). II. Pigment composition. Journal of Phycology 34, 496–503.

Wängberg, S.-Å., Wulff, A., 2004. Impact of Ultraviolet-B radiation on the development of phytoplankton communities in the eastern Atlantic sector of the Southern Ocean—results from on-deck model ecosystem experiments. Deep-Sea Research II, this issue [doi:10.1016/j.dsr2.2001.05.001].

Wright, S.W., Jeffrey, S.W., 1987. Fucoxanthin pigment markers of marine phytoplankton analysed by HPLC and HPTLC. Marine Ecology Progress Series 38, 259–266.

Wright, S.W., Jeffrey, S.W., 1997. High-resolution HPLC system for chlorophylls and carotenoids of marine phytoplankton. In: Jeffrey, S.W., Mantoura, R.F.C., Wright, S.W. (Eds.), Phytoplankton Pigments in Oceanography. UNESCO Publishing, Paris, pp. 327–342.

Wright, S.W., van den Enden, R.L., 2000. Phytoplankton community structure and stocks in the East Antarctic marginal ice zone (BROKE survey, Jan—Mar 1996) determined by CHEMTAX analysis of HPLC pigment signatures. Deep-Sea Research II 47, 2363–2400.

Wright, S.W., Thomas, D.P., Marchant, H.J., Higgins, H.W., Mackey, M.D., Mackey, D.J., 1996. Analysis of phytoplankton of the Australian sector of the Southern Ocean: comparisons of microscopy and size frequency data with interpretations of pigment HPLC data using the "CHEMTAX" matrix factorisation program. Marine Ecology Progress Series 144, 285–298.

Wright, S.W., Jeffrey, S.W., Mantoura, R.F.C., 1997. Evaluation of methods and solvents for pigment extraction. In: Jeffrey, S.W., Mantoura, R.F.C., Wright, S.W. (Eds.), Phytoplankton Pigments in Oceanography. UNESCO Publishing, Paris, pp. 261–282.

ELSEVIER

Deep-Sea Research II 51 (2004) 2715–2729

DEEP-SEA RESEARCH
PART II

www.elsevier.com/locate/dsr2

Size-fractionated phytoplankton biomass, production and biogenic carbon flux in the eastern Atlantic sector of the Southern Ocean in late austral summer 1997–1998

P.W. Froneman[a,*], E.A. Pakhomov[a,b,1], M.G. Balarin[c]

[a]*Southern Ocean Group, Department of Zoology and Entomology, Rhodes University, P.O. Box 94, Grahamstown 6140, South Africa*
[b]*Zoology Department, Faculty of Science and Technology, University of Fort Hare, Private Bag X1314, Alice 5700, South Africa*
[c]*Sea Fisheries Research Institute, Roggebaai, Private Bag X 0001, Cape Town 7700, South Africa*

Abstract

Size-fractionated chlorophyll-*a* (Chl-*a*), primary production and biogenic carbon flux in the vicinity of the Winter Ice-edge Zone (WIE), Spring Ice-edge Zone (SIE) and Antarctic Polar Front (APF) were investigated in the eastern Atlantic sector of the Southern Ocean during a collaborative Scandinavian/South African Antarctic cruise conducted in late austral summer (December 1997/January 1998). Microphytoplankton (>20 μm) dominated integrated Chl-*a* biomass in the SIE and at the APF, comprising >50% of the total at all stations. Within the WIE, nanophytoplankton (2–20 μm) dominated total integrated Chl-*a* biomass comprising on average 36% of the total. Total integrated primary production ranged between 316 and 729 mg C $m^{-2} d^{-1}$ at stations occupied in the region of the SIE, and between 292 and 317 mg C $m^{-2} d^{-1}$ within the WIE. At stations occupied in the region of the APF, total integrated production ranged between 708 and 926 mg C $m^{-2} d^{-1}$. The contribution of various size fractions to total productivity generally displayed the same pattern as integrated Chl-*a* biomass. Microphytoplankton formed the most important contributor to total production at all stations in the SIE and at two stations in the region of the APF. Within the WIE, nanophytoplankton dominated total daily production. The elevated primary production rates in the region of the SIE and APF appear to be related to favourable light environment and the availability of iron. In the SIE, the partitioning of carbon between the microbial loop and classical food web was similar. Grazing activity by metazoans resulted in 11.5% of total daily production being transported to depth. In the region of the WIE and APF, the classical food web represented the main sink for daily primary production. Within the SIE and APF, the grazer-mediated carbon flux corresponded to 8.4% and 15.4% of the total production, respectively. The low rates of biologically mediated carbon flux resulting from grazing by zooplankton in the SIE can be related to the size structure of the phytoplankton assemblages and the absence of larger macrozooplankton in the region. As a consequence of the low grazing activity, the sinking of dead/senescent phytoplankton cells appears to be the major route for the transfer of carbon from the

*Corresponding author. Tel.: +27 603 8524; fax: +27 46 622 4377.
E-mail address: w.froneman@ru.ac.za (P.W. Froneman).
[1]Present address: Department of Earth and Ocean Sciences, University of British Columbia, 6339 Stores Road, Vancouver, BC, Canada V6T 1Z4.

0967-0645/$ - see front matter © 2004 Elsevier Ltd. All rights reserved.
doi:10.1016/j.dsr2.2002.09.001

surface waters to depth in the SIE. Results of the investigation suggest that the efficiency of the biological pump in t three regions of investigation was largely determined by the zooplankton community composition and the structure the local phytoplankton community.
© 2004 Elsevier Ltd. All rights reserved.

1. Introduction

The role of the oceans in the global carbon cycle is presently a leading concern in oceanographic studies (Takahashi and Azevedo, 1982; Metzl et al., 1991; Murphy et al., 1991; Legendre and Michaud, 1998). The Southern Ocean is an immense area of close to 38 million km^2 of open water. Due to its large geographic extent and its abundant supply of nutrients, it is expected that the Southern Ocean will have a major influence on the global carbon cycle. Although the ocean is characterised by an abundant supply of nutrients in the surface waters, total phytoplankton production in the open waters of the Southern Ocean is generally low, $<0.5\,g\ C\,m^{-2}\,d^{-1}$ (Allanson et al., 1981; Hayes et al., 1984; El-Sayed, 1988; Jacques, 1989; Laubscher et al., 1993; Jochem et al., 1995). As a consequence, the Southern Ocean is regarded as a high-nutrient low-chlorophyll (HNLC) region. There are, however, areas of elevated production including the vicinity of frontal regions (Laubscher et al., 1993; Bradford-Grieve et al., 1997), the Marginal Ice-edge Zone (MIZ) (Bathmann et al., 1997; Boyd et al., 1995;El-Sayed, 1988; Smith and Nelson, 1985; Whitehouse et al., 1996; Saggiomo et al., 1998) and the neritic regions of Antarctica and oceanic islands (El Sayed, 1971; von Bodungen et al., 1981; Savidge et al., 1995; Arístegui et al., 1996; Moline and Prezelin, 1996). In these regions, total phytoplankton production may exceed $1\,g\ C\,m^{-2}\,d^{-1}$ (Sullivan et al., 1993; de Baar et al., 1995; Bradford-Grieve et al., 1997; Saggiomo et al., 1998). The factors responsible for the increased production in these regions have been reviewed in detail in El-Sayed (1988) and Priddle et al. (1992). These include the vertical stabilisation of the water column (Holm-Hansen et al., 1977; Perissinotto et al., 1990; Sakshaug and Slagstad, 1992; Laubscher et al., 1993), seawater temperature (Jacques, 1983) and chemical processes such as trace metal availabili (iron and chelators) (Martin et al., 1990; de Ba et al., 1995).

The flux of photosynthetically fixed carbon ou of the photic zone is a central element in th cycling of carbon in the oceans (Broecker an Peng, 1982; Berger et al., 1989; Priddle et al., 199 Falkowski et al., 1998). Photosynthesis and th export of organic carbon from the surface wate as dissolved or particulate organic carbon (result ing from sedimentation or grazing by zooplank ton) act as a "biological pump" which lowers th partial pressure of CO_2 in surface waters resultin in the drawdown of atmospheric CO_2 (Huntle et al., 1991; Longhurst, 1991; Wefer and Fisher 1991; Siegenthaler and Sarmiento, 1993). Th efficiency of the biological pump is determine by the rate of carbon transfer to depth, which i largely a function of the partitioning of phytogenic carbon between the various size classes of the grazers (Longhurst, 1991; Fortier et al., 1994; Legendre et al., 1993; Froneman et al., 1996a 1997). Phytoplankton production is channelled into the microbial loop or the classical food web (Longhurst, 1991; Siegenthaler and Sarmiento, 1993; Legendre and Michaud, 1998). In the microbial loop, recycling is rapid but the system is a weak exporter of organic matter to the deep layers (Longhurst and Harrison, 1989; Fahnenstiel et al., 1995). In contrast, the classical food web is generally characterised by the export of carbon to depth through the sinking of phytoplankton cells and the production of large fast-sinking faecal pellets with a high carbon content (Longhurst and Harrison, 1989; Fortier et al., 1994). The partitioning of carbon between the two food webs is largely determined by the size composition of the phytoplankton assemblages. Generally, in regions dominated by large cells, phytoplankton production is channelled into the classical food web while the microbial loop represents the sink

or production in areas dominated by small hytoplankton (Fortier et al., 1994; Froneman t al., 1997).

The role of the Southern Ocean in the global arbon cycle is a leading concern in physical and iological oceanographic studies. Several multi-isciplinary studies in different sectors of the outhern Ocean, including the Bellingshausen nd Weddell Seas, have been conducted (Turner nd Owens, 1995). However, the extreme varia-ility in the physico-chemical parameters and onsequently biological processes in the different ectors of the ocean suggest that to fully under-tand the role that frontal regions and MIZ play n the carbon cycle of the Southern Ocean, urther studies in other sectors are required. he main aims of the present study were to letermine the relative importance of various actors (including physical, chemical and biologi-al) that control primary production and to assess he consequences of these factors on the biogenic arbon flux in the eastern Atlantic sector of the outhern Ocean in austral summer 1997/1998. Within the sector, three different regions were onsidered, the Spring Ice-edge Zone (SIE), Antarctic Polar Front (APF) and Winter Ice-edge Zone (WIE).

2. Materials and methods

2.1. Size fractionated primary production

Water samples for chlorophyll-*a* (chl-*a*) and size-fractionated primary productivity were collected in the three zones along a south–north transect between 60°24.57′ S and 49°49.51′ S along 6°00′ E meridian aboard the S.A. *Agulhas* during a collaborative Scandinavian/South African Antarctic cruise conducted during December/January 1997–1998 (Fig. 1). The transect SIE was occupied from 4 to 10 January, the transect in the WIE was occupied over the period 14–16 January, while the transect in the vicinity of the APF was occupied from 28 till 31 January 1998. The APF position was defined as the northern most extent of the 2 °C isotherm (Turner et al., 2004). The SIE coincided with the ice edge which was crossed during the southbound underway transect conducted in early December 1997. Finally, the WIE represented the northern boundary of the winter ice, which coincided with the negative subsurface isotherms (Turner et al., 2004).

Conductivity, temperature and pressure measurements at each production station were made using a Neil Brown MK II CTD. Mixed layer depths were assumed to correspond to the depth where a change in ρT of 0.02 units from the stable surface value occurred (JGOFS, 1994). Daily photosynthetic active radiation (PAR, 400–700 nm) was measured using a Li-Cor 4π spherical quantum sensor (LI 1935 A) and Li-Cor data logger (LI-1000) logging 10–15 min means throughout the day. The subsurface light field was measured using the same instrument and used to calculate the sampling depths corresponding to the 100%, 50%, 25%, 10%, 5% and 1% light depths. Water samples from the corresponding depths were taken from 12 L Niskin seawater bottles mounted to a teflon-coated stainless steel rosette frame carrying the CTD.

Size-fractionated primary production, defined as the uptake of inorganic carbon into particulate matter, was measured with the method adapted from Evans et al. (1987) and JGOFS Protocols (1994). Water samples (250 mL), in triplicate for the productivity measurements, were collected and incubated with 50 μCi sodium bicarbonate ($NaH^{14}CO_3$) for 24 h on deck in light-gradient incubators. The incubators consisted of Perspex sleeves covered with neutral density screens to simulate light intensity of depth of collection. The neutral density screens were calibrated using a Biospherical Instruments quantum metre (Model QSP- 170) probe. The incubators were cooled with running surface water obtained from the scientific seawater supply. Temperatures within the incubators were maintained to within 1 °C of the sea surface temperatures.

After incubation, the water samples were gently filtered (<710 mm Hg) onto Nitex mesh (20 μm pore size) and isopore membrane (Millipore) filters (2.0 and 0.2 μm pore size). Each filter was then placed into a glass scintillation vial and 0.5 mL 3 M HCl added. The vials were then placed in a shaker under the fume hood for 2 h to ensure that

Fig. 1. Cruise track and position of primary production stations occupied during a collaborative Scandinavian/South Africa Antarctic expedition to the region of the eastern Atlantic sector of the Southern Ocean in late austral summer (December 97–Januar 98). APF = Antarctic Polar Front; SIE = Spring Ice-Edge Zone; WIE = Winter Ice-Edge Zone.

all non-biologically precipitated labelled carbon evaporated. Time-zero controls were treated as above. Packards UltraGold XR fluor (10 mL) was added to each sample and the radioactivity was determined using a Beckman LS-133 liquid scintillation system. All counts (cpm) were converted to disintegrations per minute (dpm) by the external standard ratio method.

Total areal production at each station wa estimated employing the following equation:

$$(\text{mg C m}^{-3}\,\text{d}^{-1}) = ((\text{SDPM}/\text{V})*(\text{W})/\text{TDPM})*(1.05/T),$$

where SDPM = DPMs in filtered samples, V = volume of filtered sample (L), TDPM = total ^{14}

)PMs (in 0.05 L), W = DIC concentration in amples, 1.05 = correction for the lower uptake of ^{14}C compared to ^{12}C, and T = time (days). DIC oncentrations were determined using the potenometric titration method (Almgren et al., 1983).

Size-fractionated chl-*a* concentrations at each ght depth were determined by gently (<710 mm Ig) filtering 250 mL water samples through 20 μm Nitex), 2.0 μm (Millipore) and Whatman GF/F lters, extraction in the dark in 90% acetone for 4 h at −20 °C and measuring the fluorescence efore and after acidification with 10% HCl on a urner Designs 10 AU fluorometer (Holm-Hansen nd Riemann, 1978). The fluorometer was calirated against a Chl-*a* standard (Sigma). Areal hl-*a* and productivity were obtained by trapezoial integration (Froneman et al., 2001).

.2. Biogenic carbon flux

Since the grazing impact of metazoans (meso- nd macrozooplankton) was only estimated at six tations during the investigation (three in the SIE, ne in the WIE and two in the APF), a single nodel for each region will be presented below. A ummary of the grazing impact of the various size lasses of zooplankton on daily primary production is presented in Table 1. A detailed description f the materials and methods employed to estimate he grazing impact of the zooplankton are resented in Froneman (2004) and Pakhomov nd Froneman (2004b). The grazing impact of rotozooplankton within the three regions of investigation was estimated employing the seawater dilution technique while the impact of the larger zooplankton was determined using the gut fluorescent technique (Froneman, 2004; Pakhomov and Froneman, 2004b). A carbon to chlorophyll ratio of 50 was assumed to estimate the daily production consumed by herbivorous zooplankton (Froneman et al., 1997). Grazing by protozooplankton was assumed not to contribute to the export of phytogenic carbon to depth (Longhurst, 1991; Moloney and Field, 1991; Fahnenstiel et al., 1995). An average assimilation efficiency of 70% for the entire zooplankton community was assumed (Froneman et al., 1997). No distinction was made between the sedimentation rates of meso- and macrozooplankton faecal pellets. All faecal material from the larger zooplankton (>200 μm) was assumed to sediment to depth. Only the role of herbivorous zooplankton in biogenic carbon flux was considered as they contributed up to 80% of the numerical abundance of the zooplankton in the region of investigation (Pakhomov and Froneman, 2004a). Carnivorous zooplankton were, therefore, unlikely to have made a substantial contribution to biogenic carbon flux. Finally, senescence and sinking of phytoplankton cells was assumed to correspond to 5% of the total daily production (Murphy et al., 1998).

Table 1
Average grazing impact of the protozooplankton and metazoans on total primary production at stations occupied within the SIE, WIE and APF

	Bio-stations		
	SIE	WIE	APF
Zooplankton group			
Protozooplankton	31.7 (12.6)	25.9 (5.6)	86.3 (11.8)
Metazoans	30.9 (6.4)	157.1	225.1 (73.6)

Results presented are in mg C $m^{-2} d^{-1}$. Values in brackets are standard deviation. Standard deviation values for metazoan grazing impact in the WIE are not shown as only a single bio-station was occupied.

3. Results

3.1. Hydrographical conditions

The overall hydrography of the study area is discussed elsewhere (Turner et al., 2004). Here a summary of the hydrological conditions at the primary production stations is presented (Table 2). No sea-ice was encountered during the survey. Cloud cover ranged from 4/8 to 8/8 with wind speeds ranging from 4.1 to 17.8 m s^{-1} (Table 2). Sea surface temperatures in the SIE ranged between −0.28 and 0.09 °C, between 0.12 and 0.27 °C in the WIE and between 3.52 and 3.74 °C in the region of the APF. At stations occupied in the SIE, salinities displayed a distinct trend. At the four southernmost stations (D098, D126, D134

and D162), salinity values were 33.8 in the top 30 m while at the northerly stations (D172 and D199), the values were >34.0 throughout the euphotic zone (corresponding to a depth of approx. 70 m). At stations in the WIE (D233 and D258) salinities ranged between 34.2 and 34.30 in the euphotic zone (up to 90 m depth). In the vicinity of the APF (stations D316, D341, D351, D368) salinity values of 33.8 were recorded throughout the euphotic zone (up to 105 m).

Mixed layer depths displayed a general increase along the south–north transect (Fig. 2). With the exception of stations D233 and D258 occupied within the region of the WIE, euphotic depth exceeded the mixed layer depths (MLD) (Fig. 2).

Table 2
Summary of environmental conditions at production stations occupied in the eastern Atlantic sector of the Southern Ocean (December 97–February 98)

Station	Sea temp. (°C)	Air temp. (°C)	Wind speed ($m s^{-1}$)	Cloud cover	Sea State
SIE					
D098	−0.28	0.2	7.1	6/8	3
D126	0.09	−0.2	4.5	5/8	2
D134	−0.05	−0.5	13.9	8/8	5
D162	−0.06	−0.1	17.0	3/8	6
D172	0.03	1.4	10.3	3/8	2
D199	0.06	−0.2	16.8	8/8	6
WIE					
D233	0.12	1.2	12.3	8/8	5
D258	0.27	1.3	8.1	7/8	4
APF					
D316	3.72	3.2	14.4	7/8	6
D341	3.74	2.7	8.7	8/8	3
D351	3.52	4.7	9.2	4/8	3
D378	3.56	6.4	17.8	8/8	7

SIE = Spring Ice-Edge Zone; WIE = Winter Ice Edge Zone; APF = Antarctic Polar Front.

3.2. *Size-fractionated primary production*

3.2.1. *Integrated chlorophyll*

Total areal Chl-*a* concentrations in the SIE ranged from 21.2 to 55.4 mg Chl-*a* m^{-2} (Fig. 3). Microphytoplankton formed the most important contributor to total pigments at all stations comprising between 68% and 76% of the total. Microphytoplankton integrated biomass in the SIE ranged from 15.4 to 39.7 mg Chl-*a* m^{-2}. Nanophytoplankton biomass ranged between 2.6 and 8.7 mg Chl-*a* m^{-2} and picophytoplankton between 3.1 and 5.9 mg Chl-*a* m^{-2} (Fig. 3). There were no distinct differences in the Chl-*a* profiles of the three size fractions in the euphotic depth within the three regions of investigation.

In the WIE, total integrated chlorophyll concentrations ranged from 16.7 to 23.3 mg Chl-*a* m^{-2} (Fig. 3). A considerable shift in the size composition of the phytoplankton assemblages was evident with the smaller nano- and picophytoplankton cells contributing between 71% and 73% of the total pigment. Integrated pico- and nanophytoplankton values ranged between 6.5 and 7.8 mg Chl-*a* m^{-2} and between 5.7 and 8.8 mg Chl-*a* m^{-2},

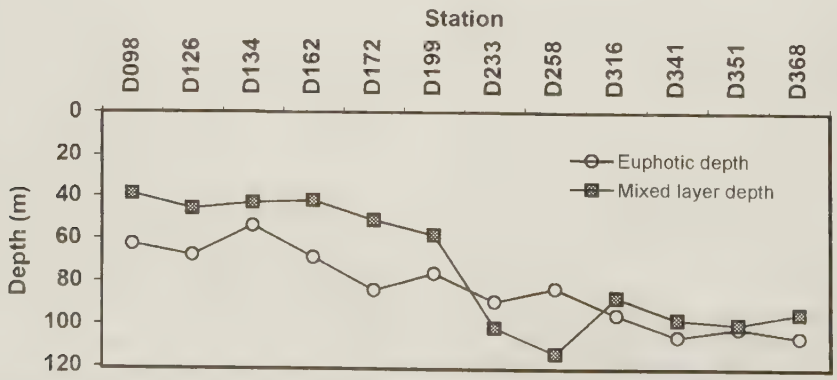

Fig. 2. Relationship between mixed-layer depth and euphotic depth at stations occupied within the three regions of investigations.

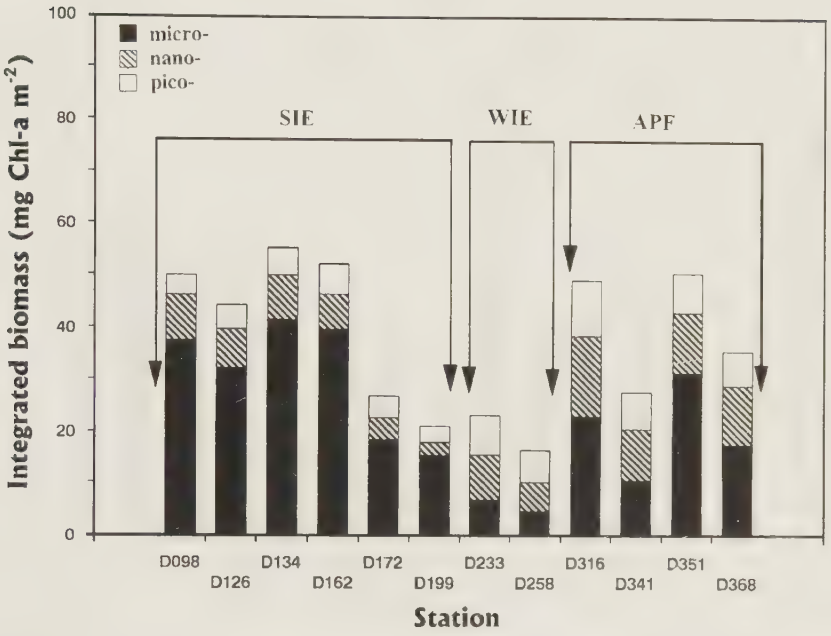

Fig. 3. Total size-fractionated phytoplankton chl-*a* concentrations at stations in the vicinity of the SIE, WIE and APF in December 1997–February 1998. All data are integrated to the 1% euphotic depth. Micro = microphytoplankton (>20 μm); Nano = nanophytoplankton (2–20 μm); Pico = picophytoplankton (<2 μm). SIE = Spring Ice-Edge Zone; WIE = Winter Ice-Edge Zone; APF = Antarctic Polar Front.

respectively (Fig. 3). Microphytoplankton comprised <29% of the total pigment at all stations occupied within the WIE. Total integrated Chl-*a* biomass at stations in the vicinity of the APF ranged between 27.9 and 50.5 mg Chl-*a* m^{-2} (Fig. 3). Microphytoplankton integrated biomass ranged between 10.8 and 23.0 mg Chl-*a* m^{-2} or between 35% and 65% of the total pigment. Nanophytoplankton represented the second most important fraction (Fig. 3). Integrated nanophytoplankton biomass ranged between 9.9 and 15.5 mg Chl-*a* m^{-2}. Picophytoplankton always contributed <25% of the total integrated biomass at all stations (Fig. 3).

3.2.2. *Integrated primary production*

Total daily integrated production within the three regions of investigation displayed the same spatial pattern as integrated biomass. Generally the highest integrated production rates were recorded at stations occupied in the vicinity of the SIE and APF (Fig. 4). Integrated primary production at stations in the SIE ranged from 317 to 887.3 mg C m^{-2} d^{-1} (Fig. 4). In this zone microphytoplankton were the most important contributor to total production comprising between 60% and 73% of the total. Total daily integrated microphytoplankton production ranged from 230.6 to 633.1 mg C m^{-2} d^{-1} (Fig. 4). Nanophytoplankton integrated production ranged between 62.3 and 246.7 mg C m^{-2} d^{-1}, while the picophytoplankton production ranged between 24.1 and 77 mg C m^{-2} d^{-1} (Fig. 4).

Total integrated production in the WIE ranged between 292.8 and 317.9 mg C m^{-2} d^{-1} (Fig. 4). In this region, nanophytoplankton was the most important contributor to total productivity comprising between 44% and 52% of the total (Fig. 4). Picophytoplankton was the second most important contributor to total production comprising up to 26% of the total. Daily integrated picophytoplankton production values ranged between 76.5 and 83.6 mg C m^{-2} d^{-1} while nanophytoplankton production ranged from 141.1 to 152.7 mg C m^{-2} d^{-1} (Fig. 4). At stations occupied in the vicinity of the APF, total daily integrated

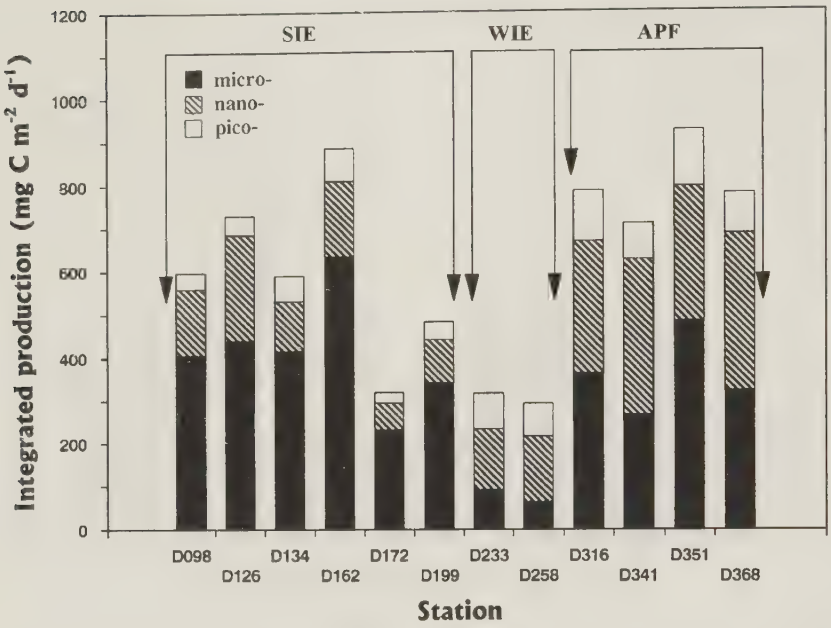

Fig. 4. Total integrated size-fractionated phytoplankton primary production measurements at stations occupied in the vicinity of the SIE, WIE and APF in December 1997 February 1998. All data are integrated to the 1% euphotic depth. Abbreviations as in Fig. 3.

production ranged from 708.5 to 926.8 mg $C\,m^{-2}\,d^{-1}$ (Fig. 4). Microphytoplankton was the most important contributor to total production at stations D316 and D351, while nanophytoplankton dominated total production at stations, D341 and D378 (Fig. 4). Total daily integrated microphytoplankton production ranged from 264.7 to 483.5 mg $C\,m^{-2}\,d^{-1}$ while nanophytoplankton production ranged between 304.5 and 364.1 mg $C\,m^{-2}\,d^{-1}$. Picophytoplankton production ranged from 84.7 to 132.3 mg $C\,m^{-2}\,d^{-1}$ (Fig. 4).

3.3. *Biogenic carbon flux*

The partitioning of phytogenic carbon between the classical food web, dominated by metazoans, and microbial loop (protozooplankton) was similar (34.9 vs. 31.7 mg $C\,m^{-2}\,d^{-1}$) in the SIE (Fig. 5). Biologically mediated carbon flux resulting from the grazing by the metazoans was equivalent to 9.3 g $C\,m^{-2}\,d^{-1}$ (Fig. 5). These rates correspond to a transfer of 1.5% of the total daily production to depth. The sinking of dead/senescent phytoplankton cells was equivalent to 30.1 mg $C\,m^{-2}\,d^{-1}$, which accounted for 74% of the total biogenic carbon flux to depth.

Within the WIE average, total daily productivity corresponded to 305 mg $C\,m^{-2}\,d^{-1}$ (Fig. 6). Microzooplankton and metazoan grazing impact was equivalent to 25.9 and 157.1 mg $C\,m^{-2}\,d^{-1}$, respectively. Collectively, metazoans were responsible for the transfer of 15.4% of the total phytoplankton production to depth. The sinking of dead/senescent phytoplankton cells contributed 15.3 mg $C\,m^{-2}\,d^{-1}$ or 24% of the total carbon transported to depth (Fig. 6).

Total average daily phytoplankton production at stations occupied in the region of the APF was the highest during the entire investigation corresponding to 799.9 mg $C\,m^{-2}\,d^{-1}$ (Fig. 7). Protozooplankton and metazoan grazing impact was equivalent to 86.3 and 225.1 mg $C\,m^{-2}\,d^{-1}$, respectively (Fig. 7). Grazing by the metazoans was responsible for the transfer of up to 67.5 mg $C\,m^{-2}\,d^{-1}$ or 8.4% of the total daily production to depth. The sinking of dead/senescent cells was responsible for transferring 40 mg $C\,m^{-2}\,d^{-1}$ to depth. This value corresponded to 37% of the total biogenic carbon transported to depth (Fig. 7).

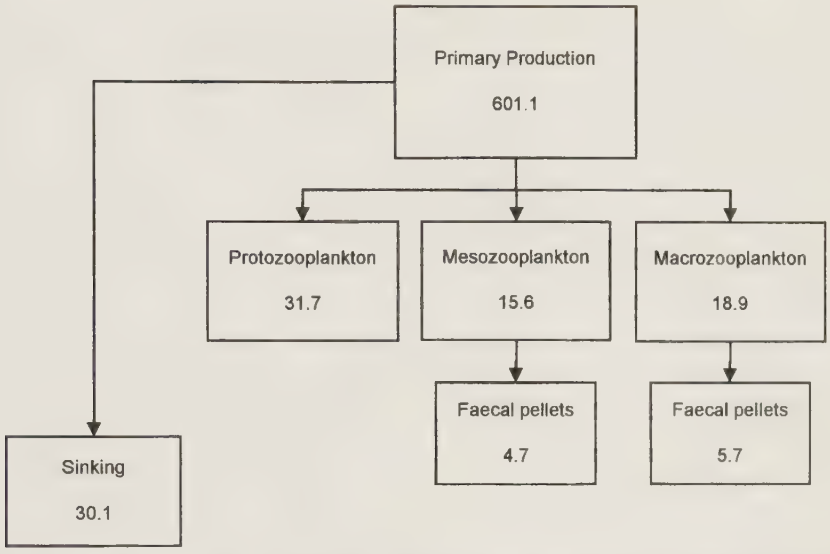

Fig. 5. Total integrated primary production and estimates of vertical carbon flux resulting from grazing activity of zooplankton and sinking of phytoplankton cells in the SIE of the eastern Atlantic sector of the Southern Ocean in austral summer (December 97–January 98). Units are mg C $m^{-2} d^{-1}$.

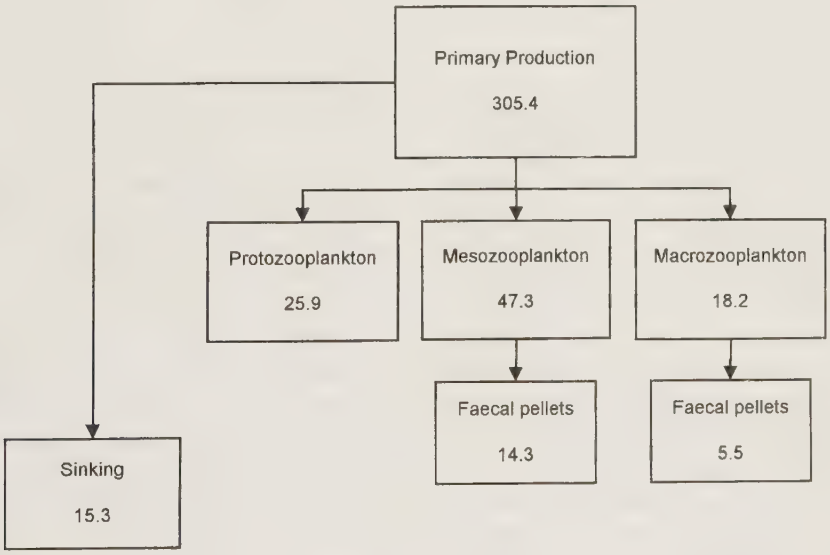

Fig. 6. Total integrated primary production and estimates of vertical carbon flux resulting from grazing activity of zooplankton and sinking of phytoplankton in the WIE of the eastern Atlantic sector of the Southern Ocean in austral summer (December 97–January 98). Units are mg C $m^{-2} d^{-1}$.

4. Discussion

4.1. Size-fractionated primary production studies

Total integrated chl-*a* biomass and production were highest in the region of the SIE and in the vicinity of the APF (Figs. 3 and 4). The estimates of integrated primary production at stations occupied within the vicinity of these two features are in agreement with previous studies conducted in the region of the APF and MIZ in different sectors of the Southern Ocean (Weber and

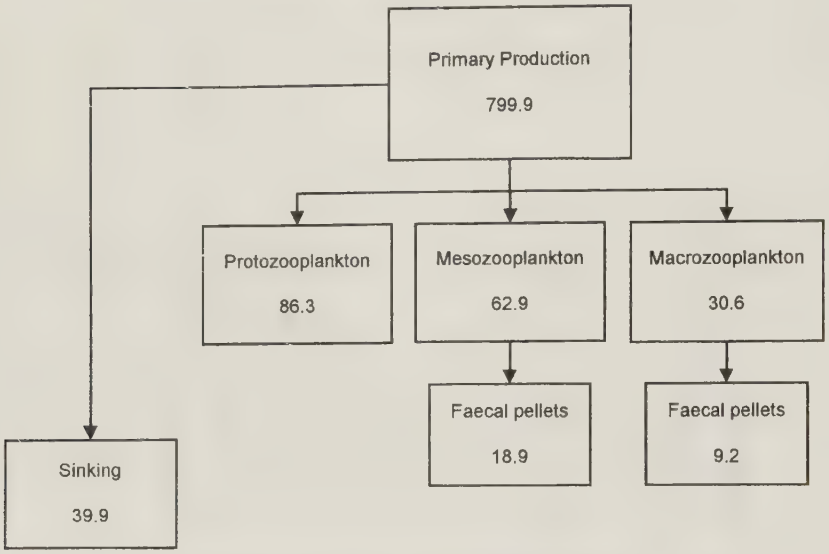

Fig. 7. Total integrated primary production and estimates of vertical carbon flux resulting from grazing activity of zooplankton and sinking of phytoplankton in the region of the APF in the eastern Atlantic sector of the Southern Ocean in austral summer (December 97–January 98). Units are mg $C\,m^{-2}\,d^{-1}$.

El-Sayed, 1987; Laubscher et al., 1993; Boyd et al., 1995; Smetacek et al., 1997; Froneman et al., 2001). It is generally accepted that macronutrient concentrations south of the APF are above the threshold, which would limit primary production (El-Sayed, 1988; Laubscher et al., 1993; Froneman et al., 2001). As a consequence, it is unlikely that the observed pattern in primary production during this study reflects the availability of macronutrients. At stations occupied in the region of the SIE and APF, the euphotic depth (Eu) exceeded the mixed layer depth (MLD) (Fig. 2). These data suggest that high production rates recorded in the region of the SIE and APF could partially be attributed to a favourable light environment. Indeed, at stations occupied in the vicinity of these two features, the ratio of Eu to MLD accounted for up to 53% of the total variance associated with total primary production ($P<0.05$). The occurrence of a shallow MLD in the region of retreating ice is well documented and can be related to the release of freshwater during the ice melt, which confers local water column stability (Laubscher et al., 1993; Froneman et al., 1997). Although no sea-ice was observed at stations in the SIE, the low salinity values recorded at stations in the SIE clearly demonstrate the continual influence of the sea-ice retreat on the water column. Water column stability in the region of the retreating ice may be further enhanced by the summer capping of the colder winter waters. It is worth noting that the increase in MLD along the south–north transect in the SIE was coupled with a general decrease in total integrated primary production (Figs. 2 and 4). These facts suggest that the effect of sea-ice melt had partially been eroded at the northern stations within the SIE. Increased water column stability in the region of the APF is thought to result from the interaction of colder Antarctic surface waters with the warmer Polar Frontal zone waters, which confers localised water column stability in the region of the front (Laubscher et al., 1993). Finally, it is not impossible that the increased primary production rates recorded in the vicinity of the APF may be associated with seawater temperature (Laubscher et al., 1993). Neori and Holm-Hansen (1982) showed that the maximum assimilation rates for Antarctic phytoplankton occurred at seawater temperatures ranging between 2 and 5 °C, well

within the temperature range spanning the APF (Table 1). Unfortunately, the spatial resolution of this study does not allow us to test this hypothesis.

Total integrated chl-*a* biomass and production at stations occupied in the WIE were <25 mg Chl-*a* m^{-2} and <320 mg C m^{-2} d^{-1}, respectively (Figs. 3 and 4). The estimates of biomass and production presented here are in the same range as those reported for open water stations in the Southern Ocean (Laubscher et al., 1993; Froneman et al., 2001). It is now generally well accepted that small nano- and picophytoplankton dominate total primary production in the open waters of the Southern Ocean (Weber and El-Sayed, 1985; Jacques, 1989; El-Sayed, 1988; Laubscher et al., 1993; Froneman et al., 2001). The predominance of small phytoplankton cells in these regions is thought to reflect the unfavourable light environment, which favours the growth of small phytoplankton cells (Fogg, 1991). The predominance of small nano- and picophytoplankton and the presence of MLD which exceeded Eu at stations occupied in the WIE suggest that this region can be considered as an open water region. It is worth noting that the production rates at stations occupied in the northern sector of the SIE are in the same range as those reported for the WIE (Fig. 4). These facts suggest that the effect of sea-ice melt on the water column had partially been eroded at the stations occupied in the northern region of the SIE. Evidence to support this hypothesis includes increased salinity values and MLD (Fig. 2).

The important role of iron (Fe) availability in limiting primary production in the Southern Ocean is now well documented (Martin et al., 1990; de Baar et al., 1995; Boyd and Law, 2001). Preliminary results of the iron study conducted in parallel to the size-fractionated primary production study indicated that Fe concentrations (10 m) were highest (up to 1.6 nM) at stations in the southern region of the SIE and lowest at the northern boundary of the APF (<0.4 nM). Intermediate concentrations, ranging between 0.4 and 1.15 nM, were recorded at the northernmost stations of the SIE, the WIE and at stations occupied at the southern boundary of the APF (Croot et al., 2004). Although the correlation between iron concentration and primary production during this study was not significant ($P<0.05$), there are several important points that require further discussion. Firstly, the decrease in total integrated primary production along the south–north transect in the SIE corresponded to the observed pattern in Fe concentration. Secondly, despite the moderately high concentrations of Fe in the WIE, total production was the lowest during the entire investigation. These facts suggest that while a favourable light environment is a prerequisite for elevated primary production in the Southern Ocean, Fe availability likely determines the magnitude of the increase.

4.2. Biogenic carbon flux

Biogenic carbon flux resulting from the grazing of zooplankton was highest at stations occupied in the region of the WIE, where up to 15.4% of the total primary production was transported to depth (Fig. 6). In contrast to the WIE, in the region of the SIE and APF, grazer-mediated carbon flux accounted for $<8\%$ of the total primary production (Figs. 5 and 7). The estimates of the contribution of zooplankton to total vertical carbon flux are in agreement with a recent study conducted in the Lazarev Sea (Pakhomov et al., 2002). The spatial variability in grazer-mediated biogenic carbon flux in the three regions of investigation appears to be related to both the phytoplankton and zooplankton community structure. A feature of the zooplankton community during the study was the virtual absence of larger macrozooplankton in the region of investigation. Indeed, mesozooplankton always accounted for $>70\%$ of the total zooplankton biomass (Pakhomov and Froneman, 2004a). In the WIE, total chl-*a* was dominated by nanophytoplankton, which is the optimum size particle for mesozooplankton (Fortier et al., 1994). The high rates of biogenic carbon flux resulting from grazing by zooplankton in the WIE are, therefore, not surprising. In contrast to the WIE, Pakhomov and Froneman (2004a) suggested that the grazing impact of mesozooplankton in the region of the SIE and APF was constrained by the size structure of the local phytoplankton assemblages. In the

APF region, microphytoplankton comprising chain forming and pennate diatom species of the genera *Chaetoceros* and *Proboscia* contributed most to phytoplankton biomass while in the region of the SIE chain forming species and the prymnesiophytes, *Phaeocystis* spp. dominated the phytoplankton community (Froneman, P.W., unpublished data).

The sinking of dead/senescent phytoplankton cells has been identified as an important mechanism for the transportation of carbon to depth in the region of the retreating sea-ice and oceanic frontal systems of the Southern Ocean (von Bodungen et al., 1986; Fischer et al., 1988; Murphy et al., 1998; Pakhomov et al., 2002). A recent study conducted in different oceanic provinces showed that the sinking of ungrazed large diatoms represented the key determinant of the magnitude of downward POC in the ocean (Boyd and Newton, 1999). During this study sinking of dead/senescent phytoplankton cells corresponded to 76% and 37% of the total biogenic carbon transported to depth in the SIE and APF, respectively (Figs. 5 and 7). In both regions, microphytoplankton comprising mainly diatoms contributed most to phytoplankton biomass (Froneman, P.W., unpublished data). In the region of the WIE where nanophytoplankton dominated total chl-*a*, the sedimentation of phytoplankton comprised only 24% of the total biogenic flux. Low rates of sedimentation of phytoplankton in the open ocean environment of the Southern Ocean have previously been documented and can be related to the predominance of small phytoplankton cells in these regions which have low sinking rates (Fischer et al., 1988).

It should be pointed out that the results presented here should be regarded with caution due to possible sources of error. For example, we have assumed an average assimilation efficiency of 70% for the entire zooplankton community. Clearly this value will vary considerably between the various groups of zooplankton. Similarly, it was assumed that grazing by protozooplankton does not contribute to the export of carbon to depth. However, a study conducted in the Weddell Sea showed that faecal pellets protozoan in origin were sampled at depths >100 m, suggesting that protozooplankton grazing may at times contribute to vertical carbon flux (Nöthig and von Bodungen, 1989). Following this, it is well documented that all the major zooplankton groups in the high Antarctic region feed on protozooplankton (Atkinson, 1996; Froneman et al., 1996b). Production originating from the microbial loop will thus be transferred to depth, increasing the local efficiency of the biological pump. The magnitude of this transfer is presently still unknown. Finally, we have not taken into account the phenomenon of copraphagy.

In conclusion, results of this study suggest that the relative efficiency of the biological pump in the three regions of investigation appeared to be related to both the size structure of the local phytoplankton assemblages and the zooplankton community structure. In both the SIE and APF regions, the local phytoplankton assemblages were too large to be efficiently grazed on by mesozooplankton which dominated the zooplankton community. As a consequence, in these regions $<8\%$ of total daily primary production was transported to depth. In contrast, in the region of the WIE, a favourable size structure of the phytoplankton community coupled with high biomass of zooplankton resulted in up to 15% of the total daily phytoplankton production being transported to depth. These facts suggest regional variability in the efficiency of the biological pump. These data are supported by pCO_2 studies conducted in parallel to this investigation, which showed that the WIE region represented a strong sink for atmospheric CO_2 while the regions of the APF and SIE were weak sinks (Chierici et al., 2004).

Acknowledgements

We would like to thank the Swedish Polar Secretariat, the Department of Environmental Affairs and Tourism, South Africa, and Rhodes University for providing funds and facilities for this study. Our thanks go the officers and crew of the research vessel S.A. *Agulhas* for their invaluable assistance at sea. Finally, the successful completion of the cruise would not have been possible without the invaluable

assistance of all our colleagues who participated in the cruise.

References

Allanson, B.R., Hart, R.C., Lutjeharms, J.R.E., 1981. Observations on the nutrients, chlorophyll and primary production of the Southern Ocean south of Africa. South African Journal of Antarctic Research 10, 3–14.

Almgren, T., Dyrssen, D., Fonselius, S., 1983. Determination of alkalinity and total carbonate. In: Grasshoff, K., Ehrhart, M., Gremling, K. (Eds.), Methods of Seawater Analysis. Springer, Weinheim, p. 419.

Arístegui, J., Montero, M.F., Ballesteros, S., Basterretxea, G., van Lenning, K., 1996. Planktonic primary production and microbial respiration measured by ^{14}C assimilation and dissolved oxygen changes in coastal waters of the Antarctic Peninsula during austral summer: implications for the carbon flux studies. Marine Ecology Progress Series 132, 191–201.

Atkinson, A., 1996. Subantarctic copepods in a oceanic, low chlorophyll environment: ciliate predation, food selectivity and impact on prey populations. Marine Ecology Progress Series 130, 85–96.

Bathmann, U.V., Scharek, R., Klaas, C., Dubischar, C.D., Smetacek, V.S., 1997. Spring development of phytoplankton biomass and composition in major water masses of the Atlantic sector of the Southern Ocean. Deep-Sea Research II 44, 51–67.

Berger, W.H., Smetacek, V.S., Wefer, G., 1989. Ocean productivity and paleoproductivity—an overview. In: Berger, W.H., Smetacek, V., Wefer, G. (Eds.), Productivity of the Ocean: Present and Past. Wiley, New York, pp. 1–34.

Boyd, P.W., Newton, P.P., 1999. Does plankton community structure determine downward particulate organic carbon flux in different oceanic provinces. Deep-Sea Research I, 63–91.

Boyd, P.W., Law, C.S., 2001. The Southern Ocean Iron RElease Experiment (SOIREE)—introduction and summary. Deep-Sea Research II 48, 2425 2438.

Boyd, P.W., Robinson, C., Savidge, G., Williams, P.J., 1995. Water column and sea-ice primary production during Austral spring in the Bellingshausen Sea. Deep-Sea Research II 42, 1177.

Bradford-Grieve, J.M., Chang, F.H., Gall, M., Pickmere, S., Richards, F., 1997. Size fractionated phytoplankton standing stock and primary production during austral winter and spring 1993 in the Subtropical Convergence region near New Zealand. New Zealand Journal of Marine and Freshwater Research 31, 201–224.

Broecker, W.S., Peng, T.H., 1982. Tracers in the Sea. Eldigio Press, Palisades, NY, 690pp.

Chierici, M., Fransson, A., Turner, D.R., Pakhomov, E.A., Froneman, P.W., 2004. Variability in pH, fCO_2, oxygen and flux of CO_2 in the surface water along a transect in the Atlantic sector of the Southern Ocean. Deep-Sea Research II, this issue [doi: 10.1016/j.dsr2.2001.03.002].

Croot, P.L., Andersson, K., Özturk, M., Turner, D.R., 2004. The distribution and speciation of iron along 6°E in the Southern Ocean. Deep-Sea Research II, this issue [doi: 10.1016/j.dsr2.2003.10.012].

de Baar, H.J.W., De Jong, J.T.M., Bakker, D.C.E., Löscher, B.M., Veth, C., Bathmann, U., Smetacek, V., 1995. Importance of iron for plankton blooms and carbon dioxide draw down in the Southern Ocean. Nature 373, 412 415.

El Sayed, S.Z., 1971. Observations on phytoplankton bloom in the Weddell Sea. In: Llano, G.A., Wallen, I.E. (Eds.), Biology of the Antarctic Seas (Ant. Res. Ser. IV), Vol. 17. American Geophysical Union, Washington, pp. 302–312.

El-Sayed, S.Z., 1988. Productivity of the Southern Ocean: a closer look. Comparative Biochemistry and Physiology 90B, 489–498.

Evans, C.A., O'Reilly, J.E., Thomas, J.P., 1987. A handbook for the measurement of chlorophyll and primary production. Biological Investigations of Marine Antarctic Systems and Stocks (BIOMASS), vol. 8. Texas A & M University, College Station, TX, USA.

Falkowski, P.G., Barber, R.T., Smetacek, V., 1998. Biochemical controls and feedbacks on ocean primary production. Science 281, 200–206.

Fahnenstiel, G.L., McCormick, M.J., Lang, G.A., Radalje, D.G., Lohrenz, S.F., Marcowitz, M., Wagoner, B., Garrick, H.J., 1995. Taxon specific growth and loss rates for dominant phytoplankton populations from the northern Gulf of Mexico. Marine Ecology Progress Series 117, 229 239.

Fischer, G., Futterer, D., Gersonde, R., Honjo, S., Ostermann, D., Wefer, G., 1988. Seasonal variability of particle flux in the Weddell Sea and its relation to ice cover. Nature 335, 426–428.

Fogg, G.E., 1991. Tansley Review No. 30. The planktonic ways of life. New Phytologist 118, 191–232.

Fortier, L., Le Fèvre, J., Legendre, L., 1994. Export of biogenic carbon to fish and to the deep ocean: the role of large planktonic microphages. Journal of Plankton Research 16, 809–839.

Froneman, P.W., 2004. Protozooplankton community structure and grazing impact in the eastern Atlantic sector of the Southern Ocean in austral summer 1998. Deep-Sea Research II, this issue [doi: 10.1016/j.dsr2.2004.09.001].

Froneman, P.W., Perissinotto, R., McQuaid, C.D., 1996a. Seasonal variations in microzooplankton grazing in the region of the Subtropical Convergence. Marine Biology 126, 433 442.

Froneman, P.W., Perissinotto, R., McQuaid, C.D., 1996b. Role of microplankton in the diet and daily ration of Antarctic zooplankton species during austral summer. Marine Ecology Progress Series 143, 15 23.

Froneman, P.W., Pakhomov, E.A., Perissinotto, R., Laubscher, R.K., McQuaid, C.D., 1997. Dynamics of the plankton communities of the Lazarev Sea (Southern Ocean)

during seasonal ice melt. Marine Ecology Progress Series 149, 201 -214.

Froneman, P.W., Laubscher, R.K., McQuaid, C.D., 2001. Size fractionated primary production in the south Atlantic and Atlantic sector of the Southern Ocean. Journal of Plankton Research 23, 611–622.

Hayes, P.K., Whitaker, T.M., Fogg, G.E., 1984. The distribution and nutrient status of phytoplankton in the Southern Ocean between 20E and 70E W. Polar Biology 3, 153–165.

Holm-Hansen, O., El-Sayed, S.Z., Franceschini, N.I., Cuhel, R.L., 1977. Primary production and the factors controlling phytoplankton growth in the Southern Ocean. In: Llano, G.A. (Ed.), Adaptations within Antarctic Ecosystems. Smithonian Institute, Washington DC, pp. 11–50.

Holm-Hansen, O., Riemann, B., 1978. Chlorophyll-a determination: improvements in methodology. Oikos 30, 438–447.

Huntley, M.E., Lópes, M.D., Karl, D.M., 1991. Top predators in the Southern Ocean: a major leak in the biological carbon pump. Science 253, 64–66.

Jacques, G., 1983. Some ecophysiological aspects of the Antarctic phytoplankton. Polar Biology 2, 27–33.

Jacques, G., 1989. Primary production in the open Antarctic Ocean during the austral summer. A review. Vie Milieu 39, 1–17.

Jochem, F.J., Mathot, S., Quéguiner, B., 1995. Size-fractionated primary production in the open Southern Ocean in austral spring. Polar Biology 15, 381–392.

JGOFS, 1994. Photosynthesis measurements task team. Report of the meeting held in Carquerianne, September 14–16, 1993.

Laubscher, R.K., Perissinotto, R., McQuaid, C.D., 1993. Phytoplankton production and biomass at frontal zones in the Atlantic sector of the Southern Ocean. Polar Biology 13, 471–481.

Legendre, L., Gosselin, M., Hirche, H.-J., Kattner, G., Rosenberg, G., 1993. Environmental control and potential fate of size-fractionated phytoplankton production in the Greenland Sea (75°N). Marine Ecology Progress Series 98, 297–313.

Legendre, L., Michaud, J., 1998. Flux of biogenic carbon in oceans: size dependant regulation by pelagic food webs. Marine Ecology Progress Series 164, 1–11.

Longhurst, A.R., 1991. Role of the marine biosphere in the global carbon cycle. Limnology and Oceanography 36, 1507–1526.

Longhurst, A.R., Harrison, W.G., 1989. The biological pump: profiles of plankton production and consumption in the upper ocean. Progress in Oceanography 22, 47–123.

Moloney, C.L., Field, J.G., 1991. The size-based dynamics of plankton food webs. I. A simulation model of carbon and nitrogen flows. Journal of Plankton Research 13, 1003–1038.

Martin, J.H., Gordon, R.M., Fitzwater, S., 1990. Iron in Antarctic waters. Nature 345, 156–158.

Metzl, N., Beauverger, C., Brunet, C., Goyet, C., Poisson, A., 1991. Surface water carbon dioxide in the southwest Indian sector of the Southern Ocean: highly variable CO_2 source/sink region in summer. Marine Chemistry 35, 85–96.

Moline, M.A., Prezelin, B., 1996. Long-term monitoring and analyses of physical factors regulating variability in coastal Antarctic phytoplankton biomass, in situ productivity and taxonomic composition over sub-seasonal, seasonal and inter-annual time scales. Marine Ecology Progress Series 145, 143–160.

Murphy, P.P., Feely, R.A., Gammon, R.H., Harrison, D.E., Kimberly, C.K., Waterman, L.S., 1991. Assessment of air–sea exchange of CO_2 in the South Pacific during austral autumn. Journal of Geophysical Research 96, 20455–20465.

Murphy, E.J., Boyd, P.W., Leakey, R.J.G., Atkinson, A., Edwards, E.S., Robinson, C., Priddle, J., Bury, S.J., Robins, D.B., Burkill, P.H., Savidge, G., Owens, N.J.P., Turner, D.R., 1998. Carbon flux in ice-ocean-plankton systems of the Bellingshausen Sea during a period of ice retreat. Journal ff Marine Systems 17, 207–227.

Neori, A., Holm-Hansen, O., 1982. Effect of temperature on rates of photosynthesis in Antarctic phytoplankton. Polar Biology 1, 33–38.

Nöthig, E., von Bodungen, B., 1989. Occurrence and vertical flux of faecal pellets probably protozoan in origin in the southeastern Weddell Sea (Antarctica). Marine Ecology Progress Series 56, 281–289.

Pakhomov, E.A., Froneman, P.W., 2004a. Zooplankton dynamics in the eastern Atlantic sector of the Southern Ocean during the austral summer 1997/1998. Part 1. Community structure. Deep-Sea Research II, this issue [doi: 10.1016/j.dsr2.2000.11.001].

Pakhomov, E.A., Froneman, P.W., 2004b. Zooplankton dynamics in the eastern Atlantic sector of the Southern Ocean during the austral summer 1997/1998. Part 2. Grazing impact. Deep-Sea Research II, this issue [doi: 10.1016/j.dsr2.2000.11.002].

Pakhomov, E.A., Froneman, P.W., Wasserman, P., Ratkova, T., Arashkevich, E., 2002. Contribution of algal sinking and zooplankton grazing to downward flux in the Lazarev Sea (Southern Ocean) during the onset of a phytoplankton bloom: a lagrangian study. Marine Ecology Progress Series 233, 73–88.

Perissinotto, R., Duncombe Rae, C.M., Boden, B.P., Allanson, B.R., 1990. Vertical stability as a controlling factor of the marine phytoplankton production at the Prince Edward Archipelago (Southern Ocean). Marine Ecology Progress Series 60, 205–209.

Priddle, J., Smetacek, V., Bathmann, U., 1992. Antarctic marine primary production, biochemical carbon cycles and climatic change. Philosophical Transactions of the Royal Society of London B 338, 289–297.

Sakshaug, E., Slagstad, D., 1992. Sea ice and wind: effects on primary productivity in the Barents Sea. Atmosphere-Ocean 30, 579–591.

Siegenthaler, U., Sarmiento, J.L., 1993. Atmospheric carbon dioxide and the ocean. Nature 365, 119–125.

Saggiomo, V., Carrada, G.C., Mangoni, O., Riebera d'Alcala, M., Russo, A., 1998. Spatial and temporal variability of

size-fractionated biomass and primary production in the Ross Sea (Antarctica) during austral spring and summer. Journal of Marine Systems 17, 115–127.

Savidge, G., Harbour, D., Gilpin, L.C., Boyd, P.W., 1995. Phytoplankton distributions and production in the Bellingshausen Sea, austral spring 1992. Deep-Sea Research II 42, 1201–1224.

Smetacek, V., de Baar, H.J.W., Bathmann, U.V., Lochte, K., van der Loeff, M.M.R., 1997. Ecology and biogeochemistry of the Antarctic Circumpolar Current during austral spring: A summary of Southern Ocean JGOFS cruise ANT X/6 of RV Polarstern. Deep-Sea Research II 44, 1–21.

Smith, W.O., Nelson, D.M., 1985. Phytoplankton bloom produced by a receding ice edge in the Ross Sea: Spatial coherence with a density field. Science 227, 163–166.

Sullivan, C.V., Arrigo, K.R., McClain, C.R., Comiso, J.C., Firestone, J., 1993. Distribution of phytoplankton blooms in the Southern Ocean. Science 262, 1832–1837.

Takahashi, T., Azevedo, A.E.G., 1982. The oceans as a CO_2 reservoir. In: Reck, R.A., Hummel, J.R. (Eds.), Interpretation of Climate and Photochemical Models, Ozone and Temperature Measurements. American Institute of Physics, New York, pp. 83–109.

Turner, D.R., Owens, N.J.P., 1995. A biochemical study in the Bellingshausen Sea: overview of the STERNA 1992 expedition. Deep-Sea Research II, 907–932.

Turner, D.R., Bertilsson, S., Fransson, A., Pakhomov, E., 2004. The SWEDARP 97/98 marine expedition: overview. Deep-Sea Research II, this issue [doi: 10.1016/j.dsr2.2003.08.006].

von Bodungen, B., Tilzer, M.M., Lutjeharms, J.R.E., 1981. Observations on the nutrients, chlorophyll and primary production of the Southern Ocean south of Africa. South. African Journal of Antarctic Research 10, 3–14.

Weber, L.H., El-Sayed, S.Z., 1987. Contributions of the net, nano- and picoplankton to the phytoplankton standing crop and primary productivity in the Southern Ocean. Journal of Plankton Research 9, 973–994.

Wefer, G., Fischer, G., 1991. Annual primary production and export flux in the Southern Ocean from sediment trap data. Marine Chemistry 35, 597–613.

Whitehouse, M.J., Priddle, J., Trathan, P.N., Brandon, M.A., 1996. Substantial open-ocean phytoplankton blooms to the north of South Georgia, South Atlantic, during summer 1994. Marine Ecology Progress Series 140, 187–197.

ELSEVIER

Deep-Sea Research II 51 (2004) 2731–2744

DEEP-SEA RESEARCH
PART II

www.elsevier.com/locate/dsr2

Impact of ultraviolet-B radiation on the development of phytoplankton communities in the eastern Atlantic sector of the Southern Ocean—results from on-deck model ecosystem experiments

S.-Å. Wängberg[a,*], A. Wulff[b]

[a] *Botanical Institute, Göteborg University, Box 461, SE-405 30 Göteborg, Sweden*
[b] *Department of Marine Ecology, Göteborg University, Box 461, SE-405 30 Göteborg, Sweden*

Abstract

Two model ecosystem experiments to assess the effects of UVB radiation (UVBR, 280–320 nm) on phytoplankton communities were performed on-deck during the SWEDARP 97/98 expedition to the eastern Atlantic sector of the Southern Ocean in January 1998. The first experiment was run in the Spring Ice Edge, around 60 S, and the second at the Antarctic Polar Front, around 50°S. The duration of the experiments were 12 and 10 days, respectively. Ambient UVBR was modified to three levels (i.e. treatments): NoUVB—shielded from UVBR (mylar foil); AMB—ambient UVBR; UVB+—enhanced UVBR. The development of the phytoplankton communities was followed by measuring primary production and composition of pigments and diatom species.

At the start of the first experiment UVB+ had lower primary production per volume, but not when normalised to chlorophyll *a*. At the end there were no differences between treatments in primary production per volume but there were differences when normalised to chlorophyll *a*. In addition, a significant increase in the stimulation of primary production for UVB+ when excluding UVBR and in chlorophyll *a* concentration was found. These changes, together with changes in species composition, are assumed to be the result of an adaptation to the enhanced UVBR. During the second experiment, the effects from changes in UVBR were generally smaller but resembled to some extent the first experiment. The chlorophyll *a* concentration increased significantly in the UVB+ treatment at the end of the experiment and there was a strong tendency towards a reduction in primary production per chlorophyll *a*, but not per volume. The results are important when estimating the effects of increased UVBR as they show variability in short-term sensitivity, and also the capacity of phytoplankton communities to adapt to UVBR and retain primary production even in enhanced UVBR.
© 2004 Elsevier Ltd. All rights reserved.

*Corresponding author. Tel.: +46 31 773 2608; fax: +46 31 773 2626.
E-mail address: swa@botany.gu.se (S.-Å. Wängberg).

0967-0645/$ - see front matter © 2004 Elsevier Ltd. All rights reserved.
doi:10.1016/j.dsr2.2001.05.001

1. Introduction

Since the discovery of the reduction in the stratospheric ozone layer over Antarctica (Farman et al., 1985), the ecological effects following the increased UVB-radiation (UVBR, 280–320 nm; see Table 1 for a list of abbreviations used) have been extensively discussed (e.g. Young et al., 1993; Häder, 1993; Weiler and Penhale, 1994; Rozema et al., 1997; Davidson, 1998). In the Southern Ocean, special attention has been paid to the effects of UVBR on microalgae, assessed primarily by measurements of carbon dioxide fixation in short-term experiments (2–8 h) of which several have been summarised in Prezelin et al. (1994). In various studies, the reduction in primary production has been estimated to be between 0% and 12% (UNEP, 1996).

That UVBR has an inhibiting effect on short-term measurements of carbon dioxide fixation does not, however, mean that UVBR reduces primary production over longer-time scales. There are several ways in which microalgal communities can adapt to changes in the radiation environment, both on the cellular level and by changes in species composition (Karentz, 1994; Davidson, 1998). The primary production can also be indirectly affected, both positively and negatively, by UVBR affecting other parts of the ecosystem, biotic or abiotic (Bushaw et al., 1996; Wetzel et al., 1995; Herndl et al., 1993).

The only way to validate the relevance of short-term measurements for long-term changes is to observe the development of natural communities in model ecosystem experiments (also called mesocosm or microcosm experiments) exposed to different levels of UVBR. Only then is it possible to test the capacity of different parameters to predict the long-term effects of UVBR. Model ecosystem experiments can also give guidance as to which variables should be measured in short-term and culture experiments, and should be used as indicators when monitoring for UVBR effects in the field. Model ecosystem experiments can, however (as any other experimental system), never exactly mimic a natural system. This fact holds true especially for deep oceans with large Upper Mixed Layers and where in situ deployment is not possible.

In this paper, we present data from two model ecosystem experiments performed on deck during the Swedish/South African expedition in the eastern part of the Atlantic sector of the Southern Ocean, January 1998. The experiments were designed to follow the long-term changes in composition (species, pigments), production and short-term sensitivity to UVBR of the phytoplankton communities in the surface layer of the Southern Ocean under ambient radiation regime, with modified UVBR. Two experiments were performed, one in the Spring Ice Edge (SIE) (60°S) and one at the Antarctic Polar Front (APF) (50°S).

Earlier phytoplankton from Antarctica have been exposed for to altered UV spectra in on-deck experiments in Antarctic waters by Helbling et al. (1992). Our experiments are, however, the first on-deck experiment in the Southern Ocean including long-term effects of reduced and enhanced UVBR.

Table 1
Major abbreviations used

PAR	Photosynthetic active radiation (400–700 nm)
UVBR	Ultraviolet B radiation (280–320 nm)
UVB_{BE}	Biological effective UVBR
P_{Vol}	Volume-specific primary production in ambient radiation ($\mu mol\,C\,l^{-1}\,h^{-1}$)
P_{Chl}	Chlorophyll *a* specific primary production ($\mu mol\,C\,\mu g\,chl\,a^{-1}h^{-1}$)
$P_{-UVB/AMB}$	Increase in primary production when UVBR is excluded (% of P_{Vol})
AMB	Aquaria with ambient radiation
UVB+	Aquaria with enhanced UVBR
NoUVB	Aquaria with no UVBR
SIE	Spring Ice Edge, around 60°S
APF	Antarctic Polar Front, around 50°S
chl *a*	Chlorophyll *a* ($\mu g\,l^{-1}$)
chl *b*	Chlorophyll *b* ($\mu g\,l^{-1}$)
chl c_1c_2	Chlorophyll c_1+c_2 ($\mu g\,l^{-1}$)
Per	Peridinin ($\mu g\,l^{-1}$)
19′-but	19′-butanoyloxyfucoxanthin ($\mu g\,l^{-1}$)
fucox	Fucoxanthin ($\mu g\,l^{-1}$)
19′-hex	19′-hexanoyloxyfucoxanthin ($\mu g\,l^{-1}$)
dt	Diatoxanthin ($\mu g\,l^{-1}$)
Allox	Alloxanthin ($\mu g\,l^{-1}$)
Zeax	Zeaxanthin ($\mu g\,l^{-1}$)

2. Materials and methods

2.1. Experimental site

The experiments were performed on-deck of the South African research vessel S.A *Agulhas* during the SWEDARP 97/98 marine expedition in Antarctica. More general descriptions of the expedition, including the meteorological and oceanographic conditions are found in other papers in this special volume. The first experiment (Exp. I), in the SIE between 61.03 and 59.3°S, was run for 12 days (December 28, 1997–January 9, 1998) and the second (Exp. II), in the APF, between 51.61 and 49.01°S, was run for 10 days (January 19–28, 1998). The longitude was 6°W in both experiments. (Fig. 1).

Fig. 1. Map of the eastern Atlantic sector of the Southern Ocean indicating the areas where the experiments were performed (each day is one dot). Arrows indicate the location of the sampling of the start communities.

2.2. The model ecosystem set-up

The model ecosystems consisted of 12 aquaria (40 l) made of UVB transparent acrylic (Altuglas CN UVD, 5 mm) (see Fig. 2 for transmittance spectra), placed in larger boxes through which seawater circulated for temperature control. A UVB transparent acrylic plate was tightly screwed on top of each box and sealed with silicone. The mean water temperature in the aquaria (measured daily in each aquarium) was 3.2 °C (±1.7 s.d.) during Exp. I and 5.8 °C (±0.8 s.d.) during Exp. II. The surface temperature in the sea was 0.2 and 4.0 °C, respectively. The inter-aquaria variation was always less than 1.0 °C.

During commencement of the experiment 500 l of seawater, screened through a 200 μm net, was filled into a polyethylene container. The water was collected with Go-Flo bottles from 10–15 m depth. In Exp. I, the container was filled between 15:45 and 17:15 on December 28 at 61.00°S, 5.56°W, and in Exp. II, at 50.30°S, 6.00°W between 23:25 and 00:20, January 18/19 (see Fig. 1). Thirty litres were distributed to each aquarium, followed by 10 l filtered (0.2 μm) seawater from the ship's non-toxic water supply. The filtration was done with a tangential-flow filter (Minikros, Microgen Inc.). Each aquarium had a tap on the side at the 30 l level through which sampling was done. At

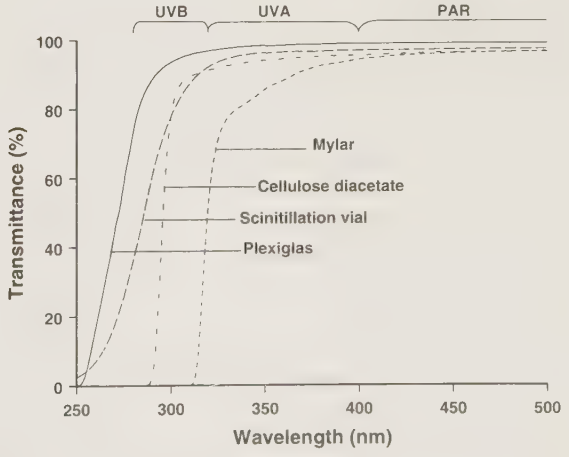

Fig. 2. Transmission spectra of the material used measured on a Shimadzu UV-2401PC spectrophotometer.

approximately 10:00, each day, the water level in all aquaria was reduced to 30 l, and 10 l filtered seawater was added. The system was thus run semi-continuously and the construction ensured that it was possible to sample and support the system even in very rough sea. The semi-continuous dilution made it possible to keep the phytoplankton community growing without increasing the standing stock. The shading from the boxes in which the aquaria were placed and the acrylic plate reduced the incoming radiation by 35%, measured with a 4π-PAR sensor (Biospherical Instruments), central in the aquaria. Using the values for albedo and attenuation in the water from Rasmus et al. (2004), the remaining 65% of the ambient radiation corresponded to the light climate at a depth of 2–3 m for 305 nm and 5–6 m for PAR.

The water turbulence within the aquaria was dependent on the vibration of the ship and its movement in the sea, and on the circulation induced at each water addition. The sea was exceptionally calm, especially during the first experiment, and even if a total turnover took place at each filling, aggregates of algae (mostly *Phaeocystis*) accumulated on the bottom.

2.3. Radiation measurement, ambient and enhanced levels

The ambient radiation was continuously measured (280–700 nm, one scan each 15 min) by a spectroradiometer (Optronics OL754) equipped with a 2π-sensor (see Chen et al., 2004 for details). The biological effective UVBR (UVB_{BE}) was calculated using a Biological Weighting Function (BWF) for the inhibition of primary production of a diatom-dominated Antarctic phytoplankton community (Boucher and Prezelin, 1996). The daily doses of PAR and UVB_{BE} are presented in Fig. 3.

The UVBR was modified to three different levels (i.e. treatments), each run in four parallels: NoUVB—covered by UVB absorbing foil (mylar-D, du Pont, for transmittance spectra, see Fig. 2); AMB—ambient UVBR; UVB+—enhanced UVBR. The enhanced UVBR was given by two UVB fluorescent tubes (Philips TL4W/12) placed on top of each aquarium (on NoUVB and AMB

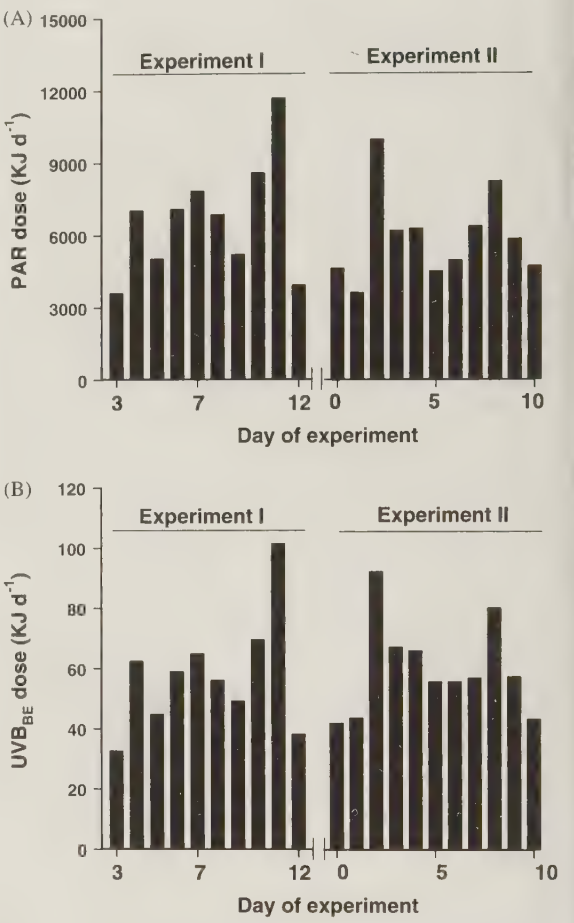

Fig. 3. Daily doses of ambient radiation. Data are not corrected for absorption and reflection by the incubators covers and walls. (A) PAR; (B) $UVBR_{BE}$.

aquaria replicas were placed to give the same degree of shading). To avoid exposure of UVC radiation, a cellulose diacetate film (for the transmittance spectra, see Fig. 2) was placed between the tube and the aquaria and changed daily. The tubes were running for 6 h each day (9:00–15:00). The radiation intensity of each tube was measured daily using a broadband UVB sensor (Vital Technologies). This was necessitated by low temperature enhancing the ageing of the tubes and some exchanges were done. New tubes, that had been preburned for 100 h were used for each experiment. Spectra of an unused tube and one that was employed in Exp. II are shown in Fig. 4. The mean enhancement of the UVBR level

during Exp. I was 0.12 W m^{-2} (s.d. 0.03), and during Exp. II, 0.17 W m^{-2} (s.d. 0.06). UVB doses added were, at the water surface in the aquaria, 2.2 and 3.7 kJ m^{-2} d^{-1} in Exps. I and II, respectively, added UVB_{BE} doses were 7.2 and 11.9 kJ m^{-2} d^{-1}. The larger doses during Exp. II were probably due to higher air temperature making the fluorescence tubes more efficient. The UVB fluorescent tubes also give some UVAR. We did not measure this radiation daily but earlier experiences have shown that the radiation energy within UVAR is about the same as within UVBR.

The resulting increase in UVB doses per day varied depending on the ambient radiation and was, on average, 6.3% (s.d. 2.4) in Exp. I and 10.1% (s.d. 4.44) in Exp. II for unweighted radiation. The ambient UVAR dose was, on average, 16 times the UVBR dose. The increase in UVAR from the tubes was thus less than 1%. For UVB_{BE} the average percentage increase during Exp. I was 20.9% (s.d. 8.2) and for Exp. II, 30.9% (s.d. 14.1) (Fig. 5). Using a Radiation Amplification Factor (RAF) of 0.8 (Boucher and Prezelin, 1996), the enhancement corresponds to a 26% and 33% reduction of the stratospheric ozone layer in Exps. I and II, respectively (corresponds to a depletion by 86 and 120 DU). In Fig. 6, the

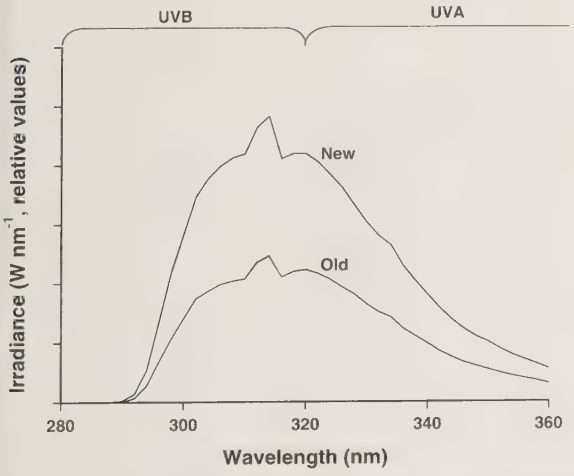

Fig. 4. Spectra of the UVB fluorescent tubes measured with an OL754 Spectroradiometer. Spectra are shown both for lamps that have not been used in the experiment (preburned for 100 h)—"New" and lamp that have been employed for 12 days experiment "Old".

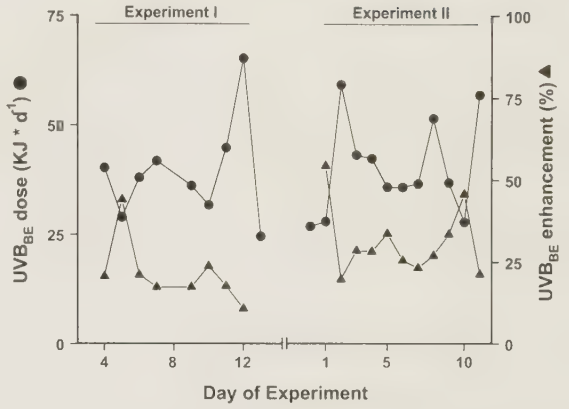

Fig. 5. Ambient UVB_{BE} dose (corrected by absorption and reflection in the incubators covers and walls) and percentage increase in the UVB+ treatment.

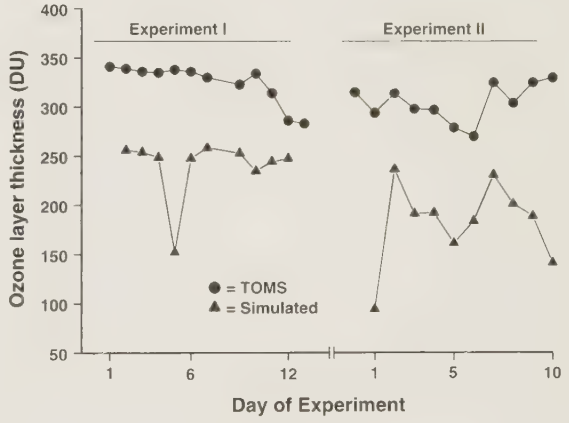

Fig. 6. Thickness of stratospheric ozone layer and the simulated reduction. The thickness of the stratospheric ozone layer is TOMS data and the simulated thickness is calculated from ambient radiation, BWF and a RAF of 0.8.

thickness of the stratospheric ozone layer during the experiments is shown, measured with the Total Ozone Mapping Spectroradiometer (TOMS) placed on the Earth Probe spacecraft (data from NASA homepage). In this figure is also shown the simulated ozone level in UVB+ treatments following the calculation described above.

It should be noted that there was no possibility of measuring the spectra of the fluorescent tubes during the experiments, and the spectra and calibration factor for the broadband sensor to UVBR was determined afterwards.

2.4. Sampling and parameters measured

Samplings were performed the day after filling the aquaria, and on three and two more occasions for Exps. I and II, respectively. The samples taken out of the aquaria were stored in a polyethylene container at 1 °C and dim light for less than 1 h. Samples for primary production were taken directly from the aquaria.

2.5. Phytoplankton species composition

For the taxonomic analysis, a 250 ml sample was taken from each aquaria and preserved in 10% buffered formalin (hexamine). The densities of phytoplankton in each sample were identified and enumerated using a Nikon TMS inverted microscope operated at ×400 magnification in a 10 ml chamber. A maximum of 500 cells was counted in each sample. Where less than 500 cells were recorded, the entire sample was counted (2500 fields = 10 ml). For the identification of phytoplankton species, the works of Priddle and Fryxell (1985) and Tomas (1996) were employed. The counting was finished within 6 months of sampling.

In addition to the quantitative analysis, qualitative measurements of the species composition were done on fresh samples after filtration on a polycarbonate filter (Poretics, pore size 3 μm) onboard. This was done for one aquarium at each sampling date.

2.6. Pigments

Two subsamples of 0.5–1.0 l from each aquarium were gently filtered onto 20 mm Whatman GF/F fibreglass filters. The filters were put in cryovials and immediately frozen in liquid nitrogen (−196 °C). The filtration was done in dim light at 1 °C. After 4–8 weeks, the filters were transferred to a low-temperature freezer (−85 °C) and stored for up to 3 months until analysed. 1.5 ml 100% methanol was added to the filters and the extraction and HPLC-analysis continued according to Wright and Jeffrey (1997). Pigments were quantified in $\mu g\,l^{-1}$ as also described in Wright and Jeffrey (1997). For further details, see Wulff and Wängberg (2004). Pigments are expressed as concentrations ($\mu g\,l^{-1}$). The following pigments were detected: chlorophyll *a* (chl *a*), chlorophyll *b* (chl *b*), chlorophyll c_3 (chl c_3), chlorophyll c_1+c_2 (chl c_1c_2), peridinin (*per*), 19′-butanoyloxyfucoxanthin (19′-*but*), fucoxanthin (*fucox*), 19′-hexanoyloxyfucoxanthin (19′-*hex*), diadinoxanthin (*dd*), diatoxanthin (*dt*), alloxanthin (*allox*), lutein, violaxanthin, zeaxanthin (*zeax*) and β-carotene. In addition, chlorophyll breakdown products were analysed, but as only very small amounts of chlorophyllide *a* was found, they will not be discussed further. To estimate the contribution of different algal classes to total chl *a*, the pigment data was interpreted using the matrix factorisation program CHEMTAX (Mackey et al., 1996; Wright et al., 1996). The program uses a steepest-descent algorithm to determine the best fit based on an estimate of pigment/chl *a* ratios for different algal classes (Mackey et al., 1996). We used an initial pigment-ratio matrix derived from a Southern Ocean data set (Mackey et al., 1996).

2.7. Primary production

Primary production was measured in on-deck incubations in separate, temperature controlled, incubators covered with UVB transparent Acrylic. One incubator was covered with mylar foil to exclude UVBR. Primary production was measured in scintillation vials (Packard, high quality, for transmittance spectra, see Fig. 2) as incorporation of ^{14}C- labelled carbon dioxide to acid stable compounds. Duplicate samples (10 ml) from each aquarium were incubated in each of the incubators. To each vial, 3 μCi ^{14}C-carbonate were added and they were incubated for 4 h. In Exp. I, the incubation started between 8:00 and 8:30 and in Exp. II, 1–1.5 h later depending on the later sunrise at that latitude (Table 2). After the incubation 300 μl formaldehyde (35%) were added and the samples were acidified with HCl to pH < 2 and placed on a shaking board overnight to dispose of inorganic carbonate and scintillation cocktail (Beckman, Ready Gel) was added. The radioactivity was measured using a Beckman scintillation counter (Beckman Mod. 1802). To correct for biotic carbon uptake, formaldehyde was added to

Table 2
Mean light intensities during the primary production incubations and the incubation times

Day of experiment	Date	Start	End	PAR ($\mu E\,m^{-2}\,s^{-1}$)	PAR ($W\,m^{-2}$)	UVB ($W\,m^{-2}$)	UVB_{BE} ($W\,m^{-2}$)	UVA ($W\,m^{-2}$)
Exp. I								
1	Dec. 29	8:15	12:30	860[a]				
4	Jan. 1	8:05	12:05	852	178	1.82	1.87	27.46
8	Jan. 5	8:03	12:00	747	156	1.63	1.68	24.79
12	Jan. 9	8:35	12:30	418	81	0.93	1.14	12.91
Exp. II								
1	Jan. 19	9:35	13:35	544	122	1.59	1.78	20.54
5	Jan. 23	9:50	13:50	557	137	1.80	2.22	22.92
10	Jan. 28	9:10	13:20	635	140	1.50	1.60	22.22

Except when indicated the radiation was measured with an Optronics OL754 spectroradiometer.
[a]Measured with a International Light cosinus calibrated broad band sensor (SUL 240).

two samples before the start of the incubations. From the scintillation counts three values of primary production were calculated. P_{Vol} is the primary production per volume, P_{Chl} is the production per chl *a* and $P_{-UVB/AMB}$ is the percentage increase in primary production when samples were shielded from ambient UVBR during the incubation. The mean radiation levels during the incubations were almost within a factor of 2 (418–852 $\mu E\,m^{-2}s^{-1}$ PAR, 1.14–2.22 $W\,m^{-2}$ $UVBR_{BE}$, Table 2).

2.8. Statistical methods

The statistical evaluations were, done with ANOVA, if necessary, after appropriate transformation. Cochran's *C*-test was used to check for heterogeneous variances. Post hoc analyses were made by the Student–Newman–Keul (SNK) test. *P*-values <0.05 were accepted as significant differences.

3. Results

3.1. General development of the communities

After an initial decrease in the chl *a* concentration, a statistically significant increase was observed at the end of Exp. I, reaching values between 0.6 and 1.2 $\mu g\,l^{-1}$ (Table 3 and Fig. 7). No initial decrease was found in Exp. II (Fig. 7) but a similar increase as in Exp. I was observed although with a higher chl *a* concentration of 1.0–1.7 $\mu g\,l^{-1}$ (Table 3 and Fig. 7). When applying the matrix factorisation program CHEMTAX (Mackey et al., 1996; Wright et al., 1996) significant shift in the algal composition was observed. In Exp. I, an initial dominance of haptophytes, contributing with 50–70% of total chl *a*, was turned over to a diatom-dominated community (80–85%) at the end of the experiment. Initially, a small contribution of cryptophytes (ca. 3%) was observed, as revealed by the pigment *allox*, but from Day 4 onwards, only very small amounts of cryptophytes were found. Instead, from Day 8 to 12, CHEMTAX indicated a presence of cyanobacteria, contributing with ca. 5% of the biomass. The seed community in Exp. II differed from Exp. I with the presence of dinoflagellates (marker pigment *per*) and chlorophytes (chl *b*). From then on, the two experimental communities showed a similar development with an increased proportion of diatoms (80–90%) at the expense of flagellates. However, a slight difference between the experiments was observed. At the end of Exp. I, haptophytes, dinoflagellates and cyanobacteria contributed with ca 10, 0, and 6%, respectively. In Exp. II, the outcome was ca. 13, 1, and 2%.

For the dominating diatom species, there was a satisfactory agreement between the analysis done

Table 3
Pigment concentrations ($\mu g l^{-1}$)

Day	EXP. I	Chl c_3	Chl c_1c_2	*per*	19′-*but*	*fucox*	19′-*hex*	*dd*	*Allox*	*Dt*	*Zeax*	chl *b*	chl *a*	β-carotene
1	NoUVB	0.032	0.076	n.d.	0.008	0.117	0.351	0.054	0.004	0.008	0.000	n.d.	0.644	—
	AMB	0.030	0.068	n.d.	0.008	0.111	0.317	0.048	0.004	0.007	0.000	n.d.	0.493	—
	+UVB	0.027	0.063	n.d.	0.006	0.116	0.255	0.050	0.003	0.005	0.000	n.d.	0.590	—
4	NoUVB	0.015	**0.043a**	n.d.	0.003	**0.099a**	0.127a	0.035	0.000	0.004	0.000	n.d.	0.492	—
	AMB	0.012	**0.034b**	n.d.	0.003	**0.082b**	0.102b	0.031	0.000	0.003	0.000	n.d.	0.465	—
	+UVB	0.012	**0.032b**	n.d.	0.002	**0.081b**	0.092b	0.030	0.000	0.004	0.000	n.d.	0.368	—
8	NoUVB	0.011	0.043	n.d.	0.002	0.150	0.059	0.047	0.000	0.002	0.016	n.d.	0.336	—
	AMB	0.009	0.036	n.d.	0.003	0.130	0.065	0.048	0.000	0.003	0.013	n.d.	0.386	—
	+UVB	0.015	0.052	n.d.	0.007	0.162	0.090	0.058	0.001	0.005	0.012	n.d.	0.446	—
12	NoUVB	0.012	**0.081ab**	n.d.	0.001	0.257	0.047	0.083	0.000	0.006	0.040	n.d.	**0.843a**	—
	AMB	0.012	**0.063a**	n.d.	0.001	0.203	0.060	0.066	0.000	0.003	0.037	n.d.	**0.613a**	—
	+UVB	0.019	**0.101b**	n.d.	0.009	0.324	0.104	0.092	0.000	0.006	0.044	n.d.	**1.137b**	—
	EXP. II													
1	NoUVB	0.024	0.066	0.032	0.034	0.174	0.236	0.087	0.005	0.007	0.004	0.014	0.609	0.000
	AMB	0.027	0.084	0.034	0.034	0.223	0.238	0.099	0.004	0.005	0.005	0.014	0.774	0.000
	UVB+	0.025	0.075	0.024	0.029	0.196	0.197	0.081	0.005	0.006	0.009	0.013	0.710	0.000
5	NoUVB	0.032	0.091	0.017	0.021	0.235	0.194	0.114	0.003	**0.006a**	0.001	0.005	0.806	0.000
	AMB	0.027	0.073	0.014	0.019	0.197	0.165	0.105	0.001	**0.004b**	0.000	0.000	0.717	0.004
	UVB+	0.027	0.078	0.016	0.021	0.227	0.174	0.114	0.002	**0.005b**	0.000	0.002	0.776	0.005
10	NoUVB	0.032	**0.223a**	0.017	0.016	**0.581a**	0.077	0.160	0.000	0.011	**0.010a**	0.000	**1.430a**	0.019
	AMB	0.023	**0.118b**	0.014	0.016	**0.359b**	0.090	0.118	0.001	0.008	**0.011a**	0.004	**0.959b**	0.005
	UVB+	0.025	**0.160b**	0.011	0.013	**0.479ab**	0.084	0.156	0.000	0.013	**0.015b**	0.000	**1.666a**	0.016

Significant differences ($p<0.05$) between treatments are indicated by labels and bold text; n.d., not detected; —, not measured; letters a and b indicate which treatments that differs in the post-hoc analysis. Treatments with one label in common are not statistically different.

on preserved samples and those done onboard. However, very few flagellates were found in the preserved samples despite the fact that several flagellates (especially *Phaeocystis* sp.) were found during Exp. I in the direct counts, and an occurrence of haptophytes was indicated by high concentrations of 19′-*hex*. The analysis of species data is thus limited to diatoms. At the start of Exp. I, *Cylindrotheca closterium* and *Pseudo-nitzschia* spp. were the most abundant diatoms while different *Chaetoceros* species dominated in the end (Table 4). Exp. II was dominated by *Chaetoceros* spp. and *Pseudonitzschia* spp. throughout the whole experiment.

The primary production was fairly constant during Exp. I when based either on volume (P_{Vol}) or chl *a*. (P_{Chl}) (Fig. 8). During Exp. II, P_{Vol} and P_{Chl} were similar to that in Exp. I on Days 1 and 5 but, P_{Vol} especially increased at the end of the experiment (Day 10) (Fig. 8). In Exp. I $P_{-UVB/AMB}$ was on average 42% on Day 1, but decreased during the experiment in the NoUVB and AMB treatments whilst increasing in UVB+. In Exp. II, $P_{-UVB/AMB}$ was 5% on Day 1, 32% on Day 5, but decreased thereafter (Fig. 9).

3.2. Changes due to UVBR

A summary of the treatment effects is given in Table 5. A significant difference in P_{Vol} between treatments was found on Day 4 of Exp. I where UVB+ had lower production than NoUVB (Fig. 8A). This difference could be explained by lower algal biomass as no difference was seen in P_{Chl} on this day. P_{Chl} was instead affected at the end of the experiment (Day 12) with a significantly

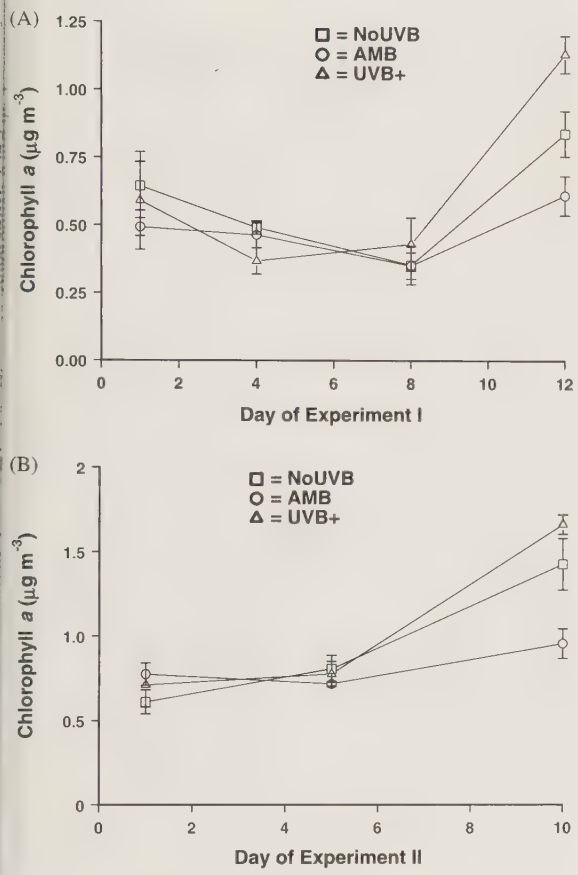

Fig. 7. Chl *a*. concentration. (A) Exp. I; (B) Exp. II. Error bars represent s.e. $n = 4$.

higher production in AMB than in both UVB+ and NoUVB (Fig. 8B). On this day, there were no effects on P_{Vol}. In Exp. II, there were no significant differences in P_{Vol} or P_{Chl} between treatments although there was a tendency to a lower P_{Chl} in the UVB+ treatment on Day 10 ($p = 0.056$) (Fig. 8C, D). The UVBR-dependent reduction in primary production measured as $P_{-UVB/AMB}$ increased from Day 8 in the UVB+ treatment of Exp. I, and reached 82% on Day 12 whilst decreasing for the other treatments (Fig. 9).

Significant treatment effects on chl *a*. concentrations were only found at the end of the experiments. In Exp. I, the chl *a* concentration was significantly higher in UVB+ than both AMB and NoUVB on Day 12. In Exp. II, both UVB+ and NoUVB had significantly more chl *a* than AMB on Day 10 (Fig. 7).

For the other pigments, significantly higher concentrations of chl c_1c_2, *fucox* and 19′-*hex* were found in NoUVB than in the other treatments on Day 4 of Exp. I (Table 3). This was, however, only transient and was not observed later in the experiment. As for chl *a*, the concentration of chl c_1c_2 was significantly higher in UVB+ than in AMB on Day 12. In Exp. II, NoUVB had significantly higher concentrations than the other treatments for *dt* on Day 5 and for chl c_1c_2 on Day 10. On Day 10, a significantly higher concentration of *fucox* was found in NoUVB compared with

Table 4
Most abundant diatom species during the experiments (cell ml^{-1})

	Exp. I				Exp. II			
Date	Dec. 29	Jan. 1	Jan. 5	Jan. 9	Jan. 19	Jan. 23	Jan. 25	Jan. 28
Day of experiment	1	4	8	12	1	5	7	9
Chaetoceros atlanticus	2.18	1.78	4.29	2.46	0.33	0.15	0.33	7.23
Chaetoceros neglectus	1.67	5.20	6.12	7.81	0.67	2.07	11.69	268.32
Chaetoceros spp.	1.34	1.28	4.19	2.72	1.22	2.96	14.57	54.41
Corethron criophilum	0.50	0.13	0.33	0.09	0.17	0.07	0.04	0.17
Cylindrotheca closterium	30.67	4.42	2.33	0.69	0.33	0	0	0.19
Fragailariopsis ribbons	5.53	1.32	0.44	0	1.44	0.15	0.59	3.24
Fragilariopsis kerguelensis	0.92	0.15	0.04	0	0.78	0	4.12	0.34
Pseudonitzschia spp.	12.27	2.44	1.53	0.43	10.61	3.85	49.09	181.56
Thalassionema spp.	0	0	0	0	0	0.15	0.35	0.94
Thalassiosira spp.	2.41	1.00	0.71	0.37	1.44	0.19	0.98	4.22

Included in the table are those species that in either of the experiments was among the 10 most abundant species. Values are the mean of all communities each day.

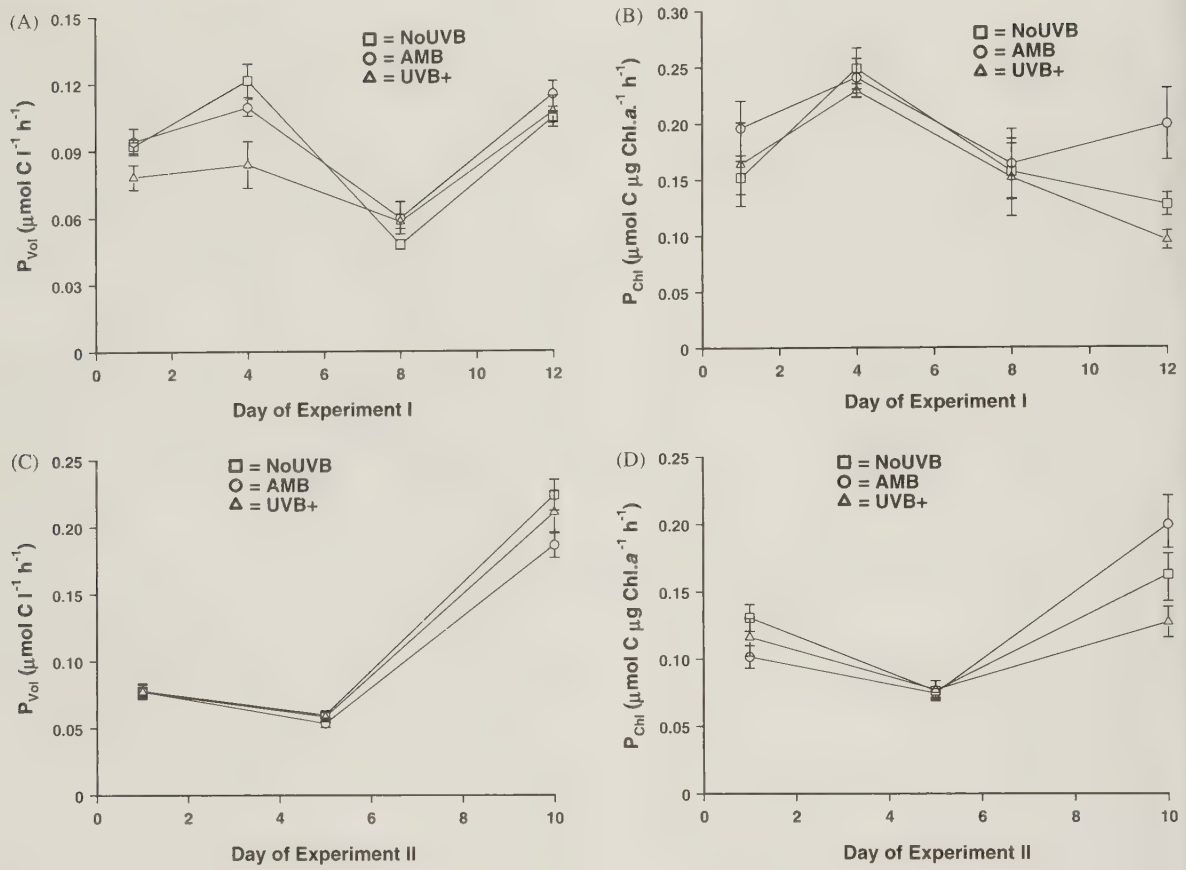

Fig. 8. Primary production during ambient radiation: incorporation of ^{14}C-carbonate to acid stable components during 4 h incubation. (A) Exp. I, volume-based, P_{Vol}; (B) Exp. I, chlorophyll-based, P_{Chl}, (C) Exp. II, volume-based P_{Vol}, (D) Exp. II, chlorophyll-based P_{Chl}. Error bars represents s.e., $n = 4$.

AMB and UVB+ had higher concentrations of *zeax* than both the other treatments.

A significant increase in cell numbers was found for *Chaetoceros* spp. in the UVB+ at the end of Exp. I compared to NoUVB on Day 8 and in both the other treatments on Day 12 (Fig. 10). A similar trend was found for *Pseudonitzschia* spp. with significantly more cells in UVB+ than in AMB on Day 8.

4. Discussion

These experiments show UVBR-mediated changes in microbial communities sampled from the upper part of the Southern Ocean and incubated on-deck for 10–12 days. With the exception of a transient effect at the start of Exp. I there was, however, no treatment effect on the primary production per volume (P_{Vol}). This contradicts those predictions, which state that an effect from the depletion of the stratospheric ozone layer would be a reduction in primary production (e.g. Prezelin et al., 1994). On the other hand we found, at the end of both experiments, treatment depending changes in the chl *a* concentration, with higher amounts in UVB+ than in AMB. The primary production per chl *a* (P_{Chl}) was consequently lower in the UVB+ treatment. Increased algal biomass due to UVBR exposure

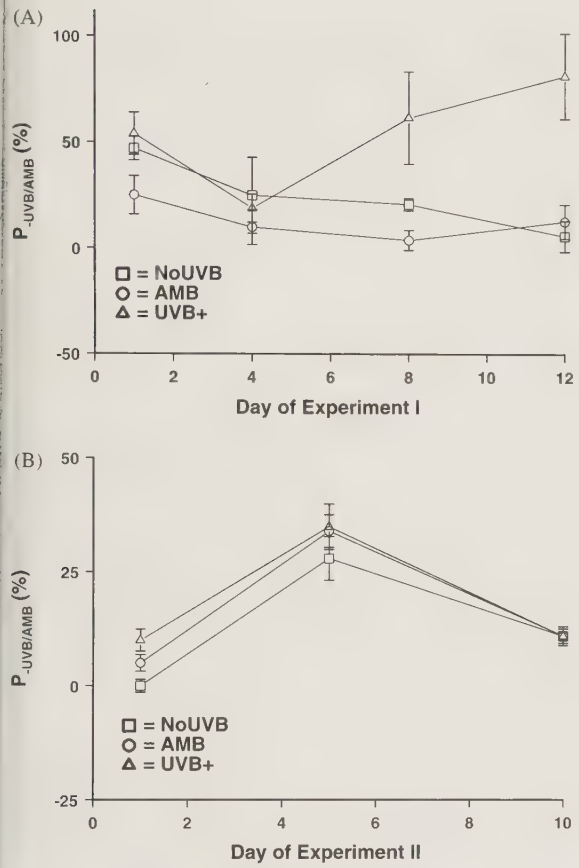

Fig. 9. Increase in primary production, $P_{-UVB/AMB}$, when shielded from UVBR compared to in ambient radiation. The three curves represent the three long-term treatments. The increase is expressed as relative primary production in ambient radiation, (A) Exp. I; (B) Exp. II. Error bars represents s.e., $n = 4$.

Table 5
Parameters that were significantly affected by the changed UVBR

	Exp. I	Exp. II
Chl *a*	+	+
Other pigments	+	+
Diatom species	+ +	–
Primary production (volume-based)	+	–
Primary production (chl *a*-based)	+	–
Stimulation in primary production by screening of UVBR	+ +	–

"–" no significant effects, "+" significant on single days, "+ +" significant effects on several consecutive days.

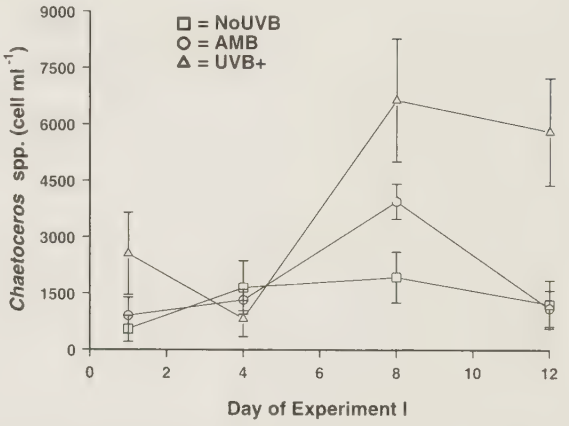

Fig. 10. Cell numbers of *Chaetoceros* spp. in Exp. I. Error bars represents s.e., $n = 4$.

has been found in several experiments and is explained either through decreased grazing pressure or UVBR-depending release of nutrient from organic matter (Bothwell et al., 1994; Mostajir et al., 1999; Wängberg et al., 1999). The lack of effect on bacterial numbers (data not shown) and similarities in primary production per volume suggest, however, that it is instead an increased chlorophyll content per biomass. This could be achieved either through a phenotypic adaptation or through changes in species composition. The effects found differ from Helbling et al. (1992), who also describe effects from on-deck experiments in the Southern Ocean. They were, however, using smaller volumes (2 l) and the communities were run as a batch for 16 days, resulting in a very high biomass in the end of the experiment. These differences in design, together with the fact that their experiment was run later in the season (February–March), makes it hard to make direct comparisons.

The chl *a* concentration in NoUVB at the end of both experiments was between AMB and UVB+ (statistically different from UVB+ in Exp. I and from AMB in Exp. II). This showed that the ambient UVBR also had effect and, at least in Exp. II, a reduced chlorophyll *a* concentration. It might seem surprising that both enhancement and reduction of UVBR increases the chl *a* concentration, but according to the content of signature pigments, the structural changes differed between

NoUVB and UVB+ at the end of Exp. II. UVB+ had, besides the higher chl *a*. concentration, a greater proportion of haptophytes and cyanobacteria compared with NoUVB. In addition, cryptophytes contributed with ca 0.5% to the total chl *a*, while they were absent in NoUVB. In Exp. I, no statistically significant treatment effects were found in any of the signature pigments after Day 4. The significantly larger cell numbers of *Chaetoceros* spp. in the UVB+ treatment show, however, changes in species composition but that these changes were found within all the major algal classes.

In Exp. I, $P_{-UVB/AMB}$ increased significantly in UVB+, a phenomenon we have earlier seen, in an experiment performed on the Swedish west-coast (Wängberg et al., 2001). A hypothetical explanation is that it is a consequence of an adaptation including an overproduction of UVBR-sensitive components within the photosynthetic machinery. If not protected from the UVBR, these components are broken down during the day, and to keep up the production, they are produced in higher quantities than needed. Consequently, if the UVBR is screened off, this results in an enhanced primary production. It is too early to speculate over which component(s) that could have been overproduced, but they could be several, as UVBR has been shown to affect both pigments, the chloroplastic electron transport and enzymes within the Calvin–Benson cycle (Strid et al., 1994; Vincent and Roy, 1993). Despite a higher chl *a* concentration in UVB+ at the end of Exp. I, we do not believe chl *a* to be that particular component. The increase in $P_{-UVB/AMB}$ was seen already on Day 8 when there where no differences in chl *a*. In addition, an increased chl *a* concentration was found also in Exp. II, but no difference was observed in $P_{-UVB/AMB}$. The overproduction could be due to either a phenotypic adaptation or a changed species composition. The fact that Helbling et al. (1996) did not find any signs of an increased UVBR sensitivity when culturing several Antarctic diatoms does not support a phenotypic adaptation.

Generally, the effects of the added UVBR on primary production and chl *a* concentration were lower during Exp. II than Exp. I, despite the fact that more UVBR was added. The most reasonable explanation is the differences in species composition. Though still dominated by haptophytes and diatoms, the seed community in Exp. II was more diverse and had a larger proportion of dinoflagellates and cryptophytes. In addition, small proportions of chlorophytes and cyanobacteria were observed. Also the pre-history of the communities might be important. The relatively high phytoplankton concentrations in the SIE depend on algae growing on the ice that earlier occupied the area. According to McMinn et al. (1994), ice-algae are extremely low-light adapted and thus potentially sensitive to UVBR. The composition of the two seed communities agreed well with other studies in the area (e.g. Smith et al., 1992; Mackey et al., 1996; Wulff and Wängberg, 2004). Though the development in the algal community composition in both experiments was similar with an increasing proportion of diatoms, a greater proportion of dinoflagellates and haptophytes was still found at the end of Exp. II.

As in all experimental systems, this system also differs from natural situations. In this case, it differs through e.g. lack of vertical circulation and that organisms $>200\,\mu m$ are excluded and we did not succeed in keeping the temperature at surface temperature in the aquaria. Grazing was simulated by the semi-continuously dilution which kept the phytoplankton biomass at levels typical of what is found in the ocean surface layer. The composition, however, deviated from what is normally found in the natural system.

Despite these artefacts, the results give new insights into potential UVBR effects on phytoplankton communities in the surface layer of the Southern Ocean that should be taken into account when assessing the effects of a reduction in the stratospheric ozone layer.

In summary, our results showed that relevant increases in UVBR had statistically significant effects on the development of the phytoplankton communities. The effect on primary production per volume was, however, found only intermittently in the beginning of one of the experiments. Primary production per chl *a* decreased in the UVB+ treatment in both experiments as did the chl *a*. concentration. There were changes in species

composition or marker pigments at the end of both experiments, indicating an interspecific adaptation to the increased UVBR. In the first experiment, the adaptation also included an increased sensitivity for ambient UVBR during short-term carbon dioxide fixation.

Acknowledgements

We would like to thank the Swedish Polar Secretariat, Göteborg Marine Research Centre (GMF), who funded the expedition. We also acknowledge the work of the crew on the Research Vessel S.A. *Agulhas* and the invaluable help from Swedish and South-African colleagues. Special thanks to Drs. William Froneman, Agneta Fransson and Anna Godhe who supported us with the data on phytoplankton species composition and carbonate concentrations.

References

Boucher, N.P., Prezelin, B.B., 1996. An in situ biological weighting function for UV inhibition of phytoplankton carbon fixation in the Southern Ocean. Marine Ecology Progress Series 144, 223–236.

Bushaw, K.L., Zepp, R.G., Tarr, M.A., SchulzJander, D., Bourbonniere, R.A., Hodson, R.E., Miller, W.L., Bronk, D.A., Moran, M.A., 1996. Photochemical release of biologically available nitrogen from dissolved organic matter. Nature 381, 404–407.

Bothwell, M.L., Sherbot, D.M.J., Pollock, C.M., 1994. Ecosystem response to solar Ultraviolet-B radiation: influence of trophic-level interactions. Science 265, 97–100.

Chen, D., Wängberg, S.-Å., Wulff, A., Borne, K., 2004. Attenuation of biologically effective UV doses under overcast skies: a case study from the eastern Atlantic sector of the Southern Ocean. Deep-Sea Research II, this issue [doi:10.1016/j.dsr2.2001.02.002].

Davidson, A.T., 1998. The impact of UVB radiation on marine plankton. Mutation Research 422, 119–129.

Farman, J.C., Gardiner, B.G., Shanklin, J.D., 1985. Large losses of total ozone in Antarctica reveal seasonal ClO_x/NO_x interaction. Nature 314, 207–210.

Häder, D.-P., 1993. Risks of enhanced solar ultraviolet radiation for aquatic ecosystems. In: Round, F.E., Chapman, D.J. (Eds.), Progress in Phycological Research. Biopress Ltd, pp. 1–45.

Helbling, E.W., Villafane, V., Ferrario, M., Holm-Hansen, O., 1992. Impact of natural ultraviolet radiation on rates of photosynthesis and on specific marine phytoplankton species, UV-B. Marine Ecology Progress Series 80, 89–100.

Helbling, E.W., Chalker, B.E., Dunlap, W.C., Holm-Hansen, O., Villafañe, V.E., 1996. Photoacclimation of Antarctic marine diatoms to solar ultraviolet radiation. Journal of Experimental Marine Biology and Ecology 204, 85–101.

Herndl, G.J., Müller-Niklas, G., Frick, J., 1993. Major role of ultraviolet-B in controlling bacterioplankton growth in the surface layer of the ocean. Nature 361, 717–719.

Karentz, D., 1994. Ultraviolet tolerance mechanisms in Antarctic marine organisms. In: Weiler, C.S., Penhale, P.A. (Eds.), Ultraviolet Radiation in Antarctica, Measurements and Biological Effects. Antarctic Research Series, vol. 62, pp. 93–110.

Mackey, M.D., Mackey, D.J., Higgins, H.W., Wright, S.W., 1996. CHEMTAX—a program for estimating class abundances from chemical markers: application to HPLC measurements of phytoplankton. Marine Ecology Progress Series 144, 265–283.

McMinn, A., Heijnis, H., Hodgson, D., 1994. Minimal effects of UVB-radiation on Antarctic diatoms over the past 20 years. Nature 370, 547–549.

Mostajir, B., Demers, S., de Mora, S., Belzile, C., Chanut, J.P., Gosselin, M., Roy, S., Villegas, P.Z., Fauchot, J., Bouchard, J., Bird, D., Monfort, P., Levasseur, M., 1999. Experimental test of the effect of ultraviolet-B radiation in a planktonic community. Limnology and Oceanography 44, 586–596.

Prezelin, B.B., Boucher, N.P., Schofield, O., 1994. Evaluation of field studies of UVB radiation effects on Antarctic marine primary productivity. In: Biggs, R.H., Joyner, M.E.B. (Eds.), Stratospheric Ozone Depletion/UV-B Radiation in the Biosphere. NATO ASI Series, vol. 118. pp. 181–194.

Priddle, J., Fryxell, G., 1985. Handbook of Common Diatoms of the Southern Ocean. Cambridge University Press, Cambridge.

Rasmus, K.E., Granéli, W., Wängberg, S.-Å., 2004. Optical studies in the Southern Ocean. Deep-Sea Research II, this issue [doi:10.1016/j.dsr2.2001.01.004].

Rozema, J., Gieskes, W.W.C., van de Geijn, S.C., Nolan, C., de Boois, H. (Eds.), 1997, UV-B and Biosphere, Advances in Vegetation Science 17, Plant Ecology 128. Kluwer Academic Publishers, Dordrecht.

Smith, R.C., Prezelin, B.B., Baker, K.S., Bidigare, R.R., Boucher, N.P., Coley, T., Karentz, D., MacIntyre, S., Matlick, H.A., Menzies, D., Ondrusek, M., Wan, Z., Waters, K.J., 1992. Ozone depletion: Ultraviolet radiation and phytoplankton biology in Antarctic waters. Science 255, 952–959.

Strid, Å., Chow, W.S., Anderson, J.M., 1994. UV-B damage and protection at the molecular level in plants. Photosynthesis Research 39, 475–489.

Tomas, C.R., 1996. Identifying Marine Diatoms and Dinoflagellates. Academic Press, San Diego.

UNEP, 1996. Environmental Effects of Ozone Depletion (Interim Report) Pursuant to Article 6 of the Montreal Protocol on Substances that Deplete the Ozone Layer.

WWW Page, http://www.gcrio.org/OnLnDoc/unepO3-sum.html

Vincent, W.F., Roy, S., 1993. Solar ultraviolet-B radiation and aquatic primary production: damage, protection, and recovery. Environment Reviews 1, 1–12.

Wängberg, S-Å., Garde, K., Gustavson, K., Selmer, J-S., 1999. Effects of UV-B radiation on marine phytoplankton communities. Journal of Plankton Research 21, 147–166.

Wängberg, S-Å., Wulff, A., Nilsson, C., Stagell, U., 2001. Impact of UVBR on microalgae and bacteria–a mesocosm study with computer modulated UVBR addition. Aquatic Microbial Ecology 25, 75–86.

Weiler, C.S., Penhale, P.A., (Eds.), 1994. Ultraviolet Radiation in Antarctica: Measurements and Biological Effects. Antarctic Research Series, vol. 62.

Wetzel, R.G., Hatcher, P.G., Bianchi, T.S., 1995. Natural photolysis by ultraviolet irradiance of recalcitrant dissolved organic matter to simple substrates for rapid bacterial metabolism. Limnology and Oceanography 40, 1369–1380.

Wright, S.W., Jeffrey, S.W., 1997. High-resolution HPLC system for chlorophylls and carotenoids of marine phytoplankton. In: Jeffrey, S.W., Mantoura, R.F.C., Wright, S.W. (Eds.), Phytoplankton Pigments in Oceanography, UNESCO Publishing, Paris, pp. 327–342.

Wright, S.W., Thomas, D.P., Marchant, H.J., Higgins, H.W., Mackey, M.D., Mackey, D.J., 1996. Analysis of phytoplankton of the Australian sector of the Southern Ocean:: comparisons of microscopy and size frequency data with interpretations of pigment HPLC data using the "CHEMTAX" matrix factorisation program. Marine Ecology Progress Series 144, 285–298.

Wulff, A., Wängberg, S-Å., 2004. Spatial and vertical distribution of phytoplankton pigments in the eastern Atlantic sector of the Southern Ocean. Deep-Sea Research II, this issue [doi:10.1016/j.dsr2.2001.01.002].

Young, A.R., Björn, L.O., Moan, J., Nultsch, W. (Eds.), 1993, Environmental UV Photobiology. Plenum Press, New York.

ELSEVIER

Deep-Sea Research II 51 (2004) 2745–2756

DEEP-SEA RESEARCH
PART II

www.elsevier.com/locate/dsr2

Variations of biochemical parameters along a transect in the Southern Ocean, with special emphasis on volatile halogenated organic compounds

K. Abrahamsson[a,*], S. Bertilsson[b], M. Chierici[a], A. Fransson[a], P.W. Froneman[c], A. Lorén[a], E.A. Pakhomov[c,1]

[a]*Department of Analytical and Marine Chemistry, Chalmers University of Technology and Göteborg University, SE-412 96 Göteborg, Sweden*

[b]*Department of Civil and Environmental Engineering, Massachusetts Institute of Technology, Cambridge MA 02139, USA*

[c]*Southern Ocean Group, Department of Zoology, Rhodes University, PO Box 94, Grahamstown 6140, South Africa*

Abstract

A number of parameters of biogeochemical interest were monitored along a north–southerly transect (S 43–S 63) in the Atlantic Sector of the Southern Ocean from the 8th to the 20th of December 1997. Changes in total dissolved inorganic carbon (C_T) and total alkalinity (A_T) were mostly dependent on temperature and salinity until the ice edge was reached. After this point only a weak correlation was seen between these. Highest mean values of C_T and A_T were observed in the Winter Ice Edge (WIE) (2195 and 2319 μmol kg^{-1}, respectively). Lowest mean A_T (2277 μmol kg^{-1}) was observed in the Sub-Antarctic Front (SAF), whereas lowest mean C_T concentration (2068 μmol kg^{-1}) was associated with the Sub-Tropical Front (STF). The pH in situ varied between 8.060 and 8.156 where the highest values were observed in the southern part of the Antarctic Polar Front (APF) and in the Summer Ice Edge (SIE) Region . These peaks were associated with areas of high chlorophyll *a* (chl *a*) and tribromomethane values. In the other areas the pH in situ was mainly dependent on hydrography. Bacterial abundance decreased more than one order of magnitude when going from north to south. The decrease appeared to be strongly related to water temperature and there were no elevated abundances at frontal zones. Microphytoplankton dominated in the SAF and APF, whereas the nano- and picoplankton dominated outside these regions.

Volatile halogenated compounds were found to vary both with regions, and with daylight. For the iodinated compounds, the highest concentrations were found north of the STF. Brominated hydrocarbons had high concentrations in the STF, but elevated concentrations were also found in the APF and SIE regions. No

*Corresponding author. Tel.: +46 31 772 2780; fax: +46 31 772 2785.

E-mail address: katarina@amc.chalmers.se (K. Abrahamsson).

[1]Present address: Department of Earth and Ocean Sciences, University of British Columbia, 6339 Stores Road, Vancouver, BC, Canada V6T 1Z4 and Faculty of Science and Technology, University of Fort Hare, Private Bag X 1314, Alice 5700, South Africa.

0967-0645/$ - see front matter © 2004 Elsevier Ltd. All rights reserved.
doi:10.1016/j.dsr2.2004.09.004

obvious correlation could be found between the occurrence of individual halocarbons and chl *a*. On some occasions trichloroethene and tribromomethane related to the presence of nano- and microplankton, respectively.
© 2004 Elsevier Ltd. All rights reserved.

1. Introduction

The Southern Ocean is characterised by a number of circumpolar currents, which are separated by a number of frontal systems. The locations of the fronts are mainly determined by topography, and to some extent by wind fields (Veth et al., 1997). These areas and Marginal Ice Zones (MIZ) are regarded to be areas with enhanced biological production (e.g. Owens et al., 1991; Nelson and Smith, 1986). The Antarctic Polar Front (APF) is considered to be a productive area, mainly because of upwelling of nutrient and iron-rich water, which is favourable for plankton growth (Veth, 1991; de Baar et al., 1997). The MIZ is an area close to the ice edge, where the upper surface layer becomes stable in spring due to low salinity melt water. This shallow surface layer, together with light penetration, favours primary production (e.g. Smith and Nelson, 1985). A number of parameters can be measured in order to assess such an enhanced biological production, (i.e. phytoplankton community structure, presence and activity of bacteria, the carbon dioxide system and nutrients concentration).

pH has been shown to be a useful parameter in the study of the oceanic carbon dioxide (CO_2) system. In particular, variations in pH are often associated with the occurrence of photosynthesis and respiration, where CO_2 is consumed/produced (Steinberg et al., 1998). Another study in the Bellingshausen Sea report high pH values associated with enhanced levels of chlorophyll *a* (chl *a*) (Bellerby et al., 1995). In contrast to pH, total alkalinity (A_T) is not directly dependent on CO_2 and is considered to be the most conservative parameter in the oceanic carbon dioxide system unless calcifying organisms are present in the seawater. A_T is the only parameter in the oceanic carbon dioxide system that can give information on the occurrence of these organisms.

An effect of phytoplankton activity is the formation of organic compounds of environmental concern, such as volatile halogenated organic compounds (halocarbons). They are involved in a number of atmospheric reactions, among them the destruction of tropospheric and stratospheric ozone (Montzka et al., 1999).

The natural production of halocarbons has been shown to be closely connected to photosynthesis, and the compounds are formed when algae reduce poisonous oxygen species such as hydrogen peroxide and superoxide radicals. During the reduction of hydrogen peroxide by haloperoxidases, hypohalous acids are formed, which readily react with organic compounds present, yielding a vast number of chlorinated, brominated and iodinated substances (Collén et al., 1994; Ekdahl et al., 1998).

Characterisation of the halocarbons in the oceans is of special concern since the oceanic flux is still an unknown factor in the atmospheric budgets of halogens. The largest problem is to find the means to make accurate global estimates of the production of halocarbons by phytoplankton. An approach that seems plausible is to relate specific photosynthetic pigments to the occurrence of halocarbons. In such a way the halocarbon production might be approximated by remote sensing by aircraft or satellite colour sensors.

Phytoplankton also produce other organic compounds that may serve as substrates for heterotrophic bacterial growth. In open oceanic environments, this is the main source of substrates for these microheterotrophs and areas of high primary production are therefore likely to be coupled to areas of high activity and biomass of heterotrophic bacteria (Azam and Cho, 1987). As these heterotrophic microorganisms are the major degraders of organic compounds in aquatic environments (Azam and Hodson, 1977; Wetzel, 1983), they may change the speciation and concentration of organic compounds significantly.

The functional capability of bacteria to degrade halogenated organic compounds is quite widespread between different bacterial taxa in nature (Fetzner, 1998: Damborsky, 1999) and it can, therefore, be suspected that high bacterial activity and abundance would influence the concentrations of such compounds negatively.

The aim of our studies was to obtain more detailed knowledge of the variation of biological important parameters across frontal regions in the Southern Atlantic Ocean. Emphasis was put on studies of the coupling between the carbon dioxide system and biological and physical parameters in the surface waters, as well as to study local variations in microbial communities and concentrations of halocarbons.

2. Material and methods

Underway stations were occupied along a north–southerly transect (S 43–S 63°) along E 12–E 4° (Fig. 1). The positions of the Sub-Tropical Front (STF), the Sub-Antarctic Front (SAF) and the APF were determined from changes in sea surface temperature (STF, SAF, APF) and salinity (SAF) (Table 1). These broadly corresponded to the historical positions of the fronts reported in the literature (Laubscher et al., 1993). The region between the APF and the Summer Ice Edge (SIE) is referred to as the Winter Ice Edge (WIE).

Water samples were collected every hour through the ship seawater supply, which was situated at approximately 4 m depth. A number of parameters were measured: the oceanic carbon dioxide system (pH, total dissolved inorganic carbon (C_T), total alkalinity (A_T)), biomass (size fractioned chlorophyll, bacterial numbers), and volatile halogenated organic compounds (Table 2).

2.1. Oceanic carbon dioxide system

C_T and A_T were analysed within an hour after sampling. pH was determined every 7 min at 15 °C (pH_{15}), and the determination was performed by the use of a semi-continuous system, where a diode-array spectrophotometer was connected to the ship's on-line supply. A more detailed description of the pH measurements are described in this issue by Chierici et al., 2004. The pH in situ was calculated for every discrete station with a CO_2 calculation programme developed by Lewis and Wallace (1998) using the parameters A_T, pH_{15} and in situ temperature. For the calculations the carbon dioxide constants from Roy et al. (1993, 1994) were used. All pH values are on the total hydrogen ion scale.

C_T was determined by gas extraction from acidified seawater samples followed by coulometric titration with photometric detection (Johnson et al., 1985, 1987). The precision was obtained by replicate analysis of the samples. The accuracy was assessed by the use of certified reference

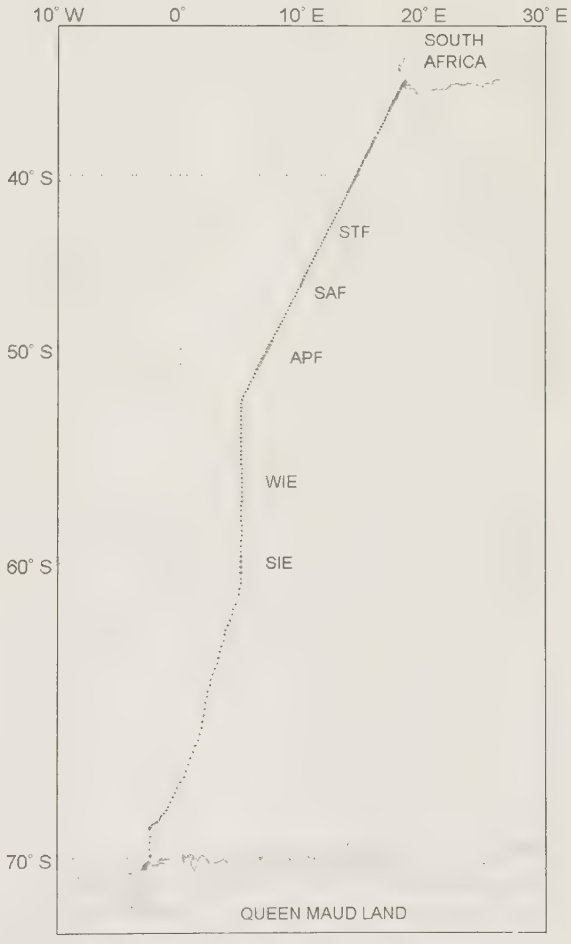

Fig. 1. Cruise track.

Table 1
The mean value and standard deviation for the different regions as defined

Parameter	STF (43–44°S)	North SAF (44–47°S)	South SAF (47–51°S)	APF (51–53°S)	South APF (53-56°S)	WIE (56–60°S)	SIE (60-63°S)
C_T	2068±6	2080±15	2113±8	2141±5	2170±18	2195±6	2174±9
A_T	2290±11	2277±3	2277±4	2286±4	2308±7	2319±6	2298±7
PH in situ	8.103±0.04	8.086±0.008	8.082±0.011	8.083±0.005	8.097±0.012	8.078±0.008	8.091±0.009
T	10.8±1.7	8.06±0.9	4.3±0.7	2.1±0.7	−0.14±0.5	−0.7±0.1	−1.5±0.3
S	34.37±0.38	34.11±0.11	33.81±0.02	33.79±0.01	34.04±0.08	34.19±0.08	33.88±0.10

C_T (total dissolved inorganic carbon) and A_T (total alkalinity) are in $\mu mol\,kg^{-1}$.
T(°C) and S (psu) corresponds to temperature and salinity respectively.

Table 2
The compound name and the chemical formula for the 14 halogenated substances measured

Compound name	Chemical formula
Iodomethane	CH_3I
Trichloromethane	$CHCl_3$
Tetrachloromethane	CCl_4
1,1,1-trichloroethane	CH_3CCl_3
Trichloroethene	$CHCl=CCl_2$
Dibromomethane	CH_2Br_2
Bromodichloromethane	$CHCl_2Br$
Chloroiodomethane	CH_2ClI
2-Iodobuthane	$CH_3CHICH_2CH_3$
Tetrachloroethene	$CCl_2=CCl$
Dibromochloromethane	$CHClBr_2$
1-Iodobuthane	$CH_2ICH_2CH_2CH_3$
2-Iodopropane	CH_3CHICH_3
Tribrommethane	$CHBr_3$

material supplied by Andrew Dickson at Scripps Institution of Oceanography, San Diego, USA. The values for C_T were corrected for the deviation from the certified value by using the ratio between the measured and the certified concentration. The precision for the C_T measurements varied within the range 1–2 $\mu mol\,kg^{-1}$. The correction factor was close to 1.004, which corresponds to a difference of approximately 10 $\mu mol\,kg^{-1}$.

Total alkalinity (A_T) was determined by titrating the seawater samples with 0.05 M HCl while the change in pH was followed by a potentiometric method (Haraldsson et al., 1997). The precision and accuracy were investigated following the same procedure as for the C_T determination. The precision of the A_T measurements was within the range $\pm 1\,\mu mol\,kg^{-1}$ and the correction made varied between 1.003 and 1.008.

2.2. The biological system

Size fractionated chl *a* concentrations were determined by gently serially filtering (<5 cm Hg) a 250 ml seawater sample obtained from the seawater supply through a serial filtration unit and fractionated into the pico- (<2.0 μm), nano- (2–20.0 μm) and microphytoplankton (>20 μm) size fractions. Chl *a* concentrations were determined fluorometrically after extraction in 90% acetone for 24 h using a Turner designs 10 AU fluorometer (Holm-Hansen and Riemann, 1978).

Bacterial cell numbers were measured with a flow cytometer (del Giorgio et al., 1996). A green–fluorescent DNA stain (Syto 13 stain, Molecular Probes) and Fluoresbrite Carboxy YG microspheres (0.92 μm diameter, Polysciences) were added to formaldehyde-preserved water samples, resulting in a final Syto 13 concentration of 50 mM, and a bead concentration of 2.2×10^5 beads ml^{-1}. Cells were counted no later than 2 days after sampling using a FACSCalibur flow-cytometer at a low sample flow-rate ($12\,\mu l\,min^{-1}$). Syto 13-stained bacterial cells and microspheres were separated in a log-log scattergram of green fluorescence intensity and side scatter. Data acquisition was terminated after 5000 microspheres had been counted, and the bacterial cell concentrations were then calculated using the added microspheres as an internal standard. The background cell counts in samples containing only beads was always less than 1×10^4

cells ml^{-1}. For comparison, selected samples were analysed microscopically after DAPI staining as described by Porter and Feig (1980).

2.3. Halocarbon measurements

The halocarbons (Table 2) were pre-concentrated with a purge-and-trap system, which was connected to a Varian 3400 gas chromatograph, equipped with an electron capture detector. All water samples were filtered through glass fiber filters (GFF, Whatman) in order to remove microorganisms prior to injection. The water (26.3 ml) was purged for 4 min in a purge chamber with ultra-pure nitrogen, and the compounds were trapped on a solid support (Porapak N, Alltech Inc.). The trap was cooled with water to 5 °C during trapping, and electrically heated to 140 °C in the desorption mode. The chromatographic conditions were: start temperature of 35 °C at a hold time of 3 min, which was then raised to 60 °C at a rate of 5 °C/min. Thereafter the temperature was increased to 180 °C at a rate of 15 °C/min. The temperature was held at 180 °C for 3 min. The chromatographic separation was made on a 60 m narrow bore column, 502.2 (Restek), with an inner diameter of 0.32 mm, and a film thickness of 1.8 μm. Ultra-pure nitrogen was used both as carrier gas and make-up gas at flow rates of 6 and 10 ml min^{-1}, respectively. Liquid standard solutions were made in acetone (p.a. Merck). The detection limits are in the fmol l^{-1} to pmol l^{-1} range, with a relative standard deviation (RSD) of 1–3%. For further details regarding the analytical method see Ekdahl and Abrahamsson (1997).

3. Results

The variation in salinity and temperature along the transect is shown in Fig. 2B. The mean temperature decreased with 12.3 °C between the STF and the SIE (Table 1). The maximum and minimum values of the salinity was 34.97 and 33.75, respectively. Major changes occurred in the STF and the south APF. At the ice edge a sharp decrease in salinity was observed, which probably was an effect of melting sea ice.

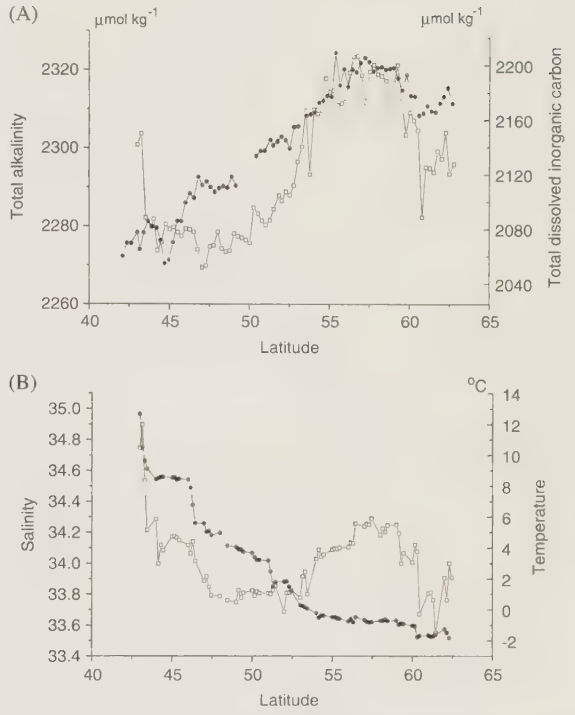

Fig. 2. (A) Total alkalinity (open squares) and total dissolved inorganic carbon (solid circles) along the transect. (B) Salinity (open squares) and temperature (solid circles) variations along the transect.

3.1. Oceanic carbon dioxide system

Mean values and standard deviations were calculated for C_T, A_T and pH in situ for the different regions and are listed in Table 1. From this table, it can be seen that C_T increased from north to south over the entire transect until the ice edge was reached, where the mean concentration was approximately 20 μmol kg^{-1} lower than in the WIE (Fig. 2A). The pH in situ (Fig. 3A) showed the opposite trend relative C_T, and decreased from the STF, where the highest mean value was observed (Table 1), until the WIE, where the lowest mean pH in situ was measured (8.078). In the SIE, the mean pH in situ had increased to 8.091.

A_T decreased rapidly between STF and the north SAF and remained constant until the beginning of the APF, where A_T increased (Fig. 2A). As the SIE was entered, A_T decreased,

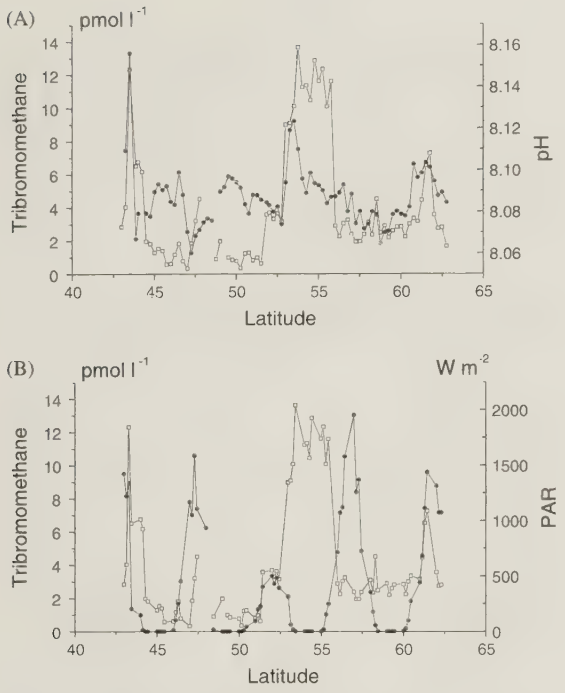

Fig. 3. (A) Tribromomethane, $CHBr_3$, (open squares, left axis) and pH (solid circles, right axis) along the transect.(B) Tribromomethane, $CHBr_3$, (open squares, left axis) and time of day of sampling as indicated by PAR (solid circles, right axis).

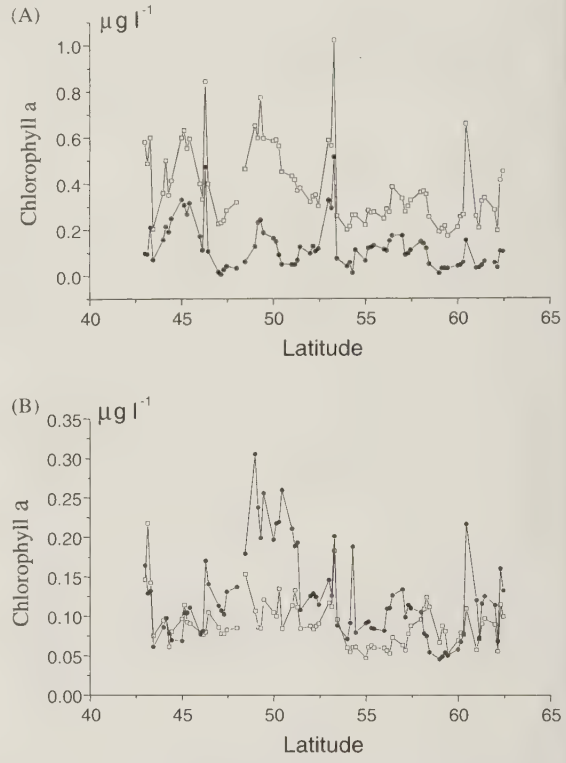

Fig. 4. (A) Total chlorophyll (open squares) and microphytoplankton chlorophyll (solid circles) along the transect. (B) Picophytoplankton chlorophyll (open squares) and nano-phytoplankton chlorophyll (solid circles) along the transect.

as C_T, with approximately 20 µmol kg^{-1} relative the A_T in the WIE (Table 1). The standard deviations for the mean values reflect the variability within the regions, and show that the largest variability in A_T and pH in situ was in the STF, whereas C_T varied the most in the north SAF and the south APF.

3.2. The biological system

Total chl *a* concentrations along the transect ranged from 0.17 to 1.0 µg l^{-1} (Fig. 4A). Peaks in total chl *a* concentration were recorded at stations occupied in the APF and in the SAF. Here total chl *a* concentrations were >0.8 µg l^{-1} (Fig. 4A). Nominal increases in total chl *a* were also recorded at stations in the north SAF and in the MIZ. Outside these regions total chl *a* concentrations were generally <0.35 µg l^{-1}.

North of the APF, total pigment concentration was dominated by microphytoplankton at stations in the SAF and APF (Fig. 4A). Outside these regions, however, total chl *a* was dominated by nano- and picophytoplankton which comprised >70% of the total pigment. South of the APF, the pattern was more complex. In the permanently open waters and at stations occupied in WIE, total chl *a* was again dominated by microphytoplankton. Here microphytoplankton comprised between 45 and 63% of total chl *a* (Fig. 4A). With the exception of the WIE stations, total chl *a* within the seasonal ice zone was always dominated by nano- and picophytoplankton which comprised >60% of total pigment at all stations (Fig. 4B).

Bacterial abundance decreased gradually with increasing latitude (Fig. 5A). The measured cell concentration in surface water varied by more than one order of magnitude, with typically very low abundances ($<2\times10^5$ cells ml^{-1}) south of S 50°. There were no indications of an elevated

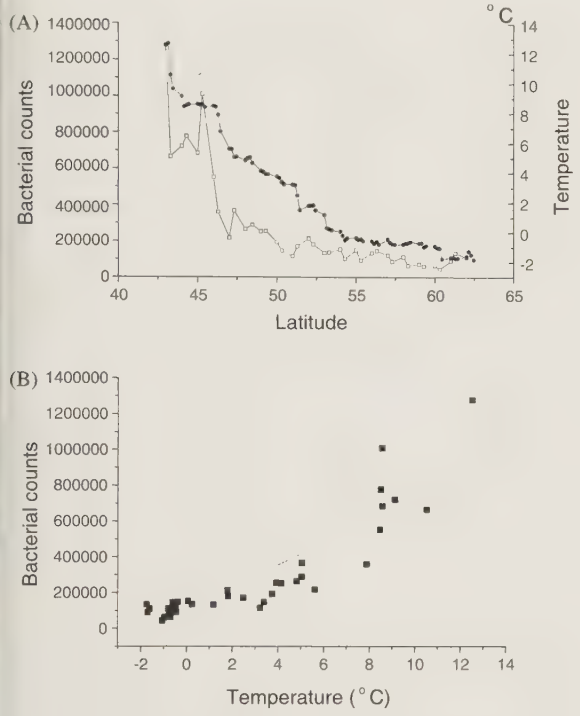

Fig. 5. (A) Abundance of bacteria (open squares, left axis) and temperature (solid circles, right axis) along the transect. (B) The correlation between abundance of bacteria and temperature ($y = 62319x + 104573$, $r^2 = 0.78$).

bacterial abundance in the high-chlorophyll frontal regions. Instead bacterial abundance was strongly correlated with temperature (Fig. 5B). Notably, the number of bacteria increased slightly when the ice-covered zone was reached (south of S 61°).

3.3. Halocarbons

It is nowadays accepted that several of the chlorinated, and some of the brominated halocarbons have both a biogenic and an anthropogenic origin. Tetrachloromethane (CCl_4) and 1,1,1-trichloroethane (CH_3CCl_3) are still regarded as being strictly anthropogenic. The concentrations of these two compounds increased to the south along the transect, which reflects their increased water solubility as the temperature decreases (Fig. 6). Similar to C_T, A_T and pH in situ, the concentrations decreased at the ice edge. The observed increase in concentration of

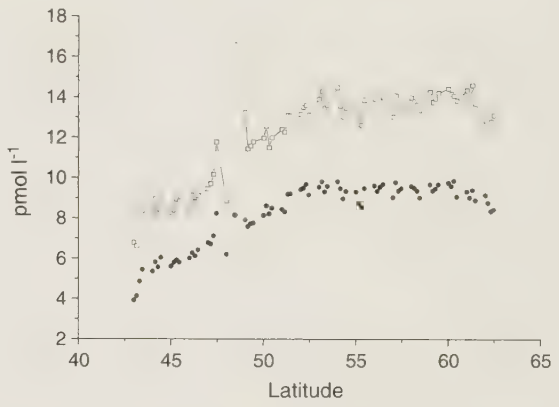

Fig. 6. 1,1,1-trichloroethane, CH_3CCl_3, (open squares) and tetrachloromethane, CCl_4, (solid circles) along the transect.

1,1,1- trichloroethane in the SAF region cannot be accounted for. None of the other measured halocarbons related to CCl_4 nor CH_3CCl_3, indicating a biogenic rather than an anthropogenic origin.

The concentrations of the halocarbons with a biogenic origin, varied significantly between the different frontal regions along the transect (Table 3). For the iodinated compounds, the average surface concentrations decreased south of the STF, and were fairly constant over the entire region. For brominated compounds, the average concentrations decreased south of the STF, as for the iodinated ones. There was a large increase in concentrations at the APF and south of the APF (Table 3) or almost all of the measured brominated compounds, most pronounced for tribromomethane (Fig. 3A). There was also a tendency for elevated concentrations as the SIE was reached.

Tribromomethane has been considered to be the largest single contributor to the concentration of organo-bromine in the oceans. However, the distribution of bromochloromethane relates well to that of tribromomethane, thus indicating a biogenic origin rather than an anthropogenic origin. As can be seen from Table 3, the concentration of bromochloromethane exceeds by far that of the other brominated compounds.

Three chlorinated compounds with proven biogenic origin were measured, trichloromethane,

Table 3
Mean concentrations of halocarbons in the different regions as defined in the text

Compound	STF (43°S–44°S)	North SAF (44°S–47°S)	SAF (47°S–51°S)	APF (51°S–53°S)	South APF (53°S–56°S)	WIE (56°S–60°S)	SIE (60°S–63°S)
CH_3I	3.9±2.5	2.0±0.29	1.8±0.31	1.5±0.04	1.1±0.33	1.6±0.41	1.4±0.55
CH_3CH_2I	1.6±0.69	0.98±0.28	1.7±1.8	1.2±0.44	0.90±0.57	6.2±22	0.86±0.42
CH_3CHICH_3	1.2±0.37	0.77±0.08	0.45±0.11	0.59±0.04	0.58±0.03	0.45±0.10	0.45±0.10
$CH_3CH_2CH_2CH_2I$	0.23±0.10	0.14±0.06	0.13±0.18	nd	nd	nd	nd
$CHCl_3$	2.1±0.43	1.6±0.12	2.4±0.49	2.2±0.16	2.3±0.25	2.3±0.21	2.3±0.19
$CHCl=CCl_2$	13±5.0	13±3.2	49±41	29±6.6	12±5.9	19±5.6	27±21
$CCl_2=CCl_2$	0.23±0.10	0.29±0.29	0.46±0.67	0.28±0.06	0.32±0.22	0.28±0.09	0.34±0.08
CH_2ClI	0.79±0.91	0.28±0.12	0.26±0.17	0.29±0.07	0.23±0.08	0.38±0.08	0.44±0.10
CH_2BrCl	170±49	140±17	95±14	110±5.1	130±3.7	98±25	100±15
$CHBrCl_2$	0.33±0.10	0.22±0.05	0.34±0.15	0.30±0.03	0.31±0.05	0.37±0.06	0.32±0.06
$CHBr_2Cl$	0.25±0.13	0.24±0.06	0.35±0.08	0.35±0.05	0.57±0.05	0.38±0.06	0.33±0.07
CH_2Br_2	5.0±0.62	3.7±0.61	4.1±0.44	4.9±0.30	5.7±0.25	4.8±1.1	5.1±0.59
$CHBr_3$	6.4±3.3	1.3±0.57	1.5±1.2	3.0±1.2	11±1.4	2.7±0.60	3.8±1.8

All values are given in pmol l^{-1}.
nd = not detectable.

trichloroethene and tetrachloroethene. Trichloromethane and tetrachloroethene did not show any significant variation in mean concentrations. But trichlorethene showed a dramatic increase at some stations in the SAF, all during high light intensities. There was also a small tendency for an increase in concentrations at the ice edge.

4. Discussion

In general we see a trend of decreasing temperature farther south as expected (Fig. 2B). A decrease in temperature leads to higher solubility of CO_2, hence a higher C_T value along the transect (Fig. 2A). To eliminate the effect of salinity we normalised C_T to a salinity of 34 (C_{T34}). The temperature effect on C_{T34} is calculated as approximately 8 μmol kg^{-1} $°C^{-1}$ (Lewis and Wallace, 1998) with constant partial pressure of CO_2 (fCO_2). This would result in a C_T difference of approximately 92 μmol kg^{-1} for the change of 11.5 °C in the observed mean temperature from the STF to the ice edge. The observed C_T change is 142 μmol kg^{-1} for the same region, hence the bias of 50 μmol kg^{-1} shows that temperature cannot entirely explain the increase in C_T. This is probably due to changes in CO_2 caused by air–sea exchange and biological processes. This is also confirmed in regions where the presence of a minimum in fCO_2 (maximum in pH in situ) is associated with enhanced Chl *a* as reported by Chierici et al., (2004, this issue).

An earlier study in the Bellingshausen Sea, which used the same method for pH measurements, obtained pH values between 8.04 and 8.25 at in situ temperatures on the same pH scale (Bellerby et al., 1995). This can be compared with the mean pH in situ of 8.081±0.008 between S 55° and S 60°, which implies that there is less variability in our study area compared to the Bellingshausen Sea. From Skirrow (1975) the pH varied between 8.05 and 8.15 units between S 60° and S 68° in another part of the Southern Ocean.

The distribution of total chl *a* along the transect is consistent with several previous studies conducted within the Atlantic sector of the Southern Ocean (Froneman et al., 1995, 1998). Peaks in total pigment at frontal features in the Southern Ocean are well documented (Lutjeharms et al., 1985; Jacques, 1989; Laubscher et al., 1993; Froneman et al., 1995, 1998). We do not have any primary production data to identify the causes of elevated production in the vicinity of the fronts. Biological enhancement at the fronts and the ice edge are thought to result from increase in situ

primary production rates primarily resulting from increased water column stability (Laubscher et al., 1993). It is also possible that the availability of the trace metal, iron, may have contributed to the elevated pigment concentrations in the SAF and in the WIE. This is also confirmed by a peak in pH in situ. These observations in combination with elevated concentrations of chl *a* are an indication of a recent primary production. At stations occupied at the ice-edge, the increase in total pigment may also have resulted from the release of epontic ice algae during the seasonal ice-melt. The preliminary analysis of the phytoplankton assemblages at stations occupied in the region of the ice edge showed that typical ice associated diatoms of the genera *Fragilariopsis* and *Chaetoceros* comprised >90% of all cells counted (Froneman and Pakhomov, unpublished).

Eynaud et al. (1999) observed the presence of coccolithophores (mainly *Emiliana huxleyi*) down to 57°S in the Atlantic sector of the Southern Ocean in austral summer 1995. During our study, the strong relationship between A_T and salinity indicated no evidence of calcifying organisms along the transect. Since no data on phytoplankton species composition was available this cannot be confirmed.

The predominance of large microphytoplankton within the seasonal ice zone of the Southern Ocean during austral summer is well documented (Lutjeharms et al., 1985; Laubscher et al., 1993; Froneman et al., 1995). Our results which showed that small nano- and picophytoplankton dominated total chl *a*–*a* within the seasonal ice zone during this investigation are, therefore, surprising (Fig. 4B). Studies conducted beneath the sea-ice in winter have shown that total chl *a* is dominated by small nano- and picophytoplankton (Garrison et al., 1993). After the retreat of the ice, however, the release of the epontic algae results in a dramatic shift in the community structure with large microphytoplankton generally dominating total pigment concentration. These facts suggest that the algal community sampled during this investigation were remnants of the winter sea-ice community. A study conducted within the same region two weeks later showed that total chl *a* was almost entirely dominated by large phytoplankton cells comprising mainly diatoms and the colonial haptophyte, *Phaeocystis* (Froneman and Pakhomov, unpublished), which partially support our findings.

In the present study, no apparent correlation between bacterial abundance and chl *a* could be observed. Hence our data do not support the hypothesis that phytoplankton play a major role as regulators of bacterial growth by acting as a source of organic substrates. Instead, the bacterial counts were correlated to water temperature, suggesting that temperature rather than phytoplankton-derived substrates regulated bacterial growth and abundance. This finding is consistent with a recent study, which indicates that temperature could be a major factor regulating bacterial abundance and activity in cold surface oceanic waters (Li, 1998). However, our findings should be interpreted with caution, since temperature could influence other processes such as phytoplankton excretion and grazing pressure on bacteria. Since bacterial counts were low south of the STF, and since no elevated bacterial counts could be observed in the regions where elevated concentrations of phytoplankton were observed (SAF and APF), it is unlikely that bacterial uptake and degradation could have influenced the spatial patterns observed for halocarbons in these frontal regions. For the halocarbons with a biogenic origin the measured concentrations vary significantly. The relatively high standard deviations (Table 3) reflect the complexity of a system with a patchy distribution of phytoplankton in combination with the relatively long environmental half-lives of the individual compounds. Surface water concentrations of halocarbons are rarely mentioned in the literature in this region. Our observed values of brominated and iodinated substances are comparable with those found by Shall et al. (1997). However, of the data presented in their work, only three stations were in the same latitudinal region.

In areas with high light intensities, it has been shown that the production of halocarbons by macroalgae is more efficient (Abrahamsson et al., 1995; Ekdahl et al., 1998). Therefore, it is not surprising to find relatively high concentrations of halocarbons in surface waters north of the STF. This has also been reported by Schall et al. (1997) and Quack and Suess (1999).

No strong relationship between the surface water concentrations of halocarbons and total chl *a* could be observed, in agreement with what has been indicated in a number of investigations (Abrahamsson and Ekdahl, 1993; Schall et al., 1997). Also, there was no pronounced relationship between the sized fractionated chl *a* measurements and the occurrence of halocarbons. On some occasions, increases of concentrations of bromoform were followed by increases in total chl *a* and microphytoplankton. Also, the relatively high concentrations of trichloroethene seen at some stations in the SAF corresponded with the presence of nano-phytoplankton (Fig. 4B). A study conducted in parallel to this investigation showed that the nano- and picoplankton are the most efficient producers of halocarbons (Abrahamsson et al., 2004, this issue). The increased levels of some of the halocarbons at the ice edge, where the nano-and picoplankton dominated, could be seen as a weak indication of such a relationship.

A relationship between tribromomethane and time of day could be observed (Fig. 3B). The levels of tribromomethane increased on several occasions during parts of the day with sunlight. The influence of daylight on the concentrations of halocarbons was also seen during this expedition (Abrahamsson et al., 2004, this issue). This has also been described earlier by Ekdahl et al. (1998), where the highest levels of halocarbons in a rock pool inhabitated with macroalgae, were found at midday when photosynthesis is at its maximum. As can be seen from Fig. 3B, the production of tribromomethane is always followed by a decrease in concentration of the same magnitude, yielding a background value (Table 3). This rapid decrease was also observed in the study of the rock pool, and this decrease is probably caused by several factors, the most important being the exchange with the atmosphere.

However, on one occasion, south of the APF, tribromomethane reached the highest levels observed at night time. This could be explained by a recent production of tribromomethane, since the environmental half-life is fairly long, some hundreds of years in seawater at prevailing water temperatures. This is also supported by the peak in pH in situ in the same region (Fig. 3A). This increase in pH in situ could be seen as an indicator of a bloom of phytoplankton. Similar to tribromomethane, the pH signal remain for a longer period of time than that of chl *a*. Another explanation could be that, since macroalgae are efficient producers of brominated compounds, the concentrations of tribromomethane are elevated in areas in the vicinity of algae belts. The transect passed relatively close to Bouvet Island (around S 54°), where elevated macroalgae densities were previously observed (Laubscher et al., 1993).

5. Conclusion

All carbon dioxide parameters follow the hydrological features along the transect. However, pH showed the highest values in areas associated with high chl *a* levels in frontal areas, especially south of the APF, where also the silicate concentrations were low. The distribution of halocarbons in surface water was shown to fluctuate both with region and time of day. No correlation with micro, nano- or picoplankton could be observed. Therefore, the use of chl *a* as a proxy for phytoplankton biomass is not sufficient for global estimates of the production of volatile halogenated substances. Also, the fact that a diurnal variation is superimposed on a regional variation makes flux calculations extremely difficult.

Acknowledgements

We would like to thank the Swedish Polar Secretariat, Göteborg Marine Research Centre (GMF), the Swedish Natural Science Research Council and the South African Department of Environmental Affairs and Tourism, who funded the expedition. Associate Professor Sten-Åke Wängberg has kindly provided the light data.

The work of the crew on the Research Vessel *SA Agulhas* is also acknowledged. A special thank is due to Chris Rohleder for handling the ship's measurements of underway salinity, temperature and wind speeds, and for a multitude of assistance with the scientific equipment.

References

Abrahamsson, K., Ekdahl, A., 1993. Gas chromatographic determination of halogenated compounds in water and sediment in the Skagerrak. Journal of Chromatography 643, 239–248.

Abrahamsson, K., Ekdahl, A., Collén, J., Pedersén, M., 1995. Marine algae—a source of trichloroethylene and perchloroethylene. Limnology and. Oceanography 40, 1321–1326.

Abrahamsson, K., Lorén, A., Wullf, A. Wängberg, S.-Å., 2004. Air–sea exchange of halocarbons: The influence of diurnal and regional variations and distributions of pigments. Deep-Sea Research II, this issue [doi:10.1016/j.dsr2.2004.09.005].

Azam, F., Cho, B.C., 1987. Bacterial utilization of organic matter in the sea. In: Fletcher, M., Gray, T.R.G., Jones, J.G. (Eds.), Ecology of Microbial Communities. Cambridge University Press, Cambridge GB.

de Baar, H.J.W., Van Leeuwe, M.A., Scharek, R., Goeyens, L., Bakker, K.M.J., Fritsche, P., 1997. Nutrient anomalies in Fragilariopsis kerguelensis blooms, iron deficiency and the nitrate/phosphate ratio (A.C. Redfield) of the Antarctic Ocean. Deep-Sea Research II 44 (1–2), 229–260.

Bellerby, G.J., Turner, D.R., Robertson, J.E., 1995. Surface pH and pCO_2 in the Bellingshausen Sea, Southern Ocean, during the early Austral summer. Deep-Sea Research II 42, 1093–1107.

Chierici, M., Fransson, A., Turner, D.R., Pakhomov, E.A., Froneman, P.W., 2004. Variability in pH, fCO_2 and fluxes of CO_2 and oxygen in the surface water along a transect in the Atlantic sector of the Southern Ocean. Deep-Sea Research II, this issue [doi:10.1016/j.dsr2.2001.03.002].

Collén, J., Ekdahl, A., Abrahamsson, K., Pedersén, M., 1994. The involvement of hydrogen peroxide in the production of volatile halogenated compounds by Meristiella gelidium. Phytochemistry 36, 1197–1202.

Damborsky, J., 1999. Tetrachloroethene degrading bacteria. Folia Microbiol 44, 247–262.

Ekdahl, A., Abrahamsson, K., 1997. A simple and sensitive method for the determination of volatile halogenated organic compounds in seawater in the amoll^{-1} to pmoll^{-1}range. Analytica Chimica Acta 357, 197–209.

Ekdahl, A., Pedersén, M., Abrahamsson, K., 1998. A study of the diurnal variation of biogenic volatile halocarbons. Marine Chemistry 63, 1–8.

Eynaud, F., Giraudeau, J., Pichon, J.-J., Pudsey, C.J., 1999. Sea surface distribution of coccolithophores, diatoms, silicoflagellates and dinoflagellates in the South Atlantic Ocean during the late austral summer 1995. Deep-Sea Research I 46, 451–482.

Fetzner, S., 1998. Bacterial dehalogenation. Applied Microbiology and Biotechnology 50, 633–657.

Froneman, P.W., Perissinotto, R., McQuaid, C.D., Laubscher, R.K., 1995. Summer distribution of netphytoplankton in the Atlantic sector of the Southern Ocean. Polar Biology 15, 77–84.

Froneman, P.W., Pakhomov, E.A., Meaton, V., 1998. Surface distribution of microphytoplankton of the south-west Indian Ocean along a repeat transect between Cape Town and the Prince Edward Islands. South African Journal of Science 94, 124–129.

Garrison, D.L., Buck, K.R., Gowing, M.M., 1993. Winter plankton assemblage in the ice-edge zone of the Weddell and Scotia Seas: composition, biomass and spatial distributions. Deep-Sea Research II 40, 311–338.

del Giorgio, P.A., Bird, D.F., Prairie, Y.T., Planas, D., 1996. The flow cytometric determination of bacterial abundance in lake plankton with the green nucleic acid stain SYTO 13. Limnology and Oceanography 41, 783–789.

Haraldsson, C., Anderson, L.G., Hassellöv, M., Hulth, S., Olsson, K., 1997. Rapid, high-precision potentiometric titration of alkalinity in the ocean and sediment pore waters. Deep-Sea Research I 44, 2031–2044.

Holm-Hansen, O., Riemann, B., 1978. Chlorophyll-*a* determination: improvements in methodology. Oikos 30, 438–447.

Jacques, G., 1989. Primary production in the open Antarctic ocean during austral summer. A review. Vie Milieu 39, 1–17.

Johnson, K.M., King, A.E., Sieburth, J.M., 1985. Coulometric TCO_2 analyses for marine studies: an introduction. Marine Chemistry 16, 61–82.

Johnson, K.M., Sieburth, J.M., Williams, P.J., Brandstrom, L., 1987. Coulometric total carbon dioxide analysis for marine studies: automation and calibration. Marine Chemistry 21, 117–133.

Laubscher, R.K., Perissinotto, R., McQuaid, C.D., 1993. Phytoplankton production and biomass at frontal zones in the Atlantic sector of the Southern Ocean. Polar Biology 13, 471–481.

Lewis, E., Wallace, D.W.R., 1998. Program Developed for CO_2 System Calculations. ORNL/CDIAC-105. Carbon Dioxide Information Analysis Center, Oak Ridge National Laboratory, US Department of Energy, Oak Ridge, Tennessee.

Li, W.K.W., 1998. Annual average abundance of heterotrophic bacteria and Synechococcus in surface ocean waters. Limnology and Ocanography 43 (7), 1746–1753.

Lutjeharms, J.R.E., Walters, N.M., Allanson, B.R., 1985. Oceanic frontal systems and biological enhancement. In: Siegfried, W.R., Condy, P.R., Laws, R.M. (Eds.), Antarctic Nutrient Cycles and Food Web. Springer, Berlin.

Montzka, S.A., Butler, J.H., Elkins, J.W., Thompson, T.H., Clarke, A.D., Lock, L.T., 1999. Present and future trends in atmospheric burden of ozone depleting halogens. Nature 398, 691–694.

Owens, N.J.P., Priddle, J., Whitehouse, M.J., 1991. Variations in phytoplanktonic nitrogen assimilation around South Georgia and in the Bransfield Strait (Southern Ocean). Marine Chemistry 35, 287–304.

Porter, K.G., Feig, Y.S., 1980. The use of DAPI for identifying and counting aquatic microflora. Limnology and Oceanography 25, 943–948.

Quack, B., Suess, E., 1999. Volatile halogenated hydrocarbons over the western Pacific between 43° and 4°N. Journal of Geophysical Research 104, 1663–1678.

Roy, R.N., Roy, L.N., Vogel, K.M., Porter-Moore, C., Pearson, T., Good, C.E., Millero, F.J., Campbell, D.M.,

1993. The dissociation constants of carbonic acid in seawater at salinities 5–45 and temperatures 0–45 °C. Marine Chemistry 44, 249–267.

Roy, R.N., Roy, L.N., Vogel, K.M., Porter-Moore, C., Pearson, T., Good, C.E., Millero, F.J., Campbell, D.M., 1994. Erratum for: The dissociation constants of carbonic acid in seawater at salinities 5–45 and temperatures 0–45 °C. Marine Chemistry 45, 337.

Schall, C., Heumann, K.G., Kirst, G.O., 1997. Biogenic volatile organoiodine and organobromine hydrocarbons in the Atlantic Ocean from 42°N to 72°S. Fresenius Journal of Analytical Chemistry 359, 298–305.

Skirrow, G., 1975. The dissolved gases. In: Riley, J.P., Skirrow, G. (Eds.), Chemical Oceanography. vol. 2. second ed. Academic Press, New York, pp. 1–181.

Smith, W.O., Nelson, D.M., 1985. Phytoplankton bloom produced by a receding ice edge in the Ross Sea: spatial coherence with the density field. Science 277, 163–166.

Steinberg, P.A., Millero, F.J., Zhu, X., 1998. Carbonate system response to iron enrichment. Marine Chemistry 62, 31–43.

Veth, C., 1991. The structure and evolution of the top layers of the water column across the marginal ice zone during spring 1988 in the Scotia–Weddell Sea sector of the Southern Ocean. Marine Chemistry 35 (1–4), 63–76.

Veth, C., Peeken, I., Scharek, R., 1997. Physical anatomy of fronts and surface waters in the ACC near the 6W meridian during austral spring 1992. Deep-Sea Research II 44 (1–2), 23–49.

ELSEVIER

Deep-Sea Research II 51 (2004) 2757–2772

DEEP-SEA RESEARCH
PART II

www.elsevier.com/locate/dsr2

Transformation of carbon and oxygen in the surface layer of the eastern Atlantic sector of the Southern Ocean

Agneta Fransson[a,b,*], Melissa Chierici[a,b], Leif G. Anderson[a], Roland David[c]

[a]*Department of Chemistry, Analytical and Marine Chemistry, Göteborg University, SE-412 96 Göteborg, Sweden*
[b]*Climate Change Research Project, National Institute for Environmental Studies, 16-2 Onogawa, Tsukuba, Ibaraki 305-8506, Japan*
[c]*CSIR, PO Box 17001, Congella 4013, Kwa-Zulu Natal, South Africa*

Abstract

The biogeochemical transformation of carbon, and the exchange of carbon dioxide and oxygen over the sea–air interface were evaluated from measurements of dissolved inorganic carbon, total alkalinity, dissolved oxygen and nitrate in the Atlantic sector of the Southern Ocean. The investigation was carried out along longitude 6 E from December 1997 to January 1998 and was focused on three areas; the Spring Ice Edge (SIE), the Winter Ice Edge (WIE) and the Antarctic Polar Front (APF). The method is based on the assumption that differences between preformed and measured concentration of any property, are attributable to biological processes and sea–air exchange. By correcting the deficit of carbon and excess of oxygen observed in the surface mixed layer for the biological activity, the sea–air exchange of carbon dioxide and oxygen is estimated. In the SIE and the APF, a net release of carbon dioxide to the atmosphere of 0.1 and 0.5 mol m^{-2}, respectively, was calculated over a time scale of several months (from austral winter to January). In the WIE a net oceanic uptake of carbon dioxide was calculated, with a sea–air exchange of -0.1 mol m^{-2}. The calculated sea–air exchange of oxygen in the APF indicated an oceanic net release of oxygen to the atmosphere of 1.2 mol m^{-2}. In the SIE and the WIE the sea–air exchange of oxygen was -0.3 and -1.4 mol m^{-2}, respectively, from austral winter to January. Averaging the integrated sea–air exchanges indicated that the entire region acted as a weak oceanic source of carbon dioxide, from austral winter to January. The corresponding oxygen sea–air exchange showed a sink.
© 2004 Elsevier Ltd. All rights reserved.

1. Introduction

The Southern Ocean is a large potential sink for atmospheric carbon dioxide (CO_2). Together with oceanic heat loss and biological primary production, which both lower the surface ocean partial pressure of CO_2 (pCO_2), the existence of high winds and rough seas favour a carbon dioxide flux

*Corresponding author. Climate Change Research Project, National Institute for Environmental Studies, 16-2 Onogawa, Tsukuba, Ibaraki 305-8506, Japan.
E-mail address: agneta.fransson@nies.go.jp (A. Fransson).

0967-0645/$ - see front matter © 2004 Elsevier Ltd. All rights reserved.
doi:10.1016/j.dsr2.2001.12.001

between the atmosphere and ocean (e.g. Robertson and Watson, 1995; Takahashi et al., 1993). However, there is still the question of whether the Southern Ocean is a source or sink for atmospheric carbon dioxide, since other processes also affect the surface water pCO_2, and the relative magnitudes of them all are not well known. Recently, many papers have appeared highlighting the sink behaviour, among others Hoppema et al. (1999), Louanchi et al. (1999), and Caldeira and Duffy (2000). One important process that increases the inorganic carbon concentration in the surface layer is mixing of water masses of high pCO_2 from below (Poisson et al., 1993). Another variable process is the cycling of carbon through the biological system, including the flux of carbon out of the euphotic zone. Changes in environmental conditions in the upper ocean, e.g. those caused by a climate change, will likely affect the productivity and sinking of particulate matter as well as vertical mixing, and thus the sea–air exchange of CO_2. Consequently there is a need for a better understanding of the Southern Ocean and its role for the carbon budget of the world oceans.

At least two areas in the Southern Ocean are considered to provide good conditions for primary production, the marginal ice zone or the ice edge, and the area of the Antarctic Polar Front (APF). The marginal ice zone, an area of sea ice formation and melting, is important in the dynamics of the Southern Ocean. Enhanced primary production has been observed as a result of the formation of a shallow, vertically stable upper layer during spring/summer when sea ice melts (Smith and Nelson, 1985; Lancelot et al., 1991). The resultant stratification enhances light conditions, favouring the start of phytoplankton growth. The APF area is considered to be a site of formation of intermediate water, where surface water sinks and thus brings CO_2 into deeper layers (Veth et al., 1997). According to Smetacek et al. (1997) the APF exhibits the highest biological activity and biogeochemical changes in the Southern Ocean, and the region is one of the most productive Antarctic oceanic ecosystems (Tréguer and Jacques, 1992; Bathmann et al., 1997).

Sea–air fluxes of CO_2 in the Southern Ocean, based on measurements of pCO_2 and wind speed, are variable and indicate both sinks and sources, depending on the area and season (Poisson et al., 1993). During spring and summer, the oceanic CO_2 is approximately at equilibrium with the atmospheric value (Takahashi, 1989; Metzl et al., 1991; Murphy et al., 1991). However, Robertson and Watson (1995) observed a strong CO_2 undersaturation in summer. Bakker et al. (1997) reported a minor oceanic sink of CO_2 with a net sea–air flux of $-0.3\,\mathrm{mmol\,m^{-2}\,day^{-1}}$ in spring and Poisson et al. (1993) reported a flux of -1.5 $(\pm 4.6)\,\mathrm{mmol\,m^{-2}\,day^{-1}}$ in summer. Stoll et al. (1999) investigated the Weddell Sea in late autumn and found a sea–air flux of $-2.0\,\mathrm{mmol\,m^{-2}\,day^{-1}}$. In this work we investigate whether the ice edge and the APF in the eastern Atlantic sector are potential sinks or sources for atmospheric CO_2 and oxygen, and estimate the sea–air exchange of CO_2 and oxygen from austral winter January. This approach to obtaining sea–air fluxes includes seasonal variability with a time scale of several months, which is different from methods such as flux calculations with fCO_2.

2. Methods

The investigation took place along longitude 6°E from 31 December 1997–27 January 1998. The positions of the stations occupied are shown in Fig. 1. Data used for the calculations were collected in the Spring Ice Edge (SIE) between 59.6°S and 60.4°S, in the winter Ice Edge (WIE) between 55.8°S and 56.7°S, and in the APF between 50°S and 51.6°S. The APF position in our study was defined as the northernmost extent of the 2 °C isotherm in the surface water. The SIE in our study coincided with the Weddell Gyre and with the ice edge during the southward transect in the beginning of December 1997. The maximum boundary for the winter ice edge was defined from historical data, which varied between latitudes 52°S and 56°S in the study area. The positions of the WIE agreed with those of the ACC-Weddell Gyre Boundary (latitude 57°S and longitude 6°W), which is a front between the Weddell Gyre and the

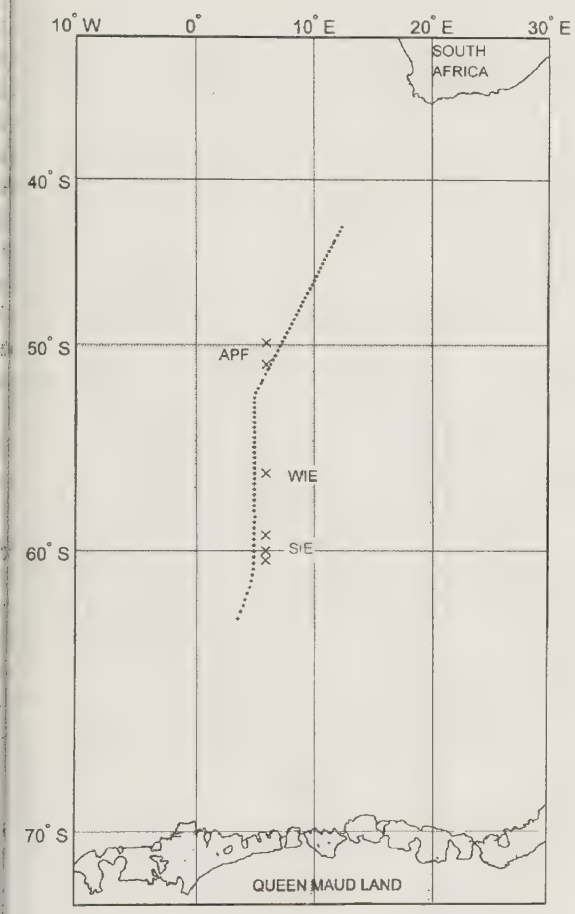

Fig. 1. Map of the Atlantic sector of the Southern Ocean with the stations occupied during the investigation in 31 December 1997–27 January 1998.

Southern Antarctic Circumpolar Current (ACC) according to Veth et al. (1997). A front called the Weddell Front was defined by Spiridonov et al. (1996) at latitude 56°30′S and longitude 0°.

Samples for the determination of total dissolved inorganic carbon (C_T), total alkalinity (A_T), dissolved oxygen (O_2) and nitrate (NO_3) were taken from a rosette with 12 Niskin bottles closed at different depths. Salinity and temperature were measured by a Seabird CTD. C_T and A_T samples were analysed within 5 hours of collection. Oxygen samples were stored about 3–5 h before analysis. All nitrate samples were refrigerated immediately and analysed in duplicate within 12 h of sampling.

The C_T was determined by gas extraction from acidified seawater samples followed by coulometric titration with photometric detection (Johnson et al., 1985, 1987). The precision varied between 1 and 2 $\mu mol\,kg^{-1}$ ($\pm 0.05\%$) and was obtained by three replicate analyses of a sample. These triplicate measurements were performed at least every hour to check the reliability of the C_T values. The accuracy was controlled against a Certified Reference Materiel (DOE, 1994) supplied by Andrew Dickson (Scripps Institution of Oceanography, San Diego, USA). These measurements were performed for each change of cell solution, i.e. every 24 h. The samples were corrected for the difference between the measured and the certified values. The correction factor was around 1.005, corresponding to a difference of about 8 $\mu mol\,kg^{-1}$. The certified reference material varied $\pm 6\,\mu mol\,kg^{-1}$ during the whole cruise. A_T was determined by potentiometric titration with 0.05 M HCl according to Haraldsson et al. (1997). The precision and accuracy were determined by the same procedure as for C_T. The precision for the A_T determinations was 1 $\mu mol\,kg^{-1}$ (0.05%), and the accuracy was obtained by the correction factor of 1.005, corresponding to a difference between measured and certified values of 12 $\mu mol\,kg^{-1}$. The variability in the certified reference material during the whole cruise was $\pm 6\,\mu mol\,kg^{-1}$. The fugacity of carbon dioxide (fCO_2) was calculated by use of the CO_2-system program of Lewis and Wallace (1998), using the carbonate system parameters A_T and C_T. For the calculations the thermodynamic dissociation constants from Mehrbach et al. (1973) was used, following the recommendation of Wanninkhof et al. (1999). However, the difference using the Mehrbach constants instead of the constants by Roy et al. (1993, 1994) is less than 1 µatm in the calculated fCO_2 for the SIE and the WIE, and less than 6 µatm for the APF. This is in the same order of magnitude as the precision and accuracy for the fCO_2 calculations, which are about 2 and 5 µatm, respectively (Dickson and Riley, 1978). Since fCO_2 is mainly used to illustrate the CO_2 concentration at the temperature minimum, and the current fCO_2 condition in the surface water in January, this

uncertainty makes no significant contribution to the results.

Oxygen was determined by an automated Winkler type titration with a photometric detection. The precision of $\pm 1.5\,\mu mol\,kg^{-1}$ (0.3%) was determined by replicate measurements of water collected from the same Niskin bottle. Thus, the uncertainty due to sampling is included in this value. The accuracy of $1\,\mu mol\,kg^{-1}$ was determined by the variation in standardization of the sodium thiosulphate during the study. All nutrients were analysed using colorimetric techniques set out by Mostert (1983), based on nutrient determination according to Koroleff (1976) and Solorzano and Sharp (1980). Nitrate was determined by the cadmium reduction method that involved passing the sample through a copperised cadmium reduction column to reduce all dissolved nitrate to nitrite. Nitrite was also analysed similarly except that the sample was not passed through the column. The difference between nitrate + nitrite and nitrite produced nitrate values in $\mu mol\,l^{-1}$. Analysis of several replicates of the same sample resulted in a precision within 4%. Accuracy was determined by spiking a sample of known concentration with a standard, determining the recovery. The accuracy in percent recovery was 98%, however, this was not corrected for.

3. Calculations

In order to evaluate the biogeochemical transformation of the different constituents during the productive season, the concept of preformed concentrations is required. Using preformed concentrations in comparison with summer surface concentrations, the assumption of little or no vertical mixing and advection, has to be applied (Jennings et al., 1984). In our study we assume that C_T, oxygen and nitrate are equally mixed from below the temperature minimum depth to the surface water. This assumption might underestimate the consumption of nitrate, however, the sea–air exchange of CO_2 and oxygen should not be changed significantly.

In our areas of investigation the summer surface water is a mixture of winter surface water and sea ice melt. The winter surface water has a remnant during summer at the temperature minimum (T_{min}) (e.g. Ishii et al., 1998; Hoppema et al., 1999), found at 100–150 m depth (Fig. 2A). To obtain the preformed concentrations, the modification by addition of sea ice melt (meteoric water can be neglected) has to be compensated for, since the concentrations of the constituents in sea ice melt is different from that in the winter surface water. We assume the precipitation to be balanced by evaporation, and therefore this contribution is neglected in the calculations. In sea ice the constituents are trapped in the brine channels until the sea ice melts, and then they are released to the surface water. The salinity in sea ice melt water is variable, depending on the age of the sea ice. In this study a salinity of 6 is used for the seasonal sea ice (Eicken, 1998). Assuming a conservative behaviour of nitrate, A_T and C_T in the sea ice bulk water (Anderson and Jones, 1985) and a salinity of 6, the resulted concentrations in the melt water are 4.3, 406 and $386\,\mu mol\,kg^{-1}$, respectively. These values are obtained by normalization of the concentrations of respective chemical constituent in the winter water to a salinity of 6. Oxygen is not related to salinity as the other constituents, and therefore we assume oxygen to be saturated in the sea ice melt water. With this assumption the oxygen concentration corresponds to $440\,\mu mol\,kg^{-1}$ in sea ice melt water ($S = 6$ and $T = -0.3\,^{\circ}C$). The fraction of sea ice melt (f_{sim}) is calculated from

$$S_{meas} = (1 - f_{sim})\,S_{ww} + f_{sim}\,S_{sim}, \quad (1)$$

where S_{ww} and S_{sim} are the salinity of the winter surface water and sea ice melt, respectively. S_{ww} is found at the depth of T_{min} and S_{sim} is set to 6 (Eicken, 1998). The different concentrations, found at T_{min}, of the constituents used in the calculations are shown in Table 1.

For each of the nitrate, oxygen, C_T and A_T data points (Fig. 2), the change of concentration (Δc) in the surface water, since winter, is calculated according to

$$\Delta c = c_{preformed} - c_{measured}, \quad (2a)$$

which can be written as

$$\Delta c = ((1 - f_{sim})c_{ww} + f_{sim}\,c_{sim}) - c_{measured}, \quad (2b)$$

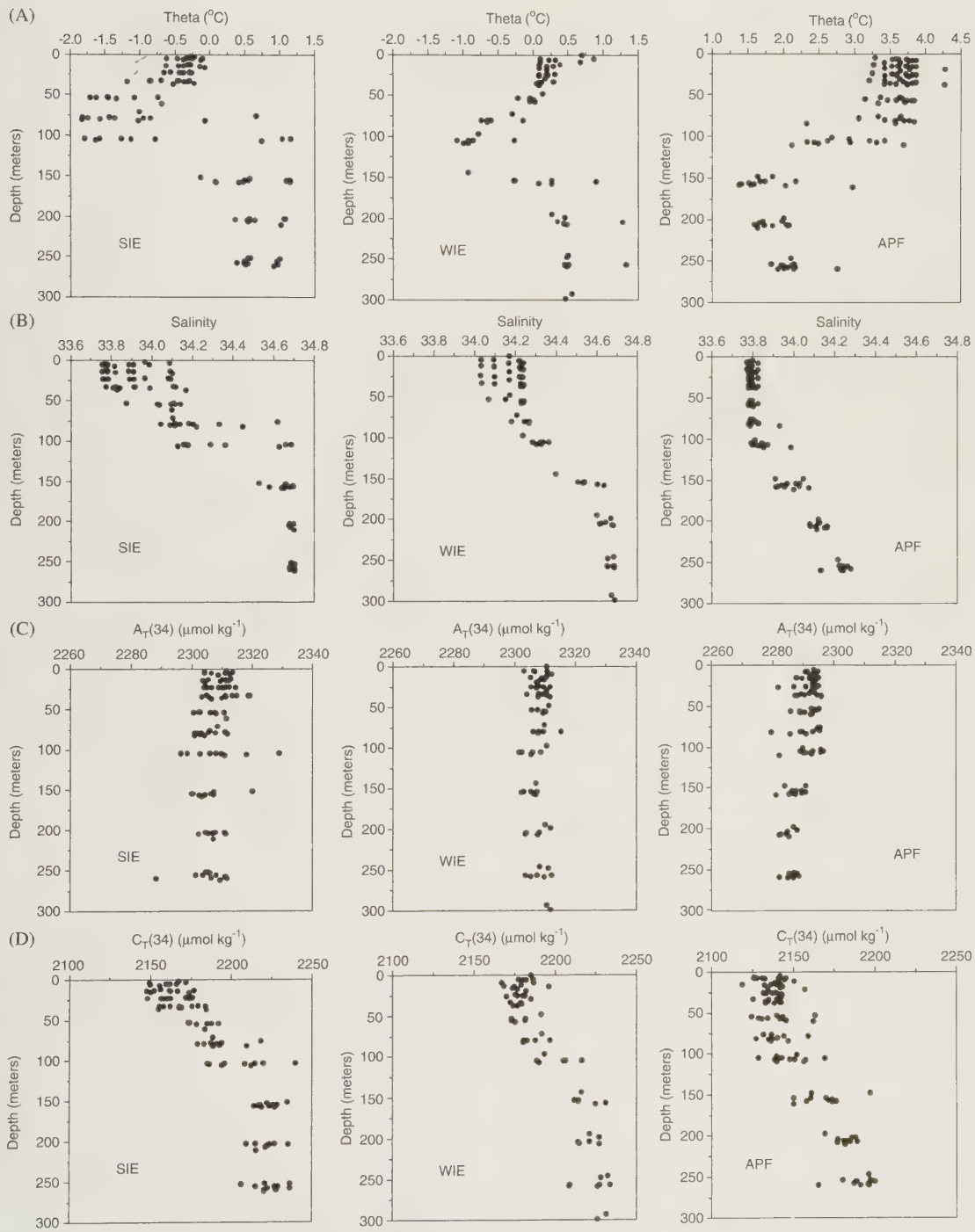

Fig. 2. Depth profiles of (A) potential temperature (theta), (B) salinity, (C) normalized A_T to a salinity of 34, (D) normalized C_T to a salinity of 34, (E) nitrate, (F) oxygen and (G) fCO_2 in the SIE, WIE and the APF, respectively.

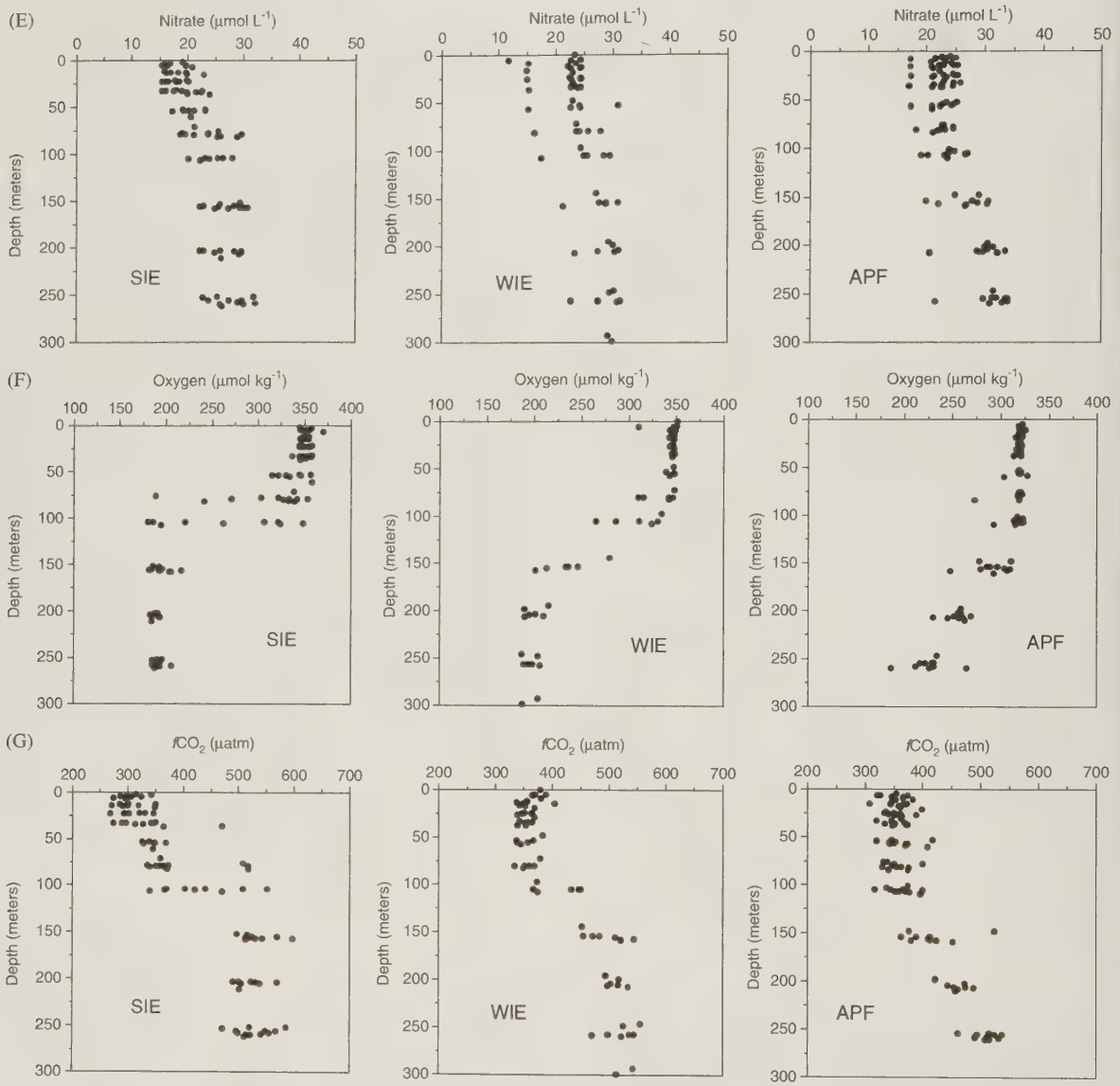

Fig. 2. (*Continued*)

where $c_{\text{preformed}}$ is the preformed concentration, c_{measured} is the measured concentration, and c_{ww} and c_{sim} are the concentrations in the winter water and sea ice melt of each constituent, respectively.

The changes (Δc) in nitrate and A_T are only due to biological activity, mainly through the following reactions representing the formation of proteins and calcium carbonate skeletons:

$$2CO_2 + NO_3^- + H^+ + H_2O \rightarrow$$

$$NHCH_2CO\ (\text{org}) + 3.5O_2 \quad (3a)$$

$$Ca^{2+} + 2HCO_3^- \rightarrow CaCO_3\ (\text{s}) + CO_2 + H_2O \quad (3b)$$

Reaction (3a) decreases nitrate and increases A_T with one equivalent, and decreases C_T by two,

Table 1
Mean values of the data at the temperature minimum (T_{min}), for each region

	SML depth (m)	T_{min} (°C)	A_T (μmol kg^{-1})	C_T (μmol kg^{-1})	NO_3 (μmol l^{-1})	O_2 (μmol kg^{-1})
SIE[a]	80±17	−1.70±0.11	2315±7	2197±4	22±2	327±14
WIE[b]	112±16	−0.91±0.11	2327±5	2221±30	25±4	303±19
APF[c]	160±18	1.71±0.23	2286±4	2171±15	27±3	288±22

n is the number of stations used for the mean values.
[a] $n = 6$.
[b] $n = 5$.
[c] $n = 6$ ($n = 5$ for oxygen).

while reaction (3b) decreases A_T by two equivalents and C_T by one. Parallel to reaction (3a) carbohydrates, lipids and phosphate ester groups are also formed. However, these reactions will not affect nitrate or A_T, only C_T and oxygen.

In this work nitrate is used as reference for the net biological uptake of CO_2, since atmospheric sources of nitrogen and ammonia can be neglected. Denitrification and nitrogen fixation are processes that also affect nitrate, but these are of insignificant importance for this evaluation.

The consumption of nitrate is converted into carbon equivalents using an empirical ratio between carbon and nitrate (C/N). This biological consumption of carbon is referred to new production (Dugdale and Goering, 1967). The ratio of C/N in the production of organic matter has been widely investigated starting with the classic Redfield ratio (RKR ratio) of 6.6 (Redfield et al., 1963). More recent studies have confirmed the validity of the RKR ratio in the Southern Ocean (Rubin et al., 1998; Gibson, 1998; Gibson and Trull, 1999; Hoppema and Goeyens, 1999). Other studies have shown C/N ratios in decaying organic matter to range between 7 and 8.5 (e.g. Jones et al., 1984; Takahashi et al., 1993; Anderson and Sarmiento, 1994; Wallace et al., 1995). Since this investigation is based on the consumption of carbon and nitrate, caused by production of organic matter the C/N ratio of 6.6 is applied.

An advantage of using nitrate compared to phosphate, representing the biological uptake of carbon, is that the C/N ratio observed in different phytoplankton species is constant, while the P/C ratio has shown an inconsistent behaviour (Bates et al., 1998; Carlson et al., 1998). The C/N ratio is consistent even at iron(II) deficit since the biological uptake of nitrogen varies as much as the uptake of carbon (Sakshaug and Holm-Hansen, 1977; de Baar et al., 1997). This is not the case for phosphate, where the C/P ratio changes with iron concentration (Sakshaug and Holm-Hansen 1977; de Baar et al., 1997).

By applying the C/N ratio of 6.6 and the changes in reactions (3), the change in C_T as a result of biological activity is calculated according to the following equations:

$$\Delta C_T^{bio} = \Delta C_T^{soft} + \Delta C_T^{hard}, \quad (4a)$$

where

$$\Delta C_T^{soft} = C/N \times \Delta NO_3^- \quad (4b)$$

and

$$\Delta C_T^{hard} = \Delta A_T^{hard} \times 0.5. \quad (4c)$$

Furthermore,

$$\Delta A_T = \Delta A_T^{soft} + \Delta A_T^{hard}, \quad (4d)$$

where

$$\Delta A_T^{soft} = -\Delta NO_3^-. \quad (4e)$$

Combining Eqs. (4c)–(4e), and together with (4b) inserted into (4a) gives

$$\Delta C_T^{bio} = C/N\,\Delta NO_3^- + (\Delta A_T + \Delta NO_3)\,0.5. \quad (5)$$

The superscripts "soft" and "hard" represent soft and hard biogenic matter as illustrated in reactions (3a) and (3b), respectively. The difference between ΔC_T and ΔC_T^{bio}, integrated over the surface mixed layer, is equal to the contribution by sea–air exchange of CO_2 ($\Delta C_T^{sea\text{-}air}$), since this is the only other source or sink of C_T. Similarly, the

contribution by sea–air exchange of oxygen, $\Delta O_2^{sea-air}$, can be calculated as the difference between ΔO_2 and ΔO_2^{bio}, where the latter equals $O/N \cdot \Delta NO_3^-$. The O/N ratio of −8.6 (−138/16) is used, according to the RKR ratio (Redfield et al., 1963).

4. Results

During our investigation all areas, including the SIE, were in open water with no sea ice. In the beginning of December 1997 there was an ice edge in the SIE, however, in January the ice had recently disappeared/melted. The results from the calculations of carbon consumption, new production and the oceanic net uptake or release of CO_2, for each region are presented in Table 2a. The corresponding results for oxygen are presented in Table 2b. The noted standard deviations reflect the variability between the stations within each of the three regions and a positive value indicates an oceanic flux to the atmosphere. The carbon consumption due to biological production, estimated from nitrate (i.e. new production), is about four times higher in the APF relative that in the SIE, where the lowest value is found.

The observed ΔC_T in the SIE and the APF minus the ΔC_T^{bio}, indicate an oceanic net release of CO_2, where the APF acts as a three times larger source, compared to the SIE. In the WIE, on the other hand the observed changes show an oceanic net uptake of CO_2 from the atmosphere. The observed changes in oxygen due to sea–air exchange show that the SIE and the WIE act as oceanic sinks for atmospheric oxygen, while a release of oxygen to the atmosphere is seen in the APF. For all stations in the entire region mean values of the sea–air exchange of CO_2 and oxygen indicated a small sea–air exchange of CO_2 of $0.2 \pm 0.5\,mol\,m^{-2}$ ($n = 17$) and of oxygen $-0.1 \pm 1.6\,mol\,m^{-2}$ ($n = 16$). However, the calculations do not consider the relative sizes (or width, from south to north) of the different regions, which is 89 km in the SIE, 100 km in the WIE and 178 km in the APF. Furthermore, the sea–air exchange is very variable within each region, resulting in a significant standard deviation of the mean sea–air exchange. This is also illustrated in Fig. 3 where oceanic net uptake or release of CO_2 and oxygen for each station is presented.

Table 2
Calculated changes of carbon and oxygen with standard deviations, representing the variability within each region

	ΔC_T^{soft} (new production)		ΔC_T	ΔC_T^{bio}	$\Delta C_T^{sea-air}$	
	$mol\,m^{-2}$	$g\,C\,m^{-2}$	$mol\,m^{-2}$	$mol\,m^{-2}$	$mol\,m^{-2}$	$g\,C\,m^{-2}$
(a) Carbon[a]						
SIE[b]	1.2±0.3	14±3.6	1.3±0.4	1.2±0.4	0.11±0.4	1.3±4.8
WIE[c]	2.0±0.8	24±9.3	1.8±1.0	1.9±0.8	−0.07±0.5	−0.8±6.0
APF[b]	4.0±0.7	48±7.9	4.4±0.9	3.9±0.5	0.54±0.7	6.5±8.4
	ΔO_2 ($mol\,m^{-2}$)	ΔO_2^{bio} ($mol\,m^{-2}$)	$\Delta O_2^{sea-air}$ ($mol\,m^{-2}$)			
(b) Oxygen[d]						
SIE[a]	−1.6±0.2	−1.5±0.4	−0.1±0.3			
WIE[b]	−3.9±2.5	−2.6±1.0	−1.4±1.7			
APF[c]	−4.0±2.7	−5.2±0.9	1.2±2.1			

n is the number of stations used for the mean values.

[a]The changes are preformed minus measured, according to Eqs. (4) and (5), and $\Delta C_T^{sea-air}$ is the difference between ΔC_T and ΔC_T^{bio}, with positive values indicating a loss from the sea.

[b]$n = 6$.

[c]$n = 5$.

[d]The changes are preformed minus measured and $\Delta O_2^{sea-air}$ is the difference between ΔO_2 and ΔO_2^{bio}, with positive values indicating a loss from the sea.

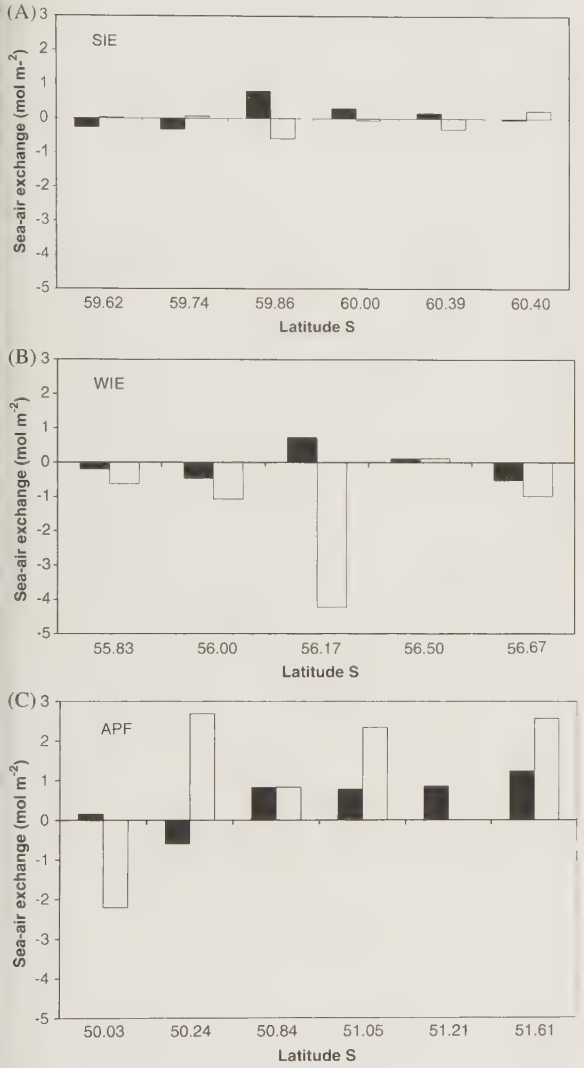

Fig. 3. Sea–air exchange of CO_2 (black bars) and oxygen (white bars) of the stations in the (A) SIE, (B) WIE, and the (C) APF. Positive sea–air exchange represents oceanic loss to the atmosphere and negative represents uptake.

5. Discussion

5.1. Biological production of soft and hard organic matter

Since the surface layer in the SIE was shallow (Table 1) and consequently more favourable for phytoplankton growth than that in the APF, the highest biological production might be expected in the SIE. However, in the SIE the previous ice cover presumably had a limiting effect on the biological productivity by hampering of the light penetration in the water column. Higher iron content in the APF relative to that in the SIE has been suggested to be one reason for the higher productivity (de Baar et al., 1995; Bathmann et al., 1997). In the WIE the estimate of new production is almost twice as high relative to that in the SIE. This can be explained by that the WIE coincides with the Weddell Front (Spiridonov et al., 1996; Veth et al., 1997), and regions in the Southern Ocean with dynamic hydrographic characteristics are considered to obtain high phytoplankton standing stock (Smetacek et al., 1990; Tréguer and Jacques, 1992; Robins et al., 1995; Bathmann et al., 1997). In this frontal area Spiridonov et al. (1996) found a maximum of chlorophyll *a* in early austral winter. In addition, the calculated new production in the SIE, WIE and the APF largely differs since the productive period does not start at the same time in the three areas. Hence, the SIE has the shortest productive period and the APF has the longest, due to the different ice conditions.

In order to estimate the daily new production and change in $\Delta C_T{}^{\text{sea–air}}$, the onset of primary production had to be known. Since primary production depends on light conditions, a function of ice cover and mixed layer depth (e.g. Smith and Nelson, 1990), the start of the biological production varies between areas and years. In an annual study of the SIE off East Antarctica, Gibson and Trull (1999) observed an increase in chlorophyll *a* and oxygen, and a decrease in nitrate in November, indicating the beginning of spring bloom. Assuming that our observed changes were built up from November to January (end of our study) i.e. 90 days, the daily new production can be calculated. The daily new production thus resulted in 0.16, 0.27 and 0.53 $g C m^{-2} day^{-1}$ for the SIE, WIE and the APF, respectively (Table 3). These values can be compared to estimates from the Weddell Sea, where the mean new production in the marginal ice zone (corresponding to the SIE) varied from 0.40 $g C m^{-2} day^{-1}$ in November to 0.25 $g C m^{-2} day^{-1}$ in March with an average of 0.32 $g C m^{-2} day^{-1}$ for the 5-month period (Smith and Nelson, 1990). Gibson and Trull (1999) suggested the productive season to end in March,

Table 3
New production and sea-air fluxes of carbon dioxide and oxygen, based on $\Delta^{sea\ air}$ from Table 2 and a 90 day period to achieve daily change

	New production		Carbon dioxide ($mmol\,m^{-2}\,day^{-1}$)	Oxygen ($mmol\,m^{-2}\,day^{-1}$)
	$mmol\,m^{-2}\,day^{-1}$	$g\,C\,m^{-2}\,day^{-1}$		
SIE	13±3	0.16±0.04	1.2±4.4	−1.1±3.3
WIE	22±9	0.27±0.10	−0.8±5.7	−16±19
APF	44±7	0.53±0.09	6.0±7.3	10±24

however, our study is based on a 3-month period (November to January). Hence, this can be a possible explanation for the lower value ($0.16\,g\,C\,m^{-2}\,day^{-1}$) in our calculation.

The effect of calcification and dissolution of calcium carbonate was considered through ΔA_T (Eqs. (4c)–(4e)). The effect of these processes on ΔC_T was evaluated to maximum 3% of ΔC_T, which was corrected for in the calculations. The observed ΔA_T did not show any significant formation of calcium carbonate or dissolution since winter. This is in agreement with Karlson and Godhe (1998) who reported that calcium carbonate producing plankton were insignificant in study area during our cruise. This is in agreement with a study by Honjo (1991). However, at some occasions coccolithophores have been found close to the Polar Front (Eynaud et al., 1999).

5.2. Fluxes

5.2.1. Carbon dioxide

During winter the surface water is enriched with CO_2, caused by mixing with deeper water. Another explanation for the high CO_2 concentration can also be a result of local mineralization of organic carbon in the water column (Gibson and Trull, 1999). In spring the summer surface water is formed due to warming, causing a supersaturation of CO_2 in the surface water. The relatively little freshening by sea ice melt has a minor effect on the solubility of gases. Continuing warming, mainly in the APF, of this water further strengthens the CO_2 supersaturation, resulting in a loss of CO_2 to the atmosphere. In spring when primary production starts, CO_2 is consumed, which lowers the CO_2 concentration and with time even results in undersaturation. Our calculations indicated that the SIE and the APF acted as net sources of CO_2, while the WIE acted as an oceanic net sink. In the WIE the primary production is the likely cause of the net CO_2 uptake in the WIE, where the new production is higher than in the SIE. However, although the highest new production is observed in the APF, the CO_2 uptake by biological production is not large enough during the 3-month period to compensate for the strong oceanic loss of CO_2 in winter/spring. This explanation is probably also valid for the SIE, where the new production is lower than in the other two areas. In both the SIE and the WIE the ice cover has a large impact on the CO_2 sea–air exchange, since the ice cover prevents the oceanic CO_2 to equilibrate with the atmospheric during winter. When the CO_2 enriched winter surface water is exposed to the atmosphere, the oceanic CO_2 escapes. Net oceanic release of CO_2 to the atmosphere was also found in the marginal ice zone (corresponds to SIE) by Bakker et al. (1997), which they attributed to the uncovering of supersaturated surface water after a recent ice retreat. Carrillo and Karl (1999) also pointed out that, despite the potential for uptake of atmospheric CO_2 in the ice-edge regions of Gerlache Strait, Antarctica, the sinks may be balanced by equally large CO_2 sources during the winter caused by respiration and upwelling of CO_2 enriched water. However, Hoppema et al. (1999) found in their study in the Weddell Sea that the upwelling of CO_2 enriched water was smaller than the drawdown of CO_2 by biological production.

Fig. 2G shows that all values at the T_{min} depth and below are higher than the atmospheric CO_2, which is 363 µatm (Chierici et al., 2004). The surface water fCO_2 is lower compared to that at the T_{min} depth (Fig. 2G), which is mainly a result of recent processes (e.g. biological production) in austral summer (in January). In the SIE there was an indication of a recent bloom of *phaeocystis* (Karlson and Godhe, 1998), consuming CO_2. In combination with lower seawater temperature in the SIE than in the WIE and the APF, these factors can explain the relatively low fCO_2 in the surface layer at SIE in January. In the study by Chierici et al. (2004) all the three areas indicated an oceanic sink of CO_2. The result from that study shows the current situation in these areas, since the parameters of the CO_2 system are instantly measured (Fig. 2G). In contrast, the study in this work includes the change in the chemical constituents during a longer time period, and is explained by both outgassing of CO_2 to the atmosphere in spring and biological production. This preformed concentration approach includes the history of all biogeochemical processes, from austral winter to January.

As for new production we assume a 90-day period for the observed changes of $\Delta C_T^{sea-air}$, giving a daily net flux of CO_2 to the atmosphere of $1.8 \pm 4.3\,mmol\,m^{-2}\,day^{-1}$ in the SIE and $6.0 \pm 7.3\,mmol\,m^{-2}\,day^{-1}$ in the APF. In the WIE the corresponding CO_2 flux is -0.8 ± 5.7 (Table 3). Computed fluxes, using ΔfCO_2 from the mesoscale survey during the same expedition, and the formulation of Wanninkhof and McGillis (1999), resulted in sea–air fluxes of CO_2 of −0.8, −0.3 and $-3.1\,mmol\,m^{-2}\,day^{-1}$ for the SIE, WIE and APF, respectively (Chierici et al., 2004). However, the fluxes in Chierici et al. (2004) represent the fluxes at the current situation in January, while our estimates are a net effect of all processes during the 3-month period.

5.2.2. Oxygen

The calculated oxygen changes (i.e. $\Delta O_2^{sea-air}$) observed in the SIE and the WIE suggest a previous net uptake of oxygen from the atmosphere during the period from austral winter to January. In the APF the ocean shows the opposite behaviour, where a net oceanic flux of oxygen to the atmosphere is calculated. During winter the oxygen concentrations are low in all areas, according to the oxygen concentrations deeper than the T_{min} depth (Fig. 2F). This deeper water is mixed with the surface layer in winter, causing low concentration of oxygen in the winter surface water. This is supported by a study of Gibson and Trull (1999), who found decreasing concentrations of oxygen in the surface water from March to early November. The low concentration in the winter surface water leads to an undersaturation in the newly formed summer surface layer, however, subsequently this signal is reduced by the seasonal warming. An additional factor is that in the SIE the recent ice cover has isolated the surface water from equilibrating with the oxygen in the atmosphere. Both the SIE and the WIE show lower new production, relative the APF, and the oxygen release during photosynthesis has probably not been high enough to compensate for the undersaturation. In the APF, conversely, the relatively intense productivity, combined with the increased seawater temperature resulted in a supersaturation of oxygen. The daily fluxes of oxygen are evaluated, assuming a 90-day period as for CO_2, resulting in fluxes to the ocean of 1.1, 16 and out of the ocean of $10\,mmol\,m^{-2}\,day^{-1}$, for the SIE, WIE and APF, respectively (Table 3).

5.2.3. Comparison of CO_2 and oxygen sea–air exchange

No clear pattern is observed comparing the sea–air exchange of CO_2 and oxygen. In the SIE, the CO_2 and oxygen sea–air exchange in almost all stations are inversely correlated (Fig. 3), and the absolute sea–air exchange of CO_2 and oxygen is about the same. This pattern might give an indication of the biological production. However, since the biological production was relatively low, this can reflect that the effect of winter water mixing and ice cover is similar. Furthermore, the result almost agrees with the Redfield O/C ratio of −1.3 (Redfield et al., 1963), where the ratio between the mean values of $\Delta O_2^{sea-air}$ and $\Delta C_T^{sea-air}$ (Table 2) is almost −1.0 (−0.1/0.11). The ratio between ΔO_2 and ΔC_T, where sea–air exchange is included, is −1.2 (−1.6/1.3), indicating

that the sea–air exchange does not effect the O/N ratio significantly in the SIE. Almost all stations in the WIE show the same direction of both the CO_2 and oxygen sea–air exchange (Fig. 3). The oxygen sea–air exchange is about twice as large as the sea–air exchange of CO_2, and both gases indicate a mean oceanic uptake from the atmosphere. In the APF there is a mean oceanic source of both CO_2 and oxygen to the atmosphere (Fig. 3). The new production is largest in this area, resulting in a relatively large oxygen production. The biological activity, in combination with increased temperature in spring, should lead to a supersaturation of oxygen in the surface water. The CO_2 concentration in the surface water, on the other hand, increases due to upwelling of CO_2-enriched water. The temperature increase further enhances the supersaturation in the surface water in spring, resulting in outgassing of CO_2. The decrease of CO_2 due to biological production has not been large enough to compensate for this oceanic release of CO_2 to the atmosphere.

5.2.4. Uncertainties in the analytical methods and calculations

One uncertainty in our calculations is attributed to the imprecision of the applied analytical methods. These deviations are combined to all determinations resulting in an uncertainty ($\mathrm{mol\,m^{-2}}$), using the following statistical formula:

$$\text{uncertainty} = (x * (y * z/1000)^2))^{-0.5},$$

where x is the number of depth interval of the surface mixed layer (m), y is the range of each depth interval (m), and z is the integrated deficit of any property ($\mathrm{mol\,m^{-2}}$). x multiplied by y is the same as the depth of the surface mixed layer (m). The maximum uncertainty in the computed $\Delta C_T{}^{\text{sea–air}}$ is $\pm 0.2\,\mathrm{mol\,m^{-2}}$, or 30–40% of the variability within each region.

Another essential uncertainty is the choice of C/N ratio used in Eq. (4b). We have used the classical C/N ratio of 6.6 (Redfield et al., 1963), which is close to other values reported from the Southern Ocean 6.9 ± 0.6 (Rubin et al., 1998) and 6.0 ± 0.2 (Gibson, 1998; Gibson and Trull, 1999). Hoppema and Goeyens (1999) confirmed the validity for the Redfield ratio in the surface layer of the Weddell Sea, where they estimated a C/N ratio of 5.7. The effect of different C/N ratios on ΔC_T^{bio} is directly proportional to the change in the ratio. Consequently a C/N ratio of 7.3, found in the Indian sector of the Southern Ocean (Tréguer et al., 1990), will result in a change of about 10% in ΔC_T^{bio}.

Respiration by zooplankton in the surface water or at T_{min} depth might increase the C/N ratio. Assuming a change in these relative concentrations, the calculated sea–air exchange might change. As a result of increased CO_2 compared to decreased nitrate due to respiration, the sink would be larger or the source smaller. Since we have no measurements on respiration, we cannot make any complements to the calculations.

The estimate of new production is based on the consumption of nitrate from austral winter to January. Other nitrogen constituents, predominantly ammonium, may also be abundant. The concentration of ammonium in winter surface water is likely small (Rönner et al., 1983; Bury et al., 1995), but during the time of investigation it can be significant in the surface water. If so, our estimated ΔC_T^{bio} is overestimated as the ammonium must have been added through decay of organic matter and respiration, which is not compensated for in our estimate. The consumption of nitrate is in the order of 5–10 $\mu\mathrm{mol\,l^{-1}}$, while the ammonium concentration in austral summer in the Southern Ocean has been reported to 0.2–0.5 $\mu\mathrm{mol\,l^{-1}}$ (Smith and Nelson, 1986; Smith, 1991; Bury et al., 1995). Hence, the maximum overestimation in our calculations is 3.5–8%, which is less than the uncertainty due to the variability within the areas.

The used productive period is suggested to end in March (Gibson and Trull, 1999). However, our study is based on a 3-month period (November–January), and we believe that the primary production has not reached its maximum during this period, which can explain the relatively low new production for the entire study. Considering the fact of an extended productive period, a higher new production might be estimated. However, at the end of the period the mineralization is more pronounced, increasing the nitrate concentration. Hence, the new production would end up lower.

Consequently, the net effect of both these hypotheses might cancel out each other.

Calculating sea–air exchange, there is an uncertainty of the effect of vertical mixing and advection. We have applied an assumption of negligible effect on the calculations of sea–air exchange. However, in the APF and the WIE this assumption might be critical since the water masses in these areas are relatively dynamic. In these areas the T_{min} depth is not pronounced by a sharp gradient, which might be a result of mixing. However, we assume that the biochemical parameters are mixed equally from the water below T_{min} to the surface layer. This would not affect the calculated sea–air exchange, but only the new production, which would be underestimated. Since we have no winter data from 1997, the winter water concentrations can be compared with winter data from 1992 (Hoppema et al., 2000), and we can investigate the validity of the model approach. In the study by Hoppema et al. (2000) the winter surface water temperatures were almost the same as those found at T_{min} in our study at SIE and APF. The temperature in the area corresponding to the WIE is lower, which is acceptable, since the underlying water is warmer. Therefore, mixing of water from below seems to be negligible. The oxygen concentrations show similar values as the winter data, but C_T in the WIE and the APF is about $\pm 10\,\mu mol\,kg^{-1}$ higher. However, this is close to the uncertainty due to the relatively large variability within the areas. For nitrate the winter values in our study are slightly lower in the SIE and the WIE than in those by Hoppema et al. (2000). Nevertheless, the two studies represent two different years, and the values cannot be expected to be exactly the same. Hoppema et al. (1999) found in their study that the temperature minimum in December/January was within 0.1 °C of the near-freezing winter surface layer, and could be considered a remnant of the surface water from previous winter. This is valid also for the temperature minimum of −1.7 °C in the SIE, which was close to the freezing point of −1.8 °C. In the study by Hoppema et al. (1999), the winter water value of C_T at 100 m was the same as the summer value in the central Weddell Sea (can be compared to the SIE). The depth profile of the winter C_T showed that the surface water was homogenous from surface down to 80 m. That depth was close to the T_{min} depth at SIE in our study, which means that we can assume that the winter water can be found at T_{min}.

The estimated total uncertainties of the $\Delta C_T^{sea\ air}$ in Table 2a, from all above effects, are significantly less than the variability within the three regions. Hence, the standard deviations also include uncertainties from analytical errors, C/N ratios and neglected biochemical processes, such as ammonium release and zooplankton respiration.

6. Conclusions

The most significant conclusion from this study is the fact that the Atlantic sector of the Southern Ocean is a weak source ($2.3 \pm 5.9\,mmol\,m^{-2}\,day^{-1}$) of atmospheric CO_2 from austral winter to January, instead of a sink. However, the variability due to both time and space is as large as the calculated fluxes, and parts of the investigated area act as sources (the SIE and the APF) and parts act as sinks (the WIE). Although assumptions about the different processes in the area, this approach gives us an important insight in the carbon cycle, where the variability due to seasonal changes over a longer time period is considered. This method minimizes the uncertainty in the calculated sea air fluxes over a longer time period, compared to methods where sea–air fluxes are calculated from measured ΔfCO_2 and wind speed, and sea–air fluxes are extrapolated over any time span.

The new production is about four times higher in the APF than in the SIE and twice as high than in the WIE, with a mean for all regions of $0.32 \pm 0.14\,g\,C\,m^{-2}\,day^{-1}$. Although there is relatively high new production in the APF, the calculated CO_2 sea–air exchange shows loss to atmosphere. The oxygen fluxes vary between the areas, with net fluxes to the sea in the SIE and the WIE, and to the atmosphere in the APF. The mean sea air flux for the whole region is for oxygen $-1.1 \pm 18\,mmol\,m^{-2}\,day^{-1}$.

Acknowledgements

The authors would like to thank the Swedish Polar Research Secretariat, the Swedish Natural

Science Research Council (NFR) and the Göteborg Marine Centre (GMF) for financial support. Thanks also to the scientific leader David Turner and to Anne-Marie Larsson, Leif Djurfeldt, Per-Ingvar Sehlstedt, Ole-Anders Nøst and Elisabeth Engum for providing salinity and temperature data. Thanks to the crew of the *SA Agulhas*, and special thanks to Chris Rohleder for all technical support.

References

Anderson, L.A., Sarmiento, J.L., 1994. Redfield ratios of remineralization determined by nutrient data analysis. Global Geochemical Cycles 8, 65–80.

Anderson, L.G., Jones, E.P., 1985. Measurements of total alkalinity, calcium and sulfate in natural sea ice. Journal of Geophysical Research 90, 7355–7360.

Bakker, D.C.E., de Baar, H.J.W., Bathmann, U.V., 1997. Changes of carbon dioxide in surface-waters during spring in the Southern Ocean. Deep-Sea Research II 44, 91–128.

Bates, N.R., Hansell, D.A., Carlson, C.A., 1998. Distribution of CO_2 species, estimates of net community production, and air–sea CO_2 exchange in the Ross Sea polynya. Journal of Geophysical Reseach 103, 2883–2896.

Bathmann, U.V., Scharek, R., Klaas, C., Dubischar, C.D., Smetacek, V., 1997. Spring development of phytoplankton biomass and composition in major water masses of the Atlantic sector of the Southern Ocean. Deep-Sea Research II 44, 51–67.

Bury, S.J., Owens, N.J.P., Preston, T., 1995. ^{13}C and ^{15}N uptake by photoplankton in the marginal ice zone of the Bellinghausen Sea. Deep-Sea Research II 42, 1225–1252.

Caldeira, K., Duffy, P.B., 2000. The role of the Southern Ocean in uptake and storage of anthropogenic carbon dioxide. Science 287, 620–622.

Carlson, C.A., Ducklow, H.W., Hansell, D.A., Smith, W.O., 1998. Organic carbon partitioning during spring phytoplankton blooms in the Ross Sea Polynya and the Sargasso Sea. Limnology and Oceanography 43, 375–386.

Carrillo, J.C., Karl, D.M., 1999. Dissolved inorganic carbon pool dynamics in northern Gerlache Strait, Antarctica. Journal of Geophysical Research 104, 15,873–15,884.

Chierici, M., Fransson, A., Turner, D.R., Pakhomov, E.A., Froneman, P.W., 2004. Variability in pH, fCO_2, oxygen and flux of CO_2 in the surface water along a transect in the Atlantic sector of the Southern Ocean. Deep-Sea Research II, this issue [doi:10.1016/j.dsr2.2001.03.002].

de Baar, H.J.W., de Jong, J.T.M., Bakker, D.C.E., Löscher, B.M., Veth, C., Bathmann, U., Smetacek, V., 1995. Importance of iron for plankton blooms and carbon-dioxide drawdown in the Southern Ocean. Nature 373, 412–415.

de Baar, H.J.W., van Leeuwe, M.A., Scharek, R., Goeyens, L., Bakker, K.M.J., Fritsche, P., 1997. Nutrient anomalies in *Fragilariopsis kerguelensis* blooms, iron deficiency and the nitrate/phosphate ratio (A.C. Redfield) of the Antarctic Ocean. Deep-Sea Research II 44, 229–260.

Dickson, A.G., Riley, J.P., 1978. The effect of analytical error on the evaluation of the components of the aquatic carbon-dioxide system. Marine Chemistry 6, 77–85.

DOE, 1994. In: Dickson, A.G., Goyet, C. (Eds.), Handbook of methods for the analysis of the various parameters of the carbon dioxide system in sea water; Version 2. ORNL/CDIAC-74.

Dugdale, R.C., Goering, J.J., 1967. Uptake of new and regenerated forms of nitrogen in primary productivity. Limnology and Oceanography 12, 196–206.

Eicken, H., 1998. Deriving modes and rates of ice growth in the Weddell Sea from microstructural, salinity and stable-isotope data. In: Jeffries, M.O. (Ed.), Antarctic Sea Ice: Physical Processes, Interactions and Variability, vol. 74. American Geophysical Union, Washington, DC, Antarctic Research Series, pp. 89–122.

Eynaud, F., Giraudeau, J., Pichon, J.-J., Pudsey, C.J., 1999. Sea-surface distribution of coccolithophores, diatoms and dinoflagellates in the South Atlantic Ocean during the late austral summer 1995. Deep-Sea Research I 46, 451–482.

Gibson, J.A.E., 1998. Carbon flow through inshore marine environments of the Vestfold Hills, East Antarctica. ANARE Reports 139, 222pp.

Gibson, J.A.E., Trull, T.W., 1999. Annual cycle of fCO_2 under sea-ice and in open water in Prydz Bay, East Antarctica. Marine Chemistry 66, 187–200.

Haraldsson, C., Anderson, L.G., Hassellöv, M., Hulth, S., Olsson, K., 1997. Rapid, high-precision potentiometric titration of alkalinity in the ocean and sediment pore waters. Deep-Sea Research I 44, 2031–2044.

Honjo, S., 1991. Particle fluxes and modern sedimentation in the polar oceans. In: Smith, W.O. (Ed.), Polar Oceanography, Part B. Academic, San Diego, CA, pp. 687–739.

Hoppema, M., Goeyens, L., 1999. Redfield behavior of carbon, nitrogen, and phosphorus depletions in Antarctic surface water. Limnology and Oceanography 44, 220–224.

Hoppema, M., Fahrbach, E., Stoll, M.H.C., de Baar, H.J.W., 1999. Annual uptake of atmospheric CO_2 by the Weddell Sea derived from a surface layer balance, including estimations of entrainment and new production. Journal of Marine Systems 19, 219–233.

Hoppema, M., Fahrbach, E., de Baar, H.J.W., 2000. Surface layer balance of the southern Antarctic Circumpolar Current (prime meridian) used to derive carbon and silicate consumption and annual air–sea exchange for CO_2 and oxygen. Journal of Geophysical Research 105, 11,359–11,371.

Ishii, M., Inoue, Y.H.Y., Matsueda, H., Tanoue, E., 1998. Close coupling between seasonal biological production and dynamics of dissolved inorganic carbon in the Indian Ocean sector and the western Pacific Ocean sector of the Antarctic Ocean. Deep-Sea Research 45, 1187–1209.

Jennings, J.C., Gordon, L.I., Nelson, D.M., 1984. Nutrient depletion indicates high primary productivity in the Weddell Sea. Nature 309, 51–54.

Johnson, K.M., King, A.E., Sieburth, J.M., 1985. Coulometric TCO_2 analyses for marine studies: an introduction. Marine Chemistry 16, 61–82.

Johnson, K.M., Sieburth, J.M., Williams, P.J., Brandstrom, L., 1987. Coulometric total carbon dioxide analysis for marine studies: automation and calibration. Marine Chemistry 21, 117–133.

Jones, E.P., Dyrssen, D., Coote, A.R., 1984. Nutrient regeneration in deep Baffin Bay with consequences for measurements of the conservative tracer NO and fossil fuel CO_2 in the oceans. Canadian Journal of Fishery Aquatic Science 41, 30–35.

Karlson, B., Godhe, A., 1998. Phytoplankton observations in the Atlantic sector of the Southern Ocean. Polarforskningssekretariatets årsbok, 69–70.

Koroleff, F., 1976. In: Grasshoff, K. (Ed.), Methods of Seawater Analysis. Verlag Chemie, New York.

Lancelot, C., Billen, G., Veth, C., Becquevort, S., Mathot, S., 1991. Modelling carbon cycling through phytoplankton and microbes in the Scotia–Weddell Sea area during sea ice retreat. Marine Chemistry 35, 305–324.

Lewis, E., Wallace, D.W.R., 1998. Program Developed for CO_2 System Calculations. ORNL/CDIAC-105. Carbon Dioxide Information Analysis Center, Oak Ridge National Laboratory, U.S. Department of Energy, Oak Ridge, Tennessee.

Louanchi, F., Hoppema, M., Bakker, D.C.E., Poisson, A., Stoll, M.H.C., de Baar, H.J.W., Schauer, B., Ruiz-Pino, D.P., Wolf-Gladrow, D., 1999. Modelled and observed sea surface fCO_2 in the southern ocean: a comparative study. Tellus 51B, 541–559.

Mehrbach, C., Culberson, C.H., Hawley, J.E., Pytkowicz, R.M., 1973. Measurement of the apparent dissociation constants of carbonic acid in seawater at atmospheric pressure. Limnology and Oceanography 18, 897–907.

Metzl, N., Beauverger, C., Brunet, C., Goyet, C., Poisson, A., 1991. Surface water carbon dioxide in the southwest Indian sector of the Southern Ocean: a highly variably variable CO_2 source/sink region in summer. Marine Chemistry 35 (1–4), 85–95.

Mostert, S.A., 1983. Procedures used in South Africa for the automatic photometric determination of micronutrients in seawater. South African Journal of Marine Science 1, 189–198.

Murphy, P.P., Feely, R.A., Gammon, R.H., Kelly, K.C., Waterman, L.S., 1991. Autumn air–sea disequilibrium of CO_2 in the South Pacific Ocean. Marine Chemistry 35, 77–84.

Poisson, A., Metzl, N., Brunet, C., Schauer, B., Bres, B., Ruiz-Pino, D., Louanchi, F., 1993. Variability of sources and sinks of CO_2 in the Western Indian and Southern Oceans during the year 1991. Journal of Geophysical Research 98, 22,759–22,778.

Redfield, A.C., Ketchum, B.H., Richards, F.A., 1963. The influence of organisms on the composition of seawater. In: Hill, M.N. (Ed.), The Sea, vol. 2. Wiley, New York, pp. 26–77.

Robertson, J.E., Watson, A.J., 1995. A summer time sink for atmospheric CO_2 in the Southern Ocean between 88°W and 80°E. Deep-Sea Research II 42, 1081–1091.

Robins, D.B., Harris, R.P., Bedo, A.W., Fernández, E., Fileman, T.W., Harbour, D.S., Head, R.N., 1995. The relationship between suspended particulate material, phytoplankton and zooplankton during the retreat of the marginal ice zone in the Bellinghausen Sea. Deep-Sea Research II 42, 1137–1158.

Rönner, U., Sörensson, F., Holm-Hansen, O., 1983. Nitrogen assimilation by photoplankton in the Scotia Sea. Polar Biology 2, 137–147.

Roy, R.N., Roy, L.N., Vogel, K.M., Porter-Moore, C., Pearson, T., Good, C.E., Millero, F.J., Campbell, D., 1993. The dissociation constants of carbonic acid in sea water at salinities 5-45 and temperatures 0–45 °C. Marine Chemistry 44, 249–267.

Roy, R.N., Roy, L.N., Vogel, K.M., Porter-Moore, C., Pearson, T., Good, C.E., Millero, F.J., Campbell, D., 1994. Erratum for: the dissociation constants of carbonic acid in sea water at salinities 5–45 and temperatures 0–45 °C. Marine Chemistry 45, 337.

Rubin, S.I., Takahashi, T., Chipman, D.W., Goddard, J.G., 1998. Primary productivity and nutrient utilization ratios in the Pacific sector of the Southern Ocean based on seasonal changes in seawater chemistry. Deep-Sea Research I 45, 1211–1234.

Sakshaug, E., Holm-Hansen, O., 1977. Chemical composition of *Skeletonema Costatum (Grev.) Cleve* and *Pavlova (Monochrystis) Lutheri (Droop) Green* as a function of nitrate-, phosphate- and iron limited growth. Journal of Experimental Marine Biology and Ecology 29, 1–34.

Smetacek, V., Scharek, R., Nöthig, E.-M., 1990. Seasonal and regional variation in the pelagial and its relationship to the life-history of krill. In: Kerry, K.R., Hempel, G. (Eds.), Antarctic Ecosystems Ecological Change and Conservation. Springer, Berlin, pp. 103–114.

Smetacek, V., de Baar, H.J.W., Bathmann, U.V., Lochte, K., Rutgers van der Loeff, M.M., 1997. Ecology and biogeochemistry of the Antarctic Circumpolar Current during austral spring: a summary of Southern Ocean JGOFS cruise ANT X/6 of R.V. Polarstern. Deep-Sea Research II 44, 1–21.

Smith, W.O., 1991. Nutrient distributions and new production in polar regions: parallels and contrasts between the Arctic and the Antarctic. Marine Chemistry 35, 245–257.

Smith, W.O., Nelson, D.M., 1985. Phytoplankton bloom produced by a receding ice edge in the Ross Sea: spatial coherence with the density field. Science 277, 163–166.

Smith, W.O., Nelson, D.M., 1986. Importance on ice edge phytoplankton blooms in the Southern Ocean. Bioscience 36, 251–257.

Smith, W.O., Nelson, D.M., 1990. Phytoplankton growth and new production in the Weddell Sea marginal ice zone in austral spring and autumn. Limnology and Oceanography 35, 809–821.

Solorzano, L., Sharp, J.H., 1980. Determination of total dissolved nitrogen in natural waters. Limnology and Oceanography 25, 751–754.

Spiridonov, V.A., Nöthig, E.-M., Schröder, M., Wisotzki, A., 1996. The onset of biological winter in the eastern Weddell Gyre (Antarctica) planktonic community. Journal of Marine Systems 9, 211–230.

Stoll, M.H.C., de Baar, H.J.W., Hoppema, M., Fahrbach, E., 1999. New early winter fCO_2 data reveal continous uptake of CO_2 by the Weddell Sea. Tellus B 51, 679–687.

Takahashi, T., 1989. The carbon dioxide puzzle. Oceanus 32 (2), 22–29.

Takahashi, T., Olafson, J., Goddard, J.G., Chipman, D.W., Sutherland, S.C., 1993. Seasonal variation of CO_2, and nutrient salts over the high latitude oceans: a comparative study. Global Biogeochemical Cycles 7, 843–878.

Tréguer, P., Jacques, G., 1992. Dynamics of nutrients and phytoplankton, and fluxes of carbon, nitrogen and silicon in the Antarctic Ocean. Polar Biology 12, 149–162.

Tréguer, P., Nelson, D.M., Gueneley, S., Zeyons, C., Morvan, J., Buma, A., 1990. The distribution of biogenic and lithogenic silica and the composition of particulate organic matter in the Scotia Sea and the Drake Passage during autumn 1987. Deep-Sea Research 37, 833–851.

Veth, C., Peeken, I., Scharek, R., 1997. Physical anatomy of fronts and surface waters in the ACC near the 6°W meridian during austral spring 1992. Deep-Sea Research II 44, 23–49.

Wallace, D.W.R., Minnett, P.J., Hopkins, T.S., 1995. Nutrients, oxygen and inferred new production in the Northeast Water Polynya. Journal of Geophysical Research 100, 4323–4340.

Wanninkhof, R., McGillis, W.R., 1999. A cubic relationship between air–sea CO_2 exchange and wind speed. Geophysical Research Letters 26, 1889–1892.

Wanninkhof, R., Lewis, E., Feely, R.A., Millero, F.J., 1999. The optimal carbonate dissociation constants for determining surface water pCO_2 from alkalinity and total inorganic carbon. Marine Chemistry 65, 291–301.

ELSEVIER

Deep-Sea Research II 51 (2004) 2773–2787

DEEP-SEA RESEARCH
PART II

www.elsevier.com/locate/dsr2

Variability in pH, fCO_2, oxygen and flux of CO_2 in the surface water along a transect in the Atlantic sector of the Southern Ocean

Melissa Chierici[a,*], Agneta Fransson[a,1], David R. Turner[a], E.A. Pakhomov[b,2], P.W. Froneman[b]

[a]*Department of Chemistry, Analytical and Marine Chemistry, Göteborg University, SE-412 96 Göteborg, Sweden*
[b]*Southern Ocean Group, Department of Zoology and Entomology, Rhodes University, P.O. Box 94, Grahamstown 6140, South Africa*

Abstract

Underway sampling and measurements of pH, fCO_2, oxygen and Chlorophyll *a* (Chl *a*) were performed in the surface waters from Cape Town (South Africa) to Queen Maud Land (Antarctica) in the Atlantic sector of the Southern Ocean during the austral summer 1997/1998. From direct measurements of these parameters and from calculated fCO_2 the oceanic carbon dioxide system was studied and related to hydrological and biological parameters. fCO_2 was in general undersaturated relative to the atmosphere and showed a large variability with values ranging from 313 to 377 µatm with a mean value of 346 ± 13 µatm. The undersaturation was more pronounced in areas associated with fronts where high Chl *a* and high pH in situ values were observed. Using shipboard wind speed data, estimates of the CO_2 flux were made along the transect and during three mesoscale surveys on the northward return transect in the area of the Spring Ice Edge (SIE), the Winter Ice Edge (WIE) and in the Antarctic Polar Front (APF). The undersaturation observed during the transect caused the ocean to act as a sink for CO_2 with a mean sea–air flux for the entire transect of -3 ± 5 mmol $m^{-2} d^{-1}$ with a large variability between -20 mmol $m^{-2} d^{-1}$ (oceanic uptake) to 1.3 mmol $m^{-2} d^{-1}$ (oceanic source). The lowest fCO_2 values (largest oceanic uptake of CO_2) were found at the southern boundary of the APF at 53°S, which coincided with a supersaturation in oxygen and high pH values. Oxygen concentrations were measured from 50°S to 63°S and varied between 324 and 359 µmol kg^{-1} with a mean value of 347 ± 9 µmol kg^{-1}. In general only small deviations from equilibrium oxygen saturation were observed (mean value $= 99 \pm 2\%$). However, in the SIE oxygen was clearly undersaturated, probably an effect of upwelling of oxygen poor deep water which had not yet been

*Corresponding author. Climate Change Research Project, National Institute for Environmental Studies, 16-2 Onogawa, Tsukuba, Ibaraki 305-8506, Japan.

E-mail address: melissa.chierici@nies.go.jp (M. Chierici).

[1]Present address. Climate Change Research Project, National Institute for Environmental Studies, 16-2 Onogawa, Tsukuba, Ibaraki 305-8506, Japan.

[2]Present address. Department of Earth and Ocean sciences, University of British Columbia, 6339 Stores Road, Vancouver, BC, Canada V6T 1Z4 and Zoology Department, Faculty of Science and Technology, University of Fort Hare, Private Bag X1314, Alice 5700, South Africa.

0967-0645/$ - see front matter © 2004 Elsevier Ltd. All rights reserved.
doi:10.1016/j.dsr2.2001.03.002

compensated for by biological production. Three weeks later, the ice edge had retreated in the SIE region and the Chl *a* concentration had increased three-fold, suggesting the start of a phytoplankton bloom. This was also seen in the oxygen concentration which had increased and showed supersaturation. This coincided with an increased oceanic uptake of CO_2 in the SIE during the mesoscale survey.
© 2004 Elsevier Ltd. All rights reserved.

1. Introduction

There is a need for more information on the carbon dioxide system in the Southern Ocean in order to better understand the oceans' role in the uptake of atmospheric carbon dioxide (Broecker et al., 1986; Tans et al., 1990; Louanchi et al., 1999). To be able to address this question it is important to consider processes that affect the sea–air exchange of carbon dioxide in this unique region. Physical processes such as deep water formation in the Weddell Sea, upwelling of deep water at the divergence zone, formation of intermediate water in the Polar Front region and the advance and retreat of the ice edge can influence the sea–air exchange of carbon dioxide (CO_2) (e.g. Bakker et al., 1997; Hoppema et al., 1995).

The Southern Ocean is an area where several frontal systems are observed and the sector between Africa and Antarctica has historically been considered to be particularly interesting for the variations in the position and strength of frontal currents (Lutjeharms and Valentine, 1984; Sparrow et al., 1996; Belkin and Gordon, 1996). Frontal zones are defined by sharp changes in temperature and salinity, and have also been reported to be areas of enhanced biological production (e.g. Tréguer and Jacques, 1992; Veth et al., 1997; Eynaud et al., 1999). Several investigators have reported enhanced Chl *a* concentrations and reduced fCO_2 values connected with frontal structures as well as in the marginal ice zone and at the ice edge (Smith and Nelson, 1986, 1990; Turner and Owens, 1995; Poisson et al., 1994). These frontal structures are thus of particular interest when addressing the oceans' role in the sea–air exchange of CO_2.

In this study we have investigated the oceanic carbon dioxide system in surface waters along a transect from Cape Town (South Africa) to Queen Maud Land, Antarctica in the Atlantic sector of the Southern Ocean (12–4°E, 43°S–63°S). In addition to the transect, three detailed studies were performed while returning north after conducting the transect, the Spring Ice Edge (SIE), the Winter Ice Edge (WIE) and the Antarctic Polar Front (APF) regions. The main aim of our study was to estimate sea–air exchange of CO_2 and oxygen, and to study their coupling to biological activity in the surface waters using Chl *a* as an indicator for photosynthetic activity. The flux of CO_2 and the oxygen saturation are estimated along the transect. We first examine the variability in the studied parameters in relation to hydrological and biological parameters for the transect and then discuss the temporal (weekly) surveys in the three regions.

2. Methods

During the Swedish–South African expedition in the Atlantic sector of the Southern Ocean in December 1997–February 1998, chemical and biological parameters were studied in addition to the hydrography. For an overview of the aims of the SWEDARP 1997/1998 expedition see Turner et al. (2004). Fig. 1 shows the cruise track of the *SA Agulhas* for the transect and for the three mesoscale studies performed in the APF (Antarctic Polar Front), WIE and SIE. In the figure the Subtropical Front (STF) and the Subantarctic Front (SAF) as well as the position of the winter and SIE are shown. The ice edge was positioned at 56°S during the winter (WIE), however, in December it had retreated to 60°S (SIE).

The measurements along the transect were performed between the 6th and 10th of December 1997 and the three mesoscale surveys were conducted between the 28th of December – 23rd of January 1998. Underway samples were taken from the ship's on-line seawater supply (intake situated

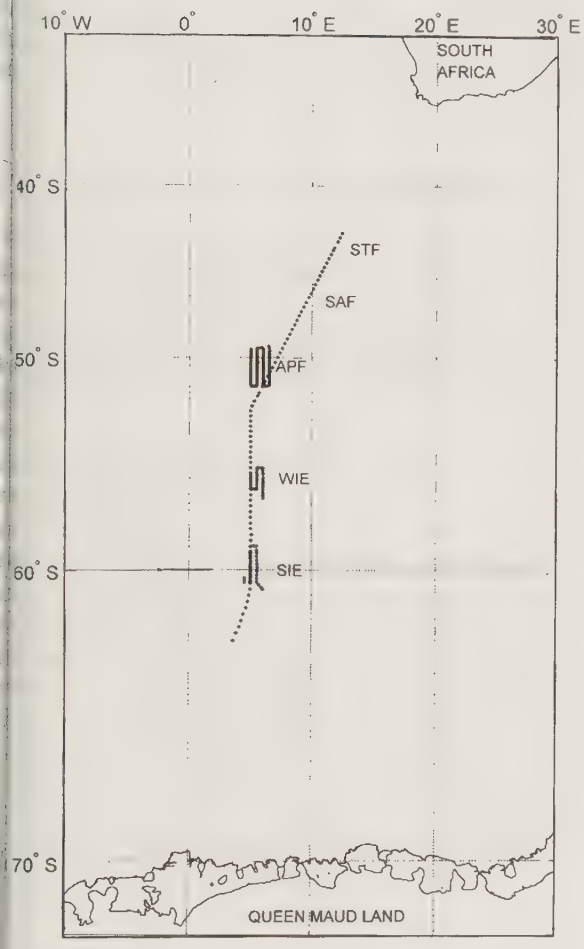

Fig. 1. Cruise track for the southward transect and the three frontal region study areas (APF 49.42–51.50°S, 4.99–6.50°E; WIE 55.50–56.92°S, 4.99–6.01°E; SIE 59.02–60.78°S, 4.50–5.97°E). The points represent individual underway sampling stations. WIE indicates the winter ice edge and SIE the summer ice edge; for other abbreviations see Table 1.

at 4 m depth) and measured directly onboard. Measurements of pH, fugacity of CO_2 (fCO_2), dissolved oxygen and total chlorophyll *a* (Chl *a*) were made. Measurements of total alkalinity (A_T) and total dissolved inorganic carbon (C_T) along the transect are used in this work for the calculation of fCO_2. A_T was determined by potentiometric titration with 0.05 M HCl according to Haraldsson et al. (1997). The precision was obtained by three replicate analyses of a sample at least every hour and was determined to $\pm 1\,\mu mol\,kg^{-1}$ (0.05%) The accuracy was controlled against a Certified Reference Material (DOE, 1994) supplied by Andrew Dickson (Scripps Institution of Oceanography, San Diego, USA) at the beginning and at the end of 12 samples (each station). The correction factor was around 1.005, corresponding to a difference of about $12\,\mu mol\,kg^{-1}$. The variation in the CRM measurements was $\pm 6\,\mu mol\,kg^{-1}$ during the entire cruise. C_T was measured as described in Abrahamsson et al. (2004).

Measurements of sea surface temperature (T) and salinity (S) were logged continuously from the ship's thermosalinograph. Wind speed data were obtained from the ship and logged continuously.

The determination of pH was performed by the use of a semi-continuous system where a diode-array spectrophotometer was connected to the ship's on-line supply and pH was analysed every 7 min, an approach similar to that used by Bellerby et al. (1995). The pH was determined by the use of the sulphonephtalein dye, *m*-cresol purple, as indicator (Clayton and Byrne, 1993; Lee and Millero, 1995), and measured in a 1 cm flowcell thermostated to 15 °C (pH_{15}). The temperature was determined in the seawater sample upstream of the flowcell. The analytical precision was estimated as ± 0.0005 pH units, which was determined by repeated analysis of a sample ($n = 3$) on a daily basis. The accuracy is determined by the accuracy of the temperature measurements and the accuracy in the determination of the equilibrium constants of the dye, which was approximately ± 0.002 (Dickson, 1993). The magnitude of the perturbation to seawater pH caused by addition of the indicator solution was calculated and corrected for by the use of the method described in Chierici et al. (1999). The pH in situ was calculated with the CO_2 calculation program developed by Lewis and Wallace (1998) by using the parameters A_T and pH_{15} for each discrete station and the in situ temperature. All pH values are reported on the total hydrogen ion scale (pH_T).

On line measurements of fCO_2 (using the same pumped surface water supply) were also performed during the southern part of the transect and for two of the survey areas using an automated fCO_2 analyser (Challenger Oceanics,

England). CO_2 was quantified by infrared absorption (Li-Cor 6262 gas analyser) in air equilibrated with the seawater supply. Surface water fCO_2 measurements were made every 10 min, and were calibrated against standard gases (286 ± 1 and 354 ± 1 µtam, traceable to NIST standards) supplied by Air Products (Sandton, South Africa).

Oxygen measurements, from samples taken between 50°S and 63°S, were performed by an automated Winkler type titration with photometric detection. The precision of $\pm 1.5\,\mu mol\,kg^{-1}$ (0.3%) was determined by replicate measurements of water collected from the same Niskin bottle. Thus, the uncertainty due to sampling is included in this value. The accuracy of $1\,\mu mol\,kg^{-1}$ was determined by the variation in standardisation of the sodium thiosulphate during the study.

The Chl *a* concentration was determined every 15 min of latitude during underway measurements, and every hour during the surveys. In the area covered by ice, water samples for Chl *a* were collected from the surface using a plastic bucket. A 250 ml water sample was gently (<50 mm Hg, i.e., <0.07 atm) filtered through a GF/C Whatman filter using a serial filtration unit. Chl *a* concentrations were then determined fluorometrically after extraction in 90% acetone for 24 h (Holm-Hansen and Riemann, 1978). The fluorometer was calibrated prior to the cruise using a chlorophyll *a* standard provided by SIGMA Chemical Co., St. Louis, USA.

2.1. Hydrography

It is necessary to study the different frontal structures within the area since they are known to affect the biological activity and thus the CO_2 system. The positions and description of the major fronts encountered during the expedition are summarised in the overview by Turner et al. (2004). Also, a description of the fronts south of Africa was reported by Lutjeharms and Valentine (1984) and in the work of Belkin and Gordon (1996), where frontal structures were marked by high gradients in sea surface temperature. With the use of data on sea surface temperature (T) from this work and the definitions of the characteristics of the major fronts south of Africa, we have recognised three major oceanic frontal structures which are marked in Fig. 2. The (STF divides warmer tropical waters and colder sub-tropical waters, and is seen in our data as a sharp temperature gradient (from 13 to 8 °C) between 43 and 44°S. The positions of the SAF and the

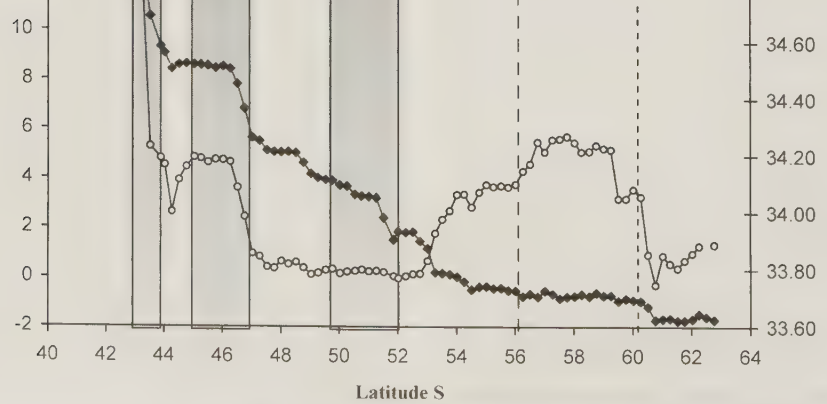

Fig. 2. Sea surface temperature (filled symbols) and salinity (open symbols) measured on the southward transect. The position of the three major fronts and the WIE and SIE are marked on the figure.

APF agreed well with earlier reports (Lutjeharms and Valentine, 1984; Belkin and Gordon, 1996; Eynaud et al., 1999). The SAF was found at an average position of 46°S and is marked by a temperature decrease of 3 °C. The APF, considered to be an important ecological boundary, was found between 49° 30′ and 52°S. Another interesting feature is seen in our sea surface temperature data centred at 53°S, indicated by a temperature drop of 2° C coinciding with an increase in salinity of 0.2. This structure was also observed by Eynaud et al. (1999) and was referred to as the southern border of the APF.

2.2. Calculating the CO_2 system

The fugacity of CO_2 (fCO_2) can be estimated either from direct measurements of fCO_2 in the water, or by calculations from two of the parameters pH, C_T or A_T together with appropriate equilibrium constants describing the oceanic carbonate system. Since direct measurements of $fCO2$ did not cover the entire transect, we used A_T and pH to calculate fCO_2 (fCO_2^{ATpH}) along the transect. For this purpose the CO_2 system program developed by Lewis and Wallace (1998), was used. We used the CO_2 constants from Roy et al., (1993, 1994), and the calculations were made on the total hydrogen ion scale.

2.2.1. Internal consistency

Clayton et al. (1995) and Dickson and Riley (1979) compared the errors arising from the use of different combinations of carbonate system pairs. The results showed that the smallest errors in calculated fCO_2 were obtained by using pH together with either A_T or C_T. The use of A_T and C_T (fCO_2^{ATCT}) as input parameters gives much larger errors. With the A_T and pH precision quoted above (A_T: $\pm 1\,\mu mol\,kg^{-1}$ and 0.0005 in pH), the precision in the calculation of fCO_2^{ATpH} is approximately 2 µatm and the estimated accuracy is approximately 5 µatm. The corresponding error estimates in the calculated values of fCO_2^{ATCT} are 5 and 9 µatm, respectively.

The linear relationship and the ratio (intercept = 0) between fCO_2^{ATpH} and direct measurements of fCO_2 (fCO_2^{meas}) for the southward transect are illustrated in Fig. 3a, and between fCO_2^{ATCT} and fCO_2^{meas} in Fig. 3b. In Fig. 3a we can see a fairly good correlation ($r^2 = 0.87$) between fCO_2^{ATpH} and fCO_2^{meas}, and the ratio is close to 1 (0.999). This gives confidence in the calculations of fCO_2 from A_T and pH and also in the comparison in the temporal study. Since no pH measurements were performed in the SIE region on the return north we have used direct measurements of fCO_2 in that region. However, from Fig. 3b we can clearly see a bias between fCO_2^{meas} with fCO_2^{ATCT} in the data set, where the ratio is 0.986 and a poor correlation ($r^2 = 0.47$). The appropriate equilibrium constants for different measurement parameter pairings when calculating fCO_2 have been a subject of discussion for many years. Recent investigations by Wanninkhof et al. (1999) and Johnson et al. (1999), came to the conclusion that the equilibrium constants of Mehrbach et al. (1973) were more appropriate when A_T and C_T were used to calculate fCO_2, while the constants of Roy et al. (1993, 1994) should be used when A_T and pH are the source data.

2.3. Sea–air exchange of CO_2

The atmospheric carbon dioxide concentration at the South Pole in January 1998 was found to be 362.5 ppmv (mole fraction in dry air) (Tans and Conway, 2000). This value was recalculated to fugacity of CO_2 in wet air (fCO_2^{wetair}) in µatm (Weiss, 1974; Beer, 1983) with the use of data for sea surface temperature (T), sea surface salinity (S), air pressure and humidity from our cruise data at latitude 70°S, giving the result 359.1 µatm. The latitudinal dependence of the atmospheric CO_2 was investigated by extrapolating January data collected at Amsterdam Island (38°S) from 1993, 1994 and 1995 (Gaudry et al., 1996) to 1998 assuming a linear increase. This value (363.1 ppmv) was then corrected for wet air with the same procedure as the South Pole data but with the use of air pressure, S, T and humidity from our stations around 40°S giving the result 365.9 µatm. Assuming a linear latitudinal variation of atmospheric fCO_2 between 38°S and 90°S, we can calculate atmospheric fCO_2 in our study area as $fCO_2 = 3'74.6 - 0.226 \times$ Latitude

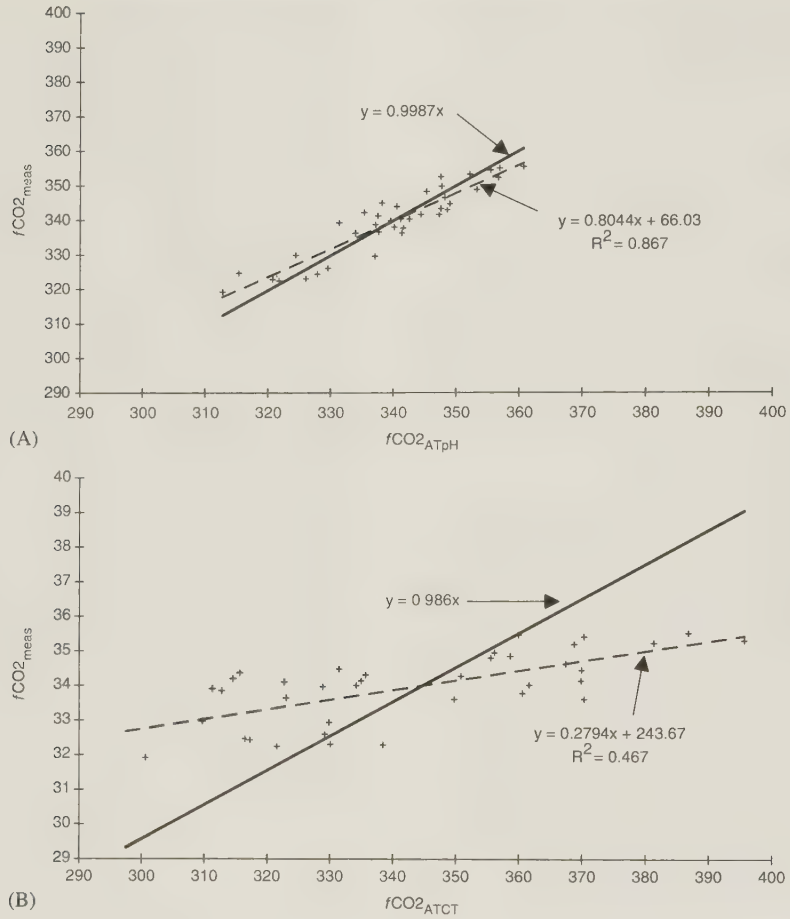

Fig. 3. Linear regressions and ratios between (A) fCO_2^{ATpH} and fCO_2^{meas} ($r^2 = 0.86$), and (B) fCO_2^{ATCT} and fCO_2^{meas} ($r^2 = 0.47$).

S, giving values of 364.9 µatm at 43°S (our most northerly station) and 360.4 µatm at 63°S (our most southerly station). In view of the uncertainties in the surface water fCO_2 data, and of the assumptions made in obtaining the atmospheric fCO_2 estimate, we have used a constant value of 363 µatm for atmospheric fCO_2 in our flux calculations.

2.4. CO_2 flux formulation

The sea–air flux of CO_2 ($Flux_{CO_2}$) is dependent on the magnitude of super/undersaturation and the wind speed, and can be calculated according to Eqs. (1–3);

$$Flux_{CO_2} = K_0^* k_{CO_2}^* (f_{CO_2}^{sw} - f_{CO_2}^{air}), \quad (1)$$

$$k_{CO_2} = 0.31u^2(660/Sc_{CO_2})^{0.5} \quad \text{(Wanninkhof, 1992)}, \quad (2)$$

$$k_{CO_2} = 0.0283u^3(660/Sc_{CO_2})^{0.5} \quad \text{(Wanninkhof and McGillis, 1999)}, \quad (3)$$

where K_0 is the solubility of carbon dioxide at the sea surface temperature in mol m^{-3} atm^{-1}, u is the in situ wind speed in m s^{-1}, k_{CO_2} is the piston velocity for carbon dioxide in cm h^{-1} and Sc_{CO_2} is

he Schmidt number for CO_2, fCO_2^{sw} (here CO_2^{ATpH}) is the fugacity in µatm for the CO_2 in he surface water, and fCO_2^{air} is the fugacity of he CO_2 in the wet atmosphere in µatm. Since he relationship between u and k_{CO_2} is still a ource of uncertainty, we have applied two lifferent formulations (Eqs. (2 and 3)) and ompared the results.

. Results

In general, the expected trend of decreasing emperature towards the south was observed Fig. 2). In the SIE region the surface water was reshened and cooled by sea ice melt water (Fig. 2). The close relationship between temperature and pH_{15} can be seen by comparing Fig. 2 and Fig. 4. However, there are features deviating from the emperature pattern, where pH_{15} values are nhanced (46°S, 49°S, 53°S and 61°S). From pH n situ and Chl *a* (Fig. 5) we can see that the ighest pH in situ values were observed in the ame areas as the Chl *a* maxima. pH in situ varied etween 8.060 and 8.123 with a mean value of 8.086 ± 0.011. The observed Chl *a* concentration varied between 0.15 and 1.02 mg m^{-3}.

The calculated values of fCO_2^{ATpH} along the transect (Fig. 6) indicate that the majority of the surface water is undersaturated in CO_2, with fCO_2 varying between 313 and 377 µatm with a mean value of 346 ± 13 µatm. The general trend is that fCO_2 tends to decrease towards the south, and when reaching the SIE fCO_2 decreases rapidly. Starting from north to south, the waters in the STF are supersaturated in CO_2, which is also the case in parts of the SAF although the mean value shows an undersaturation of CO_2 in the surface water. The APF and the WIE regions show a significant CO_2 undersaturation with mean values of 346 ± 11 and 343 ± 5 µatm, respectively. The lowest fCO_2 values are observed on entering the SIE, and the mean for the entire SIE region is 333 ± 9 µatm. This seems natural considering the decreasing temperature and the ice cover that prevents sea–air exchange of CO_2. For comparison, fCO_2^{meas} is also shown in Fig. 6 where these data are available.

The oxygen concentration was compared with oxygen saturation (calculated from S and T) and only a small disequilibrium in oxygen is observed in the APF and the WIE regions, which is considered insignificant (Fig. 7). However, in the SIE region the surface waters are significantly

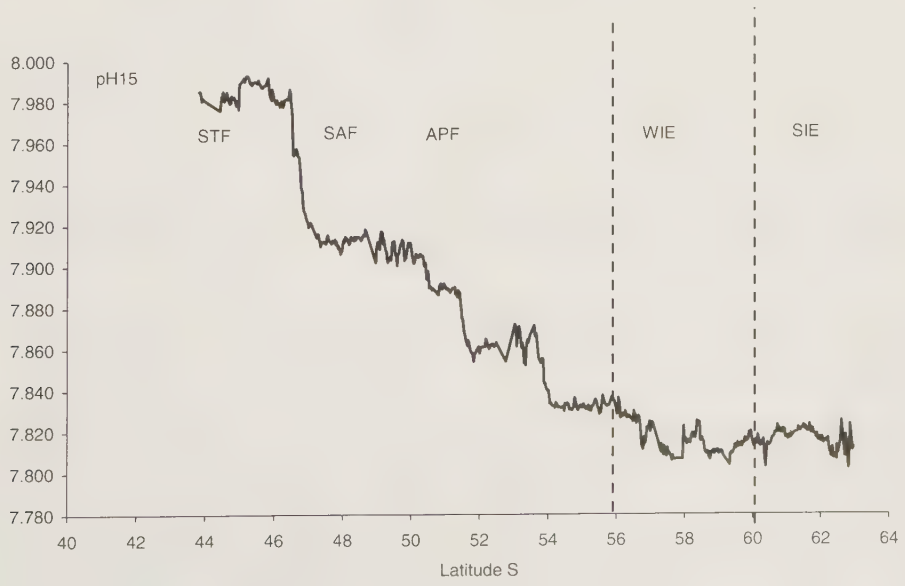

Fig. 4. Surface pH_{15} measured every 7 min on the southward transect.

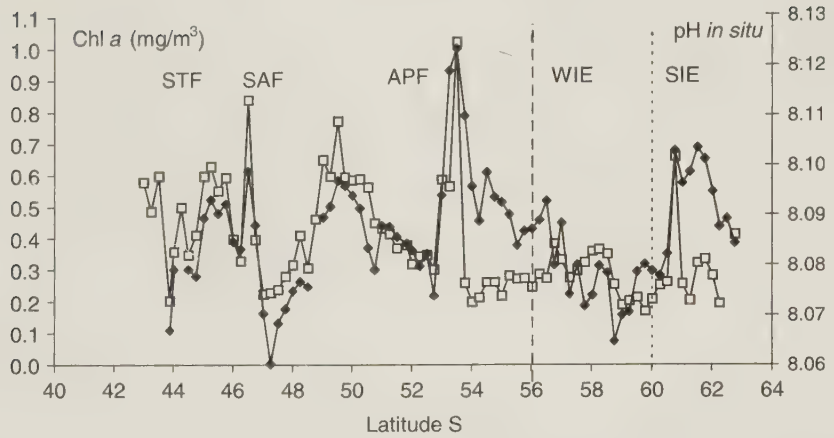

Fig. 5. Surface pH in situ (filled symbols) and Chlorophyll *a* (open symbols) measured on the southward transect.

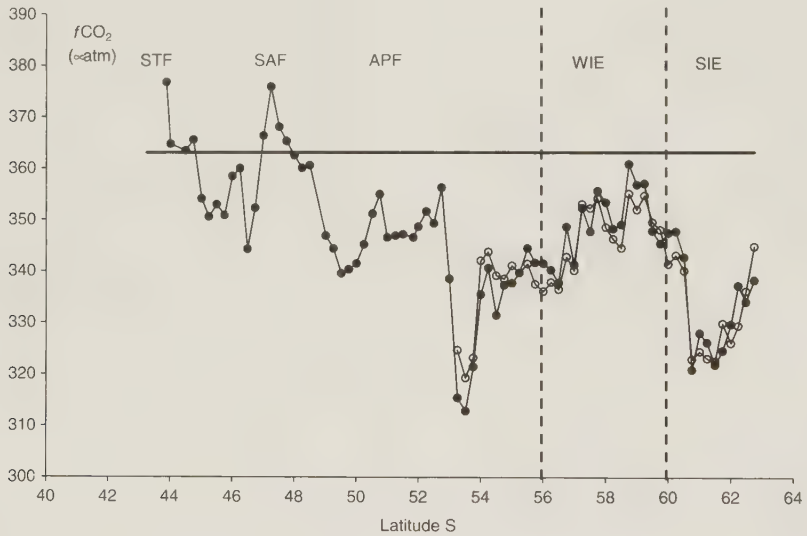

Fig. 6. Measured (fCO_2^{meas}) and calculated (fCO_2^{ATpH}) surface water fugacities of CO_2 in µatm along the southward transect. Open symbols denote fCO_2^{meas} and filled symbols fCO_2^{ATpH}. The horizontal line shows the atmospheric fCO_2 used in this study (363 µatm).

undersaturated, and the difference between the measured oxygen and saturation (ΔO_2) is eight times larger than in the WIE region.

Using shipboard wind speed measurements (Fig. 8) together with ΔfCO_2, the sea–air fluxes of CO_2, $Flux_{CO_2}$ (Fig. 9) were calculated. A large variability in CO_2 sea–air flux along the transect was calculated with values ranging from −20 to 1.3 mmol $m^{-2} d^{-1}$ with a mean value of -3 ± 5 mmol $m^{-2} d^{-1}$. The only region where an upward flux of CO_2 is observed is in the STF region where the mean sea–air flux was 0.7 mmol $m^{-2} d^{-1}$. The largest mean flux to the sea was calculated in the APF (-6 ± 4 mmol $m^{-2} d^{-1}$). The mean sea–air flux in the WIE region is −5 mmol $m^{-2} d^{-1}$. However, between the APF and the WIE a sharp maximum in sea–air flux is observed at ~53°S with a value of −20 mmol $m^{-2} d^{-1}$, which is in contrast to the large areas with negligible flux south of the WIE.

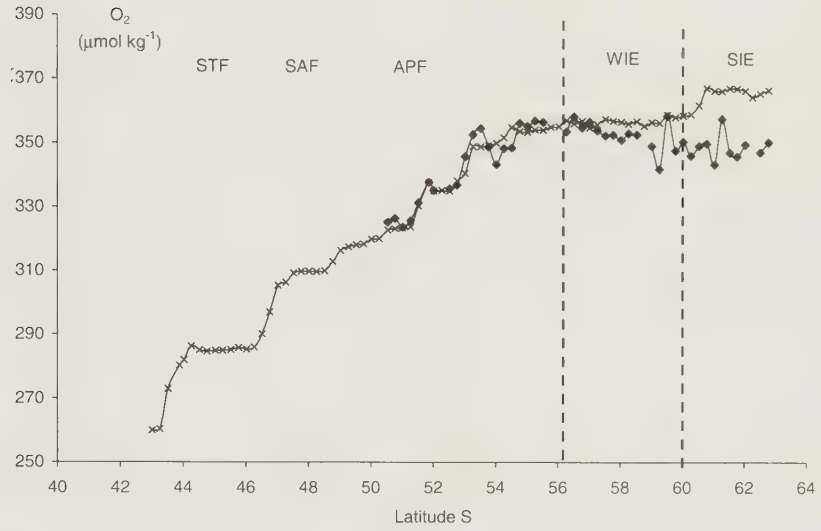

Fig. 7. O_2 concentration (filled symbols) and oxygen saturation (cross) for the southward transect.

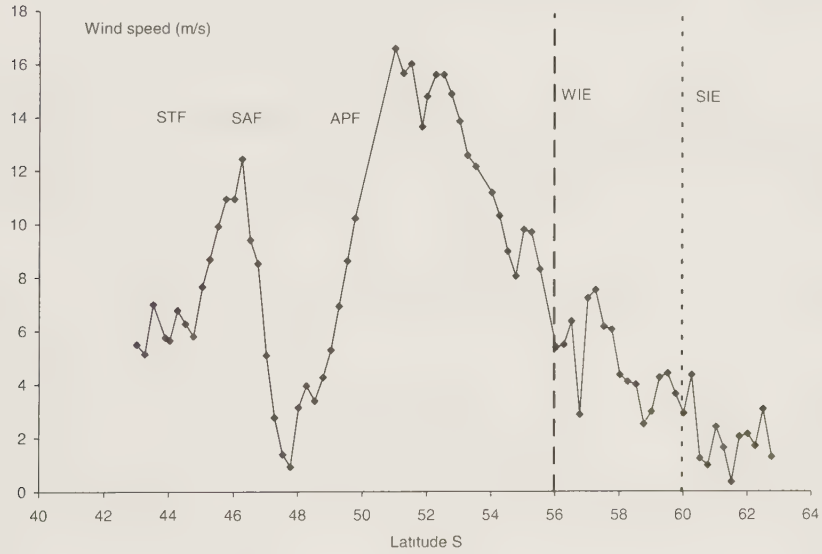

Fig. 8. Shipboard wind speed measurements (10 min averages) along the southward transect.

The sea–air flux in the SIE region is not significant even though a strong undersaturation in fCO_2 was calculated in this region, illustrating the importance of wind on the CO_2 flux. Table 1 presents a summary of the mean values and standard deviations for fCO_2^{ATpH}, ΔfCO_2 ($=fCO_2^{sw}-fCO_2^{air}$), ΔO_2, $Flux_{CO_2}$ and wind speed for different sections of the transect.

3.1. Temporal changes in fCO_2 and the flux of CO_2

Between the 28th of December 1997 and the 23rd of January 1998, three mesoscale surveys were performed in areas of the SIE, WIE and the APF while returning northwards (Fig. 1). During these surveys, pH was measured only in the WIE and APF regions, consequently the measured fCO_2

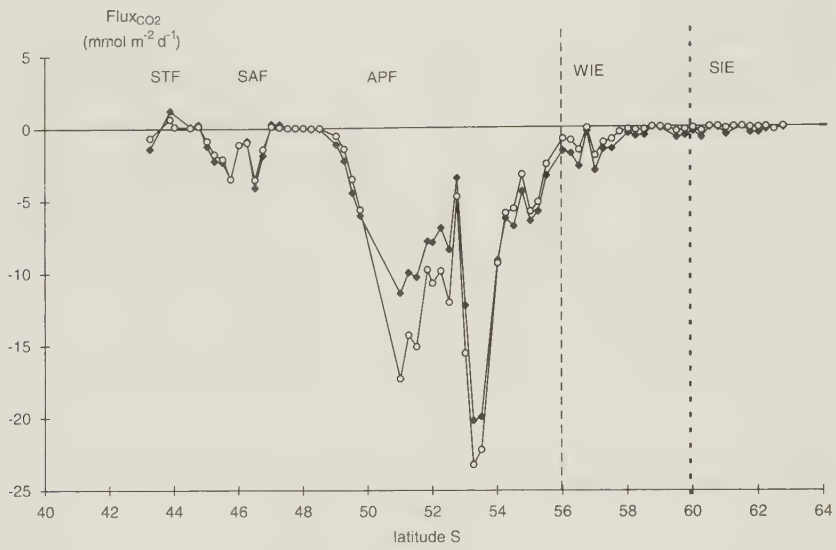

Fig. 9. Calculated sea–air fluxes of CO_2 ($Flux_{CO_2}$) in mmol m^{-2} d^{-1} for the southward transect. Filled symbols denote the CO_2 flux calculated using Eq. (2), and open symbols denote fluxes calculated using Eq. (2).

Table 1
Mean values and standard deviations for fCO_2, ΔfCO_2, ΔO_2, the fluxes of CO_2, wind speed, and surface temperature and salinity in different regions along the southward transect

Latitude range	fCO_2 (μatm)	ΔfCO_2 (μatm)	$Flux_{CO_2}$ (mmol m^{-2} d^{-1})		ΔO_2 (μmol kg^{-1})	Wind (m s^{-1})	T (°C)	S
			W92[a]	WM99[b]				
43°S–44°S	371±8	9±18	0.7±0.7	0.4±0.4	nd[c]	6±1	10.8±1.7	34.47±0.27
45°S–47°S	353±5	−9±5	−2±1	−2±1	nd[c]	10±1	7.9±1.0	34.12±0.11
49.5°S–52°S	346±5	−16±5	−6±4	−7±7	1.8±0.3	11±5	3.3±0.8	33.79±0.03
52°S–60°S	343±11	−19±11	−5±5	−5.3±6	−1.8±0.7	9±4	−0.2±0.8	34.08±0.16
60°S–63°S	333±9	−29±9	−0.3±0.2	−0.1±0.1	−16±0.3	2±1	−1.6±0.3	33.86±0.13

[a]Flux calculated according to Wanninkhof (1992) (Eq. (2)); positive fluxes are from the ocean to the atmosphere.
[b]Flux calculated according to Wanninkhof and McGillis (1999) (Eq. (3)); positive fluxes are from the ocean to the atmosphere.
[c]No data.

values (fCO_2^{meas}) were used in the SIE region for the comparison with fCO_2^{ATpH} obtained during the southward transect. For the WIE and APF surveys, fCO_2^{ATpH} was used for comparison with the southward transect. Chl *a* and oxygen data were available for the SIE region, but no measurements were made in the WIE or the APF. Table 2 shows the mean values and standard deviations for fCO_2, ΔfCO_2 (sea–air), ΔO_2, and $Flux_{CO_2}$ during the southward transect, divided into the same latitudinal areas as the mesoscale surveys.

On return to the SIE the ice cover had disappeared, and a more pronounced CO_2 undersaturation and a ΔfCO_2 of −22 μatm was observed (Table 3, cf. Table 2), This, combined with a higher wind speed, resulted in the estimated flux being three times higher. The salinity was relatively constant, although the sea surface temperature had increased by 0.6 °C, which should result in an

Table 2
Mean values and standard deviations for fCO_2, ΔfCO_2, ΔO_2, the fluxes of CO_2, wind speed, and surface temperature and salinity in different regions along the southward transect

Region latitude °S	fCO_2 data	fCO_2 (μatm)	ΔfCO_2 (μatm)	$Flux_{CO_2}$ ($mmol\,m^{-2}\,d^{-1}$)	ΔO_2 ($\mu mol\,kg^{-1}$)	Wind ($m\,s^{-1}$)	T (°C)	S	Chl a ($mg\,m^{-3}$)
SIE 59–61	fCO_2^{AtpH}	349±6	−13±6	−0.45±0.3	−12±0.3	3±1	−1±0.3	34.04±0.16	0.28±0.1
WIE 55–57	fCO_2 ^{ATpH}	342±4	−20±4	−2±1	0.8±2.5	6±2	−0.7±0.1	34.16±0.06	
APF 49–51.5	fCO_2 ^{ATpH}	346±5	−16±5	−6±4	1.8±0.3	13±4	3.4±0.8	33.79±0.01	

Fluxes are calculated according to Wanninkhof (1992); positive fluxes are from the ocean to the atmosphere.

Table 3
Mean values and standard deviations for fCO_2, ΔfCO_2, ΔO_2, the fluxes of CO_2, wind speed, and surface temperature and salinity in different regions during the surveys conducted after the southward transect

Region latitude °S	Delay[a] (weeks)	fCO_2^{AtpH} (μatm)	ΔfCO_2 (μatm)	$Flux_{CO_2}$ ($mmol\,m^{-2}\,d^{-1}$)		ΔO_2 ($\mu mol\,kg^{-1}$)	Chl a ($mg\,m^{-3}$)	Wind ($m\,s^{-1}$)	T (°C)	S
				W92[b]	WM99[c]					
SIE 59–61	3	340±12*	−22±12	−1.4±2	−0.8±2	2±0.6	0.78±0.3	5±2	−0.4±0.2	33.99±0.1
WIE 55–57	5	357±11	−5±5	−0.6±1	−0.3±0.8	nd[d]	nd[d]	4±2	0.57±0.3	34.06±0.09
APF 49–51.5	6	353±11	−9±11	−2.8±4	−3.1±5	nd[d]	nd[d]	11±4	3.5±0.4	33.78±0.05

*Denotes that fCO_2^{meas} is used in the SIE on the return survey.
[a]Time interval between measurements on the southward transect and the subsequent survey in each area.
[b]Flux calculated according to Wanninkhof (1992) (Eq. (2)); positive fluxes are from the ocean to the atmosphere.
[c]Flux calculated according to Wanninkhof and McGillis (1999) (Eq. (3)); positive fluxes are from the ocean to the atmosphere.
[d]No data.

increase in fCO_2 of around 7 μatm (Takahashi et al., 1993), in contrast to the reduction in fCO_2 that was observed. The oxygen concentration had increased and changed from an insignificant undersaturation to a clear supersaturation. These changes coincide with a three-fold increase in the Chl a concentration (from 0.28 to 0.78 $mg\,m^{-3}$).

The WIE was revisited 5 weeks after the southward transect, and the fCO_2 had increased by 15 μatm, which most probably was due to the 1 °C increase in sea surface temperature. The net oceanic uptake of CO_2 had decreased by around 50%, which is a combined result of the smaller ΔfCO_2 and the slightly lower wind speed observed on the return.

The changes in salinity and temperature during the 6 weeks between the southward transect and the survey in the APF are negligible, although slightly higher fCO_2^{ATpH} values and lower wind speeds result in a lower oceanic CO_2 uptake. Fig. 10 summarises the observed temporal changes in ΔfCO_2 and wind speed.

4. Discussion

In general, elevated Chl a levels were associated with frontal regions and were accompanied by minima in fCO_2 and maxima in pH in situ. This implies that much of the decrease in fCO_2 (and increase in pH in situ) was driven by recent biological production, which was also observed by Robertson and Watson (1995). However, although the peaks in Chl a at 46°30′, 53°S and 61°S correspond to maximum values in pH in situ, the pH signal extends into a larger area than the Chl a signal. This more extensive pH maximum (and fCO_2 minimum) may be a chemical memory effect indicating a previous primary production event which has now ceased (and where Chl a is thus low

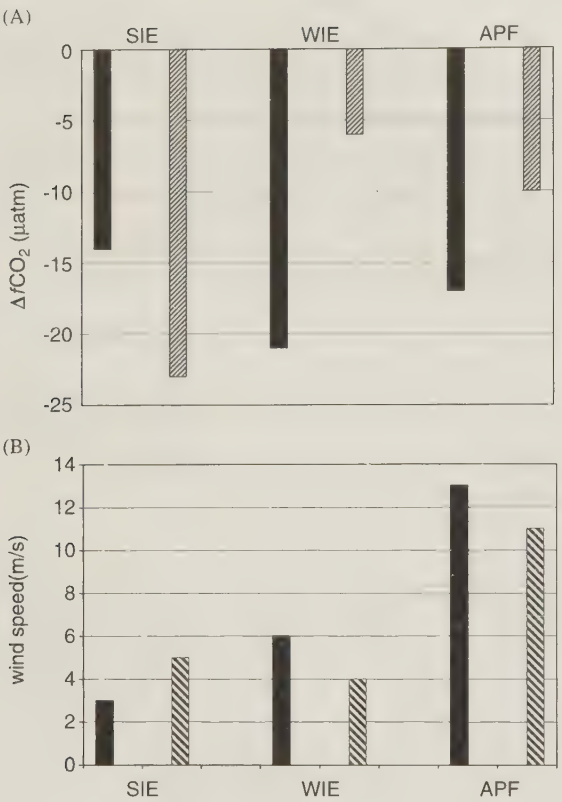

Fig. 10. Comparison between the southward transect and the mesoscale study for (A) ΔfCO_2 in µatm and (B) wind speed ($m\,s^{-1}$). Filled bars indicate data from the southward transect and hatched bars indicate data from the return surveys.

again). The indication of a phytoplankton bloom at 53°S provides an interesting parallel with the results of Eynaud et al. (1999), who reported maximum phytoplankton cell densities at 53°S, dominated by diatoms. The peak in Chl *a* observed at 61°S on the southward transect was probably caused by a dense *Phaeocystis* bloom which appeared to be already in decline (Karlson and Godhe, 1998). The highly CO_2-undersaturated surface waters in the SIE had not yet "recovered" from the bloom and re-equilibrated with the atmosphere due to the low wind speeds and resulting low CO_2 gas fluxes (Fig. 8).

The general trend along the southward transect is that fCO_2 decreases towards the south, with a sharp decrease at the ice edge. This seems natural considering the decreasing temperature and the seasonal ice cover that prevents sea–air exchange of CO_2. However, other studies have reported the opposing scenario, a rapid increase in fCO_2 when approaching the ice edge (Bakker et al., 1997; Turner and Owens, 1995). This was explained by upwelling of CO_2-rich water, which could not equilibrate with the atmosphere due to ice cover. These two studies were performed earlier in the productive season than this study (December–January): Bakker et al. (1997) investigated the CO_2 system during the austral spring (October–November) and Turner and Owens (1995) performed their study in November and December. In addition, neither of the earlier studies showed any sign of primary production at the ice edge, in contrast to this study (Fig. 4). Hoppema et al. (1995) explained that the low summer fCO_2 in the Weddell Gyre was caused by biological uptake, and the increase in fCO_2 during winter was an effect of increased mixing of subsurface water.

For comparison with the fluxes calculated using Eq. (2) (Wanninkhof, 1992), fluxes were also calculated using the cubic relationship between wind speed and CO_2 flux given in Eq. (3) (Wanninkhof and McGillis, 1999) (Fig. 8). With the cubic relationship a larger variability was seen in the mean fluxes (Table 1), and while the major sinks in the APF and WIE regions were more pronounced, the weak sink observed in the SIE region became even weaker.

4.1. Temporal changes

On return to the SIE, the observed increase in CO_2 undersaturation cannot be explained by the small changes in temperature and salinity. However, Chl *a* concentrations had increased threefold, and the ΔO_2 had changed from slight undersaturation to significant supersaturation (Tables 2 and 3). This implies that the decrease in fCO_2 was a result of enhanced biological activity. Schneider and Morlang (1995) reported that the fCO_2 distribution in high-latitude areas of the Atlantic Ocean is controlled by biological production more than by changes in temperature and salinity. One week after the SIE mesoscale survey, Froneman et al. (2004), found the highest primary production rates of the whole expedition,

d the presence of both ice-associated and open ater phytoplankton. As mentioned above, the ice d disappeared from the SIE on our return, and e loss of the ice cover resulted in water ratification and light penetration depth more vourable for primary production. This was also pported by S, T and light data obtained during e expedition, and follows the model proposed Sullivan et al. (1988), where the introduction low-salinity melt water associated with the treat of the ice stabilises the water column and sults in the development of a bloom in the ea corresponding to the SIE. The observed anges of fCO_2 in the WIE could be explained the changes in temperature, whereas in the PF, the lower wind speeds together with less dersaturation were the probable causes for e decrease in oceanic uptake of CO_2 6 weeks ter.

2. The circumpolar sink zone

In the confluence between the warmer subtropil waters and the subantarctic waters a strong O_2-sink zone has been observed between 40°S nd 50°S (Poisson et al., 1993; Takahashi et al., 993; Bakker, 1998). This is probably an effect of ne strong cooling of the warm subtropical waters nd the resulting increase of CO_2 solubility. This gion could thus be a site for a strong drawdown f CO_2. Differences in fCO_2 between surface aters and the atmosphere (ΔfCO_2) have preously been reported to range from −40 to 15 µatm (e.g. Takahashi et al., 1993). Most of ne 40–50°S area was undersaturated in this study, ith the exception of the STF and SAF close to 4°S and 47°S, respectively. These regions were lso found to be supersaturated by Robertson and Watson (1995), who ascribed the supersaturation upwelling of CO_2-rich deep waters. The ΔfCO_2 alues observed in this work range from −23 to 15 µatm with an average value of -6 ± 11 µatm.

Bakker (1998) reported a sink of 0.2 Gt C yr^{-1} etween 40°S and 55°S in the South Atlantic Ocean. Bakker et al. (1997) found a mean undersaturation of 15 µatm in the APF, which agrees ell with the mean undersaturation from this tudy of 16 µatm.

It is important to note that our flux estimates describe the situation over a limited period of time over a limited area; any extrapolation to a seasonal flux should be treated with caution. Fransson et al. (2004) show that the ocean has in fact been acting as a CO_2 source in the SIE and the APF region and as an oceanic CO_2 sink in the WIE region from winter 1997 through to January 1998. In that study, the strongest seasonal CO_2 source was observed in the APF region, where a sink was observed in this study. The result from the WIE agrees well with the result from our study where the WIE was identified as a sink region. Fransson et al.'s explanation for the SIE and the APF acting as sources is that the winter surface water is supersaturated in CO_2, and that this is enhanced by heating in the spring. These observations emphasise the importance of making observations throughout the year if reliable annual flux estimates are to be derived.

5. Conclusions

High Chl *a* was associated with frontal systems and accompanied by high pH in situ and minima in fCO_2. Hence, in these regions we assume that this was the result of relatively recent biological activity, which has also been confirmed in the SIE by other investigators. In other areas the pH and fCO_2 seemed to be controlled mainly by hydrography.

In most areas where an undersaturation of CO_2 was found the ocean acted as a sink for atmospheric CO_2 along the transect. The ice cover and the low wind speeds in the SIE region resulted in small fluxes of CO_2 despite the large undersaturation. However, when the ice cover vanished, a larger undersaturation in CO_2 coincided with a supersaturation in oxygen, which could not be explained by a change in the hydrography. This change was explained by an increase in biological activity which was supported by tripled Chl *a* levels and the highest production rates in the SIE region. The temperature of the surface waters of the WIE region had increased 5 weeks later, which explained the observed changes in the CO_2 system. In general, large variances in the calculated CO_2

fluxes in the survey areas make interpretation difficult, so that the mean fluxes should only be taken as indicative.

Acknowledgements

We thank the Swedish Polar Research Secretariat for shiptime and logistic support; Göteborg Marine Research Centre (GMF) for technical support; the Swedish Natural Science Research Council and the Knut and Alice Wallenberg Foundation for financial support. Many thanks also to Leif G Anderson for constructive criticism and support regarding the manuscript and the cruise.

Thanks also to the crew and officers at the Research vessel *SA Agulhas*. Special thanks to Chris Rohleder for handling the ship's measurements of underway salinity, temperature and wind speeds and overall making the scientific work at the cruise possible.

References

Abrahamsson, K., Bertilsson, S., Chierici, M., Fransson, A., Froneman, P.W., Lorén, A., Pakhomov, E.A., 2004. Variations of biochemical parameters along a transect in the Southern Ocean, with special emphasis on volatile halogenated organic compounds. Deep-Sea Research II, this issue [doi:10.1016/j.dsr2.2004.09.004].

Bakker, D.C.E., 1998. Process studies of the air–sea exchange of carbon dioxide in the Atlantic Ocean. Ph.D. Thesis. NIOZ, The Netherlands.

Bakker, D.C.E., de Baar, H.J.W., Bathmann, U.V., 1997. Changes of carbon dioxide in surface-waters during spring in the Southern Ocean. Deep-Sea Research II 44, 91–128.

Beer, T., 1983. Environmental Oceanography, Textbook to "The Applied Environmetrics Oceanographical Tables". Pergamon Press, Oxford.

Belkin, I.M., Gordon, A.L., 1996. Southern Ocean fronts from the Greenwich meridian to Tasmania. Journal of Geophysical Research 101, 3675–3696.

Bellerby, R.G.J., Turner, D.R., Robertson, J.E., 1995. Surface pH and pCO_2 in the Bellingshausen Sea, Southern Ocean, during the early Austral summer. Deep-Sea Research II 42, 1093–1107.

Broecker, W.S., Ledwell, J.R., Takahashi, T., Weiss, R., Merlivat, L., Memery, L.-H., Peng, T.-H., Jähne, B., Munnich, K.O., 1986. Isotopic versus micrometeorological ocean CO_2 fluxes: a serious conflict. Journal of Geophysical Research 91, 10517–10527.

Chierici, M., Fransson, A., Anderson, L.G., 1999. Influence of *m*-cresol purple indicator additions on the pH of seawater samples: correction factors evaluated from a chemical speciation model. Marine Chemistry 65, 281–290.

Clayton, T.D., Byrne, R.H., 1993. Spectrophotometric seawater pH measurements: total hydrogen ion concentration scale calibration of *m*-cresol purple and at-sea results. Deep-Sea Research I 40, 2115–2129.

Clayton, T.D., Byrne, R.H., Breland, J.A., Feely, R.A., Millero, F.J., Campbell, D.M., Murphy, P.P., Lamb, M.-F., 1995. The role of pH measurements in modern oceanic CO_2-system characterisations: Precision and thermodynamic consistency. Deep-Sea Research II 42, 411–429.

Dickson, A.G., 1993. The measurement of seawater pH. Marine Chemistry 44, 131–142.

Dickson, A.G., Riley, J.P., 1979. The estimation of acid dissociation constants in seawater from potentiometric titrations with strong base I. The ion product of water $-K_w$. Marine Chemistry 7, 89–99.

DOE, 1994. Handbook of methods for the analysis of the various parameters of the carbon dioxide system in seawater; Version 2. In: Dickson A.G., Goyet C. (Eds.), ORNL/CDIAC-74.

Eynaud, F., Giraudeau, J., Pichon, J.-J., Pudsey, C.J., 1999. Sea–surface distribution of coccolithophores, diatoms, silicoflagellates and dinoflagellates in the South Atlantic Ocean during the late austral summer 1995. Deep-Sea Research I 46, 451 482.

Fransson, A., Chierici, M., Anderson, L.G., David, R., 2004. Transformation of carbon and oxygen in the surface layer of the eastern Atlantic sector of the Southern Ocean. Deep-Sea Research II, this issue [doi:10.1016/j.dsr2.2001.12.001].

Froneman, P.W., Pakhomov, E.A., Balarin, M.G., 2004. Size-fractionated phytoplankton biomass, production and biogenic carbon flux in the eastern Atlantic sector of the Southern Ocean in late austral summer 1997–1998. Deep-Sea Research II, this issue [doi:10.1016/j.dsr2.2002.09.001].

Gaudry, A., Kazan, V., Monfray, P., 1996. Atmospheric CO_2 concentrations from Amsterdam Island. Complement to Trend's online, Carbon Dioxide Information analysis Center, Oak Ridge National Laboratory, Oak Ridge, TN, USA. WWW Page, cdiac.esd.ornl.gov/ftp/trends/co/amsterda.co$_2$

Haraldsson, C., Anderson, L.G., Hassellöv, M., Hulth, S., Olsson, K., 1997. Rapid, high-precision potentiometric titration of alkalinity in the ocean and sediment pore waters. Deep-Sea Research I 44, 2031–2044.

Holm-Hansen, O., Riemann, B., 1978. Chlorophyll-*a* determination: improvements in methodology. Oikos 30, 438–447.

Hoppema, M., Fahrbach, E., Schröder, M., Wisotzki, A., de Baar, H.J.W., 1995. Winter–summer differences of carbon dioxide and oxygen in the Weddell Sea surface layer. Marine Chemistry 51, 177–192.

Johnson, K.M., Körtzinger, A., Mintrop, L., Duinker, J.C., Wallace, D.W.R., 1999. Coulometric total carbon dioxide analysis for marine studies: measurements and internal consistency of underway TCO_2 concentrations. Marine Chemistry 67, 123–144.

arlson, B., Godhe, A., 1998. Phytoplankton observations in the Atlantic sector of the Southern Ocean. In: Polarforskningssekretariatets årsbok 1998. Polarforskningssekretariatet, Stockholm, pp. 69–70.

ee, K., Millero, F.J., 1995. Thermodynamic studies of the carbonate system in seawater. Deep-Sea Research I 42, 2035–2061.

ewis, E., Wallace, D.W.R., 1998. Program developed for CO_2 system calculations. ORNL/CDIAC-105, Carbon Dioxide Information Analysis Center, Oak Ridge National Laboratory, US Department of Energy, Oak Ridge, TN.

ouanchi, F., Hoppema, M., Bakker, D.C.E., Poisson, A., Stoll, M.H.C., de Baar, H.J.W., Schauer, B., Ruiz-Pino, D.P., Wolf-Gladrow, D., 1999. Modelled and observed sea surface fCO_2 in the southern ocean: a comparative study. Tellus 51B, 541–559.

utjeharms, J.R.E., Valentine, H.R., 1984. Southern Ocean thermal fronts south of Africa. Deep-Sea Research I 31, 1461–1475.

Mehrbach, C., Culberson, C.H., Hawley, J.E., Pytkowicz, R.M., 1973. Measurement of the apparent dissociation constants of carbonic acid in seawater at atmospheric pressure. Limnology and Oceanography 18, 897–907.

oisson, A., Metzl, N., Brunet, C., Schauer, B., Bres, B., Ruiz-Pino, D., Louanchi, F., 1993. Variability of sources and sinks of CO_2 in the western Indian and Southern Oceans during the year 1991. Journal of Geophysical Research 98, 22759–22778.

oisson, A., Metzl, N., Danet, X., Louanchi, F., Brunet, C., Schauer, B., Brès, B., Ruiz-Pino, D., 1994. Air–sea CO_2 fluxes in the Southern Ocean between 25°E and 85°E. In: Johannessen, O.M., Muench, R.D., Overland, J.E. (Eds.), The Polar Oceans and their Role in Shaping the Global Environment, pp. 273–284.

Robertson, J.E., Watson, A.J., 1995. A summer time sink for atmospheric CO_2 in the Southern Ocean between 88°W and 80°E. Deep-Sea Research II 42, 1081–1091.

Roy, R.N., Roy, L.N., Vogel, K.M., Porter-Moore, C., Pearson, T., Good, C.E., Millero, F.J., Campbell, D.M., 1993. The dissociation constants of carbonic acid in seawater at salinities 5–45 and temperatures 0–45 °C. Marine Chemistry 44, 249–267.

Roy, R.N., Roy, L.N., Vogel, K.M., Porter-Moore, C., Pearson, T., Good, C.E., Millero, F.J., Campbell, D.M., 1994. Erratum for: The dissociation constants of carbonic acid in seawater at salinities 5–45 and temperatures 0–45 °C. Marine Chemistry 45, 337.

Schneider, B., Morlang, J., 1995. Distribution of the CO_2 partial pressure in the Atlantic Ocean between Iceland and the Antarctic Peninsula. Tellus B 47, 93–102.

Smith, W.O., Nelson, D.M., 1986. Importance of ice edge phytoplankton blooms in the Southern Ocean. BioScience 36, 251–257.

Smith, W.O., Nelson, D.M., 1990. Phytoplankton growth and new production in the Weddell Sea marginal ice zone during austral spring and autumn. Limnology and Oceanography 35, 809–821.

Sparrow, M.D., Heywood, K.J., Brown, J., Stevens, D.P., 1996. Current structure of the south Indian Ocean. Journal of Geophysical Research 101, 6377–6391.

Sullivan, C.W., McClain, C.R., Comiso, J.C., Smith, W.O., 1988. Phytoplankton standing crops within an Antarctic ice-edge assessed by satellite remote sensing. Journal of Geophysical Research 93, 12487–12498.

Takahashi, T., Ólafsson, J., Goddard, J.G., Chipman, D.W., Sutherland, S.C., 1993. Seasonal variation of CO_2 and nutrients in the high-latitude surface oceans: a comparative study. Global Biogeochemical Cycles 7, 843–878.

Tans, P.P., Fung, I.Y., Takahashi, T., 1990. Observational constraints on the global atmospheric CO_2 budget. Science 247, 1431–1438.

Tréguer, P., Jacques, G., 1992. Dynamics of nutrients and phytoplankton, and fluxes of carbon, nitrogen and silicon in the Antarctic Ocean. Polar Biology 12, 149–162.

Turner, D.R., Owens, N.J.P., 1995. A biogeochemical study in the Bellingshausen Sea: Overview of the STERNA 1992 expedition. Deep-Sea Research II 42, 907–932.

Veth, C., Peeken, I., Scharek, R., 1997. Physical anatomy of fronts and surface waters in the ACC near the 6°W meridian during austral spring 1992. Deep-Sea Research II 44, 23–49.

Wanninkhof, R.H., 1992. The relationship between wind speed and gas exchange over the ocean. Journal of Geophysical Research 97, 7373–7382.

Wanninkhof, R., McGillis, W.R., 1999. A cubic relationship between air–sea CO_2 exchange and wind speed. Geophysical Research Letters 26, 1889–1892.

Wanninkhof, R., Lewis, E., Feely, R.A., Millero, F.J., 1999. The optimal carbonate dissociation constants for determining surface water pCO_2 from alkalinity and total inorganic carbon. Marine Chemistry 65, 291–301.

Weiss, R.F., 1974. Carbon dioxide in water and seawater: the solubility of a non-ideal gas. Marine Chemistry 2, 203–205.

ELSEVIER

Deep-Sea Research II 51 (2004) 2789–2805

DEEP-SEA RESEARCH
PART II

www.elsevier.com/locate/dsr2

Air–sea exchange of halocarbons: the influence of diurnal and regional variations and distribution of pigments

Katarina Abrahamsson[a,*], Anders Lorén[a], Angela Wulff[b], Sten-Åke Wängberg[b]

[a]*Department of Chemistry and Bioscience, Chalmers University of Technology, SE-412 96 Göteborg, Sweden*
[b]*The Botanical Institute, Göteborg University, Box 461, SE-405 30 Göteborg, Sweden*

Abstract

Diurnal cycles of halocarbons, except methyl bromide and methyl chloride, were observed at six 24-h stations occupied in three different regions, the Summer Ice Edge, the Winter Ice Edge, and the Antarctic Polar Front, in the Atlantic sector of the Southern Ocean during a Swedish South African expedition in 1997/1998. The diurnal cycles contained three phases; a productive phase, a phase of losses and a phase with steady state. The duration of the different phases varied for the different stations as well as for individual compounds. The measured production and losses of organo-halogens in the Antarctic Ocean based on values from each station, were in the order of a few to hundreds of $ng\,yr^{-1}$.

Bromochloromethane, tribromomethane, trichloroethene and diiodomethane were the four compounds found in highest concentrations throughout the investigation, and they were found to be the major contributors of organo-halogens. Only the presence of the photosynthetic pigment *19′-hexanoyloxyfucoxanthin*, biomarker pigment of haptophytes, could explain some of the variations in the distribution and production of halocarbons, and then only for iodinated compounds.

The flux of organo-halogens from the oceans to the atmosphere was estimated in two ways, either based on calculations according to models or based on the measured concentrations. Large discrepancies were found, which could not be explained by chemical or biological degradation or adsorption to particles. This investigation, therefore, shows the need for assessing the rates of degradation and the air–sea exchange more accurately.
© 2004 Elsevier Ltd. All rights reserved.

1. Introduction

Halogens play an important role in the depletion of ozone in polar regions. In Antarctica, a third of the ozone loss is believed to be due to bromine, which implies that in the stratosphere, bromine is about 50 times more efficient in depleting ozone than is chlorine (Wofsy et al., 1975). A synergistic effect of chlorine and bromine species has been reported, and it might account for approximately 20% of the polar stratospheric ozone depletion (Prather et al., 1984).

*Corresponding author. Tel./fax: +46 31 772 27 85.
E-mail address: katarina@amc.chalmers.se (K. Abrahamsson).

0967-0645/$ - see front matter © 2004 Elsevier Ltd. All rights reserved.
doi:10.1016/j.dsr2.2004.09.005

The ocean plays an important role in the biogeochemical cycle of organo-halogens. This group of compounds are of both biogenic and anthropogenic origin. Methyl chloride and methyl bromide have been regarded as the largest contributors of naturally produced halogens to the stratosphere (Butler and Rodriguez, 1996). However, other rather short-lived chlorinated and brominated compounds have lately been suggested as important species in atmospheric chemistry. Bromoform, has for instance been found to be a more significant contributor to atmospheric inorganic bromine at mid-latitudes than all other long-lived gases combined (Dvortsov et al., 1999). Also, chlorinated compounds with lifetimes of some months in the troposphere, have been shown to be transported to the stratosphere in significant amounts (Graedel and Keene, 1995).

Phytoplankton are regarded as the main producers of halocarbons in the oceans. Antarctic phytoplankton communities are generally dominated by flagellates from different systematic classes (Smetacek et al., 1990). Sometimes blooms of diatoms or small flagellates, such as the colonial haptophyte *Pheaocystis* sp. occur within the community (Davidson and Marchant, 1992). The rate of production of halocarbons has been shown to be species-dependent when measured in cultures (Tokarczyk and Moore, 1994). It is therefore of interest to find relationships between the size and composition of the phytoplankton community and the production of biogenic halocarbons.

The production of halocarbons by marine algae has been shown to be closely connected to the reduction of hydrogen peroxide and other reactive oxygen species by living organisms, especially marine algae (Collén et al., 1994). The suggested pathway is the formation of chlorinated, brominated and iodinated compounds through reactions with enzymatically produced hypochlorite or hypobromite (Wever et al., 1991; Abrahamsson et al., 1995; Moore et al., 1996). There is, however, a difference in formation mechanisms for the polyhalogenated compounds and the halomethanes (Wuosmaa and Hager, 1990).

It is especially important to characterise the biogenically produced halocarbons in the oceans, since the oceanic flux of most biogenic halocarbons is still an unknown factor in the atmospheric budgets of halogens. In the case of methyl bromide, the flux over the air–sea interface has been thoroughly investigated, and the ocean was found to act as a sink (Lobert et al., 1995). Several factors need to be addressed in order to accurately assess the flux such as the sources and the biotic and abiotic processes that act upon the compounds in the oceans. The rate of production and degradation of halocarbons in the oceans govern the concentration of the halocarbons in sea water and thereby the flux of these compounds between the ocean and the atmosphere. The flux calculations are usually derived from average concentrations in surface water along transects. Generally such calculations do not take the time of day into consideration (Class and Ballschmiter, 1988; Moore and Tokarczyk, 1992; Anbar et al., 1996; Schall et al., 1997; Quack and Suess, 1999). The removal of halocarbons from the upper water column has mainly been attributed to the air–sea exchange, and removal of halocarbons due to convection or chemical or biological degradation have been regarded as being slow processes of minor importance, because of their relatively long environmental half-lives reported in the literature (Vogel et al., 1987; Jeffers et al., 1989). However, an investigation of the diurnal variations of halocarbons in a rock pool suggested that the removal rates are much higher than what could be explained by a flux to the atmosphere as calculated according to accepted models (Ekdahl et al., 1998).

In this paper, we put emphasis on measurements of the concentrations of halocarbons, except methyl chloride and methyl bromide, both at the surface and at the chlorophyll maximum (chl. max) during 24-h periods. Thus, we are able to assess the flux of halocarbons from the ocean to the atmosphere more accurately. Production rates and removal rates are estimated from the measured concentrations during the 24-h period. The production rates were also determined in incubation experiments. The composition of phytoplankton communities was determined in order to find out its influence on the magnitude of the production of halocarbons as well as the distribution of halocarbons in different areas.

Experimental

1. Sampling

The Swedish–South African Expedition to the Atlantic Sector of the Southern Atlantic Ocean in 1997/1998, sampled six locations during 24-h periods. The studies were performed in three different areas along 6°E (Fig. 1). The areas were the Summer Ice Edge (SIE), the Winter Ice Edge (WIE) and the Antarctic Polar Front (APF) (Table 1). At each station the concentrations of halocarbons were measured in surface water, and water samples at the chl. max determined by in-situ fluorescence once every hour or once every 2 h.

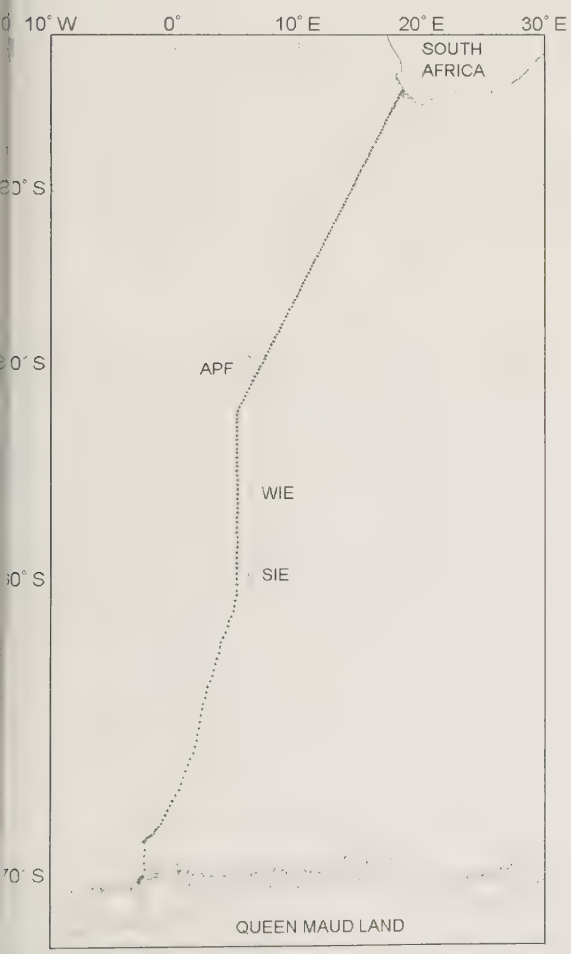

Fig. 1. The 24-h stations occupied during the investigation. The three investigated regions are indicated.

Water from these two depths was also collected on four occasions at each station, in order to measure the concentrations of phytoplankton pigments. The water samples were drawn from a rosette sampler or from Go-Flow bottles. The measurements started at 8.30 am and ended at 8.30 am the following day.

For the purpose of incubation studies, 25 l of water was drawn from the rosette sampler at chl. max on eight occasions, each at approximately 8.30 am.

2.2. Materials and methods

The halocarbons measured are listed in Table 2. Liquid standard stock solutions of the halocarbons were prepared in acetone (Baker). They were further diluted in sea water collected at 2000 m to give final concentrations of pmol l^{-1}.

The water samples, approximately 27 ml of sea water, were pre-concentrated by a purge- and trap technique. The separations were carried out with a Varian 3400 gas chromatograph equipped with a Ni^{63} electron capture detector. The identity of the compounds was established through the use of standard additions. Also, the retention times were confirmed by gas chromatography–mass spectrometry, also available on board. The chromatographic columns were identical in both systems.

The detection limits for the compounds are in amol l^{-1} to fmol l^{-1} range with relative standard deviations between 1% and 3%. The method has been described in detail in Ekdahl and Abrahamsson (1997).

2.3. Pigments

Water, 0.5–2.0 l, was drawn from the rosette sampler or the Go-Flow bottles four times during each station. The water was filtered through 20 mm Whatman GF/F fibreglass filters. The filters were put in cryovials and immediately frozen in liquid nitrogen (−196 °C). The filtration was done in dim light at 1 °C. After 4–8 weeks, the filters were transferred to a low-temperature freezer (−85°C) and stored for up to 3 months until analysed. 1.5 ml 100% methanol was added to the filters, and the extraction and the determination by

Table 1
Position and hydrographic data for the six stations occupied during the investigation

Station	Latitude	Longitude	Date	Salinity	Temperature	Sigma
MIZ 1	60°24′S	6°00′E	4–5 January	33.86±0.045	−0.39±0.31	27.20±0.04
MIZ 2	60°00′S	6°00′E	6–7 January	33.82±0.017	−0.17±0.047	27.15±0.01
MIZ 3	59°20′S	6°00′E	8–9 January	34.15±0.042	−0.29±0.44	27.44±0.05
IFR	56°30′S	6°00′E	14–15 January	34.25±0.028	−0.039±0.23	27.50±0.02
APF 1	51°00′S	6°00′E	27–28 January	33.81±0.017	3.63±0.011	26.87±0.01
APF 2	49°50′S	6°00′E	29–30 January	33.84±0.010	3.42±0.10	26.92±0.01

Table 2
The halocarbons determined in the investigation

CH_3I	Iodomethane
CH_3CH_2I	Iodoethane
CH_3CHICH_3	2-Iodopropane
$CH_3CH_2CH_2I$	1-Iodopropane
$CH_3CH_2CHICH_3$	2-Iodobuthane
$CH_3CH_2CH_2CH_2I$	1-Iodobuthane
CH_2I_2	Diiodomethane
$CHCl_3$	Trichloromethane
$CHCl=CCl_2$	Trichloroethene
$CCl_2=CCl_2$	Tetrachloroethene
CH_2ClI	Chloroiodomethane
CH_2BrCl	Bromochloromethane
$CHBrCl_2$	Bromodichloromethane
$CHBr_2Cl$	Dibromochloromethane
CH_2Br_2	Dibromomethane
$CHBr_3$	Tribromomethane
CCl_4	Tetrachloromethane
CH_3CCl_3.	1,1,1-Trichloroethane

high-performance liquid chromatography (HPLC) was performed according to Wright and Jeffrey (1997) using an absorbance diode-array detector (Spectraphysics UV6000LP). To ensure a correct identification, a spectrum (400–700 nm) was run for each sample. Pigment standards were provided by the International Agency for ^{14}C determination, Hørsholm, Denmark. Pigments are expressed as concentrations ($\mu g\,l^{-1}$). The following pigments were detected: chlorophyll *a* (chl *a*), chlorophyll *b* (chl *b*), chlorophyll c_3 (chl c_3), chlorophyll $c_1 + c_2$ (chl c_1c_2), peridinin (per), 19′-butanoyloxyfucoxanthin (19′-but), fucoxanthin (fucox), 19′-hexanoyloxyfucoxanthin (19′-hex), diadinoxanthin (dd), alloxanthin (allox), lutein, violaxanthin, zeaxanthin (zeax) and β-carotene. In addition, the breakdown/intermediate product chlorophyllide *a* (chlid *a*) was determined but not further evaluated.

To estimate the contribution of different algal classes to total chl *a*, the pigment data were interpreted using the matrix factorisation programme CHEMTAX (Mackey et al., 1996; Wright et al., 1996). The programme uses a steepest-descent algorithm to determine the best fit based on an estimate of pigment/chl *a* ratios for different algal classes. We used an initial pigment-ratio matrix derived from the Southern Ocean data set used in Mackey et al. (1996).

2.4. Incubation studies

The formation of halocarbons by pelagic organisms was determined on eight occasions. Approximately 25 l of water was filtered through a filtration unit equipped with five different sized filters (1000, 125, 20, 2 and 0.4 μm). The water retained in four different compartments was divided into 60 ml glass bottles and incubated at +2 °C and a light intensity of 100 μE. Fraction 1 is the fraction contained between the two largest filters, and fraction 4 is the fraction contained between the two smallest filters. After approximately 24 h the amounts of halocarbons were determined.

2.5. Production, loss and flux calculations

The production and disappearance rates of halocarbons during the 24-h periods were calculated from the measured water concentrations. We assumed a box with a surface area of 1 m^2 and a height of the surface mixed layer for each area

according to Fransson et al. (this volume), yielding a total volume of SIE 80, WIE 112 and APF 160 m^3. The production rates were derived by subtracting the concentration at the start of the productive period from the maximum concentration divided by the time of production, thereafter adding values for the actual loss per hour in a similar way to that used by Ekdahl et al. (1998). The time of production and the time of decrease in concentration were determined from the plotted water concentrations versus time of day at chl. max.

The flux of halocarbons across the air–sea interface was estimated according to the model described by Liss and Merlivat (1986), where the flux is controlled by the concentration gradient between water and air, as well as the mass transfer velocities in air and water, respectively. The concentrations of biogenic halocarbons in air were assumed to be zero, since it was impossible to measure air samples at the same frequency due to lack of instrument capacity. The Henry's Law constants for the individual compounds were from Moore et al. (1995), Dewulf et al. (1995) and Klick and Abrahamsson (1992). The Henry's Law constant for bromochloromethane was estimated according to Schwarzenbach et al. (1993). The wind speed was monitored continuously during each 24-h period, and used to calculate the water transfer velocities at each sampling point. Consequently, the loss to the atmosphere could be calculated for each time of sampling.

The loss due to abiotic degradation was calculated according to Anbar et al. (1996) using the environmental half-lives given by Vogel et al. (1987) and Jeffers et al. (1989).

3. Results and discussion

3.1. General picture

A considerable number of halocarbons are produced by macro- and microalgae in the oceans. The compounds listed in Table 2, except tetrachloromethane and 1,1,1-trichloroethane, have all been identified as naturally produced (Collén et al., 1994; Fogelqvist and Tanhua, 1995; Laturnus, 1996). In the studied area, the concentrations of three halocarbons exceeded by far those of the other halocarbons measured. Those were bromochloromethane, tribromomethane and diiodomethane (Table 3). The average concentrations of tribromomethane of 7.2–47 pmol l^{-1} in the different areas agree well with other investigations performed in Antarctica (Reifenhäuser and Heumann, 1992; Klick and Abrahamsson, 1992; Schall et al., 1997). However, to our knowledge, high concentrations of diiodomethane (110–170 pmol l^{-1}) and bromochloromethane (290–400 pmol l^{-1}) have not earlier been reported in the open ocean. Concentrations of diiodomethane of some 500–700 pmol l^{-1} have been found in coastal areas with macroalgae belts (Klick, 1992). Trichloroethene had the highest concentrations of the chlorinated compounds with mean concentrations of 2.5–7.5 pmol l^{-1}.

There was no obvious difference in the concentration of the halocarbons at the surface and at the chl. max (Figs. 2 and 5). The linear relationships found between tribromomethane, and dibromomethane and bromochloromethane indicate that the two latter compounds too have a natural rather than an anthropogenic origin in the investigated area (Fig. 2).

3.2. Regional variations

The APF was identified by the water temperature, whereas the position of the SIE was determined as the ship passed southwards some weeks prior to the investigation. However, at the time of sampling the ice had melted, and the entire area of investigation was free of ice. As can be seen from Table 1, there are variations in density, which is mainly due to variations in temperature. Among the three stations occupied in the SIE, SIE 3 differed considerably regarding the hydrography, and showed similarities with the stations occupied further north.

The highest concentrations of chl *a* were found within the SIE with values around 4 μg l^{-1} (Fig. 4). The phytoplankton community composition, as suggested by CHEMTAX showed a total dominance of haptophytes at all stations, an observation also made by others (Mackey et al., 1996;

Table 3
Average concentrations (pmol l^{-1}) of halocarbons at the different stations

Compound	SIE1	SIE 2	SIE 3	WIE	APF1	APF2
CH_3I	1.6±1.2	1.8±0.15	1.2±0.57	0.66±0.12	0.83±0.19	0.81±0.1
CH_3CH_2I	0.28±0.08	0.27±0.08	0.13±0.04	0.13±0.06	0.10±0.07	0.13±0.0
CH_3CHICH_3	0.20±0.04	0.15±0.1	0.07±0.05	0.11±0.08	0.09±0.05	0.09±0.0
$CH_3CH_2CH_2I$	0.97±0.2	1.0±0.10	0.90±0.31	1.5±0.21	0.84±0.21	1.4±0.5
$CH_3CH_2CHICH_3$	0.04±0.04	0.009±0.02	0.06±0.06	0.14±0.03	0.03±0.03	0.06±0.0
$CH_3CH_2CH_2CH_2I$	0.05±0.03	0.61±0.33	0.17±0.08	0.09±0.05	0.02±0.02	0.02±0.0
CH_2I_2	170±53	140±78	160±105	110±109	120±92	140±10C
$CHCl_3$	0.25±0.02	0.24±0.02	0.21±0.02	0.22±0.03	0.24±0.03	0.25±0.0
$CHCl=CCl_2$	7.5±1.6	6.7±9.3	3.2±1.5	3.6±2.3	2.5±0.94	3.9±3.1
$CCl_2=CCl_2$	0.08±0.01	0.14±0.07	0.06±0.03	0.07± 0.02	0.06±0.02	0.18±0.3
CH_2ClI	0.13±0.06	0.39±0.23	0.08±0.04	0.05±0.03	0.10±0.02	0.07±0.0
CH_2BrCl	350±48	290±16	300±67	360±46	290±39	400±80
$CHBrCl_2$	0.39±0.05	0.34±0.08	0.27±0.46	0.32±0.07	0.22±0.04	0.25±0.0
$CHBr_2Cl$	0.58±0.08	0.68±0.09	0.5±0.15	0.72±0.11	0.59±0.16	0.97±0.44
CH_2Br_2	2.5±0.08	2.3±0.17	2.1±0.15	2.2±0.27	2.1±0.21	2.3±0.18
$CHBr_3$	47±14	21±2.9	15±3.6	22±3.3	7.2±2.6	12±3.6

Values from both sampling depths are included.

Wright et al., 1996; Peeken, 1997; Wulff and Wängberg, this issue). In SIE, the haptophytes contributed with around 80% to the total chl *a*, while the diatom and dinoflagellate contribution were around 20% and 1%, respectively. A haptophyte bloom (*Phaeocystis* sp.) that appeared to be in decline was also observed during the cruise.

There was, however, a substantial variation between the three biostations occupied in the SIE, where the two most southerly stations had high values of chl *a*, while SIE 3 had concentrations of chl *a* comparable to those found in the APF. Also, the phytoplankton community composition varied between the stations in SIE. In the two southernmost stations the cryptophyte contribution was somewhat higher, and the dinoflagellate and diatom contribution were smaller compared with in SIE 3 (Fig. 3). The cryptophyte contribution could be explained by the presence of *Mesodinium rubrum*, a ciliate containing cryptophytes, which earlier have been observed in association with the ice-edge (Satoh and Watanabe, 1991). Overall, as for physical data, SIE 3 showed a greater resemblance with the northern stations than SIE 1 and 2. The lowest concentrations of chl *a* were found within the WIE with typical concentrations around 0.5 $\mu g\,l^{-1}$. This area is usually associated with low biomass (Wulff and Wängberg, this issue) due to the lack of stratification and low iron concentrations. CHEMTAX suggested a phytoplankton composition similar to the SIE, however, with the addition of cyanophytes, contributing with ca. 3% to total chl *a* (see Wulff and Wängberg, this issue). In APF, the chl *a* concentrations were around 1.7 $\mu g\,l^{-1}$ with a relatively larger biomass of dinoflagellates (ca. 5%) and chlorophytes (ca. 3%), as suggested by CHEMTAX, compared with the other areas (see discussion in Wulff and Wängberg, this issue).

The differences in concentrations of halocarbons were most pronounced for the compounds produced at the highest rates (Table 3). In general, the highest concentrations of iodinated compounds were found in the SIE, where the analysis of pigments showed that diatoms and haptophytes were dominant. Earlier investigations performed in the Southern Ocean have shown a relationship between the concentration of iodomethane and the occurrence of the most dominant haptophyte, *Phaeocystis* sp. (Abrahamsson, unpublished).

There is a tendency for the brominated and chlorinated compounds to be found at the highest concentrations in the SIE as well. However, the differences are not as pronounced as for the iodinated compounds. These small differences could be explained by the fact that the major producers of brominated and chlorinated compounds are not the microphytoplankton, but rather the nano- and picoplankton (Fig. 4), which are perhaps more evenly distributed. At WIE, the overall concentrations of pigments were low. However, the total production of organo-halogens (discussed in more detail further on), estimated from the diurnal variations at this site, was in the same order of magnitude as the other stations. This might be an indication of the effectiveness of the micro-organisms at this station as halocarbon producers.

Fig. 2 compares the water concentrations of brominated compounds between the different regions. The stations occupied in the SIE varied to a higher extent than the other two regions for bromochloromethane. This might be due to the fact that different phytoplankton are the major producers of bromochloromethane and tribromomethane, or that this region was influenced to a larger extent by different water masses. The heterogeneity of the SIE area was also seen in the pigment analysis (Table 4). The larger slope observed in the APF compared to the SIE and the WIE for dibromochloromethane and tribromomethane could be due to a more recent produc-

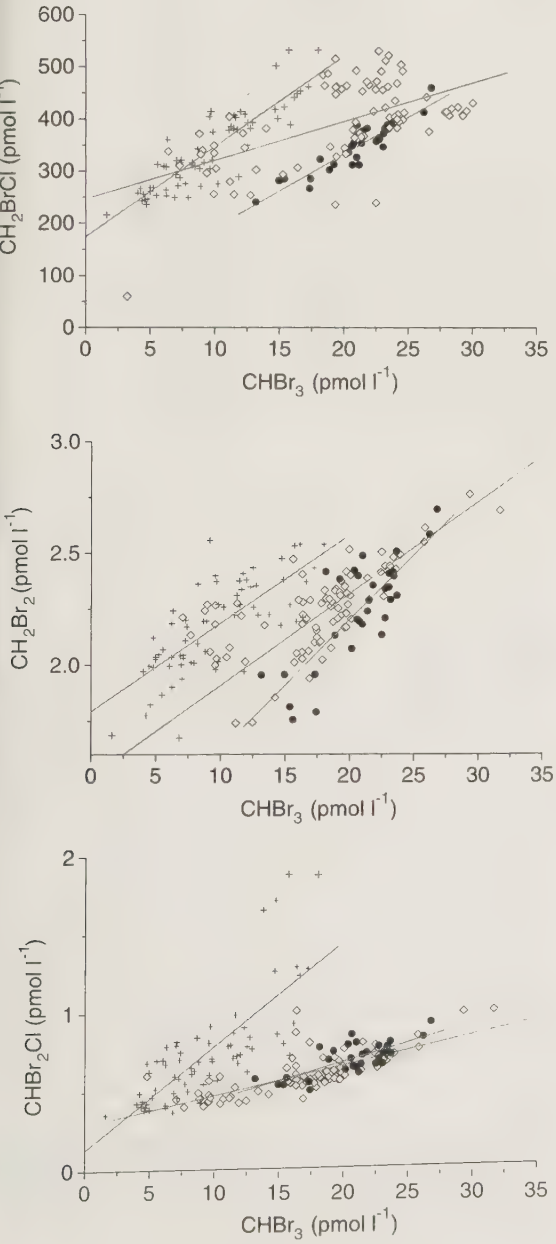

Fig. 2. Comparisons of the measured concentrations of four brominated halocarbons at the different regions. Values from both the surface and chl. max. are included. Open diamonds represent values from SIE, filled circles represent values from WIE, and crosses represents values from APF. The statistical parameters for the regression $y = kx + L$ are

$CH_2BrCl/CHBr_3$: SIE; $k = 7 \pm 1.1$, $L = 172 \pm 18$, $r^2 = 0.59$, $p < 0.0001$
WIE; $k = 14 \pm 1.1$, $L = 50 \pm 23$, $r^2 = 0.92$, $p > 0.0001$
APF; $k = 17 \pm 1.1$, $L = 173 \pm 11$, $r^2 = 0.89$, $p < 0.0001$

$CH_2Br_2/CHBr_3$: SIE; $k = 0.041 \pm 0.005$, $L = 1.5 \pm 0.086$, $r^2 = 0.69$, $p < 0.0001$
WIE; $k = 0.058 \pm 0.008$, $L = 1.0 \pm 0.17$, $r^2 = 0.81$, $p > 0.0001$
APF; $k = 0.039 \pm 0.004$, $L = 1.8 \pm 0.046$, $r^2 = 0.74$, $p < 0.0001$

$CHBr_2Cl/CHBr_3$: SIE; $k = 0.019 \pm 0.0.002$, $L = 0.29 \pm 0.034$, $r^2 = 0.75$, $p < 0.0001$
WIE; $k = 0.024 \pm 0.004$, $L = 0.21 \pm 0.083$, $r^2 = 0.75$, $p > 0.0001$
APF; $k = 0.066 \pm 0.007$, $L = 0.13 \pm 0.069$, $r^2 = 0.77$, $p < 0.0001$

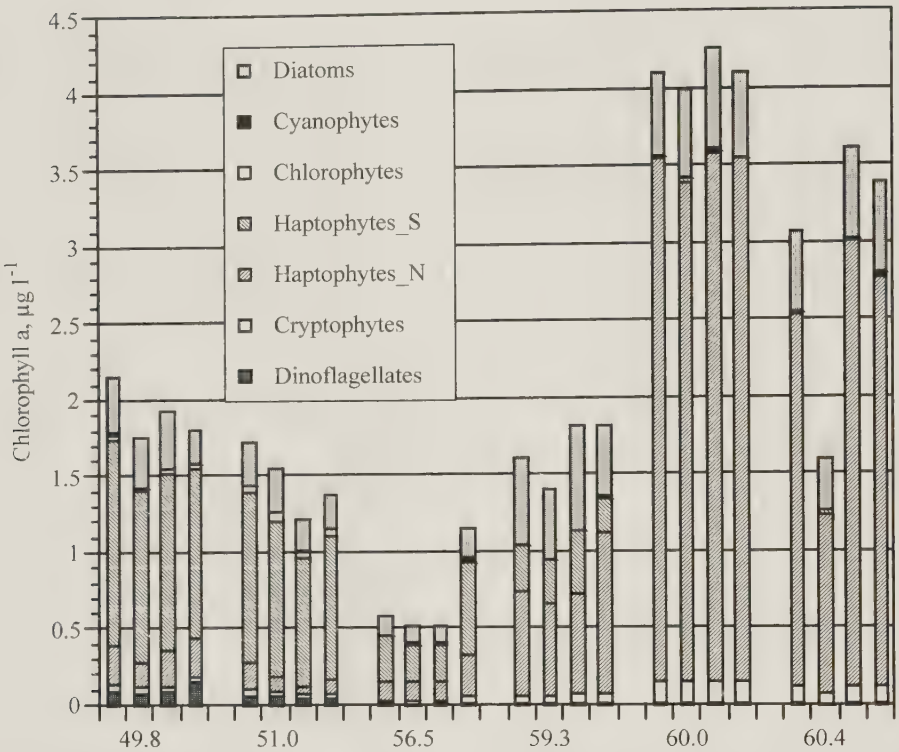

Fig. 3. Contribution of algal classes to total chlorophyll *a* according to CHEMTAX. The individual columns are average values for samples collected at the surface and at chl. max.

tion. Dibromochloromethane could be a degradation product of tribromomethane through nucleophilic substitution similar to that of the transformation of methyl iodide to methyl chloride (Zafiriou, 1975).

The production rates of the four dominating halocarbons by phytoplankton of different sizes are shown in Fig. 4. Water was filtered on two occasions at three stations. Unfortunately the filtrations at the WIE were not successful. However, the results from the filtrations at an individual station were in fairly good agreement, indicating that the filtration and the incubation procedure are reasonably reproducible. The production rates were determined as the slope of the linear increase in halocarbon concentrations with time.

The highest production rates were found at two stations, SIE 3 and APF 2, and the production rates at the other stations were one order of magnitude lower. Some similarities between SIE 3 and APF 2 were found, regarding pigments as well as hydrography. The pigment composition indicated a relatively large contribution of dinoflagellates to chl *a* at APF 2 (Fig. 3). In SIE 3 we also found higher proportion of dinoflagellates and diatoms compared to the other stations in the SIE. The two APF stations vary considerably in the amounts of halocarbons produced. However, the pigment analysis did not reveal any large differences in algal community. The production rate of trichloroethene was found to be much higher in SIE 3 compared to APF 2. This could be due to the fact that the relative abundance of diatoms was larger in SIE 3 than in the APF region.

In general, the smallest-sized fractions were the most efficient producers of individual halocarbons per chl *a* (Fig. 4), and the rates were in the same order of magnitude as those measured in late

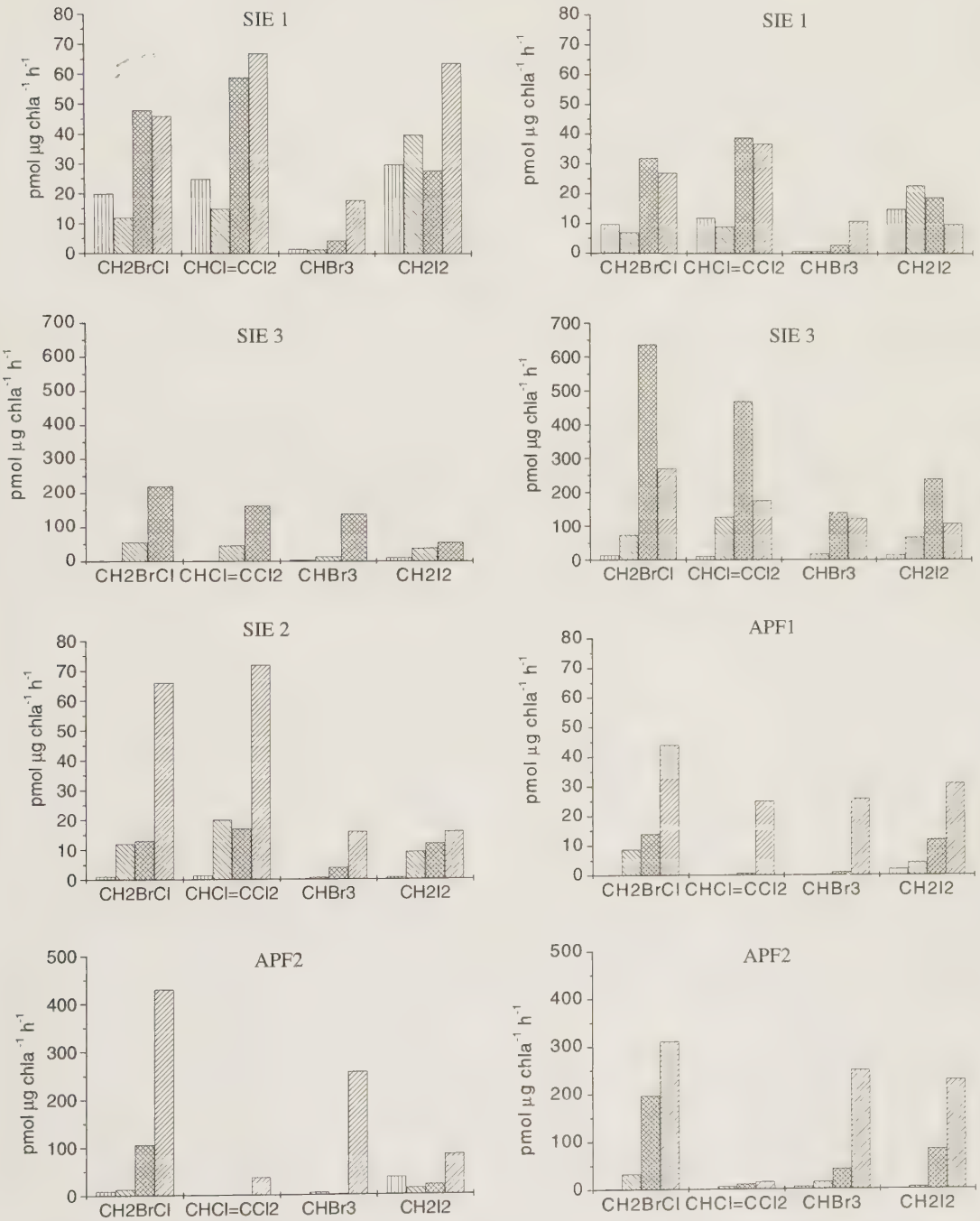

Fig. 4. Production rates of the four dominating halocarbons by phytoplankton of different sizes at the different biostations. The different sizes are from left to right for each compound: 150–1000 µm; 20–150 µm; 2–20 µm; and 0.4–2 µm. At three stations, duplicate filtrations were made. Unfortunately the filtrations were not successful at the WIE. Note the different scales on the *y*-axis.

Table 4
Pigment concentrations (±SD) for the different biostations

Area	Biostation	Per	19′-but	Fucox	19′-hex	Allox	Zeax	Chl *b*
SIE	Average SIE	17±4	26±3	469±48	1409±735	21±9	nd	0
	SIE 1	13±6	23±3	461±86	1542±407	23±4	nd	nd
	SIE 2	20±2	29±1	520±29	2067±136	29±2	nd	1±3
	SIE 3	19±6	25±7	426±56	616±267	12±6	nd	nd
WIE	WIE	11±6	23±14	151±70	227±117	6±3	6±2	nd
APF	Average APF	87±36	66±9	345±48	402±94	8±1	1±0	17±6
	APF 1	62±5	59±4	311±28	335±25	8±2	1±1	21±5
	APF 2	112±52	72±11	379±94	469±105	9±2	1±2	13±6

Concentrations are given in ng l^{-1}. nd = not detected.

autumn in the Greenland Sea, but much higher than those found in the Arctic Ocean during summer (Ekdahl, 1997). However, the production rates for diiodomethane at SIE 1 are relatively high for all fractions. This could be due to the relatively large abundance of *Phaeocystis* as mentioned above. These algae could be present in the largest fractions 1 and 2.

3.3. Diurnal variations

For most of the halocarbons a clear diurnal cycle could be seen both for samples collected at the surface and for those collected at chl. max (Fig. 5). The results show that there is a 24-h cycle with one or two productive periods, one or two periods with decrease in concentrations, and a period with steady state. The increases during mid-day could be as high as 500%, 400% and 800% for trichloroethene, tribromomethane and diiodomethane, respectively.

The highest concentrations of biogenic halocarbons were usually found at mid-day when photosynthesis was at its maximum. On some occasions a second halogen production maximum could be found in the early evening. This pattern agrees well with results from a similar investigation in a rock pool (Fig. 6) (Ekdahl et al., 1998). The second maximum found during the dark hours, is caused by biological activity other than photosynthesis, such as respiration. It has been shown that macroalgae produce halocarbons even in dark conditions (Collén et al., 1994).

The most striking feature is the rapid decrease in concentration of halocarbons observed both at the surface and at the chl. max. This implies that the amounts of halocarbons produced in the water column from the surface down to the chl. max disappear in just a few hours.

3.4. Total production and total loss

The measured increases and decreases in concentrations were used to calculate the production and the losses of halocarbons during 24-h periods at the six stations. The production times varied considerably between stations as well as between compounds. The period of production varied from 4 to 16 h, and these values were used to calculate both the total production and the total loss.

The total production was calculated both from the incubation experiments and from the measured concentrations. The incubation experiments provided production rates from fractions of different sizes. Values for the size fractioned chl *a* data are presented by Froneman and Pakhamov (this issue). Using the production rates for the individual fractions and the box described earlier the total production of organo-halogens were estimated (Fig. 7). These values were compared with the observed production, lower graph Fig. 7. The values are in fairly good agreement. However, the incubation experiments yielded higher values for organo-bromine and organo-chlorine, and lower values for organo-iodine. Earlier investigations have shown that the production of especially

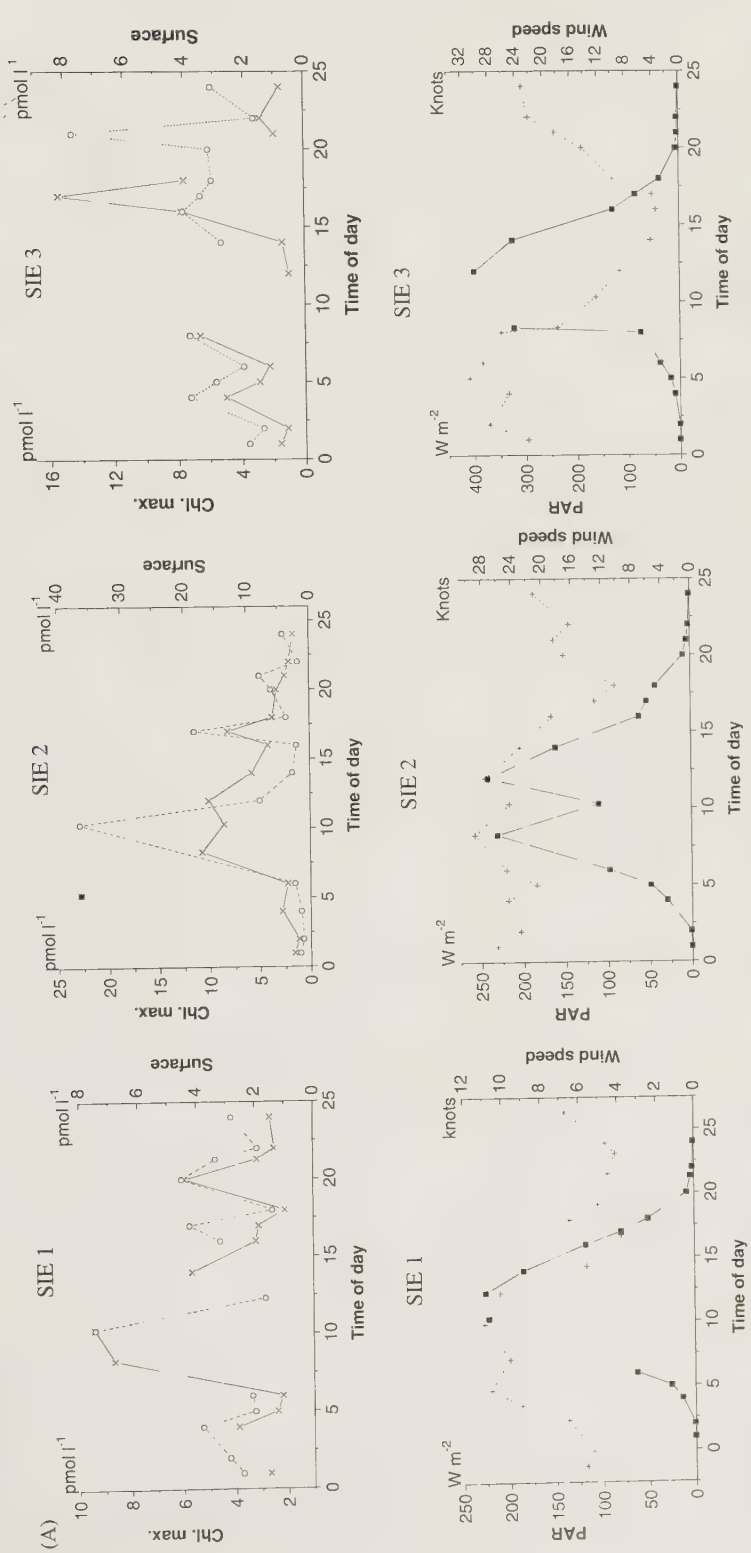

Fig. 5. The diurnal variations of trichloroethene (upper graphs) and wind speed (lower graphs, dotted line) at the six biostations. For the graphs illustrating the variations of trichloroethene, the straight line represents chl. max, whereas the dotted lines represent surface samples. The time of day with day light is given in the lower graphs (PAR, straight lines).

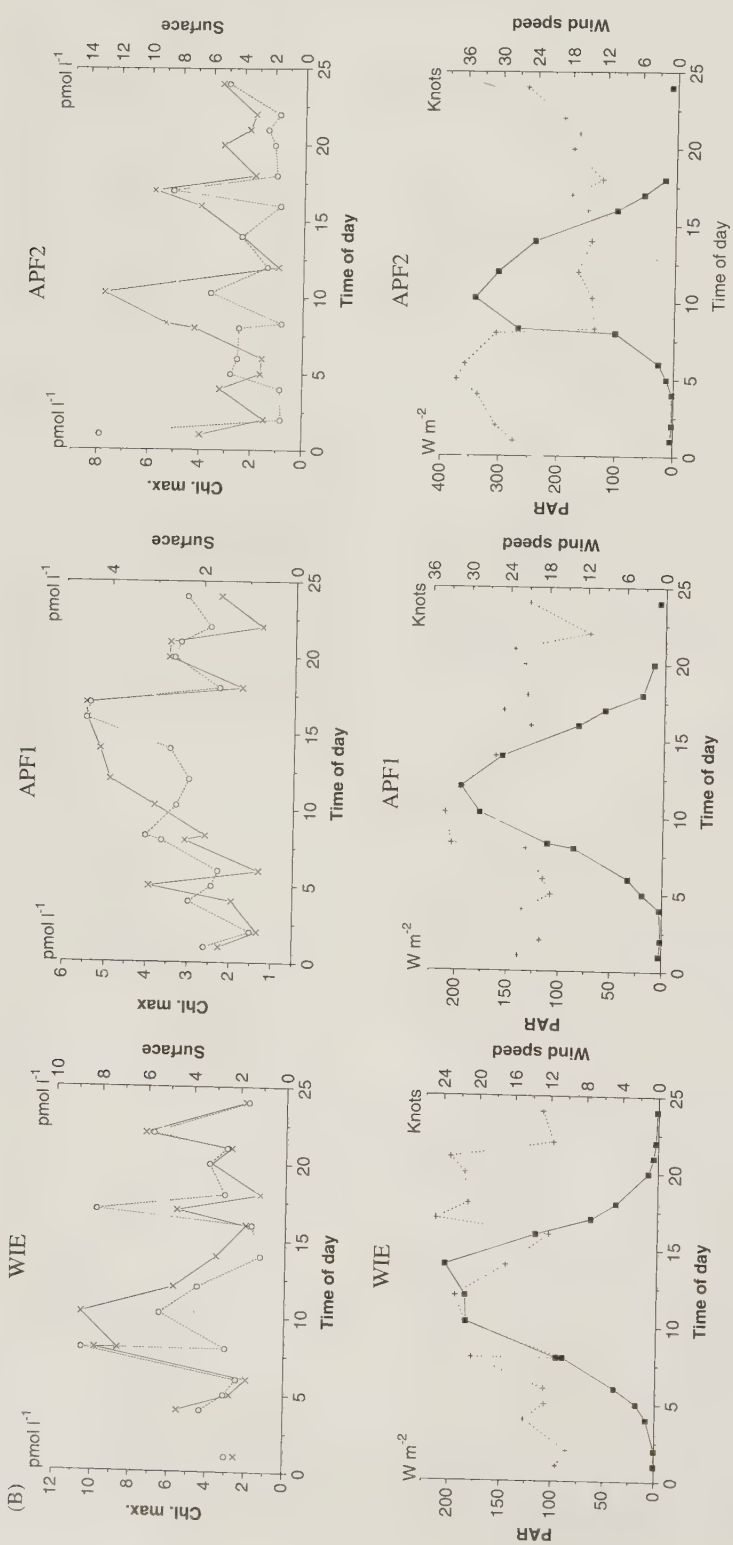

Fig. 5. (*Continued*)

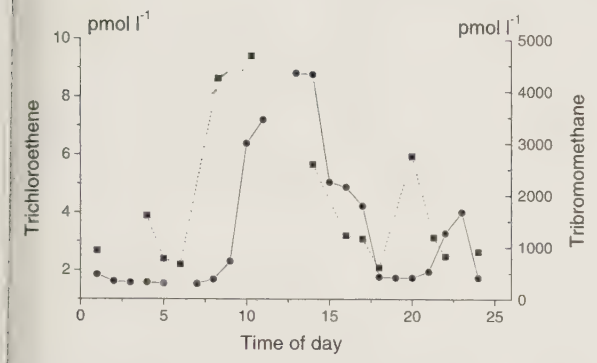

Fig. 6. Comparison of the diurnal variation of halocarbons in a rock pool (straight line, right axis) and in the open ocean (dashed line, left axis).

chlorinated and brominated compounds is due to oxidative stress and mechanical stress (Collén et al., 1994; Pedersén et al., 1996), which could be the reason for the slightly over-estimated production values (a factor of around 2) in the incubation experiments. If we use the production rates for a given station (Fig. 7) to extrapolate over the entire Antarctic Ocean, the total production of organo-halogens is in the order of Tg yr^{-1} (Table 5). The differences found in total production between the stations within a region, and in between regions can be a factor of 10, which illustrates the uncertainties in extrapolation from one station to an entire region. It should be emphasised that the main contributing compounds to the production rates reported in Table 5 are tribromomethane, bromochlormethane, trichloroethene and diiodo-methane.

If we compare the observed decrease over an hour with the calculated loss to the atmosphere, there is a large discrepancy. The diffusion rates for the halocarbons are low, and the environmental half-lives for chlorinated and brominated com-pounds are long. Thus, we have to conclude that a large amount of halocarbons are produced during a 24-h period. How, then, shall we account for the disappearance rates? The disappearance rates estimated from the variations over 24-h periods include both the loss to the atmosphere, biological and chemical degradation, and also downward mixing. We assumed that loss due to downward

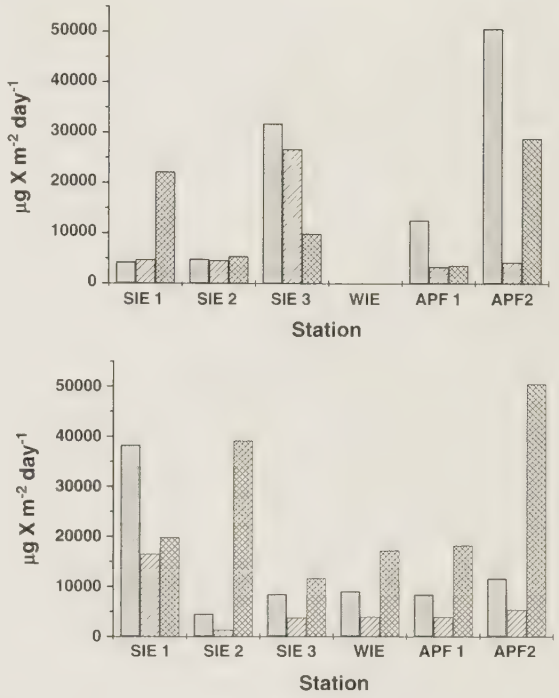

Fig. 7. The production of organo-bromine (filled box), organo-chlorine (hatched box) and organo-iodine (cross-hatched box) at the different stations. The upper graph shows the production determined from the incubation experiments, and the lower graph shows the production estimated from the measured concentrations.

Table 5
The total production of organo-halogens in the Antarctic Ocean based on the measured concentrations during 24-h periods

Station	Production 24-h variation (Tg yr^{-1})		
	Organo-Br	Organo-Cl	Organo-I
SIE 1	200	100	100
SIE 2	30	8	200
SIE 3	50	20	70
WIE	50	20	100
APF1	50	30	100
APF2	70	30	300
Average	70	30	100

The values (in nmol d^{-1}) are calculated for a box with an area of 1 m^2 and a depth given by the surface mixed layer.

mixing was negligible. Thus, biological degradation of marine bacteria could be a plausible explanation for the rapid disappearance of halocarbons. However, an investigation performed by Goodwin et al. (1997) showed that tribromomethane was not degraded by bacteria, and that dibromomethane could be degraded but could only account for $<1\%$ of the dibromomethane produced by macroalgae. Bacterial activity could be assumed to be slow in cold waters. Consequently, the explanation of the discrepancy could not be found in microbial degradation.

Chemical reactions such as hydrolysis and other nucleophilic substitution reactions are known to be slow at temperatures around 0 °C, which is reflected in the environmental half-lives given by Vogel et al. (1987) and Jeffers et al. (1989) of 0.5 to as much as 1×10^6 years for chlorinated and brominated compounds. If we try to estimate the losses due to chemical reactions according to Anbar et al. (1996) we end up with relatively low amounts (Table 6). Hence, the chemical degradation yields no explanation either. However, the relatively high disappearance rates observed for iodinated compounds could be explained by photochemical and chemical reactions. These compounds are more unstable than the other compounds.

An unknown factor that might be the explanation is sorption to particulate matter. The tendency to sorb to particulate matter can be estimated by their octanol–water partition coefficients K_{ow}. The values for halocarbons vary between $2 < \log K_{ow} < 3$, and the partition coefficients ($\log K_{om}$) between organic matter and water for different halocarbons have been found to be between 1 and 2 (Schwarzenbach et al., 1993). These values do not exclude sorption to particles, but the association tendency is weak. For instance, the removal of tetrachlorethene ($\log K_{ow} = 2.88$) to sediments was assumed to be negligible in a case study in a lake (Schwarzenbach et al., 1993).

We then turn to the exchange between the sea surface and the atmosphere as estimated from the model by Liss and Merlivat (1986). The fluxes are given in Table 6, and the values are based on estimating the flux at each sample point. Again, the numbers are too low to explain the observed losses. During the steady states, mainly observed

Table 6
The measured total loss, the loss due to chemical degradation and the estimated fluxes to the atmosphere at the different stations

Station	Trichloroethene			Tetrachloroethene			Trichloromethane			Dibromomethane			Tribromomethane		
	Total	Degradation	Flux	Total	Degradation	Flux	Total	Degradation	Flux	Total	Degradation	Flux	Total	Degradation	Flux
SIE 1	400–700	0.42	4	4	0.003	0.08	20	0.01	0.28	10–50	0.0007	1.9	400–1100	0.002	8.3
SIE 2	200	0.33	30	9	0.005	0.48	4	0.009	0.69	60	0.0006	3.6	700	0.001	19
SIE 3	80–2000	0.39	7	7 30	0.005	0.17	8	0.02	0.49	250	0.001	2.2	1900	0.002	10
WIE	1300	0.56	9	9–60	0.006	0.17	10–20	0.02	0.52	30	0.001	3	1800	0.004	18
APF 1	1700–2900	0.39	8	10–40	0.005	0.17	8	0.02	0.76	5	0.001	3.3	1300	0.001	6
APF 2	3000–3400	0.49	10	60	0.061	0.48	4–10	0.02	0.72	130	0.002	3.5	2000	0.002	11

The values (in nmol d^{-1}) are calculated for a box with an area of 1 m^2 and a depth given by the surface mixed layer.

during night time, there were no net flux over the air–sea interface. This period was sometimes as long as 20 h. From the fact that we observed the same type of behaviour in a shallow rock pool (Fig. 6), we believe that the observed losses could not be assigned to diffusion within the surface mixed layer.

The values given in Table 6 clearly show that the total loss calculated from the observed variations during a 24-h period could not be explained by the flux to the atmosphere or by chemical degradation. It has been suggested that all halocarbons produced by marine algae will eventually reach the atmosphere. Our investigation seems to yield no support to this suggestion. However, if the net flux to the atmosphere is equal to the total production minus the total aquatic loss, the explanations for the discrepancies must be found in the different terms used for the calculations.

Table 7 shows the total flux of organo-halogens to the atmosphere in the Antarctic Ocean estimated from the individual values at each station. The global annual emission of organo-chlorine has been estimated to be approximately $1\,Tg\,yr^{-1}$ (Reactive Chlorine Emission Inventory, RCEI). Our estimate, in average $0.2\,Tg\,yr^{-1}$, in contrast to RCEI, does not include methyl chloride but bromochloromethane, which was shown to constitute a large portion of the investigated halocarbons.

For organo-bromine and organo-chlorine the values between the calculated losses and the observed losses vary with a factor of 10. There was, however, a larger difference for organo-iodine.

4. Conclusions

Variations of the concentrations of halocarbons were observed at all sampling occasions during 24-h periods. The production of organo-halogens varied from a few hundred to 20,000 µg organo-halogen per day. The total losses ranged between 100 and 7000 µg organo-halogen per day. The diurnal variations were shown to consist of three phases, production, loss and steady state, describing a diurnal cycle. Only the presence of the photosynthetic pigment *19'hex*, that is, the presence of haptophytes, could explain some of the variations in the distribution and production of halocarbons, and then only for iodinated compounds. For compounds with large diurnal variations, the flux to the atmosphere varied considerably, and consequently, estimates of fluxes to the atmosphere based on only one, or a few occasions a day, are very uncertain.

The estimated losses could not be explained by air–sea exchange, microbial degradation, chemical degradation or sorption to particles. This investigation therefore shows the need for assessing the rates of degradation, as well as the air–sea exchange, more accurately.

Acknowledgements

We would like to thank the Swedish Polar Secretariat, Göteborg Marine Research Centre (GMF), the Swedish Natural Science Research Council who funded the expedition.

Table 7
The flux of organo-halogens to the atmosphere at the different stations

Station	Calculated flux organo-Br	Calculated flux organo-Cl	Calculated flux organo-I	Observed flux organo-Br	Observed flux organo-Cl	Observed flux organo-I
SIE 1	0.2	0.08	0.03	8	3	8
SIE 2	0.5	0.2	0.07	5	1	8
SIE 3	0.3	0.1	0.03	7	3	20
WIE	0.5	0.2	0.06	7	3	70
APF1	0.5	0.2	0.03	7	6	40
APF2	0.7	0.3	0.07	9	6	70
Average	0.5	0.2	0.05	7	3	40

The fluxes (in $Tg\,yr^{-1}$) are extrapolated to a surface area of $3.2 \times 10^9\,km^2$.

The work of the crew on the Research Vessel S.A. *Agulhas* is also acknowledged.

References

Abrahamsson, K., Ekdahl, A., Collén, J., Pedersén, M., 1995. Marine algae—a source of trichloroethylene and perchloroethylene. Limnology and. Oceanography 40, 1321–1326.

Anbar, A.D., Yung, Y.L., Chavez, F.P., 1996. Methyl bromide: ocean souces, ocean sinks and climate sensitivity. Global of Geochemical Cycles 110, 175–190.

Butler, J.H., Rodriguez, J., 1996. Methyl bromide in the atmosphere. In: Bell, C.H., Price, N., Chakrabarti, B. (Eds.), The Methyl Bromide Issue. Wiley, New York, pp. 28–90.

Class, T., Ballschmiter, K., 1988. Chemistry of organic traces in air VIII: sources and distribution of bromo- and bromochloromethanes in marine air and surface water of the Atlantic Ocean. Journal of Atmospheric Chemistry 6, 35–46.

Collén, J., Ekdahl, A., Abrahamsson, K., Pedersén, M., 1994. The involvement of hydrogen peroxide in the production of volatile halogenated compounds by *Meristiella gelidium*. Phytochemistry 36, 1197–1202.

Davidson, A.T., Marchant, H.J., 1992. Protist interactions and carbon dynamics of a *Phaeocystis*-dominated bloom at an Antarctic coastal site. Polar Biology 12, 387–395.

Dewulf, J., Drijvers, D., van Langenhove, H., 1995. Measurements of Henry's law constant as a function of salinity and temperature for the low temperature range. Atmospheric Environment 29, 323–331.

Dvortsov, V.L., Geller, M.A., Solomon, S., Schauffler, S.M., Atlas, E.L., Blake, D.R., 1999. Rethinking reactive halogen budgets in the midlatitude lower stratosphere. Geophysical Research Letters 26, 1699–1702.

Ekdahl, A., 1997. On the origin and assessment of biogenic halocarbons. Ph.D. Thesis, Department of Analytical and Marine Chemistry, Göteborg University, Sweden.

Ekdahl, A., Abrahamsson, K., 1997. A simple and sensitive method for the determination of volatile halogenated organic compounds in sea water in the amoll^{-1} to pmoll^{-1}range. Analytica Chimica Acta 357, 197–209.

Ekdahl, A., Pedersén, M., Abrahamsson, K., 1998. A study of the diurnal variation of biogenic volatile halocarbons. Marine Chemistry 63, 1–8.

Fogelqvist, E., Tanhua, T., 1995. A field study of the release of halogenated C_1–C_4 organics from ice algae in the Antarctica. In: Grimvall, A., deLeer, E.V.B. (Eds.), Naturally Produced Organo-halogens. Kluwer Academic Publishers, Dordrecht, Delft, The Netherlands, pp. 295–306.

Goodwin, K.D., Lidstrom, M.E., Oremland, R., 1997. Marine bacterial degradation of brominated methanes. Environmental Science and Technology 31, 3188–3192.

Graedel, T.E., Keene, W.C., 1995. Tropospheric budget of reactive chlorine. Global Biogeochemical Cycles 9, 47–77.

Jeffers, P.M., Ward, L.M., Woytowitch, L.M., Wolfe, N.I 1989. Homogeneous hydrolysis constants for select chlorinated methanes, ethanes, ethenes, and propane Environmental Science and Technology 23, 965–969.

Klick, S., 1992. Seasonal variations of biogenic and anthr pogenic halocarbons in sea water from a coastal sit Limnology and Oceanography 37, 1579–1585.

Klick, S., Abrahamsson, K., 1992. Biogenic volatile iodate hydrocarbons in the ocean. Journal of Geophysical R search 97, 12,683–12,687.

Laturnus, F., 1996. Volatile halocarbons released from Arct macro algae. Marine Chemistry 55, 359–366.

Liss, P.S., Merlivat, L., 1986. Air–sea gas exchange rate introduction and synthesis. In: Buat-Ménerad, P. (Ed.), Th Role of Air–Sea Exchange in Geochemical Cycling. D Riedel Publishing Company, Dordrecht, pp. 113–127.

Lobert, J.M., Butler, J.H., Montzka, S.A., Geller, L.S., Myers R.C., Elkins, J.W., 1995. A net sink for atmosperic CH_3B in the East Pacific Ocean. Science 267, 1002 1005.

Mackey, M.D., Mackey, D.J., Higgins, H.W., Wright, S.W. 1996. CHEMTAX—a program for estimating class abun dances from chemical markers: application to HPLC measurements of phytoplankton. Marine Ecology Progress Series 144, 265–283.

Moore, R.M., Tokarczyk, R., 1992. Volatile biogenic halocar bons in the Northwest Atlantic. Global of Geochemica Cycles 7, 195–210.

Moore, R.M., Geen, C.E., Tait, V.K., 1995. Determination o Henry's law constants for a suite of naturally occuring halogenated methanes in seawater. Chemosphere 30, 1189–1191.

Moore, R.M., Webb, M., Tokarczyk, R., Wever, R., 1996. Bromoperoxidase and iodoperoxidase enzymes and production of halogenated methanes in marine diatom cultures. Journal of Geophysical Research 101, 20,899–20,908.

Pedersén, M., Collén, J., Abrahamsson, K., Mtolera, M., Semesi, A., Gracia-Reina, G., 1996. The ice–ice deseace and oxidative stress of marine algae. In: Björk, M., Semesi, A., Pedersén, M., Bergman, B. (Eds.), Current Trends in Marine Botanical Research in the East-African Region, pp. 11–24.

Peeken, I., 1997. Photosynthetic pigment fingerprints as indicators of phytoplankton biomass and development in different water masses of the Southern Ocean during austral spring. Deep-Sea Research II 44, 261–282.

Prather, M.J., McElroy, M.B., Wofsy, S.C., 1984. Reductions in ozone at high concentrations of stratospheric halogens. Nature 312, 227–231.

Quack, B., Suess, E., 1999. Volatile halogenated hydrocarbons over the western Pacific between 43° and 4°N. Journal of Geophysical Research 104, 1663–1678.

Reifenhäuser, W., Heumann, K.G., 1992. Bromo- and bromochloromethane in the Antarctic atmosphere and the south polar sea. Chemosphere 24, 1293–1300.

Satoh, H., Watanabe, K., 1991. A red-water bloom caused by the ciliate *Mesodinium rubrum* in the Austral summer in the fast ice near Syowa station Antarctica with notes on their

photosynthetic rate. Journal of the Tokyo University of Fisheries 78, 11–18.

Schall, C., Heumann, K.G., Kirst, G.O., 1997. Biogenic volatile organoiodine and organobromine hydrocarbons in the Atlantic Ocean from 42°N to 72°S. Fresenius Journal of Analytical Chemistry 359, 298–305.

Schwarzenbach, R.P., Gschwend, P.M., Imboden, D.M., 1993. Environmental Organic Chemistry. Wiley, USA.

Smetacek, V., Scharek, R., Nöthig, E.-M., 1990. Seasonal and regional variation in the pelagial and its relationship to the life history cycle of krill. In: Kerry, K.R., Hempel, G. (Eds.), Antarctic Ecosystems: Ecological Change and Conservation. Springer, Berlin, pp. 103–114.

Tokarczyk, R., Moore, R.M., 1994. Production of volatile halogens by phytoplankton cultures. Geophysical Research Letters 21, 285–288.

Vogel, T.M., Criddle, C.S., McCarty, P.M., 1987. Transformation of halogenated aliphatic compounds. Environmental Science and Technology 21, 722–736.

Wever, R., Tromp, M.G.M., Krenn, B.E., Marjani, A., van Tol, M., 1991. Brominating activity of the seaweed *Ascophyllum nodosum*: impact of the biosphere. Environmental Science and Technology 25, 446–449.

Wofsy, S.C., McElroy, M.B., Yung, Y.L., 1975. The chemistry of atmospheric bromine. Geophysical Research Letters 2, 215–219.

Wright, S.W., Jeffrey, S.W., 1997. High-resolution HPLC system for chlorophylls and carotenoids of marine phytoplankton. In: Jeffrey, S.W., Mantoura, R.F.C., Wright, S.W. (Eds.), Phytoplankton Pigments in Oceanography. UNESCO Publishing, Paris, pp. 327–360.

Wright, S.W., Thomas, D.P., Marchant, H.J., Higgins, M.D., Mackey, M.D., Mackey, D.J., 1996. Analysis of phytoplankton of the Australian sector of the Southern Ocean: comparisons of microscopy and size frequency data with interpretations of pigment HPLC data using the CHEMTAX matrix factorisation program. Marine Ecology Progress Series 144, 285–298.

Wuosmaa, A.M., Hager, L.P., 1990. Methylchloride transferase: a carbocation route for biosynthesis of halometabolites. Science 249, 160–162.

Zafiriou, O.C., 1975. Reaction of methyl halides with sea water and marine aerosols. Journal of Marine Science 33, 75–81.

ELSEVIER

Deep-Sea Research II 51 (2004) 2807–2825

DEEP-SEA RESEARCH
PART II

www.elsevier.com/locate/dsr2

The role of mixing in an Antarctic ocean ecosystem: observations and model computations of vertical distributions of related parameters

Anne-Marie Larsson*

Oceanography, Centre of Geosciences, Göteborg University, Box 460, SE-405 30 Göteborg, Sweden

Abstract

Observations during the Swedish–South African Antarctic marine expedition, SWEDARP 97 98, from December 1997 to February 1998 along longitude 6°E in the Southern Ocean demonstrate geographical differences in vertical distributions of chlorophyll-a and salts in three special study areas between latitude 61 °S and 40 °30′S. The aim of this work is to describe the functioning of the Antarctic ecosystem with emphasis on the inter-link between physical, chemical and biological processes in surface waters (0–200 m). Model calculations of fluxes of salts provide possible explanations of measured concentrations of vertical variations regarding salinity, chlorophyll-a and nitrate. The area of investigation is described by vertical mean gradients of salinity, temperature and nitrate for the upper layer (0–400 m) in every special study area together with chlorophyll-a for 0–100 m. The model includes physical processes in terms of vertical mixing and sinking velocity together with biological processes in terms of light-dependent phytoplankton growth, zooplankton grazing and regeneration. The vertical mixing is parameterised as an eddy diffusivity (K_z), assessed from salinity measurements. Both a depth constant K_z and a depth variable K_z are used. Model computations for a high K_z (2000–15 000 $m^2 day^{-1}$) in the upper layer, rapidly decreasing below 20–50 m and then a low and constant K_z (375–600 $m^2 day^{-1}$) down to 200 m depth supply the best reproduction of measured profiles. A subsurface maximum of chlorophyll-a can be formed only at very low K_z (50 $m^2 day^{-1}$). The irradiance quanta absorption coefficient is used together with the self-absorption of light of 0.06 times the mean chlorophyll-a in the water column. The specific algal gross primary production is calculated according to Steele (Limnol. Oceanogr. 7 (1962) 137). The specific loss rates are varied between 0.15 and 0.30 day^{-1} together with a regeneration factor of 0.3. The carbon:chlorophyll ratio ranges from 75 to 150, with the highest ratios in the Antarctic Polar Front area at around 51 °S, where the integrated chlorophyll-a in the upper 200 m is highest (137 mg m^{-2}). The sinking velocity of chlorophyll-a is judged to be 1 m day^{-1}.

The result of this work implies that the vertical mixing is a major limiting factor for the total amount of chlorophyll-a in the surface layer in this part of the Southern Ocean ecosystem on a shorter time scale. Changes of the vertical mixing, for example as an effect of climate change, will induce effects on the functioning of the ecosystem. For future

*Fax: +46 31 7732888.
E-mail address: amla@oce.gu.se (A.-M. Larsson).

0967-0645/$ - see front matter © 2004 Published by Elsevier Ltd.
doi:10.1016/j.dsr2.2004.09.006

oceanographic work in this area a lot of effort should be put into research with emphasis on losses of chlorophyll an an increased knowledge about vertical mixing.
© 2004 Published by Elsevier Ltd.

1. Introduction

The environmental conditions for living organisms in the Antarctic Ocean ecosystem are unique compared to conditions in other oceans. The incoming light regime experienced by a single phytoplankton varies greatly from zero hours per day during the austral winter to 24 h per day during the summer. The water temperature is low and varies from −1.8 °C near the continent to about 4.5 °C in the Antarctic Polar Front at about 50°S latitude during the summer. The concentrations of inorganic macro nutrients are generally in excess of those required to sustain the maximum growth of primary producers. Even an intense phytoplankton bloom does not bring the concentrations to a low level, and the concentration of, for example, nitrate is usually higher than 10 mmol m^{-3}. Instead, any of the micro nutrients, especially iron, are supposed to be limiting factors for the total amount of the primary production (e.g. Sakshaug and Holm-Hansen, 1984; De Baar et al., 1990). Biotic factors of importance controlling phytoplankton growth are grazing by zooplankton, shelf absorption of light and losses of chlorophyll by downward transport (Wofsy, 1983; Sakshaug et al., 1991; Taylor et al., 1991; Bouqugneau et al., 1991; Broström, 1997). Several authors have posited that the ecosystem is strongly affected by vertical mixing processes which distribute parameters throughout the water column (Gran, 1931; Riley et al., 1949; Sverdrup, 1953; Svansson, 1991; Veth et al., 1992). Gran (1931) for example, wrote: "*My explanation is that the diatoms also move with vertical movements of the water, and that therefore no accumulation is found in the illuminated zone, with the effect that the whole production is retarded, because too many of the diatoms sink below the balance depth of the photosynthesis*". Although no solitary mechanism can be pointed out to explain the limiting factor for the total amount of phytoplankton biomass and its distribution, the role of mixing is particularly important in the Antarctic Ocean where the upper water column is usually less stable than in other oceans.

In this present work observations during SWEDARP 97/98, the Swedish–South African marine expedition in the Southern Ocean, are presented and analysed in an ecological model. The aim is to describe the functioning of the Antarctic ecosystem with emphasis on the inter-linkage between physical, chemical and biological processes in surface waters. Model calculations of fluxes of salts provide possible explanations of measured concentrations of vertical variations regarding salinity, chlorophyll-a and nitrate. The results will also contribute to the understanding of the problem of limiting factors of the primary production in short time scales in the Antarctic Ocean ecosystem.

2. Observations

Data used in this paper were collected onboard SA Agulhas in the eastern Atlantic sector of the Southern Ocean during the SWEDARP expedition in a section along 6°E between the Antarctic continent (SANAE, the South African station) and South Africa (Cape Town) from December 1997 to February 1998. Part of the goal of this expedition is to determine the relative importance of different potential controlling factors for the primary production of the Antarctic ecosystem in different frontal zones within the framework of the international JGOFS (Joint Global Ocean Flux Study).

The sampling section extends from the ice edge to the permanently open zone at the northern border of the Southern Ocean (Fig. 1). In this section three areas have been selected for closer studies, the Spring Ice Edge (SIE) at around 60°S, the Winter Ice Edge (WIE) at around 56°S and the

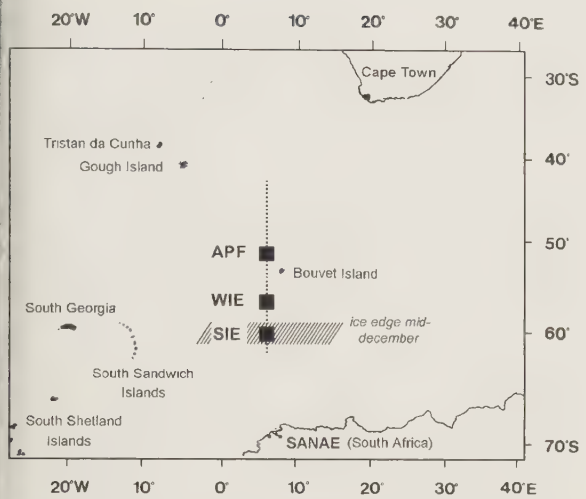

Fig. 1. Cruise track of SA Agulhas during SWEDARP 97/98 showing the CTD section along 6°E from 61°S to 41°30′S. The hatched line represents the location of the ice edge in the middle of December. The areas for closer studies are the SIE at around 60°S, the WIE at around 56°S and the APF at around 51°S. During the period of sampling all three areas were ice-free.

Antarctic Polar Front (APF) at around 51°S. The section consists of shallow CTD casts (400 m) together with a limited number of deep casts (3000 m) across the frontal features studied. The total number of CTD casts was 174. The study area is characterised by absence of the permanent pycnocline and a strongly time dependent frontal activity with several water masses involved (Lutjeharms, 1985; Veth et al., 1997). The ice edge disappeared very rapidly from around 60°S in the middle of December when only a strip of sea ice was left close to the shelf ice. SIE was situated in the expected position for the ice edge when the sampling started on December 26th.

Temperature and salinity were measured with a General Oceanics MkIIIC CTD (WOCE standard) combined with a Chlorophyll-a fluorometer (Chelsea Instruments Aquatracka). At each station a large number of measurements were conducted from discrete water samples. In addition specific observations and underway surface sampling were performed. The water samples were drawn from a Niskin bottle Rosette (24 times 7.5 l). The salinity values used in this work are selected from the 2 m means for every sampling depth. Inorganic macro nutrients were run on board using a Technicon auto analyser. Samples for analysis of chlorophyll were filtered at low temperatures (0–2 °C) in dim light and frozen in liquid nitrogen. HPLC analyses after the cruise gave the amount of chlorophyll-a (Wulff and Wängberg, 2004). A Licor LI1800UW spectroradiometer was used for parts of the optical measurements (Rasmus et al., 2004).

3. The model

This time-dependent ecological model was constructed simple enough, without too many details, to be able to compute vertical distributions of chlorophyll-a and nitrate in order to investigate the interactions between some of the physical, chemical and biological processes giving the ecosystem its character (Svansson, 1991). Fluxes of salts, including nutrients, and fluxes of gases due to biological processes could also be included (Larsson and Svansson, 1992). In this study the model was improved with a depth variable vertical mixing related to the salinity variations and only fluxes of salt (salinity) and macro nutrients were considered.

3.1. Model parameters

The present model includes the surface layer 0–200 m depth in the Antarctic Ocean. This surface water can be influenced by ice melting, but areas covered entirely by ice are not included. All parameters used in this work together with their units and, where appropriate, selected values or ranges of variations are summarised in Table 1.

3.2. Equations for chlorophyll

Changes in the concentration of chlorophyll-a (A) are a result of the specific gross algal primary production (p), the specific loss rate (L), the mixing ($\partial(K_z(\partial A/\partial z))/\partial z$) and the sinking velocity of chlorophyll (w_s). Boundary conditions for chlorophyll-a are zero at 200 m depth and no flux through the surface (no contribution from melting ice). Thus the time (t)-dependent rate of changes of

Table 1
Description of the variables with their units and values/ranges used in this paper

Variable	Value/range	Unit	Description
S	33.80–34.74		Salinity
A	0–1.9	$mg\,m^{-3}$	Concentration of chlorophyll-a (chl)
A_{av}		$mg\,m^{-3}$	Mean chl concentration for 0 to z m depth
R	12–37	$mmol\,m^{-3}$	Concentration of nitrate (NO_3–N)
z	0–200	m	Depth with the z-axis positive downwards
t		day	Time. Time step in the computations is 1 day
h		h	Hours of daylight
SUMA		$mg\,m^{-2}$	Vertical integration of chlorophyll for 0–200 m
SUMR		$mmol\,m^{-2}$	Vertical integration of nitrate for 0–200 m
K_z	50–15 000	$m^2\,day^{-1}$	Vertical diffusion coefficient
w_s	0–5	$m\,day^{-1}$	Sinking velocity of chlorophyll in phytoplankton
L	0.1–0.6	day^{-1}	Specific loss rate
k_r	0–1		Extent of regeneration
p		day^{-1}	Specific algal gross primary production
p_{max}	0.08	h^{-1}	Maximum photosynthetic rate
$I(z)/I_0$			Relative irradiance. I_0 at the surface, $I(z)$ at z
k		m^{-1}	Vertical attenuation coefficient of irradiance
k_1	0.060	$(mg/m^3\,m)^{-1}$	Self-absorption of quanta irradiance
C/A			Carbon:chlorophyll ratio by weights
k_{RA}	0.0126C/A		Factor relating nitrate to chlorophyll-a according to Redfield ratios by atoms

chlorophyll-a can be formalised as

$$\partial A/\partial t = A(p - L) + \partial(K_z \partial A/\partial z)/\partial z - w_s \partial A/\partial z.$$

The specific algal gross primary production (p) has been calculated according to Steele (1962) from a supposed maximum value for the photosynthetic rate ($p_{max} = 0.08$ per hour) in the following equation:

$$p = 2 \times 0.82(0.08h)(I(z)/I_0)\, exp(1 - 2I(z)/I_0),$$

where h is hours of daylight, I_0 is the quanta irradiance at the surface given as the total daily average light intensity during daylight hours and $I(z)$ is the corresponding quanta irradiance at each depth. In January the hours of daylight at the latitudes of the Antarctic Ocean are about 19 at 60°S, 18 at 55°S and 17 at 50°S. The relationship between irradiance and depth is given by

$$I(z)/I_0 = 0.67\ \ exp(-kz),$$

where z is the depth, k is the quanta irradiance attenuation coefficient for visible light and 0.67 is a factor compensating for k's slight deviation from being constant with depth (Svansson, 1992). Also the self-absorption of light by chlorophyll-a is important for light penetration (Kirk, 1983). The irradiance attenuation for total quanta therefore increases with increasing amount of algal biomass. In Svansson (1992) this is formalised from measurements in the Antarctic Ocean as

$$k = 0.046 + k_1/A_{av}.$$

The constant $k_1 = 0.060$ denotes the change in k for every chlorophyll-a unit and A_{av} is the mean chlorophyll-a concentration from the surface to the depth concerned. As the distribution of chlorophyll-a is depth variable, the self-absorption of light also varies with depth.

3.3. Vertical diffusion coefficient, loss rate and sinking velocity

In this model the vertical mixing is parameterised as the vertical diffusion coefficient, K_z. The vertical salinity variations, which are not affected by the biological processes but are a function of mixing and boundary fluxes, were used to provide the vertical variations of K_z. This is possible in areas where the density gradient mainly follows the salinity and the influence of temperature is

small. Already Fjeldstad (1936) used an approach of this type in Arctic waters. From mean vertical variations of salinity (S) K_z was determined at various depths. In totally well mixed surface layers K_z is very large ("infinite"). If the salinity increases linearly with depth, K_z is constant. K_z can also vary with depth with maximum values in the surface, rapidly decreasing values in the pycnocline and lower values in the deeper water. The effect of the vertical diffusion of salt, and all other parameters, is a transport from a higher concentration to a lower concentration. Horizontal salinity fluxes are not included.

The specific loss rates (L) are considered independent of depth in the model. There is a certain contribution of algal respiration and natural death, but the main part of L is the zooplankton grazing. Therefore L is far from constant in time and changes with the abundance of grazers. L is highest when micro- and mesozooplankton reach their highest density. By grazing impact of the primary production a certain part of chlorophyll-a leaves the system. In Antarctic waters L usually varies between 0.1 and 0.6 day^{-1} (G. Fransz, personal communication, 1996). This implies that the zooplankton graze 10–60% of the primary production per day. Klaas (1997) found that microprotozooplankton directly grazed from 11% to 47% of the daily primary production in October 1992, in an area corresponding to SIE.

The sinking velocity of chlorophyll-a in phytoplankton (w_s) is assumed to be 0–5 m day^{-1} (Larsson and Svansson, 1992), but can also be considerably higher. In Taylor et al. (1991) the mean sinking velocity in the north Atlantic is given to 0.9 m day^{-1}. For a nanoplankton dominated community the sinking velocity is slower, 0.3–0.5 m day^{-1} (Aksnes and Lie, 1990; Cloern, 1991).

3.4. Equation for nutrients

Throughout this work nitrate was used as representative of the nutrients. Nitrate is generally the most appropriate nutrient (e.g. Sarmiento et al., 1993) for modelling the function of an open ocean ecosystem on smaller scale.

As with chlorophyll-a, the variations of concentrations of inorganic macro nutrients and biogenic gases are a result of sinks and sources due to biological, chemical and physical processes. Thus the time variations of the concentration of nitrate ($\partial R/\partial t$) can be expressed as

$$\partial R/\partial t = -A(p - k_r L)k_{RA} + \partial(K_z \partial R/\partial z)/\partial z.$$

Apk_{RA} is the decrease of nitrate due to biological production, Ak_rLk_{RA} is the amount of nitrate which returns to the solution due to regeneration of organic material and $\partial(K_z(\partial R/\partial z))/\partial z$ is the effect of vertical mixing. The boundary condition for nitrate at the sea surface is no flux, while the boundary condition at 200 m depth is the mean value of measurements. Although not expected in the Antarctic Ocean, a nutrient limitation is built in into the model (Svansson, 1996).

k_r represents the recycling efficiency or the fraction of the nutrient from the losses of cells that return to solution. To express the extent of regeneration, $k_r = 1$ stands for total regeneration, while $k_r = 0$ stands for no regeneration. By total regeneration all nutrients and carbon fixed in organic material is set free again during oxygen consumption. In Taylor et al. (1991) a recycling efficiency of 10–20% or $k_r = 0.1$–0.2 was reported for the North Atlantic. In Larsson and Svansson (1992) $k_r = 0.3$ was used for the Weddell Sea.

The factor k_{RA} is the nitrate content of the phytoplankton biomass given in chlorophyll-a, assuming Redfield's ratios between nitrogen and carbon (16:106) to be valid for changes in concentrations as a result of biological activity (Redfield et al., 1963; Sakshaug and Holm-Hansen, 1986; De Baar et al., 1997). Thus k_{RA} (Table 1) is the ratio between carbon and chlorophyll-a (C/A) multiplied by $(16/(12 \times 106))$. The carbon to nitrogen (C/N) average ratio in Antarctic waters is reported to be 6.7 in Sakshaug and Holm-Hansen (1986), thus very close to Redfield's ratio of 6.6, while others, for example De Baar et al. (1997), found a higher C/N than stated by Redfield. If the recycling efficiency changes, C/A will also be changed. According to the model calculations C/A is assumed to be constant from the surface to 200 m depth.

3.5. Running the model

The model is time-dependent in so far as chlorophyll-a (A) and nitrate (R) are computed for 70–90 days by means of initial and boundary conditions. During that period of time the vertical mixing, the losses, the sinking of chlorophyll-a and the state of light are all time-independent. In the case of A, a steady state is attained rather quickly provided that the self-absorption condition is applied, whereas the parameter R continuously changes with time. The initial condition for chlorophyll-a is that A is approximately equal to zero at all depths. For R the measured concentrations at 200 m depth are assumed to be prevalent at all depths at the beginning of the computation. In the case of a depth constant mixing, the eddy diffusion coefficient (K_z) and the specific loss rate (L) are initially determined from the total amount of chlorophyll-a from surface to 200 m depth (SUMA) and the vertical distribution of chlorophyll-a ($A(z)$). Thereafter the relationship between carbon and chlorophyll (C/A) is varied until a good agreement between measured and computed total amount of nitrate from surface to 200 m (SUMR) is achieved. In the case of a depth variable mixing the vertical variations of K_z are assessed from the measured salinity gradients in every special study area. The level of the vertical mixing rate is then adjusted to the vertical profiles of measured parameters.

After 70–90 days of model running the last computed value of each parameter and each depth is compared to the measured counterpart. The degree of agreement between the model calculated value and the measured value is judged by means of adjusting the root mean square of depth integrated values and by graphical comparisons of model calculated and measured vertical profiles of each parameter.

4. Results

In this work results from oceanographic observations in a section along 6°E in the Southern Ocean are reported. The section includes three special study areas: (a) the SIE at about 60°S, representing the area of the ice edge in the middl of December, (b) the WIE at about 56°S and (c the APF area at about 51°S. The characteristics c the areas of investigation are described by vertica mean gradients of salinity, temperature, nitrat and chlorophyll-a in the upper layer of each stud area. When calculating the mean values (0–400 m only the stations where nutrients were analysed ar included (27 stations). For model computation the surface waters, including 0–200 m at thos stations where both nutrients and chlorophyll-a are available, are selected (11 stations).

The SWEDARP 97/98 observations are pre sented below, followed by a description of the vertical mixing. Thereafter, the effect of variations of vertical mixing on the growth of algal biomass for different losses and different settling velocities of chlorophyll-a are discussed. Vertical distributions of chlorophyll-a and nitrate are also calculated for different kinds of vertical mixing. Based on results from these calculations possible solutions for the equations are studied for the present observations in the three different study areas.

4.1. Observations of temperature and salinity

To illustrate the stability gradients of the surface layer in the CTD section the mean temperatures and mean salinities for the upper 400 m in the three different areas are shown in Fig. 2. Density gradients mainly follow the salinity as the influence of temperature is small. The temperature of the surface layer (0–75 m) is about −0.5 °C in SIE, −0.5 to +0.5 °C in WIE and about +3.5 °C in APF. Below 200 m depth the temperatures in SIE and WIE are +0.5 °C and constant with increasing depth to 400 m. In APF the temperatures between 200 and 400 m depth are slightly increasing with depth at around 2 °C. The mean salinities of the surface water are lower in SIE (33.9) and APF (33.8) compared to WIE (34.2). In APF the water at 200 m depth is less dense than in the other areas ($\sigma_t = 27.32$) due to lower salinity (34.17 in APF, 34.73 in SIE). Mean differences in salinity between 200 m and the surface (2 m) in the three areas SIE, WIE and APF are 0.81, 0.47 and 0.34, respectively. This will lead to a more stabilised water column in

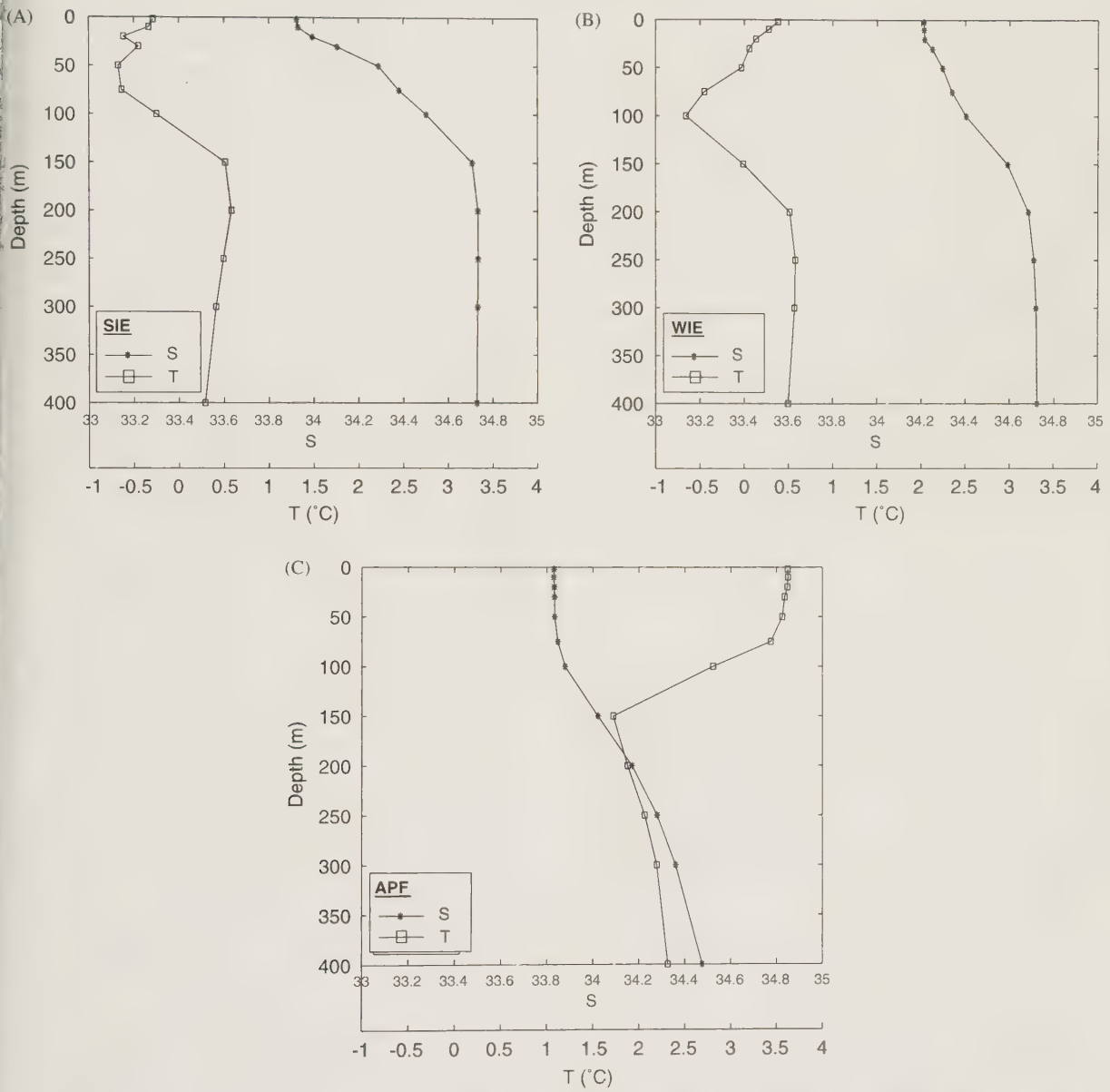

Fig. 2. Observed mean vertical profiles of temperature (T °C) and salinity (S). 0–400 m along 6° E in the Southern Ocean. The standard deviations are marked with dots: (A) SIE, at about 60°S; (B) WIE, at about 56°S; (C) APF, at about 51°S.

SIE than in WIE and APF. The depths of the well-mixed surface layers are about 20–50 m.

4.2. *Observations of chlorophyll-a and nitrate*

The typical feature of the Antarctic system, with high concentrations of nitrate even after algal primary production has started, is observed (Fig. 3). This production results in an increasing amount of chlorophyll-a in the surface layer together with a decreasing euphotic zone (Rasmus et al., 2004). The total amount of chlorophyll-a in the surface layer as integrated values from surface down to 200 m should correspond to the total

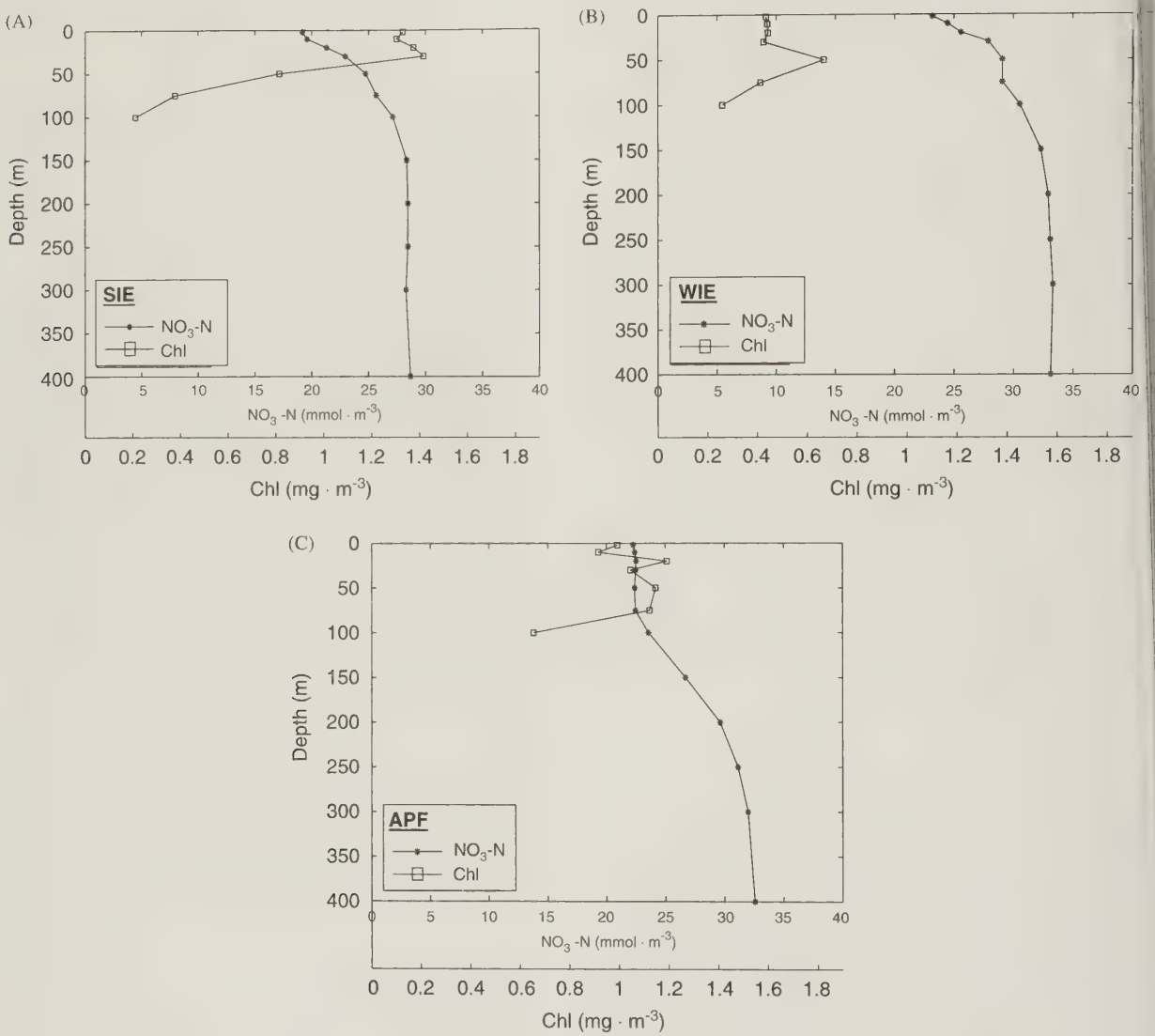

Fig. 3. Observed mean vertical profiles of nitrate (NO_3–N mmol m^{-3}) 0–400 m and chlorophyll-a (chl mg m^{-3}) 0–100 m along 6°E in the Southern Ocean. The standard deviations are marked with dots. The mean depths of the euphotic zone for stations with measurements of chlorophyll-a are 40 m in SIE, 80 m in WIE and 45 m in APF: (A) SIE, at about 60°S; (B) WIE, at about 56 S; (C) APF, at about 51°S.

amount of nutrient and carbon which are consumed and the total amount of oxygen which is released. Thus in this present 200 m thick surface layer the upper 40–80 m is a source of phytoplankton biomass, whereas the layer below is a sink for biomass. The surface (2 m) concentrations of chlorophyll-a are highest in SIE, lower in APF and lowest in WIE (Fig. 3). At 100 m depth SIE and WIE have about the same concentration of chlorophyll-a, while in APF it is three times higher. The integrated chlorophyll-a during SWEDARP 97/98 in the upper 200 m in APF (51°S) is 137 mg chl m^{-2} and thus lower than the corresponding value (177 mg chl m^{-2}) reported in

Bathmann et al. (1997) for 50°S, 6°W in November 1992.

In the surface (2 m) as well as at 200 m depth the concentration of nitrate is lowest in SIE and highest in WIE (Fig. 3). The differences in concentrations of nitrate between 200 m depth and surface (2 m) are 9 mmol m^{-3} in SIE, 10 mmol m^{-3} in WIE and 7 mmol m^{-3} in APF.

4.3. Relationships

As the distribution of concentrations of nitrate as well as of chlorophyll-a are under influence of biological processes and vertical mixing, induced by the salinity variations, all parameters are coupled together in any respect. Not only the amount of biologically created chlorophyll but also the mixing can be read from the distribution of chlorophyll-a. Some of the relationships between temperature, salinity, nitrate and chlorophyll-a are shown in Fig. 4A–D. The TS-plot in Fig. 4A shows the characteristic features of the Polar Frontal Region in APF with a temperature minimum layer in the salinity range of 33.8–34.0 as a remnant of thermohaline convection during sea-ice growth. Increasing temperatures in deeper water in APF are a result of mixing with Circumpolar Deep Water (Carmack, 1977). In SIE the low salinity surface layer is influenced by melting water. In the salinity range 34.5–34.6 this Antarctic Surface Water is mixed with the Warm Deep Water with temperatures above 0 °C and a salinity interval of 34.6–34.76 (Carmack and Foster, 1977). Upwelling of the warmer more saline water into the mixed layer supply nutrients to the surface layer (Fig. 4C). Only the surface water of WIE is characteristically an inter-frontal region as the water is warmer and more saline than in SIE. High chlorophyll-a concentrations (>0.5 mg m^{-3}) together with lower concentrations of nitrate (<25 mmol m^{-3}) were found in APF and in SIE for salinities less than 34.2 (Figs. 4B–D). The only exception to this rule is the chlorophyll-a maximum in WIE, where the concentration of chlorophyll-a is higher than 0.5 mg m^{-3} for higher salinity (>34.4) and higher concentration of nitrate (>29 mmol m^{-3}).

4.4. Data used in the modelling analysis

The illustrated SWEDARP 97/98 measurements describe three different areas of the Antarctic Ocean where the vertical profiles of salinity, nitrate and chlorophyll-a are different shapes (Figs. 2 and 3) and the co-variance between parameters are of different characters (Fig. 4). These observed differences can certainly be a consequence of the present light regime, differences in the organism communities or differences in the primary set of chemical parameters, but it can also be due to the mixing processes. Model calculations of fluxes of salts provide possible explanations of measured concentrations of vertical variations and the total amounts in the upper 200 m water layer regarding nitrate and chlorophyll-a. Data used for modelling analysis are summarised in Table 2.

4.5. Assessment of vertical mixing

The mixing process is parameterised by an eddy diffusivity (K_z), assessed from the mean salinity (S) profiles in Fig. 2. Running the model with the same depth constant mixing as in Larsson and Svansson (1992) for the Weddell Sea the SIE stations show fairly good agreement between computed and measured values. However, in WIE and especially in APF, the agreements with observations are less satisfactory. Instead, a depth variable mixing coefficient results in considerable improvements. Three layers are constructed to represent the various mixing coefficients: (1) a surface layer with the constant coefficient NYS, (2) a bottom layer with the constant coefficient NYD and (3) a layer in between (1) and (2) with a linear change from NYS at the top to NYD at its bottom. Assuming that the salt flux (SF) is constant from surface to 200 m depth, (expressed as $SF = K_z(dS/dz)$), $K_z = SF(\text{delta } z/\text{delta } S)$ are determined at a couple of depths. Several combinations of NYS and NYD are tested with different losses (L) until the total amount of chlorophyll-a (SUMA) and the best vertical profile of chlorophyll-a (A) are reproduced. Validation of the mixing coefficient is judged from SUMA and the minimum of the root mean square of A.

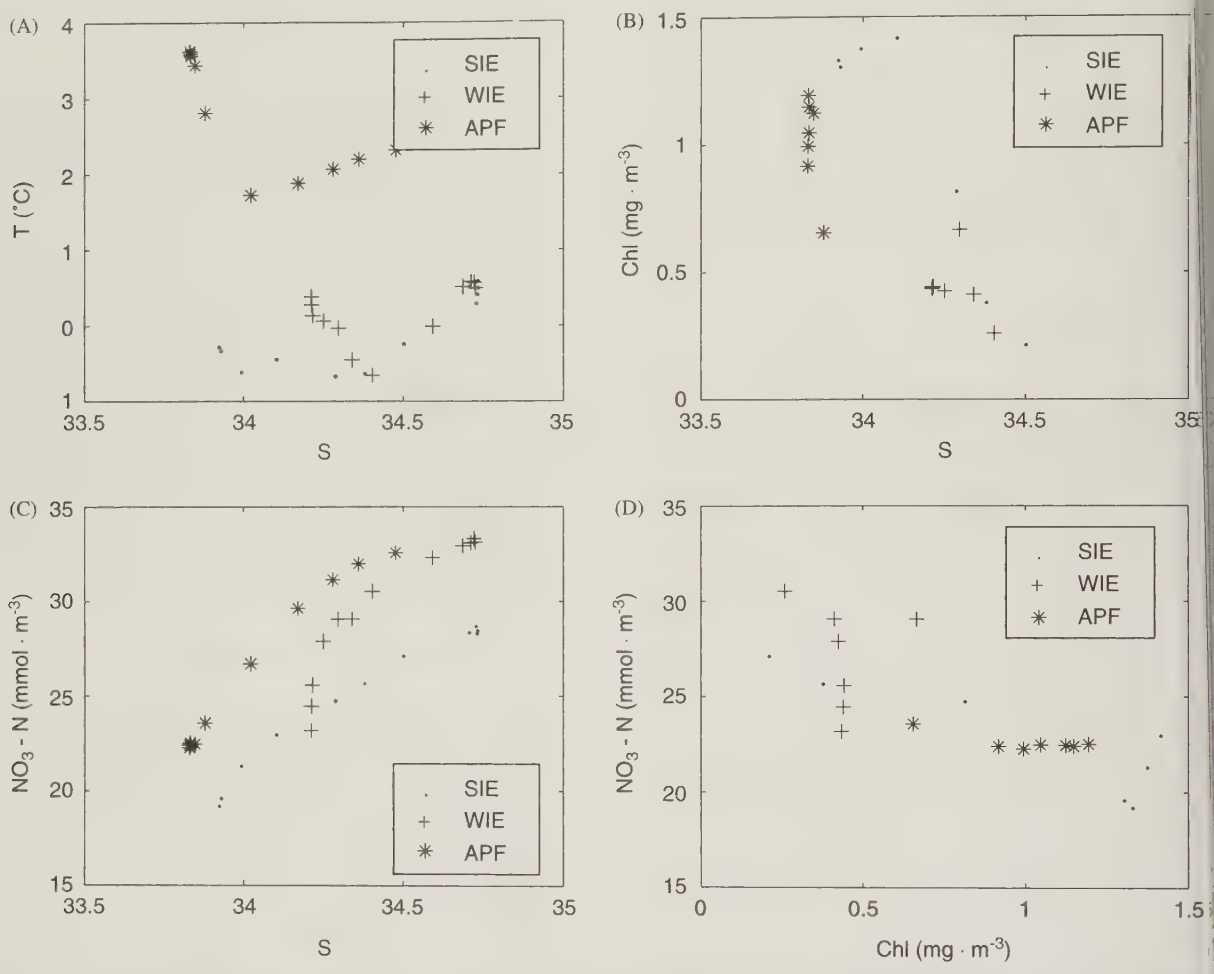

Fig. 4. The relationships between some of the observed parameters in the SWEDARP section along 6°E from 61°S to 51°S in austral summer 1997/98. Mean values for stations with measurements of nutrients are used. The diagrams include 0–400 m according to salinity and nitrate and 0–100 m according to chlorophyll-a: (A) Temperature versus salinity; (B) Chlorophyll-a versus salinity; (C) Nitrate versus salinity; (D) Nitrate versus chlorophyll-a.

To describe the standard procedure for this salinity curve method more clearly, the assessment of vertical mixing in APF is exemplified. At first (delta z/delta S) is computed from salinity measurements at $z = 15, 25, 30, 40, 62.5, 87.5, 125$ and 175 m depth. Then K_z is computed as a function of SF for every depth. These fix NYS for 0–50 m to 10 000SF and NYD to 400SF. The depth of the well mixed surface layer is estimated to 50 m and the upper depth of NYD to 80 m. Between 50 and 80 m an equation expressing a linear change from NYS to NYD is used. From these three depth intervals a mean K_z for APF is computed. Different runs of mean K_z are performed by adjusting L until SUMA = 137 mg m^{-3}. The computed vertical profile of chlorophyll-a is compared to measured values (Fig. 3) by determination of the root mean square of A. The smallest root mean square results in a mean K_z of 5300 m^2 day^{-1}, which corresponds to NYS = 15 000 m^2 day^{-1} and NYD = 600 m^2 day^{-1} (Table 3).

Table 2
Observed data used for model analyses in this paper

Parameter	SIE (60°S, 06°E)	WIE (56°S, 06°E)	APF (51°S, 06°E)
A (2 m) mg chl m^{-3}	1.33	0.43	0.99
A (100 m) mg chl m^{-3}	0.21	0.26	0.65
A (200 m) mg chl m^{-3}	0	0	0
SUMA mg chl m^{-2}	95.9	58.8	136.7
R (2 m) mmol NO_3–N m^{-3}	17.8	23.4	21.6
R (200 m) mmol NO_3–N m^{-3}	26.3	28.6	28.5
SUMR mmol NO_3–N m^{-2}	4533	5214	4794

Mean values from observations in the three study areas are calculated at 2 and 200 m depth for nitrate (R) and at 2 and 100 m depth for chlorophyll-a (A). SUMA and SUMR are vertical integrations from surface to 200 m depth. SUMA includes an extrapolation of chlorophyll-a from the measured concentration at 100 m to $A = 0$ at 200 m. The boundary conditions at the surface are $K_z\,(\partial A/\partial z) = 0$ and $K_z\,(\partial R/\partial z) = 0$. The measured value of R at 200 m and $A = 0$ are the boundary conditions of the lower border. The integrations continue for 70 days in SIE, 80 days in WIE and 90 days in APF.

Table 3
Results from model calculations based on the observed SWEDARP data which are summarised in Table 2

Parameter	SIE (60°S, 06°E)	WIE (56°S, 06°E)	APF (51°S, 06°E)
K_z (surface) $m^2\,day^{-1}$	2000	9000	15 000
K_z (deep) $m^2\,day^{-1}$	375	450	600
C/A, carbon:chlorophyll	75	80	150
L day^{-1}	0.25	0.30	0.15

The model calculated ratio between carbon and chlorophyll (C/A) and the specific loss rate of chlorophyll-a (L) are depth constant, while the mixing coefficient (K_z) varies with depth.

4.6. Loss rate, total chlorophyll-a and vertical mixing

In order to examine the effect of variations in vertical mixing on the total chlorophyll-a content in the surface layer (SUMA) at different specific loss rates (L) the model is run with APF as the initial point (Fig. 5). The maximum amount of SUMA is achieved only at moderate vertical mixing. At higher mixing rates SUMA decreases due to light limitation when the phytoplankton community is transported downwards by the vertical mixing to depths beneath the euphotic zone, where the cells cannot grow. In Antarctic waters macro nutrients do not usually have a limiting influence on primary production. To test the relevance of this, a nutrient limitation is inserted for nitrate concentrations (R) less than 8 mmol NO_3–N m^{-3}. The specific algal gross primary production (p) is thus substituted by $0.125Rp$. The result is that a nutrient limitation

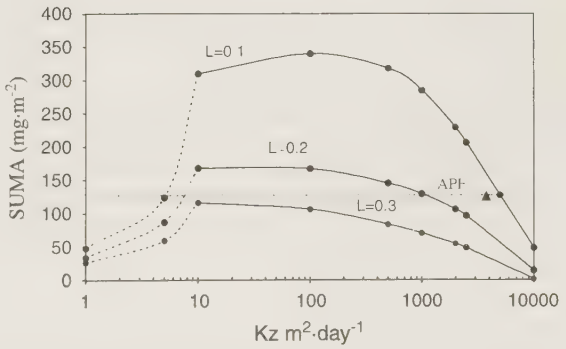

Fig. 5. Model calculations of total chlorophyll-a from surface to 200 m depth (SUMA) as a function of eddy diffusion coefficient (K_z) for three different specific loss rates (L). K_z is constant from surface downwards. Notice the logarithmic scale for K_z. Full drawn lines represent no nutrient limitation whereas dashed lines correspond to nutrient limitation. For larger K_z the curves coincide. The corresponding model computation for SWEDARP measurements in APF is marked with σ. Other possible combinations of K_z and L for APF with SUMA = 137 mg m^{-3} can be seen along the horizontal dotted line.

is reached only for smaller K_z than those usually found in the Southern Ocean. Fig. 5 shows that the SWEDARP measurements in APF correspond well to a K_z value between 1000 and 5000 m^{-2} day^{-1}(depth constant) together with loss rates of 0.1 to 0.2 day^{-1}. In SIE and in WIE the SUMAs are lower. Together with lower values of K_z this result in higher L (about 0.3 day^{-1}) in these two areas compared to APF. Measurements of macro-, meso- and microzooplankton grazing during the expedition, reported in Pakhomov and Froneman (2004) and in Froneman (2004), result in higher grazing impact of the primary production in WIE (about 70%) compared to APF (about 35%). In SIE, however, the measured grazing impact is only about 10%.

4.7. Sinking velocity, total chlorophyll-a and vertical mixing

The total amount of chlorophyll-a in the surface layer (SUMA) will of course increase with decreasing sinking velocity of chlorophyll-a (w_s). Fig. 6A and B show that this decrease is not linear and not valid for smaller K_z than 10 m^2 day^{-1}.

To decide an appropriate value for w_s, within the supposed range of 0–5 m day^{-1}, different characteristics for the mixing are tested in the model, both a depth constant K_z (Fig. 6A) and a depth variable K_z (Fig. 6B). For less depth constant mixing than 10 m^2 day^{-1} different sinking velocity is a matter of vital importance for SUMA if the system is not limited by the supply of nutrients. For situations with more mixing than 50 m^2 day^{-1} the increase of SUMA for different sinking velocities between 0 and 2 m day^{-1} is insignificant. From these curves $w_s = 1$ m day^{-1} is chosen for all further computations.

4.8. Model calculations compared with observations

In order to find the best reproduction of the measured values presented here, several attempts at running the model with different combinations of parameters for the three study areas were performed. Proceeding with APF as an example of how the calculations are carried out, now the best combination of K_z (mean = 5300 m^2 day^{-1})

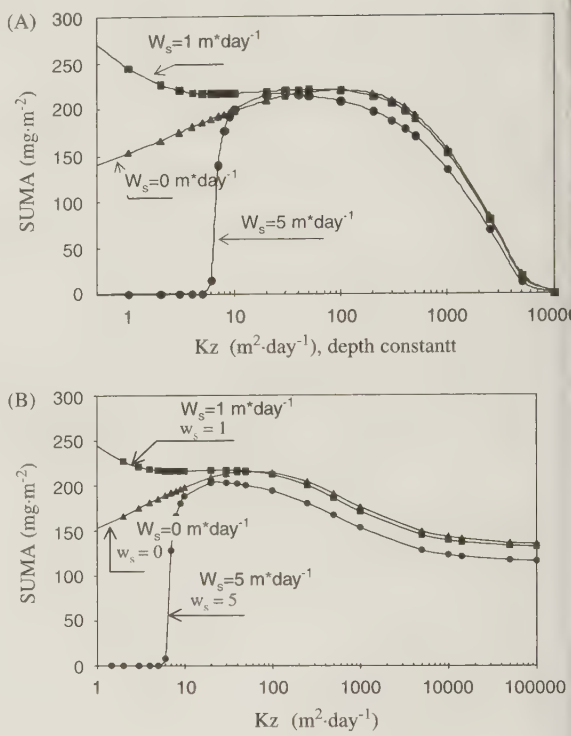

Fig. 6. Model calculations of the total amount of chlorophyll-a in the surface layer, 0–200 m (SUMA), as a function of eddy diffusion coefficient (K_z) for different chlorophyll-a sinking velocities (w_s). Notice the logarithmic scale for K_z. (A) K_z is depth constant from surface downwards, $w_s = 0$, 1, 5 m day^{-1}. (B) K_z is depth variable. In the surface water (0–50 m) K_z is variable from 5 to 100 000 m^2 day^{-1}. Then rapidly changing in the depth interval 50 to 80 m to a constant value in deeper water ($K_z = 568$ m^2 day^{-1}). The numbers on the x-axis denote K_z in the surface layer, $w_s = 0$, 1, 5 m day^{-1}.

and L (0.15 day^{-1}) are used to fix the ratio between carbon and chlorophyll (C/A). This is computed by tuning the total amount of nitrate (SUMR) to its measured value (4794 mmol NO_3–N m^{-2}). The computed vertical variation of nitrate (R) is compared to the measurements (Fig. 3) and the root mean square of R is computed as well. The computations result in C/A = 152 as the best choice.

The model-computed curves in Fig. 7A and B illustrate how the shape of the chlorophyll-a and nitrate vertical distributions shift with different eddy diffusion coefficients (K_z). To preserve a measurable subsurface maximum of chlorophyll-a,

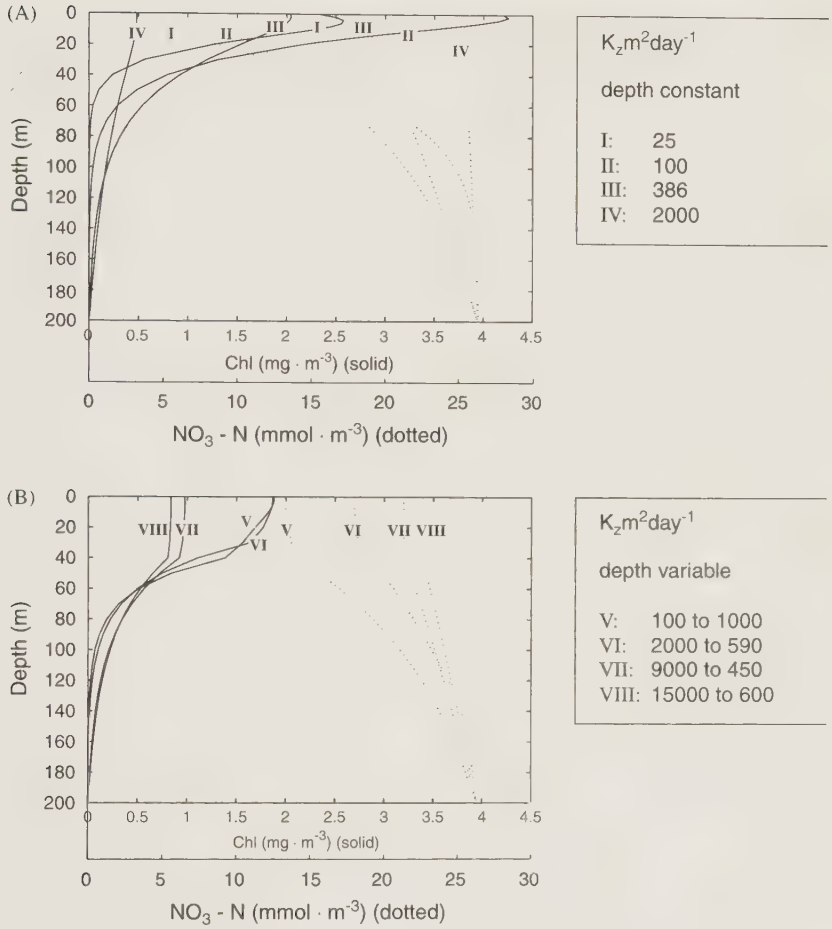

Fig. 7. Model computations of depth distributions for chlorophyll-a (solid lines) and nitrate (dotted lines) for different extent of mixing represented by the eddy diffusion coefficient (K_z) with SIE as the initial point. (A) K_z is depth constant from surface to 200 m depth. Lines denoted I for $K_z = 25$, II for $K_z = 100$, III for $K_z = 386$ and IV for $K_z = 2000\,m^2\,day^{-1}$. (B) K_z is depth variable. In the surface water (0–50 m) K_z ranges from 1000 to 15 000 $m^2\,day^{-1}$. Then rapidly changing in the depth interval 50 to 80 m to a lower value ($K_z = 100$–$600\,m^2\,day^{-1}$) down to 200 m depth. Lines denoted V for K_z (surface) = 1000 and K_z (deep) = 100, VI for K_z (surface) = 2000 and K_z (deep) = 590, VII for K_z (surface) = 9000 and K_z (deep) = 450 and VIII for K_z (surface) = 15 000 and K_z (deep) = $600\,m^2\,day^{-1}$.

K_z has to be small (Fig. 7A). In addition, an accumulation of chlorophyll-a in the surface and a depletion of macro nutrients are possible only for small K_z. Four different cases in Fig. 7B with increased depth variable mixings from 1000 to 15 000 $m^2\,day^{-1}$ in the surface and from 100 to 600 $m^2\,day^{-1}$ below 50–80 m depth result in increased amounts of nitrate in the entire water column together with less chlorophyll-a. To reproduce the vertical profiles of concentrations of chlorophyll-a and nitrate, which were measured during this expedition (Fig. 3), the vertical eddy diffusion has to be large.

Regarding the whole study area the model calculations show that the vertical mixing (K_z) is variable with depth, between 2000 and 15 000 $m^2\,day^{-1}$ in the surface layer and 375–600 $m^2\,day^{-1}$ in deeper layers (80–200 m). In between these two layers K_z decreases rapidly. The specific loss rates range from 0.14 to 0.32 day^{-1}

together with a sinking velocity of $1\,m\,day^{-1}$. The assessed ratio between carbon and chlorophyll varies between 76 and 152. Figs. 8A–C together with Table 3 show the results of the optimal combination of model settings in every different study area compared with the SWEDARP 97/98 observations. In APF the vertical eddy diffusion coefficient of $15\,000\,m^2\,day^{-1}$ in the surface and $600\,m^2\,day^{-1}$ below 80 m depth corresponds well to the measured values regarding both SUMA = $137\,mg\,m^{-2}$ and the details of $A(z)$. For SIE and especially for WIE it is much more difficult to find good agreements between the model calculations and the measurements. As mentioned before, a rather good agreement for SIE is found with a depth constant K_z. Nevertheless when a depth variable K_z is tested the result is better but still not perfect. To improve the model result for SIE for example, different values of losses were tested. Hereby it turns out, that a lower L needs a higher K_z to supply good agreements with the total amount of nitrate. This higher K_z also results in less agreement between modelling and observation of vertical profiles. An extremely low L in SIE, which would match the measured low density of zooplankton and the low grazing impact, is impossible to reproduce in the model. To reproduce the measured decrease of chlorophyll-a in the surface layer (0–50 m) in WIE the surface mixing is changed in the model within a realistic range on behalf of the salinity variations. The effects of these changes are small, for example an increase of 20% in K_z results in a marginal decrease of chlorophyll-a (1.4%).

5. Discussion and conclusions

The distribution of chemical species in the seawater is largely generated by the interaction between mixing cycles and biological cycles. In order to understand and explain the measured data during the SWEDARP expedition in austr summer 1997–1998 in the eastern Atlantic sect of the Antarctic Ocean an ecological model wa used. This model (Svansson, 1991) is especiall designed, without too many details, to be used fo a first-order study of the interaction between th physical, chemical and biological processes in volved. Results of ecosystem modelling can neve tell the whole truth, but working with the mode can provide a hint of the relative importance o some of the processes that build the system. Th model may also help to constrain ranges o different parameters and fluxes involved. Further more, it can be used to test postulated dynamics o the system, to predict possible effects of environ mental changes or to focus on fruitful future research. Of course there are a lot of aspects, some discussed below, which may be different from those stated in this paper and thus change the results. In spite of this, the model calculations clearly show that the total amount of chlorophyll-a in the upper layer is highly sensitive to the rate of vertical mixing.

In this work vertical mixing is not measured or absolutely calculated but estimated from the salinity fluxes. In the deeper layer the mean vertical diffusion coefficient (K_z) is $475\,m^2\,day^{-1}$, which is about the same as the vertical mixing, constant from surface to 200 m, used by Larsson and Svansson (1992) in the Weddell Sea. Now the magnitude of K_z in the upper layer is ten-folds and varies between 2000 and $15\,000\,m^2\,day^{-1}$. These are high numbers, but one should bear in mind that the vertical mixing coefficient in a completely homogenous water layer is very large ("infinite"). It has been demonstrated that a depth variable mixing gives the system different characteristics compared to the system with depth constant mixing (Figs. 6 and 7). For example, an extremely intense shallow surface mixing in Fig. 7B keeps the plankton biomass within the euphotic zone (Fig. 3) and does not result in a decreased amount of the

Fig. 8. Model results (dotted lines) for vertical variations of chlorophyll-a (chl) and nitrate (NO_3–N) compared to the SWEDARP measurements (solid lines) along 6 E in the three areas of observations. The total amount of chlorophyll-a from 0 to 200 m (SUMA) is given for every area. The values for K_z, L and C/A are reported in Table 3. (A) Marginal Ice Zone, at about 60 S (SIE). SUMA = $96\,mg\,m^{-2}$; (B) Inter Frontal Region, at about 56 S (WIE). SUMA = $59\,mg\,m^{-2}$; (C) Antarctic Polar Front, at about 51 S (APF). SUMA = $137\,mg\,m^{-2}$.

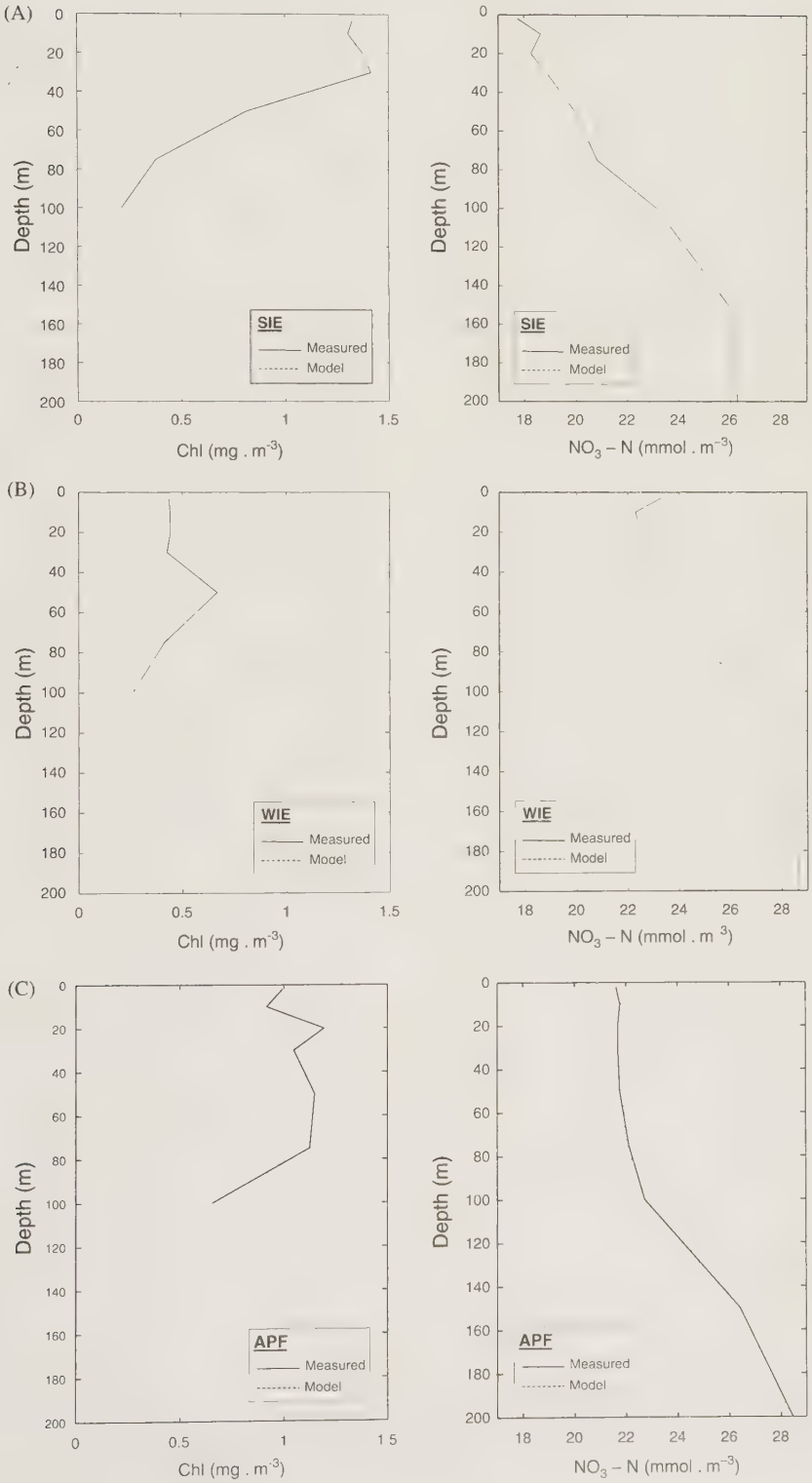
(A)
Depth (m)
Chl (mg . m-3)
SIE
Measured
Model
NO3 – N (mmol . m-3)
(B)
WIE
(C)
APF

total chlorophyll-a as in Fig. 7A with a depth constant mixing. A picture with high vertical shear in the surface water is supported by measurements with a SCANFISH, an undulating vehicle equipped with CTD and sensors for measurements of currents (ADCP), chlorophyll-a and light. The measurements, especially in WIE, show an area filled with dynamic eddy activities and local high chlorophyll-a content. Modelling of the physics in this work is obviously much simpler than the behaviour of the real ocean in this region with its hydrodynamic complexibility. For example, the salinity curve method assumes that the SFs are constant from surface to 200 m depth and horizontal fluxes are not included. This is, of course, a very great simplification, but apparently a rather useful one.

The formula used by Steele (1962) for gross algal primary production probably supplies a possible first approximation rather than an exact value. By using this formula both the hours of daylight and the number of days for the model calculations of primary production may be overestimated, as the mean values for every area are used for the whole period of integration. Model calculations show, however, that shifting from 19 to 17 h of daylight is of marginal importance. Also, changes in the number of days for integration from 90 to 70 lead to minor effects in the results. The conclusion is that the quanta irradiance and the time to develop the maximum functioning of the system are good enough and do not inhibit the system during this period of the year.

In WIE the measured vertical variations of chlorophyll-a concentrations show a subsurface maximum at 50 m depth (Fig. 8B). This is not possible to reproduce in the model and could therefore be an effect of some other factor not included in this model. In WIE the means used in the model calculations are based merely on two stations, which could imply that this subsurface maximum is not valid for the whole area. As the two stations are separated in time as well as in space and still show the same shape, the means are supposed to be valid for all the WIE-stations. Less-marked subsurface maximum concentrations of chlorophyll-a at 20–40 m depth are also observed in SIE and APF (Fig. 3C), but are not reproduced during the model calculations. Thes observations indicate that another reason for th divergent result between model calculations an measurements of subsurface maximum of chlo ophyll-a could be that the formula given b Steele does not satisfactorily supply detail of the primary production, as mentioned above Changing the bolded factor "2" in the equatio for p can force the subsurface maximum to b more or less pronounced ($p = 2 \times 0.82(0.08h)I(z)$ $I_0 \exp(1 - 2I(z)/I_0)$). Another possibility to repro duce the observed chlorophyll maxima could be t include additional processes such as micronutrien limitation or horizontal transports.

The model-computed ratios between carbon and chlorophyll (C/A) supply interesting results in this work. The variations of C/A in the oceans are complicated as C/A varies with the nutrient condition and during the season. In addition, the variations of C/A can be considerable depending on the quality of the phytoplankton community. For example a pelagic community has a different value from an ice-edge flora. In Sakshaug and Holm-Hansen (1986) C/A for Antarctic waters range between 50 and 250 with minimum values during light regimes yielding growth rates near maximum. In this work C/A is assessed from the total amount of chlorophyll-a, the vertical mixing and the losses together with the concentration of nitrate. C/A thus varies from one area to another from 76 to 152 (Table 3). The chlorophyll-a concentration in this present study is determined by HPLC quantification, which measures the amount of chlorophyll-a in living cells. This concentration is usually lower than traditional analysis including filtering and extraction followed by a photometry reading. The divergence of the two methods is variable depending on the condition of the plankton community.

A closer look at Table 3 reveals a clear difference between SIE and WIE on the one hand and APF on the other. The first two areas have about the same ratio between carbon and chlorophyll (C/A) and about the same calculated specific loss rates (L). The lower vertical integrated amount of chlorophyll-a (SUMA) in WIE combined with a higher mixing is a nice confirmation of the "Mixing hypothesis" preferential in this

paper. The model calculations of APF, however, suggest of a divergence from this hypothesis. To solve the problem of combining the high SUMA in APF with the large mixing, it is necessary to decrease L rather drastically. This reduced L can be justified by its annual variation, shifting from a minimum of 0.1 to a maximum of 0.7 day^{-1} when the zooplankton reach their highest density. The other variables follow, and e.g. a much larger C/A may be explained by annual variation.

Trying to understand the interaction between the physical, chemical and biological processes in these Antarctic subsystems we find that both the specific loss rate (L) and the vertical mixing coefficient (K_z) are very strong parameters which control the results. More vertical mixing will supply more inorganic nutrients to the euphotic zone, but will also yield less chlorophyll-a during the summer as more mixing results in less primary production. By this, L will, of course, also be changed. In addition, increased vertical mixing results in increased transport of total inorganic carbon from the sea to the air when less carbon is fixed by the primary production. As the vertical mixing varies considerably during a year, this will induce variations in the air-sea fluxes of gases. Fig. 5 shows that several combinations of L and K_z are possible in this system, but only one of these combinations will provide the very best model reproduction of the vertical variation of chlorophyll-a and the best total amount of chlorophyll-a (SUMA) for every special area. In SIE and WIE the calculated losses are close to 0.3 day^{-1}, while they are half the magnitude in APF where the total amount of chlorophyll-a is highest (Table 2). Trials with different combinations of L and K_z in the model calculations indicate that SIE had a higher primary production before the time of our observations than the measured values in APF, due to less mixing in SIE. The combination of a low L and a high SUMA is due to time variations of L with a maximum value after the phytoplankton spring bloom as reported in Larsson and Svansson (1992), where also K_z varies during the year. Variations of L and K_z during the year are not included in the present work though time variations are supposed to explain some of the divergences between measured and computed values of concentration gradients and grazing impact. However, time is indirectly involved when L changes from 0.3 in SIE and WIE to 1.5 in APF.

After a great deal of model calculations, including different combinations of parameters within natural variations, this work concludes that vertical mixing is an important limiting factor for the total amount of chlorophyll-a on shorter time scales in this system. Macro-nutrient limitation is possible only at considerably less mixing than usually found in the Antarctic Ocean. In addition, fluxes of salts and related gases are very closely connected to vertical mixing. Changes in vertical mixing, for example as an effect of climate changes, will induce effects on the functioning of the ecosystem. Future oceanographic work in this area should concentrate on research into losses of chlorophyll in the surface layer and on increasing our knowledge about vertical mixing.

Acknowledgements

I am most grateful to Artur Svansson for his support with model work, his time for discussions and help with improving the manuscript. I also thank all the participants of this expedition and the crew onboard the SA Agulhas for their work at sea. Special thanks go to my colleagues in the CTD group Per-Ingvar Sehlstedt, Ole Anders Nøst, Leif Djurfeldt, Elisabeth Engum and Chris Rohleder, to Angela Wulff who carried out the chlorophyll analysis and supplied the data, to Roland David who together with Rochelle Barath ran the autoanalyzer for determinations of nitrate, to Evgeny Pakhomov and William Froneman for their work with zooplankton and to Kai Rasmus for his optical measurements. Pontus Larsson is thanked for the computer drawing of the pictures. A. Taylor and an anonymous reviewer who improved the manuscript, are also acknowledged. This research was made possible by the work of the organisers at the Swedish Polar Research Secretariat and by our chief scientist David Turner. This part of the project was sponsored by grants from the Swedish Polar Research Secretariat, The Marine Research Centre in Göteborg, Sweden and from the Centre of Geosciences, Göteborg University, Sweden.

References

Aksnes, L., Lie, U., 1990. A coupled physical–biological pelagic model of a shallow sill fjord. Estuarine, Coastal and Shelf Science 31, 459–486.

Bathmann, U.V., Scharek, R., Klaas, C., Dubischar, C.D., Smetacek, V., 1997. Spring development of phytoplankton biomass and composition in major water masses of the Atlantic sector of the Southern Ocean. Deep-Sea Research II 44 (1–2), 51–67.

Bouqugneau, J.-M., Gieskes, W., Kraay, G., Larsson, A.-M., 1991. Influence of physical and biological processes on the concentration of O_2 and CO_2 in the ice-covered Weddell Sea in spring 1988. Polar Biology 12, 163-170.

Broström, G., 1997. Interaction between mixed layer dynamics, gas exchange and biological production in the oceanic surface layer with application to the northern North Atlantic. Ph.D. Thesis, Göteborg University, Göteborg, Sweden. ISSN 1400-3813, unpublished.

Carmack, E.C., 1977. Water characteristics of the Southern Ocean south of the Polar Front. In: Angel, M.V. (Ed.), A Voyage of Discovery, Deep-Sea Research 24 (Suppl.), 15–41.

Carmack, E.C., Foster, T.D., 1977. Water masses and circulation in the Weddell Sea. In: Dunbar, M.J. (Ed.), Polar Oceans, Proceedings of Polar Oceans Conference, Montreal, May 1974, Arctic Institute of North America, pp. 151–165.

Cloern, J.E., 1991. Tidal stirring and phytoplankton bloom dynamics in an estuary. Journal of Marine Research 49, 203–221.

De Baar, H.J.W., Buma, A.G.J., Nolting, R.F., Cadée, G.C., Jacques, G., Tréguer, P.J., 1990. On iron limitation of the Southern Ocean: experimental observations in the Weddell and Scotia Seas. Marine Ecology Progress Series 65, 105–122.

De Baar, H.J.W., Van Leeuwe, M.A., Scharek, R., Goyens, L., Bakker, K.M.J., Fritsche, P., 1997. Nutrient anomalies in *Fragilariopsis kerguelensis* blooms, iron deficiency and the nitrate/phosphate ratio (A. C. Redfield) of the Antarctic Ocean. Deep-Sea Research II 44 (1–2), 229–260.

Fjeldstad, J.E., 1936. Results of tidal observations. The Norwegian North Polar Expedition with "Maud" 1918–25, Geofysisk Institutt, Bergen, Norway. Science Research 4(4), 88.

Froneman, P.W., 2004. Protozooplankton community structure and grazing impact in the eastern Atlantic sector of the Southern Ocean in austral summer 1998. Deep-Sea Research II, this issue [doi:10.1016/j.dsr2.2004.09.001].

Gran, H.H., 1931. On the conditions for the production of plankton in the sea. Rapports et Procès-verbaux des Réunions. Conseil international pour l'Explorations de la Mer 75, 37–46.

Kirk, J.T.O., 1983. Light and Photosynthesis in Aquatic Systems. Cambridge University Press, Cambridge, 401pp.

Klaas, C., 1997. Microprotozooplankton distribution and the potential grazing impact in the Antarctic Circumpol Current. Deep-Sea Research II 44 (1–2), 375–394.

Larsson, A.-M., Svansson, A., 1992. Fluxes of gases in an ic related ecosystem in the north-western Weddell Sea. Pola Biology 12, 183–188.

Lutjeharms, J.R.E., 1985. Location of frontal systems betwee Africa and Antarctica: some preliminary results. Deep-Se Research 32 (12), 1499–1509.

Pakhomov, E.A., Froneman, P.W., 2004. Zooplankton dy namics in the eastern Atlantic sector of the Southern Ocea during the austral summer 1997/1998. Part 2. Grazin impact. Deep-Sea Research II, this issue [doi:10.1016 j.dsr2.2000.11.002].

Rasmus, K.E., Granéli, W., Wängberg, S.-Å., 2004. Optica studies in the Southern Ocean. Deep-Sea Research II, thi issue [doi:10.1016/j.dsr2.2001.01.004].

Redfield, A.C., Ketchum, B.H., Richards, F.A., 1963. The influence of organisms on composition of seawater. In: Hill M.N. (Ed.), The Sea, vol. 2. Wiley, New York, pp. 26–77.

Riley, G.A., Stommel, H., Bumpus, D.F., 1949. Quantitative ecology of the plankton of the Western-North Atlantic. Bulletin of the Bingham Oceanographic Collection 12 (3), 1–169.

Sakshaug, E., Holm-Hansen, O., 1984. Factors governing pelagic production in polar oceans. In: Holm-Hansen, O., Bolis, L., Gilles, R. (Eds.), Marine Phytoplankton and Productivity. Springer, New York, pp. 1–18.

Sakshaug, E., Holm-Hansen, O., 1986. Photoadaptation in the Antarctic phytoplankton: variations in growth rate, chemical composition and P versus I curves. Journal of Plankton Research 8, 459–473.

Sakshaug, E., Slagstad, D., Holm-Hansen, O., 1991. Factors controlling the development of phytoplankton blooms in the Antarctic Ocean—a mathematical model. Marine Chemistry 35, 259–271.

Sarmiento, J.L., Slater, R.D., Fasham, M.J., Ducklow, H.W., Toggweiler, J.R., Evans, G.T., 1993. A seasonal three-dimensional ecosystem model of nitrogen cycling in the North Atlantic euphotic zone. Global Biogeochemical Cycles 7, 417-450.

Steele, J.H., 1962. Environmental control of photosynthesis in the sea. Limnology and Oceanography 7, 137-150.

Svansson, A., 1991. A simple primary production model for the NW Weddell Sea. Marine Chemistry 35, 347–354.

Svansson, A., 1992. The Antarctic Ocean Expedition 1988/89, EPOS-LEG 2 Cruise report: Optics. Report no. 17, ISSN 0280-6932, Oceanography, Göteborg University, Sweden.

Svansson, A., 1996. A diffusion model for the primary production of phytoplankton. Deep-Sea Research II 43 (1), 37–46.

Sverdrup, H.U., 1953. On conditions for vernal blooming of phytoplankton. Journal du Conseil International pour l'Explorations de la Mer 18, 287–295.

Taylor, A.H., Watson, A.J., Ainsworth, M., Robertson, J.E., Turner, D.R., 1991. A modelling investigation of the role of phytoplankton in the balance of carbon at the surface of the

North Atlantic. Global Biogeochemical Cycles 5 (2), 151–171.

Veth, C., Lancelot, C., Ober, S., 1992. On processes determining the vertical stability of surface waters in the marginal ice zone of the north-western Weddell Sea and their relationship with phytoplankton bloom development. Polar Biology 12, 237–243.

Veth, C., Peeken, I., Scharek, R., 1997. Physical anatomy of fronts and surface waters in the ACC near the 6°W meridian during austral spring 1992. Deep-Sea Research II 44, 23–49.

Wofsy, S.C., 1983. A simple model to predict extinction coefficients and phytoplankton biomass in eutrophic waters. Limnology and Oceanography 28, 1144–1155.

Wulff, A., Wängberg, S.-Å., 2004. Spatial and vertical distribution of phytoplankton pigments in the eastern Atlantic sector of the Southern Ocean. Deep-Sea Research II, this issue [doi:10.1016/j.dsr2.2001.01.002].

ELSEVIER

Deep-Sea Research II 51 (2004) 2827–2839

DEEP-SEA RESEARCH
PART II

www.elsevier.com/locate/dsr2

Diurnal variability in the oceanic carbon dioxide system and oxygen in the Southern Ocean surface water

Agneta Fransson*,[1], Melissa Chierici[1], Leif G. Anderson

Department of Chemistry, Analytical and Marine Chemistry, Göteborg University, SE-412 96 Göteborg, Sweden

Abstract

During the *SWEDARP* cruise to the Atlantic sector of the Southern Ocean 1997/1998 six 24-hour stations were occupied in the areas of the Spring Ice Edge (SIE1, SIE2 and SIE3), the Winter Ice Edge (WIE), and the Antarctic Polar Front (APF1 and APF2). Samples were taken at the surface (2 m) every second hour and analyzed for total dissolved inorganic carbon, total alkalinity, pH and dissolved oxygen. By the use of wind speed measurements, calculated fugacity of carbon dioxide, fCO_2, and oxygen concentrations in the surface water, sea–air fluxes of carbon dioxide (CO_2) and oxygen were calculated. These fluxes and the diurnal change in the chemical properties are discussed in relation to changes in biological activity. The fluctuations in wind speed showed a larger impact on the variability of the calculated fluxes than the fluctuations in surface water fCO_2 or oxygen saturation. The calculated fluxes and the variability also showed large differences depending on how the wind speed was used, instantaneously or averaged over 24 hours. The calculated sea–air CO_2 fluxes using instantaneous wind speed varied between -0.012 and $-0.11\,mmol\,m^{-2}\,h^{-1}$ in the SIE1, -0.0073 and $-0.30\,mmol\,m^{-2}\,h^{-1}$ in the WIE and -0.043 and $-1.65\,mmol\,m^{-2}\,h^{-1}$ in the APF2. The mean values of sea–air CO_2 fluxes were calculated to -0.046 ± 0.044, -0.10 ± 0.094 and $-0.52\pm0.64\,mmol\,m^{-2}\,h^{-1}$ for the SIE1, WIE and the APF2, respectively. The mean values of sea–air oxygen fluxes were calculated to 0.072 ± 0.073, -0.12 ± 0.54 and $1.4\pm1.3\,mmol\,m^{-2}\,h^{-1}$ for the corresponding regions.
© 2004 Elsevier Ltd. All rights reserved.

1. Introduction

Studies of variability of carbon dioxide (CO_2) in time, both in the atmosphere and in sea surface water have mostly been on a seasonal or annual time scale (e.g. Peng et al., 1987). However, Inoue and Sugimura (1988) investigated the diurnal variation of the partial pressure of CO_2, pCO_2 (or fugacity of CO_2, fCO_2), in the surface water of the Southern Ocean (45–65°S, 115–150°E), which they compared with surface water temperature. Poisson et al. (1993) studied the daily variations in fCO_2 over a 3-day period at 50–58°S, 62–85°E. Robertson et al. (1993) investigated the daily change in fCO_2 and oxygen in the surface waters

*Corresponding author.
E-mail address: agneta.fransson@nies.go.jp (A. Fransson).
[1]Present address: Climate Change Research Project, National Institute for Environmental Studies, 16-2 Onogawa, Tsukuba, Ibaraki 305-8506, Japan.

0967-0645/$ - see front matter © 2004 Elsevier Ltd. All rights reserved.
doi:10.1016/j.dsr2.2001.01.001

in the North Atlantic while Oudot and Andrié (1989) showed the daily changes in the surface waters fCO_2 of the tropical Atlantic Ocean. In recent works seasonal and daily variability in fCO_2 in the Sargasso Sea are described by Bates et al. (1998) and in coastal waters by Borges and Frankignoulle (1999).

Three factors can simultaneously alter fCO_2; temperature, biological activity and sea–air exchange of CO_2, all of which have a 24-hour variability. There are also factors such as advection, horizontal and vertical mixing of water masses that could change fCO_2, especially in frontal zone areas.

The frontal systems, the ice edge and the marginal ice zone in the Southern Ocean support elevated biological activity. In spring, when ice melts, the ice edge and the marginal ice zone are characterized by a shallow surface layer, which favors primary production (e.g. Smith and Nelson, 1985). De Baar et al. (1995) found that a correlation of enhanced biological activity and iron was shown in the Antarctic polar front. According to Coale et al. (1996), areas with iron-enriched water show increased phytoplankton production and a more pronounced daily variability in the chemical constituents. Steinberg et al. (1998) found in their iron experiment that the oceanic carbonate system was intensely influenced by the response of the photosynthesis to the light cycle and zooplankton grazing.

Global flux estimates of CO_2 are generally based on few data, often not representing the whole year in any given area. This is a well-known problem that is much discussed. On a short time scale, the 24-hour cycle also has effects on sea–air fluxes. In this work we show how much the calculated CO_2 and oxygen fluxes are dependent on the time of the day, in combination with wind speed and CO_2 and oxygen surface water concentrations. Here we also present the total variability in the chemical constituents of dissolved inorganic carbon, total alkalinity, pH in situ, fCO_2 and dissolved oxygen over a 24-hours period in three different areas.

2. Analytical methods and sampling

The investigation was performed in the Southern Ocean in January 1998 along 6°E during the Swedish–South African Expedition to the eastern Atlantic sector of the Southern Ocean. Six 24-hour stations (Table 1) were occupied in the areas of the Spring Ice Edge (SIE1, SIE2 and SIE3), the Winter Ice Edge (WIE) and the Antarctic Polar Front (APF1 and APF2). The WIE was positioned at 56°S, however, in December it had retreated to 60°S (i.e. SIE). In this study the SIE coincides with the Weddell Gyre. The position for the WIE coincides with a front at latitude 56°30′S and longitude 0°, called the Weddell Front, previously defined by Spiridonov et al. (1996). Veth et al. (1997) defined the area close to latitude 57°S and longitude 6°W as the ACC-Weddell Gyre Boundary, which is a front between the Weddell Gyre and the Southern Antarctic Circumpolar Current (ACC). The APF, found between 50°S and 52°S, was defined by the temperature limit of 2 °C in the surface water, and a temperature minimum at 400 m depth. These positions agree with the positions found in the Atlantic sector by Lutjeharms and Valentine (1984) and Belkin and Gordon (1996). Fig. 1 shows the three study areas, and detailed information about location and time for each station is given in Table 1.

Water samples were collected every second hour for the study of the oceanic carbon dioxide system and oxygen. At each station the sampling started and ended at around 8.00 a.m. Samples for the determination of total dissolved inorganic carbon (C_T), total alkalinity (A_T), dissolved oxygen (O_2) and pH were taken from a rosette with Niskin bottles in the upper surface (2 m). Salinity and temperature were measured by a Seabird CTD. Wind speed data was obtained from the ship's meteorological measurements.

Table 1
Positions and date for each 24-hour station

Station	Latitude	Longitude	Date
SIE 1	60°24′S	6°00′E	4–5 January
SIE 2	60°00′S	6°00′E	6–7 January
SIE 3	59°20′S	6°00′E	8–9 January
WIE	56°30′S	6°00′E	14–15 January
APF 1	51°00′S	6°00′E	27–28 January
APF 2	49°50′S	6°00′E	29–30 January

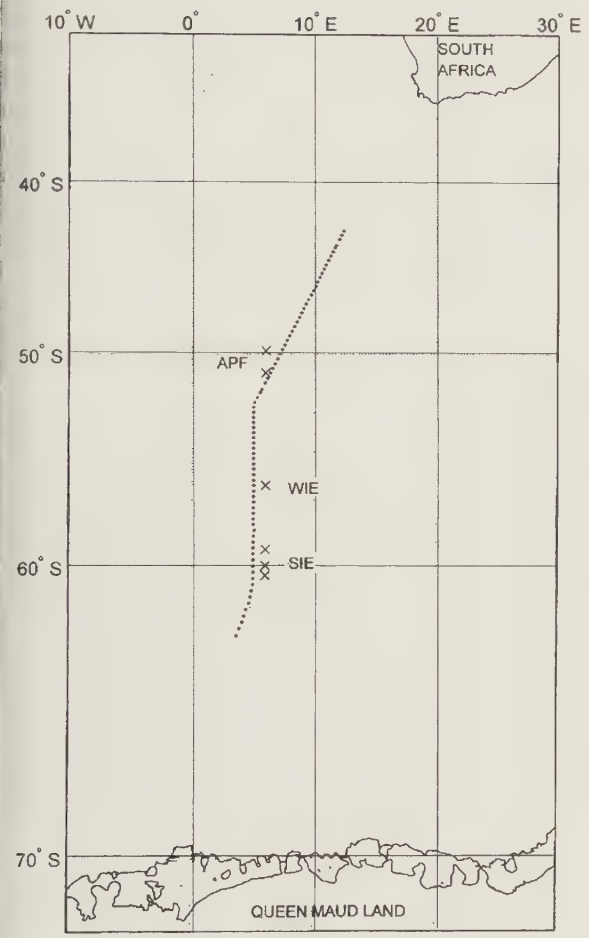

Fig. 1. Map of the Atlantic sector of the Southern Ocean with notations of the six 24-hours stations occupied in the SIE, WIE and the APF.

C_T and A_T samples were determined within an hour, pH within 30 min and oxygen after 3–5 h. The C_T was determined by gas extraction from acidified seawater samples followed by coulometric titration with photometric detection (Johnson et al., 1985, 1987). A_T was determined by potentiometric titration with 0.05 M HCl according to Haraldsson et al. (1997). The precision was $\pm 1\,\mu mol\,kg^{-1}$ for both C_T and A_T, and was obtained by replicate analysis of samples. The accuracy for C_T and A_T was controlled against a certified reference material supplied by Andrew Dickson (Scripps Institute of Oceanography, San Diego, USA) and the samples were corrected for the bias between measured and certified values. The correction was about $8\,\mu mol\,kg^{-1}$ for C_T and $12\,\mu mol\,kg^{-1}$ for A_T. The measurements of the certified reference material for both C_T and A_T varied with $\pm 6\,\mu mol\,kg^{-1}$ throughout the entire study. Oxygen measurements were performed by the use of an automated Winkler type titration with a photometric detection. The precision of oxygen measurements, where duplicate samples from the same depth, was estimated to $\pm 1.5\,\mu mol\,kg^{-1}$ (i.e. 0.3%). The uncertainty due to sampling from the Niskin bottles is thus included in this value. The accuracy of $1\,\mu mol\,kg^{-1}$ was determined by the variation in standardization of the sodium-thiosulphate during the study. The determination of pH was performed by the use of a diode-array spectrophotometer using a sulphonephtalein dye, *m*-cresol purple, as indicator (Clayton and Byrne, 1993; Lee and Millero, 1995), and measured in a 1 cm flowcell thermostated to 15 °C (pH_{15}). The precision and accuracy for the pH_{15} measurements were ± 0.0005 and ± 0.002 pH units, respectively. pH in situ was calculated from A_T, pH_{15} and in situ temperature by using the CO_2-system program by Lewis and Wallace (1998). For these calculations the carbon dioxide constants of Roy et al. (1993, 1994) were applied, and the pH was on the total hydrogen ion scale.

3. Calculations

3.1. CO_2 and oxygen fluxes

The calculated flux of CO_2 over the sea–air interface is a function of the difference in fugacity and wind speed (Eqs. (1)–(3)). Since no measurements of the fugacity of CO_2 (fCO_2) in the surface water were performed in this specific study, fCO_2^{sw} was calculated from A_T and pH_{15} using a CO_2-system program (Lewis and Wallace, 1998). The precision in the calculation of fCO_2 is approximately 2 μatm and the accuracy is about 5 μatm (Dickson and Riley, 1978). The difference between the calculated fCO_2 and that measured by an underway system (Chierici et al., 2004) was maximum 6 μatm, which is similar to the

uncertainty of the calculation of fCO_2. Internal consistency of the oceanic carbon dioxide system, accuracy and choice of parameters are discussed further in Chierici et al. (2004).

Our calculated surface water fCO_2 was compared with an atmospheric fCO_2 (fCO_2^{air}) of 363 µatm. This value was obtained from the observed atmospheric CO_2 content in mole fraction (in dry air) at the South Pole (Keeling and Whorf, 1999), recalculated to fugacity of CO_2 in wet air using surface water temperature, salinity, air pressure and humidity (Chierici et al., 2004).

The difference between fCO_2^{sw} and fCO_2^{air} is denoted ΔfCO_2 (µatm). The sea–air exchange of CO_2 is computed, according to the following equations:

$$\mathrm{Flux}_{CO_2} = K_0 k_{CO_2}(fCO_2^{sw} - fCO_2^{air}), \quad (1)$$

$$k_{CO_2} = 0.31u^2(Sc_x/660)^{-0.5}, \quad (2)$$

$$k_{CO_2} = 0.0283u^3(Sc_x/660)^{-0.5}, \quad (3)$$

where K_0 is the solubility of CO_2 at the in situ temperature, mol m^{-3} atm^{-1} (Weiss, 1974), k_{CO_2} is the piston velocity for CO_2, cm h^{-1}, u is the wind speed, m s^{-1}, Sc_x is the Schmidt number for either CO_2 or oxygen, defined from Wanninkhof (1992). The Schmidt number is obtained from $Sc = A - Bt + Ct^2 - Dt^3$ where t is the temperature in degrees Celsius. The alphabetic symbols correspond to $A = 2073.1$, $B = 125.62$, $C = 3.6276$ and $D = 0.043219$ for CO_2, and $A = 1953.4$, $B = 128$, $C = 3.9918$ and $D = 0.050091$ for oxygen (Wanninkhof, 1992). The number 660 is the Schmidt number for CO_2 at 20 °C (Wanninkhof, 1992). The wind speed was during our study measured every hour from the ship meteorological instrument, and for the flux calculations we have used two relationships, Eqs. (2) and (3), for comparison. In our calculations these equations are used for both hourly and daily average wind speed.

In order to calculate the oxygen flux, the piston velocity for oxygen, k_{CO_2} (cm h^{-1}) at in situ temperature, is calculated from that of CO_2 (Robertson et al., 1993) using the following expression:

$$k_{O_2} = k_{CO_2}(Sc_{O_2}/Sc_{CO_2})^{-0.5} \quad (4)$$

Eq. (4), together with Eqs. (2) and (3), is then used to calculate the oxygen flux according to the following expression:

$$\mathrm{Flux}_{O_2} = k_{O_2}(O_2^{meas} - O_2^{sat}), \quad (5)$$

where O_2^{meas}, µmol kg^{-1}, is the measured oxygen and O_2^{sat}, µmol kg^{-1}, is the oxygen saturation calculated from salinity and temperature.

4. Results

4.1. Regional characteristics

From the potential temperature–salinity ($\Theta - S$) plot in Fig. 2 we can see that the characteristics of SIE3 resemble the properties observed in the station occupied in the WIE more than those in SIE1 and SIE2. SIE3 is the northernmost SIE station and hence has water properties most similar to the water in the WIE, i.e. the Weddell Front, which is also confirmed in the chemical properties (Fig. 3). In Fig. 3 we can also see that the two APF stations have similar CO_2 and oxygen conditions. Since SIE3 is different from the other SIE stations and the two APF stations are similar, we choose SIE1, WIE and APF2 as representative for the three regions and thus also in the following calculations and discussions.

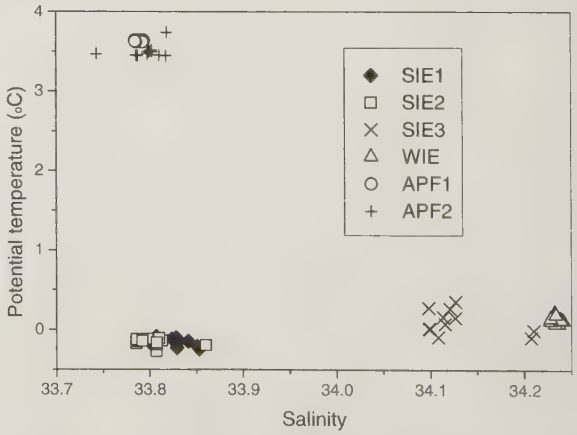

Fig. 2. $\Theta - S$ diagram of the surface water for the six stations occupied in the SIE, WIE and the APF.

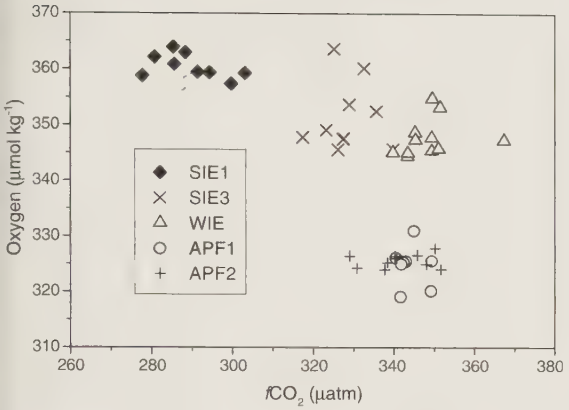

Fig. 3. fCO_2 versus oxygen for the stations occupied in the SIE, WIE and the APF. SIE2 is missing since no pH data were available for the fCO_2 calculation.

4.2. Diurnal variability in the chemical properties

CO_2 and oxygen are affected by temperature, sea–air exchange, mixing of water masses and biological processes. In all areas the light intensity increased rapidly from about 6 a.m., reached maximum at noon and decreased to low levels at around 8 p.m. (Fig. 4). These variable light conditions have the potential to influence the balance of photosynthesis and respiration (Steinberg et al., 1998). During photosynthesis the CO_2 is consumed and oxygen produced and during respiration vice versa. At the time of the investigation in January there was no ice in the areas, although, in the SIE the ice had only recently (in December) disappeared. The diurnal variability of A_T, C_T, fCO_2, pH in situ and oxygen in SIE1, WIE and APF2 is illustrated in Fig. 4.

4.3. Diurnal variability in the calculated fluxes

The wind speeds and calculated fluxes of CO_2 are shown in Table 2 and oxygen fluxes in Table 3. The wind speed varied with time and between areas, and the highest wind speeds were recorded at APF2. The following presentations of the instantaneous CO_2 and oxygen fluxes are calculated for every data point, based on Eq. (3).

4.3.1. Carbon dioxide

Variability in the calculated fluxes of CO_2 is seen in all areas. The calculated fluxes and the wind speed varied significantly at all times of the day, and the maximum fluxes were mostly observed at highest wind speed (Table 2). At all times of the day the ΔfCO_2 at SIE1 showed variability between -59 and $-84\,\mu atm$. This resulted in a general oceanic sink of CO_2 throughout the entire day, with maximum oceanic uptake of 0.11 $mmol\,m^{-2}\,h^{-1}$ and minimum uptake of 0.0063 $mmol\,m^{-2}\,h^{-1}$ using the flux formulation of Wanninkhof and McGillis (1999). Hence, the calculated fluxes varied by a factor of 17 between lowest and highest flux. In the WIE the ΔfCO_2 was -11 to $-22\,\mu atm$ throughout the entire day, which resulted in a maximum oceanic uptake of 0.30 $mmol\,m^{-2}\,h^{-1}$ and a minimum of 0.0073 $mmol\,m^{-2}\,h^{-1}$ (Table 2b), or a difference by a factor of about 30. APF2 was undersaturated at all times of the day and the ΔfCO_2 varied between -10 and $-33\,\mu atm$. The corresponding maximum computed uptake was 1.6 $mmol\,m^{-2}\,h^{-1}$ and the minimum 0.043 $mmol\,m^{-2}\,h^{-1}$ (Table 2c), a factor of about 40 between the highest and lowest. Mean values of the calculated hourly sea–air fluxes over a day in SIE1, WIE and APF2 are presented in Table 2, where the standard deviations reflect the variability throughout the 24 h. The corresponding daily mean values, simply multiplied by 24, are -1.1 ± 0.94, -2.6 ± 2.1 and -12 ± 14 mmol $m^{-2}\,d^{-1}$ for SIE1, WIE and APF2, respectively, based on Eqs. (1) and (3).

To investigate the influence of wind speed and ΔfCO_2 on the calculated CO_2 fluxes, the variability of the different fluxes throughout the day are compared. First, we average the different instantaneous wind speed for each area, and together with the calculated variable ΔfCO_2 new CO_2 fluxes can be calculated (Table 2) using Eq. (3). Then we use the average of the calculated ΔfCO_2 for each area together with instantaneous wind speed to calculate more CO_2 fluxes (Table 2). These newly calculated CO_2 fluxes with standard deviation (i.e. variability) are compared to the CO_2 fluxes, calculated with both instantaneous wind speed and variable ΔfCO_2. It is seen that constant wind speed gives significantly less variability, in absolute

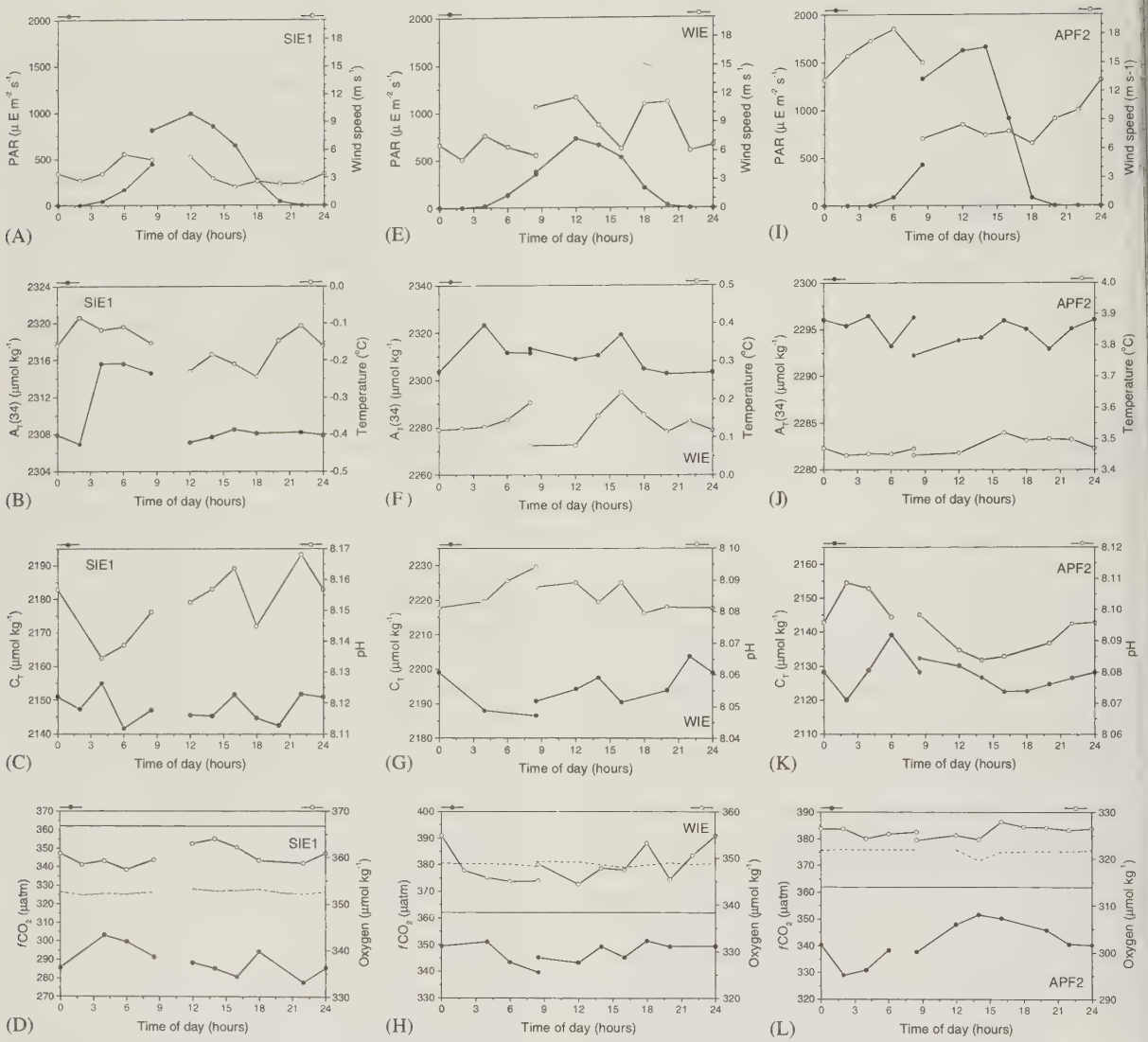

Fig. 4. The 24-hour variability of (A) light intensity (PAR) (Abrahamsson et al., 2004) (left axis, filled circles) and wind speed (right axis, open circles), (B) C_T (left axis, filled circles) and pH in situ (right axis, open circles) and (C) fCO_2 (left axis, filled circles) and oxygen (right axis, open circles), in the surface layer of SIE1. 4(D–F) are corresponding plots for the WIE, and (G–I), for APF2. The filled line is the atmospheric fCO_2 and the dotted line is the saturation degree of oxygen. Note that sampling both started and ended at 8 a.m.

numbers, in the calculated fluxes than using constant ΔfCO_2 in the calculations (Table 2). The calculated flux variability is larger in absolute numbers when the wind speed is higher, but the relative variability in wind speed is comparable to the relative variability in ΔfCO_2. The relative variability of the calculated CO_2 fluxes using constant wind speed and variable ΔfCO_2 is about 10–50% for all areas, which is smaller than the relative variability of the calculated CO_2 fluxes (80–110%) using variable wind speed and constant ΔfCO_2. Thus, the result from this study shows that the variability in wind speed affects the calculated CO_2 fluxes more than the variability in ΔfCO_2.

Table 2
Calculated CO_2 fluxes, using different equations and wind speeds

Time of day	ΔfCO_2 (μatm)	Wind speed ($m\,s^{-1}$)	CO_2 flux ($mmol\,m^{-2}\,h^{-1}$)[a]	CO_2 flux ($mmol\,m^{-2}\,h^{-1}$)[b]	CO_2 flux ($mmol\,m^{-2}\,h^{-1}$)	CO_2 flux ($mmol\,m^{-2}\,h^{-1}$)
(a) For SIE1						
08.30	n.d.	n.d.	n.d.	n.d.	n.d.[c]	n.d.[d]
10	n.d.	n.d.	n.d.	n.d.	n.d.[c]	n.d.[d]
12	−74	5.2	−0.23	−0.11	−0.021[c]	−0.11[d]
14	−77	2.9	−0.072	−0.019	−0.022[c]	−0.018[d]
16	−81	2.0	−0.035	−0.0063	−0.023[c]	−0.0056[d]
18	−68	2.6	−0.051	−0.012	−0.019[c]	−0.013[d]
20	n.d.	n.d.	n.d.	n.d.	n.d.[c]	n.d.[d]
22	−84	2.4	−0.054	−0.012	−0.024[c]	−0.0099[d]
24	−76	3.4	−0.10	−0.032	−0.021[c]	−0.031[d]
02	n.d.	n.d.	n.d.	n.d.	n.d.[c]	n.d.[d]
04	−59	3.4	−0.077	−0.024	−0.017[c]	−0.029[d]
06	−62	5.5	−0.21	−0.11	−0.018[c]	−0.12[d]
08.30	−71	4.9	−0.20	−0.089	−0.020[c]	−0.090[d]
Mean value	−72±8	3±1	−0.11±0.077	−0.046±0.044	−0.021±0.0023[c]	−0.047±0.046[d]
(b) For WIE						
08.30	−17	11	−0.21	−0.21	−0.089[e]	−0.18[f]
10	n.d.	n.d.	n.d.	n.d.	n.d.[e]	n.d.[f]
12	−19	12	−0.28	−0.30	−0.099[e]	−0.24[f]
14	−13	8.7	−0.11	−0.086	−0.067[e]	−0.10[f]
16	−17	6.2	−0.073	−0.042	−0.089[e]	−0.037[f]
18	−11	11	−0.14	−0.14	−0.056[e]	−0.20[f]
20	−13	11	−0.18	−0.18	−0.067[e]	−0.21[f]
22	n.d.	6.0	n.d.	n.d.	n.d.[e]	n.d.[f]
24	−13	6.6	−0.062	−0.038	−0.066[e]	−0.045[f]
02	n.d.	5.1	0.016	0.0073	0.028[e]	−0.021[f]
04	−11	7.6	−0.071	−0.049	−0.058[e]	−0.067[f]
06	−19	6.4	−0.087	−0.051	−0.099[e]	−0.041[f]
08.30	−22	5.5	−0.077	−0.039	−0.12[e]	−0.026[f]
Mean value	−15±3.8	8.0±2.4	−0.12±0.082	−0.10±0.094	−0.071±0.039[e]	−0.11±0.084[f]
(c) For APF2						
08.30	−24	7.0	−0.13	−0.086	−0.33[g]	−0.074[h]
10	n.d.	n.d.	n.d.	n.d.	n.d.[g]	n.d.[h]
12	−14	8.5	−0.11	−0.088	−0.19[g]	−0.13[h]
14	−10	7.4	−0.063	−0.043	−0.14[g]	−0.086[h]
16	−12	7.8	−0.079	−0.056	−0.16[g]	−0.10[h]
18	n.d.	6.5	−0.17	−0.10	−0.48[g]	−0.059[h]
20	−16	9.1	−0.15	−0.12	−0.22[g]	−0.16[h]
22	−21	10	−0.24	−0.22	−0.29[g]	−0.21[b]
24	−22	13	−0.42	−0.51	−0.29[g]	−0.49[h]
02	−33	16	−0.90	−1.3	−0.44[g]	−0.82[h]
04	−31	17	−1.0	−1.6	−0.42[g]	−1.1[h]
06	−24	18	−0.90	−1.5	−0.32[g]	−1.34[h]
08.30	n.d.	15	n.d.	n.d.	n.d.[g]	n.d.[h]
Mean value	−21±8	11±4	−0.38±0.38	−0.52±0.64	−0.30±0.11[g]	−0.42±0.46[h]

Negative values indicate fluxes to the ocean from the atmosphere. The fluxes are the momentary (hourly) fluxes. To obtain daily fluxes, 24 are multiplied to these values. n.d. indicates no data.

[a] CO_2 flux calculated from Eqs. (1) and (2) by Wanninkhof (1992), using instantaneous wind speed.
[b] CO_2 flux calculated from Eqs. (1) and (3) by Wanninkhof and McGillis (1999), using instantaneous wind speed.
[c] CO_2 flux calculated from Eqs. (1) and (3) by Wanninkhof and McGillis (1999), using daily average wind speed of $3\,m\,s^{-1}$.
[d] CO_2 flux calculated from Eqs. (1) and (3) by Wanninkhof and McGillis (1999), using daily average ΔfCO_2 of −72.
[e] CO_2 flux calculated from Eqs. (1) and (3) by Wanninkhof and McGillis (1999), using daily average wind speed of $8\,m\,s^{-1}$.
[f] CO_2 flux calculated from Eqs. (1) and (3) by Wanninkhof and McGillis (1999), using daily average ΔfCO_2 of −15.
[g] CO_2 flux calculated from Eqs. (1) and (3) by Wanninkhof and McGillis (1999), using daily average wind speed of $11\,m\,s^{-1}$.
[h] CO_2 flux calculated from Eqs. (1) and (3) by Wanninkhof and McGillis (1999), using daily average ΔfCO_2 of −21.

Table 3
Calculated oxygen fluxes, using different equations and wind speeds

Time of day	ΔO_2 ($\mu mol\,kg^{-1}$)	O_2^{sat} (%)	Wind speed ($m\,s^{-1}$)	$Flux_{O_2}$ ($mmol\,m^{-2}\,h^{-1}$)[a]	$Flux_{O_2}$ ($mmol\,m^{-2}\,h^{-1}$)[b]	$Flux_{O_2}$ ($mmol\,m^{-2}\,h^{-1}$)	$Flux_{O_2}$ ($mmol\,m^{-2}\,h^{-}$
(a) *for SIE1*							
08.30	n.d.	n.d.	n.d.	n.d.	n.d.	n.d.[c]	n.d.[d]
10	n.d.	n.d.	n.d.	n.d.	n.d.	n.d.[c]	n.d.[d]
12	9.8	103	5.2	0.48	0.23	0.043[c]	0.37[d]
14	11	103	2.9	0.17	0.044	0.049[c]	0.11[d]
16	9.2	103	2.0	0.063	0.011	0.041[c]	0.053[d]
18	6.2	102	2.6	0.073	0.017	0.027[c]	0.091[d]
20	n.d.	n.d.	n.d.	n.d.	n.d.	n.d.[c]	n.d.[d]
22	6.8	102	2.4	0.068	0.015	0.030[c]	0.077[d]
24	8.4	102	3.4	0.18	0.056	0.037[c]	0.16[d]
02	6.6	102	n.d.	0.088	0.022	0.029[c]	0.10[d]
04	7.1	102	3.4	0.15	0.046	0.032[c]	0.16[d]
06	5.3	102	5.5	0.28	0.14	0.024[c]	0.41[d]
08.30	7.0	102	4.9	0.31	0.14	0.031[c]	0.34[d]
Mean value	7.7±1.8	102±0.5	3±1	0.19±0.13	0.072±0.073	0.034±0.0079[c]	0.19±0.13[d]
(b) for WIE							
08.30	−0.51	100	11	−0.10	−0.10	−0.043[e]	0.15[f]
10	n.d.	n.d.	n.d.	n.d.	n.d.	n.d.[e]	n.d.[f]
12	−4.8	99	12	−1.2	−1.2	−0.41[e]	0.18[f]
14	−0.72	100	8.7	−0.099	−0.079	−0.061[e]	0.10[f]
16	−0.60	100	6.2	−0.042	−0.024	−0.051[e]	0.053[f]
18	4.7	101	11	1.0	1.0	0.40[e]	0.16[f]
20	−3.5	99	11	−0.79	−0.80	−0.30[e]	0.17[f]
22	1.9	101	6.0	0.13	0.070	0.16[e]	0.050[f]
24	5.9	102	6.6	0.47	0.28	0.50[e]	0.060[f]
02	−1.6	100	5.1	−0.074	−0.034	−0.13[e]	0.036[f]
04	−3.0	99	7.6	−0.31	−0.22	−0.26[e]	0.079[f]
06	−3.7	99	6.4	−0.28	−0.16	−0.31[e]	0.057[f]
08.30	−3.2	99	5.5	−0.17	−0.087	−0.27[e]	0.042[f]
Mean value	−0.76±3.4	100±1.0	8±2	−0.12±0.55	−0.12±0.54	−0.065±0.29[e]	−0.095±0.055[f]
(c) For APF2							
08.30	2.1	101	7.0	0.21	0.14	0.52[g]	0.42[h]
10	n.d.	n.d.	n.d.	n.d.	n.d.	n.d.[g]	n.d.[h]
12	3.2	101	8.5	0.46	0.36	0.77[g]	0.62[h]
14	4.5	101	7.4	0.50	0.34	1.1[g]	0.47[h]
16	6.6	102	7.8	0.80	0.57	1.6[g]	0.51[h]
18	5.2	102	6.5	0.45	0.27	1.3[g]	0.36[h]
20	5.1	102	9.1	0.85	0.70	1.2[g]	0.70[h]
22	4.6	101	10	0.93	0.84	1.1[g]	0.85[h]
24	4.6	101	13	1.6	2.0	1.1[g]	1.5[h]
02	4.4	101	16	2.2	3.2	1.1[g]	2.1[h]
04	2.4	101	17	1.4	2.3	0.59[g]	2.6[h]
06	3.4	101	18	2.3	3.9	0.83[g]	2.9[h]
08.30	3.8	101	15	1.7	2.4	0.93[g]	1.9[h]
Mean value	4.2±1.3	101±0.4	11±4	1.1±0.72	1.41±1.28	1.0±0.31[g]	1.2±0.92[h]

$\Delta O_2 = O_2^{meas} - O_2^{sat}$. Negative values indicate fluxes to the ocean from the atmosphere. The fluxes are the momentary (hourly) fluxes. To obtain daily fluxes, 24 are multiplied to these values. n.d. indicates no data.

[a]O_2 flux calculated from Eqs. (4), (5) and (2) by Wanninkhof (1992), using instantaneous wind speed.

[b]O_2 flux calculated from Eqs. (4), (5) and (3) by Wanninkhof and McGillis (1999), using instantaneous wind speed.

[c]O_2 flux calculated from Eqs. (4), (5) and (3) by Wanninkhof and McGillis (1999), using daily average wind speed of $3\,m\,s^{-1}$.

[d]O_2 flux calculated from Eqs. (4), (5) and (3) by Wanninkhof and McGillis (1999), using daily average oxygen saturation of $7.7\,\mu mol\,kg^{-1}$.

[e]O_2 flux calculated from Eqs. (4), (5) and (3) by Wanninkhof and McGillis (1999), using daily average wind speed of $8\,m\,s^{-1}$.

[f]O_2 flux calculated from Eqs. (4), (5) and (3) by Wanninkhof and McGillis (1999), using daily average oxygen saturation of $0.76\,\mu mol\,kg^{-1}$.

[g]O_2 flux calculated from Eqs. (4) and (3) by Wanninkhof and McGillis (1999), using daily average wind speed of $11\,m\,s^{-1}$.

[h]O_2 flux calculated from Eqs. (4) and (3) by Wanninkhof and McGillis (1999), using daily average oxygen saturation of $4.2\,\mu mol\,kg^{-1}$.

The effect of the wind speed and magnitude of ΔfCO_2 on the calculated fluxes is also seen when comparing the areas. Despite the three times larger mean undersaturation in SIE1 compared to APF2, the calculated mean flux is about ten times lower. This is caused by the four times higher average wind speed in APF2. As a result of wind speed, the maximum CO_2 uptake in APF2 is 15 times that in SIE1 and the minimum uptake 7 times larger.

4.3.2. Oxygen

The calculated oxygen fluxes also show variability throughout the day. In SIE1 the calculated oxygen flux, using Wanninkhof and McGillis (1999), was driven from the ocean to the atmosphere, and the most intense fluxes were observed in the morning, where also the highest wind speeds were recorded (Table 3a). The surface water in the WIE was mainly undersaturated in oxygen or close to saturation throughout the entire day, and the calculated fluxes showed varied direction, both towards the ocean and to the atmosphere (Table 3b). As for SIE1 the oxygen was supersaturated at APF2, and a release of oxygen to the atmosphere was calculated at all times of the day (Table 3c). The calculated fluxes varied by a factor of 20 between the highest and lowest in the SIE1, and in the APF2 by a factor of about 30. In the WIE the most intense calculated sea–air flux to the ocean is as large as the calculated sea–air flux to the atmosphere.

Investigations of the influence of wind speed and oxygen saturation on the calculated oxygen fluxes are performed, as for CO_2. The average wind speed for each area together with variable ΔO_2 (Table 3) is used to calculate the new oxygen fluxes using Eq. (3). Then we average the different ΔO_2 for each area, and calculate the oxygen fluxes together with instantaneous wind speed (Table 3). The calculated fluxes were lower in absolute numbers when constant (average) wind speed was applied in combination with variable ΔO_2, which is similar to the result for the calculated CO_2 fluxes.

The relative variability of the calculated oxygen fluxes using constant wind speed and variable ΔO_2 was about 20% and 30% in the SIE1 and APF2, respectively. In the WIE the relative variability was 450%. The relative variability of the calculated oxygen fluxes using variable wind speed and constant ΔO_2 was about 70%, 60% and 80% in the SIE1, WIE and APF2, respectively. However, the relative variability, using both variable wind speed and variable ΔO_2, in the three areas was almost 100% in the SIE1, 450% in the WIE and 90% in the APF2.

Although the ΔO_2 is twice as large in the SIE1 than in the APF2, the calculated mean oxygen flux in the SIE1 are 20 times smaller than in the APF2. This can be explained by the four times larger flux in the APF2 than in the SIE1. The statement valid for the CO_2 fluxes that wind speed has most effect on the calculated fluxes also holds for the calculated oxygen fluxes in the SIE1 and APF2, but not in the WIE. However, the difference between both fluxes and variability calculated using variable (instantaneous) wind speed combined with constant ΔO_2 or ΔfCO_2 and those calculated with both variable wind speed and variable ΔO_2 or ΔfCO_2, was larger for the oxygen fluxes than for the corresponding CO_2 fluxes. This implies that wind speed has a larger impact on the oxygen fluxes than on the CO_2 fluxes. This might be explained by that the surface water oxygen is closer to saturation than CO_2, and that the sea–air exchange of oxygen is faster than that of CO_2.

5. Discussion

5.1. Biogeochemical uncertainties

In the investigated areas the chemical constituents were expected to follow the diel cycle, which in turn follows the light intensity. The pattern of biological production during high light intensity and respiration during the night can be discerned in oxygen and fCO_2 at SIE1, and in C_T and pH in situ at WIE. In other parameters the signal of these biological processes is not clearly seen throughout the entire day, and an irregularity and ancillary distribution is observed in the data. In particular, at APF2, decreased C_T and fCO_2 were noticed in the night and increased fCO_2 in the afternoon. The reason for this opposite pattern could be due either to high zooplankton respiration (during daylight),

temperature change, sea–air flux of CO_2, change of water mass by advection or by horizontal or vertical water mass mixing. The measurements of zooplankton biomass and abundance were performed twice during each of the 24-hour studies (at 8.00 a.m), and the respiration and consequently the variability in total biomass and total abundance throughout the entire day cannot be investigated. The total biomass was higher in the APF2 than in the SIE1 and WIE, indicating that there might be a significant grazing pressure in the APF2. However, the total abundance was lower than in the WIE, where the highest value was found (Pakhomov and Froneman, 2004). In the SIE1 both total biomass and total abundance were relatively low, according to Pakhomov and Froneman (2004). These values only give an indication of the zooplankton activity in the different areas. The temperature variability throughout the entire day was maximum $\pm 0.08\,^{\circ}C$ in all areas. The temperature effect on C_T is calculated to $8\,\mu mol\,kg^{-1}\,^{\circ}C^{-1}$ (Lewis and Wallace, 1998) at constant partial pressure of CO_2, and thus corresponds to a maximum of $\pm 0.6\,\mu mol\,kg^{-1}$ in C_T. This effect is within the uncertainties of the analytical method, and therefore can be neglected. For fCO_2 the temperature effect is $13\,\mu atm\,^{\circ}C^{-1}$ (Takahashi et al., 1993), which corresponds to a change in fCO_2 by $\pm 1\,\mu atm$ during the 24-hour period. The effect of the oceanic CO_2 uptake on the change in C_T (during a short time scale) in the surface layer can be investigated assuming a homogeneous surface mixed layer. The mixed layer depth, MLD, is here defined as the depth where the density has increased by more than 0.01 sigma units above that of the surface mixed layer. They were found to reach down to 15 m in the SIE1, 25 m in the WIE and 80 m in the APF2. The averaged hourly fluxes for all areas are $-0.005 \pm 0.005\,mmol\,m^{-3}\,h^{-1}$ when the calculated momentary fluxes are divided by the MLD. The average increase or decrease in C_T per hour is $2–4\,mmol\,m^{-3}\,h^{-1}$ in all areas. These values show that the oceanic uptake of CO_2 in general would contribute less than 1% to the change in C_T. The calculated maximum flux, $0.02\,mmol\,m^{-3}\,h^{-1}$, is observed in the APF2 during the morning, giving a change in C_T of about 1%. Hence, the sea–air flux has a negligible effect on the change in C_T during our experiments.

The most likely uncertainty for the 24-hour study is the change of water mass, which can be due to either advection or horizontal or vertical water mass mixing. In addition, the research vessel was positioned at station, but especially in high wind speed and high current areas (such as APF2) the ship drifted relative to the surface water. Thus one explanation for the trends in concentrations which are not associated with biological processes can be an effect of change of water mass by advection or water mass mixing. Robertson et al. (1993) reported a difference of 0.03 in salinity that probably was an effect of horizontal or vertical mixing. However, they could not see any change in fCO_2 associated with a salinity change of 0.03. In our study the salinity change in the surface water was less than ± 0.03 in all areas throughout the entire day. The assumption that horizontal mixing is negligible is somewhat strengthened by this finding, though mixing of waters or advection might have influenced the surface water in some areas. In the Southern Ocean investigation by Inoue and Sugimura (1988) no clear diurnal variation was seen in fCO_2 (or pCO_2). They suggested that temperature, vertical mixing, upwelling and biological activity were responsible to the fluctuations in fCO_2. They also found that an increase of fCO_2 in the surface water was a result of air–sea exchange of CO_2 (Inoue and Sugimura, 1988), which was not the case in our study.

5.2. Uncertainties in the methods and calculations

The flux parameterization is one uncertainty that has been discussed extensively in the literature (e.g. Murphy et al., 1991; Bakker et al., 1997; Bates et al., 1998). We do not address this issue in any detail but only compare the results using the quadratic relation to wind speed (Wanninkhof, 1992) with those using a cubic relation to wind speed (Wanninkhof and McGillis, 1999). The calculated daily mean CO_2 fluxes (mean hourly flux multiplied by 24), using the quadratic relation (Eq. (2)), resulted in a sink of CO_2 of $2.6 \pm 1.8\,mmol\,m^{-2}\,d^{-1}$ in SIE1. This is about two times larger than the CO_2 sink of

1.1 ± 0.94 mmol $m^{-2} d^{-1}$ calculated using the cubic relation (Eq. (3)). In the WIE the two calculated fluxes are quite equal, while the calculated CO_2 sink in the APF2 using Eq. (2) is 9.1 ± 9.1 mmol $m^{-2} d^{-1}$ and 11.5 ± 13.9 mmol $m^{-2} d^{-1}$ using Eq. (3). The shift from higher flux using the quadratic relation in the SIE1 to higher flux using the cubic relation in the APF2, is a function of the higher wind speed in the APF2 relative to the SIE1. For the calculated oxygen fluxes there is a difference between using Eqs. (2) and (3) of almost a factor 3 in the SIE1 (4.6 and 1.7 mmol $m^{-2} d^{-1}$). The calculated oxygen fluxes in the WIE are equal (-2.9 mmol $m^{-2} d^{-1}$), and for the APF2 the calculated oxygen fluxes are 27 and 34 mmol $m^{-2} d^{-1}$ using Eqs. (2) and (3), respectively. The following discussion of the fluxes is based on the calculations using the cubic relation to wind speed (Eq. (3)).

The calculated CO_2 and oxygen fluxes differ in the choice of wind speed data used for the calculations, instantaneous wind speed or daily average wind speed. In SIE1 and APF2 the calculated mean CO_2 fluxes, using the daily mean wind speed, differ by a factor of 2 from the mean flux, using instantaneous wind speed (Table 2). The wind speed effect has also been investigated in other studies by, for example, Murphy et al. (1991) and Bakker et al. (1997).

Calculating the CO_2 flux, there are uncertainties in the chemical parameters used, derived from the uncertainty in the analytical methods. With the A_T and pH precision and accuracy quoted in the method chapter, the estimated accuracy in the calculation of fCO_2^{sea} is approximately 5 µatm (Dickson and Riley, 1978). The uncertainties in the calculated daily sea–air CO_2 fluxes (the momentary fluxes multiplied by 24), caused by the analytical precision and calculations, correspond to 0.036 ± 0.015 mmol $m^{-2} d^{-1}$ (0.0015 ± 0.0006 mmol $m^{-2} h^{-1}$) in the SIE1 and 0.37 ± 0.039 mmol $m^{-2} d^{-1}$ (0.015 ± 0.0016 mmol $m^{-2} h^{-1}$) in the APF2. Hence, these uncertainties correspond to an error of an average of 3% in the mean calculated CO_2 fluxes. The largest uncertainty is about 12% in the SIE1, where the lowest calculated flux is -0.063 mmol $m^{-2} h^{-1}$. In the APF2 the uncertainty corresponds to a maximum of 30% for the lowest calculated CO_2 flux of -0.043 mmol $m^{-2} h^{-1}$. In the flux calculations there is also an uncertainty in the fCO_2^{air} (362 µatm) value used. However, this uncertainty is less than 1 µatm in fCO_2^{air} (Chierici et al., 2004), which is less than the uncertainty in the calculated fCO_2^{sea}, and is therefore considered negligible.

Using the carbon dioxide constants of Roy et al. (1993, 1994) in the calculations of fCO_2 instead of other constants, for instance the constants of Mehrbach et al. (1973), has intensively been discussed (e.g. Johnson et al., 1999; Wanninkhof et al., 1999). The use of either of the two constants resulted in a difference in the calculated fCO_2 of maximum 15 µatm, where using the Mehrbach et al. (1973) constants resulted in higher fCO_2 than using the Roy et al. (1993) constants. This difference corresponds to a change between 8% and 10% of the mean calculated CO_2 fluxes in the SIE1 and APF2, respectively. However, we found that the calculated fCO_2, using the Roy constants, were consistent with our direct measurements of fCO_2 (Chierici et al., 2004). In addition, the trends of the calculated fCO_2 using the Roy constants showed good agreements with those of Mehrbach at low temperatures, according to Wanninkhof et al. (1999), which is also the case in our study. Clayton et al. (1995) and Lee et al. (1997) maintain that the constants of Roy are preferable with good agreements in the internal consistency when using A_T and pH for the fCO_2 calculations.

6. Conclusion

Sea–air fluxes are only of minor importance for the daily variations in C_T and oxygen as compared to biological activity and mixing processes at this time of investigation and in these regions. As an effect of variable wind speed and surface water concentrations of CO_2 and oxygen, the calculated sea–air flux of CO_2 and oxygen vary significantly throughout the entire day. In the high wind speed area, APF2, the maximum calculated flux of CO_2 was 40 times higher than the minimum, whereas in SIE1 (low wind speed area) the maximum calculated flux was about 17 times higher than minimum flux. Short-term variability in wind speed has a larger impact on sea–air fluxes than

the variability in surface water concentrations of CO_2 and oxygen. The calculated fluxes also showed significant differences depending on how the wind speed was used, as instantaneous wind speed or as daily mean value. The variability of wind speed showed a slightly larger effect on the variability of the calculated oxygen than that of CO_2. This might be explained by that the surface water oxygen is closer to saturation than CO_2 at this time of investigation.

The variability in the calculated sea–air CO_2 fluxes throughout the entire day, as a result of fluctuations in both ΔfCO_2 and wind speed, are larger than the variability in fluxes using different flux equations. Hence, estimates of CO_2 sinks/sources in the Southern Ocean and in areas and seasons with strong diurnal cycles in temperature and productivity preferably have to account for this short time variability by performing measurements at different times of the day. The use of a tracer might be a useful tool in order to elucidate the role of advection and mixing of water masses over the time period studied. We also support the idea of drifting buoys, following the movement of the water, where daily and seasonal variability in the oceanic carbon dioxide system can be studied and accounted for in future budgets of sea–air fluxes of CO_2.

Acknowledgements

The authors would like to thank the Swedish Polar Research Secretariat, the Swedish Natural Science Research Council (NFR) and the Göteborg Marine Centre (GMF) for financial support. Thanks also to the scientific leader David Turner, and to Anne-Marie Larsson, Leif Djurfeldt, Per-Ingvar Sehlstedt, Ole-Anders Nøst and Elisabeth Engum for providing CTD data. Thanks to the crew of the *SA Agulhas*, and special thanks to Chris Rohleder for wind speed data and for all technical support.

References

Abrahamsson, K., Bertilsson, S., Chierici, M., Fransson, A., Froneman, P.W., Lorén, A., Pakhomov, E.A., 2004. Variations of biochemical parameters along a transect in the Southern Ocean, with special emphasis on volatile halogenated organic compounds. Deep-Sea Research II this issue [doi:10.1016/j.dsr2.2004.09.004].

Bakker, D.C.E., de Baar, H.J.W., Bathmann, U.V., 1997. Changes of carbon dioxide in surface-waters during spring in the Southern Ocean. Deep-Sea Research II 44, 91–128.

Bates, N.R., Takahashi, T., Chipman, D.W., Knap, A.H., 1998. Variability of pCO_2 on diel to seasonal timescales in the Sargasso Sea near Bermuda. Journal of Geophysical Research 103, 15567–15585.

Borges, A.V., Frankignoulle, M., 1999. Daily and seasonal variations of the partial pressure of CO_2 in surface seawater along Belgian and southern Dutch coastal areas. Journal of Marine Systems 19, 251–266.

Belkin, I.M., Gordon, A.L., 1996. Southern Ocean fronts from the Greenwich meridian to Tasmania. Journal of Geophysical Research 101, 3675–3696.

Chierici, M., Fransson, A., Turner, D.R., Pakhomov, E.A., Froneman, P.W., 2004. Variability in pH, fCO_2, oxygen and flux of CO_2 in the surface water along a transect in the Atlantic sector of the Southern Ocean. Deep-Sea Research II, this issue [doi:10.1016/j.dsr2.2001.03.002].

Clayton, T.D., Byrne, R.H., 1993. Spectrophotometric seawater pH measurements: total hydrogen ion concentration scale calibration of m-cresol purple and at-sea results. Deep-Sea Research I 40, 2115–2129.

Clayton, T.D., Byrne, R.H., Breland, J.A., Feely, R.A., Millero, F.J., Campbell, D.M., Murphy, P.P., Lamb, M-F., 1995. The role of pH measurements in modern oceanic CO_2-system characterisations: precision and thermodynamic consistency. Deep-Sea Research II 42, 411–429.

Coale, K.H., Johnson, K.S., Fitzwater, S.E., Gordon, R.M., Tanner, S., Chavez, F., Ferioli, L., Sakamoto, C., Rogers, P., Millero, F.J., Steinberg, P., Nightingale, P., Cooper, D., Cochlan, W., Landry, M., Constantinou, J., Rollwagen, G., Tavina, A., 1996. The IronEx II mesoscale experiment produces massive phytoplankton bloom in the equatorial Pacific. Nature 383, 495–501.

de Baar, H.J.W., de Jong, J.T.M., Bakker, D.C.E., Löscher, B.M., Veth, C., Bathmann, U., Smetacek, V., 1995. Importance of iron for plankton blooms and carbon-dioxide drawdown in the Southern Ocean. Nature 373, 412–415.

Dickson, A.G., Riley, J.P., 1978. The effect of analytical error on the evaluation of the components of the aquatic carbon-dioxide system. Marine Chemistry 6, 77–85.

Haraldsson, C., Anderson, L.G., Hassellöv, M., Hulth, S., Olsson, K., 1997. Rapid, high-precision potentiometric titration of alkalinity in the ocean and sediment pore waters. Deep-Sea Research I 44, 2031–2044.

Inoue, H., Sugimura, Y., 1988. Distribution and variations of oceanic carbon dioxide in the western North Pacific, eastern Indian, and Southern Ocean south of Australia. Tellus 40B, 308–320.

Johnson, K.M., King, A.E., Sieburth, J.M., 1985. Coulometric TCO_2 analyses for marine studies: an introduction. Marine Chemistry 16, 61–82.

Johnson, K.M., Sieburth, J.M., Williams, P.J., Brandstrom, L., 1987. Coulometric total carbon dioxide analysis for marine studies: automation and calibration. Marine Chemistry 21, 117–133.

Johnson, K.M., Körtzinger, A., Mintrop, L., Duinker, J.C., Wallace, D.W.R., 1999. Coulometric total carbon dioxide analysis for marine studies: measurements and internal consistency of underway TCO_2 concentrations. Marine Chemistry 67, 123–144.

Keeling, C.D., Whorf, T.P., 1999. Atmospheric CO_2 concentrations from South Pole. Complement to Trend's online; Carbon Dioxide Information analysis Center, Oak Ridge National Laboratory, Oak Ridge, TN, USA. WWW Page, cdiac.esd.ornl.gov/ftp/trends/co2/sposio.co2.

Lee, K., Millero, F.J., 1995. Thermodynamic studies of the carbonate system in seawater. Deep-Sea Research I 42, 2035 2061.

Lee, K., Millero, F.J., Wanninkhof, R., 1997. The carbon dioxide system in the Atlantic Ocean. Journal of Geophysical Research 102, 15693 15707.

Lewis, E., Wallace, D.W.R., 1998. Program Developed for CO_2 System Calculations. ORNL/CDIAC-105. Carbon Dioxide Information Analysis Center, Oak Ridge National Laboratory, US Department of Energy, Oak Ridge, Tennessee.

Lutjeharms, J.R.E., Valentine, H.R., 1984. Southern Ocean thermal fronts south of Africa. Deep-Sea Research 31, 1461–1475.

Mehrbach, C., Culberson, C.H., Hawley, J.E., Pytkowicz, R.M., 1973. Measurement of the apparent dissociation constants of carbonic acid in seawater at atmospheric pressure. Limnology and Oceanography 18, 897–907.

Murphy, P.P., Feely, R.A., Gammon, R.H., Harrison, D.E., Kelly, K.C., Waterman, L.S., 1991. Assessment of the air–sea exchange of CO_2 in the Southern Pacific during austral autumn. Journal of Geophysical Research 96, 20455–20465.

Oudot, C., Andrié, C., 1989. Short-term changes in the partial pressure of CO_2 in eastern tropical Atlantic surface seawater and in atmospheric CO_2 mole fraction. Tellus 41B, 537–553.

Pakhomov, E.A., Froneman, P.W., 2004. Zooplankton dynamics in the eastern Atlantic sector of the Southern Ocean during the austral summer 1997/1998. Part 1. Community structure. Deep-Sea Research II, this issue [doi:10.1016/j.dsr2.2000.11.001].

Peng, T.H., Takahashi, T., Broecker, W.S., Ólafsson, J., 1987. Seasonal variability of carbon dioxide, nutrients and oxygen in the northern North Atlantic surface water: observations and a model. Tellus B 39, 439–458.

Poisson, A., Metzl, N., Brunet, C., Schauer, B., Bres, B., Ruiz-Pino, D., Louanchi, F., 1993. Variability of sources and sinks of CO_2 in the western Indian and Southern Oceans during the year 1991. Journal of Geophysical Research 98, 22759–22778.

Robertson, J.E., Watson, A.J., Langdon, C., Ling, R.D., Wood, J.W., 1993. Diurnal variation in surface pCO_2 and O_2 at 60°N, 20°W in the North Atlantic. Deep-Sea Research II 40, 409–422.

Roy, R.N., Roy, L.N., Vogel, K.M., Porter-Moore, C., Pearson, T., Good, C.E., Millero, F.J., Campbell, D.M., 1993. The dissociation constants of carbonic acid in seawater at salinities 5–45 and temperatures 0–45 °C. Marine Chemistry 44, 249–267.

Roy, R.N., Roy, L.N., Vogel, K.M., Porter-Moore, C., Pearson, T., Good, C.E., Millero, F.J., Campbell, D.M., 1994. Erratum for: the dissociation constants of carbonic acid in seawater at salinities 5 to 45 and temperatures 0 to 45 °C. Marine Chemistry 45, 337.

Smith, W.O., Nelson, D.M., 1985. Phytoplankton bloom produced by a receding ice edge in the Ross Sea: spatial coherence with the density field. Science 277, 163 166.

Spiridonov, V.A., Nöthig, E.-M., Schröder, M., Wisotzki, A., 1996. The onset of biological winter in the eastern Weddell Gyre (Antarctica) planktonic community. Journal of Marine Systems 9, 211–230.

Steinberg, P.A., Millero, F.J., Zhu, X., 1998. Carbonate system response to iron enrichment. Marine Chemistry 62, 31–43.

Takahashi, T., Ólafsson, J., Goddard, J.G., Chipman, D.W., Sutherland, S.C., 1993. Seasonal variation of CO_2 and nutrients in the high-latitude surface oceans: a comparative study. Global Biogeochemical Cycles 7, 843–878.

Veth, C., Peeken, I., Scharek, R., 1997. Physical anatomy of fronts and surface waters in the ACC near the 6°W meridian during austral spring 1992. Deep-Sea Research II 44, 23–49.

Wanninkhof, R.H., 1992. The relationship between wind speed and gas exchange over the ocean. Journal of Geophysical Research 97, 7373–7382.

Wanninkhof, R., McGillis, W.R., 1999. A cubic relationship between air–sea CO_2 exchange and wind speed. Geophysical Research Letters 26, 1889–1892.

Wanninkhof, R., Lewis, E., Feely, R.A., Millero, F.J., 1999. The optimal carbonate dissociation constants for determining surface water pCO_2 from alkalinity and total inorganic carbon. Marine Chemistry 65, 291–301.

Weiss, R.F., 1974. Carbon dioxide in water and seawater: the solubility of a non-ideal gas. Marine Chemistry 2, 203–205.

ELSEVIER

Deep-Sea Research II 51 (2004) 2841–2856

DEEP-SEA RESEARCH
PART II

www.elsevier.com/locate/dsr2

Iron enrichment and photoreduction of iron under UV and PAR in the presence of hydroxycarboxylic acid: implications for phytoplankton growth in the Southern Ocean

Murat Öztürk[a,*], Peter L. Croot[b,1], Stefan Bertilsson[c,2], Katarina Abrahamsson[d], Bengt Karlson[e,3], Roland David[f], Agneta Fransson[g,4], Egil Sakshaug[a]

[a]*Trondheim Biological Station, Norwegian University of Science and Technology, Bynesvägen 46, N-7018 Trondheim, Norway*
[b]*Department of Chemistry, Analytical and Marine Chemistry, Göteborg University, SE-412 96 Göteborg, Sweden*
[c]*Department of Water and Environmental Studies, Linköping University, SE-581 83 Linköping, Sweden*
[d]*Department of Chemistry and Bioscience, Chalmers University of Technology, SE-412 96 Göteborg, Sweden*
[e]*Botanical Institute, Göteborg University, Box 461, SE-405 30 Göteborg, Sweden*
[f]*CSIR, PO Box 17001, Congella 4013, Kwa-Zulu Natal, South Africa*
[g]*Department of Chemistry, Analytical and Marine Chemistry, Göteborg University, SE-412 96 Göteborg, Sweden*

Abstract

Iron(III) photoreduction and the responses of phytoplankton under ultraviolet (UV) and photosynthetically available radiation (PAR) were investigated with the presence of hydroxycarboxylic acid (glucaric acid (GA), a model compound for organic acids excreted by phytoplankton). The incubation experiments were carried out on board using seawater samples collected in the location of the winter ice edge (WIE) and the spring ice edge (SIE) of the Southern Ocean. In this paper, we focus on the results of experiment in WIE. Throughout the experiments, dissolved Fe(II), major nutrients and in vivo fluorescence were monitored regularly. In addition, Chl-*a*, POC/PON, cell densities of phytoplankton and bacteria, bacterial production, organic peroxide, hydrogen peroxide and total CO_2 were measured.

The results from the WIE show that iron enrichment had a substantial effect on phytoplankton growth rate. Fe(III) addition in the presence of GA (FeGA) gave higher Fe(II) concentration and higher growth rate of phytoplankton than those in controls. Our results suggest that hydroxycarboxylic acid had a significant chemical and biological impact. The presence of GA influenced iron photochemistry and iron availability to phytoplankton. Phytoplankton growth responses to iron enrichments in incubations under UV and PAR were completely dissimilar. It seems that FeGA

*Corresponding author. Tel.: +47 7359 1595; fax +47 7359 1597.
E-mail address: murato@bio.ntnu.no (M. Öztürk).
[1]Present address: Leibniz-Institut Marine Sciences at Kiel University (IFM-GEOMAR), Düsternbrooker Weg 20, D-24105 Kiel, Germany.
[2]Present address: Department of Evolutionary Biology/Limnology, Uppsala University, Norbyv. 20, SE-75236 Uppsala, Sweden.
[3]Present address: SMHI, Building 31, Nya Varvet, SE-426 71 Västra Frölunda, Sweden.
[4]Present address: Climate Change Research Project, National Institute for Environmental Studies, 16-2 Onogawa, Tsukuba, Ibaraki 305-8506, Japan.

0967-0645/$ - see front matter © 2004 Elsevier Ltd. All rights reserved.
doi:10.1016/j.dsr2.2000.10.001

addition prominently changes the harmful effect of UV on the phytoplankton population. This study provide preliminary information on how the photoreduction of iron(III) and the phytoplankton growth are affected by iro enrichment in the presence of hydroxycarboxylic acid.
© 2004 Elsevier Ltd. All rights reserved.

1. Introduction

The Southern Ocean is distinguished by being far from the major terrestrial and anthropogenic sources of iron, and its cold surface waters are separated from other major oceans by the Antarctic Polar Front. Due to its remoteness from continents, iron concentrations are very low in the surface layers of the Southern Ocean (Löscher et al., 1997). Furthermore, the Southern Ocean is known to be an important area in the world's oceans in regulating the oceanic carbon cycle, thus playing a significant role in regulating atmospheric CO_2 (Bakker et al., 1997). Nitrate, phosphate and silicate concentrations in the Southern Ocean may reach above 30, 2.5 and 100 mmol m^{-3}, respectively (Sakshaug et al., 1991). In addition, the concentrations of chlorophyll *a* (Chl-*a*) and the standing stock of phytoplankton are low, on average 0.4 mg m^{-3} and <3 mg m^{-3} Chl-*a* in the ice-free and deep-sea regions of the Southern Ocean, respectively (El Sayed, 1988; Holm-Hansen et al., 1989). Hence, the Southern Ocean, as well as the equatorial Pacific, is a major high-nutrient and low-chlorophyll (HNLC) zone.

This HNLC situation may result in light limitation due to wind-induced deep mixing (Sakshaug and Holm-Hansen, 1984; Sakshaug et al., 1991) or iron limitation (Martin et al., 1990) and grazing control (Banse, 1990). Light and iron limitation may have a similar impact (Sakshaug et al., 1991), while grazing is always more or less important as a controlling factor at certain times and in different locations. These explanations are not mutually exclusive.

The importance of iron limitation of marine phytoplankton has become increasingly apparent in recent years. A breakthrough for the iron hypothesis was the in situ iron enrichment experiments with waters in the equatorial Pacific Ocean (IronEx I & II) (Martin et al., 1994; Behrenfeld et al., 1996; Coale et al., 1996). These mesoscale in situ Fe experiments showed that Fe is a limiting element in the equatorial Pacific Ocean. Fe enrichment stimulates phytoplankton production in the Southern Ocean (van Leeuwe et al., 1997; Scharek et al., 1997).

Iron can exist in two different oxidation states in seawater: Fe(III) and Fe(II). Fe(III) is thermodynamically stable in oxic waters. Fe(II) may be produced by photochemical reduction of Fe(III) in surface seawater (Miller and Kester, 1994a). It is believed that Fe(II) in seawater exists mainly as "free" Fe^{2+} ions and is much more soluble than Fe (III) (Stumm and Morgan, 1996). Therefore it may be effectively available for phytoplankton. However, it has been argued that Fe(II) in seawater oxidizes too rapidly with half life of a few minutes (Millero et al., 1987; Morel et al., 1991) to be important. Nevertheless, significant concentrations of Fe(II) have been observed in coastal waters (Kuma et al., 1992; Zhuang et al., 1995). Dissolved organic matter (DOM) such as humic acids and hydroxycarboxylic acids, which inpart is released by phytoplankton (Kuma et al., 1992, 1995), may play an important role in the photoreduction of Fe(III) by providing an electron source. Some DOM components can slow down the re-oxidation rate by complexation with Fe(II) (Hudson et al., 1992). However, it is not yet clear to what extent this is important in seawater. On the other hand, photochemically produced radicals, for example, $O_2^{\bullet -}$, H_2O_2, $HO_2^{\bullet}$ and $OH^{\bullet}$, can participate in secondary oxidation and reduction of Fe species in seawater (Faust and Zepp, 1993; King et al., 1995; Voelker et al., 1997).

In photoreduction experiments, it has been shown that the fastest rate of Fe(III) reduction is achieved in the presence of certain DOM components such as glucaric acid (GA), which can act as an electron donor (Kuma et al., 1992, 1995). A similar type sugar acid, 0.8 μM gluconic acid, was

detected in surface water during a spring bloom in Funka Bay (Japan) (Kuma et al., 1992, and references therein). GA can form strong complexes with Fe(III) in seawater (Log $K_{FeL} = 24$; Kuma et al., 1995).

In a system containing GA, a simplified photoreduction scheme might be

$$\text{Fe(III)}-\text{GA complex} + h\nu \Rightarrow \text{Fe(II)} + \text{GA}* \quad (1)$$

(ligand to metal charge transfer (LMCT)). GA* is oxidation product of GA.

$$\text{Fe(II)} + \text{GA}* \Rightarrow \text{soluble Fe(III)}-\text{GA} \quad (2)$$

(Kuma et al., 1995).

DOM is both a potentially important electron source for photoreductive Fe(II) production and an important source for secondary reducing radicals such as $O_2^{\bullet-}$ (Faust and Zepp, 1993), while at the same time being important for the re-oxidation of Fe(II) to Fe(III). This duality results from DOM being a source of many photoproduced radicals (e.g. H_2O_2, $HO_2^{\bullet\prime}$, $O_2^{\bullet-}$ and $OH^{\bullet}$) that can oxidize Fe(II).

The roles of DOM and light on the speciation, photochemistry and complexation of iron necessarily has a profound impact on iron availability for phytoplankton. We therefore designed a deck experiment on HNLC water from the Southern Ocean. In these experiments we tested the effect of iron enrichment and photoreduction on the phytoplankton growth rate in the presence of GA under natural light with different wavelength ranges: PAR (400–700 nm), and UVAB and PAR (280–700 nm). In this paper we have focused on the results of experiments from WIE water. The results of experiments from SIE have not been presented here, but mentioned only briefly for the purpose of giving a more holistic picture.

2. Materials and methods

The incubation experiments were performed on S.A. *Agulhas* during a cruise in December 1997 and January 1998. The study area was in the locations of the winter ice edge (WIE) and the spring ice edge (SIE) (see Fig. 1 in Turner et al., 2004). The position and depths for water samples to be incubated were determined based on in vivo Chl-*a* and light transmittance measurements. Seawater samples at the WIE (at station D233: 56°30′S, 6°E) were collected from 15 m depth using a peristaltic pump with acid-washed tubes attached to a Kevlar hydrowire. Seawater samples, at station D013 (60°54′S, 05°54′E) in the SIE, were collected from 30 m depth (Chl-*a* maximum) using an acid-washed 30 l Go-Flo sampler deployed on Kevlar hydrowire.

The incubation carboys had been sequentially washed, first with microdetergents, then with Milli-Q water, methanol, Milli-Q water and 3 M HCl and kept for 2 weeks in 0.1 M Ultrapure HCl. Finally, all carboys were rinsed with copious amounts of Milli-Q water.

Incubations were performed in 12 l polycarbonate (PC) carboys (for PAR) and polyethylene (PE) bags (for UVAB–PAR). PE bags and PC carboys transmitted wavelengths >220 nm and >370 nm, respectively. The enrichments were iron (Fe), iron + glucaric acid (FeGA), and no addition (control, C) replicates (two carboys or bags for each treatment) for PAR and UVAB PAR irradiance, respectively. Additional incubations under UVA PAR were performed in addition to PAR and UVAB–PAR in SIE. In these incubations, UVB was excluded by using a Mylar filter (which transmits wavelength >320 nm). The GA solution was cleansed of iron by passing it through a Chelex-100 column, which was previously prepared and washed with 1 l of Milli-Q water to minimize the possible leakage of functional groups of Chelex-100 into GA solution. In order to outcompete other natural organic complexes in seawater, at least at the beginning of the experiments, the FeGA mixture was prepared 2 days before addition. First additions of Fe, and FeGA to the incubation carboys were done after 24 h of phytoplankton acclimatization to deck conditions. Iron was added as $FeCl_3$ solution (pH 2) to make a final concentration of $\geqslant$5 nM. Iron–GA mixture was added to a final concentration of $\geqslant$5 nM Fe and to make a final GA concentration of 1.2 μM. For every light treatment, there were Fe, FeGA and control treatments. Additions of Fe and FeGA to WIE water were done at the beginning

of the experiment and on day 10 (+3 nM Fe and 1.2 μM GA) of the 14-day-long experiment. The amount of added Fe was determined according to natural iron fluxes to the oceans. The atmospheric fluxes to the Atlantic Ocean range from 18 mmol $m^{-2} y^{-1}$ west of North Africa to 0.02 mmol $m^{-2} y^{-1}$ in the Atlantic sector of the Southern Ocean (Duce and Tindale, 1991). Similarly, fluxes of iron to the Pacific Ocean also ranged from ca. 18 mmol $m^{-2} y^{-1}$ east of Japan to 0.02 mmol $m^{-2} y^{-1}$ in the equatorial Pacific. For 50 m mixing-layer depth, the maximum natural atmospheric input of Fe to the ocean would be ca. 1 nmol $l^{-1} d^{-1}$. Additions of 5+3 nM iron for 14-day incubations (ca. 0.5–0.6 nmol $l^{-1} d^{-1}$) lie between the range of atmospheric iron inputs found in the Pacific and Antarctic Oceans. Moreover, the added iron may have been removed by precipitation or by adsorption onto the wall of carboys and become less available to phytoplankton. Additionally, photochemically produced Fe(II) may have been re-oxidized quickly. Therefore, we added extra iron and GA to meet the increased demand of iron when phytoplankton began growing. The amount of added GA (1.2 μmol l^{-1}) was chosen higher than the detected value of similar hydroxycarboxylic acid in nature (ca. 0.8 μmol l^{-1}; Nakabayashi et al., 1993, cited in Kuma et al., 1995) in order to ensure the presence of GA during incubations. The carboys were incubated on the helicopter deck. All incubation carboys and PE bags were covered by PE bags and carefully sealed to prevent contamination. PVC grey mosquito nets were used for irradiance adjustment. Incubation light was kept around 50% of ambient PAR. Running seawater was used to keep the incubation temperature close to the ambient level (1 °C). On occasions it rose to 1–2 °C higher than ambient temperature.

PC carboys and PE bags had tap systems that were tightly closed during incubation. All samples were drawn either by an all-polypropylene (PP) syringe connected to a Teflon tube or by a peristaltic pump without opening the carboys, through the sample out port. The air input taps were connected with a double 0.2 μm Teflon filter to keep out contamination in the air during sampling and kept closed during incubations. All tubing was previously acid-washed Teflon o Bevaline. Sampling during the experiment witl WIE water was done in a dust-free (class 100 container through tapping tubes, without openin the carboys and bags. Fe(II) was determined wit a stopped-flow luminol chemiluminescence mete (SFL-CL) (O'Sullivan et al., 1995; King et al. 1995; Powell et al., 1995) immediately after sampling and filtration through a 0.4 μm filter in an all-PP syringe filter holder in a clean container This method has a detection limit of 0.06 nM Fe Measurements of in vivo fluorescence were done immediately by using a Turner Design fluorometer. Ten replicates were done repeatedly for each sample. Samples for POC and PON and Chl-*a* were filtered on pre-combusted GF/F filters, packed in pre-combusted aluminum foil, and stored at −18 °C until analysis in the shore laboratory. POC and PON were determined on a CHN Analyzer (Carlo Erba). For Chl-*a* determinations, samples filtered onto GF/F filters were extracted with 90% methanol for 12 h and analyzed by a Turner Design fluorometer. Total peroxides (H_2O_2 and organic peroxides) concentrations were measured with a spectrofluorometer (excitation: 313 nm; emission: 400 nm) using horseradish peroxidase and dimerization of *p*-hydroxyphenylacetic acid (Miller and Kester, 1994b, and references therein). Organic peroxides were measured similarly with the addition of enzyme catalase together with horseradish peroxidase.

Nano- and picophytoplankton were counted by flow cytometry. The microphytoplankton were counted by light optical microscope. Phytoplankton samples from the incubation carboys were fixed by Lugol and formaline solutions (20%) in 500 and 150 ml bottles. After arrival at Trondheim Biological Station, samples were transferred to the sedimentation chambers. Volumes of 2, 10, 30 and 50 ml were selected depending on phytoplankton abundance. The samples were kept in sedimentation chambers for at least 3 days. Counting and species determination were done by inverse microscopy. At least 24 repeated counts were done for each sedimentation chamber.

Samples for bacterial abundance were preserved in formaldehyde (2% final concentration) and

were analyzed by flow cytometry as described by del Giorgio et al. (1996). All analyses were performed on board within 1 week of sampling. Bacterial production was measured according to the Leucine incorporation method (Smith and Azam, 1992).

3. Results and discussion

The total background Fe concentration at a depth of 15 m in WIE was 0.47 ± 0.13 nM ($n = 3$). Daily maximum irradiation of UVA, UVB and PAR was in the range of 21.1–53.8, 1.6–4.2 and 125–415 W m^{-2}, respectively (Wängberg et al., 2004).

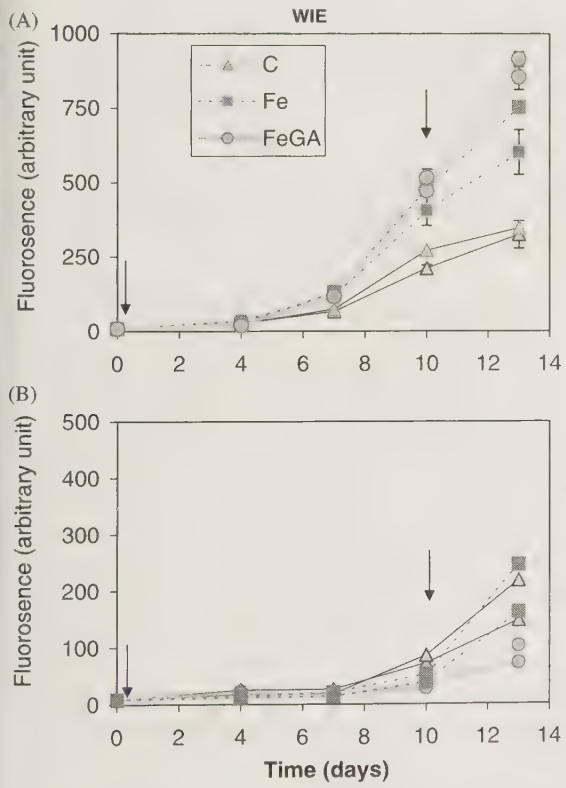

Fig. 1. In vivo fluorescence (IVF) data for phytoplankton growth following incubations in the location of the winter ice edge (WIE) of the Southern Ocean under IVF data for phytoplankton growth following the incubations of WIE seawater under PAR (A) and UVAB-PAR (B). The arrows indicate additions of Fe and FeGA.

3.1. *In vivo fluorescence and phytoplankton response to iron addition*

In vivo fluorescence of different treatments started to diverge on day 7 (Fig. 1A). There was a very clear response from Fe and FeGA treatments compared to the controls. In vivo fluorescence was significantly higher in Fe and FeGA treatments (t-test, $P<0.05$). FeGA treatments yielded the highest in vivo fluorescence at the end of the experiments (t-test, $P<0.05$). In UVAB–PAR treatments, the highest in vivo fluorescence was observed up to day 10 in the control (Fig. 1B) and the lowest in vivo fluorescence in the FeGA treatments. Differences of in vivo fluorescence between control and FeGA treatments after day 10 were siginificant ($P<0.05$). At the end of the 14-day-long incubations, in Fe and FeGA treatments under PAR, the dominating phytoplankton species were *Pseudonitzschia* spp., *Nitzschia* spp. and *Phaeocystis* spp. A considerable increase in the number of *Rhizosolenia* spp. was observed in FeGA–PAR treatment. In the control treatments, the predominant species was *Phaeocystis* spp. A shift from nano–picophytoplankton to microphytoplankton was evident in Fe and FeGA treatments under PAR (Fig. 2A and B). Under UVAB–PAR, *Phaeocystis* spp. was dominant. After the enrichment with Fe and FeGA, the number of nano–picophytoplankton also increased considerably (Fig. 2B).

These data suggest that Fe and FeGA additions dramatically alter the species composition from nano–pico to diatoms $>20\,\mu$m in the WIE (Fig. 2). This was particularly pronounced in FeGA treatments. The increase in diatoms after the addition of Fe is in agreement with previous Fe enrichment studies in HNLC regions (Coale, 1991; van Leeuwe et al., 1997; Scharek et al., 1997).

Our results suggest that microphytoplankton (mainly diatoms $>20\,\mu$m) respond favorably to the addition of FeGA and Fe in the WIE waters. Presumably, nano–pico plankton has an advantage under Fe-limited conditions, due partially to their relatively low iron requirements (Sunda et al., 1991) and/or their greater surface area : cell volume ratio, ensuring more efficient Fe uptake. Under UVAB–PAR, however, FeGA treatments

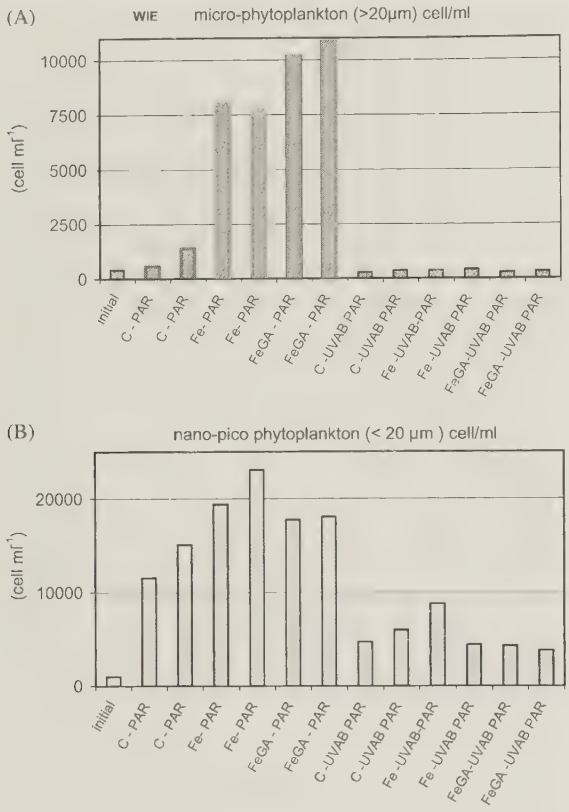

Fig. 2. Initial and final cell densities (cell ml^{-1}) for micro-phytoplankton (A) and nano–picophytoplankton (B) for each treatment and controls for incubation in WIE.

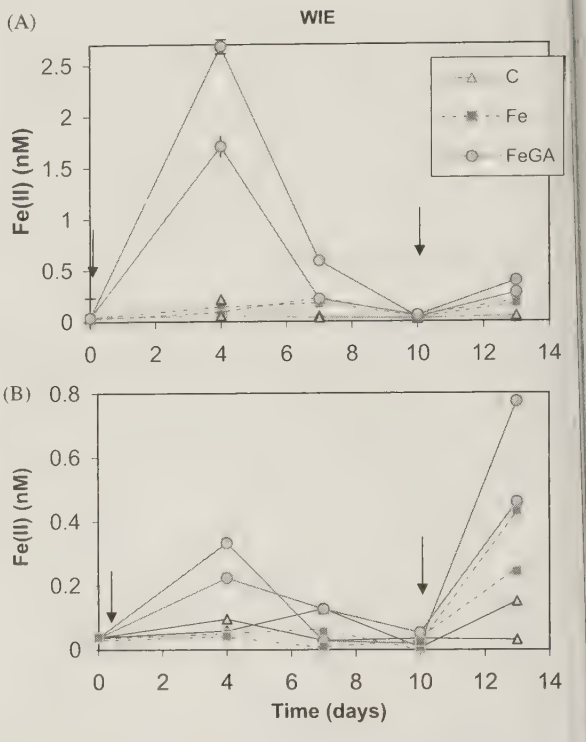

Fig. 3. Photoproduction of Fe(II) in the incubations of WIE seawater under PAR (A) and UVAB–PAR (B). Vertical arrows indicate additions of Fe and FeGA.

yielded the lowest phytoplankton biomass. This has also been observed in the SIE (data not shown). Under UVAB–PAR, FeGA may enhance the harmful effects of UV, probably due to photochemical reactions in which FeGA plays a role. It has also been reported that nutrient stress may cause increased release of organic matter (Lancelot and Billen, 1985; Verity et al., 1988), that is, after enrichment with FeGA, under UVAB–PAR, phytoplankton may release less UV-protective organic matter, thus less protection against UV.

3.2. *Fe(II), organic peroxides and H_2O_2*

After the addition of FeGA, Fe(II) increased dramatically (Fig. 3A), especially under PAR. On day 4, concentrations of Fe(II) were 1.7 and 2.6 nM in the FeGA treatments under PAR. The high level of Fe(II) on day 4 indicates photoreductive Fe(II) production due to the presence of GA. When the phytoplankton began growing, the Fe(II) concentration started to decrease, reaching the detection limit on day 10. Then, new additions (+3 nM Fe, +3 nM−1.2 µM FeGA) were made to meet the increased Fe demand. Fe(II) was still detectable 3 days after the second addition (Fig. 3A and B). Fe(II) concentrations in the FeGA treatment under UVAB–PAR varied similar to those of PAR treatments, albeit Fe(II) concentrations under UVAB—PAR–FeGA treatments were much lower than under PAR–FeGA treatments (Fig. 3B).

Peroxide concentration (H_2O_2 + organic peroxides) under PAR was low at the beginning and then increased to 150–250 µmol m^{-3} on day 10, and decreased to 15–40 µmol m^{-3} on day 13 (Fig. 4A and C) in all treatments. In the controls, organic peroxides were a little higher than in iron

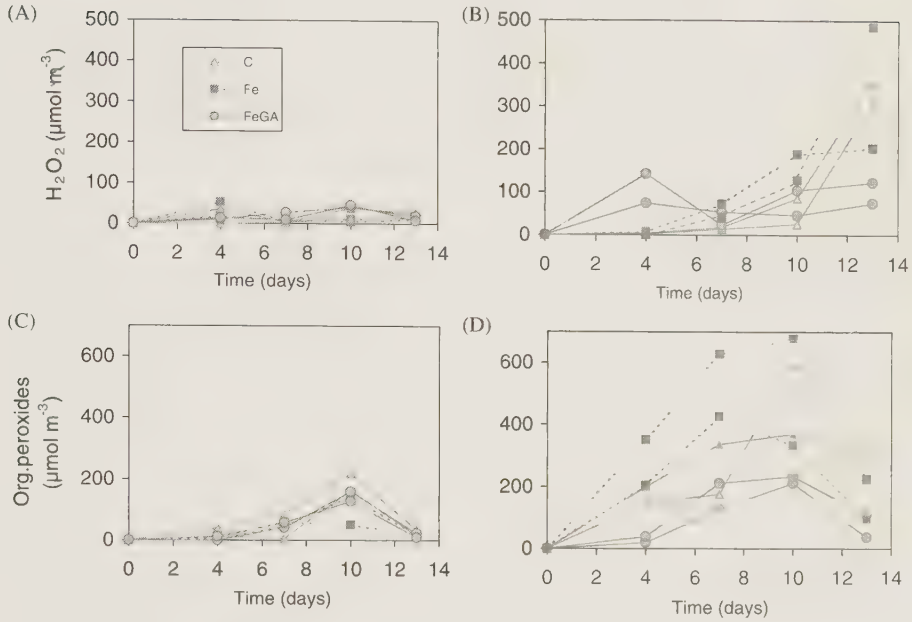

Fig. 4. Concentration of H_2O_2 under PAR (A) and UVAB–PAR (B), and organic peroxides under PAR (C) and UVAB (D) in the incubations of WIE seawater.

treatments. Under UVAB–PAR, the highest concentrations of H_2O_2 and organic peroxides were observed in the Fe treatments (Fig. 4B and D). The lowest concentrations of H_2O_2 and organic peroxides were observed in FeGA treatments. The organic peroxides concentration increased when there was little phytoplankton activity and started to decrease at the end of incubations in all treatments under UVAB–PAR. Concentrations of H_2O_2 and organic peroxides in all treatments of SIE were almost one order of magnitude lower than in the treatments of WIE.

After the formation of Fe(II), components of DOM, in addition to GA, might be responsible for keeping Fe(II) in solution. Some DOM compounds which are produced from phytoplankton could be important for Fe(III) photoreduction and some others could cause retardation of oxidation of Fe(II) and keep Fe(II) in solution by complexation. In order to understand the extent of primary photochemical reduction of Fe by the help of GA it is necessary to estimate the rate of oxidation/reduction reactions. We adopted first-order reversible photochemical oxidation/reduction reaction equations suggested by Kuma et al. (1995):

$$\text{Fe(III)GA (dissolved)} + h\nu \leftarrow k_{ox}\ k_{red} \rightarrow \text{Fe (II)} + \text{GA}*. \quad (3)$$

The Fe(II) concentration as a function of time can be written as

$$[\text{Fe(II)}]_t = \{\{k_{red}[\text{Fe(III)GA}]_0\}/(k_{red} + k_{ox})\}\ [1 - \exp\{-(k_{red} + k_{ox})\ t\}], \quad (4)$$

where $[\text{Fe(III)GA}]_0$, $[\text{Fe(II)}]_t$, k_{red} (min^{-1}) and k_{ox} (min^{-1}) are the concentrations of Fe(III)GA at $t = 0$ and Fe(II) at time t, and the rate constants of the forward (reduction) and reverse (oxidation) reactions, respectively. Kuma et al. (1995) reported values of k_{ox} and k_{red} at different temperatures (5, 10 and 15 °C) and different irradiances (1400, 1900 and 2300 µmol m^{-2} s^{-1}). k_{red} is independent of temperature and increases linearly with increasing irradiance (I_L). We obtained k_{red} dependence on irradiance ($k_{red} = 0.00004 I_L - 0.022$; $R^2 = 0.996$) and k_{ox} dependence to temperature ($k_{ox} = 0.0087T + 0.03$; $R^2 = 0.99$) from the data of Kuma et al. (1995). These estimations depend

on the assumptions that k_{red} and k_{ox} are linearly related to irradiance (I_L) and temperature (T), respectively, in extrapolated zones. From these approximations we calculated that maximum steady-state concentration of Fe(II) could reach 40–50% of added FeGA concentrations at 0 and −1 °C under 50% of ambient irradiance.

In the WIE, steady-state Fe(II) concentrations were ca. 32–50% and 5% of the added Fe(III) in PAR–FeGA and in UVAB–FeGA treatments, respectively. These results imply that Fe photoreduction under PAR seems to be more efficient than the secondary oxidation of Fe(II) by photochemically produced radicals. The difference in Fe(II) at the beginning of incubations between PAR and UV treatments was probably related to re-oxidation of photoreduced Fe(II) by photochemically produced radicals under UV treatments. Relatively high levels of H_2O_2 and organic peroxides in UV treatments both in WIE and SIE (data not shown) support this.

At high pH (typical for strong photosynthesis), the rate of secondary reduction of Fe(III) by the photochemically produced radical ($HO_2^{\bullet}/O_2^{\bullet -}$) increases (Voelker et al., 1997). This rate is at least 15 times higher than that of the Fe(II) re-oxidation reaction with $HO_2^{\bullet}/O_2^{\bullet -}$ (King et al., 1995), implying that, at natural conditions under PAR, Fe(III)GA could be a considerable source of Fe(II) and a sink for $HO_2^{\bullet}/O_2^{\bullet -}$. The presence of Fe does not seem to have been significant for the formation of H_2O_2 and $HO_2^{\bullet}/O_2^{\bullet -}$.

Our results under PAR neither suggest that organic peroxide formation depends on the presence of Fe, nor that there is a relationship between phytoplankton activities and organic peroxides in WIE or SIE. However, in the WIE experiments under UVAB–PAR, the H_2O_2 concentration generally shows increase with phytoplankton productivity. In the SIE experiments, despite the fact that the concentrations of H_2O_2 and organic peroxides in all treatments of SIE were almost one order of magnitude lower than in WIE, the trends of H_2O_2 and organic peroxides variations, especially under UVAB–PAR treatments, are almost the same as in WIE. The lowest levels of H_2O_2 and organic peroxides were observed in FeGA as the lowest values of POC and Chl-*a*. Organic peroxides levels increase when there was no phytoplankton activity an decreased with increasing phytoplankton growt at the end of incubations in all treatments unde UVAB–PAR. Thus, FeGA may have inhibited th formation of organic peroxides, or some organi peroxides may have been used to oxidize Fe(II back to Fe(III) by photochemically produce radicals originating from organic peroxides. Thi interpretation is supported by the relatively lo concentration of Fe(II) in FeGA treatments unde UVAB–PAR compared to under PAR. In the FeGA treatments under UVAB–PAR, the same process probably acted as a sink for photochemically produced peroxides and Fe(II). The most probable reaction is

$$Fe\ (II) + H_2O_2 \Rightarrow Fe\ (III) + OH^- + OH^{\bullet -}. \quad (5)$$

It seems that, in FeGA treatments, the oxidation of Fe(II) with H_2O_2 (Fenton reaction) may have been an important source of $OH^{\bullet}$ under UVAB–PAR. Hence, it may have caused oxidation of UV-protective DOM. This is also supported by the relatively low concentrations of H_2O_2 and organic peroxides, and the low phytoplankton productivity and biomass in the FeGA treatment compared to Fe and the control treatments.

The secondary reducing mechanisms, such as fast reduction of dissolved Fe(III) by the superoxide radical (Voelker and Sedlak, 1995), may also contribute to a build-up of the high steady-state Fe(II).

On the other hand, some DOM fractions may inhibit the re-oxidation of Fe(II) by oxidative radicals in two possible ways: (a) Organic matters are themselves oxidized by photochemically produced radicals, that is, Fe(II) oxidation by photochemically produced radicals is out-competed by oxidation of DOM by photochemically produced radicals. (b) Fe(II) is stabilized by organic complexation against oxidation by photochemically produced radicals.

3.3. Carbon and nitrogen assimilation: POC and PON

Under PAR, particulate organic carbon (POC) in all treatments began to diverge on day 7 until

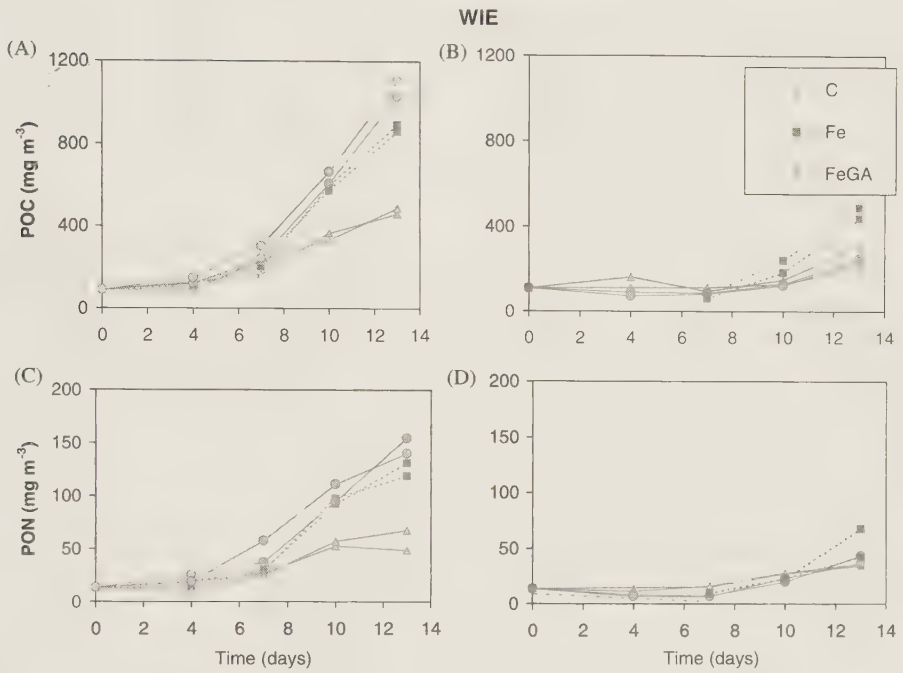

Fig. 5. Concentrations of POC under PAR (A) and UVAB–PAR (B), and PON under PAR (C) and UVAB–PAR (D) over time in iron-enrichment experiments in water from WIE.

the end of the experiments (Fig. 5A) and POC levels were significantly higher in Fe and FeGA treatments (t-test, $P<0.05$) compared to controls. POC values on day 13 in FeGA and Fe treatments were about. 2.2 and 1.9 times higher, respectively, than the POC in the controls ($P<0.05$). Moreover, on day 13, POC levels were significantly higher in FeGA ($P<0.05$) compared to POC levels in Fe treatments (Fig. 5A). Under UVAB–PAR, carbon build-up was very low in all treatments. However, POC in Fe treatments was ca. 1.8 times higher than that in both FeGA and control treatments ($P<0.05$). The lowest POC was detected in FeGA treatment under UVAB–PAR (Fig. 5B).

Particulate organic nitrogen (PON) showed similar trends as POC. The final PON levels were significantly higher in Fe and FeGA treatments ($P<0.05$). Under PAR, the difference of PON ($90\,mg\,m^{-3}$) between FeGA and controls on day 13 was higher than that between Fe and control treatments ($67\,mg\,m^{-3}$) (Fig. 5C). PON values on day 13 in FeGA and Fe treatments were ca. 2.6 and 2.2 times higher than that in the control, respectively. Under UVAB-PAR, the build-up of N was also very low in all treatments (Fig. 5D)

Primary production rates (based on increases in POC) in Fe and FeGA treatments under PAR were similar and ca. 2.5 times higher than that in the control on day 10. (Fig. 6). On day 13, the primary production rates in the Fe treatments were again ca. 2.5 times higher than that in the control. On the other hand, production rates in the FeGA were ca. 3.5 times higher than the controls. In the SIE, under UVAB–PAR, FeGA and control treatments also yielded the lowest and highest POC buildup, respectively, as in FeGA and C treatments in WIE under UVAB–PAR.

3.4. Chlorophyll-a

Under PAR, Chl-a enhancement clearly resulted from the additions of Fe and especially FeGA in our experiments (Fig. 7A). The levels of Chl-a on days 10 and 13 were significantly higher than the levels of Chl-a in the controls ($P<0.05$). Fe and FeGA treatments showed the largest Chl-a

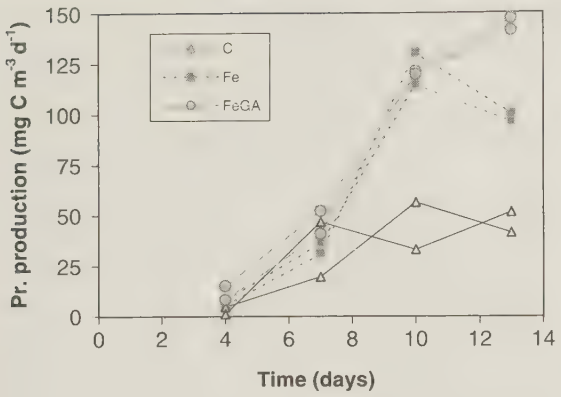

Fig. 6. Estimation of primary production as a function of time based on POC data for all phytoplankton communities in WIE incubations for all PAR treatments.

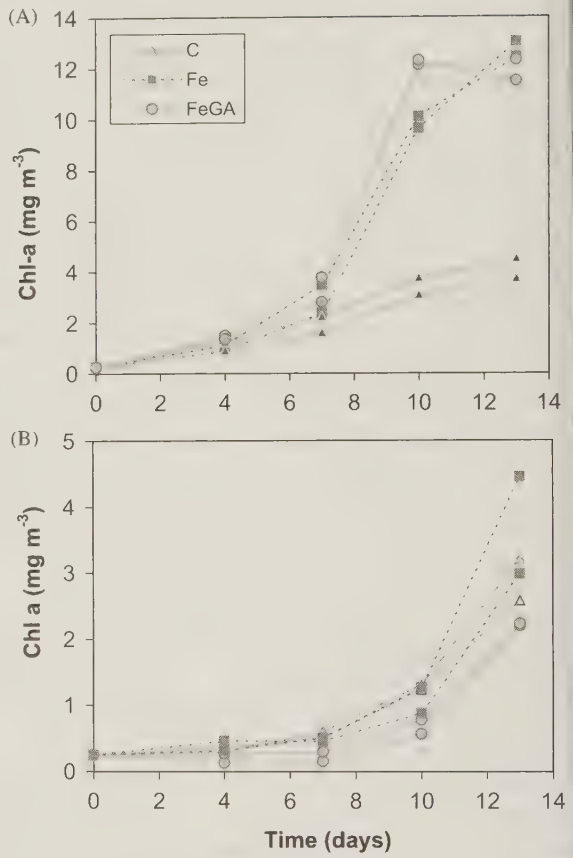

Fig. 7. Chl-*a* increase under PAR (A) and UVAB–PAR (B) in water from WIE.

increase between days 7 and 10. After day 10, the increase was tempered in the Fe treatments and stopped in the FeGA treatments. Chl-*a* concentrations in day 10 in the FeGA and Fe treatments were ca. 3.6 and 2.9 times higher than in the controls, respectively. The highest Chl-*a* production rate ($3.16\,\mathrm{mg\,Chl\text{-}a\,m^{-3}\,d^{-1}}$) was observed between days 7 and 10 in the FeGA treatments, and was ca. 2.3 and $0.5\,\mathrm{mg\,Chl\text{-}a\,m^{-3}\,d^{-1}}$ in the Fe and control treatments, respectively. That is, Chl-*a* production rates in the FeGA and Fe treatments between days 7 and 10 were ca. 6 and 4.6 times higher than that in the control, respectively.

Chl-*a* synthesis was apparently enhanced by Fe enrichment (Fe and FeGA) (Fig. 8A). However, Chl-*a* values under UVAB–PAR are quite low relative to values for corresponding treatments under PAR. In contrast to under PAR treatments, the Chl-*a* concentration began to increase after day 10. FeGA treatments under UVAB–PAR yielded the lowest Chl-*a* build up (Fig. 7B).

Chl-*a* increases resulting from the addition of Fe and FeGA were also evident in SIE PAR and UVA–PAR incubations (data not shown). The enhanced Fe(II) concentration apparently also had an impact on phytoplankton growth in SIE although it does not change the species composition. In SIE incubations, under UVAB–PAR, the highest Chl-*a* build-up was observed in control treatments, and the lowest Chl-*a* build-up was in FeGA treatment as it was in FeGA treatments in WIE incubations under UVAB–PAR.

The ratio of Chl-*a* production rates (PR-Chl-*a*) between FeGA and the control, and between Fe and the control treatments (FeGA/control and Fe/control) during exponential growth in WIE under PAR were higher than the corresponding ratios for carbon production rates (PR-POC):

$$\{PR-Chl-a_{FeGA} : PR-Chl-a_{cont.}\} : \{PR-POC_{FeGA} : PR-POC_{cont.}\} \cong 2.4$$

and

$$\{PR-Chl-a_{Fe} : PR-Chl-a_{cont.}\} : \{PR-POC_{Fe} : PR-POC_{cont.}\} \cong 1.8.$$

This possibly indicates that Fe enrichment first triggered Chl-*a* synthesis and then the biomass

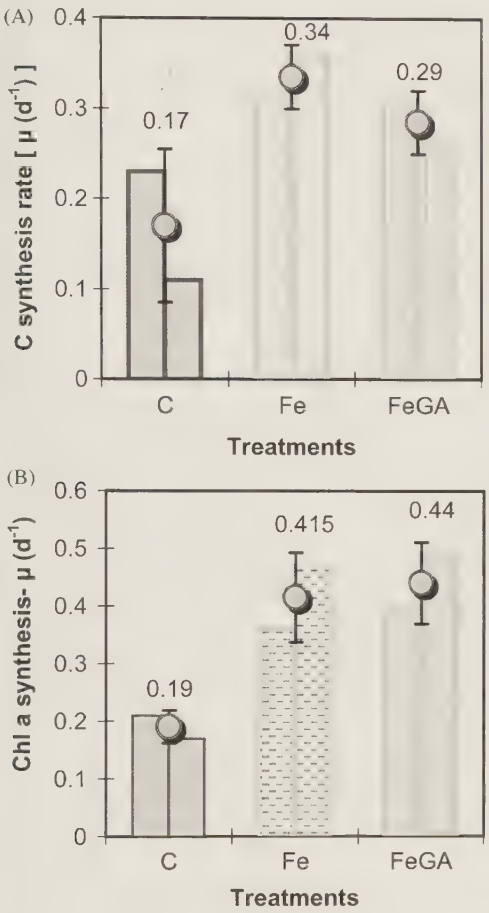

Fig. 8. Rates of Chl-*a* (A) and carbon synthesis during exponential growth in water from WIE under PAR.

increase. This effect was most pronounced in the FeGA treatments in WIE under PAR. Moreover, the rates of Chl-*a* synthesis in FeGA were slightly higher than those in the Fe treatments (Fig. 8A). The C:Chl-*a* ratios indicate that production of Chl-*a* is fastest in the Fe treatments, especially in the FeGA treatments in WIE under PAR.

3.5. Nutrients

Our results showed a significant increase of nutrient uptake by phytoplankton in Fe and FeGA treatments compared to the controls under PAR (Fig. 9A and B) (*t*-test, $P<0.05$ for both NO_3+NO_2 and Si). Towards the end of the experiment (day 13), removal of NO_3+NO_2 in FeGA, Fe, and control treatments were ca. 24, 23 and 12 mmol m^{-3}, respectively. Similarly, Si in FeGA, Fe and controls treatments decreased from ca. 60 mmol m^{-3} to ca. 15, 21 and 33 mmol m^{-3}, respectively (Fig. 9B). The removal of Si in FeGA was significantly higher than the removal of Si in Fe treatments ($P<0.05$). Despite the fact that diatoms species were not dominant in the controls under PAR, removal of Si was considerably high in control treatments (Fig. 9B). During the incubations under PAR, Si removal values against C build-up (ΔSi:ΔPOC) are 0.9 ± 0.03, 0.6 ± 0.02 and 0.57 ± 0.01 for control, Fe and FeGA treatments, respectively. The highest ΔSi:ΔPOC ratio in control indicates that Si uptake is increased with Fe stress. This is in agreement with the observation that diatoms from low-Fe waters do have high Si cell quotas (Hutchins and Bruland, 1998; Boyle, 1998). The decrease of NO_3+NO_2 was between ca. 5 (in FeGA) and 8 mmol m^{-3} (in Fe and control) under UVAB–PAR (Fig. 9C). These were quite low values compared to the decrease in NO_3+NO_2 in all treatments under PAR. Removals of Si under UVAB–PAR are ca. 10, 8 and 7 mmol m^{-3} in the control, Fe and FeGA treatments. These are low, nevertheless considerable values. Although the diatom community was not high in these treatments UV stress might have caused heavier silicification per diatom as light, temperature, N and iron stress (Flynn and Martin-Jézéquel, 2000) in the treatments under UVAB–PAR.

3.6. Bacteria

Under PAR, both the FeGA and the Fe treatments resulted in an enhanced yield of bacterial cells. The average cell counts were approximately 2.4-and 2-fold of the control levels, respectively (Fig. 10A). At the end of experiment, bacterial production in Fe and FeGA treatments was significantly higher than that of controls ($P<0.05$). There was a strong increase in bacterial productivity in Fe treatments compared to the production in the FeGA treatment and in the controls (Fig. 10c). This increase in bacterial production coincided with a decrease in primary

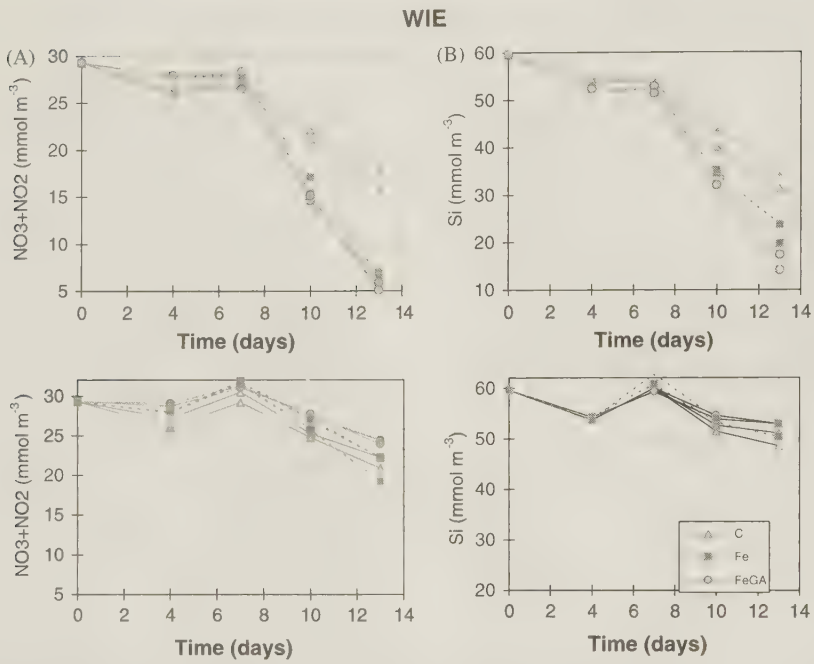

Fig. 9. The decrease in concentrations of $NO_3 + NO_2$ (A) and Si (B) under PAR, and $NO_3 + NO_2$ (C) and Si (D) under UVAB–PAR over time in water from WIE.

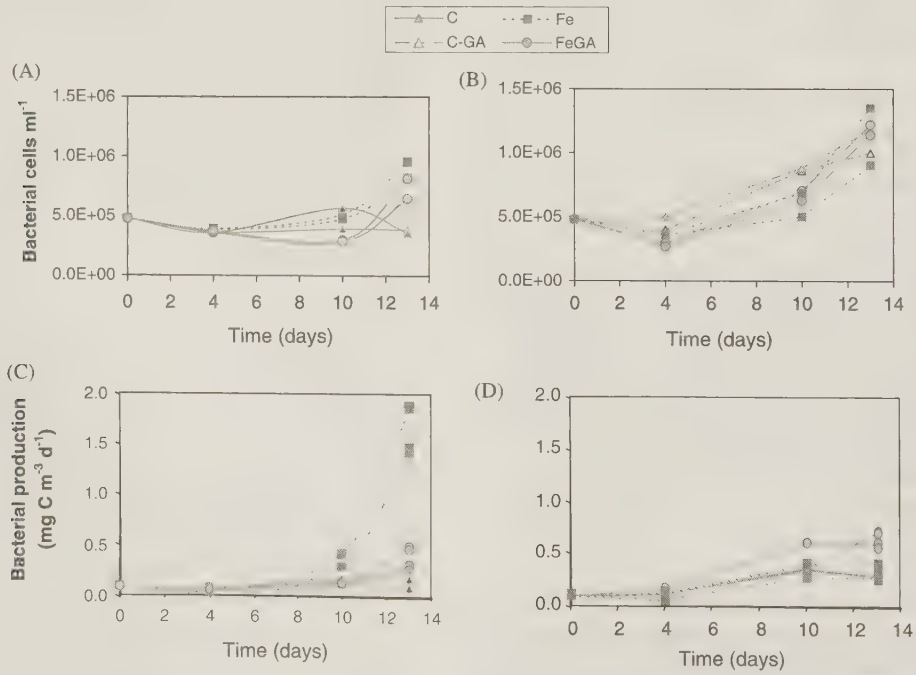

Fig. 10. Bacterial cell numbers under PAR (A) and UVAB PAR (B) in water from WIE, and bacterial production under PAR (C) and UVAB–PAR (D) in water from WIE.

roductivity in incubations enriched with Fe under 'AR (Fig. 6).

Under UVAB–PAR, bacterial density (Fig. 10B) id not differ between treatments. On the other and, at the end of experiment, bacterial productivity in FeGA (Fig. 10D) was significantly higher ($P<0.05$) than that in the Fe treatments and ontrols. A moderate increase both in bacterial cell lensity and bacterial productivity was observed in he last part of the incubation period for all reatments.

The role of bacteria in the elemental cycles, the egeneration of nutrients, and in the trophodynamics of marine ecosystems is widely recognized Pakulski et al., 1996; Tortell et al., 1999). However, in most of the deck experiments related o iron-deficient HNLC zones, data on bacterial esponses to addition of Fe have been obtained in very few studies (Pakulski et al., 1996; Tortell et al., 1999). The stimulatory effects of iron enrichment on bacterial growth could be both direct and indirect results of the Fe enrichment; Fe could directly increase the bacterial growth by being an essential nutrient, while it also increases the amount of bioavailable organic matter as a result of Fe-induced phytoplankton growth and organic matter release.

In Fe treatments under PAR in the WIE, there was much stronger bacterial response to the iron enrichment compared to the FeGA treatments, even though the FeGA treatments were enriched with extra organic matter (glucaric acid). However, the considerably higher phytoplankton growth in this treatment (compared to the Fe treatment) suggests that bacteria and phytoplankton may compete for iron, and that the speciation of iron influences the ability of these organisms to compete for this nutrient. There are some reports showing an increase in bacterial growth rate with iron experiments conducted in the dark (no extra organic matter from enhanced photosynthetic production) (Pakulski et al., 1996). Hence, it is likely that the direct effect of iron (especially Fe (III) in Fe treatments) on bacterial production is important. Our data are not sufficient to make conclusive suggestions on the role of Fe on bacterial growth and the role of bacteria in the cycling of Fe in the euphotic layer of the Southern Ocean. However, we believe that the role of bacteria in the biogeochemical cycling of Fe deserves further attention, particularly with respect to possible competition between bacteria and phytoplankton for iron as a scarce resource.

3.7. Total dissolved inorganic carbon (ΣCO_2)

ΣCO_2 was determined only for the WIE experiments. The significant decrease in ΣCO_2 was observed in FeGA treatments (ca. 140 mmol m^{-3} during incubation) and in Fe (ca. 100 mmol m^{-3}) treatments under PAR (Fig. 11). ΣCO_2 decrease in control treatments was around 40 mmol m^{-3}. Under UVAB–PAR, a small decrease in ΣCO_2, ca. 13 mmol m^{-3} ,was observed in the controls. Fe additions did not cause any change in ΣCO_2.

When we compare POC accumulation and decrease in ΣCO_2 in all treatments in WIE experiments, the ratio of POC accumulation to ΣCO_2 decrease in FeGA, Fe and control under PAR is found to be 0.59, 0.64 and 0.73, respectively. The difference between ΣCO_2 decrease and accumulated POC can be attributed to the production of dissolved organic carbon (DOC), implying that DOC production in FeGA, Fe and control under PAR in WIE experiments may constitute 41%, 36% and 27% of total fixed carbon, respectively. This is important to understand the effect of Fe enrichments on CO_2 flux in euphotic zones. Since biologically labile DOC will eventually turn back relatively quickly into the pool

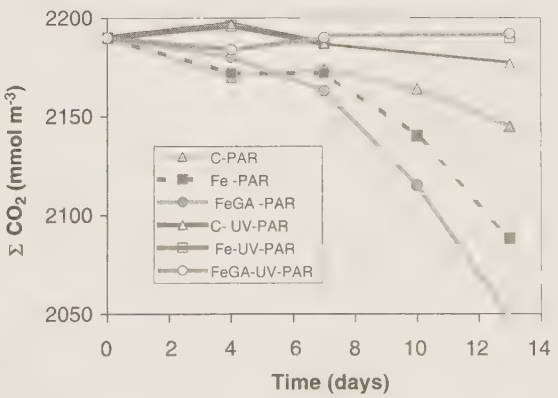

Fig. 11. Decreases in total dissolved inorganic carbon (ΣCO_2) under PAR and UVAB–PAR in iron-enrichment experiments in water from WIE.

of ΣCO_2, and only refractory DOC and sinkable POC contributes to the export of ΣCO_2 from surface water to deep water and sediment as a POC, it is important to understand the qualitative and quantitative DOC production compared to POC production due to enhancement of phytoplankton productivity with the enrichment of Fe.

4. Conclusions

Our enrichment experiments indicate that Fe and FeGA enrichments significantly increase phytoplankton biomass build-up and cause a higher growth rate compared to control treatments in the WIE under PAR (and, to some extent, in SIE under UVA–PAR). This implies that iron has an important role as a limiting factor, especially in the WIE of the Southern Ocean. Most of the biomass increase in Fe and FeGA treatments was due to diatoms $>20\,\mu m$, suggesting that this diatom community was particularly limited by the supply of Fe.

In the WIE under PAR, Fe stimulated Chl-*a* synthesis prior to carbon build-up. The effect of GA on the availability of Fe appears to be considerable. This could be explained by the effects of GA on the Fe(III) photoreduction by primary photochemical processes. Secondary processes (by photochemically produced radicals) may play some role for observable Fe(II) but their mechanisms are not yet fully understood. These mechanisms may enhance the production of available iron and make Fe(II) available from a pool of Fe(III) which is already present.

Apparently, the primary and secondary photochemical reduction of Fe(III) and re-oxidation of Fe(II) by photochemically produced radicals are affected by the spectral quality of light, speciation of Fe(III) and DOM, as well as by competitive reactions of DOM, Fe(III) and Fe(II) with photochemically produced radicals.

The role of iron for the formation of peroxide and hydroxide–superoxide radicals seems insignificant under PAR. On the contrary, under UV secondary oxidation of Fe(II) by photochemically produced radicals probably is an important sink for both Fe(II) and H_2O_2.

Related to UV and PAR dependence of iro photoreduction, our preliminary data did not sho whether any particular wavelength band can reduc Fe(III) more effectively than others. Contrary t expectations of more effective photoreduction c Fe(III) in both UVB and UVA (based on dat from inorganic Fe photoreduction experiments Stumm and Morgan, 1996), our results show tha the presence of GA causes efficient photoreductio of Fe(III) under PAR as well as in UV.

Both in the WIE and SIE, in incubation exposed to UVAB–PAR, FeGA treatments in variably yielded the lowest phytoplankton produc tivity. Thus the protective mechanism o phytoplankton to UV seems to be affected b FeGA. Fe photoreduction may enhance the negative effects of UV, contrary to the anticipation that the detrimental effects of UVB in the South ern Ocean could be counteracted by the photo reduction of iron (Palenik et al., 1991) as a result of increased photoreductive dissolution of Fe(III) under UV. This point needs further investigation.

Acknowledgments

We thank and acknowledge Sten-Åke Wängberg for providing us with his light data. We thank chief scientist David Turner and the rest of the scientific party, especially Wilhelm Granéli and Fred Sörensson for their help. We are indebted to Melissa Chierici for her involvement in the total inorganic carbon determination. We thank Eiliv Steinnes for critically reviewing the manuscript and Can Bizsel for his help for the statistical work. We are grateful to the crew of S.A. *Agulhas* for the pleasant cooperation during the cruise. The funding for this work was provided by grants from the Norwegian Polar Institute, Project No. NARE 97/98-3824. Finally, we are grateful to the two anonymous referees for their helpful comments concerning the first version of this paper.

References

Bakker, D.C.E., de Baar, H.J.W., Bathmann, U.V., 1997. Changes of carbon dioxide in surface waters during spring in the Southern Ocean. Deep-Sea Research II 44, 91–127.

Banse, K., 1990. Does iron really limit phytoplankton production in the offshore subarctic Pacific? Limnology and Oceanography 35, 772–775.

Behrenfeld, M.J., Bale, A.J., Kolber, Z.S., Aiken, J., Falkowski, P.G., 1996. Confirmation of iron limitation of phytoplankton photosynthesis in the equatorial Pacific Ocean. Nature 383, 508–511.

Boyle, E., 1998. Pumping iron makes thinner diatoms. Nature 393, 733–734.

Coale, K.H., 1991. Effects of iron, manganese, copper, and zinc enrichments on productivity and biomass in the subarctic Pacific. Limnology and Oceanography 36, 1851–1864.

Coale, K.H., Johnson, K.S., Fitzwater, S.E., Gordon, R.M., Tanner, S., Chavez, F.P., Ferioli, L., Sakamoto, C., Rogers, P., Millero, F., Steinberg, P., Nightingale, P., Cooper, D., Cochlan, W.P., Landry, M.R., Constantinou, J., Rollwagen, G., Trasvina, A., Kudela, R., 1996. A massive phytoplankton bloom induced by an ecosystem-scale iron fertilization experiment in the equatorial Pacific Ocean. Nature 383, 495–501.

del Giorgio, P., Bird, D., Prairie, Y.T., Planas, D., 1996. Flow cytometric determination of bacterial abundance in lake plankton with the green nucleic acid stain Syto 13. Limnology and Oceanography 41, 783–789.

Duce, R.A., Tindale, N.W., 1991. Atmospheric transport of iron and its deposition in the ocean. Limnology and Oceanography 36, 1715–1726.

El Sayed, S.Z., 1988. Productivity of the Southern Ocean: a closer look. Comparative Biochemistry and Physiology 90, 489–498.

Faust, B.C., Zepp, R.G., 1993. Photochemistry of aqueous iron(III)-polycarboxylate complexes: roles in the chemistry of atmospheric and surface waters. Environmental Science and Technology 27, 2517–2522.

Flynn, K.J., Martin-Jézéquel, V., 2000. Modelling Si-N-limited growth of diatoms. Journal of Plankton Research 22, 447–472.

Holm-Hansen, O., Mitchell, B.G., Hewes, C.D., Karl, D.M., 1989. Phytoplankton blooms in the vicinity of Palmer Station, Antarctica. Polar Biology 10, 49–57.

Hudson, R.J.M., Covault, D.T., Morel, F.M.M., 1992. Investigations of iron coordination and redox reactions in seawater using iron-59 radiometry and ion-pair solvent extraction of amphiphilic iron complexes. Marine Chemistry 38, 209–235.

Hutchins, D.A., Bruland, K.W., 1998. Iron-limited diatom growth and Si/N uptake ratios in a coastal upwelling regime. Nature 393, 561–564.

King, D.W., Lounsbury, H.A., Millero, F.J., 1995. Rates and mechanism of Fe(II) oxidation at nanomolar total iron concentrations. Environmental Science and Technology 29, 818–824.

Kuma, K., Nakabayashi, S., Suziki, Y., Kudo, I., Matsunaga, K., 1992. Photo-reduction of iron(III) by dissolved organic substances and existence of iron(II) in seawater during spring blooms. Marine Chemistry 37, 15–27.

Kuma, K., Nakabayashi, S., Matsunaga, K., 1995. Photoreduction of Fe(III) by hydroxycarboxilic acids in seawater. Water Research 29, 1559–1569.

Lancelot, C., Billen, G., 1985. Carbon–nitrogen relationships in nutrient methabolism of coastal marine ecosystems. Advances in Aquatic Microbiology 3, 263–321.

Löscher, B.M., de Baar, H.J.W., de Jong, J.T.M., Veth, C., Dehairs, F., 1997. The distribution of Fe in the Antarctic Circumpolar Current. Deep-Sea Research II 44, 143–187.

Martin, J.H., Gordon, R.M., Fitzwater, S.E., 1990. Iron in Antarctic waters. Nature 345, 156–158.

Martin, J.H., Coale, K.H., Johnson, K.S., Fitzwater, S.E., Gordon, R.M., Tanner, S.J., Hunter, C.N., Elrod, V.A., Nowicki, J.L., Coley, T.L., Barber, R.T., Lindley, S., Watson, A.J., Van Scoy, K., Law, C.S., Liddicoat, M.I., Ling, R., Stanton, T., 1994. Testing the iron hypothesis in ecosystems of the equatorial Pacific Ocean. Nature 371, 123–129.

Miller, W.L., Kester, D., 1994a. Photochemical iron reduction and iron bioavailability in seawater. Journal of Marine Research 52, 325–343.

Miller, W.L., Kester, D., 1994b. Peroxide variations in the Sargasso Sea. Marine Chemistry 48, 17–29.

Millero, F.J., Sotolongo, S., Izaguirre, M., 1987. The kinetics of oxidation of Fe(II) in seawater. Geochimica et Cosmochimca Acta 51, 793–801.

Morel, F.M.M., Hudson, R.J.M., Price, N.M., 1991. Limitation of productivity by trace metals in the sea. Limnology and Oceanography 36, 1742–1755.

O'Sullivan, D.W., Hanson, A.K., Kester, D.R., 1995. Stopped flow luminol chemiluminescence determination of Fe(II) and reducible Fe in seawater at subnanomolar levels. Marine Chemistry 49, 65–77.

Pakulski, J.D., Coffin, R.B., Kelley, C.A., Holder, S.L., Downer, R., Aas, P., Lyons, M.M., Jeffrey, W.H., 1996. Iron stimulation of Antarctic bacteria. Nature 383, 133–134.

Palenik, B., Price, N.M., Morel, F.M.M., 1991. Potential effects of UV-B on the chemical environment of marine organism: a review. Environmental Pollution 70, 117–130.

Powell, R.T., King, D.W., Landing, W.M., 1995. Iron distributions in surface waters of the South Atlantic. Marine Chemistry 50, 13–20.

Sakshaug, E., Holm-Hansen, O., 1984. Factors governing pelagic production in Polar Oceans. In: Holm-Hansen, O., Bolis, L., Gilles, R. (Eds.), Marine Phytoplankton and Productivity, Lecture Notes on Coastal and Estuarine Studies, vol. 8. New York, Springer, pp. 1–18.

Sakshaug, E., Slagstad, D., Holm-Hansen, O., 1991. Factors controlling the development of phytoplankton blooms in the Antarctic Ocean–a mathematical model. Marine Chemistry 35, 259–271.

Scharek, R., van Leeuwe, M.A., de Baar, H.J.W., 1997. Responses of Antarctic Ocean phytoplankton to the addition of trace metals. Deep-Sea Research II 44, 209–227.

Smith, D.C., Azam, F., 1992. A simple economical method for measuring bacterial protein synthesis rates in seawater using 3H Leucine. Marine Microbial Food Webs 6, 107–109.

Stumm, W., Morgan, J.J., 1996. Aquatic Chemistry, third ed. Wiley, New York, 1022pp.

Sunda, W.G., Swift, D.G., Huntsman, S.A., 1991. Low iron requirement for growth in oceanic phytoplankton. Nature 351, 55–57.

Tortell, P.D., Maldonado, M.T., Granger, J., Price, N.M., 1999. Marine bacteria and biogeochemical cycling of iron in the oceans. FEMS Microbiology Ecology 29, 1–11.

Turner, D.R., Bertilsson, S., Fransson, A., Pakhomov, E., 2004. The SWEDARP 97/98 marine expedition: overview. Deep-Sea Research II, this issue [doi:10.1016/j.dsr2.2003.08.006].

van Leeuwe, M.A., Scharek, R., de Baar, H.J.W., de Jong, J.T.M., Goeyens, L., 1997. Iron enrichment experiments in the Antarctic Ocean: physiological responses of plankton communities. Deep-Sea Research II 44, 189–207.

Verity, P.E., Villareal, T.A., Smayda, T.J., 1988. Ecological investigations of blooms of colonial *Phaecystis pouchetii*- I- Abundance, biochemical composition, and metabolic rate Journal of Plankton Research 10, 219–248.

Voelker, B.M., Sedlak, D.L., 1995. Iron reduction by phot produced superoxide in seawater. Marine Chemistry 5 93–102.

Voelker, B.M., Morel, F.M.M., Sulzberger, B., 1997. Irc redox cycling in surface waters: effects of humic substanc and light. Environmental Science and Technology 3 1004–1011.

Wängberg, S.-Å., Wulff, A., 2004. Impact of Ultraviolet- radiation on the development of phytoplankton commu nities in the eastern Atlantic sector of the Southern Ocean– results from on-deck model ecosystem experiments. Deep Sea Research II, this issue [doi:10.1016/j.dsr2.2001.05.001]

Zhuang, G., Zhen, Y., Wallace, G.T., 1995. Iron(II) i rainwater, snow, and surface seawater from a coasta environment. Marine Chemistry 50, 41–50.

ELSEVIER

Deep-Sea Research II 51 (2004) 2857–2879

DEEP-SEA RESEARCH
PART II

www.elsevier.com/locate/dsr2

The distribution and speciation of iron along 6°E in the Southern Ocean

Peter L. Croot[a,*], Karen Andersson[a], Murat Öztürk[b], David R. Turner[a]

[a]*Department of Chemistry, Analytical and Marine Chemistry, Göteborg University, SE-412 96 Göteborg, Sweden*
[b]*Trondheim Biological Station, Norwegian University of Science and Technology, Bynesvägen 46, N-7018 Trondheim, Norway*

Abstract

The distribution and speciation of iron was determined along a transect in the eastern Atlantic sector (6 E) of the Southern Ocean during a collaborative Scandinavian/South African Antarctic cruise conducted in late austral summer (December 1997/January 1998). Elevated concentrations of dissolved iron (>0.4 nM) were found at 60 S in the vicinity of the Spring Ice Edge (SIE) in tandem with a phytoplankton bloom, chiefly dominated by *Phaeocystis* sp. This bloom had developed rapidly after the loss of the seasonal sea ice cover. The iron that fuelled this bloom was mostly likely derived from sea ice melt. In the Winter Ice Edge (WIE), around 55°S, dissolved iron concentrations were low (<0.2 nM) and corresponded to lower biological productivity, biomass. In the Antarctic Polar Front, at approximately 50°S, a vertical profile of dissolved iron showed low concentrations (<0.2 nM); however, a surface survey showed higher concentrations (1 3 nM), and considerable patchiness in this dynamic frontal region. The chemical speciation of iron was dominated by organic complexation throughout the study region. Organic iron-complexing ligands ([L]) ranged from 0.9 to 3.0 nM Fe equivalents, with complex stability $\log K'_{Fe'L} = 21.4-23.5$. Estimated concentrations of inorganic iron (Fe′) ranged from 0.03 to 0.79 pM, with the highest values found in the *Phaeocystis* bloom in the SIE. A vertical profile of iron-complexing ligands in the WIE showed a maximum consistent with a biological source for ligand production and near surface minimum possibly consistent with loss via photodecomposition. This work further confirms the role iron that has in the Southern Ocean in limiting primary productivity.
© 2004 Elsevier Ltd. All rights reserved.

1. Introduction

Iron, one of the most important trace metals in marine biogeochemistry, is now known to be a potentially limiting element in the ocean. Iron limitation has been shown to control phytoplankton stocks in high nutrient low chlorophyll (HNLC) regions (Boyd et al., 2000; Coale et al.,

*Corresponding author. Present address: Leibniz-Institut für Meereswissenschaften, Düsternbrooker Weg 20, D-24105 Kiel, Germany. Tel.: +49 431 600 4207; fax: +49 431 600 4202.
E-mail address: pcroot@ifm-geomar.de (P.L. Croot).

0967-0645/$ - see front matter © 2004 Elsevier Ltd. All rights reserved.
doi:10.1016/j.dsr2.2003.10.012

1996a; Martin et al., 1989), in some coastal regions (Hutchins et al., 1998), and possibly also in some oligotrophic oceans (Behrenfeld and Kolber, 1999). Iron limitation in the Australian sector of the Southern Ocean has recently been dramatically demonstrated during the Southern Ocean IRon Enrichment Experiment (SOIREE) (Boyd et al., 2000), where a large phytoplankton bloom was initiated after iron fertilization.

The Southern Ocean is an important component of the global climate system, particularly in its role in buffering heat and atmospheric CO_2, in the formation of Antarctic Bottom water. Its influence on the biological pump is currently of considerable interest, as the Southern Ocean could potentially remove some anthropogenic CO_2 from the atmosphere into deep waters (Watson et al., 2000). Iron fertilization of the Southern Ocean has also been suggested as a possible mechanism for the decrease in atmospheric CO_2 during the last glacial maximum (Martin, 1990). The Southern Ocean is the largest of the HNLC regions on the globe; the high levels of nitrate (and phosphate) south of the Polar Front that persist have suggested many potential limiting processes for the low biomass maintained (Smetacek et al., 1997). In the Southern Ocean, the complex relationships between iron, light and mixed layer depth create a dynamic environment, which control phytoplankton biomass, upon which the presence of grazers exerts a further influence. The present study, which was undertaken in the framework of the international Joint Global Ocean Flux Study (JGOFS), seeks to address the cycling of carbon in different regions of the Southern Ocean. In particular, this work seeks to examine the role of iron in controlling phytoplankton biomass and productivity.

Our understanding of the marine biogeochemistry of iron has undergone a major revision in the past two decades (Wells et al., 1995). Iron in oxic seawater exists as either of the two redox species, Fe^{II} or Fe^{III}, with Fe^{III} being the thermodynamically favoured form, but it is only weakly soluble in seawater compared to Fe^{II}. Fe^{II}, the more readily bioavailable form, is presently thought to be a reactive intermediate in iron cycling, primarily generated by photochemical processes (Johnson et al., 1994), existing at extremely low concentrations (picomolar or less) in oxic seawater because of rapid oxidation by O_2 and H_2O_2 in warm waters (Millero and Sotolongo, 1989; Millero et al. 1987). However, recent work (Croot et al., 2001) performed during SOIREE has shown evidence for the persistance and production of Fe^{II} in the cold Southern Ocean waters, where oxidation rates are significantly lower. The oxidation of Fe^{II} to the less soluble Fe^{III} species leads to the formation of colloidal oxyhydroxide (Kuma et al., 1996) species which coagulate and form particulate iron (Johnson et al., 1997).

Dissolved iron is strongly complexed (Croot and Johansson, 2000; Gledhill and van den Berg, 1994; Rue and Bruland, 1995) by organic chelators, probably produced by iron-limited heterotrophic bacteria or phytoplankton (Rue and Bruland, 1997). The presence of these ligands increases the solubility of iron in seawater (Croot et al., 2001; Kuma et al., 1996), thus maximizing the dissolved iron concentration; in this way, it may act as a mechanism to maintain bioavailable iron for phytoplankton/bacteria. However, Hutchins et al. (1999) reported that prokaryotic and eukaryotic phytoplankton have different abilities to obtain iron bound to siderophores and porphyrin complexes, suggesting a competitive advantage for algal species that can obtain iron from specific ligands. In the HNLC regions, bacteria compete directly with phytoplankton for iron and can account for 20–45% of the uptake (Kirchman, 1996). Particulate iron can also be transformed into dissolved or bioavailable iron by ligand promoted dissolution (Croot and Johansson, 2000), protozoan (Barbeau et al., 1996) or zooplankton grazing (Hutchins and Bruland, 1994). Thus, interactions between microbial processes and iron chemistry appear to determine the biogeochemistry of iron in oceanic waters (Geider, 1999; Kirchman, 1996).

There have been several previous studies on the distribution of iron in the Southern Ocean (Bucciarelli et al., 2001; de Baar et al., 1999; de Jong et al., 1997; Löscher et al., 1997; Martin et al., 1990; Sarthou et al., 1997; Sedwick and DiTullio, 1997; Sedwick et al., 1997; Sohrin et al., 2000). In the Southern Ocean, dissolved iron in the near surface water is generally found at very low

oncentrations (<0.2 nM) throughout the circum-olar ocean. Only in island wakes (Bucciarelli t al., 2001), coastal shelves (Sedwick and DiTullio, 1997) and in the vicinity of the Polar Front in the Atlantic sector (Löscher et al., 1997) ignificantly high values (>0.6 nM) have been ncountered. There have been only a few iron peciation studies performed in Southern Ocean vaters (Boye et al., 2001; Croot et al., 2001; Nolting et al., 1998). In all these studies, the researchers found that there was an excess of iron-complexing ligands, and that the chemical specia-ion of iron was dominated by organic complexa-ion. In this work, we present data on the upper ocean distribution and speciation of iron along a ransect at 6°E in the Atlantic sector of the Southern Ocean.

2. Materials and methods

2.1. Sampling

2.1.1. Study area

Samples were collected during the austral summer, from December 31, 1997 to January 25, 1998, during the joint Scandinavian/South African expedition aboard the S.A. *Agulhas*. The research area was situated in the Atlantic sector of the Southern Ocean, along a survey transect along the 6°E meridian from south to north (Turner et al., 2004). The stations sampled for Fe are shown in Fig. 1.

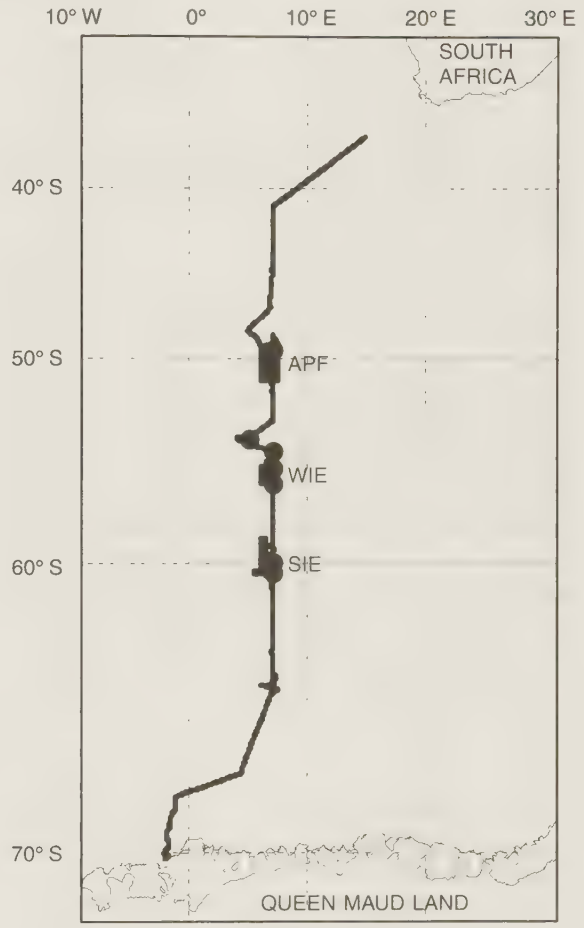

Fig. 1. Cruise track showing stations sampled for Fe.

2.1.2. Sampling-vertical profiles

Seawater samples were taken with pre-cleaned GoFlo samplers (8 L) mounted on an 8 mm Kevlar hydrowire. At each station, eight samples were collected with Kevlar wire at standard depths (10–30–50–100–150–200–300–400 m). Each cast consisted of only two GoFlo bottles, so four casts were needed to complete each station.

Immediately upon recovery, the GoFlo sampler was wrapped in clean plastic bags and transferred into a Class-100 clean air laboratory container (Danielsson and Westerlund, 1983). All sample manipulations were undertaken inside the Class-100 clean air laboratory. Pressure lines with high-purity nitrogen gas passing over fine particle arrestance filters were attached to the top of the samplers to allow for filtration by an over pressure of ≈0.5 bar. Seawater was filtered over acid-cleaned Nuclepore membrane filters (47 mm, 0.4 μm), mounted in all-Teflon filter holders (Savillex). In addition, seawater samples were taken without filtering. The filtered or unfiltered seawater was collected into 500 mL or 1 L acid-cleaned PE bottles. All sample manipulations were carried out inside a Class-100 portable laminar flow hood (Interflow B.V., The Netherlands). All sample bottles were double bagged (Ziplok) and quick frozen for subsequent analysis in the laboratory in Sweden.

2.1.3. Sampling-underway samples collected by towed fish

In the polar frontal region, surface samples were collected using a towed fish (V-fin, Endeco/YSI, USA). The V-fin was towed at 6–8 knots from the starboard CTD winch, approximately amidships, onboard the S.A. *Agulhas*. The V-fin was kept at 1–2 m depth and adjusted so that it was always 6 m or more from the side of the ship at all times. The V-fin was equipped with an all-Teflon sampling nozzle, which was located at the front of the fin, so as to continually sample clean water. Seawater samples were pumped to the deck from the V-fin, using a peristaltic pump (Masterflex, L-07591-15) and acid-cleaned polyethylene tubing. All sample manipulations were carried out inside a Class-100 portable laminar flow hood (Interflow B.V., The Netherlands). Sub-samples (unfiltered) of the continuous flowing seawater were taken at the appropriate time by filling an acid-cleaned 500 mL PE bottle. The bottle was then double bagged (Ziplok) and quick frozen for later analysis in the laboratory in Sweden.

2.1.4. Reagents and plasticware

All solutions were prepared using 18 MΩ Milli-Q water (Millipore system), denoted hereafter as MQ water. Quartz distilled acids (denoted by prefix Q) were made by re-distillation of Merck trace-metal grade acids in a quartz sub-boiling still. In this way, Q-HNO_3 (12 M), Q-HCl (6 M) and Q-acetic acid (17.4 M) were prepared and stored in clean double bagged Teflon bottles. Ultra-clean isothermally distilled ammonium hydroxide was purchased from J.T. Baker. All the plasticwares (LDPE, Teflon) used in this study were cleaned by a sequential soaking procedure, modified from early work by Bruland et al. (1979). In brief, the protocol was as follows: detergent rinse, MQ rinse, soak, soak in cold 10% (v/v) hydrochloric acid for at least 1 month, MQ rinse and finally store with a 1% Q-HCl solution. Nitric acid was not used in the cleaning procedure for the LDPE bottles for fear that residual nitric acid in the plastic may leach out, altering the redox speciation of the samples (Landing and Lewis, 1991).

2.1.5. Nutrients and CTD

Salinity and temperature profiles were measure on separate CTD casts at each station using a Ne Brown MK II CTD. Separate salinity measure ments were made on samples from the GoFlo From the CTD casts, samples were analysed fo the macronutrients (nitrate, nitrite, silicate) using Technicon II Autoanalyser following the method of (Strickland and Parsons, 1968). NH_4^+ was no measured at these stations. Chlorophyll *a* (Chl *a*) accessory pigments were measured by standard HPLC techniques (Wulff and Wängberg, 2004). O_2 data were measured by an automated Winkler titration (Chierici et al., 2004).

2.1.6. Satellite data

SeaWiFS images (level 2, browse) were obtained from the SeaWiFS website and the images were reprocessed using SeaDAS (Baith et al., 2001). Daily satellite passes through the study region was combined into a single composite image for each day, these composites were then combined and averaged to produce weekly or monthly images.

2.2. Measurement of iron concentration and speciation

2.2.1. Measurement of dissolved and total iron

During this cruise and in the land-based laboratory, Fe measurements were made using a luminol-based chemiluminescent flow injection technique modified from the one used by Powell et al. (1995). This method is based on the catalytic oxidation of luminol by Fe(II) emitting blue light ($\lambda_{max} \sim 440$ nm) (Bowie et al., 1998; Croot and Laan, 2002). For the analysis of total iron, Fe(III) is first reduced to Fe(II) using the reducing agent sodium sulfite and then Fe(II) is extracted from the sea salt matrix and pre-concentrated in-line onto an 8-hydroxyquinoline resin. Fe(II) is then eluted from the column with a weak acid prior to detection of the light on mixing with the luminol reagent system. Full details of the method used here can be found in the work by Croot et al. (2002).

In this study, the frozen seawater samples were first thawed and then acidified with 1 mL Q-HCl per litre of seawater. The samples were then kept

acidified for a minimum of a week, though typically 2 months, before analysis. Immediately prior to analysis the samples were buffered to pH 4.5 with ammonium acetate and the sulphite-reducing reagent was added. After a suitable time for the complete reduction of Fe(III) to Fe(II), 1–2 h, the samples were measured in triplicate using the method of standard additions. Analysis of the certified reference materials NASS 4 (our value: 1.87 ± 0.08; certified value: 1.88 ± 0.29), NASS 5 (our value: 3.65 ± 0.27; certified value: 3.71 ± 0.63) were undertaken as an internal check. The system blank was determined to be 0.04 ± 0.02 nM (3 s.d.) and sample values were corrected for the system blank. Precision on replicate samples was found to be better than 7% at the 0.4 nM level.

2.2.2. Electrochemical measurements

The voltammetric equipment consisted of a Metrohm VA 663 Stand, with a hanging mercury drop electrode (HMDE), glassy carbon working electrode, Ag/AgCl reference electrode and an Ecochemie μAutolab voltammeter. The potentiostat setting as well as stirring, de-aeration, timing and the HMDE was computer controlled (Ecochemie, General Purpose Electrochemical system, version 4.4, 1997). The iron speciation reagents, 2-(2thiazolylazo)-*p*-cresol (TAC) and 1-nitroso-2-napthol (1N2N), were purchased from Sigma, and prepared as described in Croot and Johansson (2000) and Gledhill and van den Berg (1994), respectively. Trace-metal clean buffers were prepared according to the protocols found in the work by Croot and Johansson (2000).

2.2.3. Determination of iron speciation using competitive ligand exchange cathodic stripping voltammetry (CLE-CSV)

In this study, two competitive ligands (TAC, 1N2N) were used separately to determine iron speciation in the water samples. The same overall procedure was used for both ligands, except for the stripping parameters which were in accordance with the previously published protocols for TAC (Croot and Johansson, 2000) and 1N2N (Gledhill and van den Berg, 1994). A brief description of the procedure for TAC is listed here: sub-samples (20 mL) of seawater were pipetted into a series of pre-cleaned Teflon bottles (125 mL) and 100 μL of 1 M EPPS added. Iron was added to all but two of the bottles, yielding concentrations from 0 to 12 nM. The added Fe was allowed to equilibrate with the natural ligands for 1 h at laboratory temperature. At the end of this equilibration period, 20 μL of 10 mM TAC (or 1N2N) was added, and the sample was left to equilibrate for a minimum of 5 h, though typically overnight. The samples were then transferred to the Teflon cell cup, the sample de-aerated for 4 min with dry nitrogen gas and subsequently, the $Fe(TAC)_2$ complexes in the sample were adsorbed onto a fresh Hg drop at an applied potential of −0.40 V for 10 min, while the sample was stirred. At the completion of the adsorption period, the stirrer was stopped, and the potential scanned using the fast linear sweep mode from −0.40 to −0.90 V at $10.1\ V\ s^{-1}$ and the and stripping current from the adsorbed $Fe(TAC)_2$ was recorded. The Teflon cups were rinsed only with MQ between analyses, and the samples were run in the order of increasing Fe additions. Duplicate runs of each sample were made, and if there was no agreement (>10% of current) between duplicates, a further run was made. For each sample run, two +0 samples were run, as a check for possible contamination of the cell. Each Teflon bottle was consistently used for a constant Fe addition.

2.2.4. Theory CLE-ACSV

The theory behind the CLE-ACSV approach was introduced by Ruzic (1982) and van den Berg (1982), and in the specific case for iron by Gledhill and van den Berg (1994) and Rue and Bruland (1995). A brief outline of the theory for determining dissolved iron speciation is presented below.

For iron in ambient seawater, a mass balance can be constructed

$$[Fe_T] = [Fe'] + [FeL_i], \quad (1)$$

where [Fe′] represents the sum of all the inorganic species (predominantly $Fe(OH)_x^{(3-x)+}$), and $[FeL_i]$ represents the organically bound iron with L_i being classes of natural organic ligands. The speciation of Fe(II) is not considered, as in most cases the long equilibration times used in these

experiments should have seen the oxidation of any Fe(II) present. Reactions between one class of the natural ligands and Fe′ can be expressed as

$$Fe' + L' = FeL, \tag{2}$$

where L' is the Fe-binding ligand not already bound to Fe(III). The equilibrium expression is then

$$K'_{FeL} = \frac{[FeL]}{[Fe'][L']}, \tag{3}$$

where $K'_{Fe'L}$ is the conditional stability constant with respect to Fe′ under these specific conditions (in this case pH 8.0 seawater). To convert $K'_{Fe'L}$ to K'_{FeL}, the conditional stability constant for FeL with respect to free Fe^{3+}, the relationship between Fe′ and Fe^{3+}, $\alpha_{Fe'} = [Fe']/[Fe^{3+}]$, can be used (e.g. $K'_{FeL} = \alpha_{Fe'} K'_{Fe'L}$).

Upon addition of the competing ligand TAC, a new equilibrium is established between TAC, the natural organic ligands and iron. The new mass balance can be described as

$$[Fe_T] = [Fe'] + [FeL_i] + [Fe(TAC)_2]. \tag{4}$$

The complexation of Fe′ by TAC can be described as

$$\beta'_{Fe(TAC)_2} = \frac{[Fe(TAC)_2]}{[Fe'][TAC']_2}. \tag{5}$$

The side-reaction coefficient for $Fe(TAC)_2$ with respect to Fe′ is then denoted by

$$\alpha_{Fe(TAC)_2} = \frac{[Fe(TAC)_2]}{[Fe']} = \beta'_{Fe(TAC)_2}[TAC']_2. \tag{6}$$

As $[TAC'] \gg [Fe_T]$ for this method, the assumption $[TAC'] = [TAC_T]$ can be used.

The sensitivity, S, is the relationship between the peak current (i_p, in nA) and the concentration of Fe-TAC is given by

$$S = \frac{i_p}{[Fe(TAC)_2]}, \tag{7}$$

where S is determined from the titration data by plotting peak current vs. Fe concentration, measuring the slope in the linear region at the high Fe end of the titration, where naturally occurring ligands are no longer competing with TAC for the added Fe. Generally, the value of S obtained in this manner for open ocean samples is the same as that obtained by adding Fe to UV-irradiated samples.

The relationship between S and [Fe′] is then

$$[Fe'] = \frac{i_p}{S\alpha'_{FeTAC_2}}. \tag{8}$$

Titrations performed using CLE-ACSV yield the fraction of Fe complexed by TAC at different Fe concentrations. This fraction is related to the side-reaction coefficient by the following relationship (all relative to Fe′):

$$\frac{[Fe(TAC)_2]}{[Fe_T]} = \frac{\beta'_2[TAC]_2}{1 + \Sigma K'_i L_i + \beta'_2[TAC]_2} = \frac{\alpha_{Fe(TAC)_2}}{1 + \alpha_{Fe\,org} + \alpha_{Fe(TAC)_2}}, \tag{9}$$

K_i is the conditional stability constant, L_i is the concentration of the ith natural ligand, $\alpha_{Fe\,org}$ is the side-reaction coefficient for the naturally occurring ligands and $\beta'_2[TAC]^2$ the side-reaction coefficient for TAC complexes, which was previously determined against well-characterized model ligands (EDTA, DTPA: Croot and Johansson, 2000). The side-reaction coefficient for all naturally occurring ligands (including inorganic ligands) is related to the concentration of [Fe′] by the relationship

$$\frac{[Fe']}{[Fe_T][Fe(TAC)_2]} = \frac{1}{1 + \Sigma K_i L'_i}. \tag{10}$$

Data in this study were analysed with a single ligand model that was a nonlinear fit to a Langmuir adsorption isotherm. This model has been described previously by Gerringa et al. (1995). Those workers made a convincing case from a statistical perspective for selecting a nonlinear fit over linearization plots, such as van den Berg/Ruzic or Scatchard plots. The single ligand model is derived from Eq. (3), where $[L_T] = [L'] + [FeL]$. Rearranging Eqs. (3), (4) and (10) yields a reciprocal Langmuir isotherm

$$\frac{[FeL]}{[Fe']} = \frac{K[L_T]}{1 + K[Fe']}. \tag{11}$$

We used the computer program ORIGIN (Microcal software) to solve Eq. (11) for K, $[L]$ by nonlinear regression analysis with Fe′ as the independent variable and [FeL]/[Fe′] as the

dependent variable. In the case of multiple ligands, a more correct form of the equation is

$$\frac{\Sigma[\mathrm{Fe}L_i]}{[\mathrm{Fe}']} = \Sigma K'_i L_{i(i>1)} + \frac{[L_1]K'_1}{1 + K'_1[\mathrm{Fe}']}, \quad (12)$$

$\Sigma K_i L_{i(i>1)}$ is the side-reaction coefficient for the weaker ligands, and K_1 and L_1 represent K and L in Eq. (9). Speciation data were also calculated for K', L using the van den Berg/Ruzic linearization of this Langmuir approach, also using the matrix optimization program FITEQL (Westall, 1982). The ambient [Fe′] was estimated by solving Eq. (11), using the calculated values of K' and L_T at the ambient dissolved iron concentration. Error estimates were constructed for all calculated parameters by applying a full and complete error analysis on each parameter, including instrumental detection limits.

Conditional stability constants were calculated using $\beta'_{\mathrm{Fe(TAC)_2}} = 10^{12.4}\,\mathrm{M}^{-2}$ (in $\mathrm{Fe}^{\mathrm{III}}$ notation $\beta_{\mathrm{Fe(TAC)_2}} = 10^{22.4}\,\mathrm{M}^{-2}$) (Croot and Johansson, 2000), $\beta'_{\mathrm{FeNN}} = 10^{18.42}$ (in $\mathrm{Fe}^{\mathrm{III}}$ notation $\beta_{\mathrm{Fe(TAC)_3}} = 10^{28.4}\,\mathrm{M}^{-3}$) and $\alpha_{\mathrm{Fe'}}$ of $10^{10.0}$ from the work of Kuma et al. (1996), Millero (1998) and Hudson et al. (1992). There is still some debate, however, over the value of $\alpha_{\mathrm{Fe'}}$; other researchers have used different values, 10^{10} (Rue and Bruland, 1995), 10^{11} (Rue and Bruland, 1997), $10^{11.9}$(Nolting et al., 1998) and $10^{11.6}$ (Gledhill and van den Berg, 1994).

3. Results

3.1. Hydrography

In the Spring Ice Edge (SIE), there was a strong temperature minimum (−1.8 °C) at 80–100 m, associated with winter water (Whitworth and Nowlin, 1987). Salinities in the SIE, which were slightly depressed at the southern stations, may have been related to recent sea ice melt. The effect of this was also seen in the mixed layer depths which were shallow (30–40 m) in the southern section and increased in the north (50 m). In the Winter Ice Edge (WIE), the temperature minimum (−0.9 °C) was also present but was found much deeper (100–150 m) than in the SIE. Salinities were fairly uniform across the WIE and so were mixed layer depths (50–60 m). The highest surface water temperatures (3–4 °C) were found in the Antarctic Polar Front (APF) where no winter water was present. Surface temperatures and salinities increased northwards, while mixed layer depths were the deepest encountered (75–90 m). Upper ocean hydrographic sections in the SIE, WIE and APF study areas can be found in Turner et al. (2004).

3.2. Macronutrients

In the SIE, both nitrate (>15 μM) and silicate (>50 μM) were plentiful in the surface waters, whose values were the maximum that was encountered during this investigation. In the WIE, surface concentrations of nitrate (14–22 μM) and silicate (40 μM) showed a trend of decreasing levels northwards from the SIE. The APF region had the lowest silicate concentrations encountered (8–14 μM), while nitrate remained high (17–23 μM). Macronutrient data associated with each station sampled for iron can be found in Table 1. A more complete description of the macronutrient distribution, and the CO_2 system at this time is found in the work by Fransson et al. (2004).

3.3. Sea ice and Chl

Satellite sea ice data, in agreement with sea truth observations, show a rapid disappearance of sea ice south of the SIE at 60°S during December 1997 (Turner et al., 2004). SeaWiFS Chl images (Fig. 2) show the development of a large bloom along the SIE at 60°S in the days following the retreat of the ice. In the 2 weeks between December 15 and 30, Chl concentrations apparently increased from 0.5 to 2–4 $\mu g\,L^{-1}$ in the vicinity of the Biostations 1 and 2 occupied during the present work. Higher Chl values were seen by SeaWiFS, in the Weddell Sea, in mid-January 1998. Fig. 2 also shows low Chl values (<0.4 $\mu g\,L^{-1}$) found throughout the WIE during the summer, while slightly higher values (0.5–1.4 $\mu g\,L^{-1}$) are encountered in the vicinity of the APF. The SeaWiFS values are in good agreement with the surface Chl measurements made during SWEDARP (Wulff and Wängberg, 2004).

Table 1
Surface water stations of SWEDARP 97/98 with data on nutrients, dissolved and total dissolvable iron

Station/ position/date	Depth (m)	Salinity GoFlo	Temperature (°C)	O_2 (μM)	Nitrate (μM)	Silicate (μM)	Dissolved Fe (nM)	Total Fe (nM)
D072/D077	10	33.769	−0.270	354.6	15.8	50.6	1.46	1.54
60°0.2′S	20	33.771	−0.271	354.1	15.8	50.6	0.58	1.59
6°0.5′E	50	33.787	−1.660	321.9	16.0	51.2	0.48	1.21
Jan. 2, 98	100	34.401	0.928	185.6	18.7	71.4	(0.90)	1.63
(BIO 2)	150	34.686	1.157	185.4	23.1	87.5	0.42	1.82
BD 5360 m	200	33.859[a]	1.073	189.2	22.9	91.9	(1.01)	(c)
MLD 32 m	300	34.702	0.895	193.9	22.7	96.4	0.46	1.05
	400	34.701	0.712	192.6	23.2	101.4	0.51	1.58
D089/D091	10	33.895	−0.362	347.4	19.7	51.0	0.35	—
60°23.8′S	30	33.900	−0.374	337.0	22.5	54.5	0.33	—
6°0.3′E	50	33.993	−1.320	330.2	23.1	55.7	0.24	—
Jan. 3, 98	100	34.148	−1.814	220.8	28.0	89.9	(0.56)[b]	—
(BIO 1)	150	34.492	−0.112	186.1	29.5	103.5	0.20	
BD 5380 m	200	34.671	0.563	184.4	29.7	107.6	0.36	
MLD 35 m	300	34.688	0.490	184.0	30.0	110.3	0.29	—
	400	34.685	0.412	183.9	31.8	113.2	(0.51)[b]	–
D203/D208	10	34.030	0.459	348.3	22.0	39.0	0.23	0.40
55°49.8′S	30	34.031	0.337	346.6	23.3	39.2	0.19	0.39
6°1.0′E	50	34.032	0.234	—	24.2	39.0	0.04	0.38
Jan. 12, 98	100	34.249	−0.427	265.6	28.3	49.8	0.12	0.39
(BIO 4)	150	34.542	0.896	213.1	28.7	55.5	0.14	0.47
BD 4520 m	200	34.066[a]	1.289	195.1	27.3	58.6	0.20	(c)
MLD 49 m	300	34.677	1.380	209.5	27.3	61.1	0.17	0.60
	400	34.689	1.253	263.4	27.6	62.3	0.18	0.83
D219/D223	10	34.233	0.113	343.1	14.8	42.0	—	0.83
56°30.1′S	30	34.233	0.104	346.0	15.3	41.8	—	0.41
6°3.1′E	50	34.235	0.003	343.4	15.3	41.0	—	0.29
Jan. 13, 98	100	34.332	−0.856	324.5	17.5	48.2	—	0.34
	150	34.489	0.096	201.7	21.3	71.4	—	0.22
BD 4920 m	200	34.661	0.440	190.2	23.3	75.2	—	0.32
MLD 60 m	300	34.686	0.454	196.7	25.2	78.2	—	0.22
	400	34.686	0.399	217.4	23.5	79.3	—	0.31
D265/D267	30	34.091	0.609	339.5	—	—	—	1.15
55°0.1′S	50	34.098	0.589	—	—	—	—	0.51
6°1.5′E	100	34.215	−0.545	—	—	—	—	0.96
Jan. 16, 98	150	34.410	−0.026	228.4	—	—	—	0.94
	200	34.555	1.016	—	—	—	—	0.55
BD 3150 m	300	34.625	1.197	—	—	—	—	0.62
MLD 50 m	400	34.675	1.202	191.2	—	—	—	0.31
D270/D272	10	33.867	0.304	340.9	—	—	—	0.31
54°22.7′S	30	33.867	0.307	341.0	—	—	—	0.78
4°0.0′E	50	33.933	0.049	344.4	—	—	—	0.55
Jan. 17, 98	100	34.051	−0.751	329.2	—	—	—	0.59
(Bouvet)	150	34.390	−0.204	262.3	—	—	—	1.15
BD 2410 m	200	34.547	1.055	201.3	—	—	—	2.69
MLD 45 m	300	34.616	1.522	193.9	—	—	—	1.05
	400	34.657	1.438	222.9	—	—	—	0.93

Table 1 (*continued*)

tation/ osition/date	Depth (m)	Salinity GoFlo	Temperature (°C)	O_2 (μM)	Nitrate (μM)	Silicate (μM)	Dissolved Fe (nM)	Total Fe (nM)
)293	10	—	3.814	322.4	17.2	14.3	0.31	0.68
9°49.8′S	30	—	3.811	320.8	16.9	13.8	(0.84)	—
°59.4′E	50	—	3.809	318.9	17.3	14.3	0.07	0.25
an. 24, 98	100	—	2.549	314.5	19.1	15.5	0.10	0.18
BIO 6)	150	—	2.091	289.3	20.0	19.7	0.04	0.39
BD 3570 m	200	—	2.054	257.2	20.6	24.2	0.06	—
MLD 76 m	300	—	2.280	212.5	21.7	34.3	(0.68)	(0.96)
)306/308	10	—	3.724	320.1	23.0	10.9	—	0.18
1°2.6′S	30	—	3.698	317.6	22.7	8.9	—	(2.81)
°49.1′E	50	—	3.673	317.8	22.9	8.9	—	0.21
an. 26, 98	100	—	3.411	318.2	23.7	10.0	—	0.50
BIO 5)	150	—	1.754	296.7	27.9	13.3	—	0.44
BD 3490 m	200	—	2.012	259.0	30.5	17.4	—	0.25
MLD 89 m	300	—	2.259	207.4	33.5	30.7	—	0.67
	400	—	2.395	186.4	33.9	38.6	—	0.58

Note: O_2 data kindly provided by M. Chierici and A. Fransson and other nutrient data from R. David.

BD denotes the bottom depth from the hull mounted echo-sounder on the S.A. *Agulhas*.

MLD denotes the mixed layer depth as determined from the CTD profile at the same station and the MLD is defined as a change in σ_t of 0.1 kg m^{-3} from that at 5 m depth.

(c) Denotes the sample that was grossly contaminated, and typically this was [Fe] > 3 nM.

( ) denotes the sample thought to be contaminated from comparison with the rest of the profile.

[a]Sample bottle closed at the wrong depth.

[b]Contamination from GoFlo bottle #4 suspected, after the sampling in the SIE; the GoFlos were acid washed again, and this problem seems to have been alleviated for this bottle.

Vertical profiles for Chl and related pigments were also made during this study (Wulff and Wängberg, 2004) at the Biostations, and selected CTD stations. In brief, the highest Chl concentrations were found in the SIE (1–2 μg L^{-1}), particularly at Biostations 1 and 2, at the southern end of the survey transect. This bloom was dominated by both small diatoms (*Chaetceros* sp., *Pseudonitzchia* sp.), large diatoms (*Fragilariopsis kergulensis*, *Cylindrotheca* sp.) and haptophytes (as identified by pigment signature); microscopy confirmed the presence of both colonial and single cell *Phaeocystis* sp. (Karlson and Godhe, 1998). In the WIE, a similar split between haptophytes and diatoms was found at station D226, while at D204 the diatoms were more dominant. The overall Chl was very low (0.2–0.4 μg L^{-1}) in the WIE, with deep Chl maxima (50–60 m). The APF had elevated Chl (0.7–1 μg L^{-1}) levels compared to the WIE and showed a transition in the phytoplankton community structure towards more dominance by diatoms, though other taxa also were important, noticeably dinoflagellates and cryptophytes. Haptophytes were still present in the APF, though now as coccolithophorid species.

3.4. Dissolved and total Fe in Antarctic surface waters—vertical profiles

Iron data from the vertical casts are shown in Figs. 3–5, collated in Table 1. Dissolved (0.2–0.5 nM) and total dissolvable iron concentrations (1–1.8 nM) were enriched in the SIE (Fig. 3), relative to the rest of the survey. Vertical profiles in the SIE showed surface enrichment, perhaps from ice melt, which removed the expected nutrient-like profile typically expected for iron. In the WIE (D203/208, Fig. 5) dissolved concentrations were low (< 0.2 nM), showed slight surface enrichment: a minimum at 50 m, consistent with the Chl maximum, then increasing iron values at the O_2 minimum. Total iron in the WIE also showed surface enrichment but was also low throughout (0.3–0.4 nM).

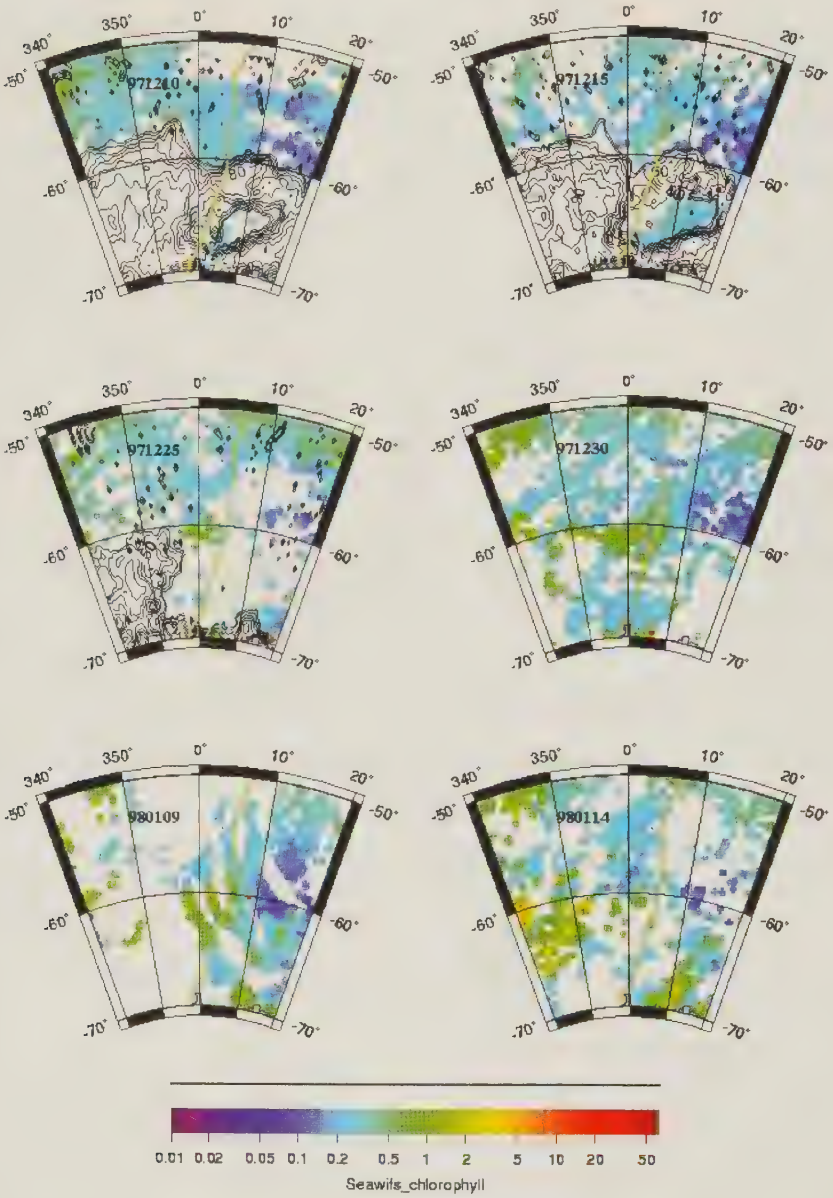

Fig. 2. Chl distribution during December 1997–January 1998 in the Atlantic sector of the Southern Ocean. Each panel is a daily composite image from SeaWiFS; white regions in the maps indicate cloud cover. The black contour lines in the maps indicate the percentage sea ice cover during the mapping period. The cruise track of the S.A. *Agulhas* is also shown on each map.

The station near Bouvet Island (D270/272) showed remarkable enrichment in total iron at around 200 m depth. The station was located at some distance away to the northeast, downstream of Bouvet, which may represent material being transported from the shelf sediments. Examination of the transmission profile at this station, however, shows little evidence of any significant turbidity current. Further north in the APF (Fig. 5), dissolved iron concentrations were very low

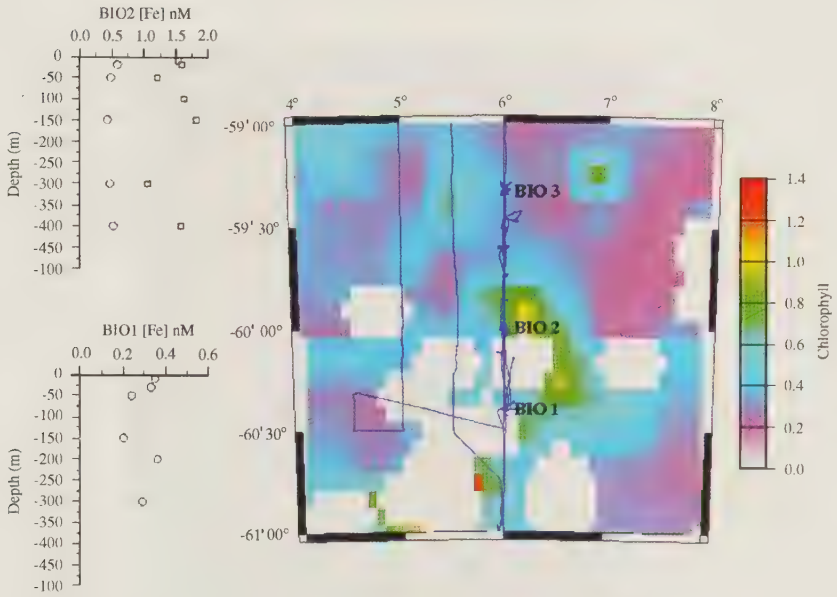

Fig. 3. Vertical profiles of dissolved (circles) and total dissolvable (squares) iron from stations in the SIE, superimposed on a SeaWiFS Chl composite image for the region and averaged over the period December 1997–January 1998.

(<0.1 nM) and below the near surface, total iron values were also relatively low (0.2–0.5 nM).

3.5. Total Fe in Antarctic surface waters—horizontal profile

A small-scale surface survey for total iron was performed in the APF (Table 2, Fig. 6) using a sub-surface underway pumping system. Total iron was found to be highly variable in both time and space through the APF. Two survey lines were conducted, 2 days apart along 6°E. On the January 18, 1998 we found total iron concentrations of around 1.4 nM, while for the same area 2 days later the values were only at 0.4–0.7 nM. The regions of high iron concentrations were often accompanied by floating seaweed, which sometimes was caught around the sampling equipment, but did not compromise the sampling. Seaweed is often observed in the Atlantic sector of the APF despite being at a long-distance away from any landmass (Croot and de Jong, 2000; de Jong et al., 1997). Higher surface iron concentrations were also found in the vicinity of the Polar Front itself (around 50°S) after rain events (January 18 and 22).

3.6. Fe complexation in Antarctic surface waters

The results of the organic speciation work are collated in Tables 3–5. In this work, we found no justification for using a two-ligand system, so all data presented have been calculated assuming only one class of iron-binding ligand. In general, all the samples for the iron speciation analysis came from the Chl maximum, and were filtered within an hour of collection with complete analysis after 24 h. Some duplicate samples were frozen after filtration and analysed back in the laboratory; these showed little difference from the original titrations performed at sea.

Only a few samples are reported from the SIE, as at Biostation 1; thiol-like compounds (this may include DMS and glutathione) were present in high concentrations and these interfered with the CSV measurements by adsorbing to the Hg drop, producing a peak and thus, making it difficult to identify the Fe peak. For Biostation 2 this

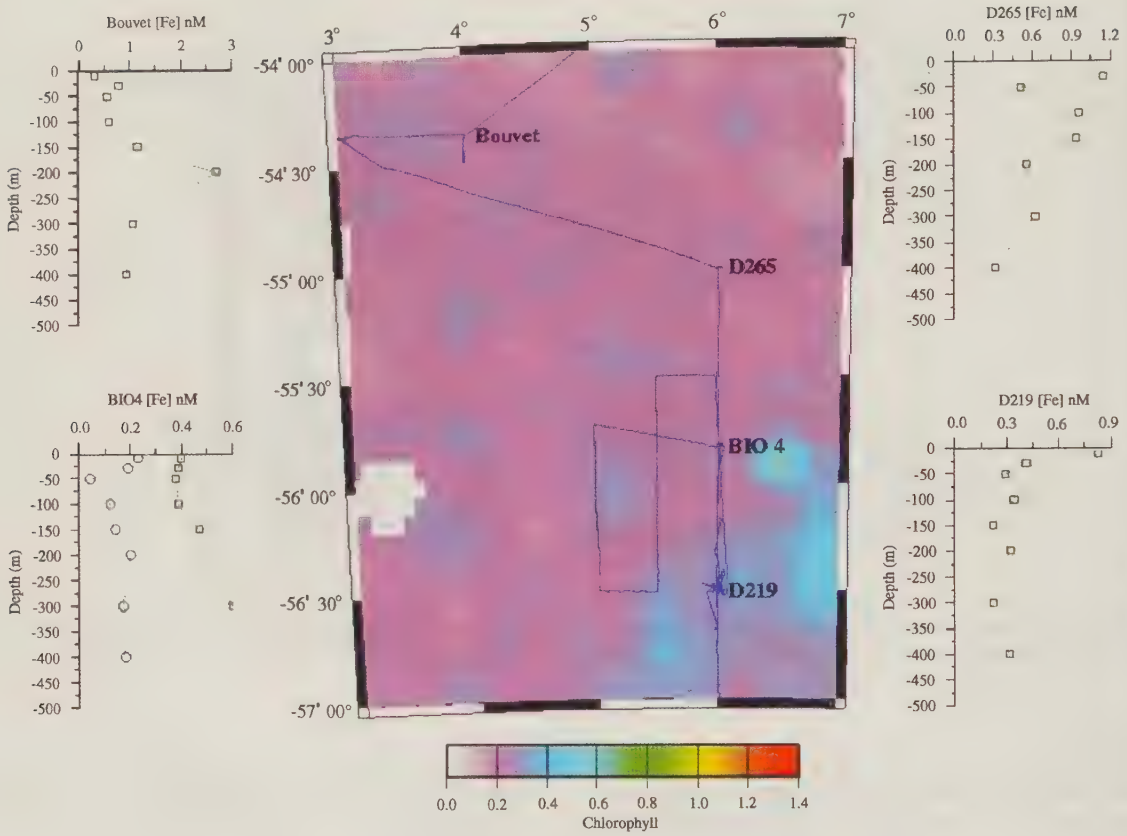

Fig. 4. Vertical profiles of dissolved (circles) and total dissolvable (squares) iron from stations in the WIE, superimposed on a SeaWiFS Chl composite image for the region and averaged over the period December 1997–January 1998.

interfering substance was still a problem but could be overcome at Biostation 3; at all other stations this phenomenon did not occur. Iron-binding ligand concentrations were relatively similar at both Biostation 2 (1.7–2.5 nM) and Biostation 3 (2.1–3.0 nM). Estimated values of Fe′ were high at Biostation 2 (0.69–0.79 pM), while they were considerably low at Biostation 3 (0.03–0.13 pM), indicating that there was more labile iron at Biostation 2.

A vertical profile for iron-complexing ligands was obtained at Biostation 4 in the WIE (Fig. 7). Ligand concentrations showed a maximum at 30 m (2.5 nM) and decreased with depth. Values of $\log \alpha_{Fe\,org}$ are included in Table 4, indicating that the organic species of iron are the dominant fraction throughout the water column. Estimated values of Fe′ ranged from 0.53 pM at 200 m, near the O_2 minimum, to 0.037 pM at 50 m, near the Chl maximum. Fe′ at Biostation 4 also indicated possible near surface enrichment, which may be consistent with photochemical degradation of the iron-binding ligands, hence their decrease near surface, with subsequent release of labile iron (Barbeau et al., 2001; Croot et al., 2001; Johnson et al., 1994).

Samples were also obtained in the APF from the BIO5 and BIO6. At these stations, a more detailed comparison was made between the two CSV techniques and different detection windows. There was very good agreement between TAC and 1N2N on the same samples (Table 5). An intermediate water sample was also obtained from 1500 m at Biostation 5; this was found to have a high Fe′ (0.61 pM), significantly higher than the waters at 60–100 m (0.013–0.019 pM).

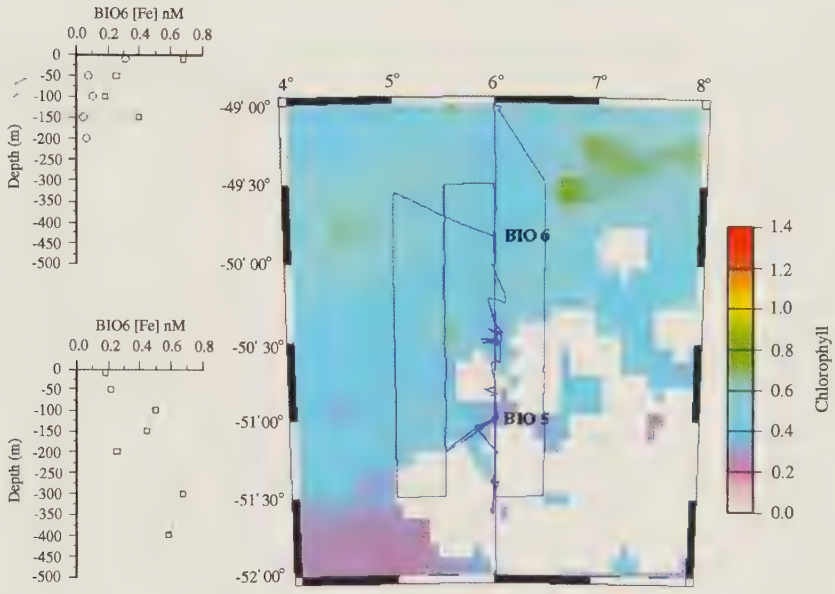

Fig. 5. Vertical profiles of dissolved (circles) and total dissolvable (squares) iron from stations in the APF, superimposed on a SeaWiFS Chl composite image for the region and averaged over the period December 1997–January 1998.

In general, there was no significant variation in $[L]$ with concentrations in all regions ranging from 0.9 to 3.0 nM. Values of $\log K'$ ranged from 21.5 to 23.5, but as this parameter is somewhat dependent on the detection window $[L]$ used the variations are not statistically significant.

4. Discussion

4.1. Sources of iron

Understanding the supply and removal of iron from the Southern Ocean is of critical importance for interpreting biological productivity in this key region of the globe. Iron has been shown to be an important limiting or colimiting factor for phytoplankton growth in the Southern Ocean (Boyd et al., 2000). For the macronutrients, supply to the surface waters of the Southern Ocean is chiefly from upwelling and vertical mixing of deep water, while for iron there are several possible sources: (i) upwelling and vertical mixing; (ii) atmospheric deposition of dust; (iii) icebergs and ice rafts and (iv) continental and island margins. Though the present study is limited to the upper 400 m of the water column, here we will compare these possible sources to answer the question—where is the iron coming from?

4.1.1. Vertical input from below by upwelling and mixing

For the present study we have very little dissolved iron data for the concentration at depth, below the influence of the wind and transient surface effects. At station D345 in the APF, we were able to obtain one sample from 1500 m which contained 0.24 nM dissolved iron. Recently, a series of deep casts were obtained along 20°E during ANT 16/3 onboard the *Polarstern*. In the study where the dissolved iron concentration, below 1000 m, ranged from 0.26 to 0.4 nM (Boye et al., 2001). Previous estimates of the upwelling flux of iron in this region have used much higher values for iron below the mixed layer (Löscher et al., 1997), with a resulting flux estimate of $1.7\,\mathrm{pmol\,m^{-2}\,s^{-1}}$. In the present study, we take the same approach as Löscher et al. to estimate the upwelling flux of iron. Using the same upwelling velocity of $15 \times 10^{-5}\,\mathrm{cm\,s^{-1}}$ as Löscher et al.—our

Table 2
Total iron (unfiltered) measurements underway in the APF during Jan. 18–22, 1998

Station	Time:date	Latitude	Longitude	T_{insitu}	S_{insitu}	[Fe] (nM
	0835:J018	51°58.6′S	6°00.8′E	—	—	1.53
	0935:J018	51°53.9′S	6°01.1′E	2.92	33.749	1.36
	1335:J018	51°30.8′S	6°01.2′E	3.47	33.785	0.50
	1435:J018	51°25.1′S	6°00.7′E	3.5	33.787	1.05
	1535:J018	51°18.2′S	6°00.7′E	3.62	33.776	–
	1630:J018	51°10.8′S	6°01.1′E	3.66	33.767	0.34
	1730:J018	51°04.3′S	6°00.5′E	3.75	33.774	—
	1830:J018	50°57.3′S	6°00.3′E	3.85	33.778	1.30
	1930:J018	50°49.9′S	6°00.2′E	3.71	33.791	1.46
U232	2030:J018	50°42.9′S	6°00.2′E	3.79	33.733	1.35
	2130:J018	50°35.6′S	6°00.0′E	4.01	33.777	1.40
	2230:J018	50°30.6′S	6°00.0′E	3.88	33.781	1.48
U239	1100:J020	49°25.2′S	6°25.5′E	3.73	33.815	0.58
U240	1200:J020	49°31.0′S	6°29.8′E	3.66	33.837	0.61
U241	1310:J020	49°39.5′S	6°30.1′E	3.62	33.793	0.80
U242	1400:J020	49°44.7′S	6°30.1′E	3.58	33.794	1.97
U247	1900:J020	50°17.8′S	6°29.9′E	3.72	33.760	0.23
U248	2000:J020	50°25.0′S	6°29.9′E	3.69	33.764	0.17
U249	2100:J020	50°31.7′S	6°00.1′E	4.05	33.732	1.16
U266	1400:J021	50°50.9′S	6°00.3′E	3.82	33.779	0.72
U267	1500:J021	50°45.8′S	6°00.4′E	3.72	33.827	0.54
U268	1600:J021	50°39.4′S	6°00.1′E	3.99	33.778	0.39
U270	1800:J021	50°25.7′S	6°00.1′E	3.98	33.789	0.50
U271	1900:J021	50°19.7′S	6°00.1′E	3.94	33.781	2.73
U272	2000:J021	50°13.4′S	6°00.0′E	3.91	33.767	3.12
U273	2100:J021	50°06.3′S	6°00.0′E	3.92	33.792	2.00
U274	2200:J021	49°59.6′S	6°00.0′E	3.58	33.809	2.88
U275	2300:J021	49°52.2′S	6°00.1′E	3.68	33.781	1.38
U276	2400:J021	49°46.5′S	6°00.0′E	3.96	33.811	1.86
U277	0100:J022	49°39.5′S	5°59.7′E	4.19	33.765	1.07
U278	0200:J022	49°32.7′S	5°54.3′E	4.23	33.763	0.40
U279	0300:J022	49°29.9′S	5°31.9′E	3.64	33.945	0.78
U281	0500:J022	49°30.3′S	5°29.9′E	4.17	33.777	1.75
U282	0600:J022	49°32.3′S	5°30.5′E	3.50	33.886	2.28
U284	0800:J022	49°45.2′S	5°30.1′E	3.60	33.788	1.66
U285	0900:J022	49°52.2′S	5°30.5′E	4.03	33.777	0.90
U286	1000:J022	49°58.5′S	5°30.1′E	3.70	33.866	0.85
U287	1100:J022	50°17.8′S	5°31.9′E	3.58	33.828	2.11
U288	1200:J022	50°05.6′S	5°29.9′E	3.48	33.801	0.95
U289	1300:J022	50°12.3′S	5°30.5′E	3.42	33.788	1.50
U290	1400:J022	50°15.7′S	5°30.3′E	3.52	33.778	0.69
U291	1500:J022	50°19.6′S	5°30.7′E	3.54	33.752	1.39
U292	1600:J022	50°24.0′S	5°30.1′E	3.96	33.730	0.65

deep water value of 0.24 nM—we obtain an advective flux of 0.36 pmol $m^{-2} s^{-1}$, five times lower than the estimate of Löscher et al. From the data of WIE (D203/208) we can obtain an estimate of the diffusive flux at that station of 0.048 pmol $m^{-2} s^{-1}$, assuming $K_z = 0.3 \times 10^{-4}$ $m^2 s^{-1}$ (typical value for Southern Ocean) and estimating $\partial[Fe]/\partial z = 1.6$ nmol m^{-4} (50–100 m depth). Combining these estimates leads to a total vertical flux of 0.41 pmol $m^{-2} s^{-1}$, which is comparable to estimates for Ocean Station Papa (Löscher et al., 1997).

4.1.2. Atmospheric input

The Southern Ocean receives the lowest atmospheric dust loads anywhere on the globe (Duce and Tindale, 1991; Mahowald et al., 1999). The transportation and deposition of mineral dust is highly variable due to the episodic nature of dust generation, transport and deposition. Recent estimates of iron flux to the Atlantic sector of the Southern Ocean range from 1.7 pmol $m^{-2} s^{-1}$ (Duce and Tindale, 1991) to 10 pmol $m^{-2} s^{-1}$ (Mahowald et al., 1999). The main source region for this dust is believed to be from Patagonia (Mahowald et al., 1999). Also, not all the iron deposited as dust will be soluble, and hence bioavailable to phytoplankton. Estimates vary but typically 10% of this dust is made soluble, though this can vary due to mineralogy, photochemistry and mode of deposition (Spokes and Jickells, 1996). Thus, the soluble iron flux estimate for atmospheric deposition is 0.17–1 pmol $m^{-2} s^{-1}$, which is similar in magnitude to the upwelling flux.

The episodic pulse nature of atmospheric deposition can also be seen in the iron profiles from the WIE (Fig. 4) and the APF (Fig. 5), where snows and rain events, respectively, elevated the near surface concentrations of dissolved iron. Similarly, during the surface survey in the APF (Fig. 6), we also encountered intermittent rain events which could have elevated the near surface

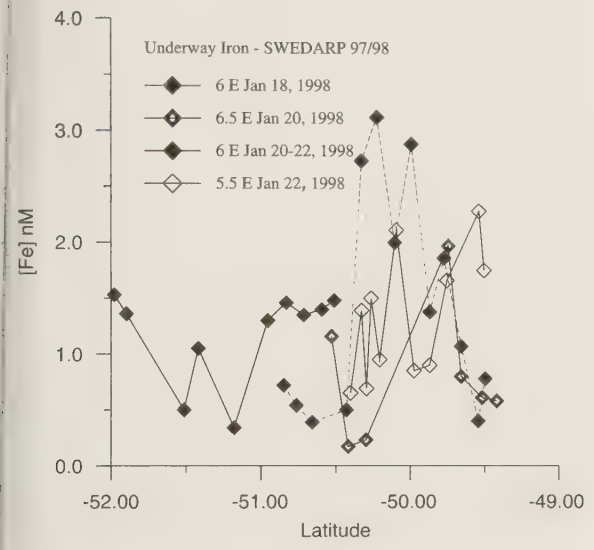

Fig. 6. Plot of surface iron measured during transect survey in APF during January 18–22, 1998.

Table 3
Biostations from SIE in SWEDARP 97/98 with data on iron speciation

Station/position/date	Depth (m)	Log K	L (nM)	Dissolved Fe (nM)	Fe′ (pM)
SIE					
D145 BIO2	25	21.9	1.7±0.2	0.60	0.69±0.27
60°0.7′S					
5°57.5′E					
Jan. 6, 98					
D166 BIO2	25	21.5	2.5±1.0	0.50	0.79±0.55
60°0.0′S					
6°0.0′E					
Jan. 7, 98					
D174 BIO3	50	22.1	3.0±0.5	0.42	0.13±0.05
59°20.4′S	100	22.7	2.1±0.5	0.45	0.054±0.027
5°59.4′E					
Jan. 8, 98					
D201 BIO3	50	22.9	2.9±0.2	0.60	0.033±0.010
59°20.0′S					
6°1.9′E					
Jan. 9, 98					

Note: Detection window employed in this work: 10 μM TAC.
The error in log K is ±0.1, unless stated.

Table 4
Depth profile of Fe-binding ligands in the WIE at Biostation 4 (D203/D208)

Station/position/date	Depth (m)	Dissolved Fe (nM)	Log K	L (nM)	Log $\alpha_{Fe\ org}$	Fe′ (pM)
D203/D208	10	0.23	22.1	1.0	12.99	0.24±0.0
55°49.8′S	30	0.19	21.7	2.5	13.06	0.16±0.0
6°1.0′E	50	0.04	21.7	2.2	13.03	0.04±0.0
Jan. 12, 98	100	0.12	22.1	1.6	13.27	0.06±0.02
	150	0.14	22.2	1.6	13.36	0.06±0.02
	200	0.20	21.4	1.7	12.58	0.53±0.16
	300	0.17	21.8	1.2	12.81	0.26±0.09
	400	0.18	22.7	1.3	13.75	0.03±0.01

Note: Detection window employed in this work: 10 μM TAC.
The error in log K is ±0.1, for $[L]$±0.1, unless stated.
Determined using CLE-CSV with 10 μM TAC.

Table 5
Biostations from APF in SWEDARP 97/98 with data on iron speciation

Station/position/date	Depth (m)	Log K	L (nM)	Dissolved Fe (nM)	Fe′ (pM)
APF					
D318 BIO5	60	23.1	2.1±0.1[a]	0.40	0.019±0.006
50°59.6′S		23.1	2.3±0.1[b]	0.40	0.019±0.005
5°59.4′E		23.5	1.4±0.2[c]	0.40	0.013±0.005
Jan. 27, 98					
D324 BIO5	100	23.4	0.9±0.1[a]	0.26	0.016±0.007
50°59.6′S					
5°59.4′E					
Jan. 27, 98					
D345 BIO5	1500	21.4	1.8±0.3[a]	0.24	0.61±0.24
50°59.8′S					
5°59.7′E					
Jan. 28, 98					
D353 BIO6	60	21.9	2.6±1.2[d]	0.40	0.23±0.17
49°50.4′S		22.6	2.3±0.1[a]	0.40	0.053±0.016
6°0.2′E					
Jan. 29, 98					

Note: Multiple detection windows employed in this work: concentration, ligand and detection window.
The error in log K is ±0.1, for $[L]$±0.1, unless stated.
[a] 10 μM TAC–$10^{12.4}$, 251.
[b] 10 μM NN–$10^{13.4}$, 2510.
[c] 20μM NN–$10^{14.3}$, 20100.
[d] 5 μM NN–$10^{12.5}$, 314.

concentrations of dissolved iron for some time until vertical mixing reduced the rain-induced gradients.

4.1.3. Icebergs and ice-rafting debris

Previous work at 6°W, during 1992, found an anomalously high number of icebergs in the APF but suggested that iceberg melt would be only a minor source of iron to this region (Löscher et al., 1997). During the present work, we encountered many large icebergs in the SIE, a few in the WIE but only rarely in the APF. The iron content of Southern Ocean icebergs and sea ice has previously been found to be in the range 10–60 nM

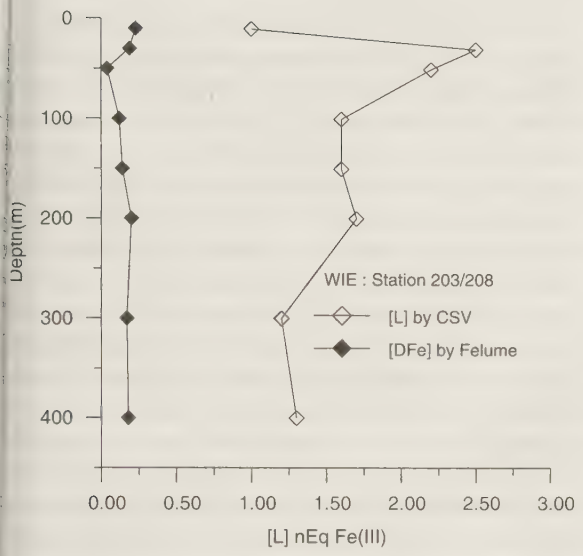

Fig. 7. Vertical profile of ligand concentration and dissolved iron in the WIE.

(Löscher et al., 1997), similar to that found in Antarctic glacial ice—0.5–120 nM (Edwards et al., 1998) and surface snow—0.3–32 nM (Edwards, 1999). The source of the iceberg is also important, as those coming directly from floating ice shelves will contain lower iron levels than bergs that had previously been grounded and accumulated sedimentary material, the so-called 'dirty' bergs. Icebergs found during the present study, most likely originated along the coast from Dronning Maud Land to Enderby Land (Swithinbank et al., 1980).

Thus, for the SIE during this study, in the vicinity of the intense phytoplankton bloom (Fig. 2), surface salinities were depressed to 33.8 (Biostation 2) from 34.1 (Biostation 3), just outside the bloom. Not all the salinity differences may be due to ice melt, implying a 0.88% dilution of surface seawater by ice melt (pure water); however, sea ice often typically has a salinity of 6.6 (Worby et al., 1998) which would imply a 1.1% dilution. On the transect through the SIE to SANAE in December 1997, the sea ice thickness in this region was between 30 and 80 cm; this ice was a mix of sea ice and overlying snow, which have typical densities of 0.9 and 0.36 $kg\,dm^{-3}$, respectively (Worby et al., 1998). Complete melting of this sea ice over a 35 m mixed layer would correspond to a dilution of 0.3–2%, in agreement with the salt budget. In the SIE, this corresponds to an annual iron flux of 0.03–1.4 $pmol\,m^{-2}s^{-1}$ from sea ice melt, though this is in reality a single pulse event and is perhaps more a measure of the atmospheric iron flux to the region (see below). For the water column, this would then correspond to a total iron addition of between 0.09 and 0.67 nM throughout the mixed layer, based on simply sea ice melt. Our observed values at station D072/077 (Table 1, Fig. 3) are higher, ranging from 1 to 1.8 nM, and are also elevated over the upper 400 m and not just the mixed layer. This may indicate the passage of one of the many large icebergs, which was previously grounded; thus, it may have higher iron content, though this region. Several icebergs in the SIE had obviously broken from the ice shelf and were 30–40 m above the water line, suggesting a draft of 180 m or more. Previous work in the SIE of the Ross Sea by Sedwick and DiTullio (1997) has also shown the effect of iron from sea ice melt on the development of phytoplankton blooms. Similar calculations for the WIE and the APF show no effect of sea ice, as mixed layers were deeper, suggesting that the passage of storms had eroded what little ice melt signal there was away.

One important question that arises from the SIE is how the iron gets into the sea ice. While the source of iron for icebergs is either from snow accumulation prior to calving or incorporation from grounding on the sea bottom, for sea ice formation in autumn there is very low iron in the seawater from which it is being formed (Croot and de Jong, 2000), so the only viable source is from the dust blown out from the Antarctic continent and Patagonia during the polar winter and spring. The sea ice then acts to accumulate mineral dust (iron) over the winter and spring, and release it in an intense pulse during ice melt. This iron pulse coupled with the water column stability provided by the ice melt provides fuel for a receding ice edge phytoplankton bloom.

4.1.4. Supply of iron from continental margins and islands

The fast-flowing currents of the ACC downstream of the Drake Passage have been proposed

as a vector for transporting iron derived from diagenetic input from shelf sediments of the Antarctic Peninsula and South America to the Atlantic APF region (Löscher et al., 1997). Despite the great distance from the source region, studies at 6°W found, over 2000 km downstream, elevated concentrations of particulate Al and dissolved Fe consistent with such transport (Löscher et al., 1997). Similar studies in the eastern Equatorial Pacific Ocean have shown enhanced signals for dissolved Fe, particulate Al in the equatorial undercurrent some 6000 km from the source region near New Guinea (Coale et al., 1996b). In the present study, we found high concentrations of total iron in the surface waters and vicinity of the Polar Frontal Jet at 6°E (Fig. 6), consistent with this type of transport mechanism. Unfortunately, we did not take samples for Al during this work, and so have no alternative chemical tracer for this process. The presence of seaweed (kelp: *Macrosystis* sp.) in the Polar Front, however, does act as a potential tracer, as this material requires an anchoring point to grow and which is not suited for growth in a pelagic environment. For the seaweed observed during this work, the nearest possible source region is South Georgia, South Sandwich or the Falkland Islands indicating considerable long-distance transport.

Phytoplankton blooming downstream of islands, a phenomenon known as the "island mass effect", have been studied for many years, and recently several studies were conducted in the Atlantic sector of the Southern Ocean, noticeably around Kerguelen (Blain et al., 2000; Bucciarelli et al., 2001), Bouvet (Perissinotto et al., 1992) and the South Sandwich Islands (Perissinotto et al., 1992). This effect has been ascribed to two main factors (Perissinotto et al., 1992): (1) micronutrient (iron) availability and (2) dynamic interactions between oceanic circulation and shelf topography. In the case of Kerguelen, Bucciarelli et al. (2001) showed elevated Fe and Mn in the wake of the islands, while Blain et al. (2000) showed that Chl standing stocks around the islands were related to the circulation, iron concentration and grazing pressure.

For Bouvet, previous work by Perissinotto et al. (1992) had found high primary production and phytoplankton blooms (maximum 7.3 μg Chl L^{-1}) during the austral summer and argued for water column stabilization as the primary factor for bloom development. In the present work, we found increased surface Chl fluorescence to the southeast of the island only (data not shown) and our station, situated to the northeast of the island, showed high concentrations of total iron below the pycnocline, perhaps consistent with transport of material from the shelf sediments. The inactive volcano of Bouvet lies close to the triple junction of three tectonic plate systems, and glaciers cover 93% of the island such that bird nesting is confined to the only beach landing on the west coast of the island (Rubin, 1996). The predominantly granite rocks would presumably provide little bioavailable iron to the surrounding waters, so the more likely iron source is from diagenesis in shelf sediments.

Alternatively, one potential source of iron is from hydrothermal vents, which are known to be important local sources of iron (Field and Sherrell, 2000). Though no evidence close to Bouvet has yet been found this, its proximity to the triple junction could make the probability quite high. Similar processes may occur in the South Sandwich Islands, where a 1962 underwater eruption of pumice occurred and the resulting pumice raft was tracked for several years as it made its way completely around the Southern Ocean (Gass et al., 1963; Sutherland, 1965).

4.2. *Iron speciation in the Southern Ocean*

The chemical speciation of iron in seawater has been shown to be dominated by organic complexing ligands in both the open ocean (Gledhill and van den Berg, 1994; Rue and Bruland, 1995) and coastal seas (Croot and Johansson, 2000). The use of speciation information has provided valuable help on examining the questions related to what chemical species of iron are bioavailable and it how these can impact on the phytoplankton community structure. The speciation work presented here is used to examine in detail the role of iron on phytoplankton growth in the SIE, WIE and APF during December 1997–January 1998.

4.2.1. Ligand distribution

Previous studies in the Southern Ocean have been undertaken in the western Pacific sector (Croot et al., 2001), the eastern Pacific sector (Nolting et al., 1998) and the Atlantic sector (Boye et al., 2001). Difficulties exist in making comparisons between studies because of different operating conditions; however, some trends can be observed. Nolting et al. (1998) used unfiltered seawater with a low detection window and found high ligand concentrations of 2–12 nM throughout their study area. At the beginning of SOIREE, Croot et al. (2001) found initial ligand concentrations of 3–4 nM, while Boye et al. (2001) in a study along 20°E in austral autumn had a much lower value of 0.72 ± 0.23 nM. Previous studies have not used more than one detection window or two separate CSV methods (1N2N, TAC), so the data here are considerably more robust.

The vertical profile of [*L*] obtained from the WIE (Fig. 7) shows a distinct maximum at 50 m, close to the Chl maximum, hinting at a potential biological origin for these iron-binding ligands, as was originally suggested by Rue and Bruland (1995). Vertical profiles for [*L*] from the APF at 20°E obtained by Boye et al. (2001) also show the same general trends as that from the WIE in the current work. In general, it has been believed that prokaryotes (such as bacteria and cyanobacteria) produce iron-specific siderophores in response to iron stress while eukaryotic organisms do not (Geider, 1999), though there are some exceptions (Fuse et al., 1993). For the present work, we cannot distinguish between ligand production from prokaryotes or eukaryotic organisms.

4.2.2. The role of L in the Fe(II) cycle

The presence of lowered ligand concentrations in the upper 40 m of the water column has also been seen in profiles in the Equatorial Pacific (Rue and Bruland, 1997) and in the Southern Ocean (Boye et al., 2001); in both cases the tentative explanation was for photochemical breakdown of the ligands. Recently, laboratory studies have demonstrated this effect for a class of iron-binding microbial siderophores (Barbeau et al., 2001). This photochemical process could lead to the reduction and release of Fe^{II} into the upper water column; such a process is believed to have happened during the latter part of the SOIREE experiment (Croot et al., 2001). This process could be important in the Southern Ocean, as the half-life of Fe^{II} is extended because of two main factors: (1) The cold temperatures lead to slower kinetics for the oxidation step (Millero and Sotolongo, 1989; Millero et al., 1987). (2) The low H_2O_2 concentrations in the Southern Ocean (Sarthou et al., 1997) lead to slower overall oxidation rates and can lead to reactions with O_2 being the major sink for Fe^{II}. Significant concentrations of Fe^{II} could therefore persist in oxic seawater in the Southern Ocean, particularly if there was a strong organic complexation of Fe^{II} to further retard the oxidation step (Santana-Casiano et al., 2000). During the present work, we made measurements of the half-life of Fe^{II} at ambient temperature (Croot and Laan, 2002), but never detected any appreciable concentrations of Fe^{II} in the seawater directly, despite a 10 pM detection limit.

4.2.3. Effects of organic complexation on iron biogeochemistry

Estimates of Fe′, the inorganic dissolved iron concentration, provide an indication of the most labile iron pool available to bacteria and phytoplankton. While evidence exists for the ability of phytoplankton to access iron from some iron organic complexes (Hutchins et al., 1999; Maldonado, 1999), currently we have no method to analyse either the complexes directly or identify the members of the bacteria/phytoplankton community that utilize them. Comparison of [Fe′] between Biostations 2 and 3 in the SIE (Table 3) reveals high Fe′ at Biostation 2, which could partly explain the phytoplankton bloom that formed there but not at Biostation 3. Overall, in general there was only a weak relationship between Fe′ and the measured integrated primary productivity during this cruise (Froneman, 2004). In the APF, primary production was high but Fe′ low, perhaps indicating that the phytoplankton were obtained Fe from organic complexes.

Estimates of the iron requirement, growth rate of phytoplankton at ambient iron concentrations for the Southern Ocean are rare. Recently (Timmermans et al., 2001) performed experiments

on both a large (*Chaetceros dichaeta*) and a small (*Chaetceros brevis*) Antarctic diatom. *C. dichaeta* was also found in the present study in significant numbers in both the SIE and APF. Timmermans et al. (2001) determined the iron half saturation constants (K_s) for growth for both species, with the large diatom (*C. dichaeta*, $K_s = 1.1$ nM dissolved Fe, $K_s = 0.46 \times 10^{-9}$ M Fe′) having a significantly higher K_s than the smaller diatom (*C. brevis*, $K_s =$ 0.6 nM dissolved Fe, $K_s = 1 \times 10^{-15}$ M Fe′). The growth of a small diatom, *C. brevis*, was only reduced in the presence of a strong iron chelating agent desferrioxamine B. Applying the results of the Timmermans et al. study to the present work, we can see that *C. brevis* may not have been iron limited in any of the regions. *C. dichaeta* would have been under iron limitation in the WIE, consistent with the microscopic evidence (Karlson, Godhe, 1998). In the APF, *C. dichaeta* should also have been under iron limitation, yet it was reasonably abundant. This highlights problems with interpreting data taken at a location at only one time; it is quite possible that in the APF the bloom was coming to an end, the iron concentration was at a minimum and *C. dichaeta* numbers at a maximum.

Examination of the vertical profile of [Fe′] obtained in the WIE suggests several processes at work: (i) near surface enrichment from direct supply of inorganic iron derived from rain/snow or from photochemical reduction of iron organic complexes, (ii) minimum associated with the Chl maximum, presumably due to the dual effect of uptake of Fe′ by phytoplankton, the production of ligands and subsequent complexation of Fe′ and (iii) maximum at 200 m, possibly related to either the O_2 minimum and/or the zone of zooplankton NH_4 production. The latter process could be related to the regeneration of dissolved Fe from particulate forms after passing through a grazer (Barbeau et al., 1996; Hutchins and Bruland, 1994; Hutchins et al., 1995). At this station in the WIE, both salps (*Salpa thompsoni*) and krill (*Euphausia superba*) overlapped, and consumed up to 86% of daily primary production (Pakhomov, 2004). Vertical migration of these zooplankton and excretion at depth may have caused this maximum in [Fe′].

5. Conclusions

The role of iron has been investigated in the Southern Ocean along 6°E during the austral summer. A large phytoplankton bloom in the SIE was apparently driven by sea ice melt which provided both iron and water column stability; whose bloom developed rapidly when fine weather hastened the ice melt. In the vicinity of the WIE, phytoplankton productivity and biomass were low, due to low iron concentrations and high grazing pressure. While in the APF, despite deep mixed layers, low dissolved iron concentrations and integrated primary productivity were high. Chemical speciation data for iron in the Southern Ocean hint at the importance of zooplankton grazing as a source of labile inorganic iron. Estimates of Fe supply to this region indicate that atmospheric deposition and upwelling are of similar magnitude, and the timing of the pulses are of key importance for phytoplankton growth. Time series data similar to that of BATS and HOTS would greatly improve our understanding of the key processes that control iron distribution and speciation in the Southern Ocean.

Acknowledgements

Special thanks to the officers and crew of the S.A. *Agulhas* who made this work possible. Thanks also to the Swedish Polar Research Secretariat for ship-time and logistical support, Göteborg Marine Research Center (GMF) and Kristineberg Marine Research Station (KMF) for technical support and the Knut and Alice Wallenberg Foundation for their financial support. PLC was funded via a New Zealand Foundation for Research, Science, Technology (FORST) postdoctoral fellowship.

We also thank Roland David (nutrients), Melissa Chierici and Agneta Fransson (O_2 data), the Physical Oceanography group onboard, Per-Ingvar Sehlstedt, Ole Anders Nøst, Anne-Marie Larsson, Leif Djurfeldt and Elisabeth Engum. The technical help of Whitney King (Colby College, USA), Ken Bruland (UCSC) and George Luther III (U Delaware) is greatly appreciated. Help

provided by the SeaWiFS community contributed to this work. The editorial assistance of Leif Anderson and the comments of two anonymous reviewers are gratefully appreciated.

References

Baith, K., Lindsay, R., Fu, G., McClain, C.R., 2001. SeaDAS: a data analysis system for ocean colour satellite sensors. Eos, Transactions of the American Geophysical Union 82, 202.

Barbeau, K., Moffett, J.W., Caron, D.A., Croot, P.L., Erdner, D.L., 1996. Role of protozoan grazing in relieving iron limitation of phytoplankton. Nature 380, 61–64.

Barbeau, K., Rue, E.L., Bruland, K.W., Butler, A., 2001. Photochemical cycling of iron in the surface ocean mediated by microbial iron(III)-binding ligands. Nature 413, 409–413.

Behrenfeld, M.J., Kolber, Z.S., 1999. Widespread iron limitation of phytoplankton in the South Pacific Ocean. Science 283, 840–843.

Blain, S., Tréguer, P., Belviso, S., Bucciarelli, E., Denis, M., Desabre, S., Fiala, M., Jézéquel, V., Fèvre, J.L., Mayzuad, P., Marty, J.-C., Razouls, S., 2000. A biogeochemical study of the island mass effect in the context of the iron hypothesis: Kerguelen Islands and Southern Ocean. Deep-Sea Research I 48, 163–187.

Bowie, A.R., Achterberg, E.P., Mantoura, R.F.C., Worsfold, P.J., 1998. Determination of sub-nanomolar levels of iron in seawater using flow injection with chemiluminescence detection. Analytica Chimica Acta 361, 189–200.

Boyd, P.W., Watson, A., Law, C.S., Abraham, E., Trull, T., Murdoch, R., Bakker, D.C.E., Bowie, A.R., Buesseler, K.O., Chang, H., Charette, M., Croot, P.L., Downing, K., Frew, R., Gall, M., Hadfield, M., Hall, J., Harvey, M., Jameson, G., LaRoche, J., Liddicoat, M., Ling, R., Maldonado, M., McKay, R.M., Nodder, S., Pickmere, S., Pridmore, R., Rintoul, S., Safi, K., Sutton, P., Strzepek, R., Tannenberger, K., Turner, S., Waite, A., Zeldis, J., 2000. Mesoscale iron fertilisation elevates phytoplankton stocks in the polar Southern Ocean. Nature 407, 695–702.

Boye, M., van den Berg, C.M.G., de Jong, J.T.M., Leach, H., Croot, P.L., de Baar, H.J.W., 2001. Organic complexation of iron in the Southern Ocean. Deep-Sea Research I 48, 1477–1497.

Bruland, K.W., Franks, R.P., Knauer, G.A., Martin, J.H., 1979. Sampling and analytical methods for the determination of copper, cadmium, zinc and nickel at the nanogram per liter level in seawater. Analytica Chimica Acta 105, 233–245.

Bucciarelli, E., Blain, S., Treguer, P., 2001. Iron and manganese in the wake of the Kerguelen Islands (Southern Ocean). Marine Chemistry 73, 21–36.

Chierici, M., Fransson, A., Turner, D.R., Pakhomov, E.A., Froneman, P.W., 2004. Variability in pH, fCO_2, oxygen and flux of CO_2 in the surface water along a transect in the Atlantic sector of the Southern Ocean. Deep-Sea Research II, this issue [doi:10.1016/j.dsr2.2001.03.002].

Coale, K.H., Fitzwater, S.E., Gordon, R.M., Johnson, K.S., Barber, R.T., 1996a. Control of community growth and export production by upwelled iron in the equatorial Pacific Ocean. Nature 379, 621–624.

Coale, K.H., Johnson, K.S., Fitzwater, S.E., Gordon, R.M., Tanner, S., Chavez, F.P., Ferioli, L., Sakamoto, C., Rogers, P., Millero, F., Steinberg, P., Nightingale, P., Cooper, D., Cochlan, W.P., Landry, M.R., Constantinou, J., Rollwagen, G., Trasvina, A., Kudela, R., 1996b. A massive phytoplankton bloom induced by an ecosystem-scale iron fertilization experiment in the equatorial Pacific Ocean. Nature 383, 495–501.

Croot, P.L., de Jong, J.T.M., 2000. Field distribution of iron in a section of the Antarctic Polar Frontal Zone. Berichte zur Polarforschung, Alfred-Wegener-Institut für Polar- und Meeresforschung 364, 44–50.

Croot, P.L., Johansson, M., 2000. Determination of iron speciation by cathodic stripping voltammetry in seawater using the competing ligand 2-(2Thiazolylazo)-*p*-cresol (TAC). Electroanalysis 12, 565–576.

Croot, P.L., Laan, P., 2002. Continuous shipboard determination of Fe(II) in Polar waters using flow injection analysis with chemiluminescence detection. Analytica Chimica Acta 466, 261–273.

Croot, P.L., Bowie, A.R., Frew, R.D., Maldonado, M., Hall, J.A., Safi, K.A., La Roche, J., Boyd, P.W., Law, C.S., 2001. Retention of dissolved iron, Fe^{II} in an iron induced Southern Ocean phytoplankton bloom. Geophysical Research Letters 28, 3425–3428.

Croot, P.L., Karlson, B., Wulff, A., Linares, F., Andersson, K., 2002. Trace metal/phytoplankton interactions in the Skagerrak. Journal of Marine Systems 35, 39–60.

Danielsson, L-G., Westerlund, S., 1983. Clean room container for Ymer 80. Ocean Science and Engineering 8, 53–61.

de Baar, H.J.W., de Jong, J.T.M., Nolting, R.F., Timmermans, K.R., van Leeuwe, M.A., Bathmann, U., Rutgers van der Loeff, M., Sildam, J., 1999. Low dissolved Fe and the absence of diatom blooms in remote Pacific waters of the Southern Ocean. Marine Chemistry 66, 1–34.

de Jong, J.T.M., den Das, J., Timmermans, K., de Baar, H.J.W., 1997. Field distribution of iron in a section of the Antarctic Polar Frontal Zone. Berichte zur Polarforschung 221, 53–60.

Duce, R.A., Tindale, N.W., 1991. Atmospheric transport of iron and its deposition in the ocean. Limnology and Oceanography 36, 1715–1726.

Edwards, P.R., 1999. Iron in modern and ancient east Antarctic snow: implications for phytoplankton production in the Southern Ocean. Ph.D. Thesis, University of Tasmania, Australia, Hobart.

Edwards, P.R., Sedwick, P.N., Morgan, V., Boutron, C.F., Hong, S., 1998. Iron in ice cores from Law Dome and East Antarctica: implications for past deposition of aerosol iron. Annals of Glaciology 27, 365–370.

Field, M.P., Sherrell, R.M., 2000. Dissolved and particulate Fe in a hydrothermal plume at 9°45′N, East Pacific Rise: slow Fe(II) oxidation kinetics in Pacific plumes. Geochimica et Cosmochimica Acta 64, 619–628.

Fransson, A., Chierici, M., Anderson, L.G., David, R., 2004. Transformation of carbon and oxygen in the surface layer of the eastern Atlantic sector of the Southern Ocean. Deep-Sea Research II, this issue [doi:10.1016/j.dsr2.2001.12.001].

Froneman, P.W., 2004. Protozooplankton community structure and grazing impact in the eastern Atlantic sector of the Southern Ocean in austral summer 1998. Deep-Sea Research II, this issue [doi:10.1016/j.dsr2.2004.09.001].

Fuse, H., Takimura, O., Kamimura, K., Yamaoka, Y., 1993. Marine algae excrete large molecular weight compounds keeping iron dissolved. Bioscience Biotechnology and Biochemistry 57, 509–510.

Gass, I.G., Harris, P.G., Holdgate, M.W., 1963. Pumice eruption in the areas of the South Sandwich Islands. Geological Magazine 100, 321–330.

Geider, R.J., 1999. Complex lessons of iron uptake. Nature 400, 815–816.

Gerringa, L.J.A., Herman, P.M.J., Poortvliet, T.C.W., 1995. Comparison of the linear van den Berg/Ruzic transformation and a non-linear fit of the Langmuir isotherm applied to Cu speciation data in the estuarine environment. Marine Chemistry 48, 131–142.

Gledhill, M., van den Berg, C.M.G., 1994. Determination of complexation of iron(III) with natural organic complexing ligands in seawater using cathodic stripping voltammetry. Marine Chemistry 47, 41–54.

Hudson, R.J.M., Covault, D.T., Morel, F.M.M., 1992. Investigations of iron coordination and redox reactions in seawater using ^{59}Fe radiometry and ion-pair solvent extraction of amphiphilic iron complexes. Marine Chemistry 38, 209–235.

Hutchins, D.A., Bruland, K.W., 1994. Grazer-mediated regeneration and assimilation of Fe, Zn and Mn from planktonic prey. Marine Ecology Progress Series 110, 259–269.

Hutchins, D.A., Wang, W.-X., Fisher, N.S., 1995. Copepod grazing and the biogeochemical fate of diatom iron. Limnology and Oceanography 40, 989–994.

Hutchins, D.A., DiTullio, G.R., Zhang, Y., Bruland, K.W., 1998. An iron limitation mosaic in the California upwelling system. Limnology and Oceanography 43, 1037–1054.

Hutchins, D.A., Witter, A.E., Butler, A., Luther III, G.W., 1999. Competition among marine phytoplankton for different chelated iron species. Nature 400, 858–861.

Johnson, K.S., Coale, K.H., Elrod, V.A., Tindale, N.W., 1994. Iron photochemistry in seawater from the equatorial Pacific. Marine Chemistry 46, 319–334.

Johnson, K.S., Gordon, R.M., Coale, K.H., 1997. What controls dissolved iron concentrations in the world ocean? Marine Chemistry 57, 137–161.

Karlson, B., Godhe, A., 1998. Phytoplankton observations in the Atlantic sector of the Southern Ocean. Polarforskingssekretariatets årsbok 1998, 69–70.

Kirchman, D.L., 1996. Microbial ferrous wheel. Nature 38[illegible] 303–304.

Kuma, K., Nishioka, J., Matsunaga, K., 1996. Controls o[illegible] iron(III) hydroxide solubility in seawater: the influence [illegible] pH and natural organic chelators. Limnology and Ocean[illegible] graphy 41, 396–407.

Landing, W.M., Lewis, B.L., 1991. Collection, processing, an[illegible] analysis of marine particulate and colloidal material fo[illegible] transition metals. In: Hurd, D.C., Spencer, D.W. (Eds.), Marine Particles: Analysis, Characterization. Geophysica[illegible] Monograph Series. American Geophysical Union.

Löscher, B.M., de Baar, H.J.W., de Jong, J.T.M., Veth, C[illegible] Dehairs, F., 1997. The distribution of Fe in the Antarcti[illegible] Circumpolar Current. Deep-Sea Research II 44, 143–187.

Mahowald, N., Kohfeld, K., Hansson, M., Balkanski, Y[illegible] Harrison, S.P., Prentice, I.C., Schulz, M., Rodhe, H., 199[illegible] Dust sources and deposition during the last glacia[illegible] maximum and current climate: a comparison of mode[illegible] results with paleodata from ice cores and marine sediments[illegible] Journal of Geophysical Research 104, 15895–15916.

Maldonado, M.T., 1999. Utilization of iron bound to strong[illegible] organic ligands by plankton communities in the subarctic[illegible] Pacific Ocean. Deep-Sea Research II 46, 2447–2473.

Martin, J.H., 1990. Glacial–interglacial CO_2 change: the iron[illegible] hypothesis. Paleoceanography 5, 1–13.

Martin, J.H., Gordon, R.M., Fitzwater, S.E., Broenkow[illegible] W.W., 1989. VERTEX: phytoplankton/iron studies in the[illegible] Gulf of Alaska. Deep-Sea Research 36, 649–680.

Martin, J.H., Gordon, R.M., Fitzwater, S.E., 1990. Iron in[illegible] Antarctic waters. Nature 345, 156–158.

Millero, F.J., 1998. Solubility of Fe(III) in seawater. Earth and Planetary Science Letters 154, 323–329.

Millero, F.J., Sotolongo, S., 1989. The oxidation of Fe(II) with H_2O_2 in seawater. Geochimica et Cosmochimica Acta 53, 1867–1873.

Millero, F.J., Sotolongo, S., Izaguirre, M., 1987. The oxidation kinetics of Fe(II) in seawater. Geochimica et Cosmochimica Acta 51, 793–801.

Nolting, R.F., Gerringa, L.J.A., Swagerman, M.J.W., Timmermans, K.R., de Baar, H.J.W., 1998. Fe(III) speciation in the high nutrient and low chlorophyll Pacific region of the Southern Ocean. Marine Chemistry 62, 335–352.

Pakhomov, E.A., 2004. Salp/krill interactions in the eastern Atlantic sector of the Southern Ocean. Deep-Sea Research II, this issue [doi:10.1016/j.dsr2.2001.03.001].

Perissinotto, R., Laubscher, R.K., McQuaid, C.D., 1992. Marine productivity enhancement around Bouvet and the South Sandwich Islands (Southern Ocean). Marine Ecology Progress Series 88, 41–53.

Powell, R.T., King, D.W., Landing, W.M., 1995. Iron distributions in surface waters of the south Atlantic. Marine Chemistry 50, 13–20.

Rubin, J., 1996. Antarctica. Lonely Planet Travel Survival Kit. Lonely Planet Publications, Hawthorn, Vic., Australia (368pp).

Rue, E.L., Bruland, K.W., 1995. Complexation of iron(III) by natural organic ligands in the Central North Pacific as

determined by a new competitive ligand equilibration/adsorptive cathodic stripping voltammetric method. Marine Chemistry 50, 117–138.

Lue, E.L., Bruland, K.W., 1997. The role of organic complexation on ambient iron chemistry in the equatorial Pacific Ocean and the response of a mesoscale iron addition experiment. Limnology and Oceanography 42, 901–910.

Luzic, I., 1982. Theoretical aspects of the direct titration of natural waters and its information yield for trace metal speciation. Analytica Chimica Acta 140, 99–113.

Santana-Casiano, J.M., Gonzalez- Davila, M., Rodriguez, M.J., Millero, F.J., 2000. The effect of organic compounds in the oxidation kinetics of Fe(II). Marine Chemistry 70, 211–222.

Sarthou, G., Jeandel, C., Brisset, L., Amouroux, D., Besson, T., Donard, O.F.X., 1997. Fe and H_2O_2 distributions in the upper water column in the Indian sector of the Southern Ocean. Earth and Planetary Science Letters 147, 83–92.

Sedwick, P.N., DiTullio, G.R., 1997. Regulation of algal blooms in Antarctic shelf water by the release of iron from melting sea ice. Geophysical Research Letters 24, 2515–2518.

Sedwick, P.N., Edwards, P.R., Mackey, D.J., Griffiths, F.B., Parslow, J.S., 1997. Iron and manganese in surface waters of the Australian Subantarctic region. Deep-Sea Research I 44, 1239–1253.

Smetacek, V., de Baar, H.J.W., Bathmann, U.V., Lochte, K., Rutgers van de Loeff, M.M., 1997. Ecology and biogeochemistry of the Antarctic Circumpolar Current during austral spring: a summary of Southern Ocean JGOFS cruise ANT X/6 of R.V. *Polarstern*. Deep-Sea Research II 44, 1–21.

Sohrin, Y., Iwamoto, S., Matsui, M., Obata, H., Nakayama, E., Suzuki, K., Handa, N., Ishii, M., 2000. The distribution of Fe in the Australian sector of the Southern Ocean. Deep-Sea Research I 47, 55–84.

Spokes, L.J., Jickells, T.D., 1996. Factors controlling the solubility of aerosol trace metals in the atmosphere and on mixing into seawater. Aquatic Geochemistry 1, 355–374.

Strickland, J.D.H., Parsons, T.R., 1968. A Manual of Sea-Water Analysis. Fisheries Research Board of Canada, Ottawa, 302pp.

Sutherland, F.L., 1965. Dispersal of pumice and supposedly from the 1962 South Sandwich Islands eruption, on Southern Australian shores. Nature 207, 1332–1335.

Swithinbank, C., McClain, P., Little, P., 1980. Drift tracks of Antarctic icebergs. Polar Record 18, 495–501.

Timmermans, K.R., Gerringa, L.J.A., de Baar, H.J.W., van der Wagt, B., Veldhuis, M.J.W., de Jong, J.T.M., Croot, P.L., Boye, M., 2001. Growth rates of large and small Southern Ocean diatoms in relation to availability of iron in natural seawater. Limnology and Oceanography 46, 260–266.

Turner, D.R., Bertilsson, S., Fransson, A., Pakhomov, E., 2004. The SWEDARP 97/98 marine expedition: overview. Deep-Sea Research II, this issue [doi:10.1016/j.dsr2.2003.08.006].

van den Berg, C.M.G., 1982. Determination of copper complexation with natural organic ligands in seawater by equilibration with MnO_2. I. Theory. Marine Chemistry 11, 307–322.

Watson, A.J., Bakker, D.C.E., Ridgewell, A.J., Boyd, P.W., Law, C.S., 2000. Effect of iron supply on Southern Ocean CO_2 uptake and implications for glacial atmospheric CO_2. Nature 407, 730–733.

Wells, M.L., Price, N.M., Bruland, K.W., 1995. Iron chemistry in seawater and its relationship to phytoplankton: a workshop report. Marine Chemistry 48, 157–182.

Westall, J.C., 1982. FITEQL: a Program for the Determination of Chemical Equilibrium Constants from Experimental Data. Oregon State University, Corvallis, OR.

Whitworth III, T., Nowlin, W.D., 1987. Water masses and currents of the Southern Ocean at the Greenwich Meridian. Journal of Geophysical Research 92, 6462–6476.

Worby, A.P., Massom, R.A., Allison, I., Lyttle, V.I., Heil, P., 1998. East Antarctic sea ice: a review of its structure properties and drift. In: Jeffries, M.O. (Ed.), Antarctic Sea Ice. Physical Processes, Interactions and Variability. Antarctic Research Series. American Geophysical Union, Washington, DC, pp. 41–67.

Wulff, A., Wängberg, S.-Å., 2004. Spatial and vertical distribution of phytoplankton pigments in the eastern Atlantic sector of the Southern Ocean. Deep-Sea Research II, this issue [doi:10.1016/j.dsr2.2001.01.002].

Deep-Sea Research Part II – Instructions to Authors

A more detailed set of instructions can be found in the journal's home page at http://www.elsevier.com/locate/dsr2

1. Submission of Papers

Authors are requested to submit their original manuscript and figures with two copies to the Guest Editor of their Special Issue. Authors should ensure that they submit manuscripts and meet any additional requirements in line with deadlines set by the Guest Editor(s) to ensure that the entire issue can be published in a timely fashion. In most instances, revised manuscripts must be resubmitted within six months of receipt by the author. Failure to do so may lead to additional review, in some instances, rejection of the paper. Submission of a paper implies that it has not been published previously, that it is not under consideration for publication elsewhere, and that if accepted it will not be published elsewhere in the same form, in English or in any other language, without the written consent of the publisher.

2. Manuscript Preparation

General: Manuscripts must be typewritten, double-spaced with wide margins on one side of white paper. Good quality printouts with a font size of 12 or 10 pt are required. The corresponding author should be identified (include a Fax number and E-mail address). Full postal addresses must be given for all co-authors. Authors should consult a recent issue of the journal for style if possible. An electronic copy of the paper should accompany the final version. The Editors reserve the right to adjust style to certain standards of uniformity. Authors should retain a copy of their manuscript since we cannot accept responsibility for damage or loss of papers. Original manuscripts are discarded one month after publication unless the Publisher is asked to return original material after use.

Paper Length: Authors should try to confine the text to no more than 25–30 pages, with a total manuscript length (including figures and tables) of 45–50 pages.

Abstracts: The essential contents of each paper should be recapitulated briefly in an abstract of no more than 500 words at the head of the paper.

Keywords: Please provide up to six subject keywords, plus regional index terms. At least four of the subject keywords should be selected from the *Aquatic Science & Fisheries Thesaurus*. An eletronic version of the Thesaurus can be found at: http://www.csa.com/ helpV3/ ab.html. The Regional terms should be provided as a hierarchical string, eg; USA, California, Monterey Bay.

Text: Follow this order when typing manuscripts: Title, Authors, Affiliations, Abstract, Keywords, Main text, Acknowledgements, Appendix, References, Vitae, Figure Captions and then Tables. The corresponding author should be identified with an asterisk and footnote. All other footnotes (except for table footnotes) should be identified with superscript Arabic numbers.

Units: In general, metric units should be used, preferably the Systeme International (SI). If other units are used (fathoms, F, knots, etc), the metric equivalents must be given in parentheses ( ) or by presenting the dimensionally correct conversion factors as a footnote.

References: All publications cited in the text should be presented in a list of references following the text of the manuscript. In the text refer to the author's name (without initials) and year of publication (e.g. "Since Peterson (1993) has shown that ..." or "This is in agreement with results obtained later (Kramer, 1994)". For three or more authors use the first author followed by "et al.", in the text. The list of references should be arranged alphabetically by authors' names. The manuscript should be carefully checked to ensure that the spelling of authors' names and dates are exactly the same in the text as in the reference list. The title of the journal should not be abbreviated; titles of journals in Russian language should be transliterated and not translated. References should be given in the following form:

Gooday, A.J., Bett, B.J., Shires, R., Lambshead, P.J.D., 1998. Deep-sea benthic foraminiferal species diversity in the NE Atlantic and NW Arabian Sea: a synthesis. Deep-Sea Research Part II 45 (1–3), 165–201.

Hessler, R.R., Wilson, G.D.F., 1983. The origin and biogeography of malacostracan crustaceans in the deep sea. In: Sims, R.W., Price, J.H., Whalley, P.E.S. (Eds.), Evolution, time and space: the emergence of the biosphere. Academic Press. London, pp. 227–254. Thiel, H., 1983. Benthos size classification. Deep-Sea Newsletter 20, 8–11.

References to unpublished literature should be set out in the format detailed below. The following information needs to be provided: Names and initials of all authors., year. Title of work. All other relevant information needed to identify items (e.g., technical report, Ph.D. Thesis, institute, current status, i.e. in press/unpublished, etc).

Marstakas, N., 1990. Relationships of morphological and physicochemical properties of vertisols under Greek climate conditions. Ph.D. Thesis, Agricultural University Athens, unpublished.

Examples of appropriate citation formats for non-text and electronic-only information can be found in the Guide for Authors at the Deep-Sea Research Part II website. However, it is requested that a web site address, or listserver message is given as a reference only where the information is unavailable in a more permanent form. If such sources are given, then please give as complete information as is possible. All references to such material in the text of the article must be supported by a full entry in the bibliography.

Illustrations: All illustrations should be provided in camera-ready form, suitable for reproduction (which may include reduction) without retouching. Photographs, charts and diagrams are all to be referred to as "Figure(s)" and should be numbered consecutively in the order to which they are referred. They should accompany the manuscript, but should not be included within the text. All illustrations should be clearly marked on the back with the figure number and the author's name. All figures are to have a caption. Captions should be supplied on a separate sheet.

Line drawings: Good quality printouts on white paper produced in black ink are required. All lettering, graph lines and points on graphs should be sufficiently large and bold to permit reproduction when the diagram has been reduced to a size suitable for inclusion in the journal. Dye-line prints or photocopies are not suitable for reproduction. Do not use any type of shading on computer-generated illustrations.
Photographs: Original photographs must be supplied as they are to be reproduced (e.g. black and white or colour). If necessary, a scale should be marked on the photograph. Please note that photocopies of photographs are not acceptable. Half-tone illustrations should be kept to a minimum.
Fold-charts: The cost of fold-charts or diagrams must be borne by the author or his institution. *Colour:* Authors will be charged for colour reproduction as follows: €350 (or US$350) for the first page, €175 (or US$175) for subsequent pages.
Submit colour illustrations as original photographs, high-quality computer prints or transparencies, close to the size expected in publication, or as 35 mm slides. Polaroid colour prints are not suitable. If, together with your accepted article, you submit usable colour figures then Elsevier will ensure, at no additional charge, that these figures will appear in colour on the web (e.g., ScienceDirect and other sites) regardless of whether or not these illustrations are reproduced in colour in the printed version. For colour reproduction in print, you will receive information regarding the costs from Elsevier after receipt of your accepted article. For further information on the preparation of electronic artwork, please see *Artwork Instructions*. Please note: Because of technical complications which can arise by converting colour figures to 'grey scale' (for the printed version should you not opt for colour in print) please submit in addition usable black and white prints corresponding to all the colour illustrations.
Tables: Tables should be numbered consecutively and given a suitable caption and each table typed on a separate sheet. Footnotes to tables should be typed below the table and should be referred to by superscript lowercase letters. No vertical rules should be used. Tables should not duplicate results presented elsewhere in the manuscript, (e.g. in graphs).

Authors in Japan kindly note: Upon request Elsevier Japan will provide a list of people who can check and improve the English of an article (*before submission*). Please contact our Tokyo office: Elsevier Japan K.K., 1-9-15 Higashi Azabu, Minato-ku, Tokyo 106-0044, Japan; tel.: +81-3-5561-5032; fax: +81-3-5561-5045; e-mail: jp.info@elsevier.com

3. Electronic Submission

Authors should submit an electronic copy of their paper with the final version of the manuscript. The electronic copy should match the hardcopy exactly. For authors using LaTex, the document style files, as well as the instructions "Preparing articles with LaTex" in the form of a dvi file, can be obtained free of charge from any host on the Comprehensive Tex Archive Network (CTAN) using anonymous ftp. The primary CTAN hosts are ftp.dante.de and ftp.tex.ac.uk. The Elsevier macros are in /pub/tex/macros/latex/contrib/supported/elsevier. These can also be downloaded from the Internet site http://www.tex.ac.uk. Always keep a back up copy of the electronic file for reference and safety. Full details of electronic submission and other formats can be obtained from http://authors.elsevier.com or from Author Support at Elsevier.

4. Proofs

Proofs will be sent to the author (first named author if no corresponding author is identified of multi-authored papers) and should be returned within 48 hours of receipt. Corrections should be restricted to typesetting errors; any others may be charged to the author. Any queries should be answered in full. Please note that authors are urged to check their proofs carefully before return, since the inclusion of late corrections cannot be guaranteed. If authors are expecting to be away from their office when the proofs arrive, arrangements should be made with colleagues for the proofs to be checked in the authors absence. Proofs are to be returned to the Log-in Department, Elsevier, Stover Court, Bampfylde Street, Exeter, Devon EX1 2AH, UK.

5. Offprints

Twenty-five offprints and a copy of the issue will be supplied free of charge to each corresponding author of a paper. Additional offprints can be ordered at a specially reduced rate using the order form sent to the corresponding author after the manuscript has been accepted. Orders for reprints will incur a 50% surcharge.

6. Copyright

All authors must sign the "Transfer of Copyright" agreement before the article can be published. This transfer agreement enables Elsevier Ltd to protect the copyrighted material for the authors, but does not relinquish the author's proprietary rights. The copyright transfer covers the exclusive rights to reproduce and distribute the article, including reprints, photographic reproductions, microfilm or any other reproductions of similar nature and translations. Includes the right to adapt the article for use in conjunction with computer systems and programs, including reproduction or publication in machine-readable form and incorporation in retrieval systems. Authors are responsible for obtaining from the copyright holder permission to reproduce any figures for which copyright exists.

7. Author Enquiries

For enquiries relating to the submission of articles (including electronic submission), the preparation of electronic artwork, the status of accepted articles, author Frequently Asked Questions and any other enquiries relating to Elsevier Science, please consult http://authors.elsevier.com
Contact details for questions arising after acceptance of an article, especially those relating to proofs, are provided when an article is accepted for publication.
Authors can also keep a track on the progress of their accepted article, and setup e-mail alerts informing them of changes to their manuscripts status, by using the "Track a paper" feature of Elsevier's Author gateway (http://authors.elsevier.com).

(*Continued from outside back cover*)

D. Chen, S.-Å. Wängberg, A. Wulff and K. Borne	2673	Attenuation of biologically effective UV doses under overcast skies: a case study from the eastern Atlantic sector of the Southern Ocean
T. Tanhua, K.A. Olsson and E. Fogelqvist	2683	A first study of SF_6 as a transient tracer in the Southern Ocean
A. Wulff and S.-Å. Wängberg	2701	Spatial and vertical distribution of phytoplankton pigments in the eastern Atlantic sector of the Southern Ocean
P.W. Froneman, E.A. Pakhomov and M.G. Balarin	2715	Size-fractionated phytoplankton biomass, production and biogenic carbon flux in the eastern Atlantic sector of the Southern Ocean in late austral summer 1997–1998
S.-Å. Wängberg and A. Wulff	2731	Impact of ultraviolet-B radiation on the development of phytoplankton communities in the eastern Atlantic sector of the Southern Ocean—results from on-deck model ecosystem experiments
K. Abrahamsson, S. Bertilsson, M. Chierici, A. Fransson, P.W. Froneman, A. Lorén and E.A. Pakhomov	2745	Variations of biochemical parameters along a transect in the Southern Ocean, with special emphasis on volatile halogenated organic compounds
A. Fransson, M. Chierici, L.G. Anderson and R. David	2757	Transformation of carbon and oxygen in the surface layer of the eastern Atlantic sector of the Southern Ocean
M. Chierici, A. Fransson, D.R. Turner, E.A. Pakhomov and P.W. Froneman	2773	Variability in pH, fCO_2, oxygen and flux of CO_2 in the surface water along a transect in the Atlantic sector of the Southern Ocean
K. Abrahamsson, A. Lorén, A. Wulff and S.-Å. Wängberg	2789	Air–sea exchange of halocarbons: the influence of diurnal and regional variations and distribution of pigments
A.-M. Larsson	2807	The role of mixing in an Antarctic ocean ecosystem: observations and model computations of vertical distributions of related parameters
A. Fransson, M. Chierici and L.G. Anderson	2827	Diurnal variability in the oceanic carbon dioxide system and oxygen in the Southern Ocean surface water
M. Öztürk, P.L. Croot, S. Bertilsson, K. Abrahamsson, B. Karlson, R. David, A. Fransson and E. Sakshaug	2841	Iron enrichment and photoreduction of iron under UV and PAR in the presence of hydroxycarboxylic acid: implications for phytoplankton growth in the Southern Ocean
P.L. Croot, K. Andersson, M. Öztürk and D.R. Turner	2857	The distribution and speciation of iron along 6°E in the Southern Ocean

CONTENTS Direct This journal is part of **ContentsDirect**, the *free* alerting service which sends tables of contents by e-mail for Elsevier books and journals. You can register for **ContentsDirect** online at: **www.elsevier.com/locate/contentsdirect**

Indexed/abstracted in: *Curr Cont/Agri Bio Env Sci. Cirr Cont/Phys. Chem. Earth Sci, Curr Cont Sci Cit Ind, Res Alert, Global Change, Curr Aware BioSci, Geobase, Ocean Lit Rev, Awuat Sci. Fish Abstr, Meteor, Geoastrophys Abstr*

ISSN 0967-0645

ELSEVIER

DEEP-SEA RESEARCH PART II

Topical Studies in Oceanography

The SWEDARP 1997/98 Expedition

Volume 51, Numbers 22–24, 2004

CONTENTS

D.R. Turner, S. Bertilsson, A. Fransson and E. Pakhomov	2543	The SWEDARP 1997/98 marine expedition: overview
S. Bertilsson, P. Carlsson and W. Granéli	2557	Influence of solar radiation on the availability of dissolved organic matter to bacteria in the Southern Ocean
W. Granéli, P. Carlsson and S. Bertilsson	2569	Bacterial abundance, production and organic carbon limitation in the Southern Ocean (39–62°S, 4–14°E) during the austral summer 1997/1998
K.E. Rasmus, W. Granéli and S.-Å. Wängberg	2583	Optical studies in the Southern Ocean
E.A. Pakhomov and P.W. Froneman	2599	Zooplankton dynamics in the eastern Atlantic sector of the Southern Ocean during the austral summer 1997/1998—Part 1: Community structure
E.A. Pakhomov and P.W. Froneman	2617	Zooplankton dynamics in the eastern Atlantic sector of the Southern Ocean during the austral summer 1997/1998—Part 2: Grazing impact
P.W. Froneman	2633	Protozooplankton community structure and grazing impact in the eastern Atlantic sector of the Southern Ocean in austral summer 1998
E.A. Pakhomov	2645	Salp/krill interactions in the eastern Atlantic sector of the Southern Ocean
L.M. Jantunen, H. Kylin and T.F. Bidleman	2661	Air–water gas exchange of α-hexachlorocyclohexane enantiomers in the South Atlantic Ocean and Antarctica

(*Continued on inside back cover*)

Visit our home page:
http://www.elsevier.com/locate/dsr2

Printed in Great Britain by Alden Press Ltd., Osney Mead, Oxford OX2 OEF

Also available on
SCIENCE DIRECT®
www.sciencedirect.com